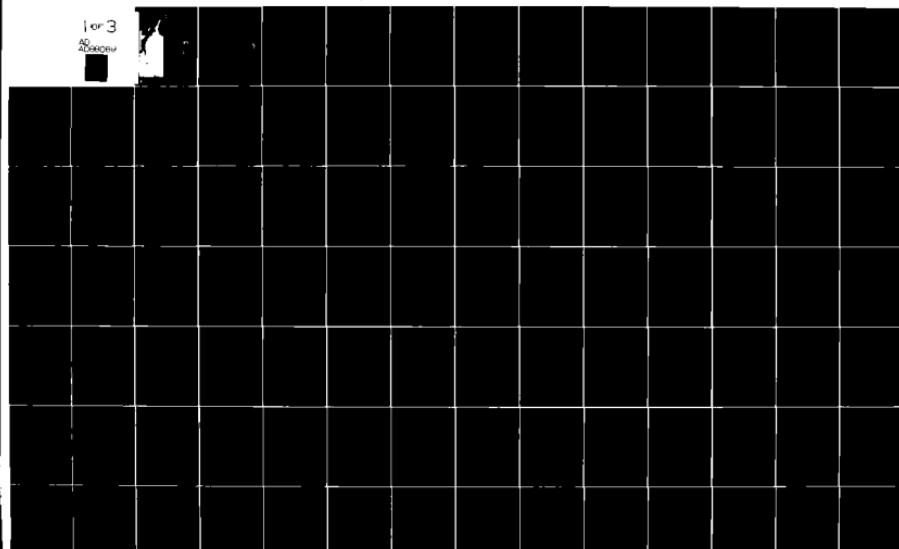
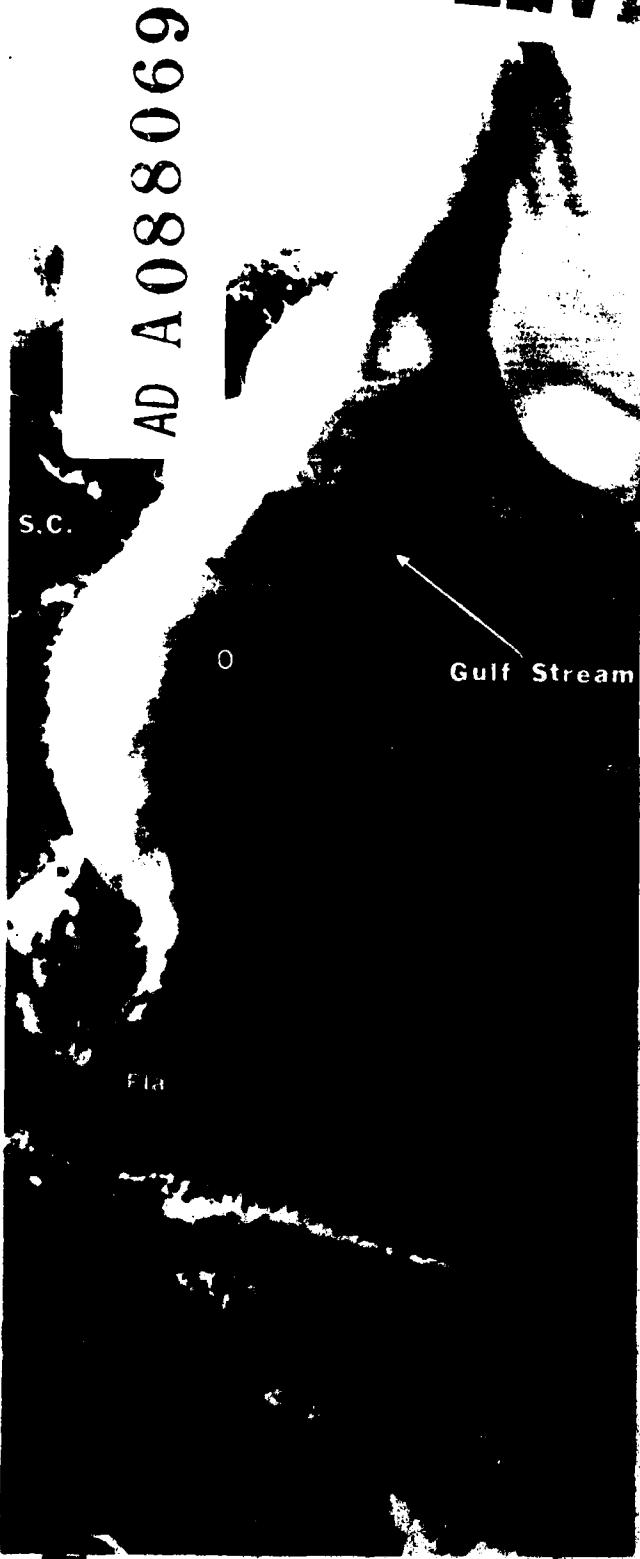


DO-A088 069

TEXAS A AND M UNIV COLLEGE STATION DEPT OF OCEANOGRAPHY F/0 8/3
THE GULF STREAM MEANDERS EXPERIMENT, CURRENT METER, ATMOSPHERIC--ETC(U)
JUL 80 D A BROOKS, J M BANE, R L COHEN N00014-77-C-0354
UNCLASSIFIED TANU-REF-80-7-T NL

1 or 3
Scanned





LEVEL

12

THE GULF STREAM MEANDERS EXPERIMENT

Current Meter, Atmospheric,
and Sea Level Data Report
for the January to May, 1979

Mooring Period

by

DTIC
SELECTED
AUG 20 1980
S

David A. Brooks

John M. Bane

Robert L. Cohen

Paul Blankinship

This document has been approved
for public release and sale; its
distribution is unlimited.

Texas A&M University

Reference 80-7-T

July 1980

80 8 19 001

12

THE GULF STREAM MEANDERS EXPERIMENT

Current Meter, Atmospheric, and
Sea Level Data Report for the
January to May, 1979 Mooring Period.

9/1/80

by

10

David A. Brooks
John M. Bane¹
Robert L. Cohen
Paul Blankinship²

DTIC
SELECTED
AUG 20 1980
S C D

15 NCOO14-77-C-0354
[] 4277
VNSF-OC673-06719

Texas A&M University
Reference 80-7-T
July 1980

This document has been approved
for public release and sale. Its
distribution is unlimited.

¹ University of North Carolina at Chapel Hill.
² North Carolina State University at Raleigh

401003

FOREWORD

This is the second in a sequence of seven reports from the Gulf Stream Meanders Experiment. The field phases of the experiment were implemented as a joint project of principal investigators at Texas A&M University (DAB), and at the University of North Carolina at Chapel Hill (JMB). The complete set of reports, not necessarily listed in their order of availability, is expected to be:

1. Hydrographic Data Report, EN-031 (Jan 79) and EN-037 (May 79).
TAMU Technical Report 80-1-T, January 1980, 145 pp.
2. Current Meter, Atmospheric, and Sea Level Data Report for the
January to May 1979 Mooring Period. TAMU Technical Report
80-7-T, July 1980, 264 pp.
3. Hydrographic Data Report, EN-040 (Aug 79) and EN-045 (Nov 79)
4. Current Meter, Atmospheric, and Sea Level Data Report for the
August to November 1979 Mooring Period.
5. Air-dropped XBT survey data report, Feb 79.
6. Air-dropped XBT survey data report, Nov 79.
7. Final project technical report.

Reports number 4, 5, and 6 will be issued at the University of North Carolina.

Accession For	
NTIS GRA&I	
DDC TAB	
Unannounced	
Justification _____	
By _____	
Date _____	
Availability _____	
Comments _____	
Initials _____	Date _____

A

Contents

	<i>page</i>
FOREWORD	ii
SECTION 1. Setting and Design of the Experiment	1
1.1. Historical Aspects	1
1.2. The Moored Instrument Array	3
1.3. Supporting Observations	9
SECTION 2. Data Sources, Processing, and Basic Statistics	10
2.1. Transcription of Aanderaa Data Tapes	10
2.2. Instrument Calibration	10
2.3. Aanderaa Data Editing	28
2.4. Ancillary Data Sources	28
2.5. Data Processing	29
2.6. Basic Statistics of the Current Meter Data Set	31
2.7. Data Presentation Formats	47
SECTION 3. Raw and 40 HRLP Data for Each Instrument	48
SECTION 4. 3-40 HRBP Data for Each Instrument	99
SECTION 5. 40 HRLP Data for Each Mooring	149
SECTION 6. 40 HRLP Current Vector "Stick" Plots for Each Mooring	170
SECTION 7. 40 HRLP Atmospheric Data from Cape Hatteras and NDBO Buoy 41004	191
SECTION 8. Comparison of 40 HRLP Wind Stress and Current Vector "Sticks"	199
SECTION 9. 40 HRLP Sea Level Height, Wind Stress, and Current Velocity Components	206
SECTION 10. Spectrum Calculations for Various Combinations of 40 HRLP Data Sets	212
Acknowledgments	262
References	263

List of Tables

<i>Table</i>	<i>page</i>
1. Instrument identification, start and stop times, depths, and mooring locations.	8
2. Aanderaa-supplied (Aa) and calibration-produced (Cal) coefficients for the conversion of recorded binary numbers to scientific units. The general formula $V = A + BN + CN^2 + DN^3$ was used, where V is the variable, and N is decimal equivalent (0 - 1023) of the recorded binary number.	15
3. First-order and variance statistics of temperature (T) and velocity components (u, v) from each instrument, shown from 3 HRLP, 3-40 HRLP, and 40 HRLP filtered data sets.	32
4. Sub-band variance ratios for temperature (T) and velocity components (u, v) from each instrument. The sub-bands approximately divide the principal tidal and inertial spectrum (3-40 HRBP) for the low frequency spectrum (40 HRLP).	35

List of Figures

<i>Figure</i>	<i>page</i>
1. Map of the South Atlantic Bight, showing the location of the Gulf Stream Meanders Experiment (inset box). Atmospheric data from moored NOAA buoy NDB0-4 and from Cape Hatteras are shown in this report. [NDB0-2 data were not available in time for this report, but will be shown in a subsequent one.]	2
2. Cross-shelf section of the Gulf Stream off Cape Fear, showing two-month mean summer isotachs. The position of the A and B mooring current meters have been projected about 10 km upstream onto this section.	4
3. Detailed map of the experiment area (the inset box Fig. 1), showing the locations of moorings "A" through "D", with the record-long mean current vectors at the top (T), middle (M), and bottom (B) instruments. The mooring "D" position is shown displaced (inset box) for clarity.	5
4. Typical mooring design, showing the position of Aanderaa current meters (Aa) in the wire held taut by a large main float and a train-wheel anchor. The C and D moorings also supported Aanderaa thermographs (Ther. Aa), but early thermistor string failures occurred in both cases. AMF (now EG&G) sea-link acoustic releases were used.	7
5. Speed and conductivity calibration graphs, using the cubic coefficients supplied by Aanderaa (Aa), which were applied to all instruments.	16
6. Calibration curves for compass direction, based on coefficients supplied by Aanderaa (-) and coefficients based on directly measured calibration data (----). The latter were used for calibration of all instruments except numbers 3423, 3332 and 3337.	17
7. Calibration curves for temperature, based on coefficients supplied by Aanderaa (-), and coefficients based on directly measured calibration data (----). The latter were used for calibration of all instruments.	21

8. Calibration curves for pressure, based on coefficients supplied by Aanderaa (-) and coefficients based on directly measured calibration data (----) over the range 0 to 500 PSIG. The two curves diverge and were not used for pressures higher than 500 PSIG because of the curve-fitting process. The highest *in-situ* pressures were less than 500 PSIG. 27
9. Response function for the 40 hour low pass Lanczos filter. 30
10. Polar histogram for instrument A-top showing the normalized magnitude distribution of the 3 HRLP velocity, accumulated vectorially in ten degree sectors. The downstream (+ v) direction of the rotated coordinate system is shown by the radial tick mark. 37
11. Polar histogram for instrument A-bot showing the normalized magnitude distribution of the 3 HRLP velocity, accumulated vectorially in ten degree sectors. The downstream (+ v) direction of the rotated coordinate system is shown by the radial tick mark. 38
12. Polar histogram for instrument B-top showing the normalized magnitude distribution of the 3 HRLP velocity, accumulated vectorially in ten degree sectors. The downstream (+ v) direction of the rotated coordinate system is shown by the radial tick mark. 39
13. Polar histogram for instrument B-bot showing the normalized magnitude distribution of the 3 HRLP velocity, accumulated vectorially in ten degree sectors. The downstream (+ v) direction of the rotated coordinate system is shown by the radial tick mark. 40
14. Polar histogram for instrument C-top showing the normalized magnitude distribution of the 3 HRLP velocity, accumulated vectorially in ten degree sectors. The downstream (+ v) direction of the rotated coordinate system is shown by the radial tick mark. 41
15. Polar histogram for instrument C-mid showing the normalized magnitude distribution of the 3 HRLP velocity, accumulated vectorially in ten degree sectors. The downstream (+ v) direction of the rotated coordinate system is shown by the radial tick mark. 42
16. Polar histogram for instrument C-bot showing the normalized magnitude distribution of the 3 HRLP velocity, accumulated vectorially in ten degree sectors. The downstream (+ v) direction of the rotated coordinate system is shown by the radial tick mark. 43

17. Polar histogram for instrument D-top showing the normalized magnitude distribution of the 3 HRLP velocity, accumulated vectorially in ten degree sectors. The downstream (+ v) direction of the rotated coordinate system is shown by the radial tick mark. 44
18. Polar histogram for instrument D-mid showing the normalized magnitude distribution of the 3 HRLP velocity, accumulated vectorially in ten degree sectors. The downstream (+ v) direction of the rotated coordinate system is shown by the radial tick mark. 45
19. Polar histogram for instrument D-bot showing the normalized magnitude distribution of the 3 HRLP velocity, accumulated vectorially in ten degree sectors. The downstream (+ v) direction of the rotated coordinate system is shown by the radial tick mark. 46
20. Raw and 40HRLP salinity, velocity component, and temperature data from instrument A-top. The positive (v, u) directions are (downstream, offshore). 49
21. Raw and 40HRLP salinity, velocity component, and temperature data from instrument A-bot. The positive (v, u) directions are (downstream, offshore). 54
22. Raw and 40HRLP salinity, velocity component, and temperature data from instrument B-top. The positive (v, u) directions are (downstream, offshore). 59
23. Raw and 40HRLP salinity, velocity component, and temperature data from instrument B-bot. The positive (v, u) directions are (downstream, offshore). 64
24. Raw and 40HRLP salinity, velocity component, and temperature data from instrument C-top. The positive (v, u) directions are (downstream, offshore). 69
25. Raw and 40HRLP salinity, velocity component, and temperature data from instrument C-mid. The positive (v, u) directions are (downstream, offshore). 74
26. Raw and 40HRLP salinity, velocity component, and temperature data from instrument C-bot. The positive (v, u) directions are (downstream, offshore). 79
27. Raw and 40HRLP salinity, velocity component, and temperature data from instrument D-top. The positive (v, u) directions are (downstream, offshore). 84
28. Raw and 40HRLP salinity, velocity component, and temperature data from instrument D-mid. The positive (v, u) directions are (downstream, offshore). 89

29.	Raw and 40HRLP salinity, velocity component, and temperature data from instrument D-bot. The positive (v, u) directions are (downstream, offshore).	94
30.	3 to 40 HRBP salinity, velocity component, and temperature data for instrument A-top.	100
31.	3 to 40 HRBP salinity, velocity component, and temperature data for instrument A-bot.	105
32.	3 to 40 HRBP salinity, velocity component, and temperature data for instrument B-top.	110
33.	3 to 40 HRBP salinity, velocity component, and temperature data for instrument B-bot.	115
34.	3 to 40 HRBP salinity, velocity component, and temperature data for instrument C-top.	120
35.	3 to 40 HRBP salinity, velocity component, and temperature data for instrument C-mid.	125
36.	3 to 40 HRBP salinity, velocity component, and temperature data for instrument C-bot.	129
37.	3 to 40 HRBP salinity, velocity component, and temperature data for instrument D-top.	134
38.	3 to 40 HRBP salinity, velocity component, and temperature data for instrument D-mid.	139
39.	3 to 40 HRBP salinity, velocity component, and temperature data for instrument D-bot.	144
40.	Pressure, salinity, velocity component, and temperature data shown jointly for all instruments on the "A" mooring. All data shown are 40 HRLP filtered except for the pressure (topmost instrument only), which is unfiltered.	150
41.	Pressure, salinity, velocity component, and temperature data shown jointly for all instruments on the "B" mooring. All data shown are 40 HRLP filtered except for the pressure (topmost instrument only), which is unfiltered.	155
42.	Pressure, salinity, velocity component, and temperature data shown jointly for all instruments on the "C" mooring. All data shown are 40 HRLP filtered except for the pressure (topmost instrument only), which is unfiltered.	160
43.	Pressure, salinity, velocity component, and temperature data shown jointly for all instruments on the "D" mooring. All data shown are 40 HRLP filtered except for the pressure (topmost instrument only), which is unfiltered.	165

44.	Vector or "stick" plots of 40 HRLP currents shown jointly for all instruments on the "A" mooring. The downstream direction is toward the top of the figure.	171
45.	Vector or "stick" plots of 40 HRLP currents shown jointly for all instruments on the "B" mooring. The downstream direction is toward the top of the figure.	176
46.	Vector or "stick" plots of 40 HRLP currents shown jointly for all instruments on the "C" mooring. The downstream direction is toward the top of the figure.	181
47.	Vector or "stick" plots of 40 HRLP currents shown jointly for all instruments on the "D" mooring. The downstream direction is toward the top of the figure.	186
48.	Wind stress vectors, atmospheric pressure, and temperature at Cape Hatteras and at the NDBO-4 buoy. The NDBO sea surface temperature is also shown.	192
49.	Comparison of the NDBO wind stress vector "sticks" with the current vector "sticks" at the top instruments.	200
50.	Barometrically-adjusted sea level height at Beaufort and Southport, NDBO wind stress vector components, and current vector components at the top instruments on the A, B and D moorings. All data shown are 40 HRLP filtered.	207
51.	Spectrum, phase, and coherence calculations for $A_T V / B_T V$ Winter 40 HRLP	214
52.	Spectrum, phase, and coherence calculations for $B_T V / C_T V$ Winter 40 HRLP	215
53.	Spectrum, phase, and coherence calculations for $B_T V / D_M V$ Winter 40 HRLP	216
54.	Spectrum, phase, and coherence calculations for $B_T V / B_B V$ Winter 40 HRLP	217
55.	Spectrum, phase, and coherence calculations for $B_T U / B_T V$ Winter 40 HRLP	218
56.	Spectrum, phase, and coherence calculations for $A_T U / B_T U$ Winter 40 HRLP	219
57.	Spectrum, phase, and coherence calculations for $A_B U / B_B U$ Winter 40 HRLP	220
58.	Spectrum, phase, and coherence calculations for $C_M V / D_M V$ Winter 40 HRLP	221

59.	Spectrum, phase, and coherence calculations for C _M U / D _M U Winter 40 HRLP	222
60.	Spectrum, phase, and coherence calculations for V-Stress _{NDB0} / V-Stress _{NDB0} Winter 40 HRLP	223
61.	Spectrum, phase, and coherence calculations for U-Stress _{NAT} / U-Stress _{NDB0} Winter 40 HRLP	224
62.	Spectrum, phase, and coherence calculations for ADJ SL _{SPT} / ADJ SL _{SPT} Winter 40 HRLP	225
63.	Spectrum, phase, and coherence calculations for V-Stress _{NDB0} / ADJ SL _{SPT} Winter 40 HRLP	226
64.	Spectrum, phase, and coherence calculations for V-Stress _{NDB0} / ADJ SL _{SPT} Winter 40 HRLP	227
65.	Spectrum, phase, and coherence calculations for V-Stress _{NDB0} / A _T U Winter 40 HRLP	228
66.	Spectrum, phase, and coherence calculations for V-Stress _{NDB0} / A _T V Winter 40 HRLP	229
67.	Spectrum, phase, and coherence calculations for V-Stress _{NDB0} / B _T U Winter 40 HRLP	230
68.	Spectrum, phase, and coherence calculations for V-Stress _{NDB0} / B _T V Winter 40 HRLP	231
69.	Spectrum, phase, and coherence calculations for V-Stress _{NDB0} / C _M U Winter 40 HRLP	232
70.	Spectrum, phase, and coherence calculations for V-Stress _{NDB0} / C _T U Winter 40 HRLP	233
71.	Spectrum, phase, and coherence calculations for V-Stress _{NDB0} / C _T V Winter 40 HRLP	234
72.	Spectrum, phase, and coherence calculations for V-Stress _{NDB0} / C _M V Winter 40 HRLP	235
73.	Spectrum, phase, and coherence calculations for V-Stress _{NDB0} / D _M U Winter 40 HRLP	236
74.	Spectrum, phase, and coherence calculations for V-Stress _{NDB0} / D _M V Winter 40 HRLP	237
75.	Spectrum, phase, and coherence calculations for V-Stress _{NDB0} / A _B U Winter 40 HRLP	238
76.	Spectrum, phase, and coherence calculations for V-Stress _{NDB0} / A _B V Winter 40 HRLP	239

77.	Spectrum, phase, and coherence calculations for V-Stress _{NDB0} / B _B U Winter 40 HRLP	240
78.	Spectrum, phase, and coherence calculations for V-Stress _{NDB0} / B _B V Winter 40 HRLP	241
79.	Spectrum, phase, and coherence calculations for U-Stress _{NDB0} / ADJ SL _{SPT} Winter 40 HRLP	242
80.	Spectrum, phase, and coherence calculations for U-Stress _{NDB0} / ADJ SL _{SPT} Winter 40 HRLP	243
81.	Spectrum, phase, and coherence calculations for U-Stress _{NDB0} / A _T U Winter 40 HRLP	244
82.	Spectrum, phase, and coherence calculations for U-Stress _{NDB0} / A _T V Winter 40 HRLP	245
83.	Spectrum, phase, and coherence calculations for U-Stress _{NDB0} / B _T U Winter 40 HRLP	246
84.	Spectrum, phase, and coherence calculations for U-Stress _{NDB0} / B _T V Winter 40 HRLP	247
85.	Spectrum, phase, and coherence calculations for U-Stress _{NDB0} / D _T U Winter 40 HRLP	248
86.	Spectrum, phase, and coherence calculations for U-Stress _{NDB0} / C _T V Winter 40 HRLP	249
87.	Spectrum, phase, and coherence calculations for U-Stress _{NDB0} / A _B U Winter 40 HRLP	250
88.	Spectrum, phase, and coherence calculations for U-Stress _{NDB0} / A _B V Winter 40 HRLP	251
89.	Spectrum, phase, and coherence calculations for U-Stress _{NDB0} / B _B U Winter 40 HRLP	252
90.	Spectrum, phase, and coherence calculations for U-Stress _{NDB0} / B _B V Winter 40 HRLP	253
91.	Spectrum, phase, and coherence calculations for A _T U / ADJ SL _{SPT} Winter 40 HRLP	254
92.	Spectrum, phase, and coherence calculations for A _T V / ADJ SL _{SPT} Winter 40 HRLP	255
93.	Spectrum, phase, and coherence calculations for B _T U / ADJ SL _{SPT} Winter 40 HRLP	256
94.	Spectrum, phase, and coherence calculations for B _T V / ADJ SL _{SPT} Winter 40 HRLP	257

SECTION 1

Setting and Design of the Experiment

1.1 HISTORICAL ASPECTS

The principal objective of the Gulf Stream Meanders Experiment was to kinematically and dynamically describe the nature of meanders. The upper continental slope region off Onslow Bay, North Carolina (inset box, Fig. 1) was chosen for the experiment site because several previous investigations in that area provided a baseline data set giving some ideas about time and space variability scales within and a several-month mean view of the Stream (Webster, 1961a, b; Richardson, *et al.*, 1969). In addition, earlier observations ranging from reports in centuries-old ship logs to recent satellite infrared imagery made it apparent that Gulf Stream meandering was more intense between Charleston and Cape Hatteras than elsewhere in the South Atlantic Bight (Fig. 1). For more details on the historical aspects and preliminary interpretation of the data presented here, see Brooks and Bane (1980).

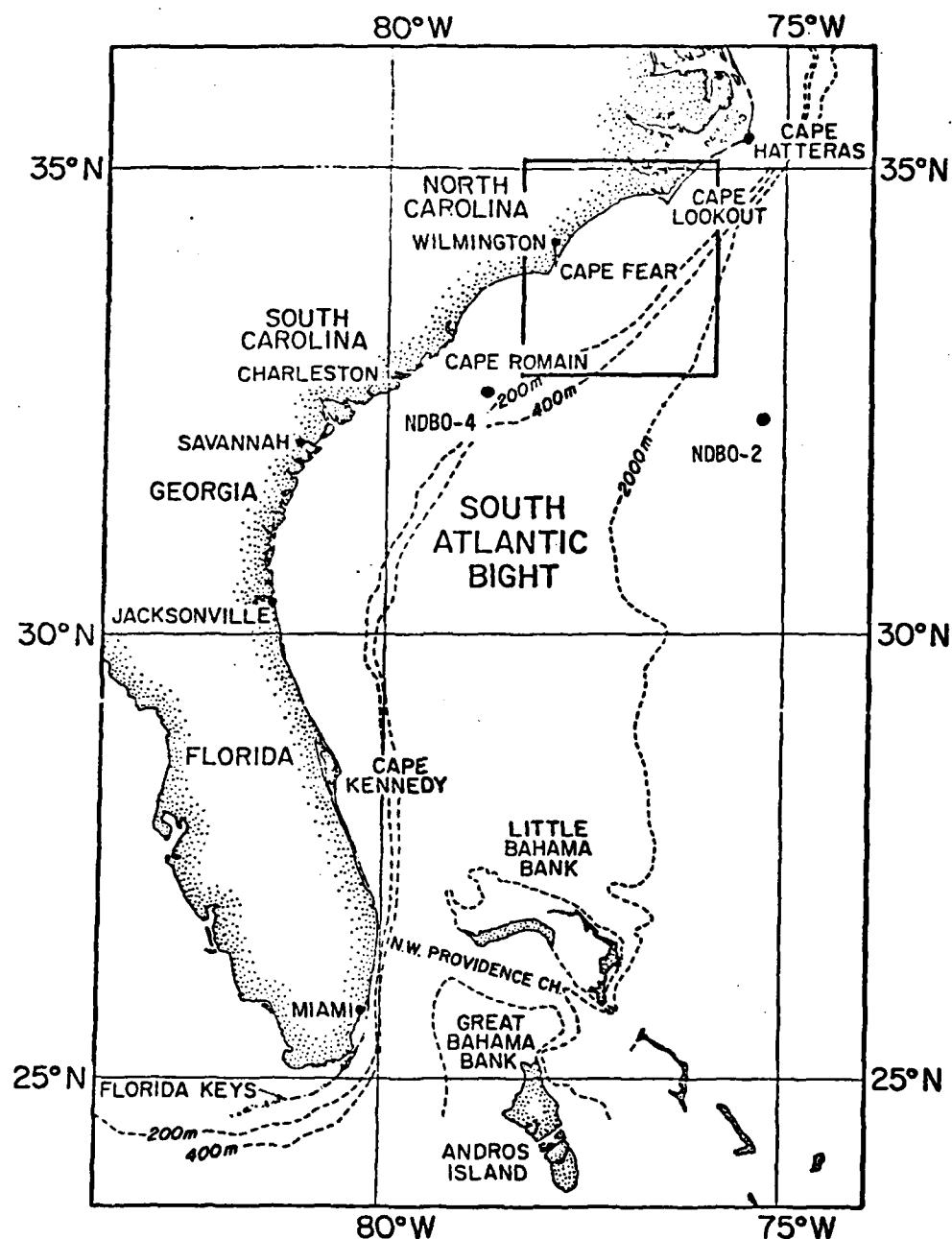


Figure 1. Map of the South Atlantic Bight, showing the location of the Gulf Stream Meanders Experiment (inset box). Atmospheric data from moored NOAA buoy NDBO-4 and from Cape Hatteras are shown in this report. [NDBO-2 data were not available in time for this report, but will be shown in a subsequent one.]

1.2 THE MOORED INSTRUMENT ARRAY

Averaged over two months, the Gulf Stream current speed on a section perpendicular to the topography off Cape Fear shows a broad, surface-intensified core (Richardson, *et al.*, 1969) extending over most of the upper continental slope (Fig. 2). Viewed on shorter time scales, however, the Stream core may be much narrower, with surface speeds considerably higher than those shown in Fig. 2. The Stream core wanders laterally over the upper slope with excursions of tens of kilometers (Webster, 1961a). Such a dynamically active region poses severe practical constraints on an experiment employing moored instruments, because the intense and highly variable current forces tend to push moorings over in the water column. Drawing on previous mooring experience in the Florida Current (Düing, 1973), we decided to deploy an L-shaped array consisting of four high-tension, subsurface moorings, each supporting two or three Aanderaa RCM-4 current meters in the lower half of the water column. The array was aligned with the local topography, with the long (75 km) leg of the "L" on the 400 m isobath. For perspective, the two moorings forming the short (15 km) leg of the "L" are shown projected about 10 km upstream onto Fig. 2. The plan view of the array is shown in Fig. 3, which is a more detailed map of the region in the inset box of Fig. 1. Mooring "D" is shown displaced for clarity.

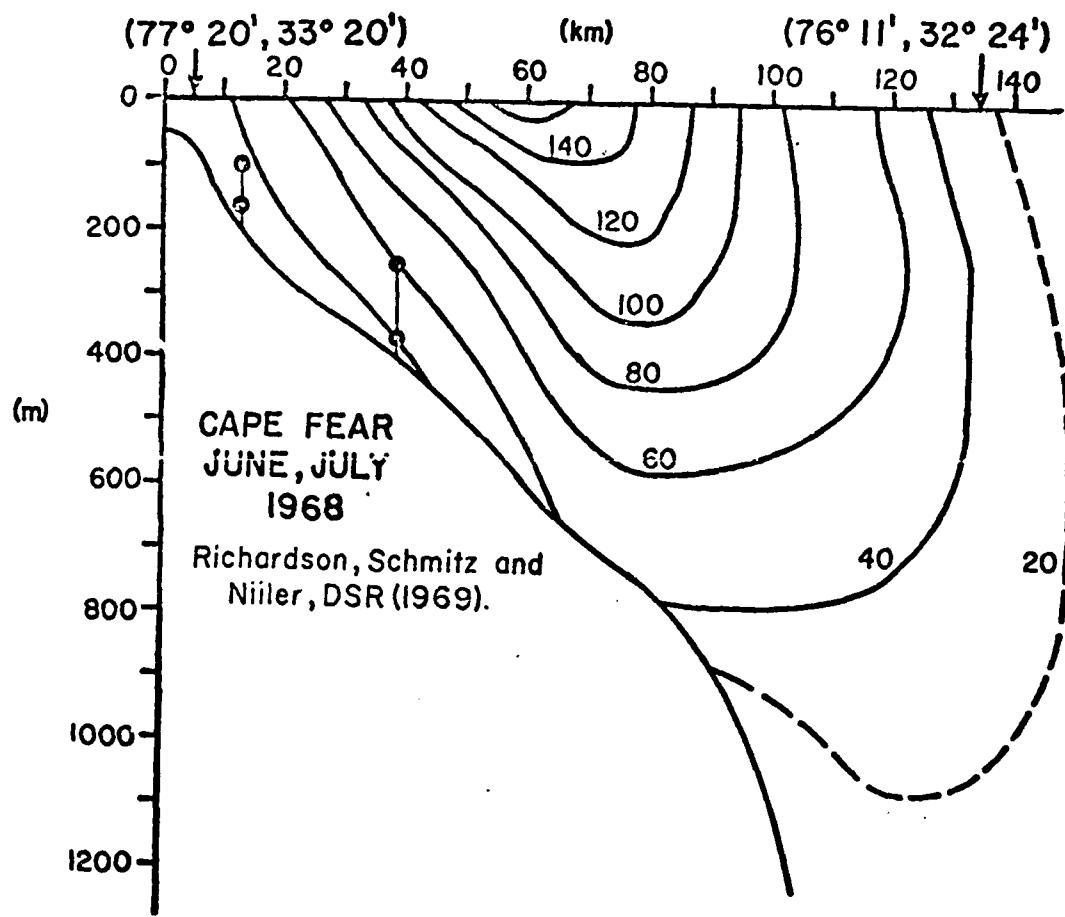


Figure 2. Cross-shelf section of the Gulf Stream off Cape Fear, showing two-month mean summer isotachs. The position of the A and B mooring current meters have been projected about 10 km upstream onto this section.

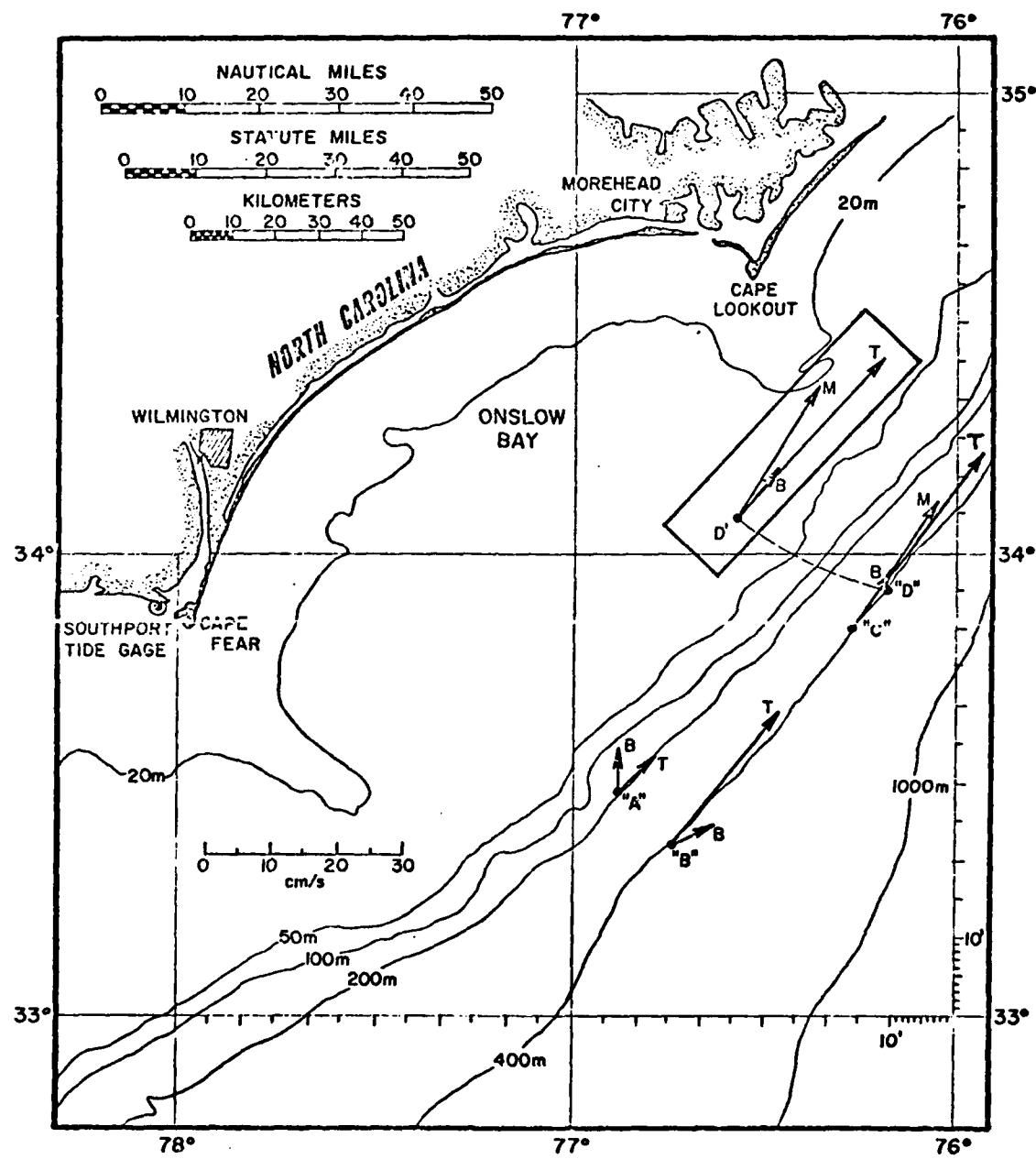


Figure 3. Detailed map of the experiment area (the inset box Fig. 1), showing the locations of moorings "A" through "D", with the record-long mean current vectors at the top (T), middle (M), and bottom (B) instruments. The mooring "D" position is shown displaced (inset box) for clarity.

Each mooring was supported by a single 37" (0.94m) diameter ORE float, yielding buoyancy in excess of 200 kg. The A and B moorings each supported two current meters, and the C and D moorings each supported three current meters. The vertical mooring design was similar to that given by Lee and Schutts (1977); a typical arrangement is shown in Fig. 4. The mooring coordinates, instrument start and stop times, instrument depths, and water depths are given in Table 1. The "winter" data set reported here spans the period from 16 January to 15 May 1979, or 120 days. Data from a similar experiment in the fall of 1979 will be presented in a future data report.

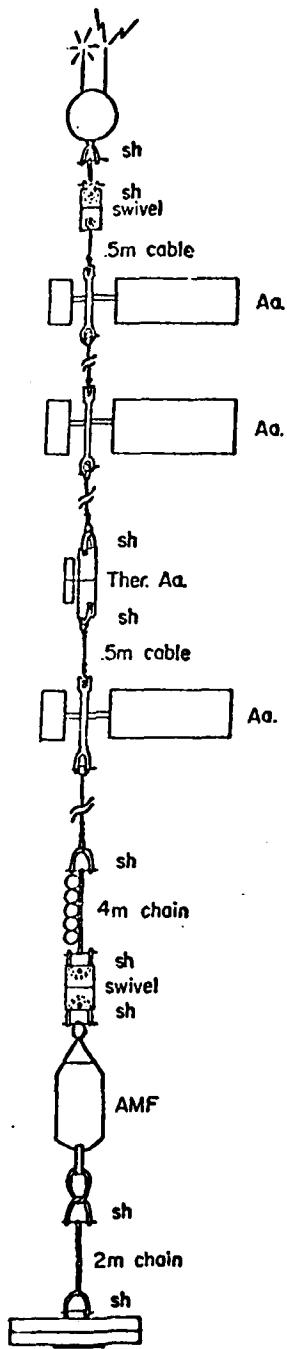


Figure 4. Typical mooring design, showing the position of Aanderaa current meters (Aa.) in the wire held taut by a large main float and a train-wheel anchor. The C and D moorings also supported Aanderaa thermographs (Ther. Aa.), but early thermistor string failures occurred in both cases. AMF (now EG&G) sea-link acoustic releases were used.

Table 1. Instrument identification, start and stop times, depths, and mooring locations.

Instr. name	Instrument no.	Instrument type	Reference no.	Coordinates	Water depth (m)	Instr. depth (m)	Sample interval (min)	Anchor deployment Start date (1979) Day-No.-Hr. (GMT)	Anchor release End date (1979) Day-No.-Hr. (GMT)	On time (GMT) (16 Jan 79)	Off time (GMT) (1979)
A TOP	3425	AA	655	Lat 33°27.96' Long 76°52.3'	198	98	20	16 Jan 0831	15 May 1030	0600	15 May 1118
A BOT	3343	AA	41		198	178	20			0600	15 May 1119
B TOP	3426	AA	622	Lat 33°21.46' Long 76°41.71'	390	250	20	16 Jan 1040	15 May 1258	0600	15 May 1342
B BOT	3423	AA	286		390	370	20			0600	15 May 1337
C TOP	3332	AA	500	Lat 33°50.75' Long 76°15.50	385	265	20	16 Jan 1532	15 May 1800	0600	16 May 2209
C MID	3345	AA	30		385	305	20			0600	16 May 2216
C BOT	3344	AA	624		385	365	20			0600	16 May 2217
D TOP	3337	AA	67	Lat 33°55.44' Long 76°11.57'	376	236	20	16 Jan 1718	15 May 2021	0600	16 May 2217
D MID	3427	AA	733		376	296	20			0600	16 May 2219
D BOT	3424	AA	840		376	356	20			0600	16 May 2220

1.3 SUPPORTING OBSERVATIONS

Hydrographic and other observations collected during the winter array launch and recovery operations were reported by Brooks *et al.* (1980). Most of the at-sea operations were conducted in R/V *Endeavor*. The moorings were recovered using R/V *John deWolfe*.

SECTION 2

Data Sources, Processing, and Basic Statistics

2.1 TRANSCRIPTION OF AANDERAA DATA TAPES

The raw data on Aanderaa magnetic tapes consist of a sequence of pulse width modulated (PCM) binary numbers. Two binary words are recorded for each sensor sampled, plus two words for an internal reference number. The binary PCM data tapes were read by a reel-to-reel tape deck, then transcribed to computer-compatible binary words by a hardware interface device built by Mr. Lawrence Ives of North Carolina State University. The decoded raw data consist of time series of numbers in the range of 0 to 1023 (decimal equivalent).

2.2 INSTRUMENT CALIBRATION

The ten Aanderaa RCM-4 recording current meters used in the Gulf Stream Meanders Experiment were subjected to calibration procedures for direction and temperature. The four meters which were positioned at the top of the moorings contained pressure sensors, which were also calibrated. The calibration values supplied by the manufacturer for speed and conductivity were used; no other laboratory calibration was performed for these variables. In this section the calibration procedures and results are presented, along with the manufacturer's calibration information. The calibration data, either measured or supplied by Aanderaa, were used to convert from the internally

recorded binary number, N, which ranges in decimal equivalent from 0 to 1023, into scientific units.

Speed

The conversion from N to speed, in cm/sec, was accomplished with the linear formula

$$\text{Speed} = 1.5 + 0.14 N.$$

The values 1.5 and 0.14 were supplied by Aanderaa. A graph of this calibration relationship is given in Fig. 5.

Conductivity

Aanderaa calibration values for conductivity were used for all meters. The coefficients in the linear formula

$$\text{Conductivity (mmho/cm)} = A + BN$$

are listed in Table 2. Although slight differences in the coefficients exist among the meters, the graphs of conductivity vs. N all appear essentially the same; thus, Fig. 5 is applicable for all instruments.

Direction

Each RCM-4 compass was calibrated as follows: The instrument was mounted on a non-magnetic bracket located away from known magnetic interference. With the internal digitizing and recording mechanisms set to continuously record, the instrument was turned through 360°, indexing by ten degrees, allowing the compass to stabilize at each position and to record at least six cycles of the direction reading. A cubic equation of the form

$$\text{Direction (magnetic)} = A + BN + CN^2 + DN^3$$

was fitted to the 36 calibration values. The coefficients A through D for each meter are listed in Table 2. The direction values from the cubic equation differed by less than one degree from the measured calibration values. Graphs

of the calibration curve and the Aanderaa curve for seven meters are shown in Fig. 6. Recording problems resulted in unuseable calibration information for meters 3423, 3332 and 3337, so the Aanderaa formula

$$\text{Direction (magnetic)} = 1.5 + 0.349 N$$

was used for these instruments.

Temperature

All temperature sensors were calibrated as follows: With all meters sealed and recording at 15 minute intervals, they were immersed in an icewater bath. The ice was allowed to slowly melt, and then the water to warm to room temperature (~25°C). Stirring was provided throughout the warming period by two small pumps. Four independent Hewlett-Packard quartz-crystal thermometers were placed around the bath for temperature measurement. A continuous record (strip chart) of the temperature measured by one of the quartz sensors was made and used as the calibration standard. Temperature readings around the bath using the other three sensors showed the temperature differences to be always less than 0.05°C,¹ insuring that all meters were recording essentially the same temperature. Calibration temperatures at known times of RCM-4 recordings were compared with the corresponding recorded values of N. A number (ca. 15 to 19) of Temperature-N pairs were used to determine the best fit to the cubic equation:

$$\text{Temperature } (^{\circ}\text{C}) = A + BN + CN^2 + DN^3$$

The coefficients A through D are listed for each meter in Table 2, along with the coefficients supplied by Aanderaa. The difference between the temperature calibration values computed from the cubic equation and those directly measured was in all cases less than the stated accuracy of the temperature sensor (0.15 °C). Graphs of Temperature vs. N are given for 9

¹ After all ice had melted.

instruments in Fig. 7. Recording problems during the bath calibration in instrument number 3423 did not permit the construction of a calibration curve; thus, the Aanderaa coefficients were used for the field data conversion for this meter.

Pressure

The pressure transducers on instruments 3425, 3426, 3332 and 3337 were calibrated using a manual hydraulic pump. Calibration data were collected in the range 0 to 500 PSIG at intervals of 50 PSIG. These points were fitted to the cubic equation

$$\text{Pressure (PSIG)} = A + BN + CN^2 + DN^3.$$

The coefficients in the cubic equation for each meter are listed in Table 2, along with the Aanderaa coefficients. Graphs of Pressure vs. N for the four meters are shown in Fig. 8. The calibration curve departs from the Aanderaa curve for values of pressure greater than 500 PSIG, because the highest pressure used in the calibration curve-fitting procedure was 500 PSIG. Since the highest pressures encountered *in situ* did not exceed 500 PSIG the upper part of the pressure calibration curves in Fig. 8 were not used and should be ignored.

Salinity

Salinity values were calculated from the temperature and conductivity time series in scientific units as follows: The conductivity that seawater with a salinity of 35 ‰ would have at the measured temperature was calculated using the formula

$$\begin{aligned} \text{Cond (T, 35)} &= 29.01067 + 0.8677579 T \\ &+ 0.4074545 \times 10^{-2} T^2 - \\ &0.1437152 \times 10^{-4} T^3. \end{aligned}$$

where T is the measured temperature ($^{\circ}\text{C}$) and Cond is in mmho/cm . This formula is the best-fit cubic equation calculated from information presented by Weyl (1964). The conductivity ratio at the measured temperature was calculated by

$$R_T = \text{Cond (meas)} / \text{Cond (T, 35)},$$

where Cond (meas) is the measured conductivity in mmho/cm . The difference, Δ_{15} , between the conductivity ratio at 15°C and R_T was calculated with the formula (National Institute of Oceanography of Great Britain and Unesco, 1971)

$$\begin{aligned} \Delta_{15} = 10^{-5} R_T (R_T - 1) (T - 15) & [96.7 - 72.0 R_T \\ & + 37.3 R_T^2 - (0.63 + 0.21 R_T^2) (T - 15)]. \end{aligned}$$

The salinity in parts per thousand was then calculated using the formula (*ibid.*)

$$\begin{aligned} S(\%) = -0.08996 + 28.29720 R_{15} + 12.80832 R_{15}^2 \\ - 10.67869 R_{15}^3 + 5.98624 R_{15}^4 \\ - 1.32311 R_{15}^5, \end{aligned}$$

where $R_{15} = R_T + \Delta_{15}$.

Table 2. Aanderaa-supplied (Aa) and calibration-produced (Cal) coefficients for the conversion of recorded binary numbers to scientific units. The general formula $V = A + BN + CN^2 + DN^3$ was used, where V is the variable, and N is decimal equivalent (0 - 1023) of the recorded binary number.

Number	Variable	Speed (cm sec ⁻¹)		Direction (degrees mag)		Conductivity (mmho cm ⁻¹)		Temperature (°C)		Pressure (kg cm ⁻²) (PSI)	
		Aa	Cal	Aa	Cal	Aa	Cal	Aa	Cal	Aa	Cal
3332	A	1.5		1.5		0		-0.885	-0.4144	-4.365C7	-53.4979
	B	0.14		0.349	No calibration data	0.07593		0.03587	0.0361	0.0770611	1.1150
	C							-0.8388 × 10 ⁻⁵	-0.8734 × 10 ⁻⁵	-0.2331 × 10 ⁻³	
	D							0.4300 × 10 ⁻⁸	0.4470 × 10 ⁻⁸	0.3127 × 10 ⁻⁶	
3337	A	1.5		1.5		0.076		-0.8905	-0.3128	-3.78849	-67.9111
	B	0.14		0.349	No calibration data	0.07607		0.03587	0.0375	0.0758634	1.3195
	C							-0.8388 × 10 ⁻⁵	-0.1230 × 10 ⁻⁵	-0.5994 × 10 ⁻³	
	D							0.4300 × 10 ⁻⁸	0.6655 × 10 ⁻⁸	0.9220 × 10 ⁻⁶	
3343	A	1.5		1.5	- 9.9327	-0.084		-0.9103	-0.3176		
	B	0.14		0.349	0.3904	0.07593		0.03587	0.0375		
	C				- 0.8870 × 10 ⁻⁴			-0.8388 × 10 ⁻⁵	-0.1260 × 10 ⁻⁵		
	D				0.4451 × 10 ⁻⁷			0.4300 × 10 ⁻⁸	0.6858 × 10 ⁻⁸		
3344	A	1.5		1.5	-10.9572	-0.084		-0.0905	-0.2421		
	B	0.14		0.349	0.4032	0.07593		0.03587	0.0372		
	C				- 1.1658 × 10 ⁻⁴			-0.8380 × 10 ⁻⁵	-0.1226 × 10 ⁻⁵		
	D				0.6087 × 10 ⁻⁷			0.4300 × 10 ⁻⁸	0.7004 × 10 ⁻⁸		
3345	A	1.5		1.5	- 6.3311	0.076		-0.0773	-0.2877		
	B	0.14		0.349	0.3514	0.07597		0.03587	0.0367		
	C				0.0054 × 10 ⁻⁴			-0.8388 × 10 ⁻⁵	-0.1044 × 10 ⁻⁵		
	D				- 0.0469 × 10 ⁻⁷			0.4300 × 10 ⁻⁸	0.5516 × 10 ⁻⁸		
3423	A	1.5		1.5		0		-0.9511		No calibration data	
	B	0.14		0.349	No calibration data	0.07574		0.03587			
	C							-0.8388 × 10 ⁻⁵			
	D							0.4300 × 10 ⁻⁸			
3424	A	1.5		1.5	- 4.8337	0		-0.8781	-0.079		
	B	0.14		0.349	0.3653	0.07650		0.03587	0.0386		
	C				- 0.4181 × 10 ⁻⁴			-0.8388 × 10 ⁻⁵	-0.1790 × 10 ⁻⁵		
	D				0.2383 × 10 ⁻⁷			0.4300 × 10 ⁻⁸	1.1579 × 10 ⁻⁸		
3425	A	1.5		1.5	- 2.7682	0.07574		-0.8551	-0.2713	-3.922C4	-65.2533
	B	0.14		0.349	0.3460	0.07574		0.03587	0.0377	0.0757081	1.2345
	C				- 0.0683 × 10 ⁻⁴			-0.8388 × 10 ⁻⁵	-1.3034 × 10 ⁻⁵	-0.5164 × 10 ⁻³	
	D				0.0824 × 10 ⁻⁷			0.4300 × 10 ⁻⁸	0.7184 × 10 ⁻⁸	0.5934 × 10 ⁻⁶	
3426	A	1.5		1.5	- 3.1920	0		-0.8827	-0.2922	-4.20412	-72.1725
	B	0.14		0.349	0.3571	0.07598		0.03587	0.0375	0.0761238	1.3555
	C				- 0.2174 × 10 ⁻⁴			-0.8388 × 10 ⁻⁵	-1.2131 × 10 ⁻⁵	-1.0377 × 10 ⁻³	
	D				0.1214 × 10 ⁻⁷			0.4300 × 10 ⁻⁸	0.6462 × 10 ⁻⁸	1.0679 × 10 ⁻⁶	
3427	A	1.5		1.5	- 3.1797	0.07612		-0.9121	-0.3606		
	B	0.14		0.349	0.3330	0.07612		0.03587	0.0380		
	C				0.3754 × 10 ⁻⁴			-0.8388 × 10 ⁻⁵	-1.3525 × 10 ⁻⁵		
	D				- 0.2328 × 10 ⁻⁷			0.4300 × 10 ⁻⁸	0.7438 × 10 ⁻⁸		

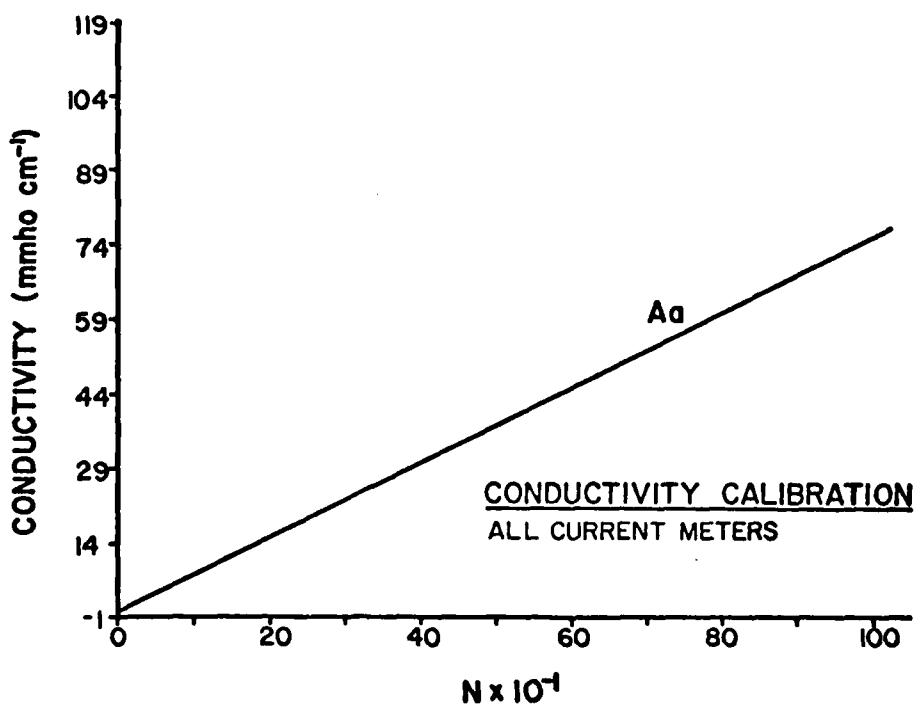
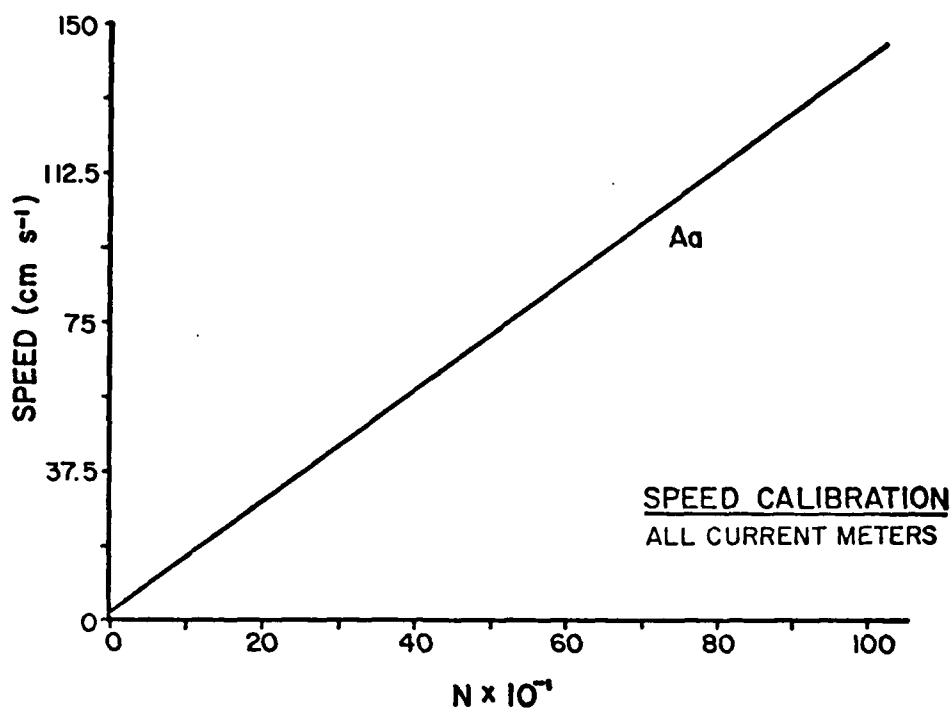


Figure 5. Speed and conductivity calibration graphs, using the cubic coefficients supplied by Aanderaa (Aa), which were applied to all instruments.

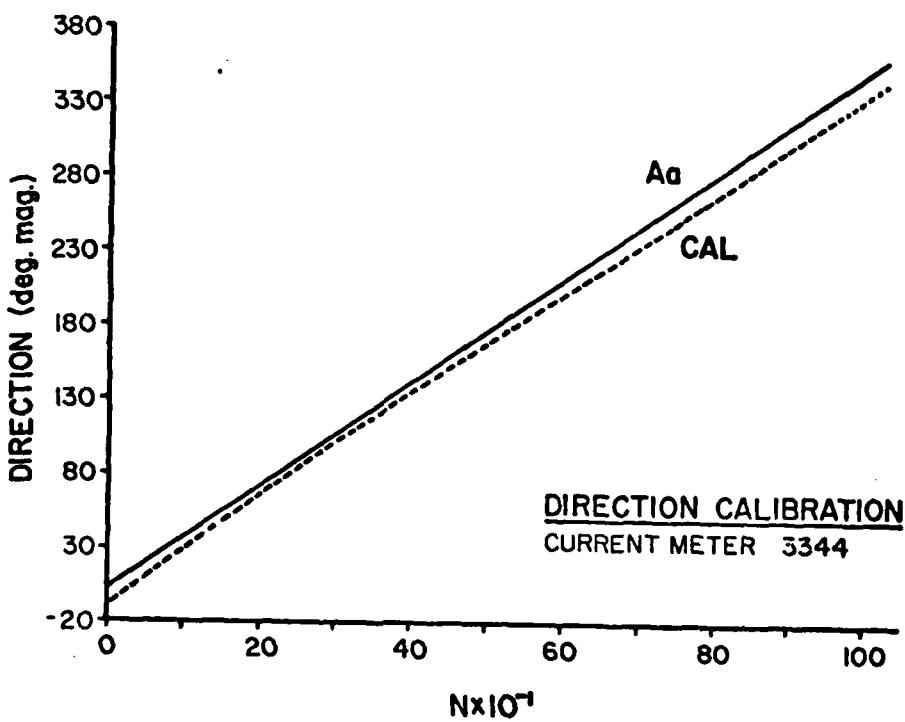
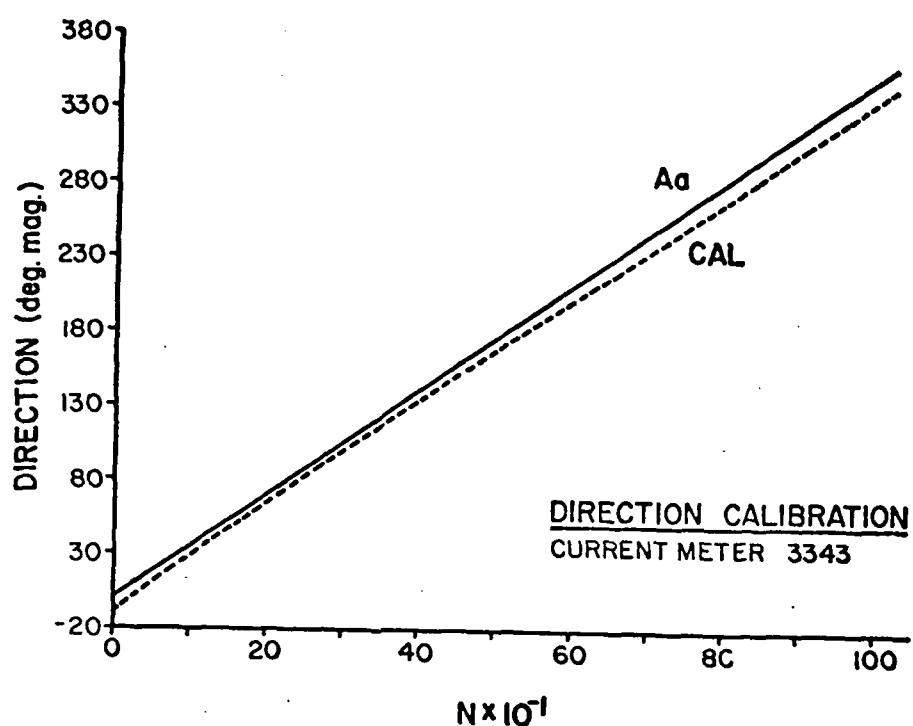
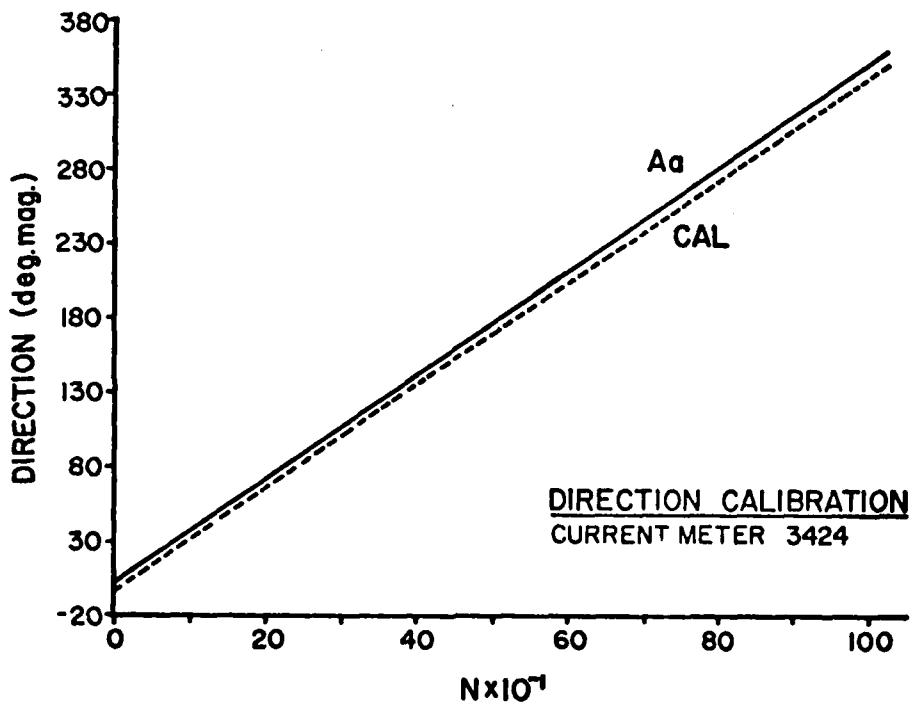
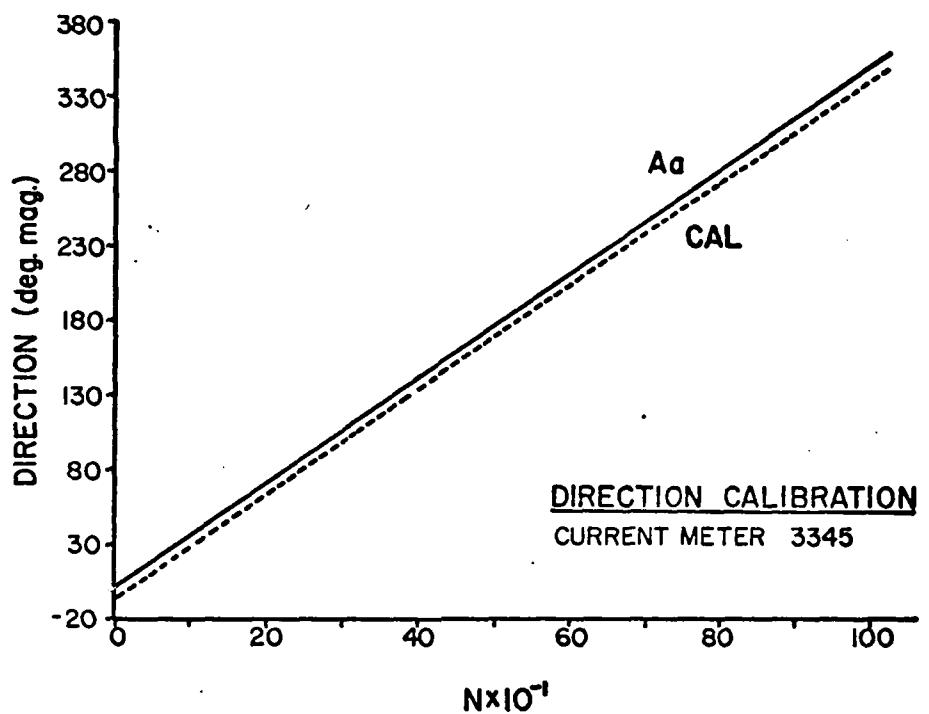
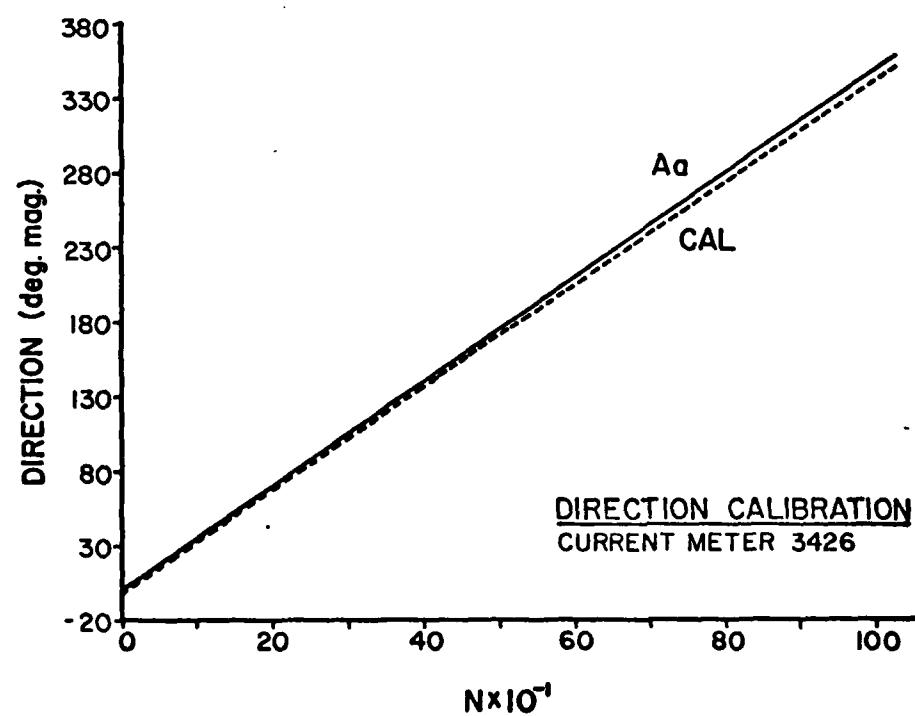
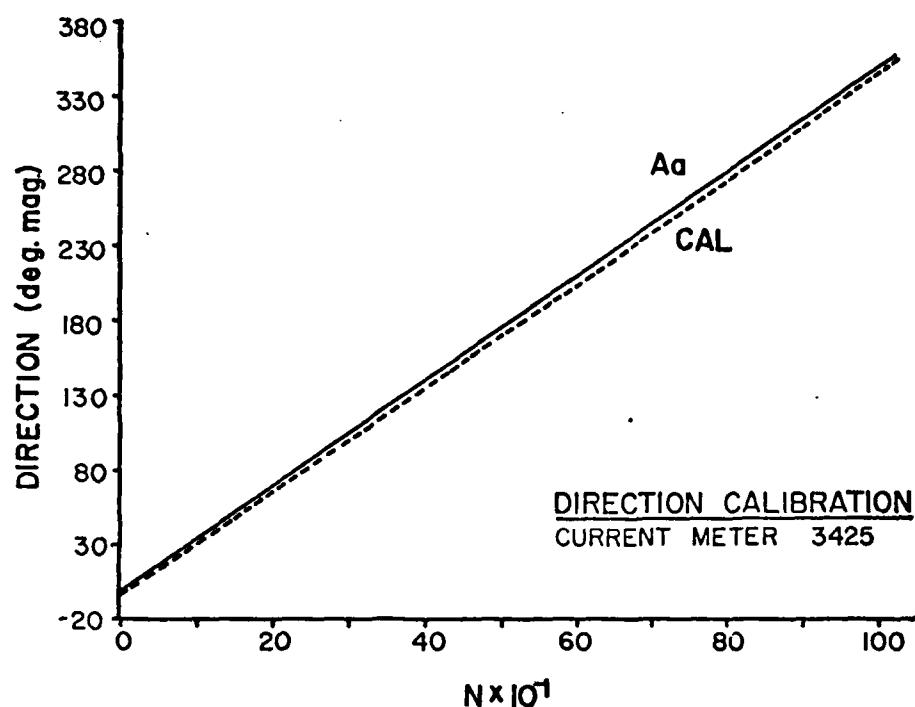
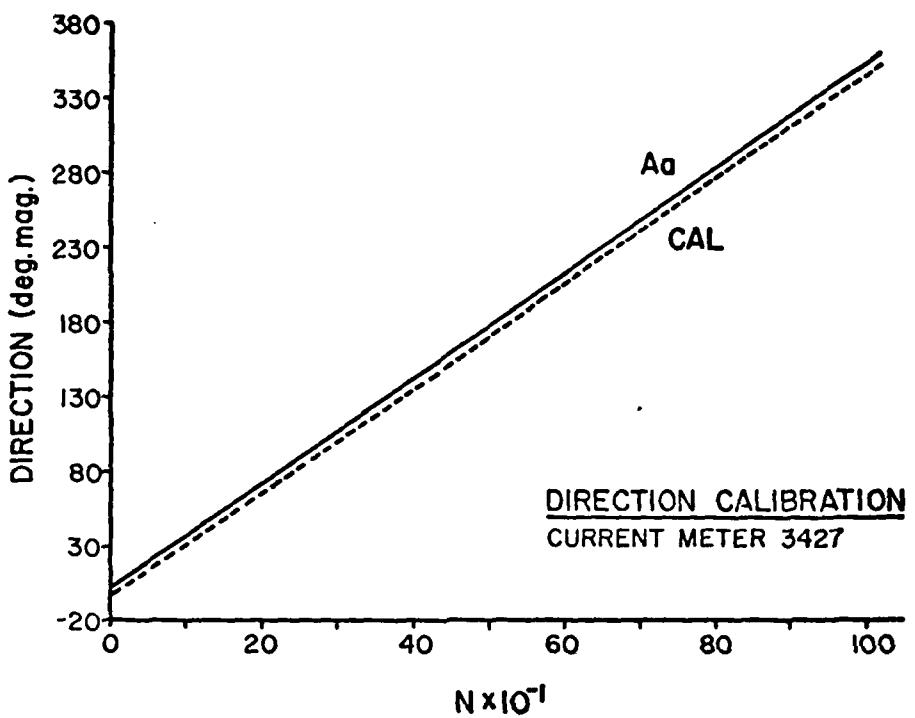


Figure 6. Calibration curves for compass direction, based on coefficients supplied by Aanderaa (-) and coefficients based on directly measured calibration data (---). The latter were used for calibration of all instruments except numbers 3423, 3332 and 3337.







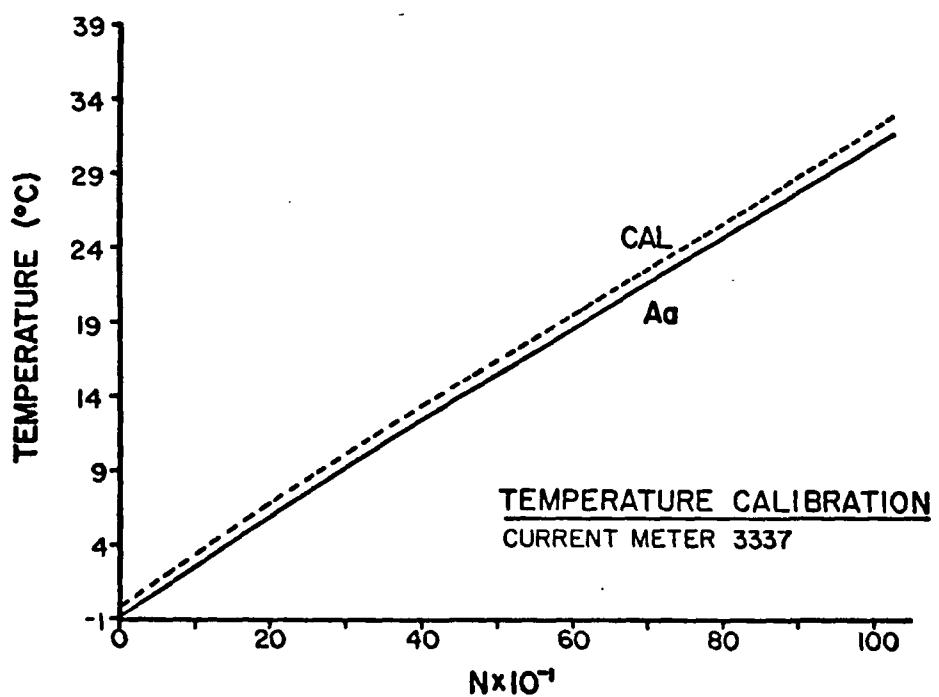
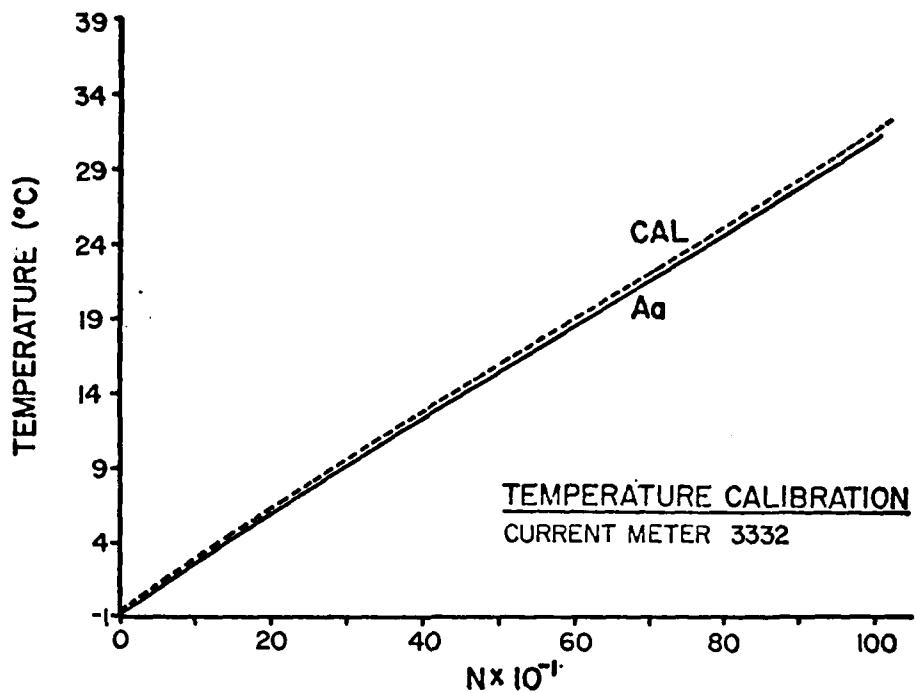
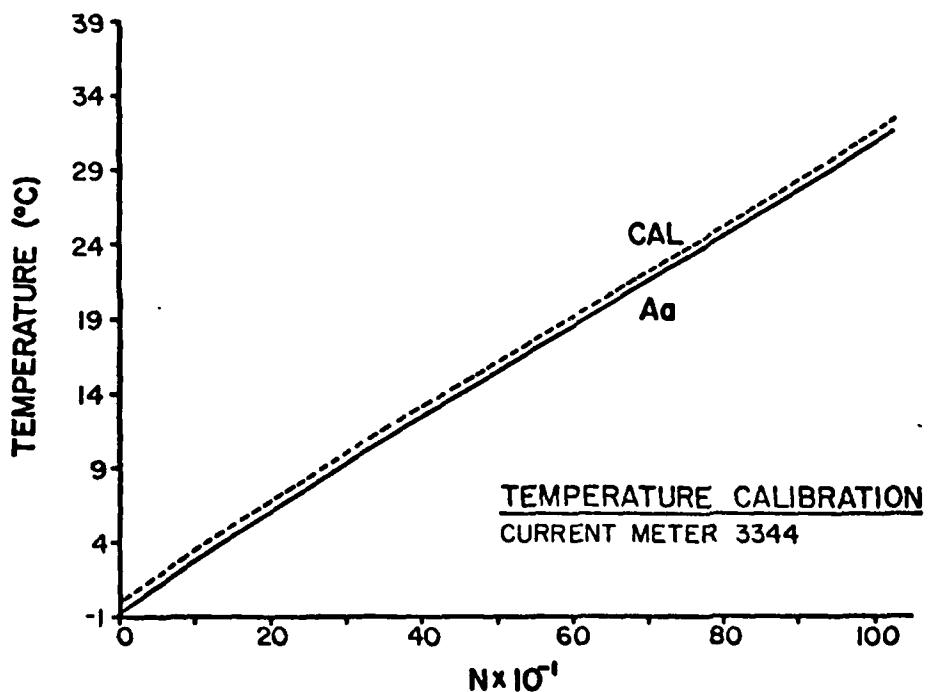
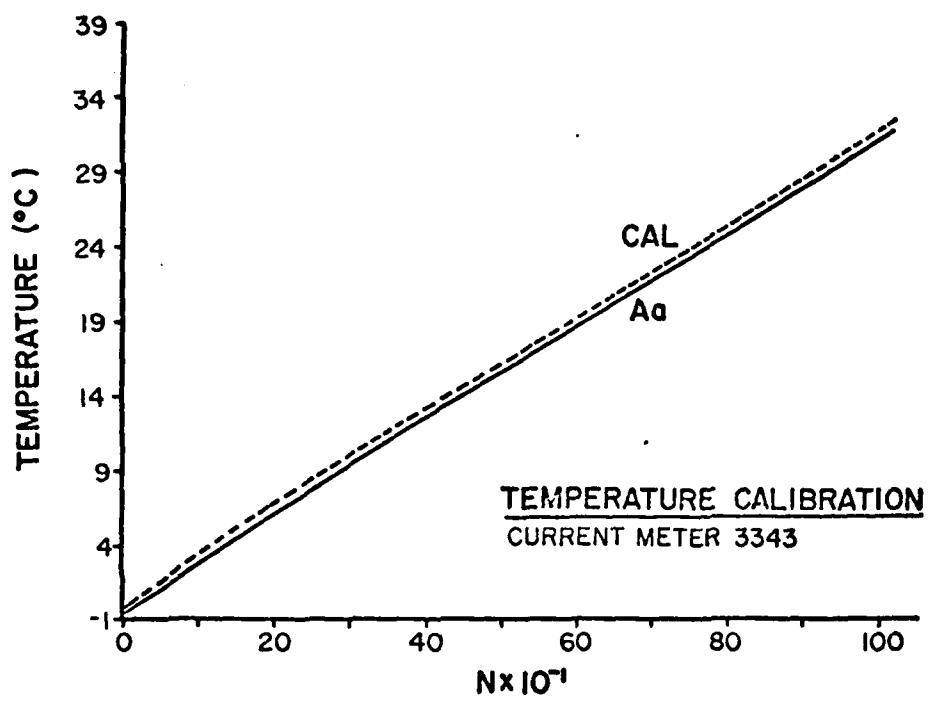
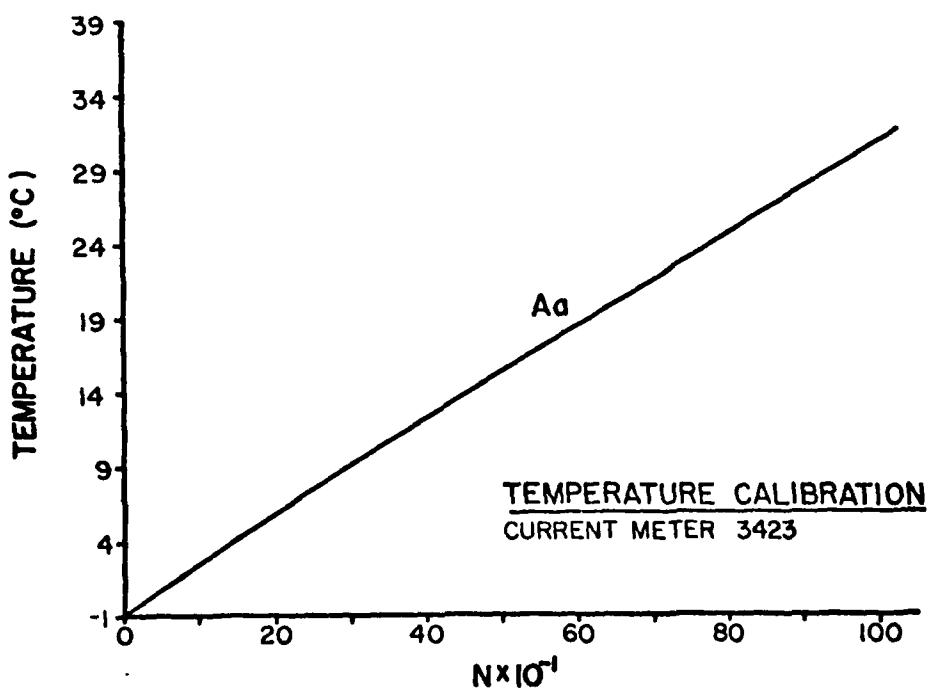
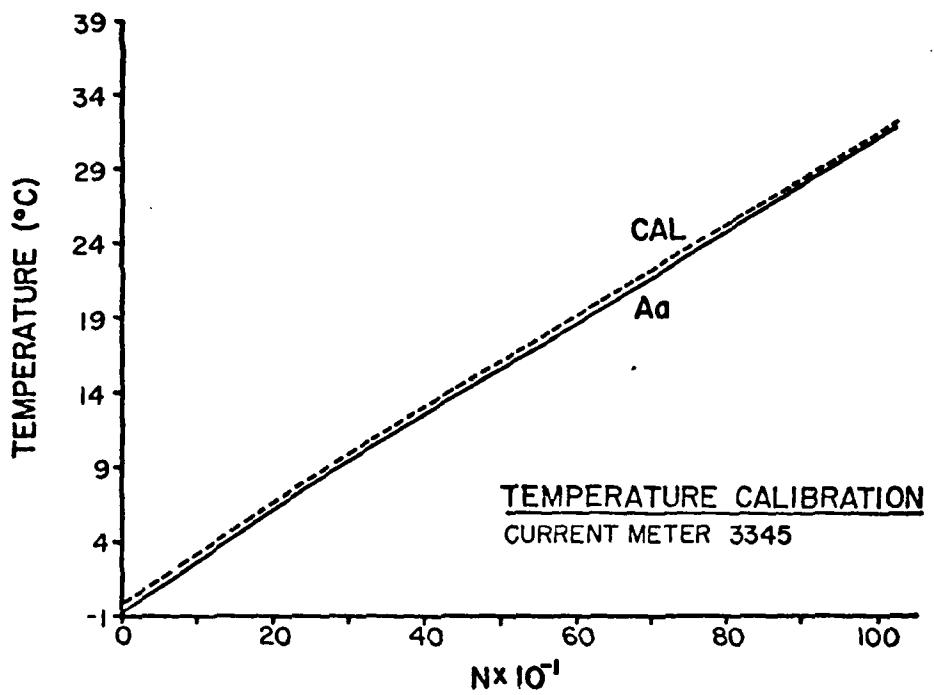
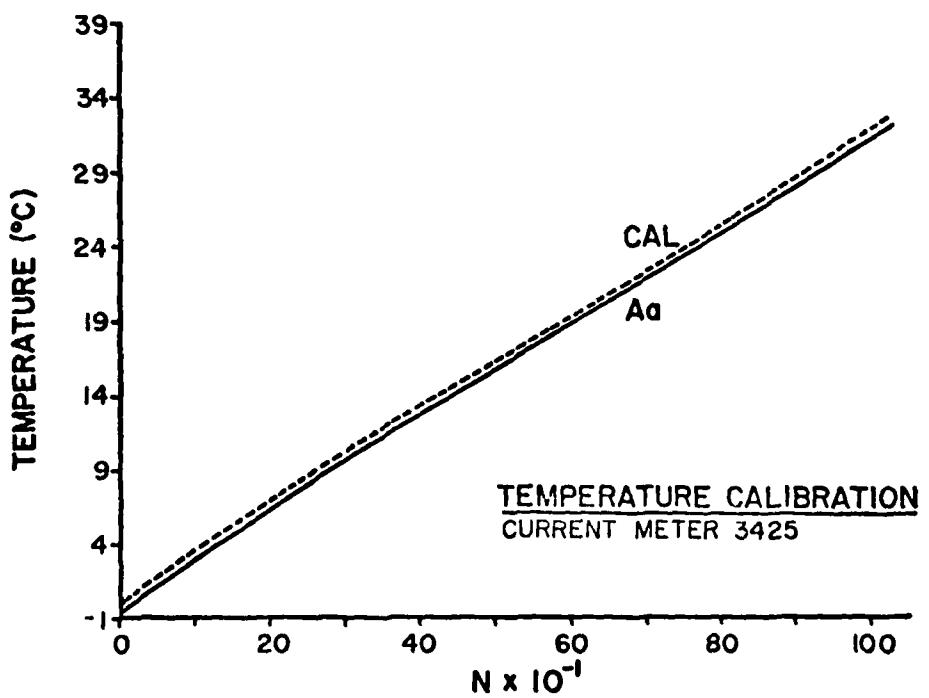
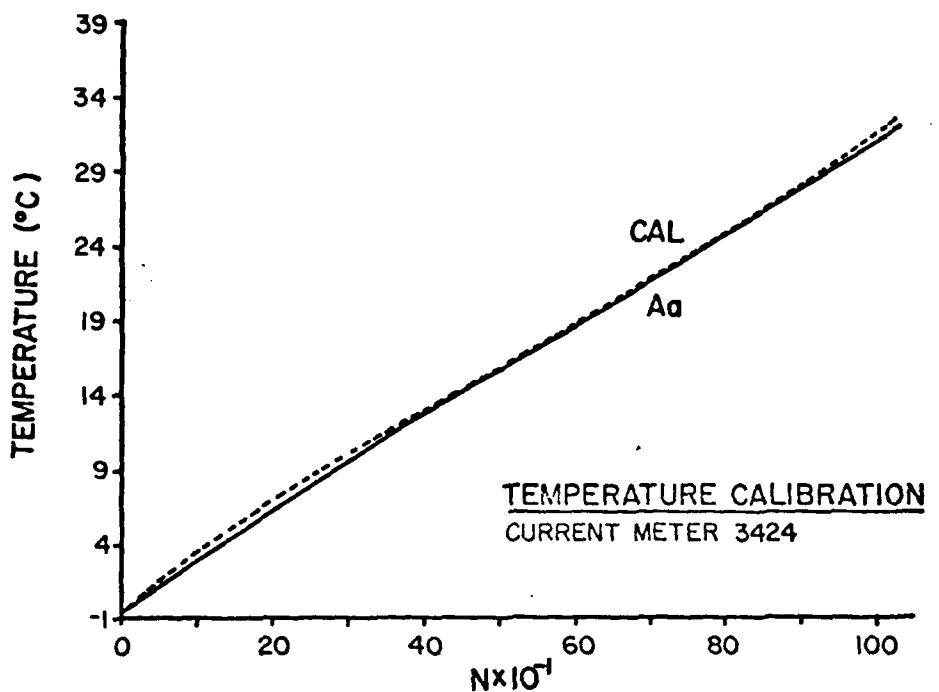
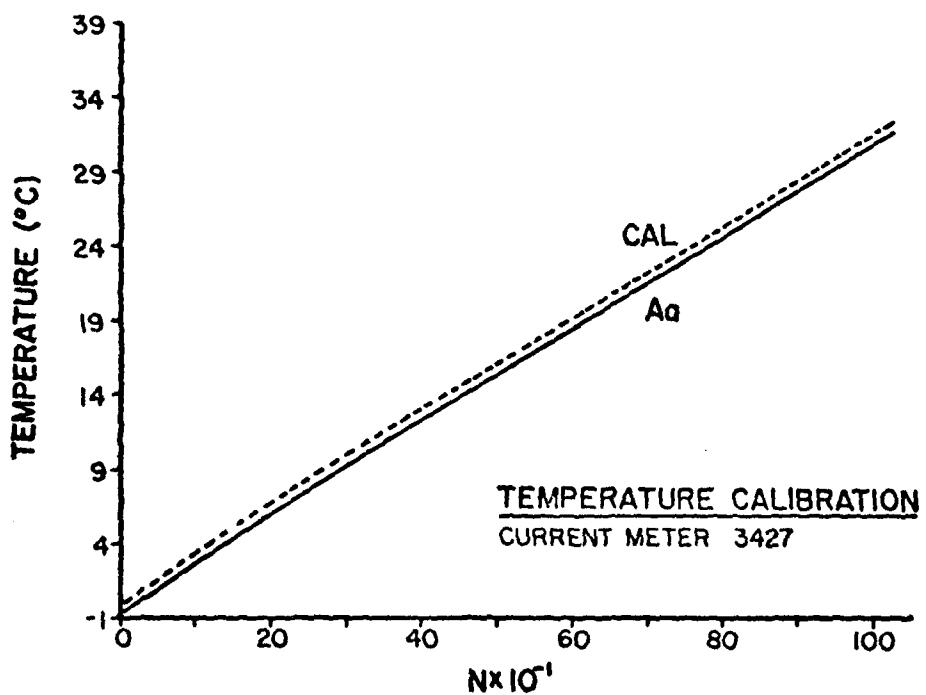
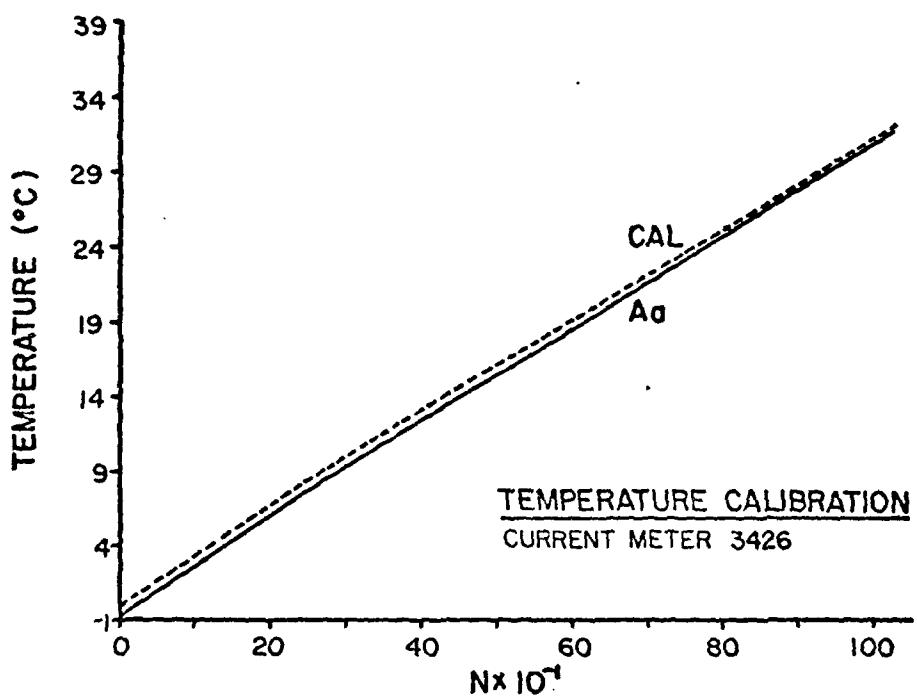


Figure 7. Calibration curves for temperature, based on coefficients supplied by Aanderaa (-), and coefficients based on directly measured calibration data (----). The latter were used for calibration of all instruments.









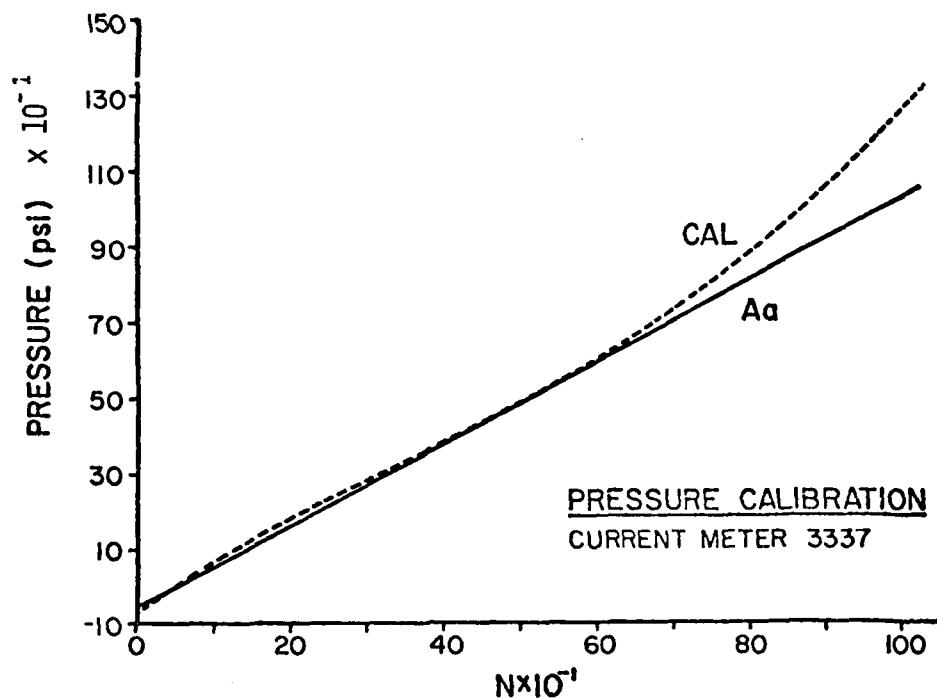
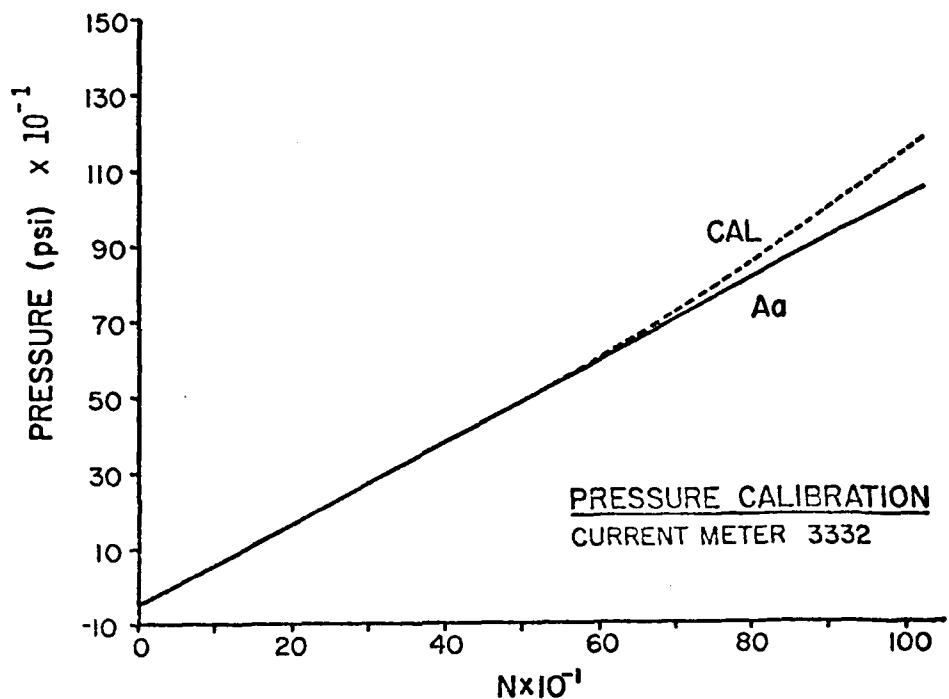
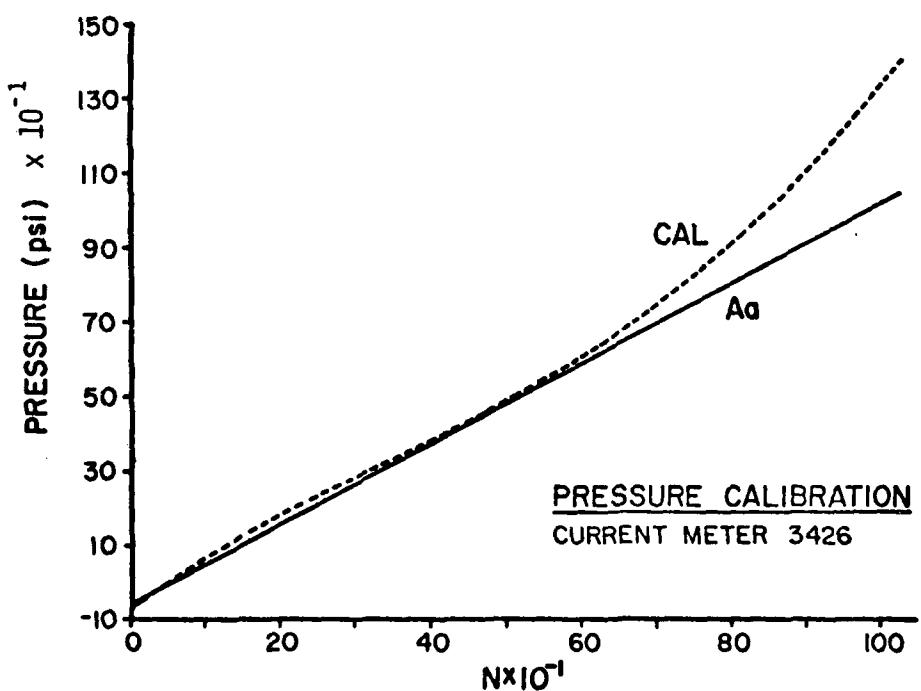
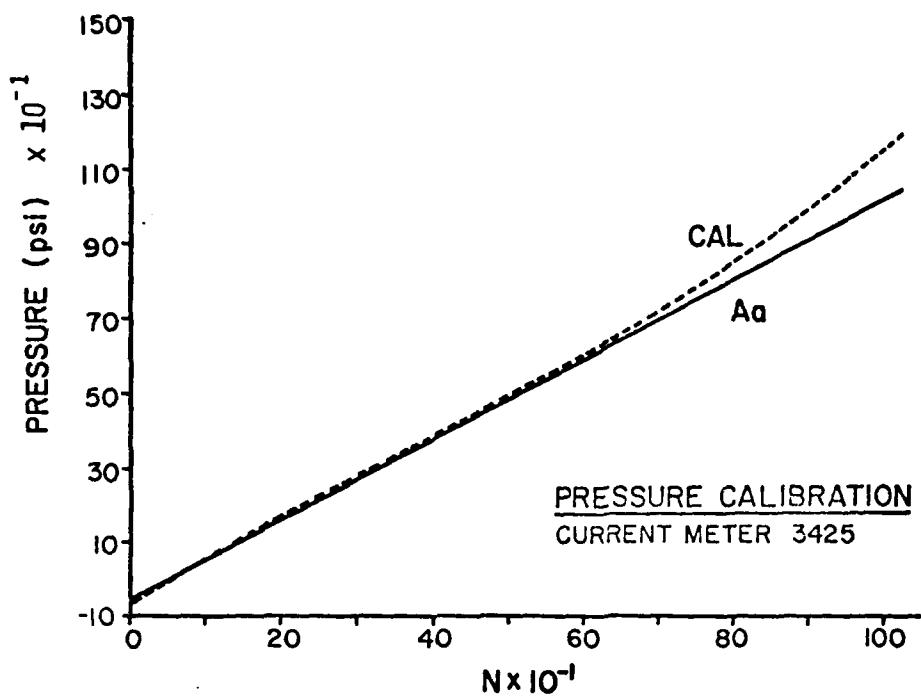


Figure 8. Calibration curves for pressure, based on coefficients supplied by Aanderaa (—) and coefficients based on directly measured calibration data (----) over the range 0 to 500 PSIG. The two curves diverge and were not used for pressures higher than 500 PSIG because of the curve-fitting process. The highest *in-situ* pressures were less than 500 PSIG.



2.3 AANDERAA DATA EDITING

The calibrated Aanderaa data files were machine-edited for extreme values exceeding reasonable upper and lower bounds on each variable. Bad points were replaced by values linearly interpolated between the preceding and succeeding good points. The data were then plotted, and further editing of unreasonable values was done by operating on the data files interactively using a computer terminal. All edited points were replaced by interpolated values, as in the machine-edited case.

2.4 ANCILLARY DATA SOURCES

Sea level height from tide gages at Southport and Beaufort (near Morehead City), Fig. 3, and atmospheric surface observations at Cape Hatteras and at NDBO moored buoy number 41004, Fig. 1, were obtained from the National Archives for the winter array period. The Hatteras atmospheric data shown here are wind velocity vector components, air temperature, and atmospheric pressure. In addition, the wind stress vector components were computed, using a constant drag coefficient $C_D = 1.5 \times 10^{-3}$. The NDBO buoy (NDBO-4 on Fig. 1) was located at 32.6°N , 78.7°W , approximately on the 100 m isobath, several hundred km upstream from our array area. The NDBO data presented are wind velocity vector components, air and sea surface (water) temperatures, and atmospheric pressure. The NDBO wind stress components are also shown. The sea level height data shown here have been corrected for static barometric pressure changes by adding 1.01 cm to sea level height for each mb of atmospheric pressure increase relative to its mean at the nearest atmospheric station (Wilmington for Southport and Cape Hatteras for Beaufort).

2.6 DATA PROCESSING

The raw, calibrated data from the current meters consisted of time series of current speed and direction, temperature, salinity, and (only for top instruments) pressure. The basic sampling interval for all current meters was 20 minutes. Current speed and direction were converted to (u , v) vector velocity components in an (offshore, downstream) coordinate frame rotated clockwise 34 degrees from true north to align with the 400 m isobath. The same coordinate frame was used for all vector data sets, which facilitates direct comparison between them.

Standard digital filtering techniques based on the FESTSA time series analysis system (Brooks, 1976) were used to subdivide the frequency domain of the data sets. First, a 3-hour low pass filter (3 HRLP) was applied to reduce sampling noise and possible aliasing. Then a 40-hour low pass filter (40 HRLP) was applied to separate the daily and semidaily tidal and inertial motions from those with periods of several days and longer. For both filters, the specified cutoff period is the period at which the filter energy response is 0.25 times its long period response (-6db point). A Lanczos taper was used in each case, and the smoothed response function of the 40 HRLP filter is shown in Fig. 9. The response at the semidaily (dominant) tidal period is less than 10^{-7} . In addition, a 3 to 40 hours bandpass (3-40 HRBP) data set was obtained by subtracting the 40 HRLP set from the 3 HRLP set. The final sample interval was 1 hour for the 3 HRLP and 3-40 HRBP sets and 6 hours for the 40 HRLP set.

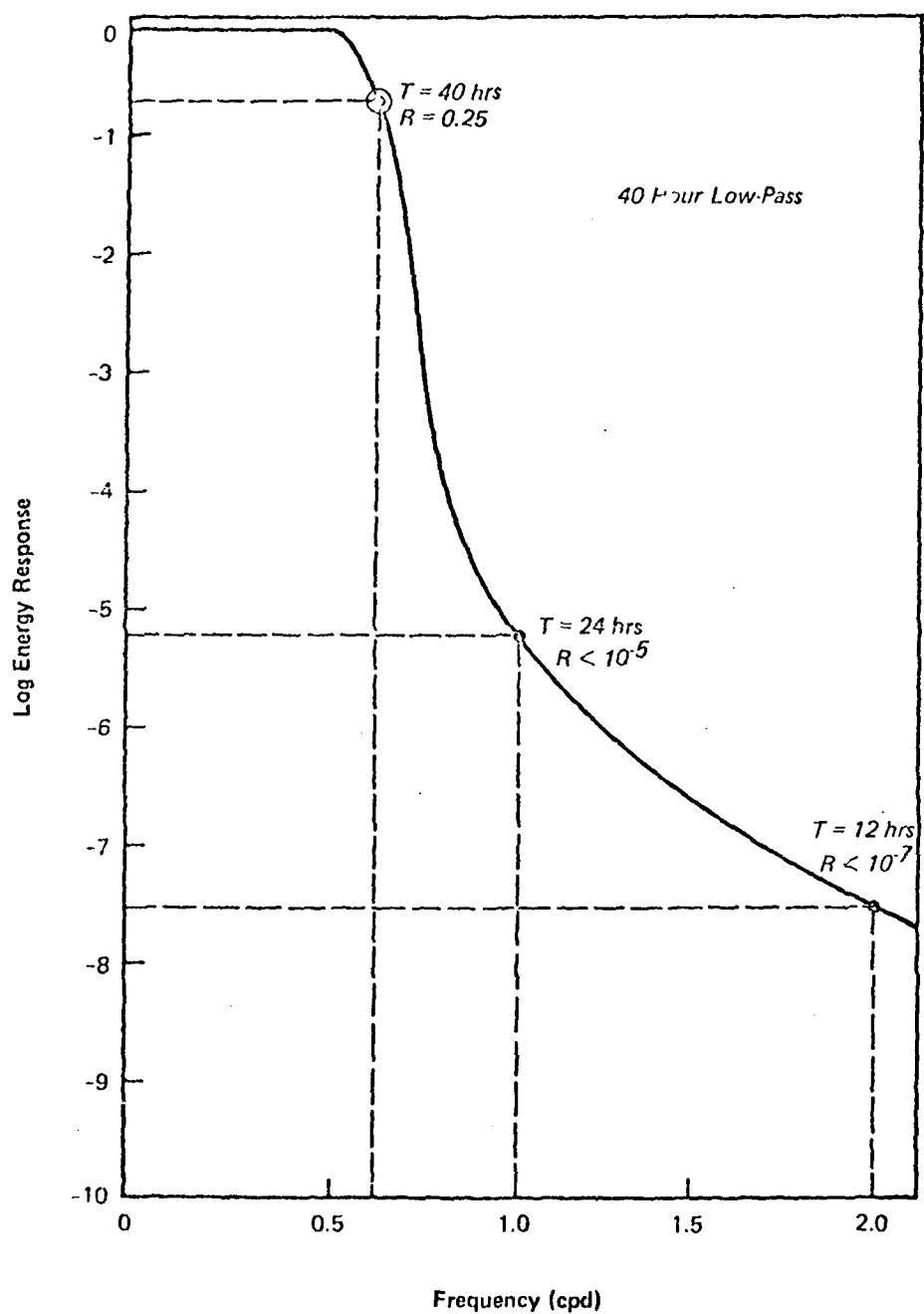


Figure 9. Response function for the 40 hour low pass Lanczos filter.

2.6 BASIC STATISTICS OF THE CURRENT METER DATA SET

First order and variance statistics for u, v, and T (temperature) from each current meter are shown in Table 3. Table 4 shows the variance ratios 3-40 HRBP/3 HRLP and 40 HRLP/3 HRLP, which approximately represent the division of total spectrum energy between the tidal-inertial band and the long period band, respectively. Departure of their sum from unity for each variable is a measure of filtering imperfection. The tidal-inertial band motions were strongest in the cross-shelf (u) component, particularly at the deepest instruments. The downstream (v) component fluctuations predominantly had periods of several days and longer.

Table 3. First-order and variance statistics of temperature (T) and velocity components (u, v) from each instrument, shown from 3 HRLP, 3-40 HRLP, and 40 HRLP filtered data sets.

3 HRLP

Current meter	Parameter	N	Min	Max	Mean	SD	Var
A TOP	T	2842	12.5	23.8	17.2	1.8	3.2
	U	2842	-38.6	48.8	0.2	9.8	96.0
	V	2842	-70.6	116.8	7.0	33.9	1149.2
A BOT	T	2842	3.9	19.5	11.5	3.3	10.9
	U	2842	-31.5	44.4	-2.7	9.1	82.8
	V	2842	-58.5	74.7	4.0	21.0	441.0
B TOP	T	2842	8.8	18.7	12.6	2.5	6.3
	U	2842	-55.6	63.8	1.3	15.7	246.5
	V	2842	-49.5	134.0	25.1	29.3	858.5
B BOT	T	2842	6.2	14.4	8.9	1.5	2.3
	U	2842	-33.6	39.5	2.3	11.0	121.0
	V	2842	-62.6	53.4	4.7	17.3	299.3
C TOP	T	2837	9.2	18.1	12.8	2.1	4.4
	U	2837	-33.2	54.3	4.3	11.5	133.2
	V	2837	-44.0	135.1	32.3	33.6	1143.3
C MID	T	2532	3.2	29.5	11.2	1.8	3.2
	U	2661	-98.8	83.2	-0.2	16.1	259.2
	V	2661	-45.7	112.6	22.9	26.6	707.6
C BOT	T	2842	7.2	14.4	9.4	1.1	1.2
	U	2842	-33.4	48.0	-0.5	9.5	90.3
	V	2842	-39.8	74.4	9.3	19.8	392.0
D TOP	T	2823	8.5	18.8	13.2	2.0	4.0
	U	1655	-28.1	48.2	4.0	10.2	104.0
	V	1655	-34.9	121.6	31.5	28.7	841.0
D MID	T	2842	7.6	19.0	11.3	1.7	2.9
	U	2842	-29.5	41.9	-1.3	8.8	77.4
	V	2842	-46.0	116.0	24.3	28.8	829.4
D BOT	T	2842	6.7	13.6	9.3	1.1	1.2
	U	2842	-26.9	34.8	0.1	7.8	60.8
	V	2842	-38.2	55.1	7.9	16.8	282.2

3-40 HRBP

Current meter	Parameter	N	Min	Max	Mean	SD	Var
A TOP	T	2650	-3.9	3.1	0.0	0.5	0.3
	U	2650	-41.6	33.9	0.0	7.3	53.3
	V	2650	-28.1	37.2	0.0	8.2	67.2
A BOT	T	2650	-7.6	8.0	0.0	1.1	1.2
	U	2650	-37.5	37.9	0.0	7.4	54.8
	V	2650	-29.9	39.1	0.0	6.7	44.9
B TOP	T	2650	-1.9	2.3	0.0	0.4	0.2
	U	2650	-29.5	28.4	0.0	6.6	43.6
	V	2650	-33.7	27.2	0.0	7.2	51.8
B BOT	T	2650	-1.9	3.4	0.0	0.3	0.1
	U	2650	-24.4	23.8	0.0	6.3	39.7
	V	2650	-20.4	18.1	0.0	5.2	27.0
C TOP	T	2645	-2.2	2.0	0.0	0.4	0.2
	U	2645	-26.8	32.7	0.0	6.4	40.7
	V	2645	-27.1	35.6	0.0	7.1	51.0
C MID	T	2340	-1.9	4.5	0.0	0.5	0.3
	U	2469	-65.5	31.2	0.0	6.9	47.6
	V	2469	-25.5	63.7	0.0	6.8	46.2
C BOT	T	2650	-2.2	4.1	0.0	0.5	0.3
	U	2650	-29.2	35.8	0.0	8.3	68.9
	V	2650	-21.5	26.0	0.0	6.2	38.4
D TOP	T	2631	-3.1	4.8	0.0	0.6	0.4
	U	1463	-28.4	28.1	0.0	6.2	38.4
	V	1463	-27.2	29.2	0.0	7.3	53.3
D MID	T	2650	-2.1	3.7	0.0	0.5	0.3
	U	2650	-21.5	22.8	0.0	5.8	33.6
	V	2650	-21.9	27.6	0.0	6.5	42.3
D BOT	T	2650	-2.3	2.6	0.0	0.4	0.2
	U	2650	-28.6	30.7	0.0	6.9	47.6
	V	2650	-22.1	23.4	0.0	5.4	29.2

40 HRLP

Current meter	Parameter	N	Min	Max	Mean	SD	Var
A TOP	T	442	13.4	22.8	17.1	1.7	2.9
	U	442	-24.2	19.6	0.1	6.5	42.3
	V	442	-58.1	102.6	5.7	32.4	1049.8
A BOT	T	442	46.5	16.9	11.6	3.0	9.0
	U	442	-19.5	10.1	-2.6	5.0	25.0
	V	442	-42.4	61.7	3.0	19.3	372.5
B TOP	T	442	8.8	18.6	12.6	2.5	6.3
	U	442	-41.9	40.3	1.2	14.1	198.8
	V	442	42.6	128.4	24.5	28.4	806.6
B BOT	T	442	6.5	13.0	8.9	1.4	2.0
	U	442	-23.9	26.1	2.2	8.8	77.4
	V	442	-52.8	44.0	3.9	16.2	262.4
C TOP	T	441	9.7	17.5	12.9	2.0	4.2
	U	441	-26.3	28.8	4.0	9.5	89.3
	V	441	-41.1	114.7	31.9	32.9	1083.7
C MID	T	390	8.8	15.5	11.2	1.6	2.6
	U	412	-41.2	64.3	0.9	13.2	174.2
	V	412	-44.4	95.4	22.6	26.1	681.2
C BOT	T	442	7.4	12.5	9.4	1.0	1.0
	U	442	-15.1	14.2	0.6	4.6	21.2
	V	442	-40.0	53.0	9.3	19.1	364.8
D TOP	T	439	9.8	18.0	13.3	1.9	3.6
	U	244	-21.1	31.1	4.0	8.3	68.9
	V	244	-26.7	95.0	31.4	28.7	823.7
D MID	T	442	8.6	15.9	11.4	1.6	2.6
	U	442	-24.3	26.1	1.4	6.4	41.0
	V	442	-43.1	102.1	24.3	28.4	806.6
D BOT	T	442	7.6	12.3	9.4	1.0	1.0
	U	442	-12.3	12.6	0.2	3.8	14.4
	V	442	-32.2	49.1	8.1	16.2	262.4

Table 4. Sub-band variance ratios for temperature (T) and velocity components (u, v) from each instrument. The sub-bands approximately divide the principal tidal and inertial spectrum (3-40 HRBP) for the low frequency spectrum (40 HRLP).

Current meter	Parameter	Variance ratio	
		3-40 HR BP 3 HRLP	40 HRLP 3 HRLP
A TOP	T	0.09	0.91
	U	0.56	0.44
	V	0.06	0.91
A BOT	T	0.11	0.83
	U	0.66	0.30
	V	0.10	0.84
B TOP	T	0.03	1.00
	U	0.18	0.81
	V	0.06	0.94
B BOT	T	0.04	0.87
	U	0.33	0.64
	V	0.09	0.88
C TOP	T	0.05	0.95
	U	0.31	0.67
	V	0.05	0.96
C MID	T	0.09	0.81
	U	0.18	0.67
	V	0.07	0.96
C BOT	T	0.25	0.83
	U	0.76	0.23
	V	0.10	0.93
D TOP	T	0.10	0.90
	U	0.37	0.66
	V	0.06	0.98
D MID	T	0.10	0.90
	U	0.43	0.53
	V	0.05	0.97
D BOT	T	0.17	0.83
	U	0.78	0.24
	V	0.10	0.93

The 3 HRLP mean velocity vectors are shown on the mooring array plan view. (Fig. 3). The largest mean departure from the downstream direction occurred for the A-bottom instrument, possibly reflecting the importance of bottom topography as the meandering Stream moved in and out of shoaling waters.

Polar histograms giving the distribution of the normalized, cumulative 3 HRLP vector magnitude are shown in Figs. 10 through 19. All of the bottom instruments and A-top had significant times of countercurrents. The fluctuations were more or less rectilinear, except at A-bot, where the distribution has an asymmetric property. It is apparent from Figs. 10 through 19 (and *not* from Fig. 3) that the onshore mean component primarily results from the correlation of onshore flow with only the downstream flow component. The coordinate rotation angle is shown in Figs. 10 through 19 by the radial tick mark at 34° clockwise from north.

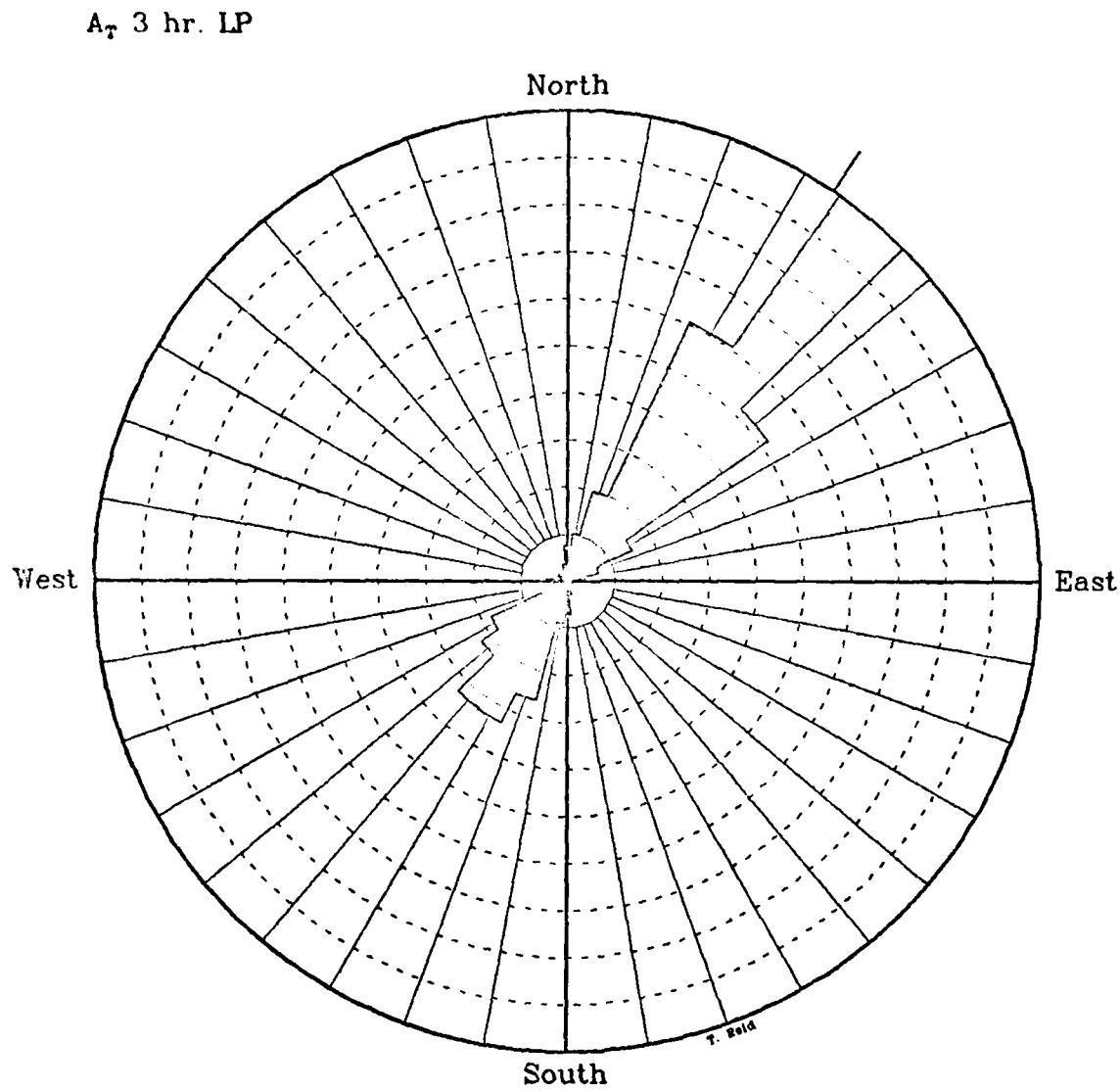


Figure 10. Polar histogram for instrument A-top showing the normalized magnitude distribution of the 3 HRLP velocity, accumulated vectorially in ten degree sectors. The downstream (+ v) direction of the rotated coordinate system is shown by the radial tick mark.

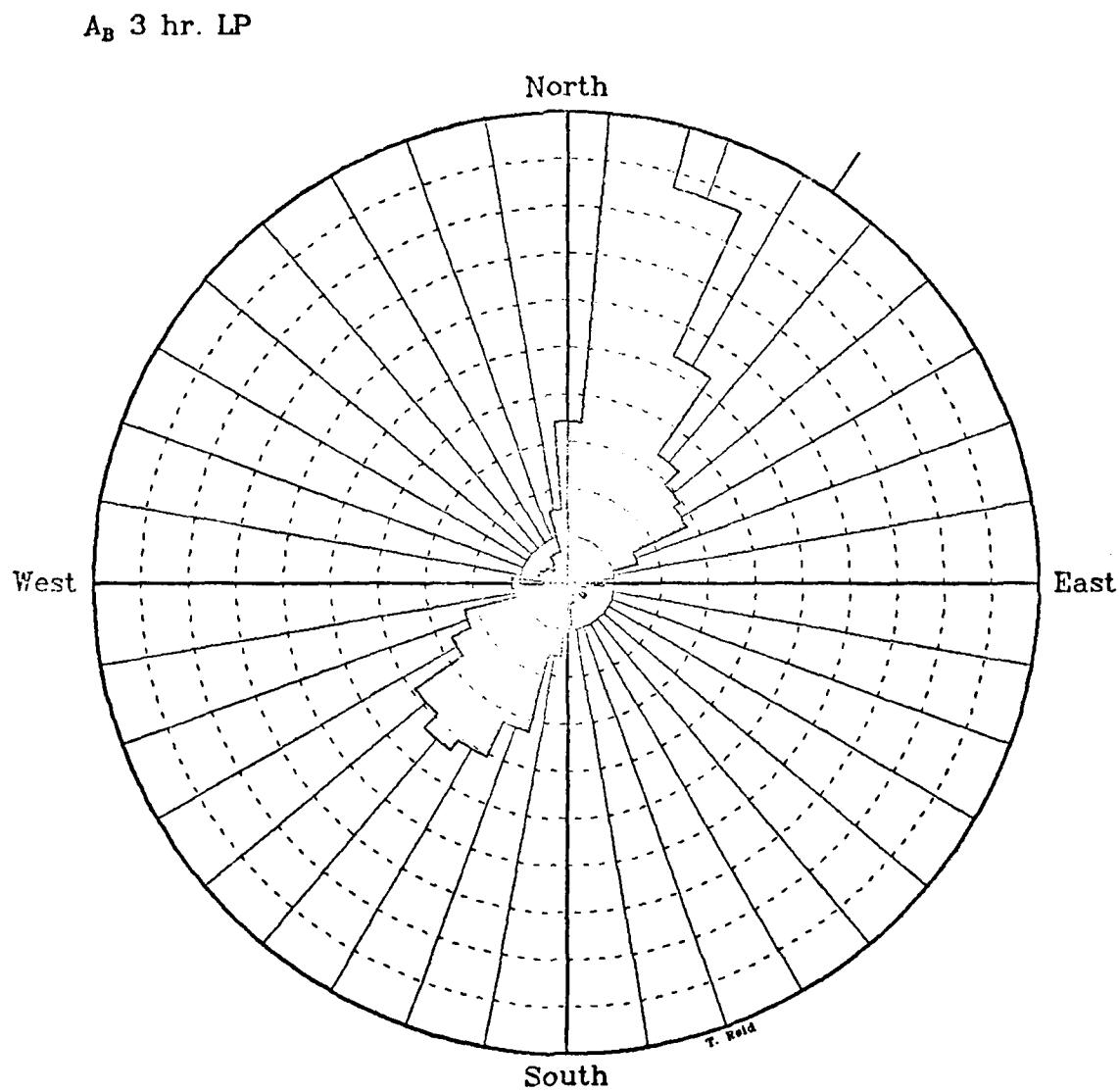


Figure 11. Polar histogram for instrument A-bot showing the normalized magnitude distribution of the 3 HRLP velocity, accumulated vectorially in ten degree sectors. The downstream (+ v) direction of the rotated coordinate system is shown by the radial tick mark.

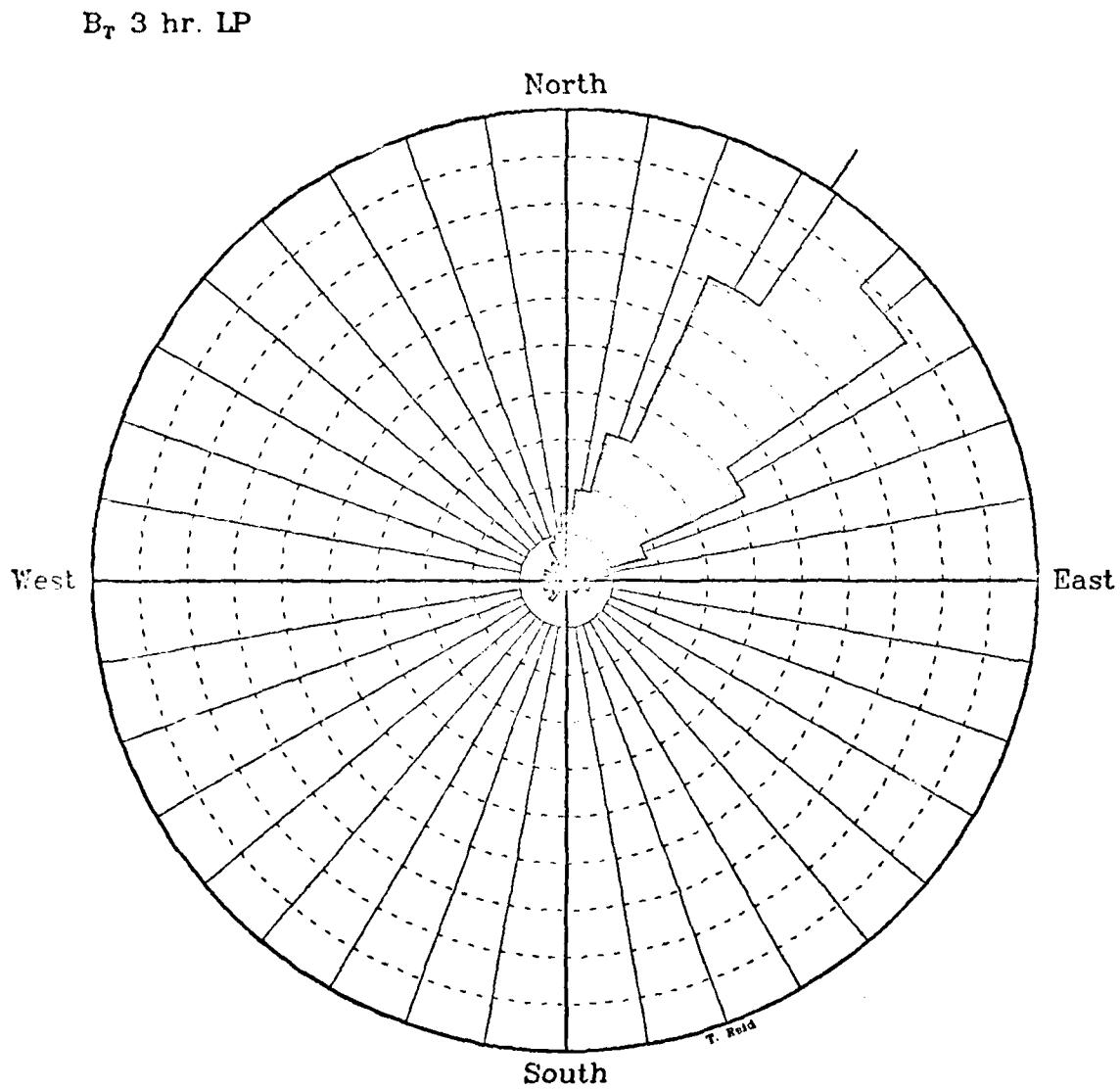


Figure 12. Polar histogram for instrument B-top showing the normalized magnitude distribution of the 3 HRLP velocity, accumulated vectorially in ten degree sectors. The downstream (+ v) direction of the rotated coordinate system is shown by the radial tick mark.

B_b 3 hr. LP

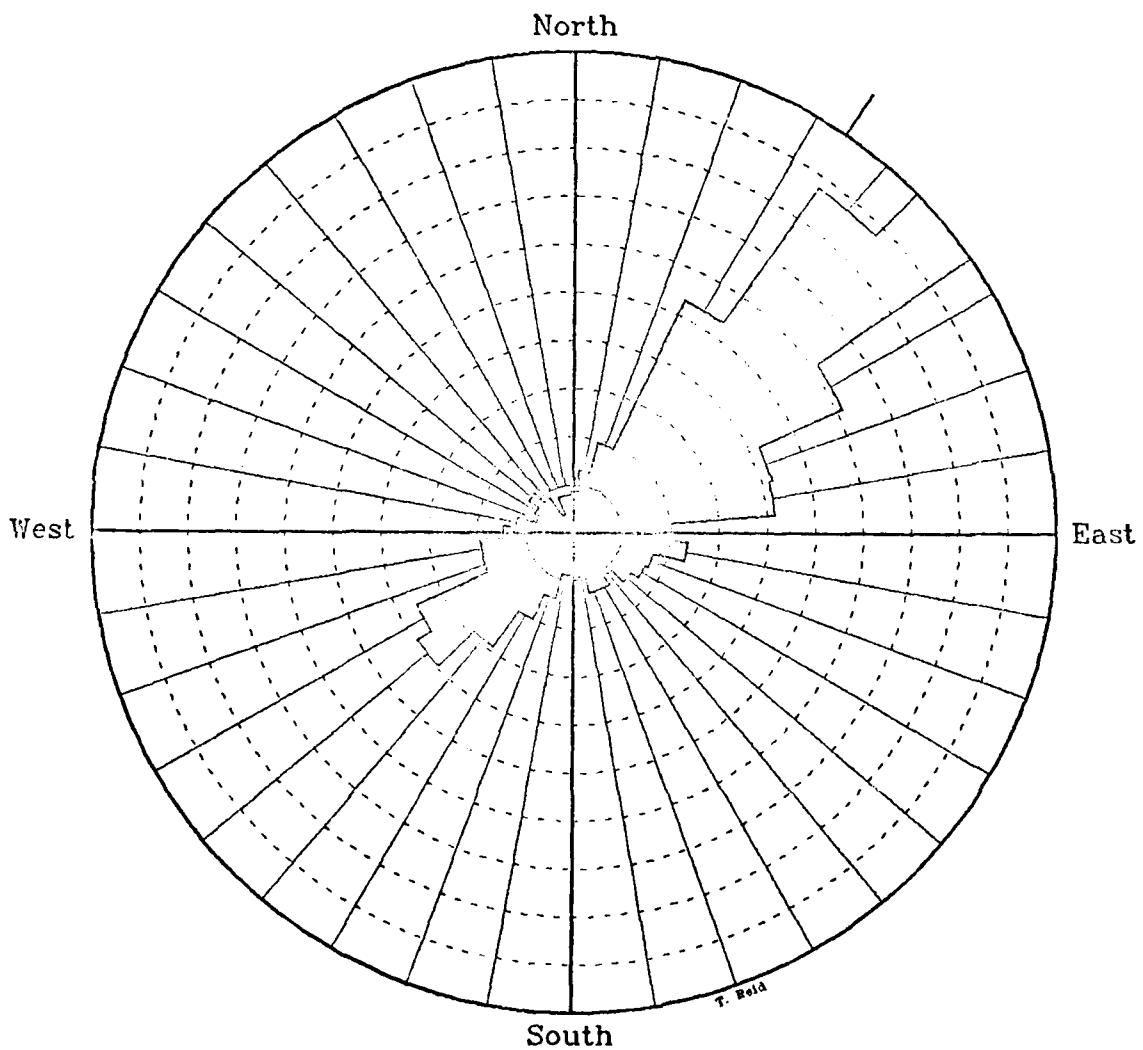


Figure 13. Polar histogram for instrument B-bot showing the normalized magnitude distribution of the 3 HRLP velocity, accumulated vectorially in ten degree sectors. The downstream (+ v) direction of the rotated coordinate system is shown by the radial tick mark.

C_T 3 hr. LP

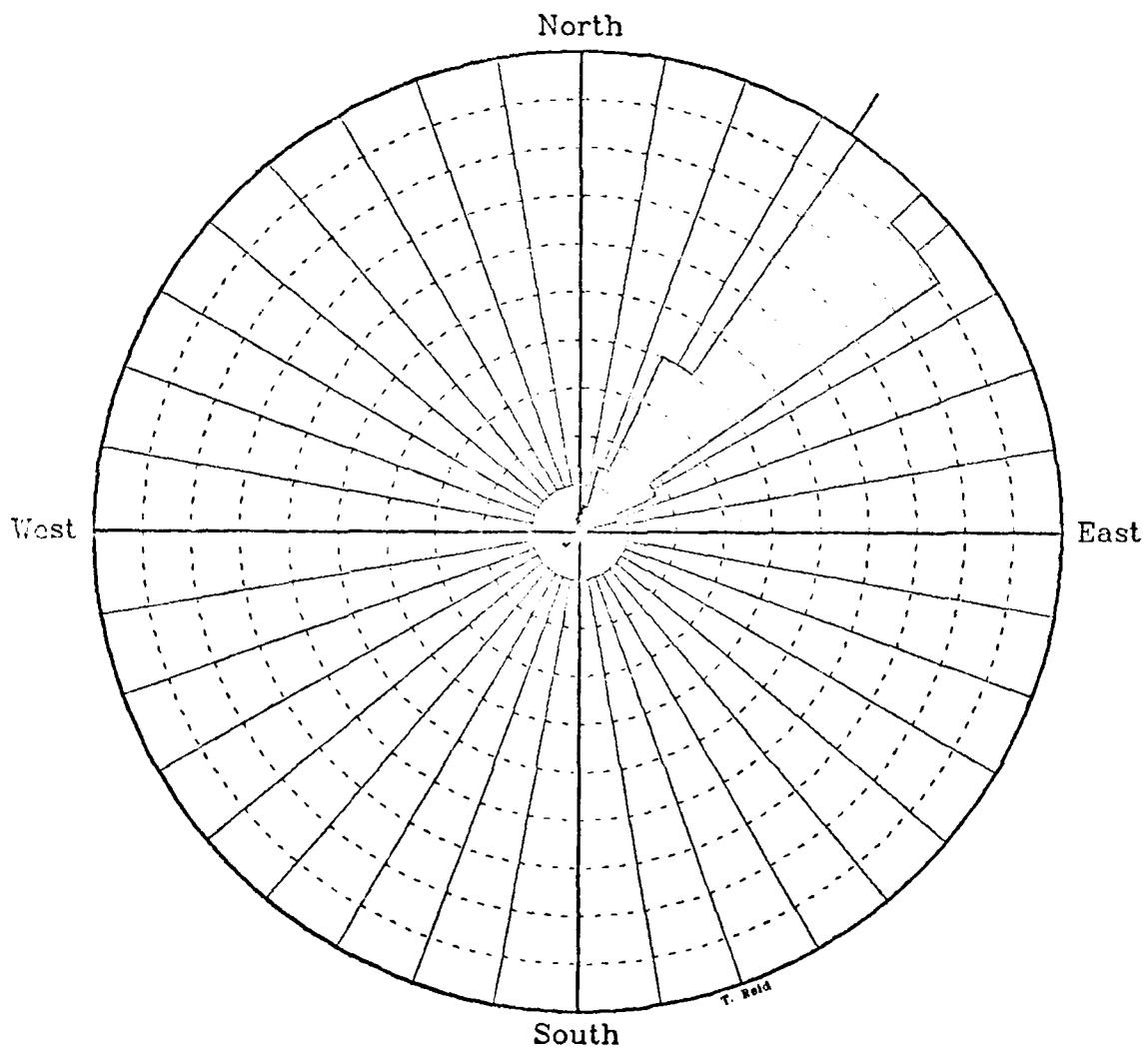


Figure 14. Polar histogram for instrument C-top showing the normalized magnitude distribution of the 3 HRLP velocity, accumulated vectorially in ten degree sectors. The downstream (+ v) direction of the rotated coordinate system is shown by the radial tick mark.

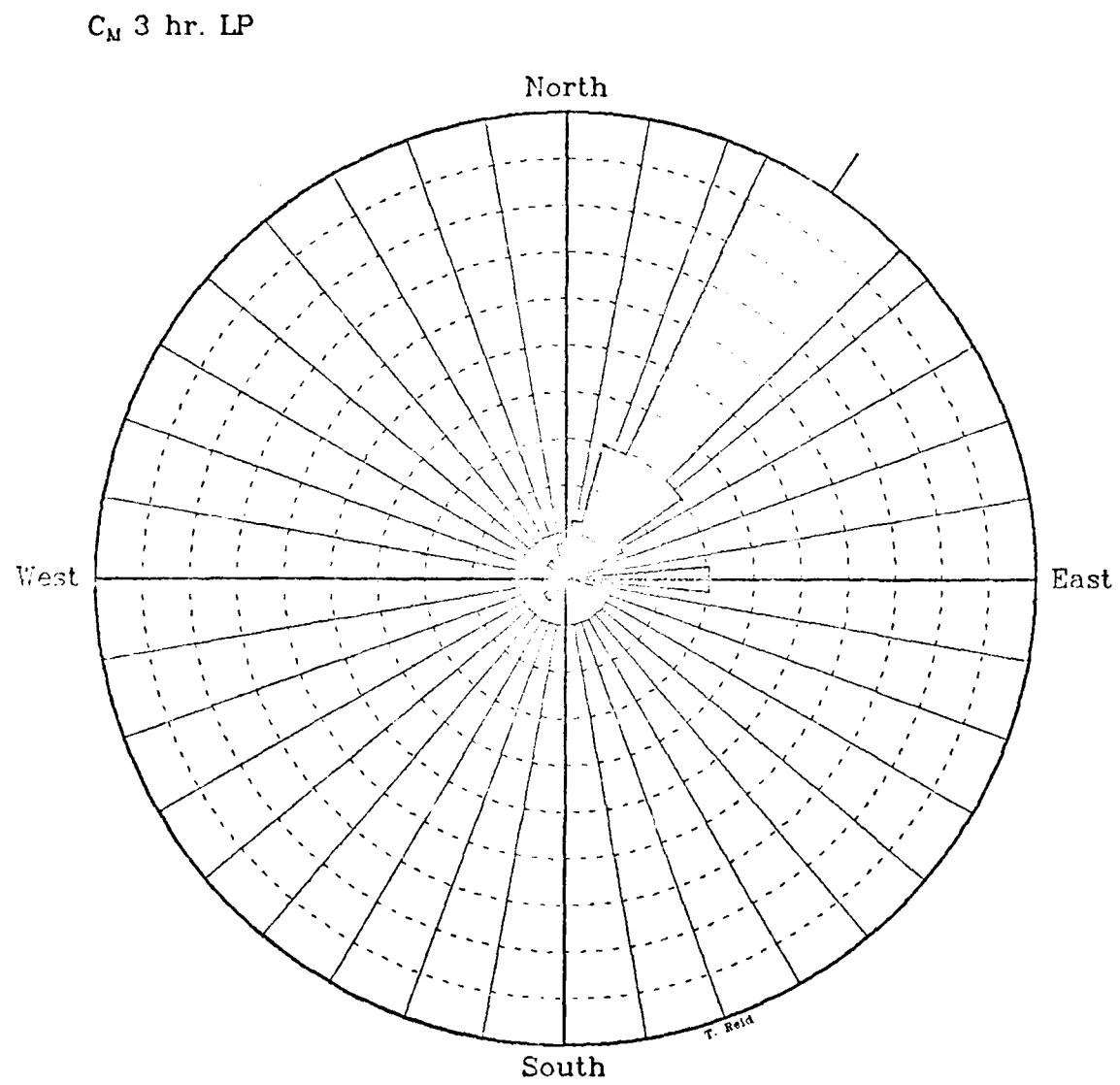


Figure 15. Polar histogram for instrument C-mid showing the normalized magnitude distribution of the 3 HRLP velocity, accumulated vectorially in ten degree sectors. The downstream ($+v$) direction of the rotated coordinate system is shown by the radial tick mark.

C_B 3 hr. LP

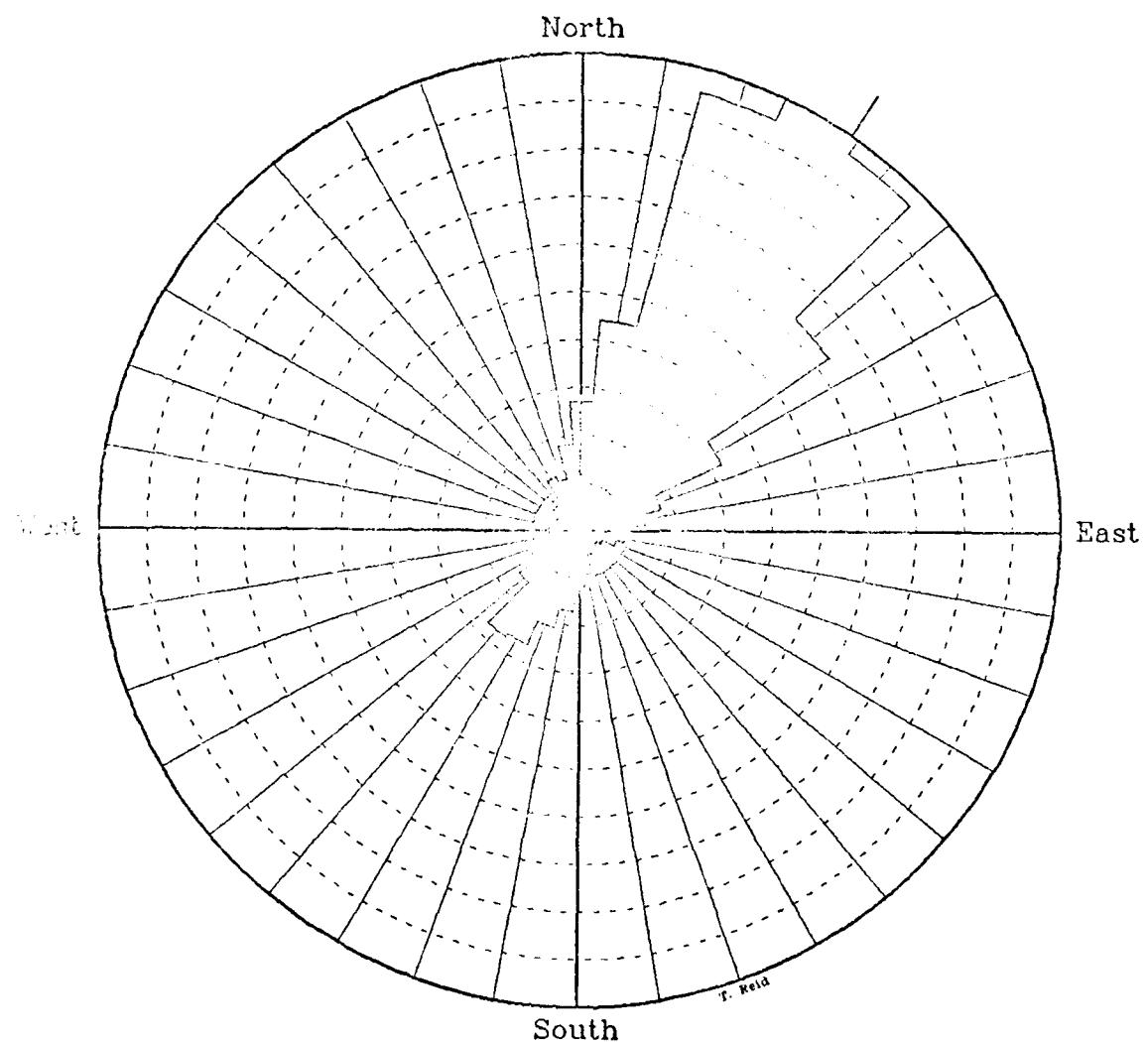


Figure 16. Polar histogram for instrument C-bot showing the normalized magnitude distribution of the 3 HRLP velocity, accumulated vectorially in ten degree sectors. The downstream (+ v) direction of the rotated coordinate system is shown by the radial tick mark.

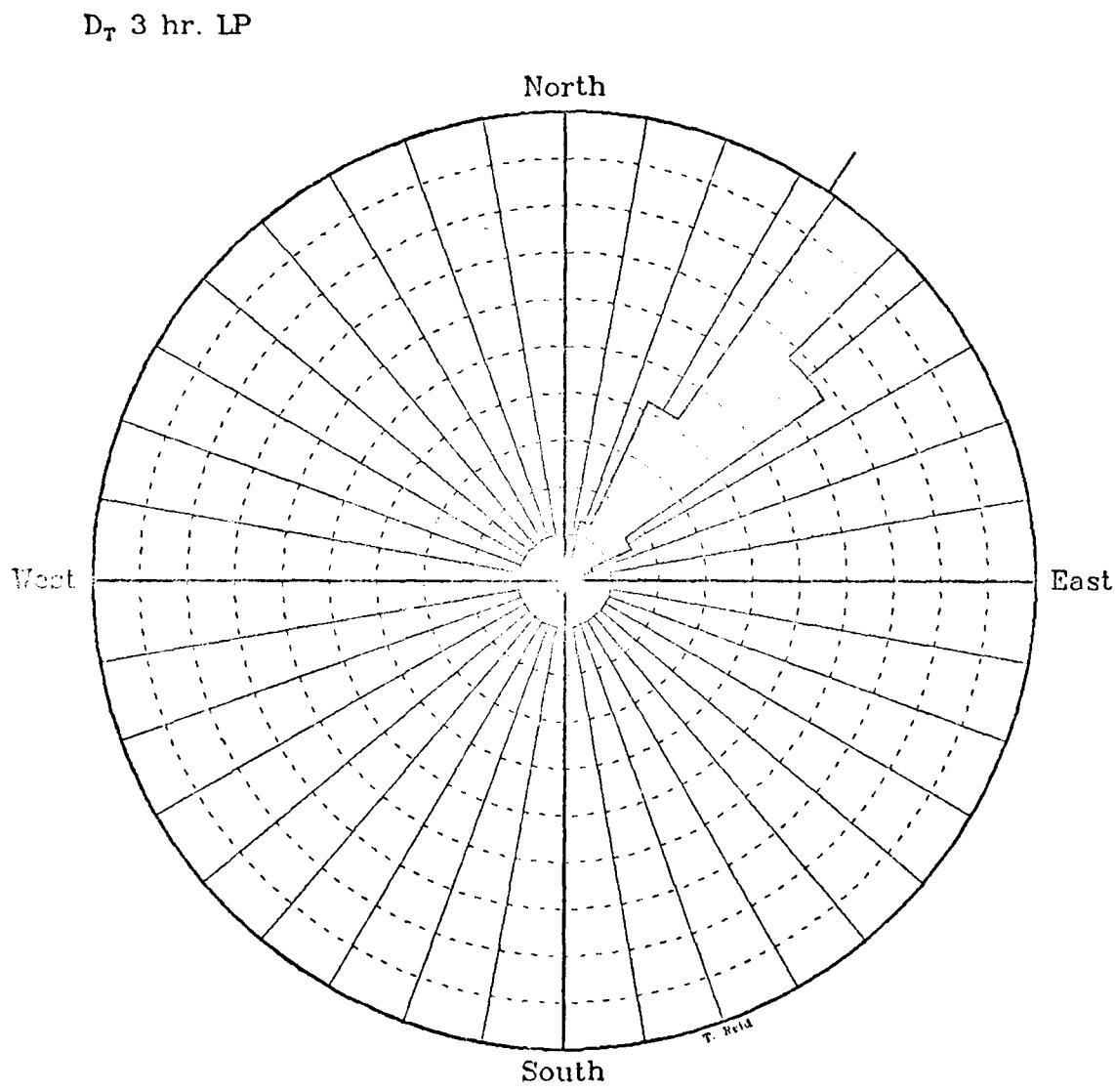


Figure 17. Polar histogram for instrument D-top showing the normalized magnitude distribution of the 3 HRP velocity, accumulated vectorially in ten degree sectors. The downstream (+ v) direction of the rotated coordinate system is shown by the radial tick mark.

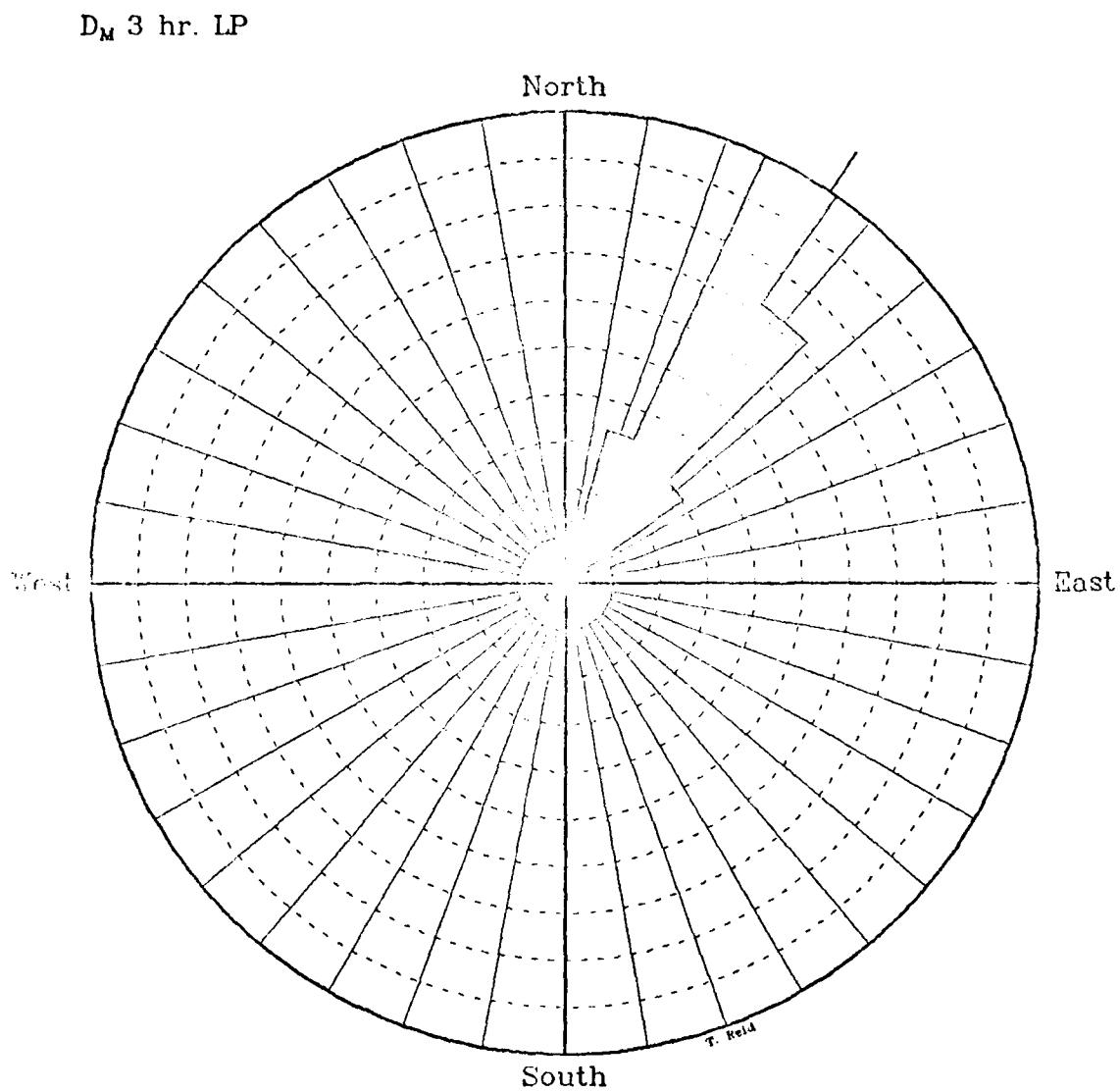


Figure 18. Polar histogram for instrument D-mid showing the normalized magnitude distribution of the 3 BLRP velocity, accumulated vectorially in ten degree sectors. The downstream (+ v) direction of the rotated coordinate system is shown by the radial tick mark.

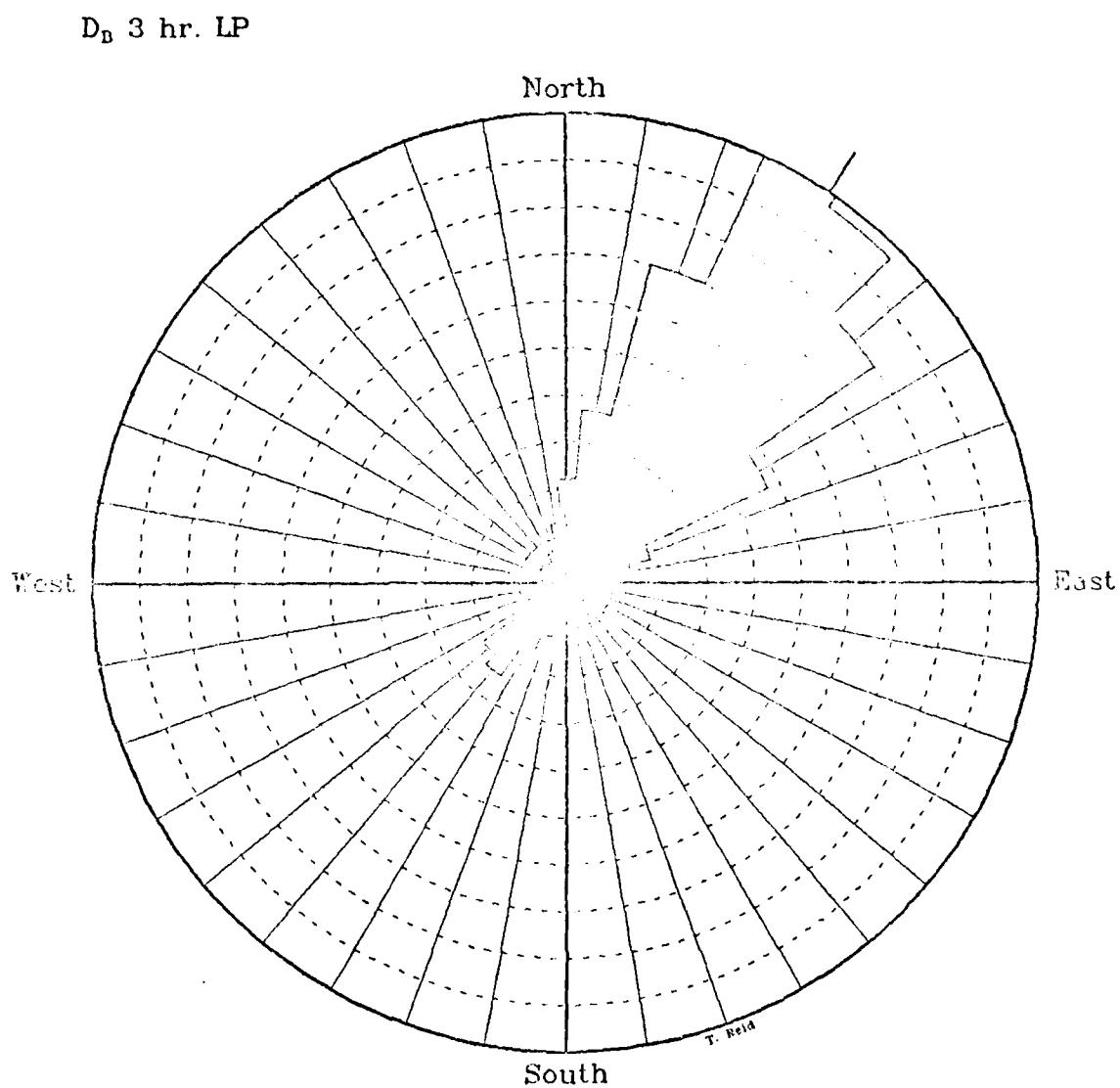


Figure 19. Polar histogram for instrument D-bot showing the normalized magnitude distribution of the 3 HRLP velocity, accumulated vectorially in ten degree sectors. The downstream (+ v) direction of the rotated coordinate system is shown by the radial tick mark.

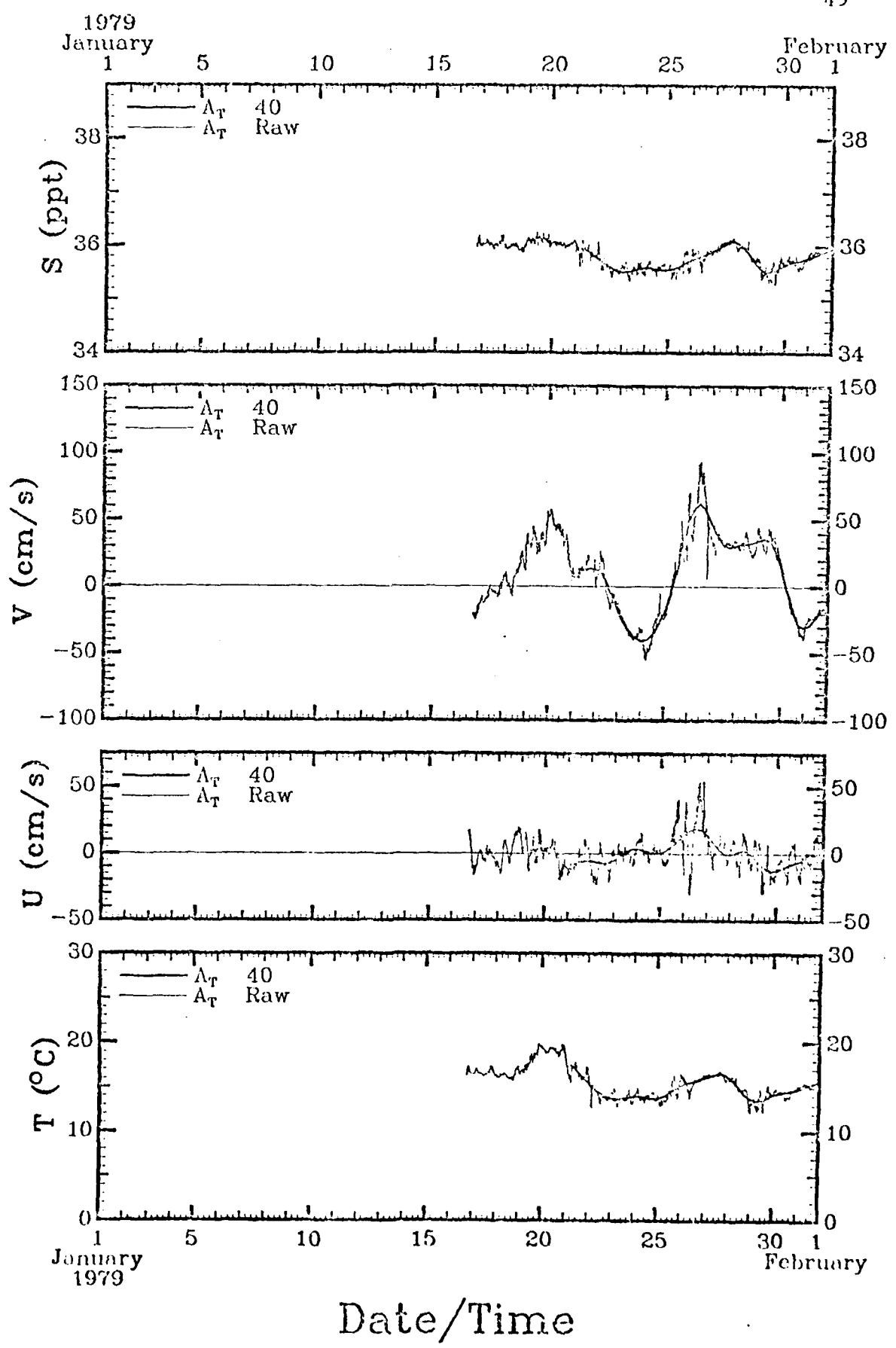
2.7 DATA PRESENTATION FORMATS

The current meter, sea level height, and atmospheric data sets are presented in the remainder of the report. Sections 3 through 5 show the current meter data in time series format and Section 6 shows the currents in "stick" plot format. Sections 7 through 9 show various combinations of the three data sets in time series format. All times in this report are given in Greenwich Mean Time (GMT). Section 10 shows the current meter data separately and in combination with other data sets in the frequency domain, giving spectrum, cross-spectrum, phase, and coherence information. All spectrum calculations employed the Cooley-Tukey method; that is, Fourier transformation of correlation functions. All frequency domain calculations in this report were carried out with an effective bandwidth of 0.033 cycles per day (CPD), to facilitate intercomparison. Current meter spectrum estimates nominally carry 15 degrees of freedom (DOF), although this number varies somewhat because of early termination of several records. For 15 DOF, the 95% confidence interval on phase estimates is about $\pm(27, 18, 12)$ degrees for coherence squared values of (0.4, 0.6, 0.8).

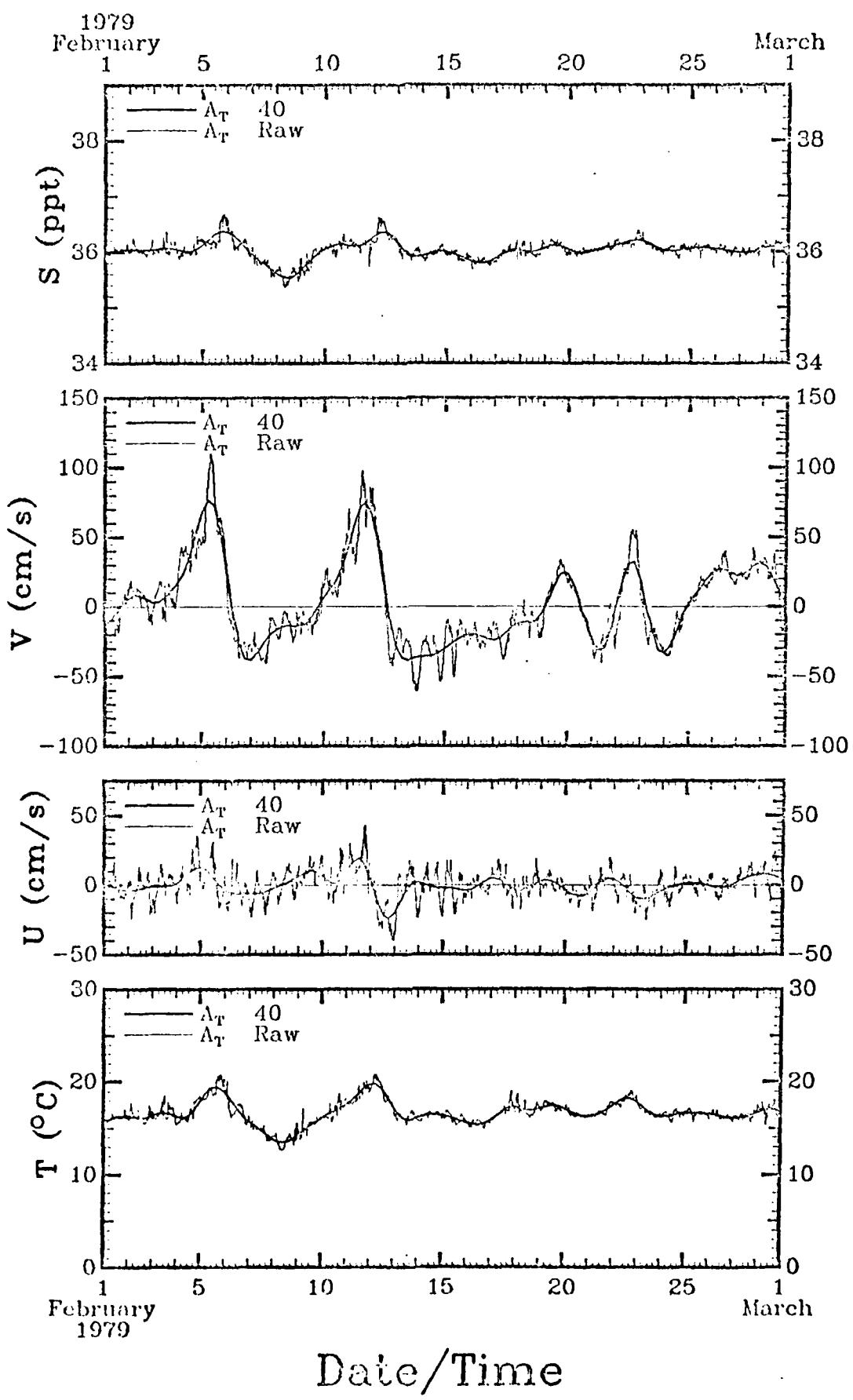
SECTION 3

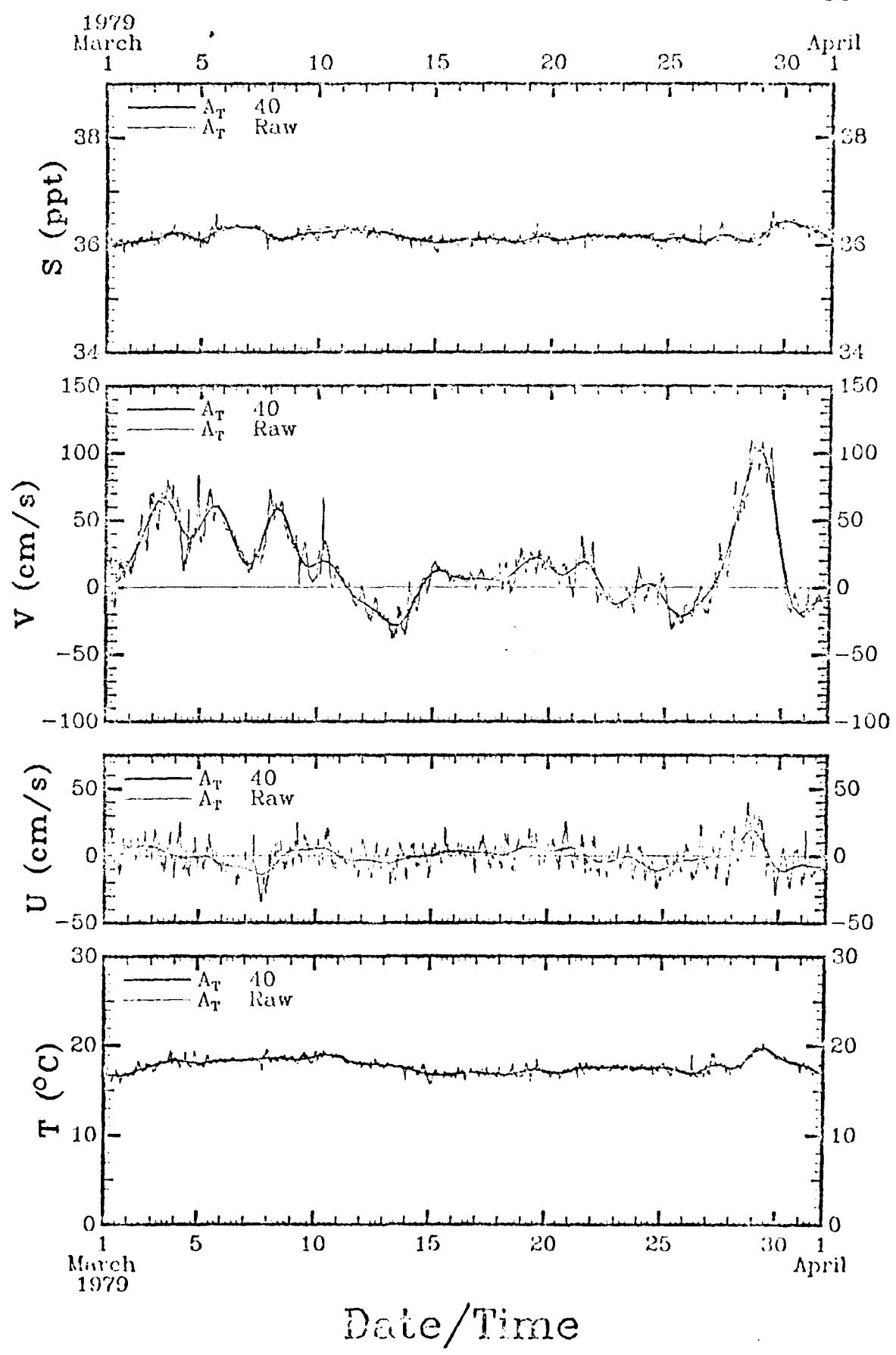
Raw and 40 HRLP Data for Each Instrument

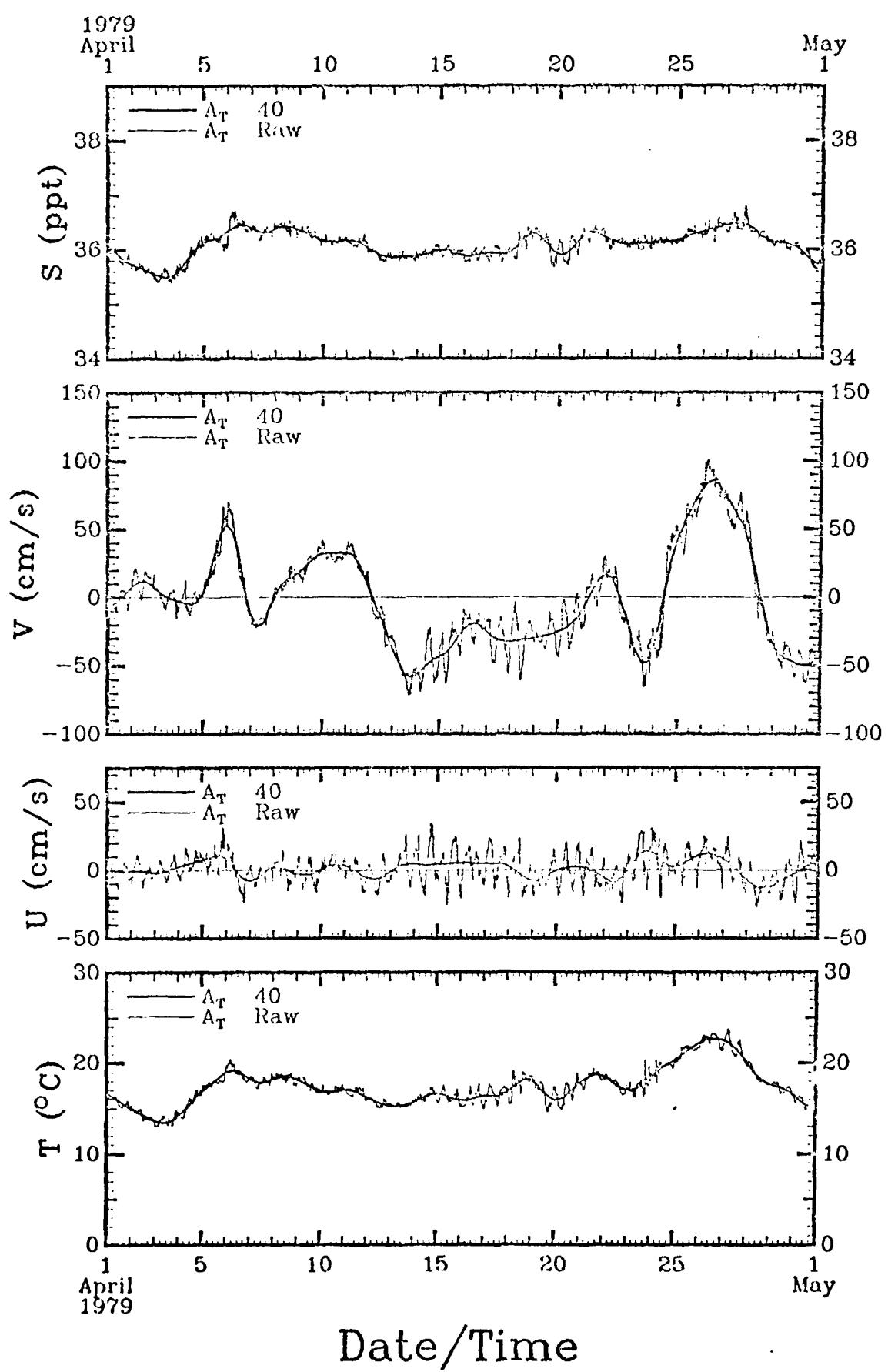
Figures 20 through 29 show the raw and superimposed 40 HRLP current meter data separately by month for each instrument. Common scaling of similar data has been used throughout this section.

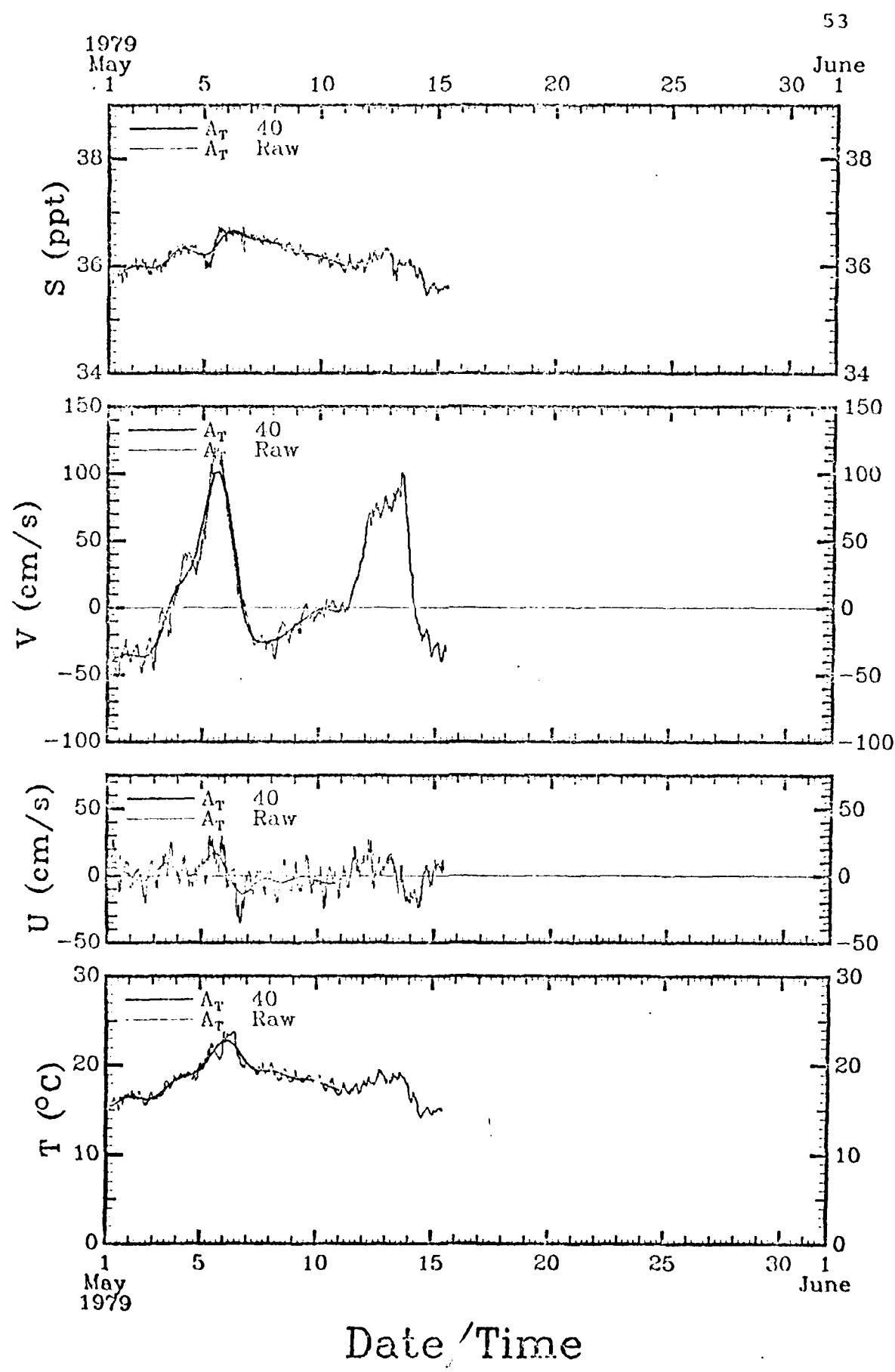


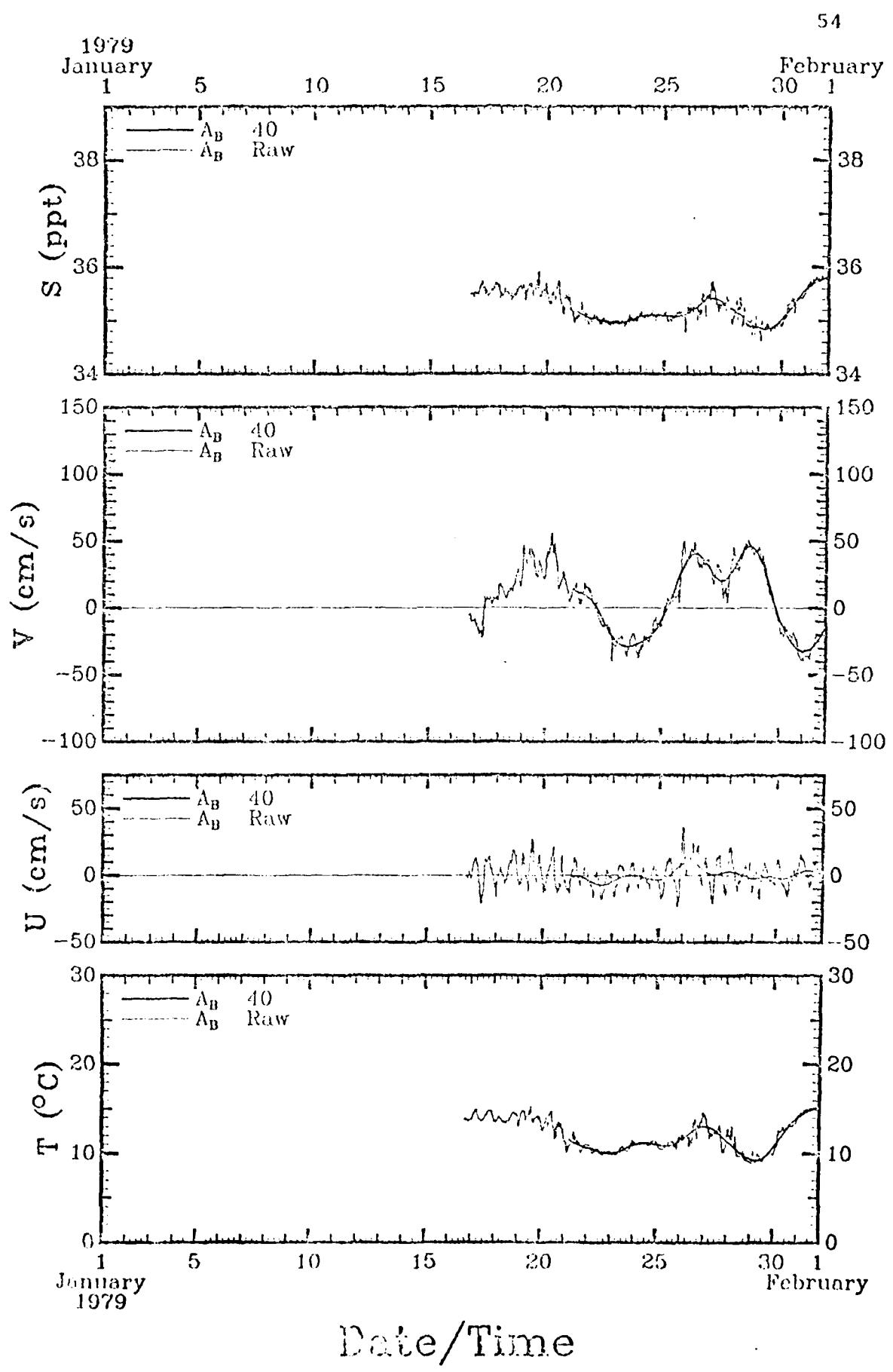
50

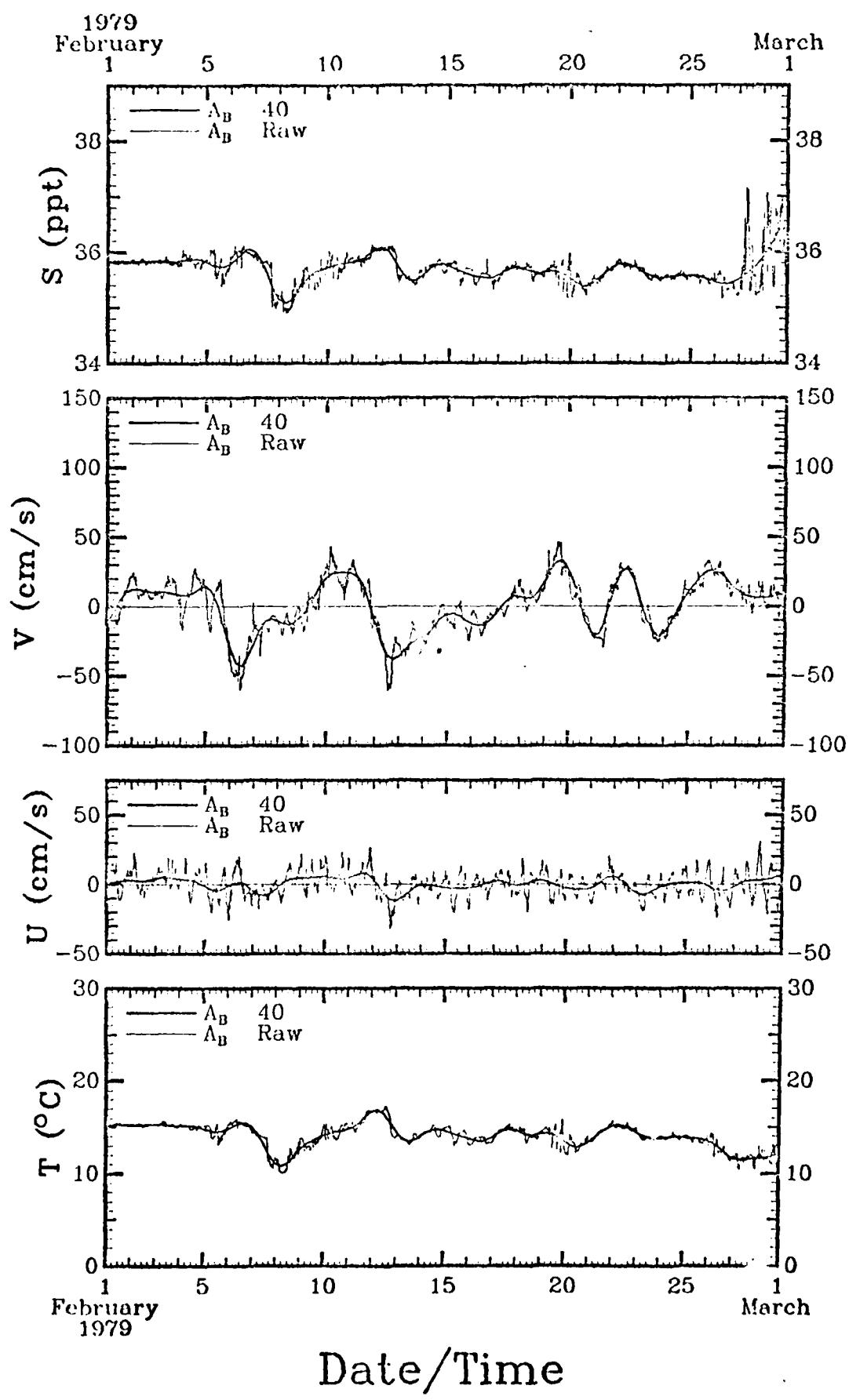


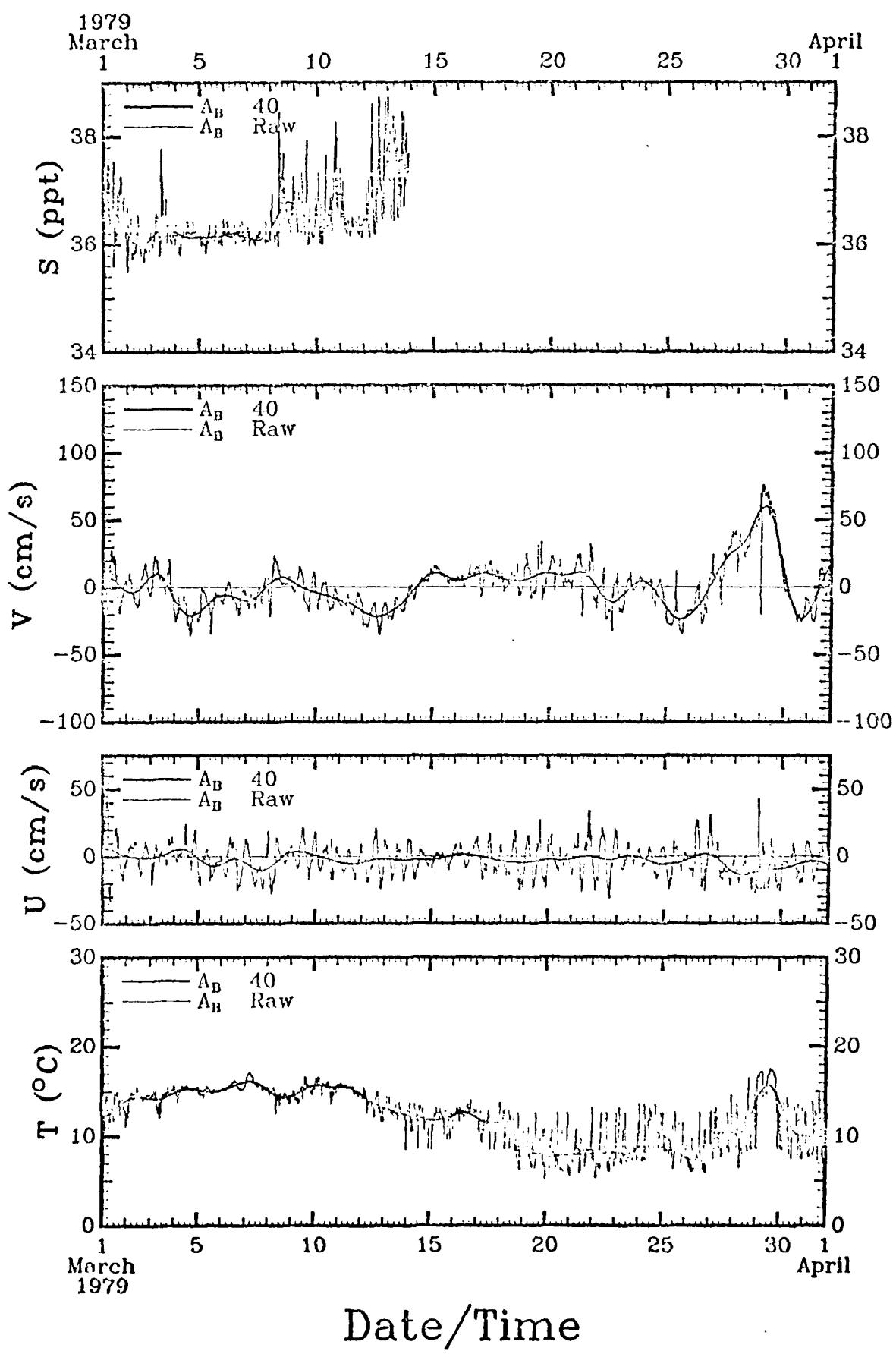


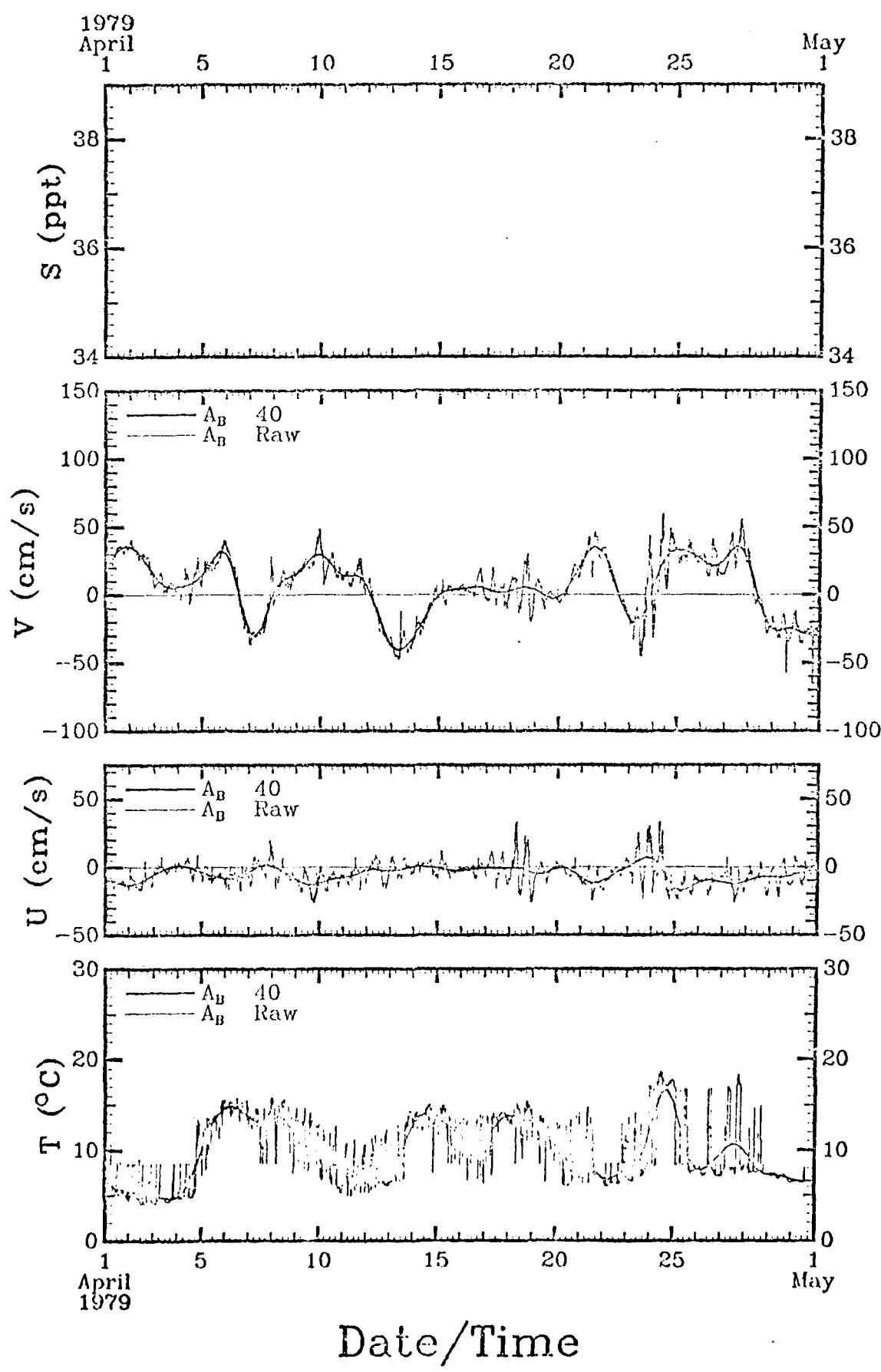


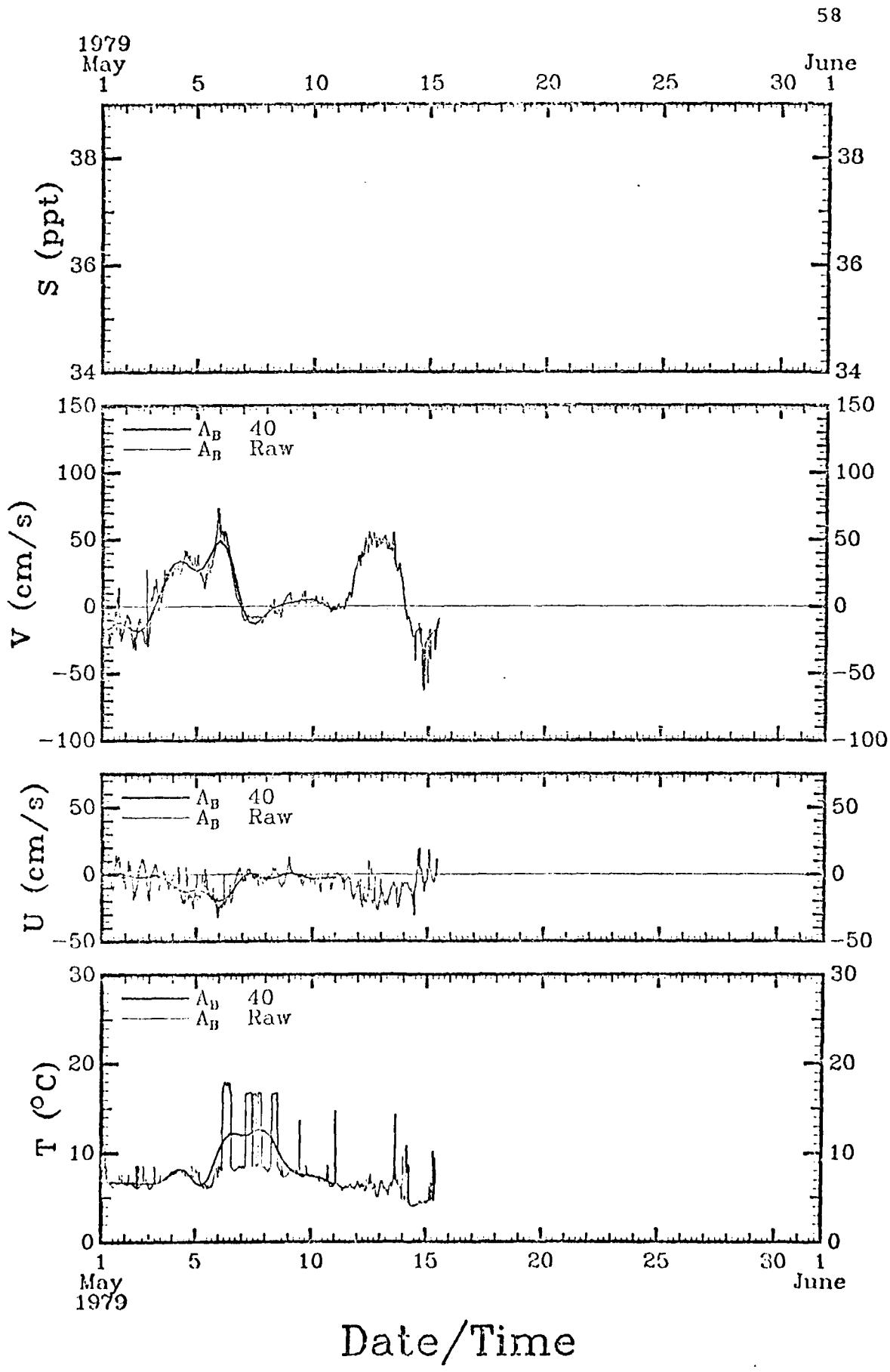


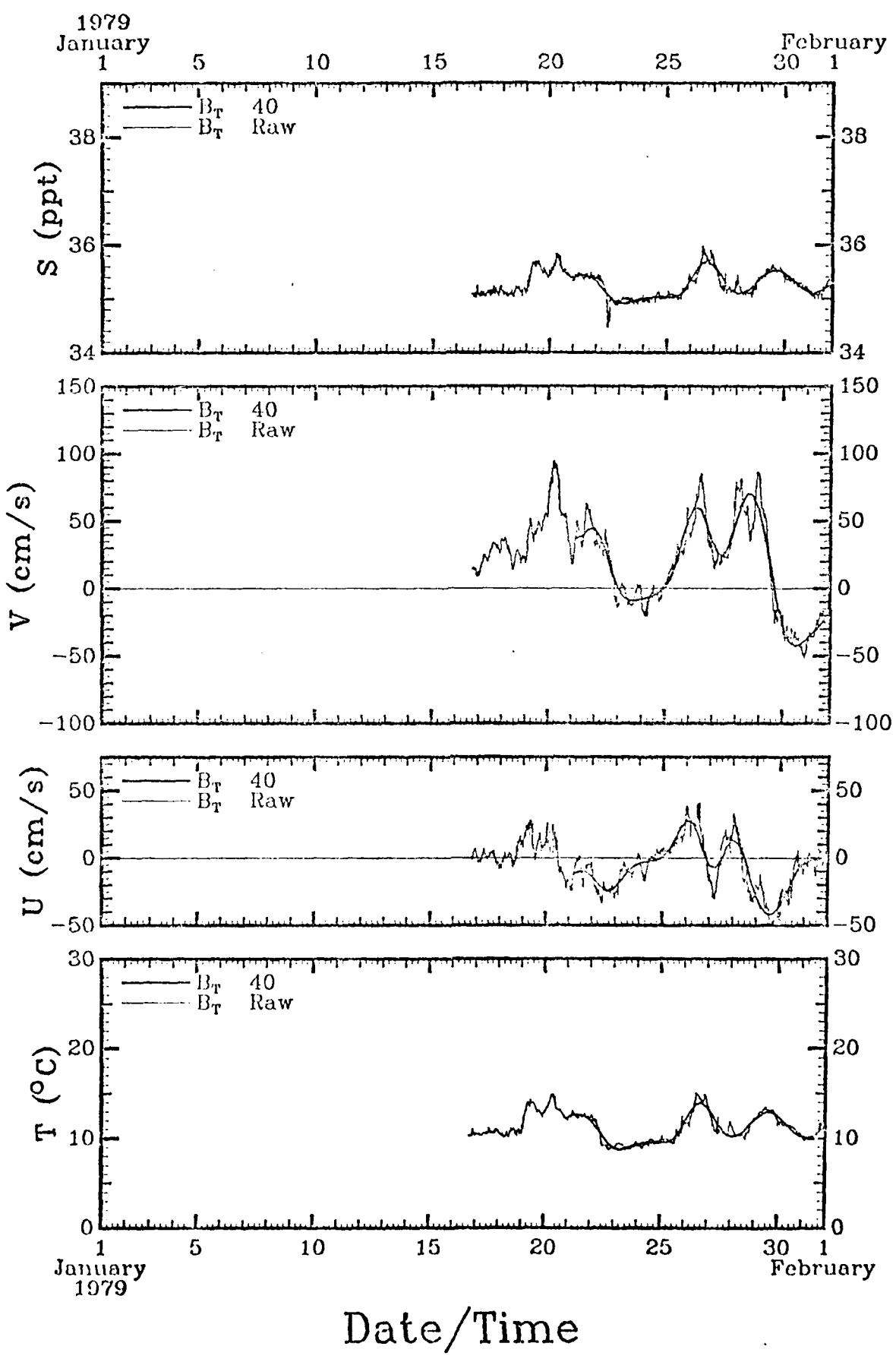


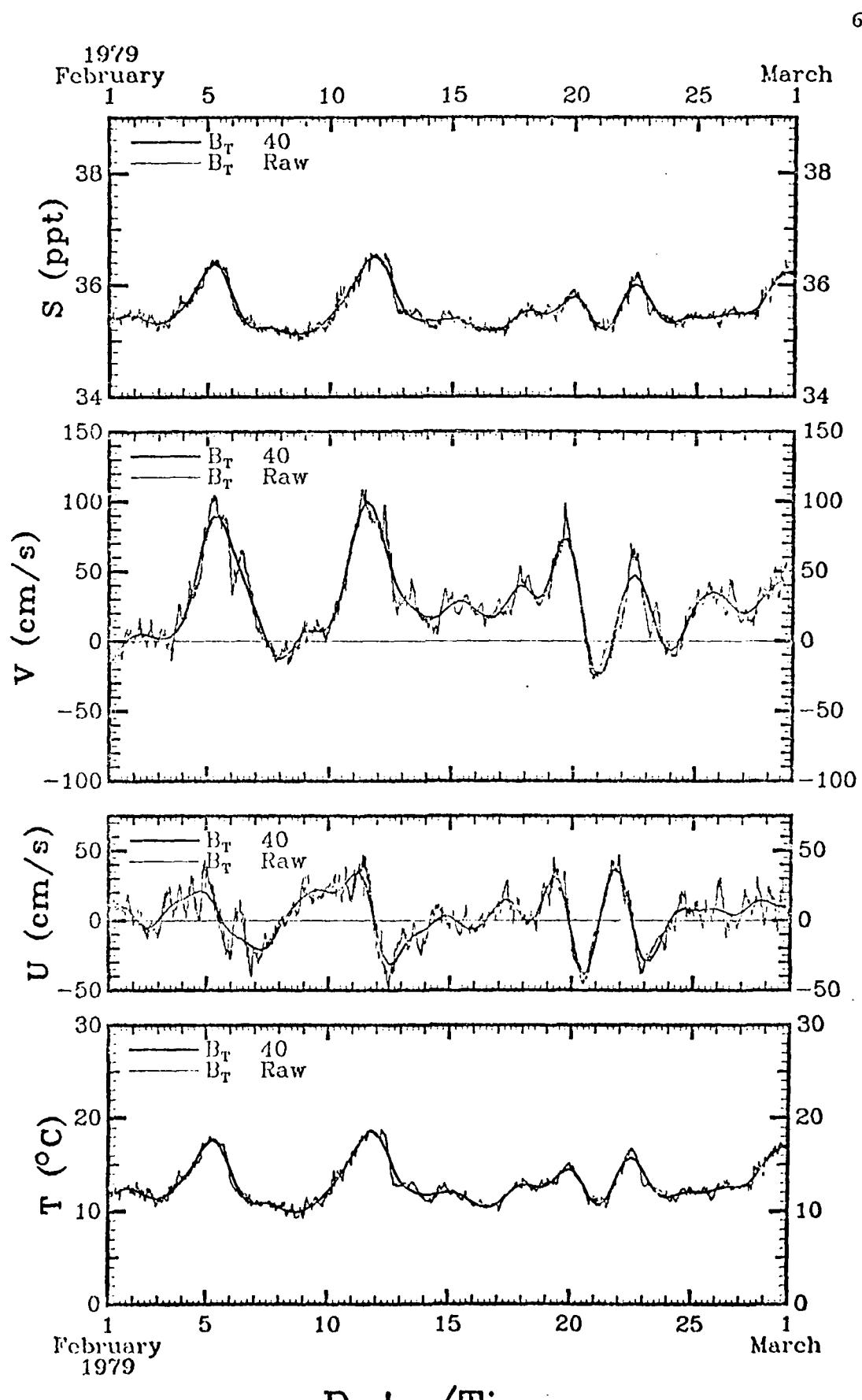




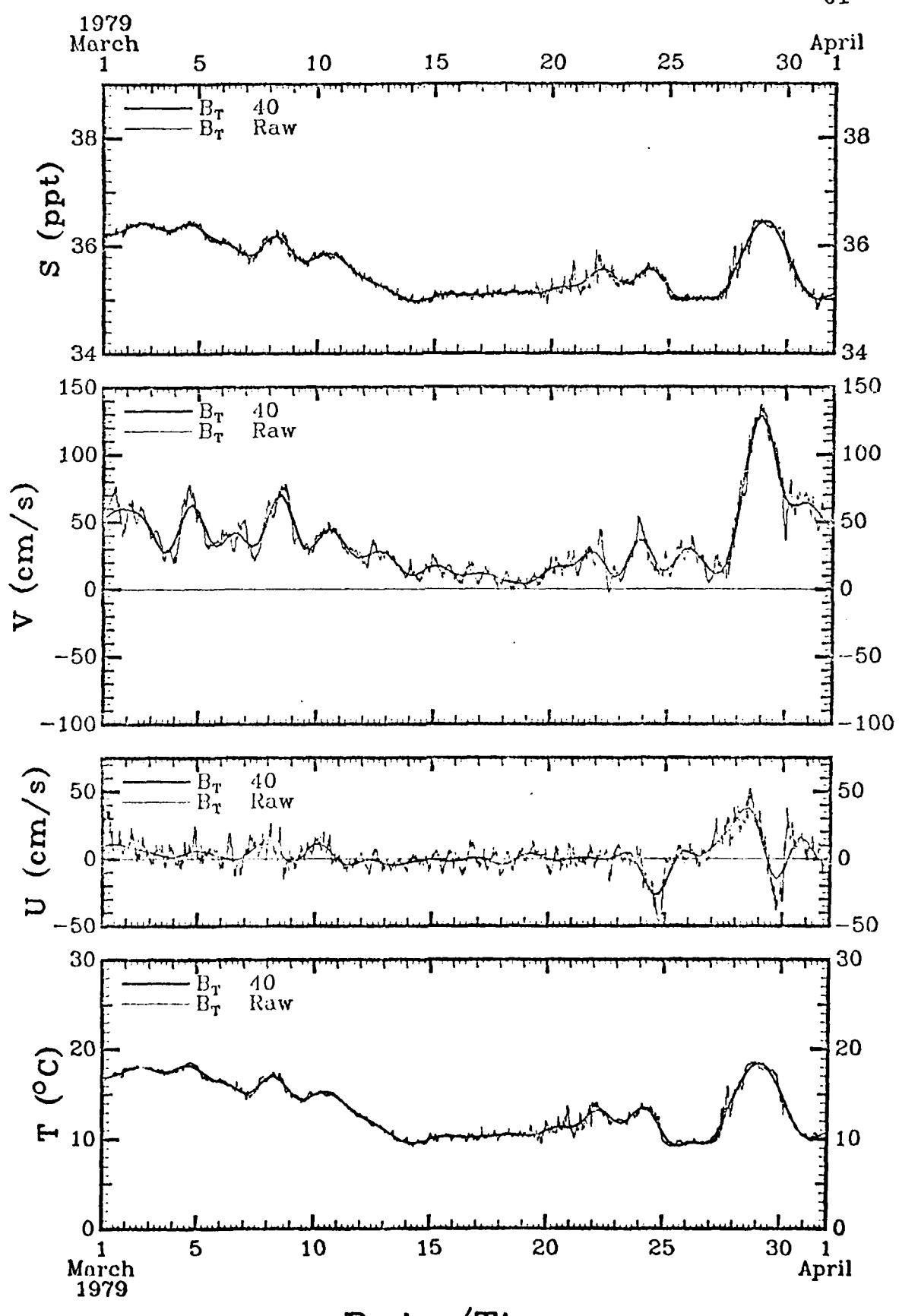


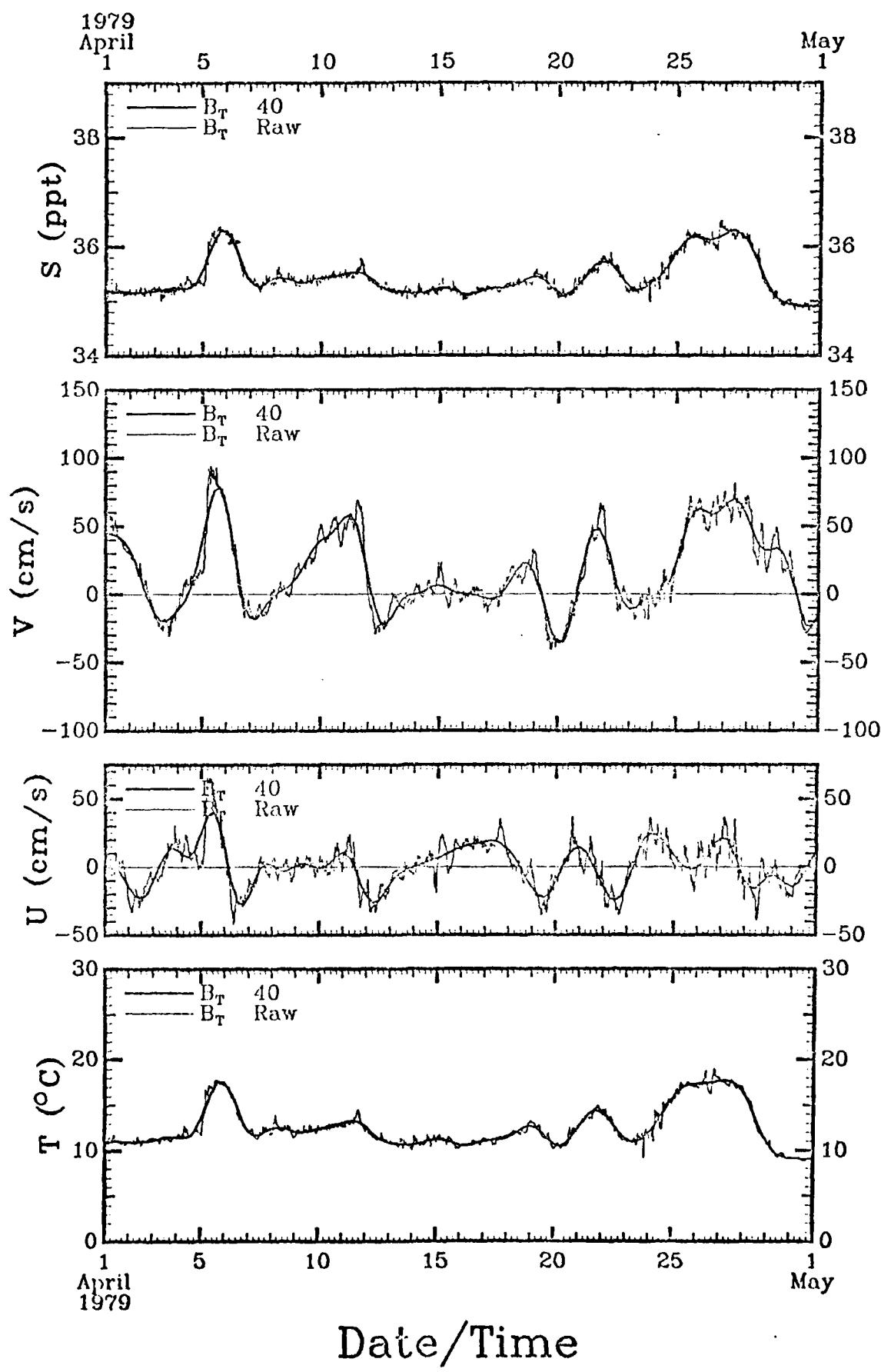


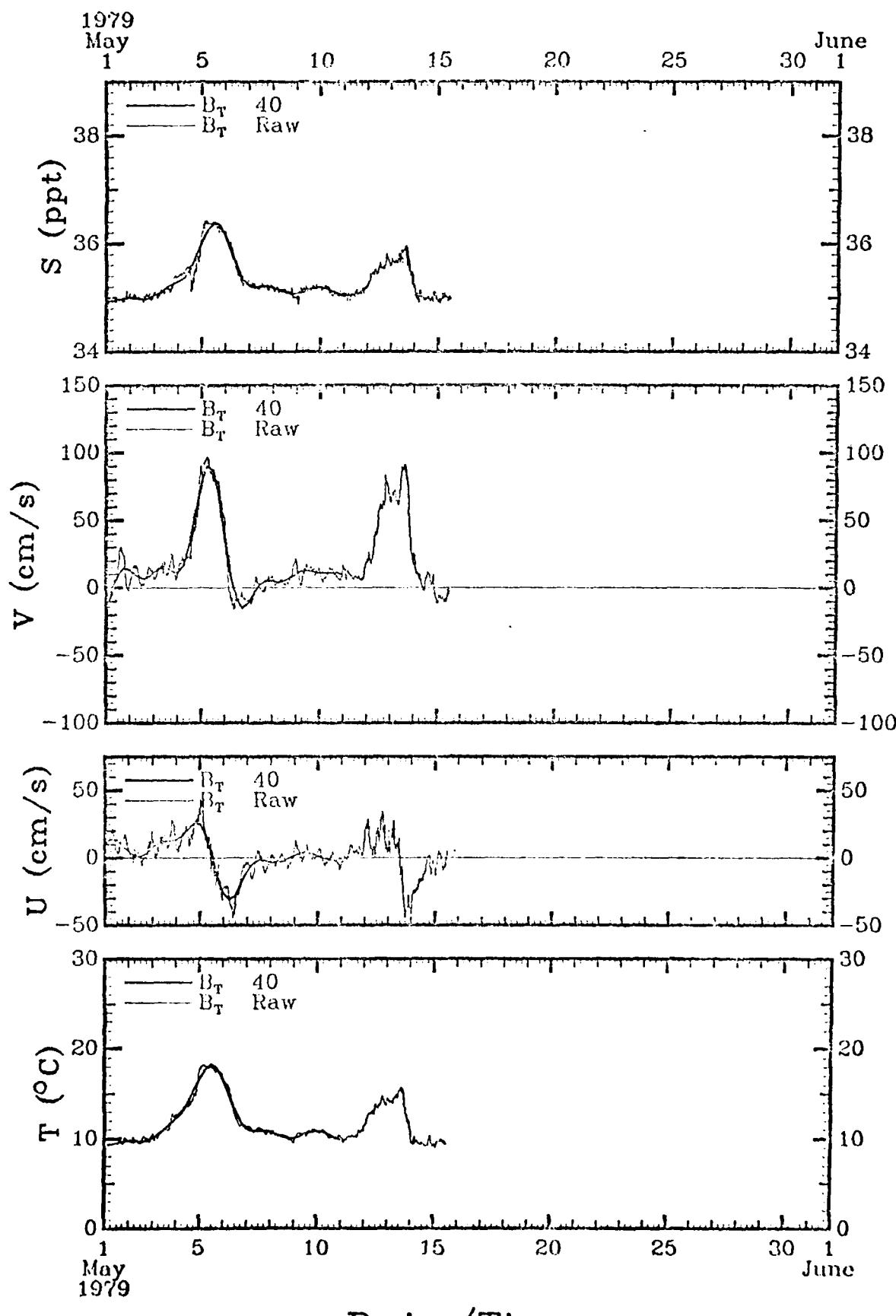




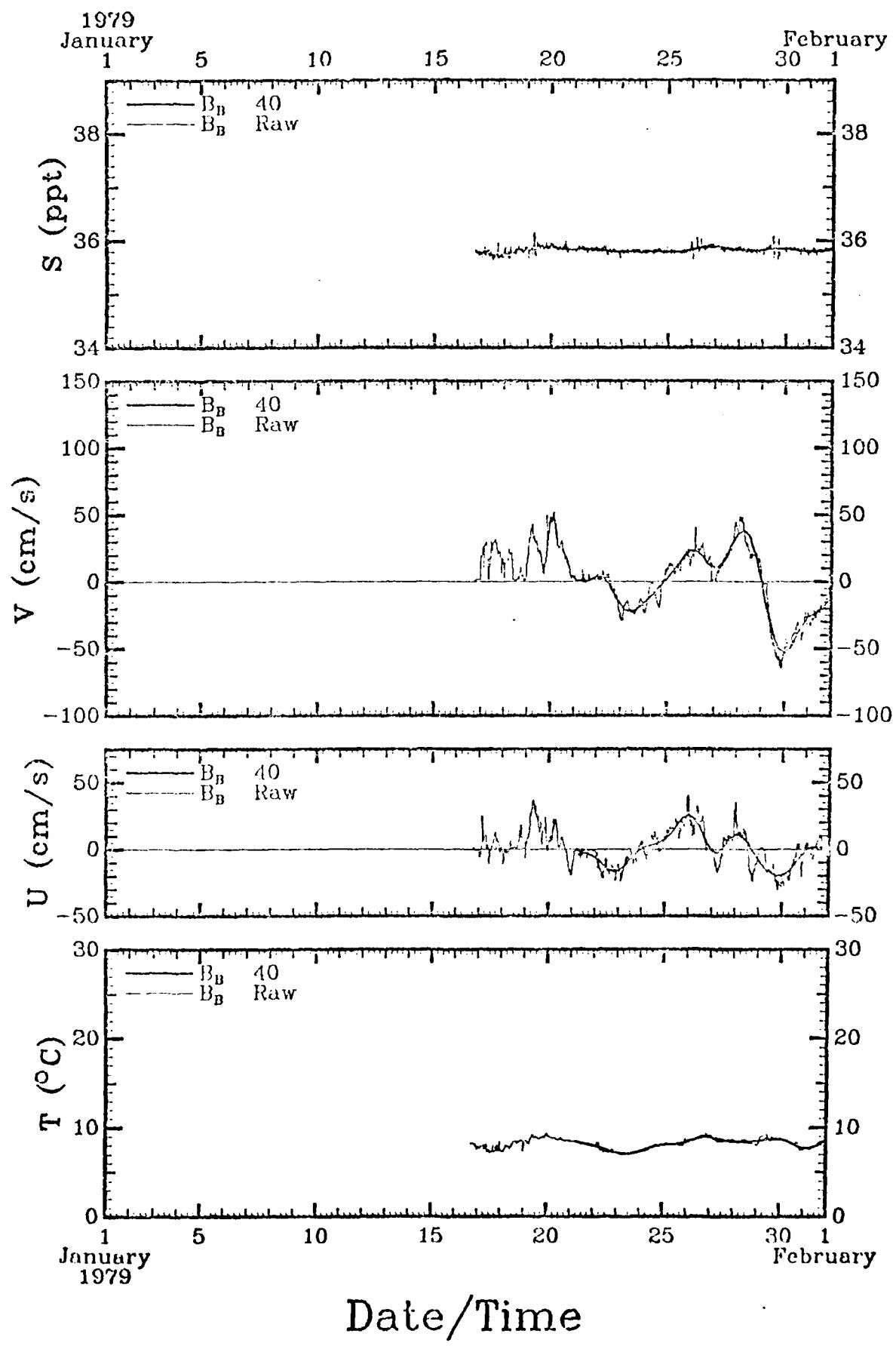
Date/Time

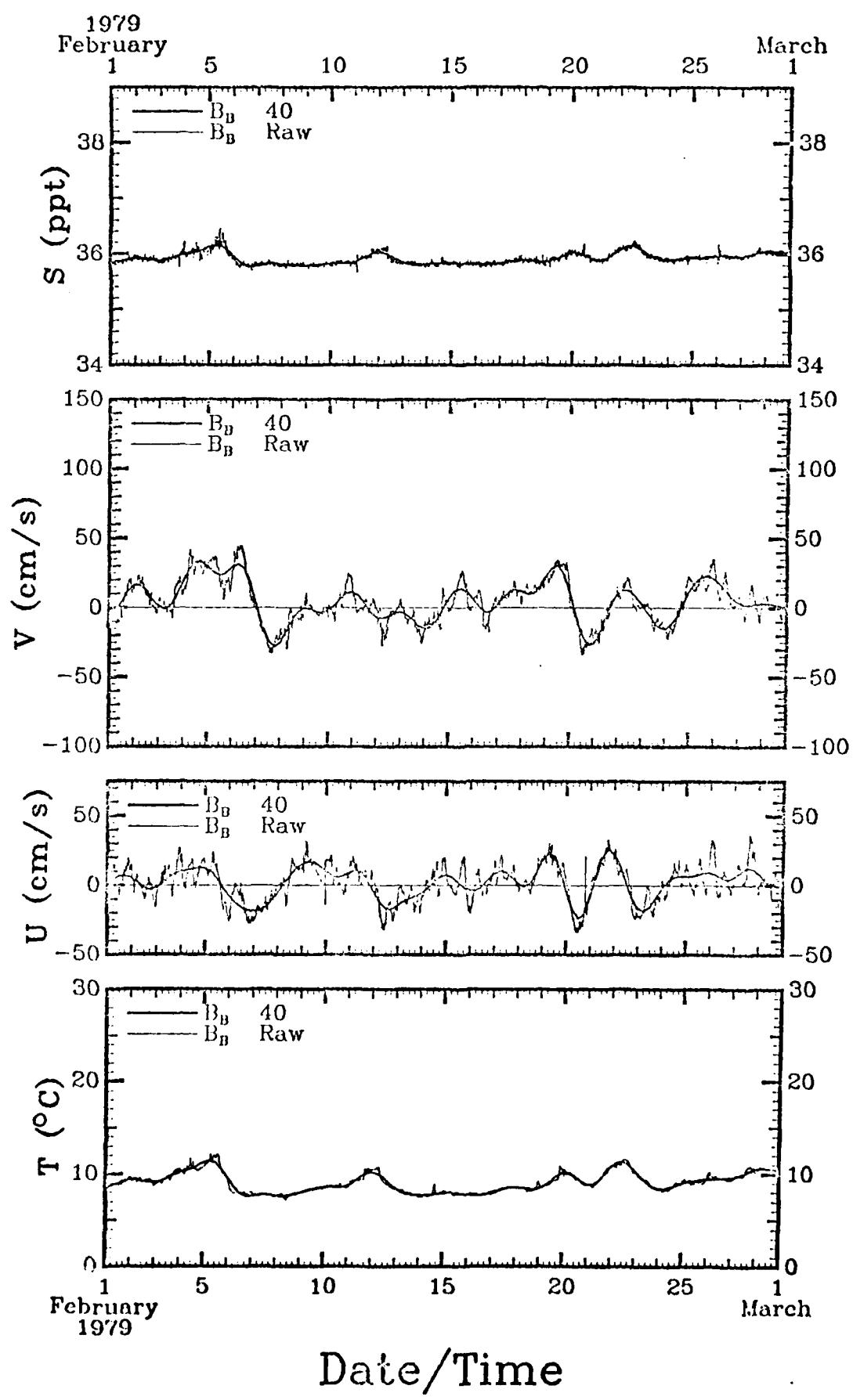


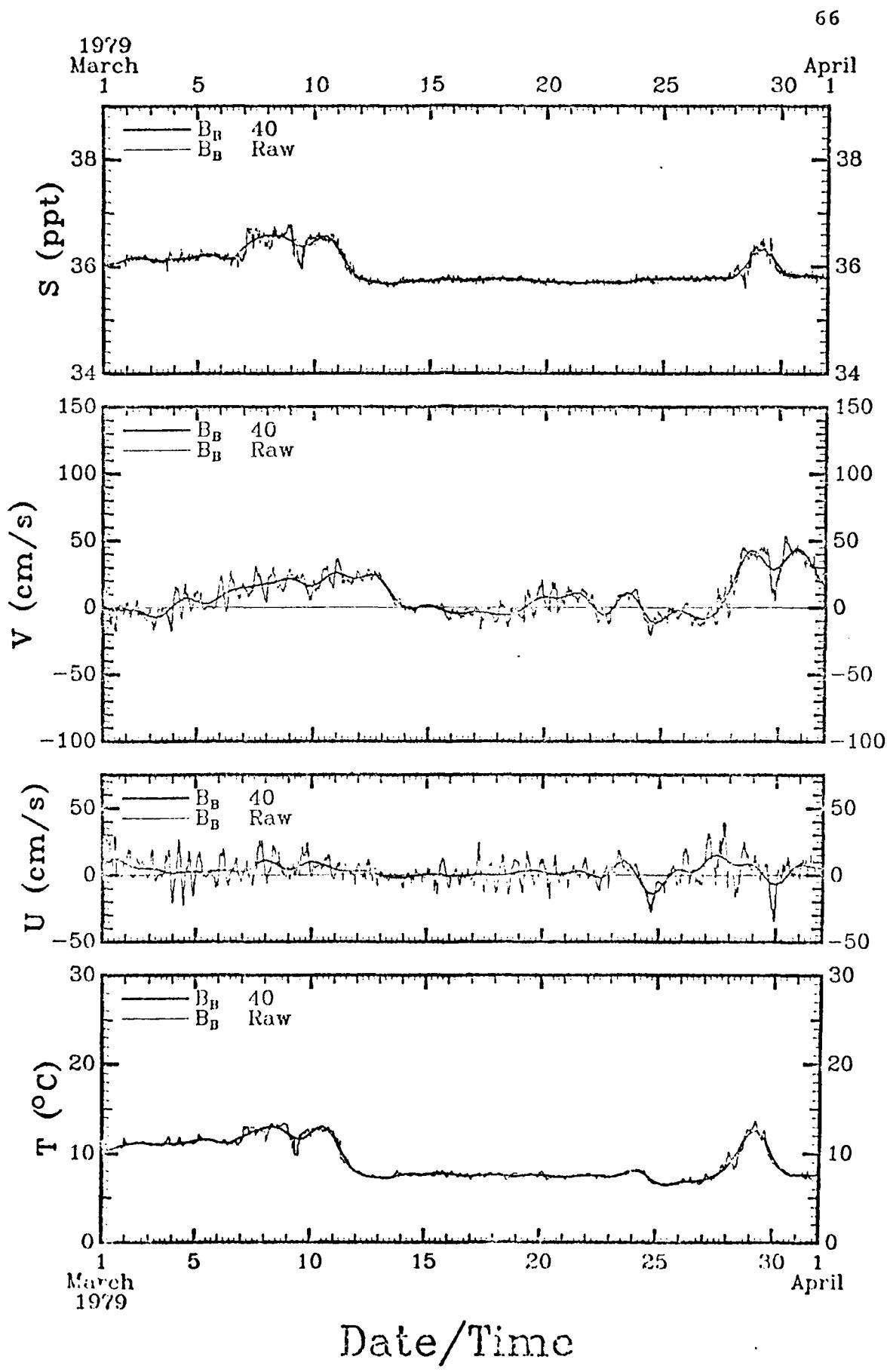


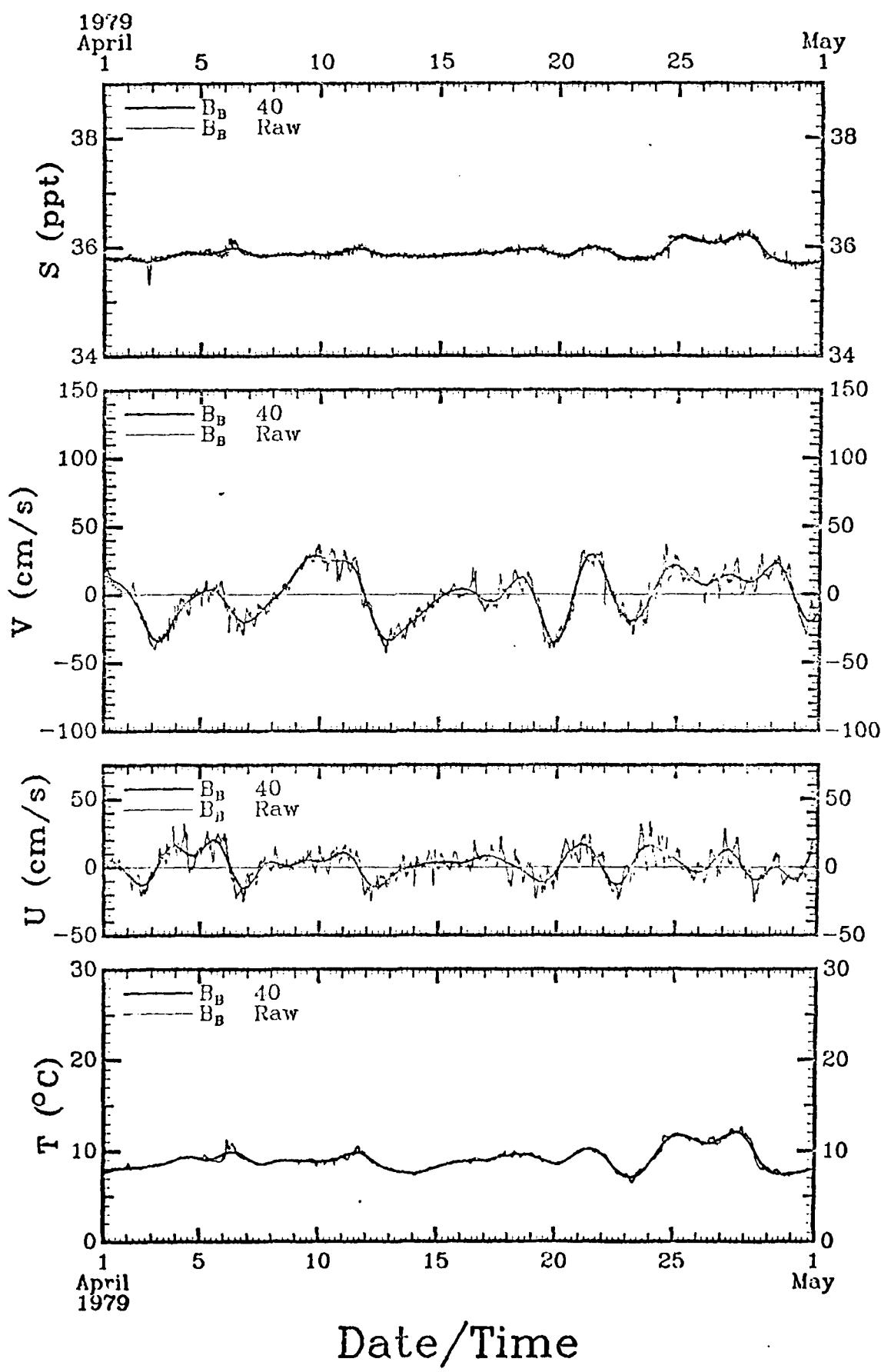


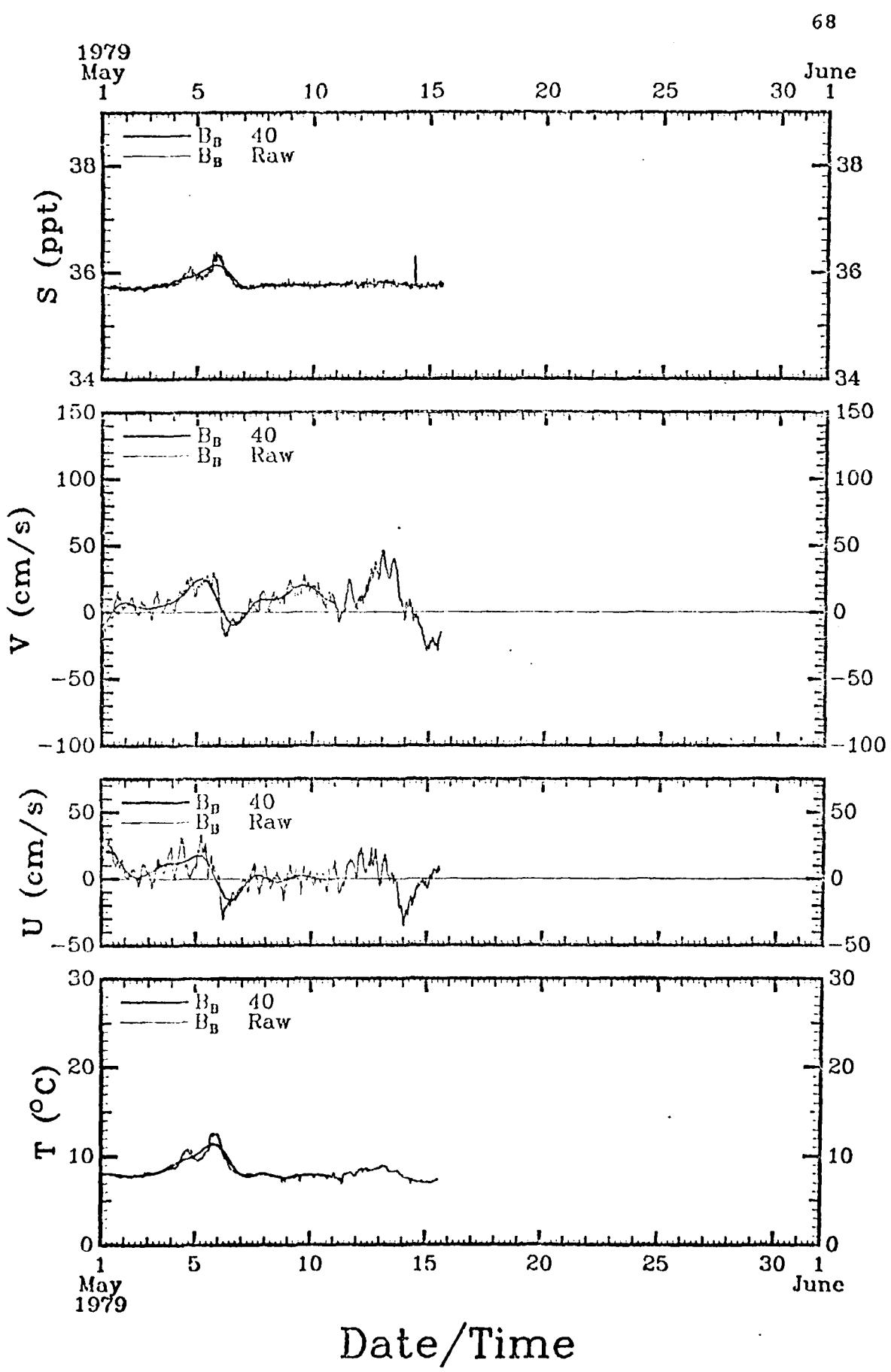
Date/Time

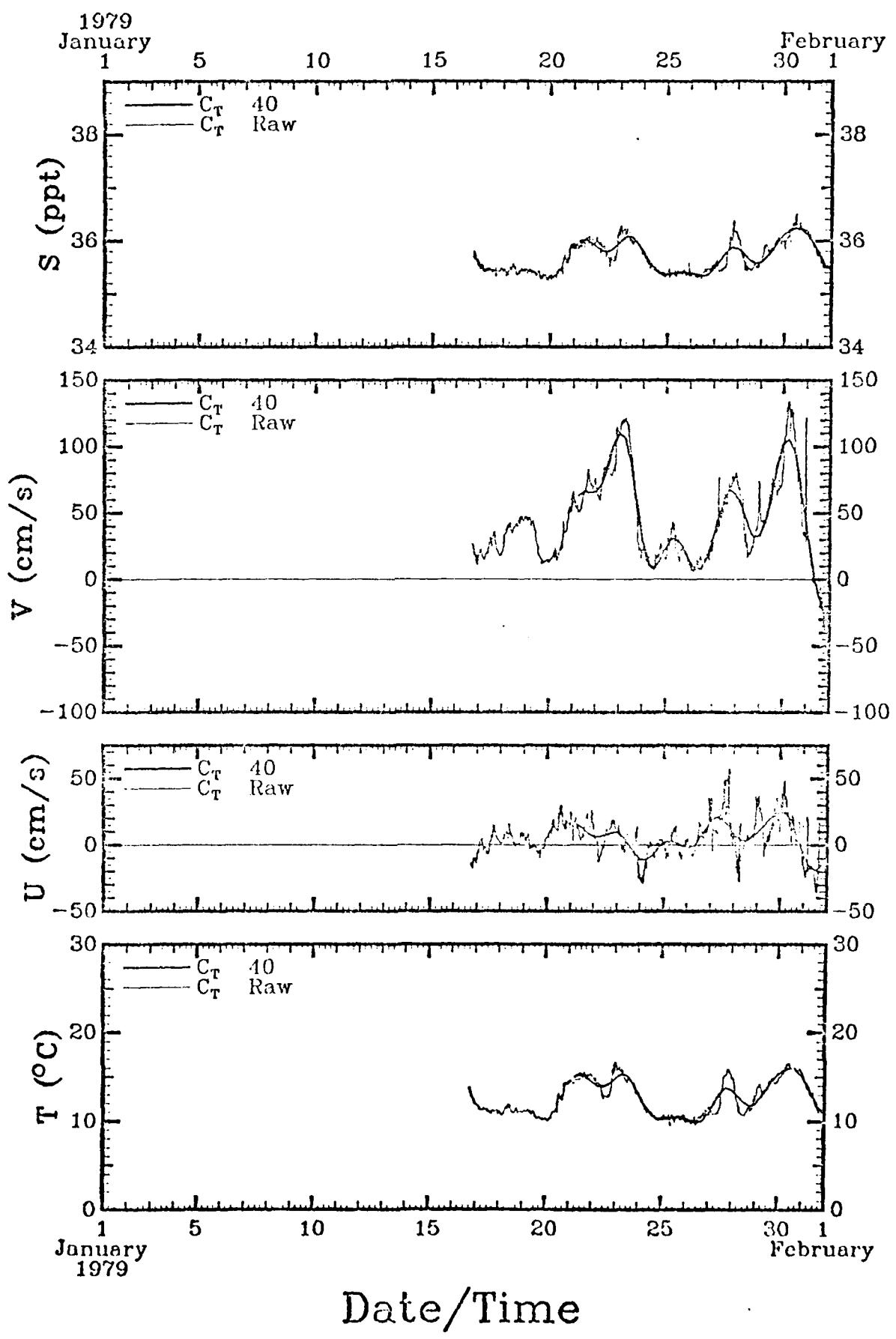


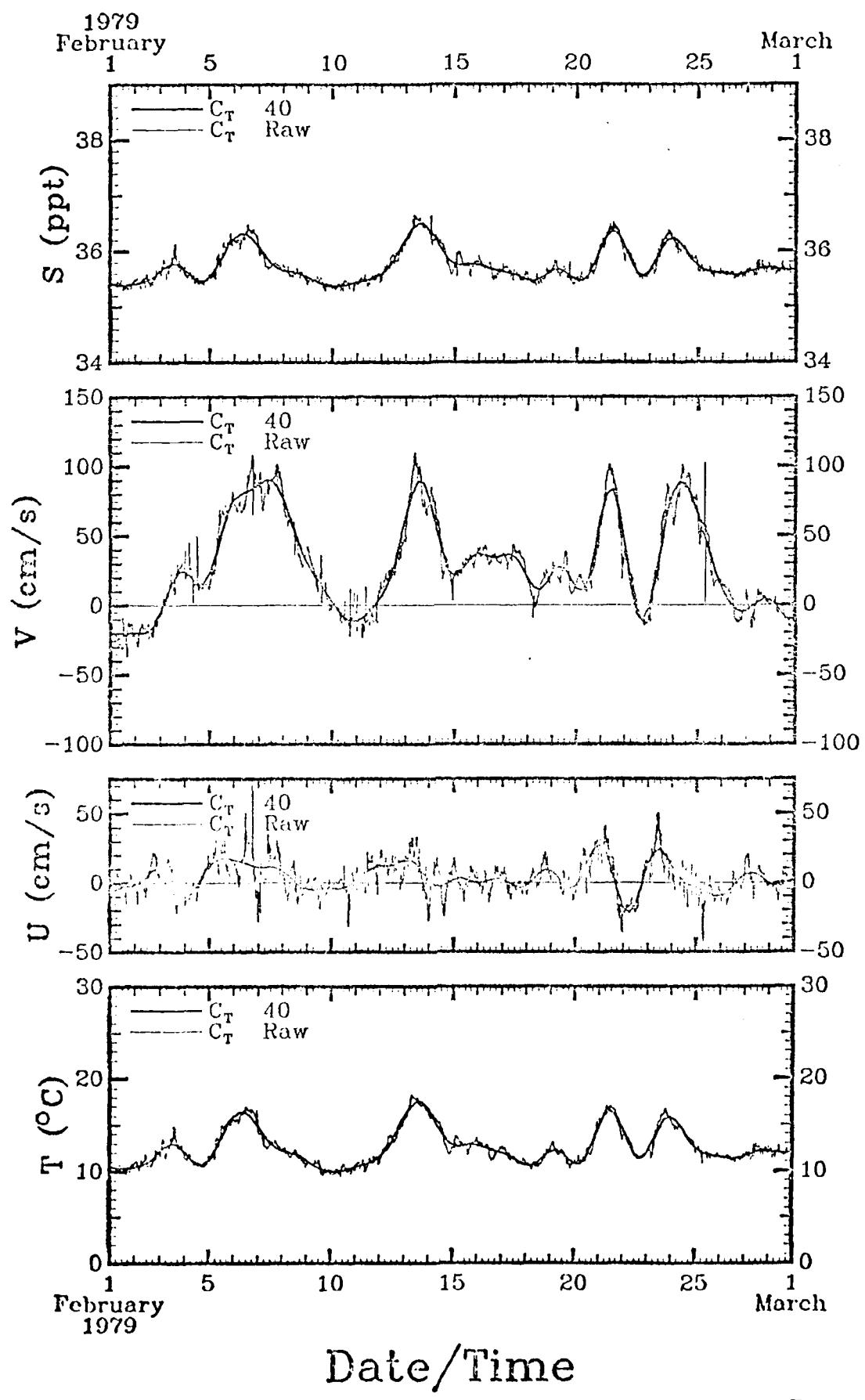


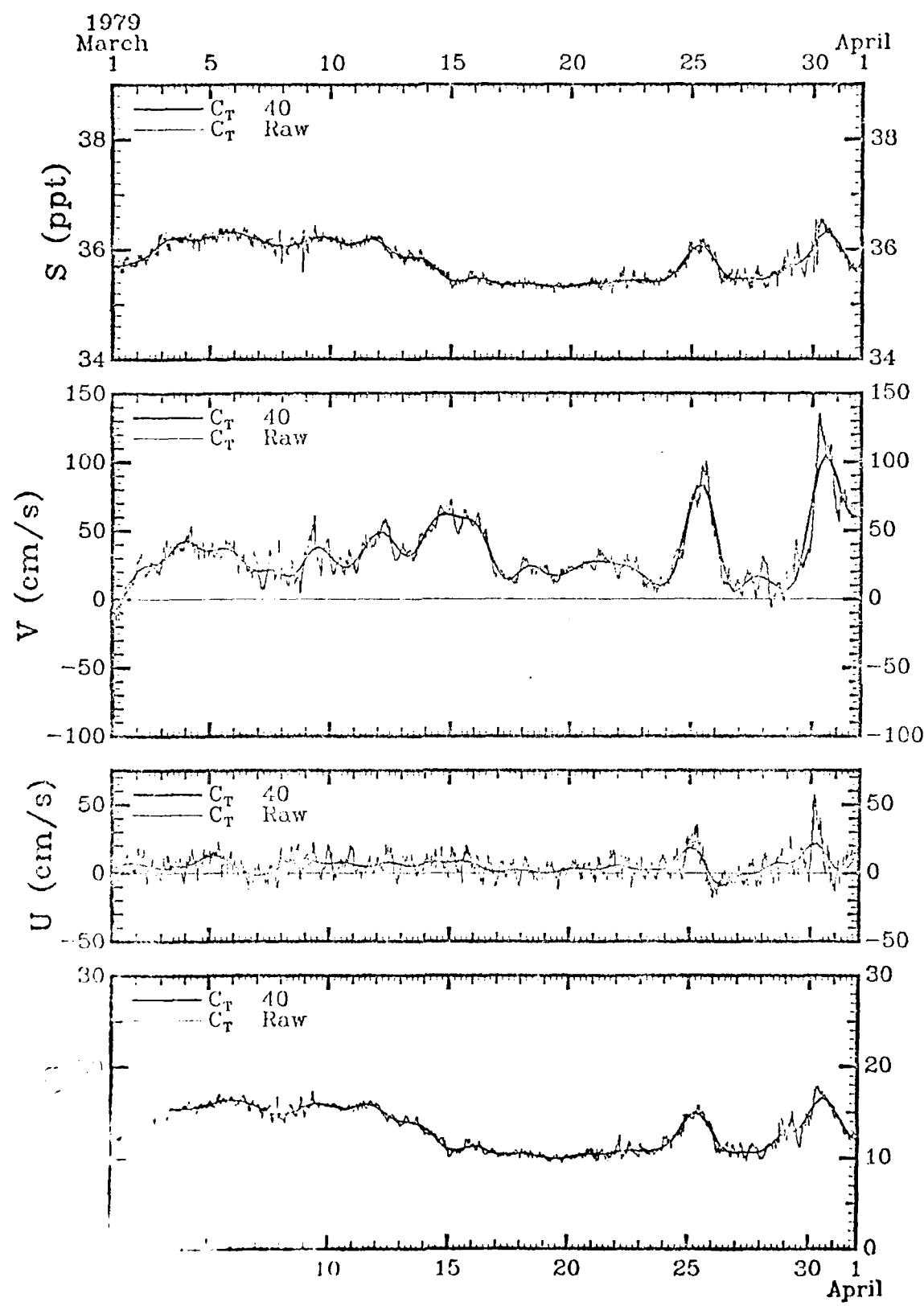




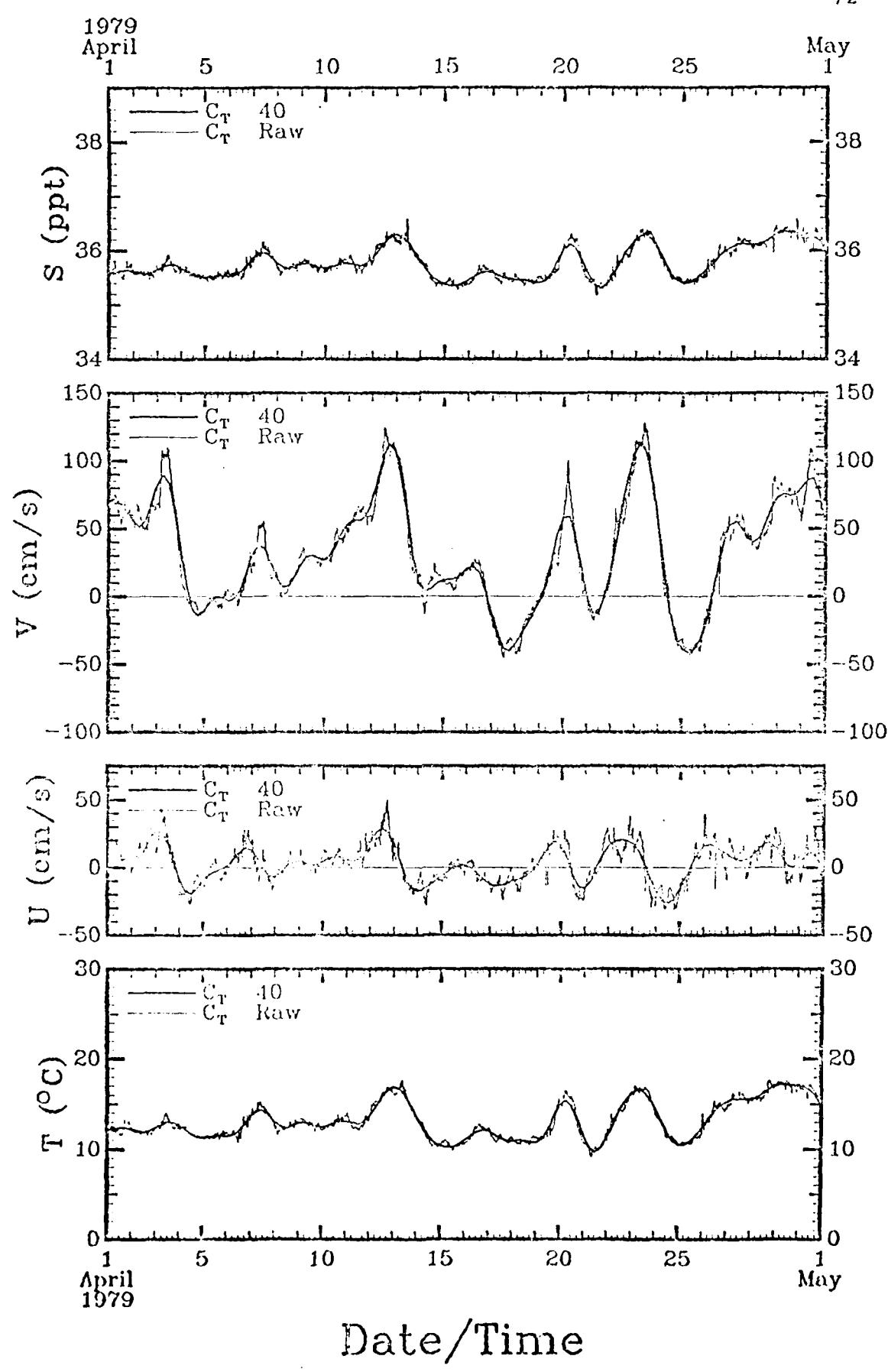


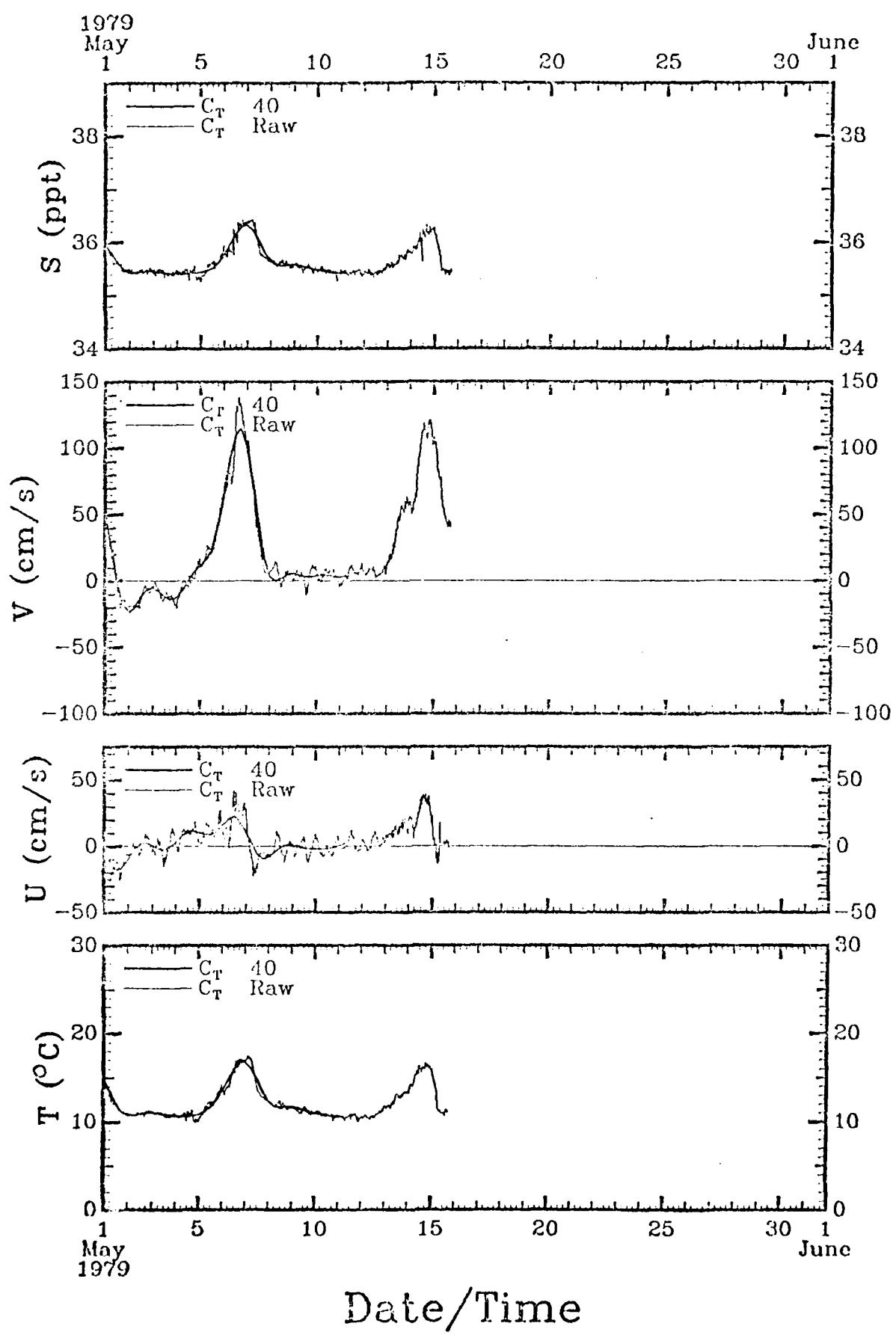


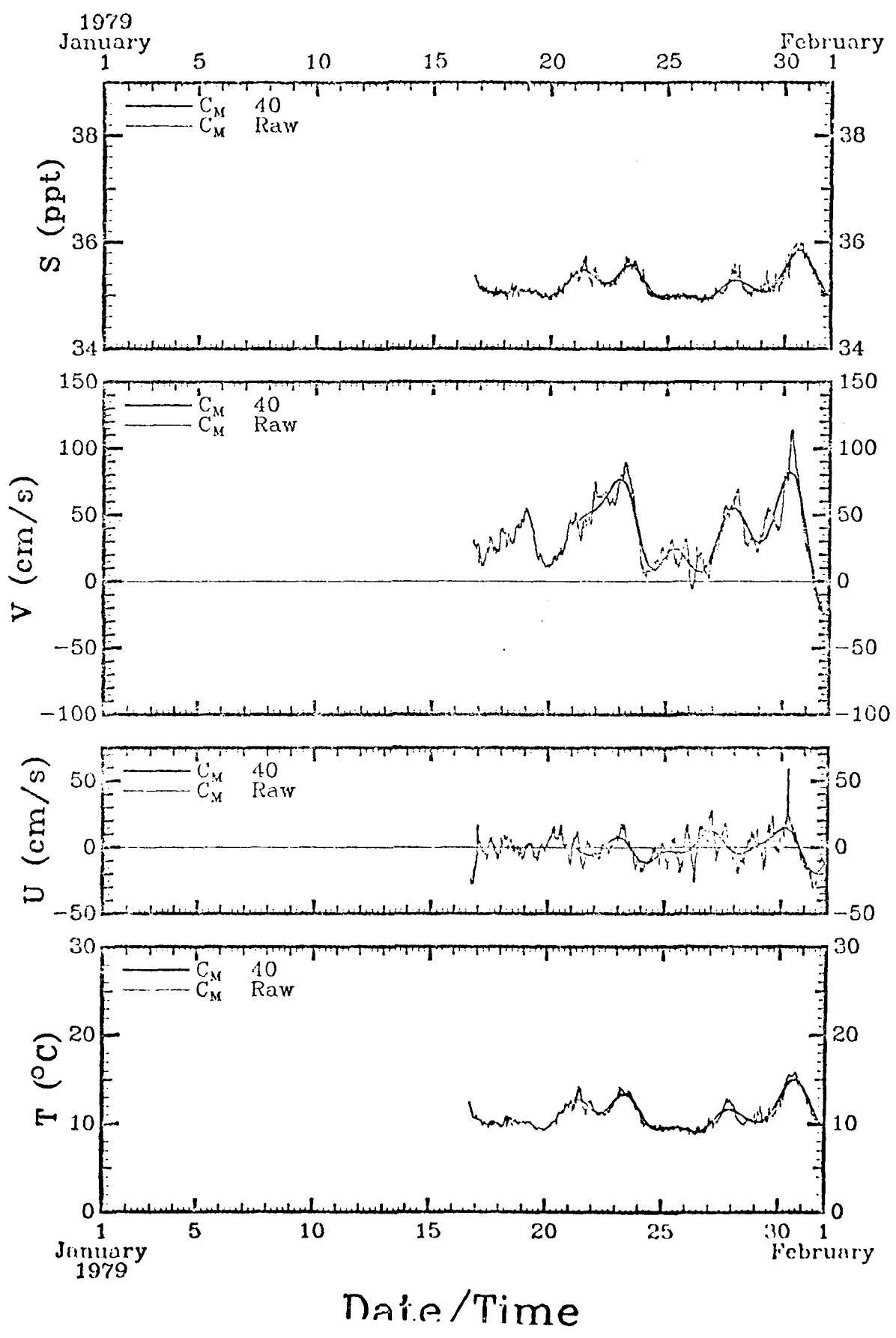


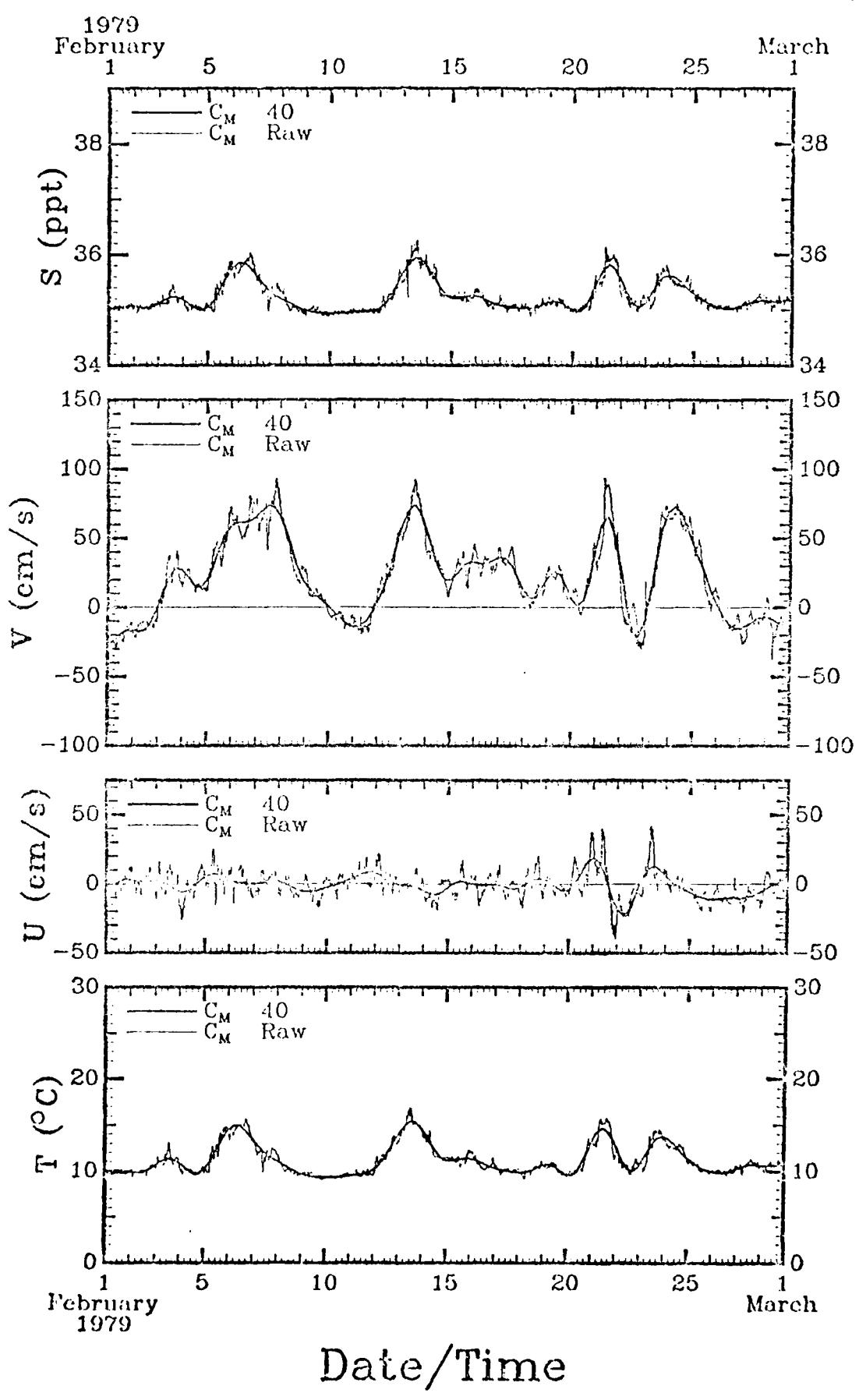


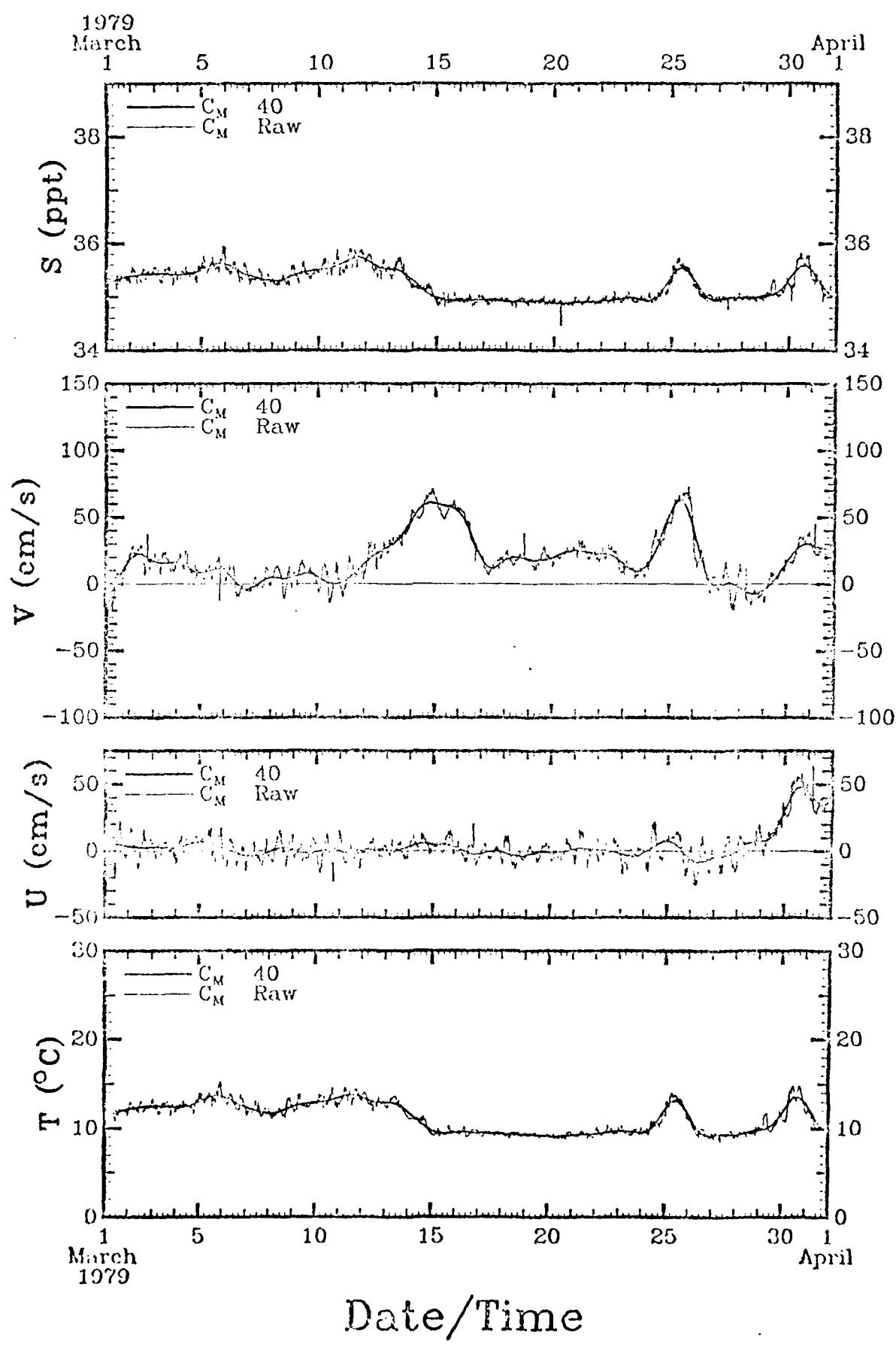
Date/Time

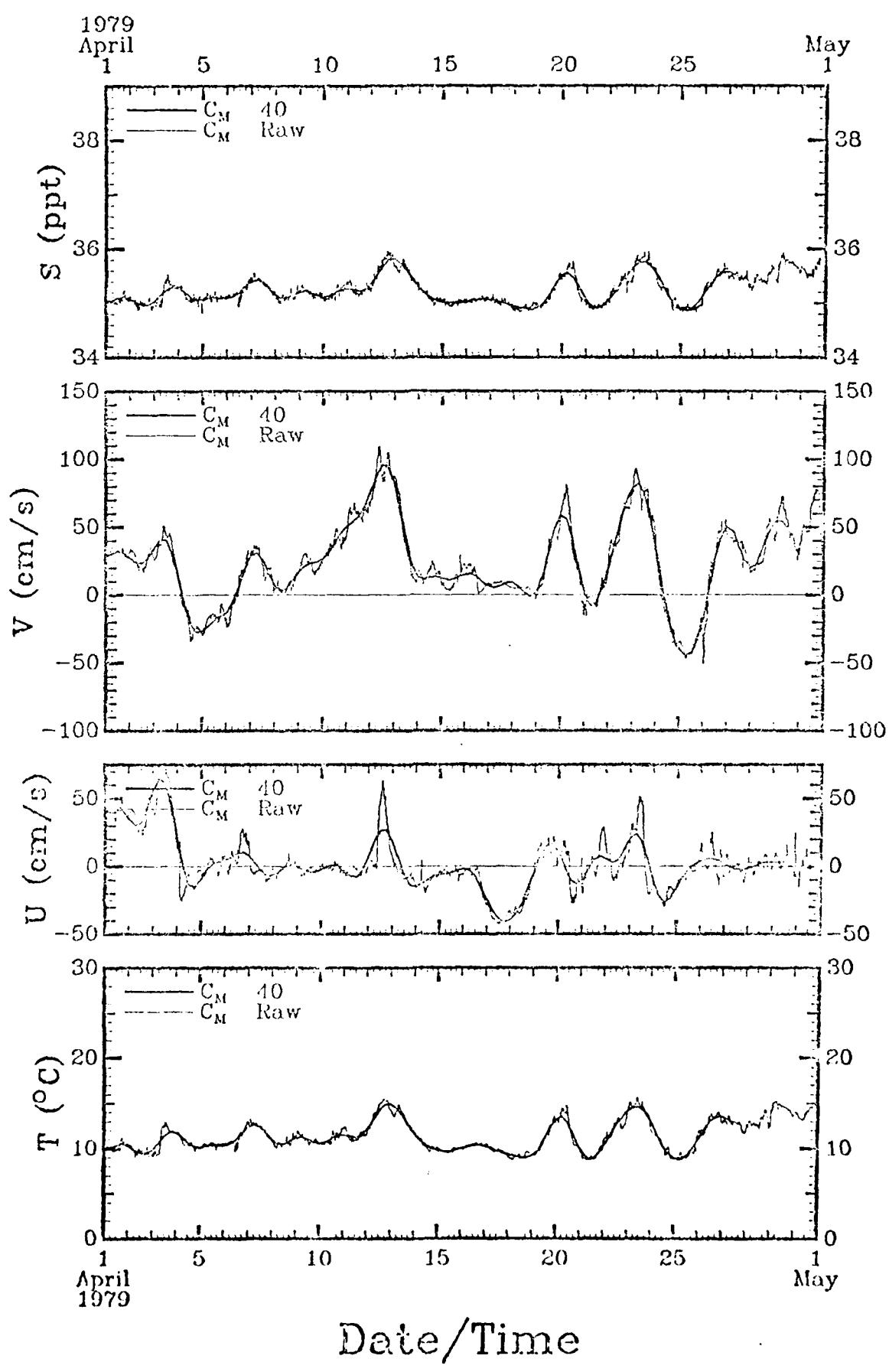


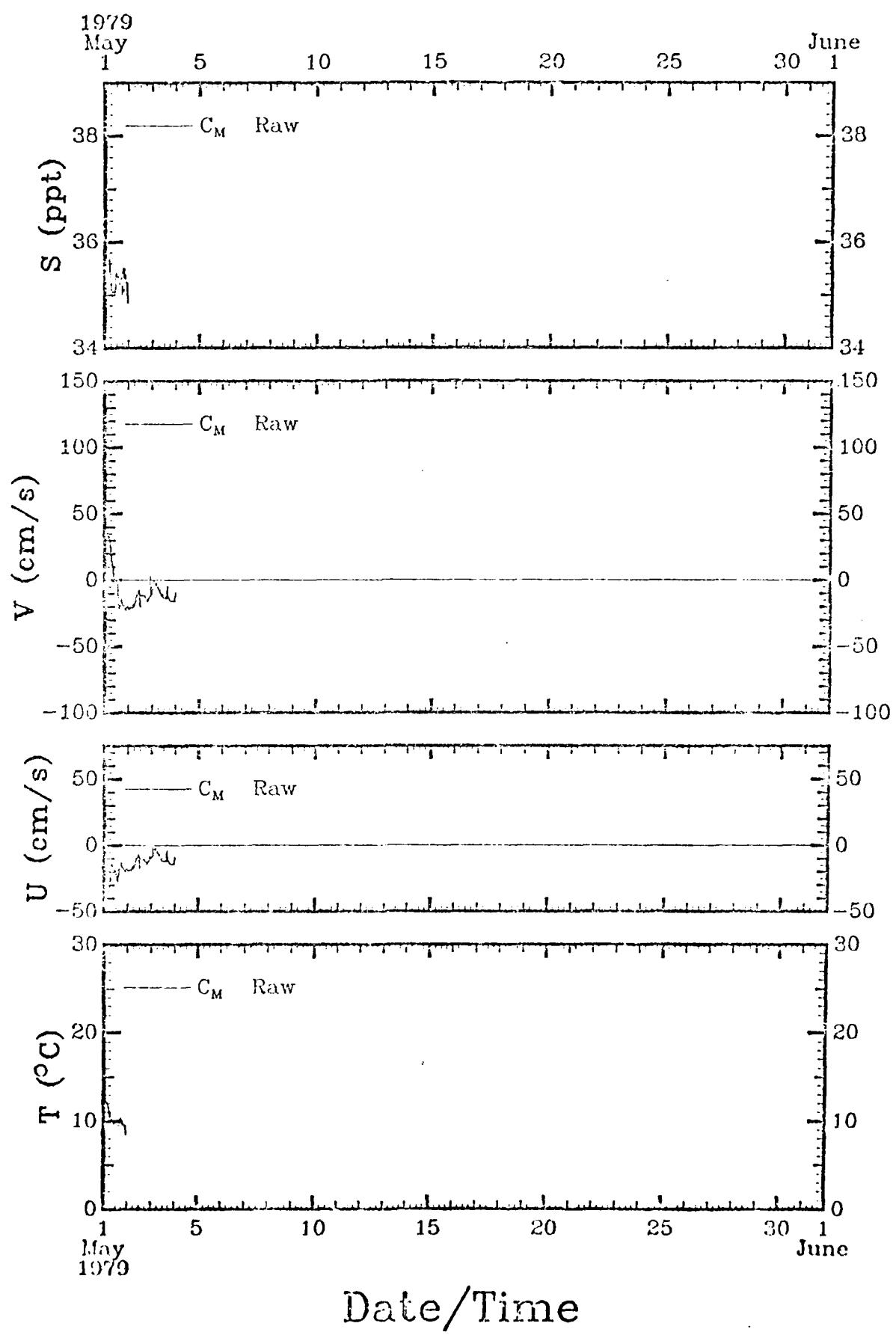


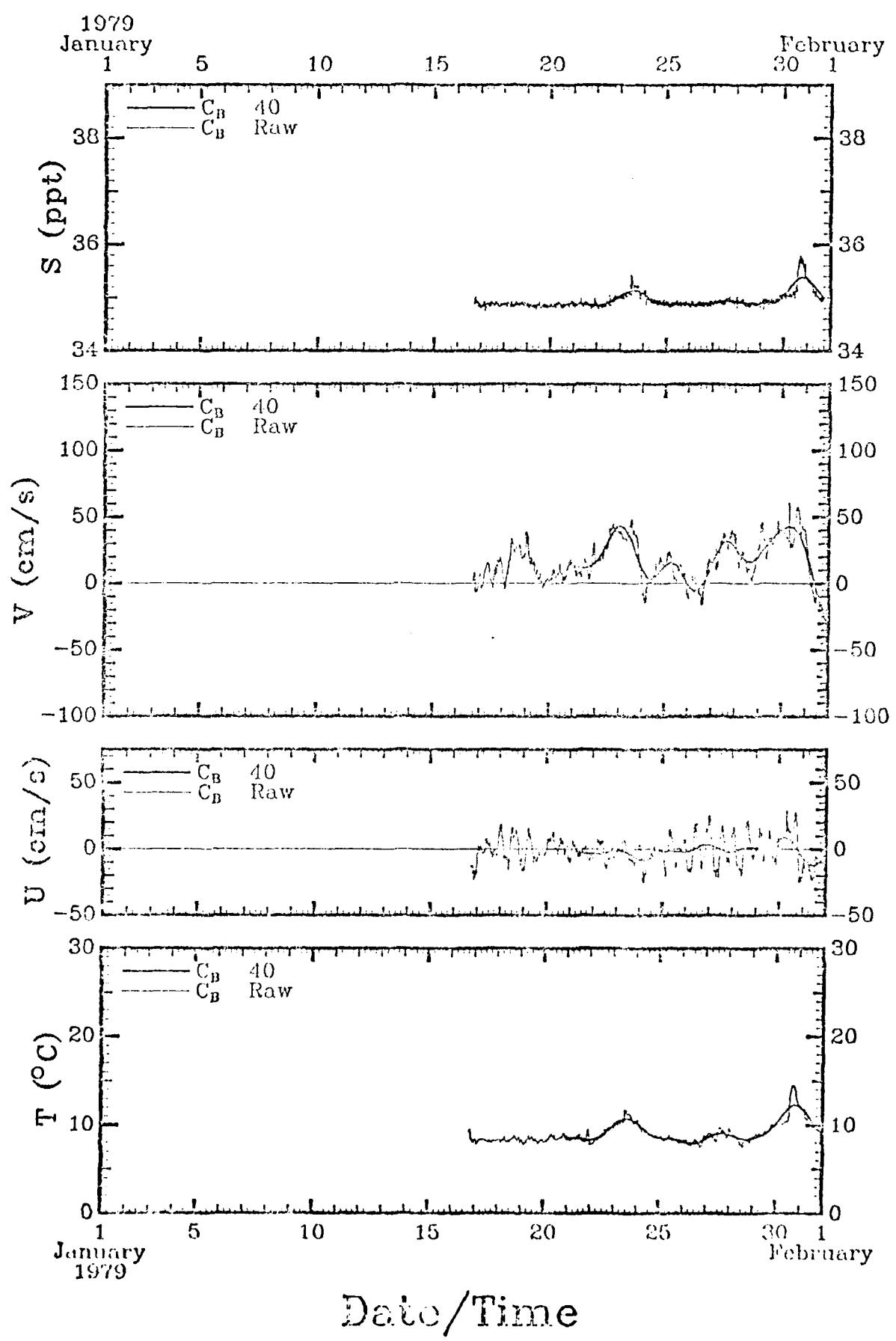


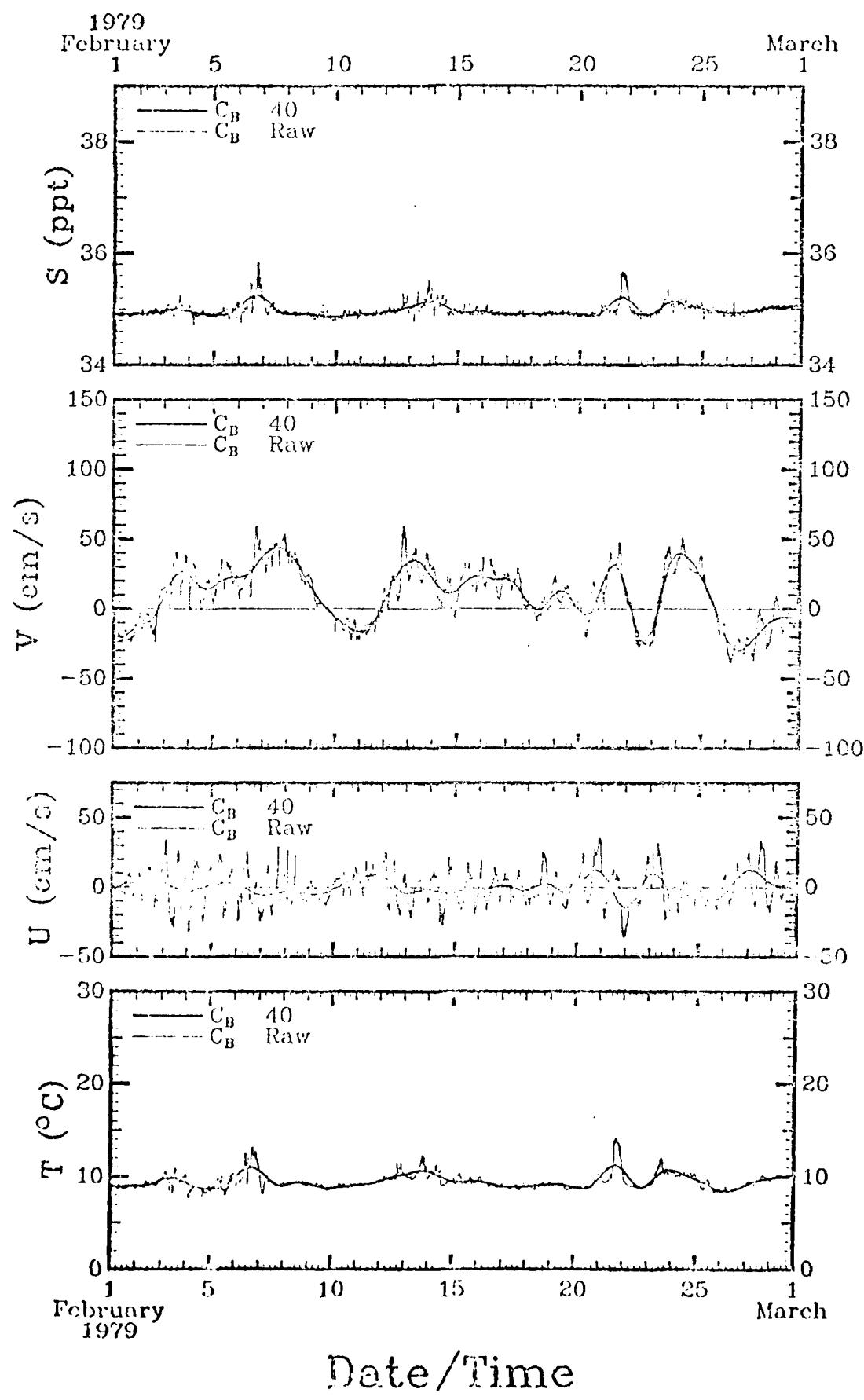


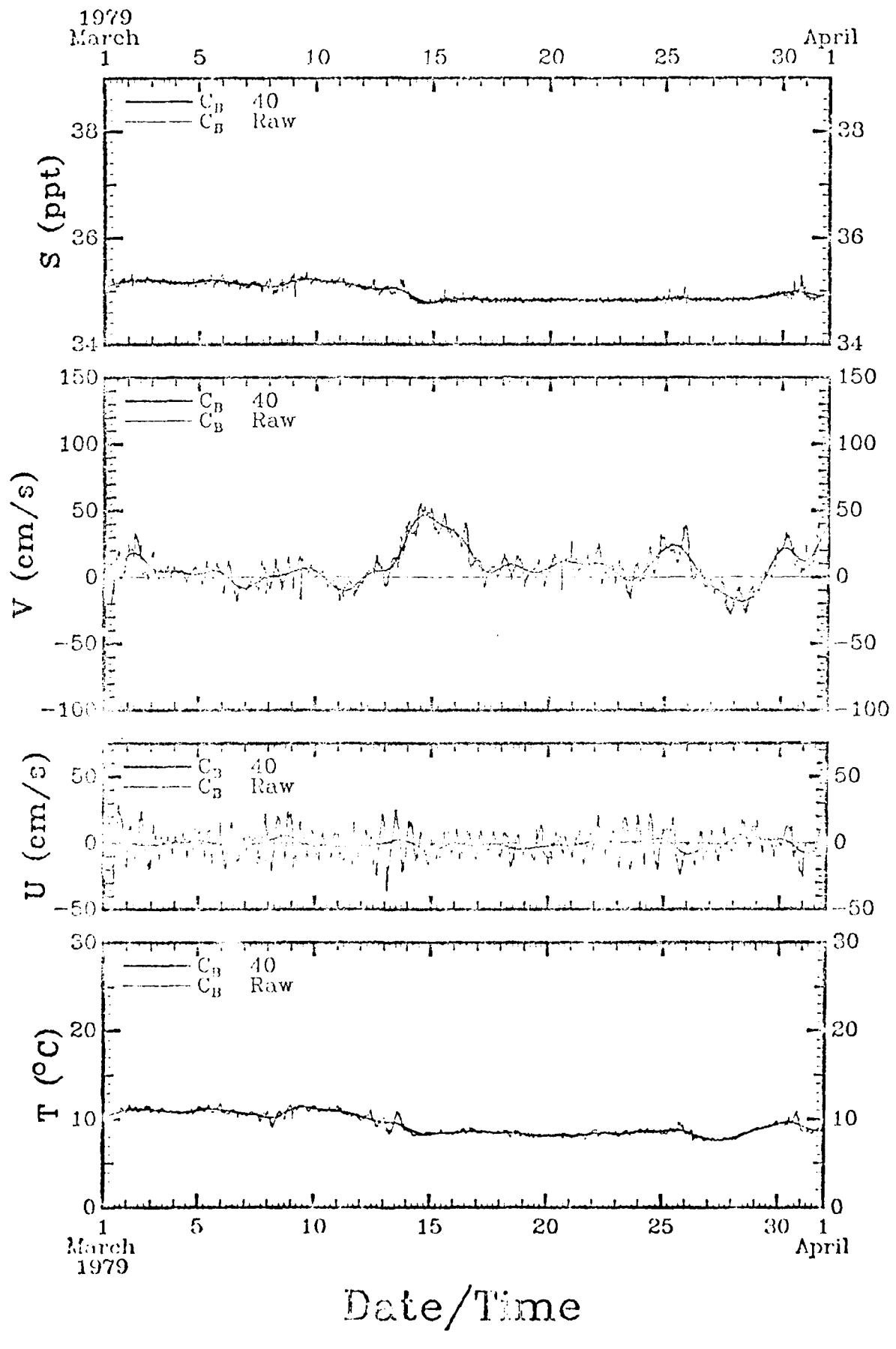


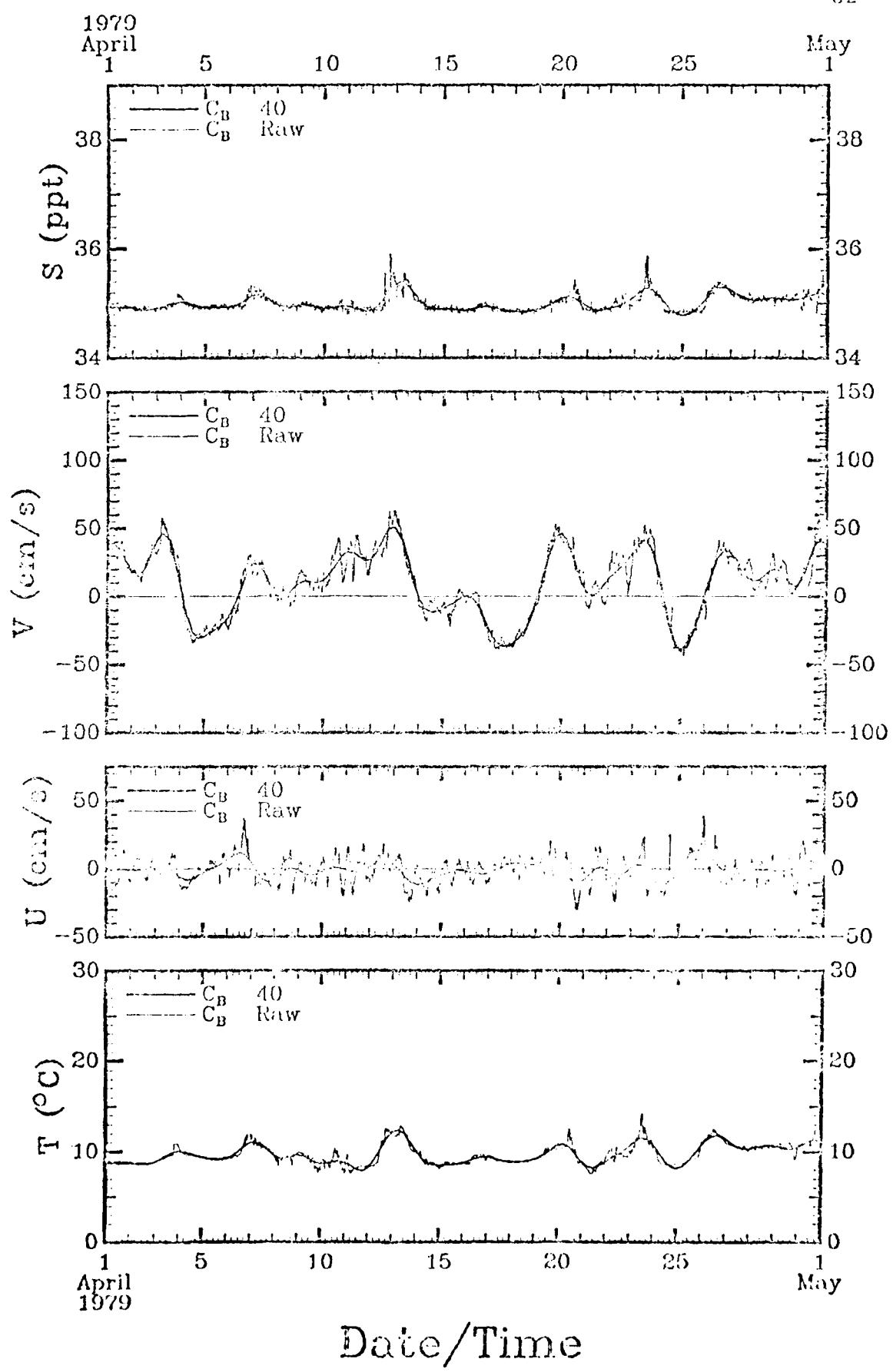


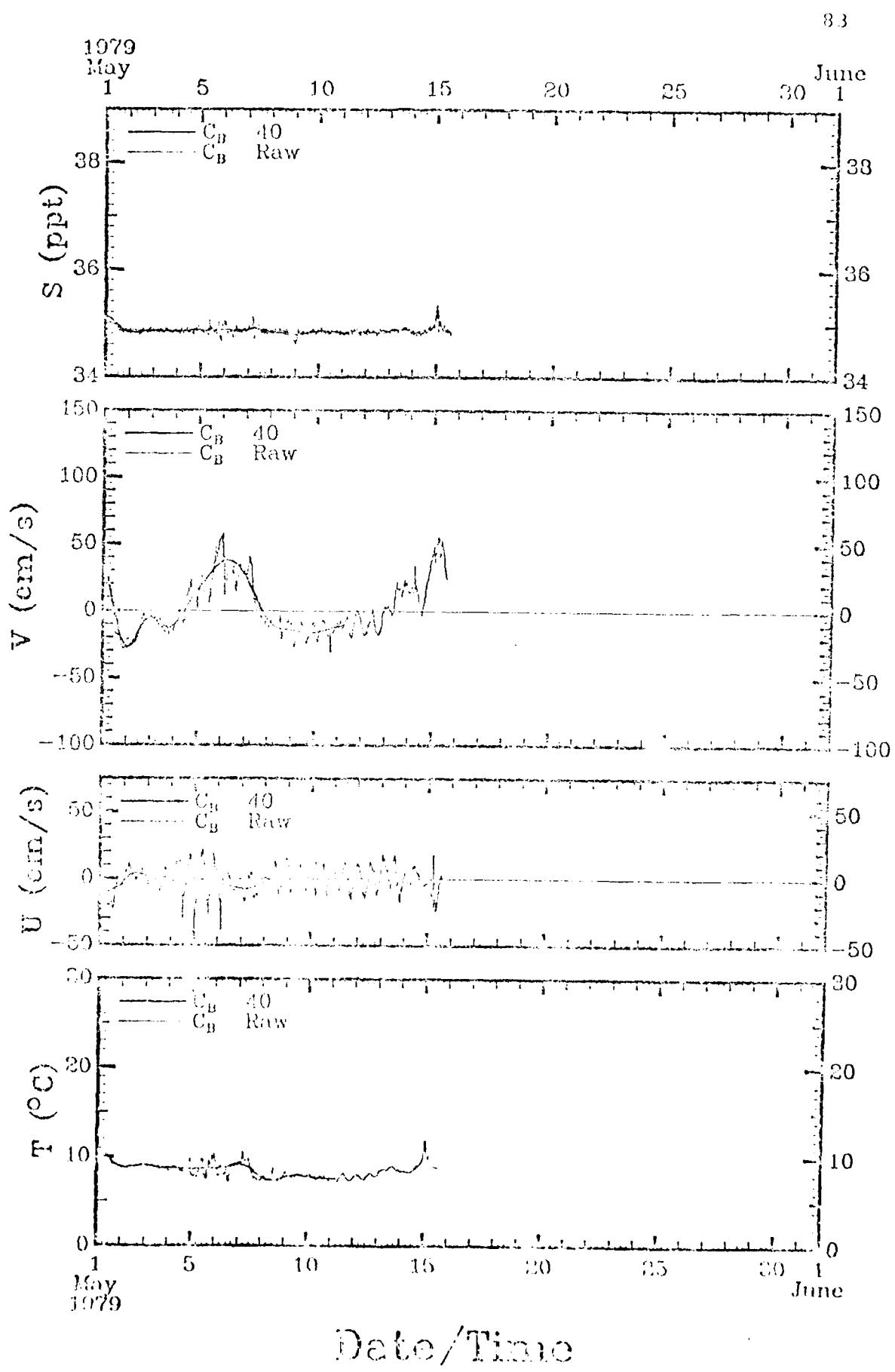


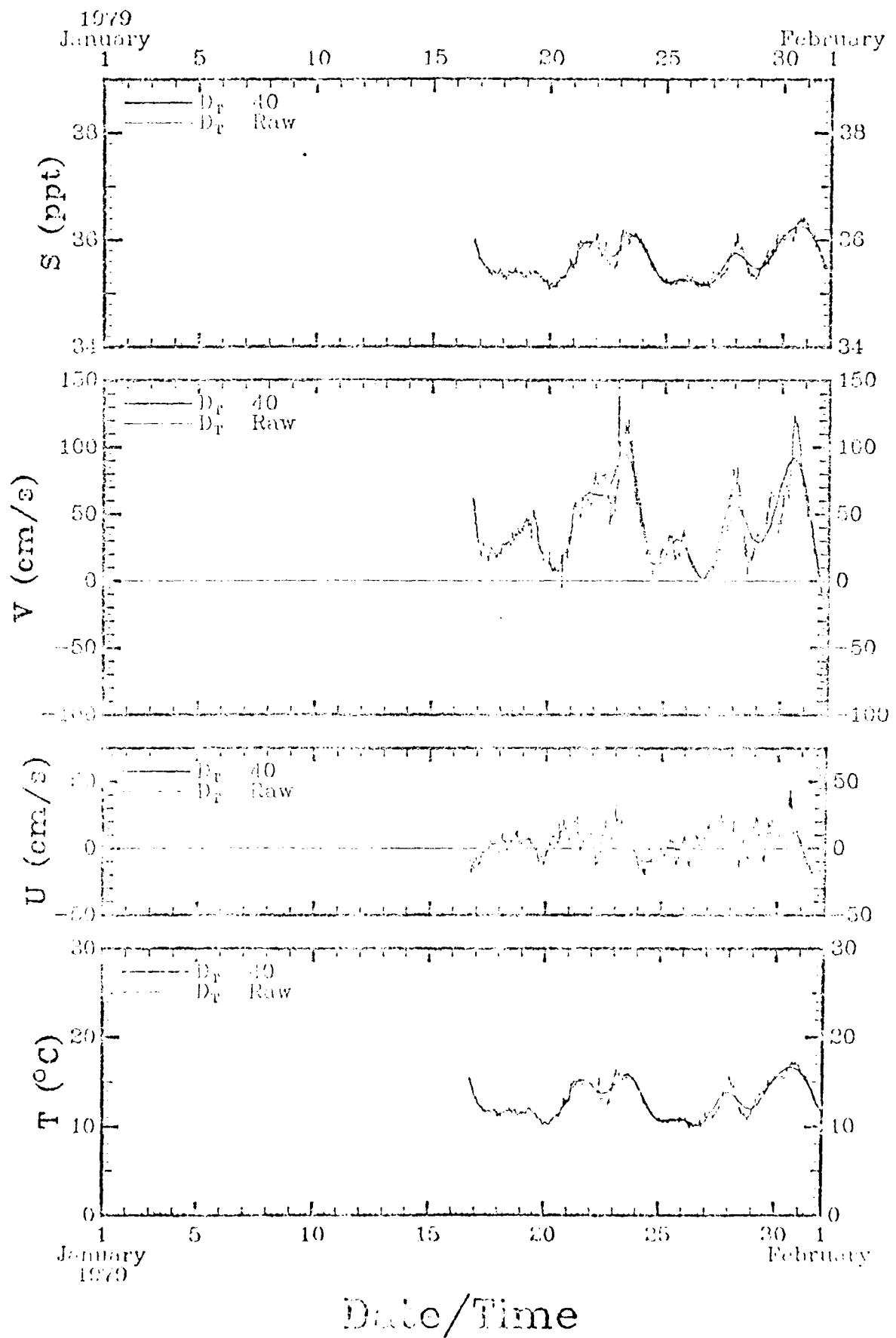








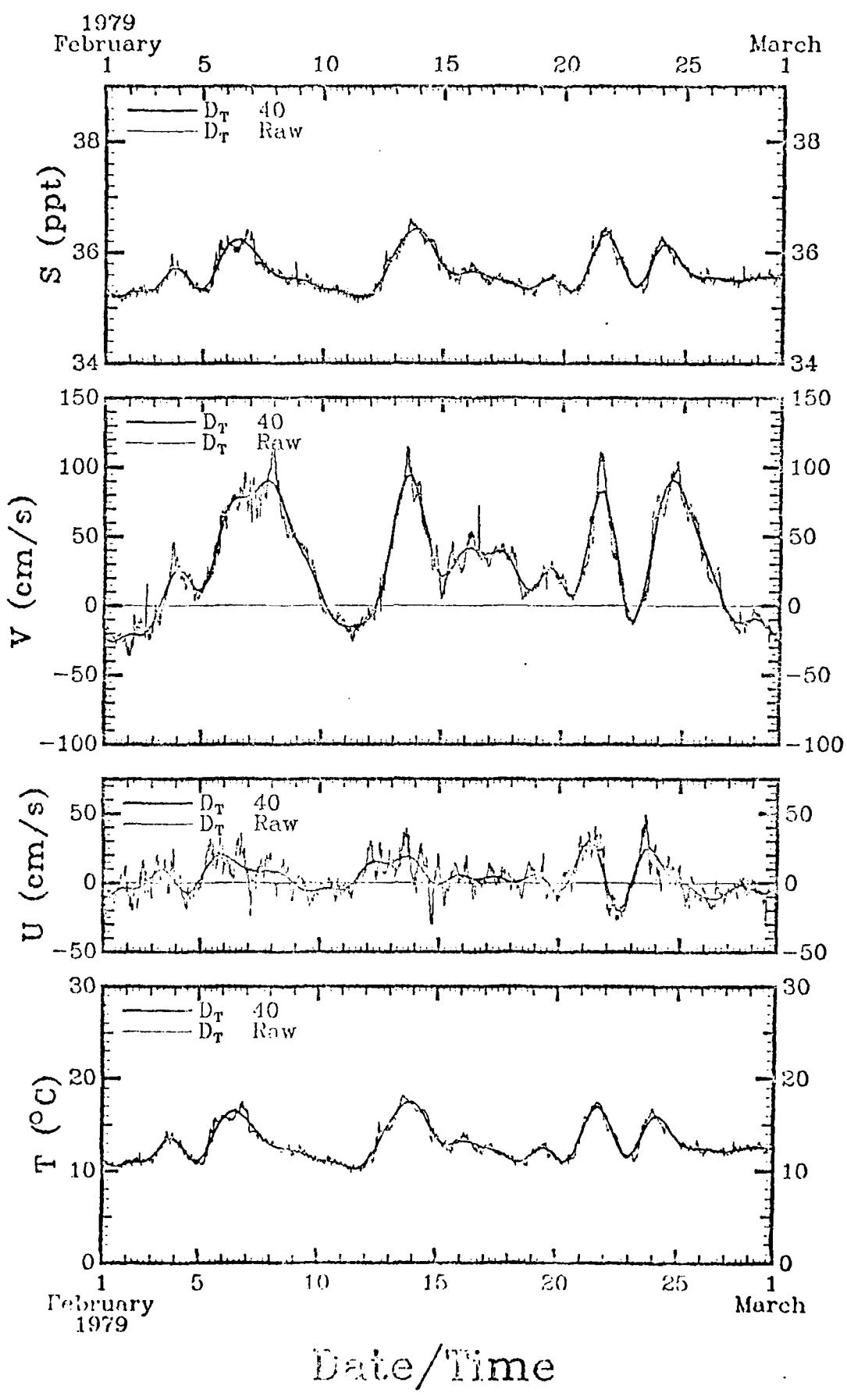


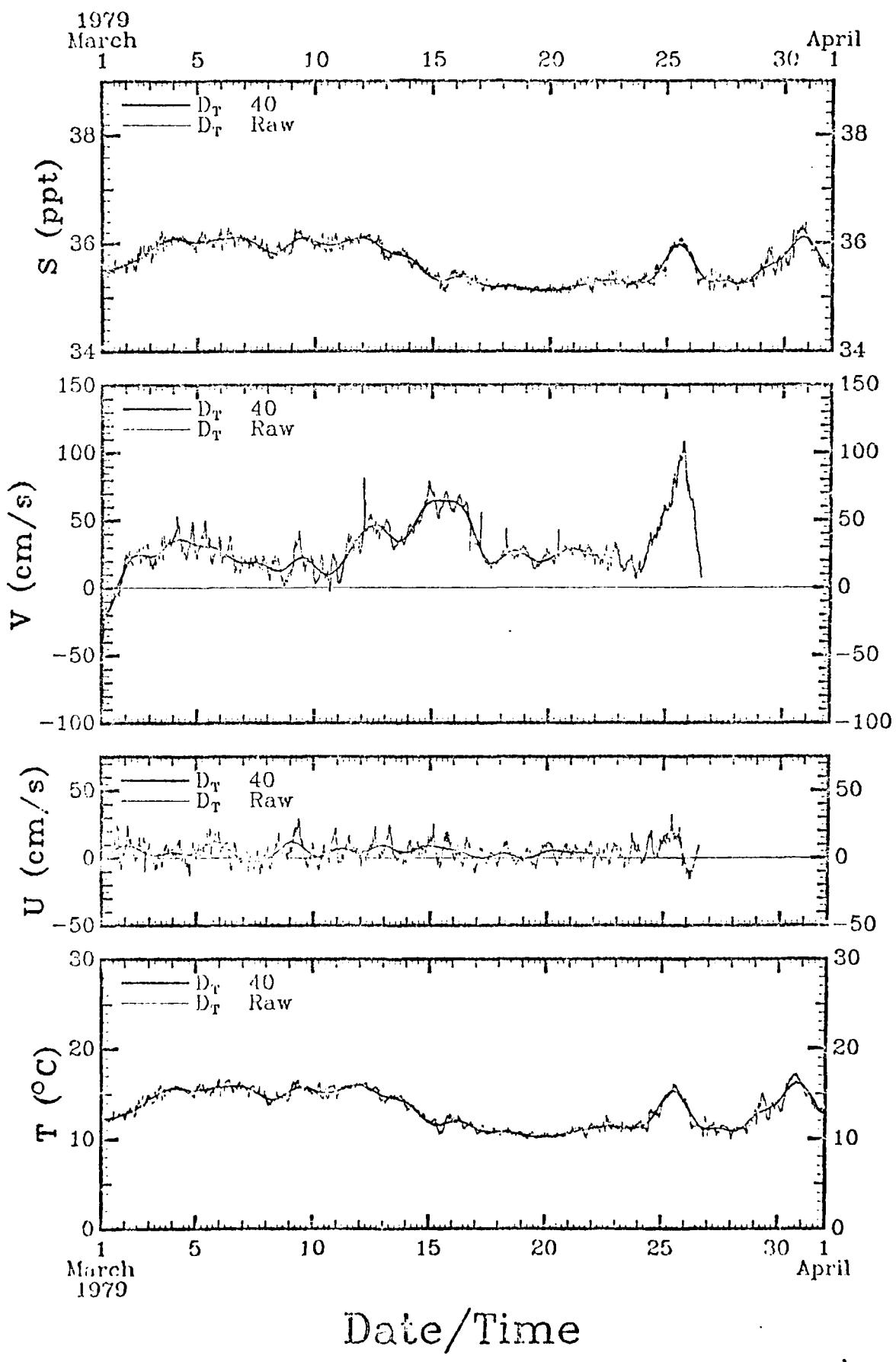


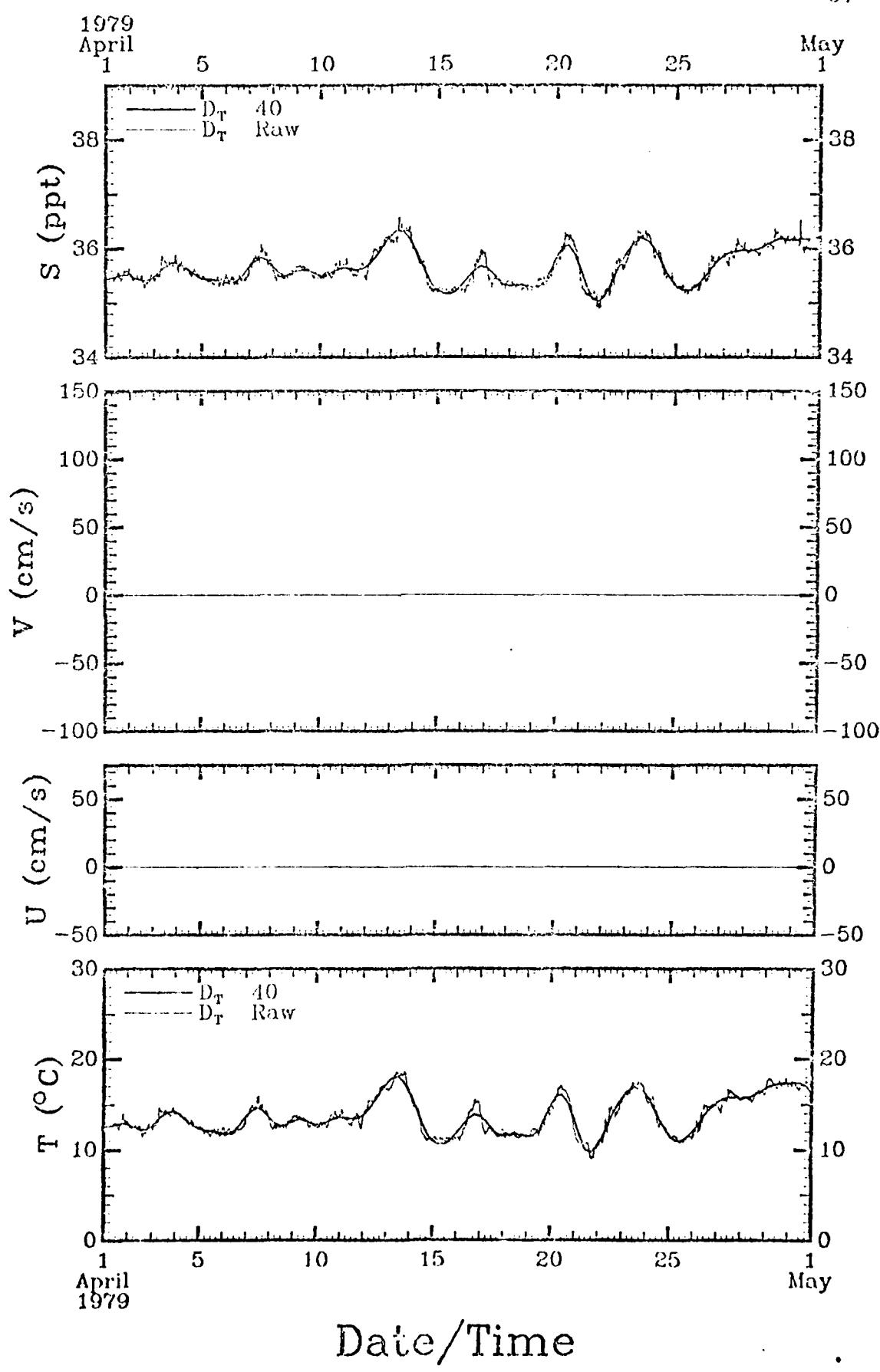
W-A088 069

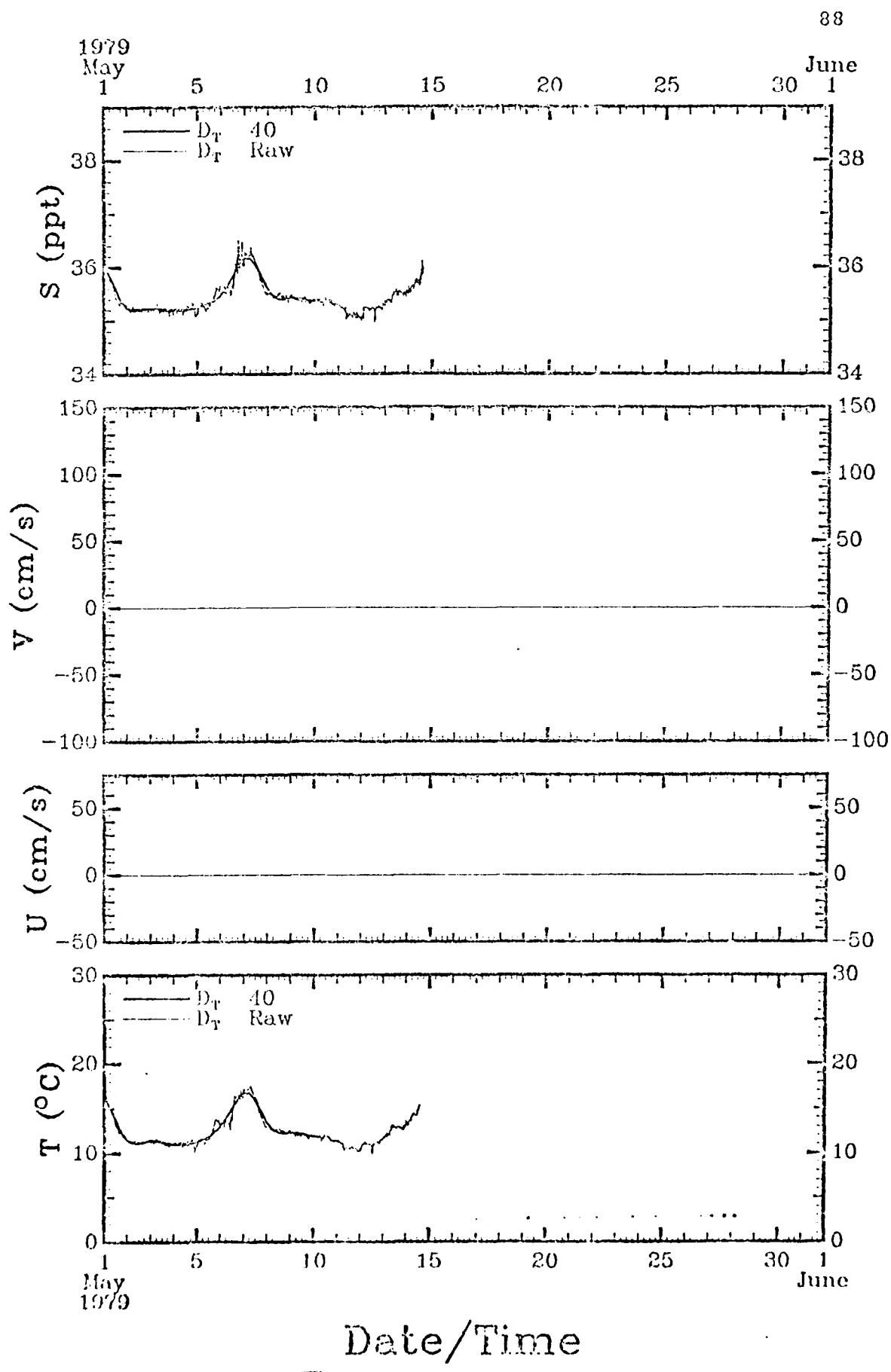
TEXAS A AND M UNIV COLLEGE STATION DEPT OF OCEANOGRAPHY F/8 8/3
THE GULF STREAM MEANDERS EXPERIMENT, CURRENT METER, ATMOSPHERIC--ETC(U)
JUL 80 D A BROOKS, J M BANE, R L COHEN N00014-77-C-0354
UNCLASSIFIED NL
TAMU-REF-80-7-T

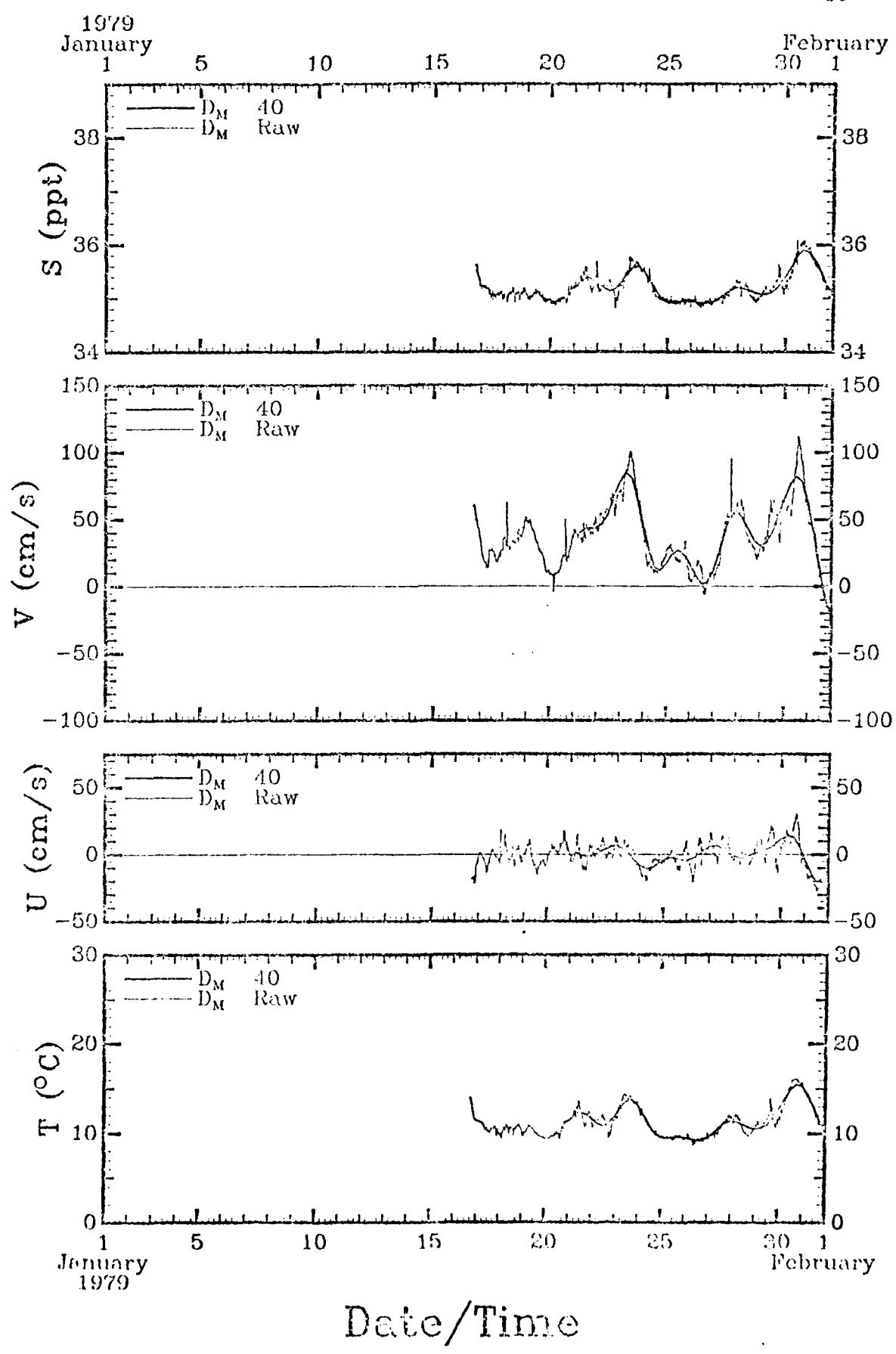
2 of 3
No copies

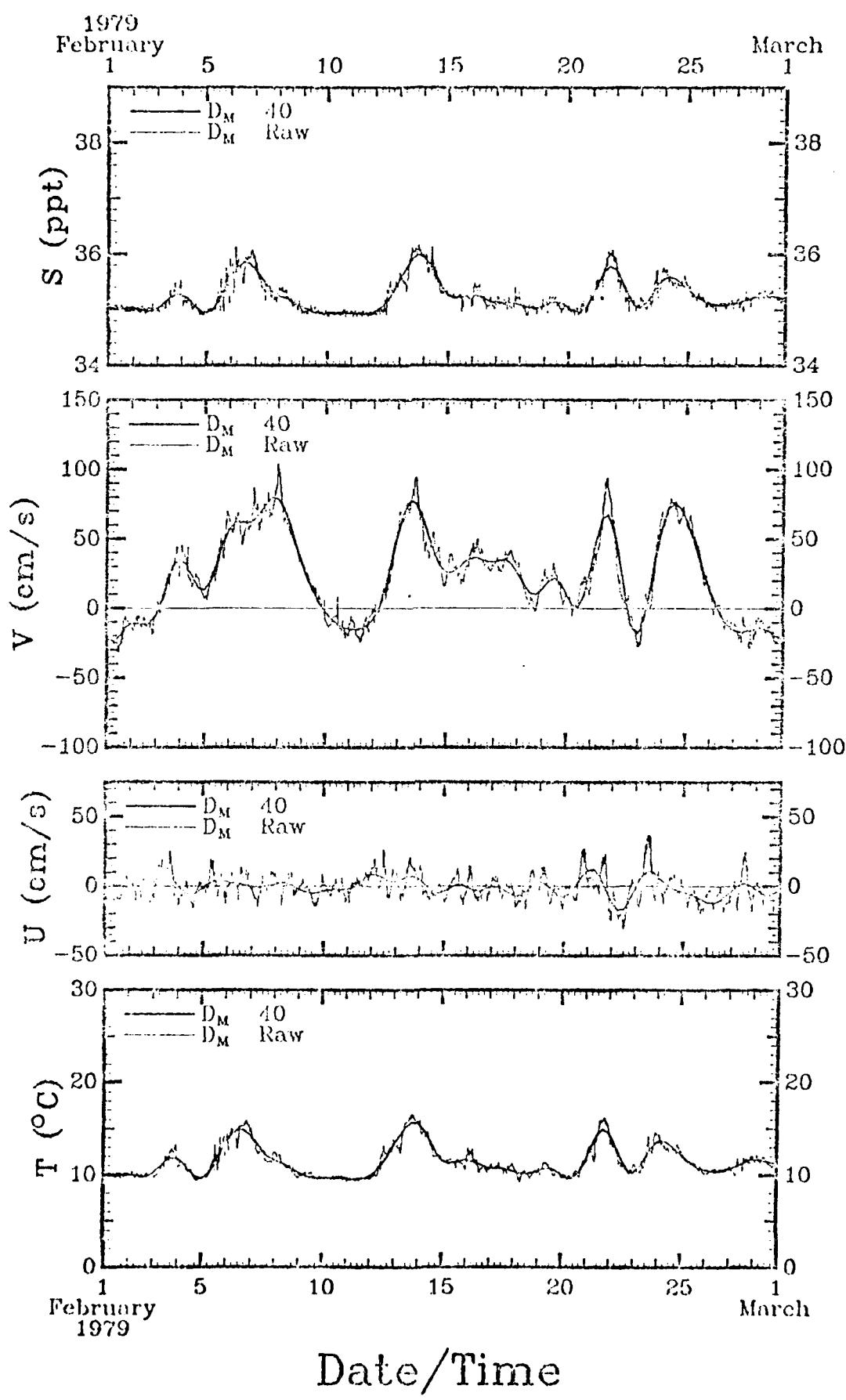



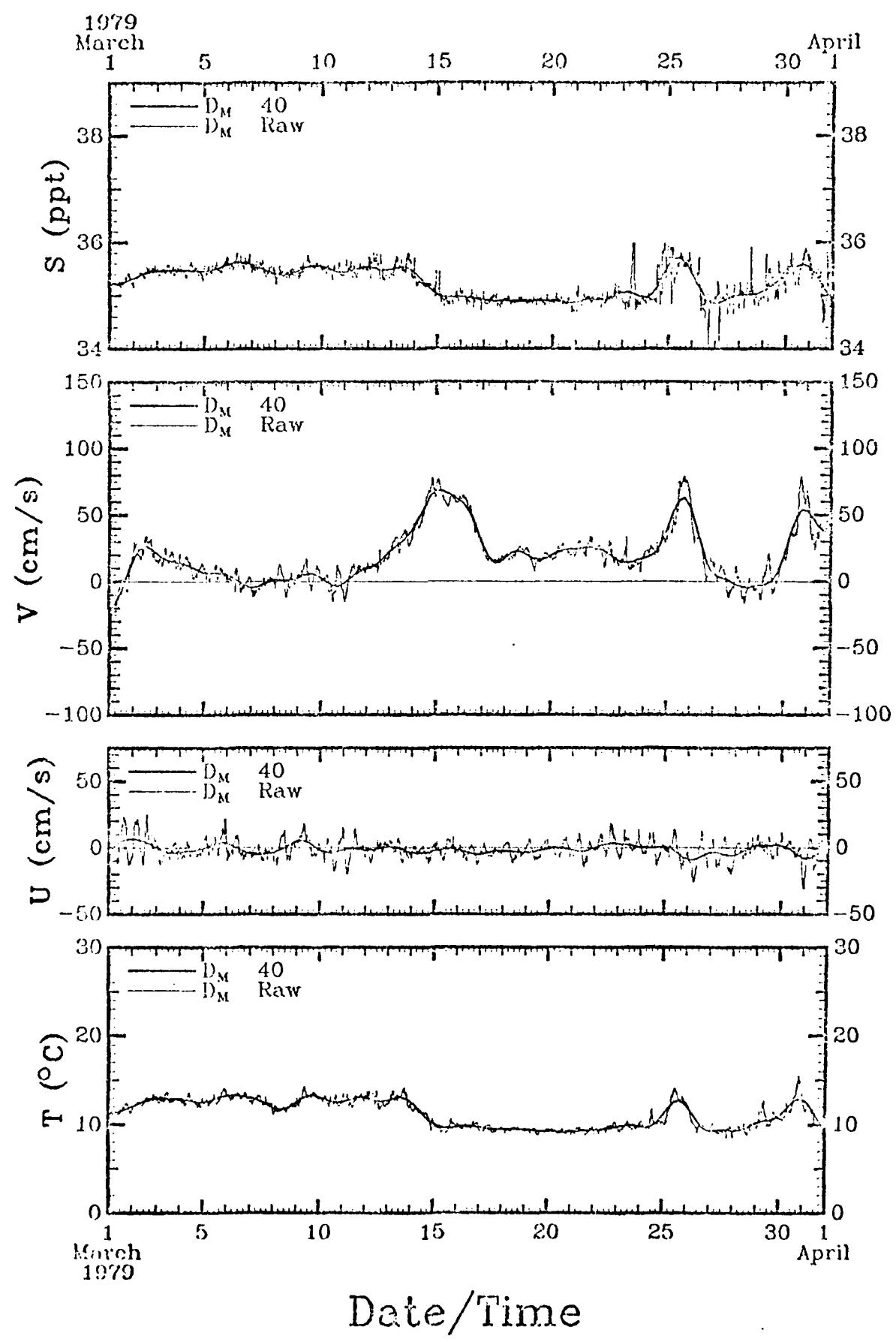


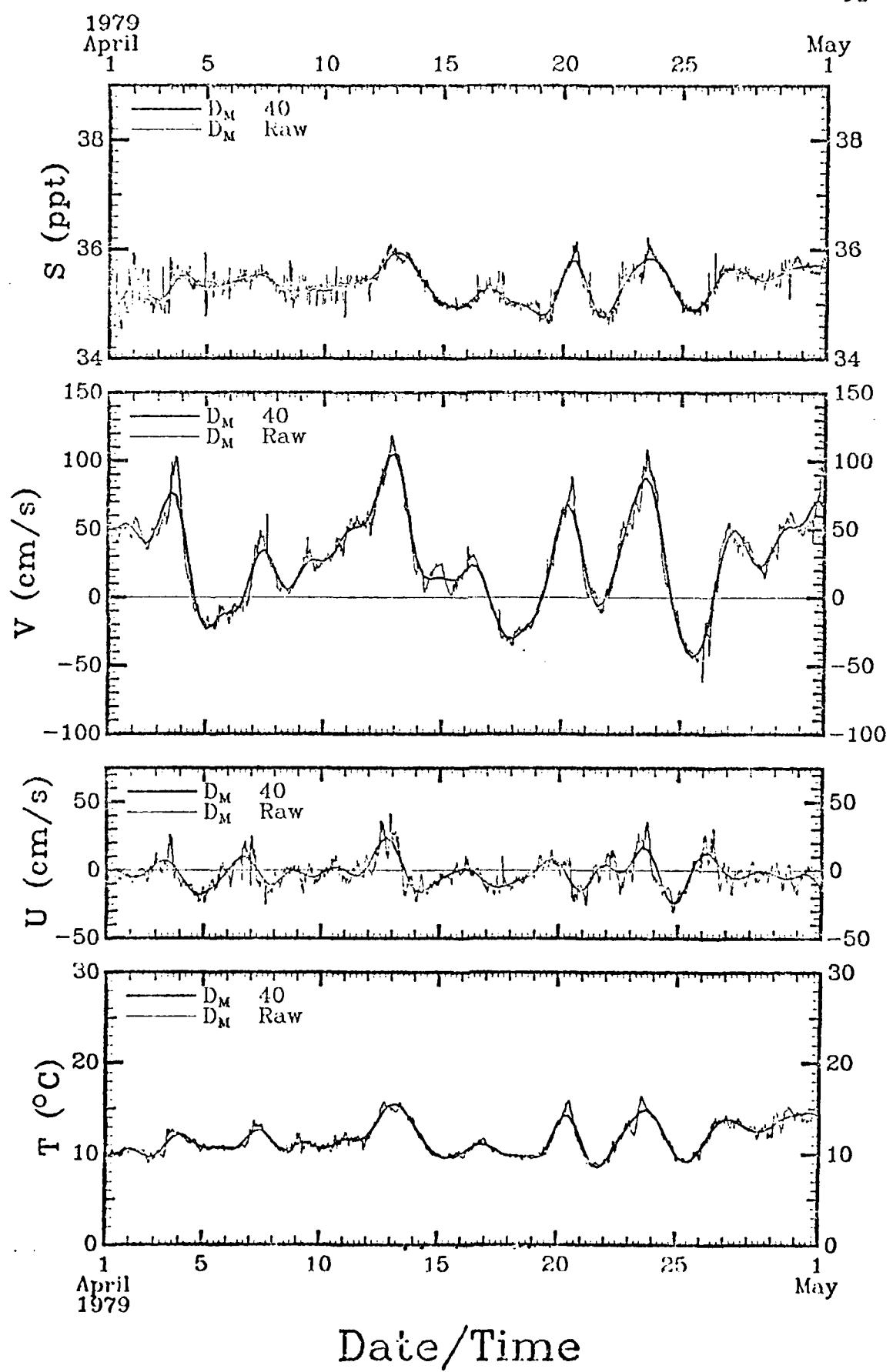


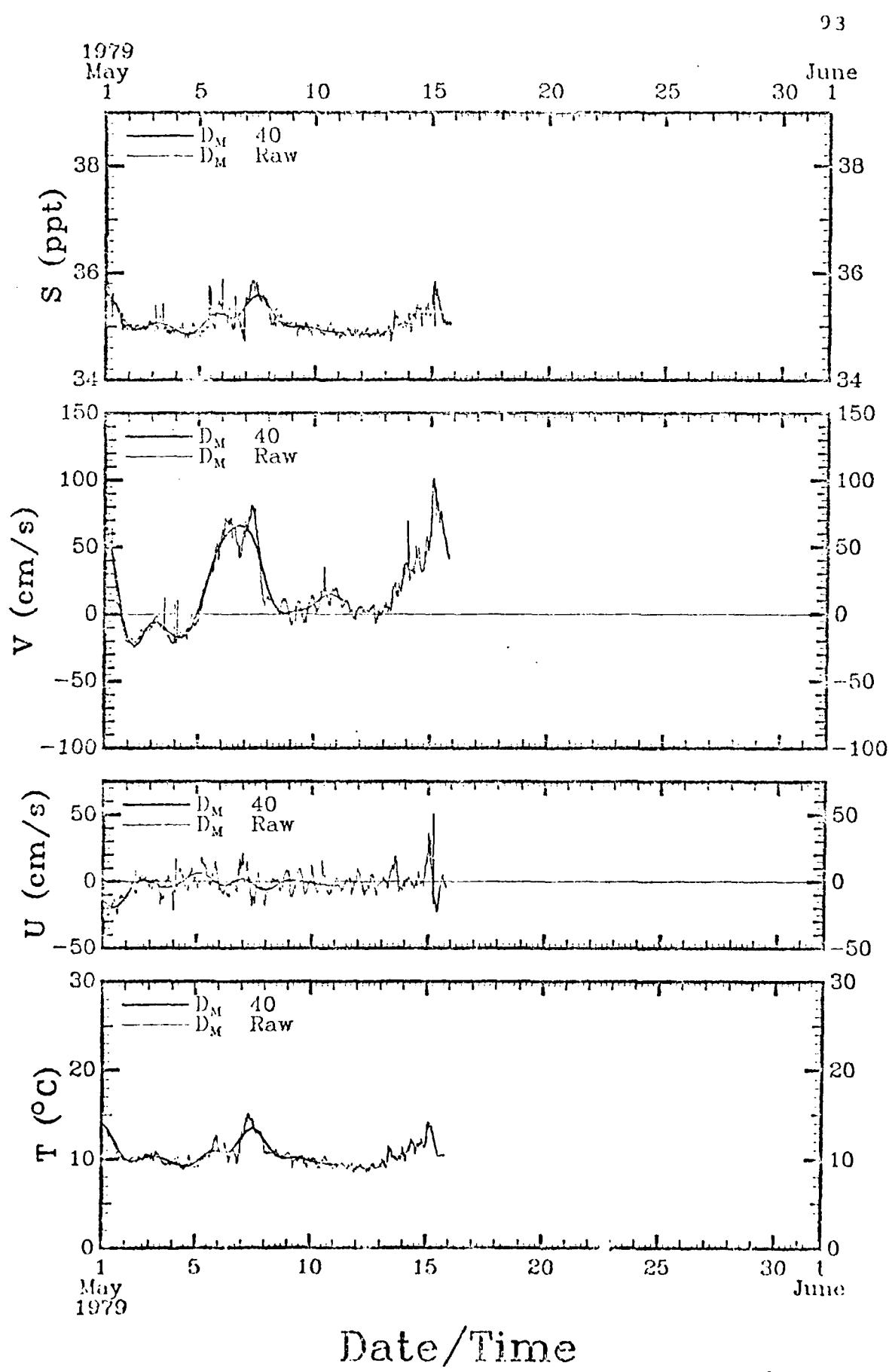


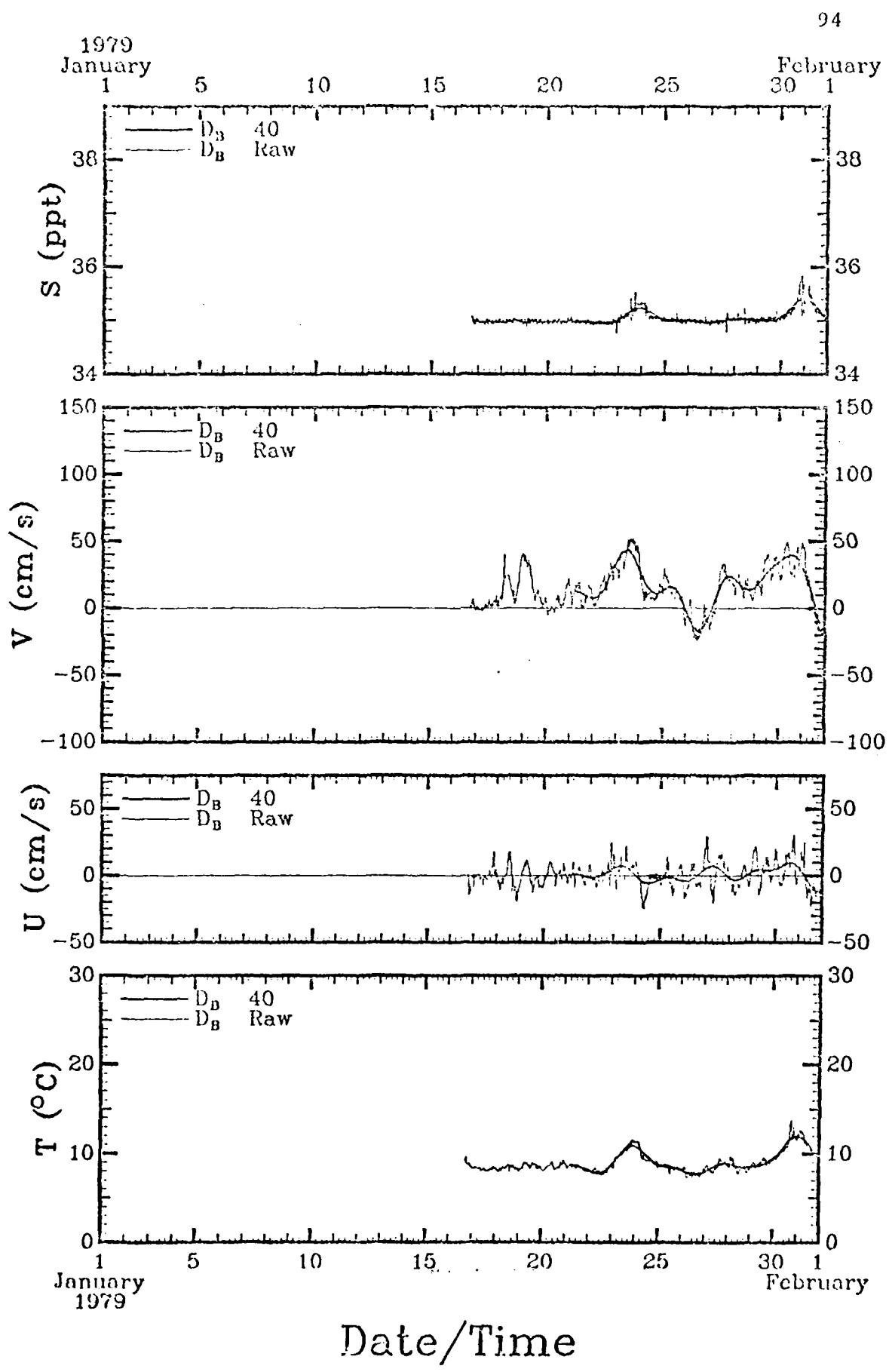


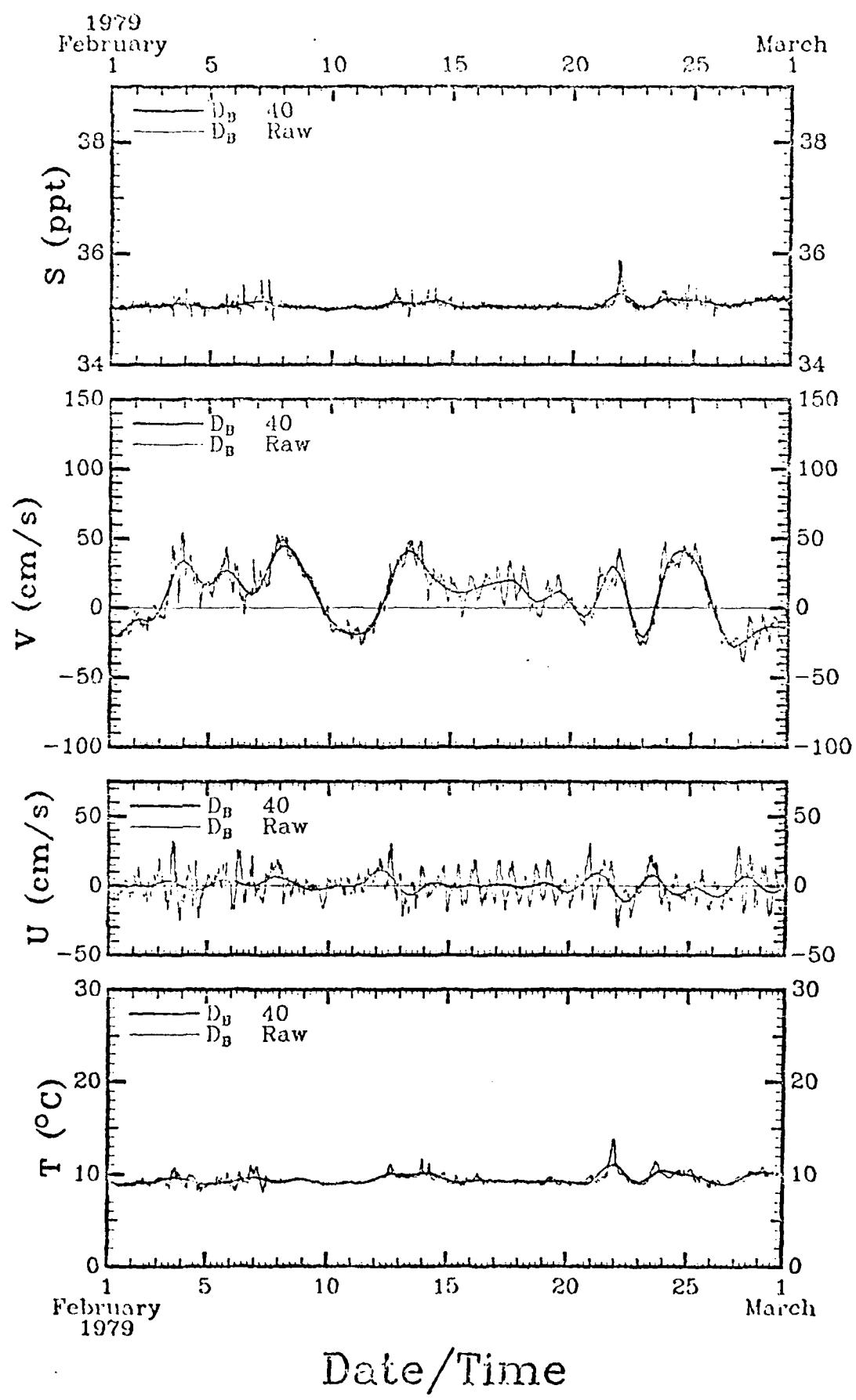


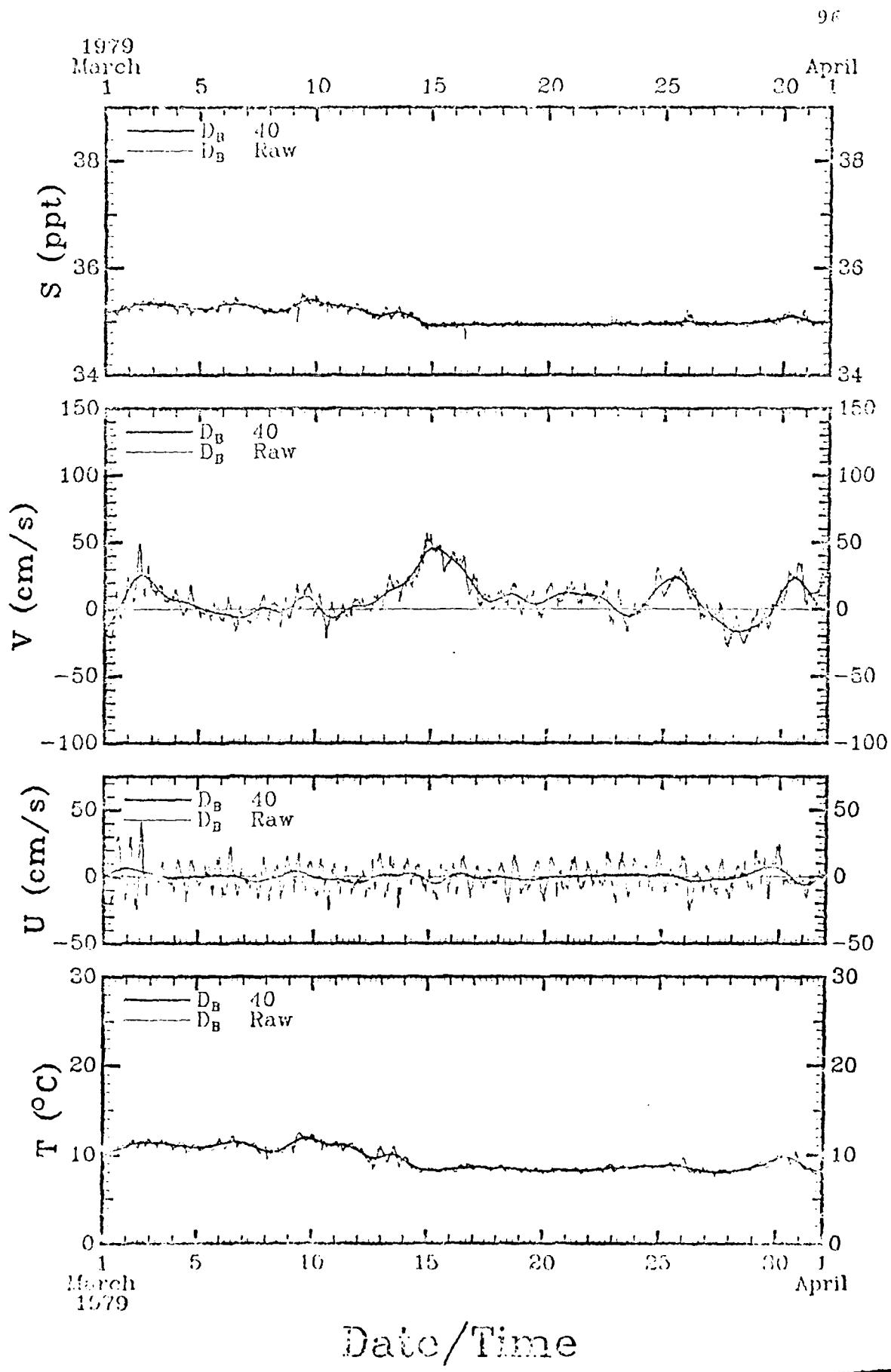


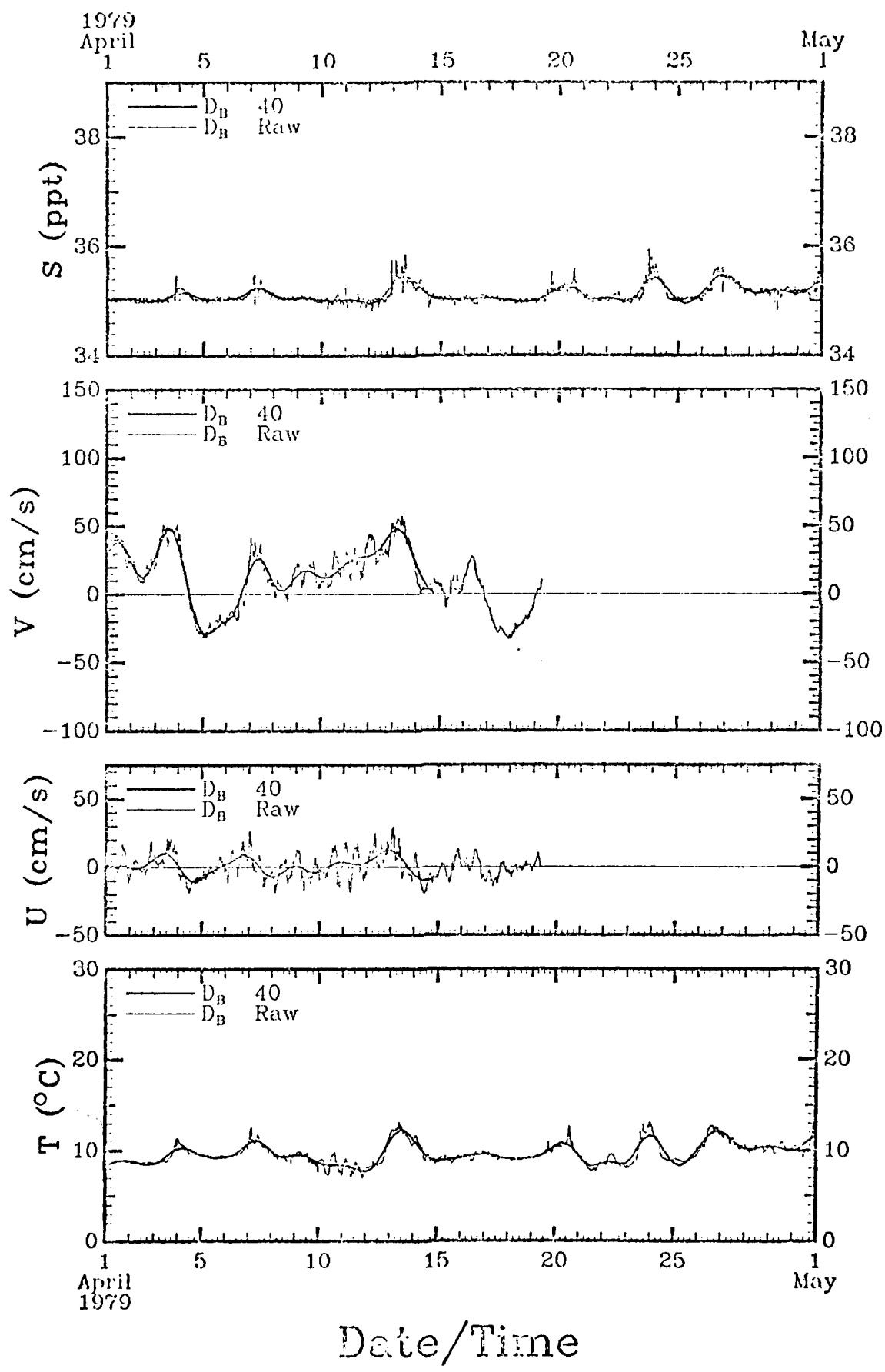




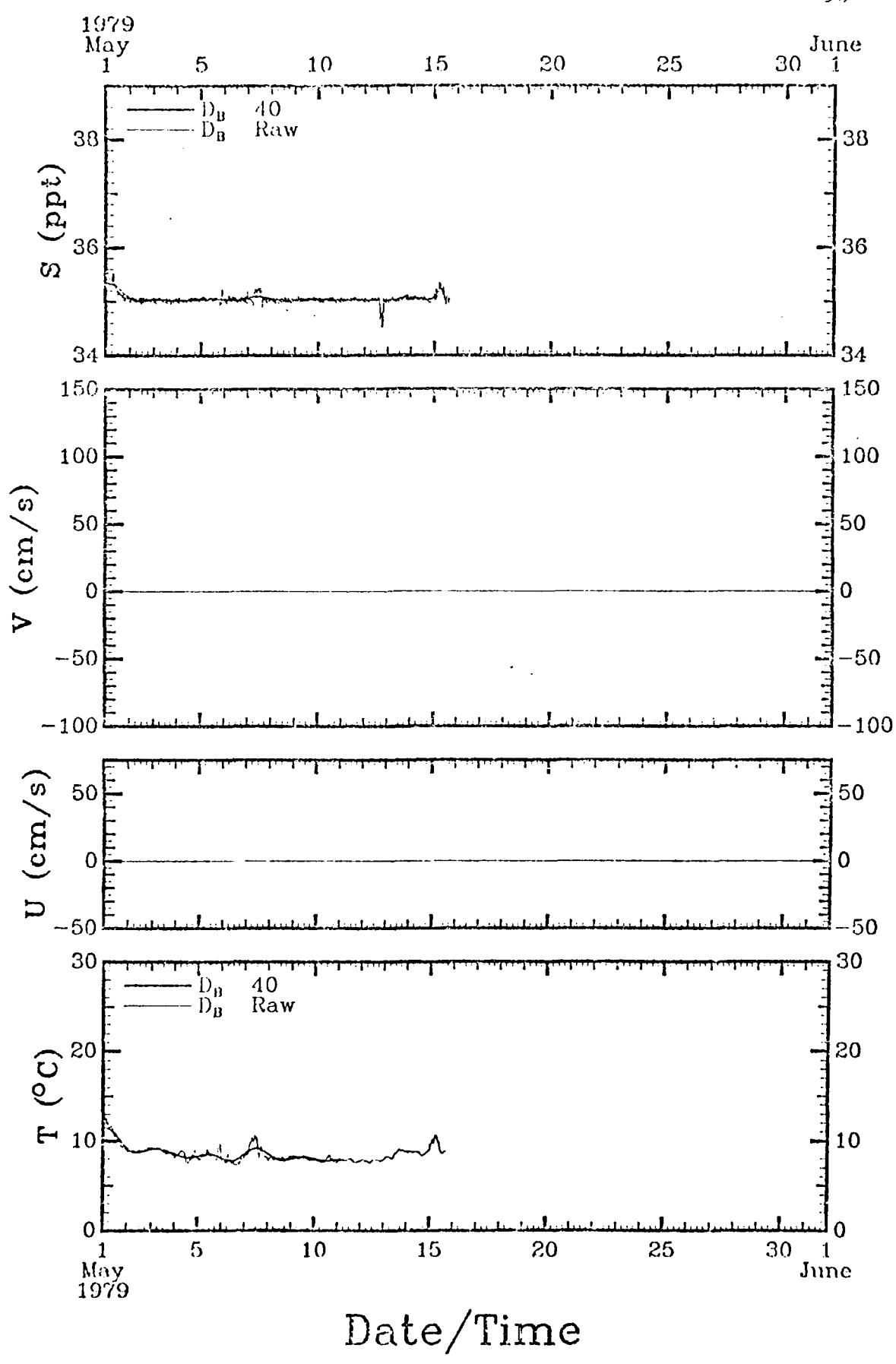








98

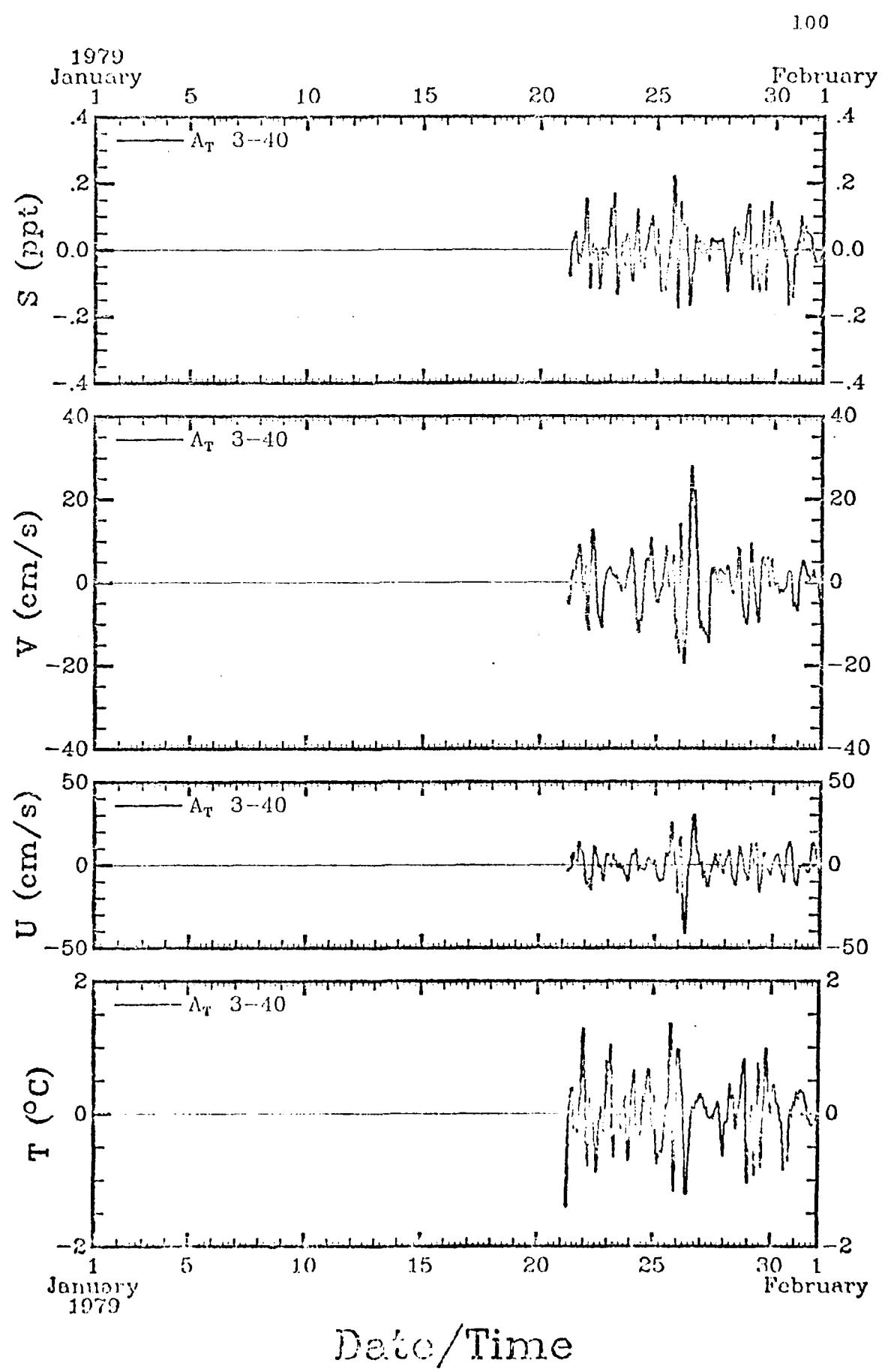


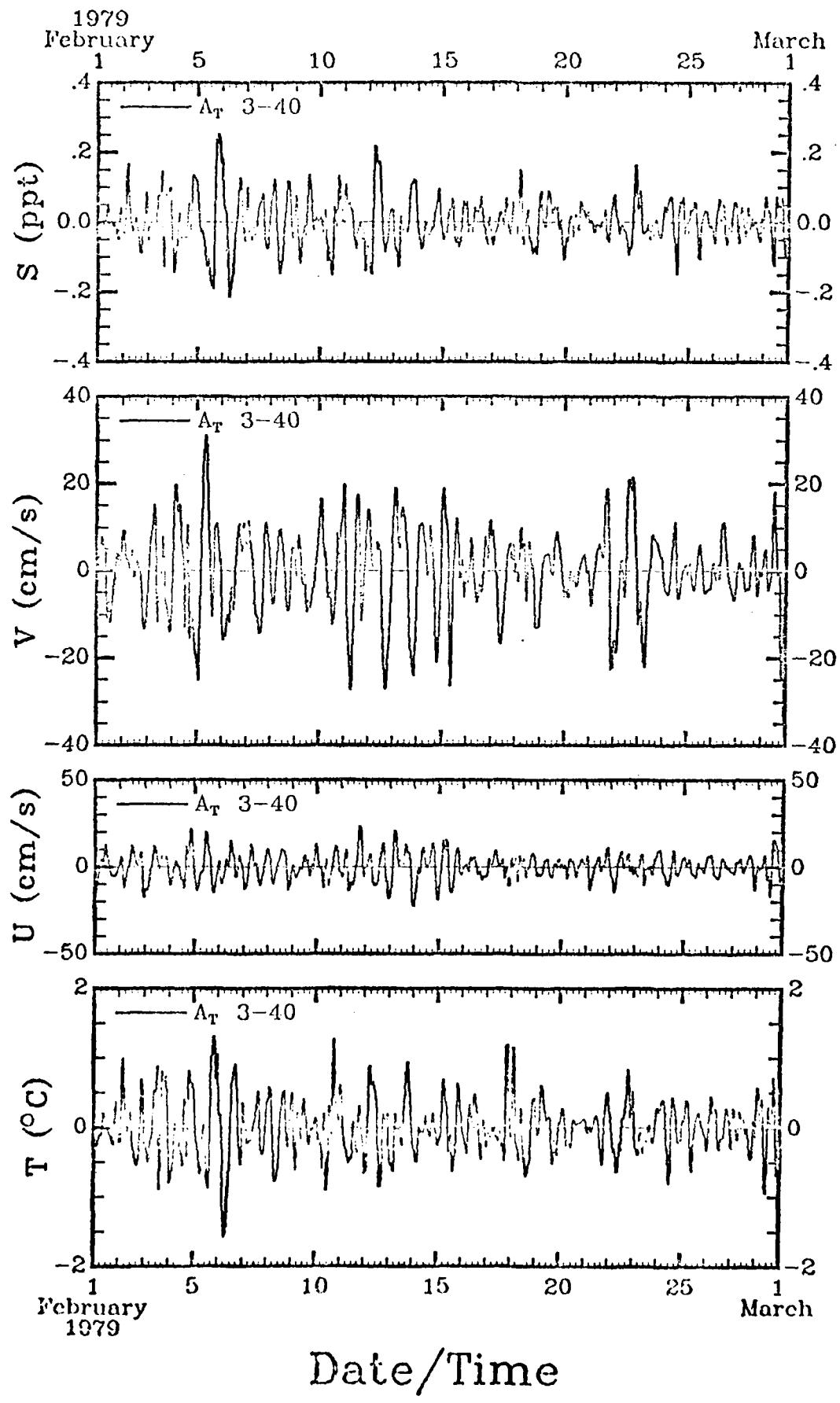
Date/Time

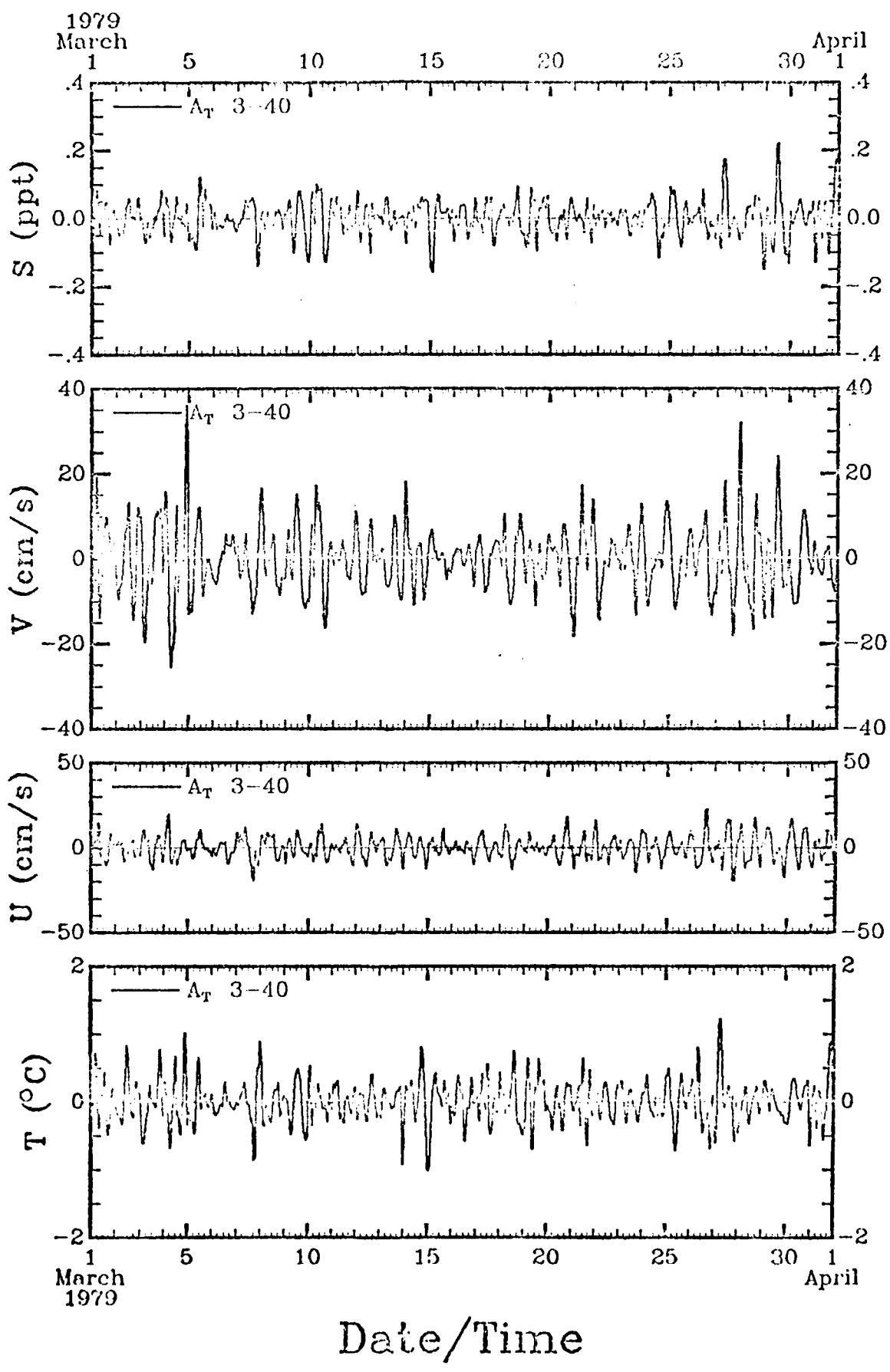
SECTION 4

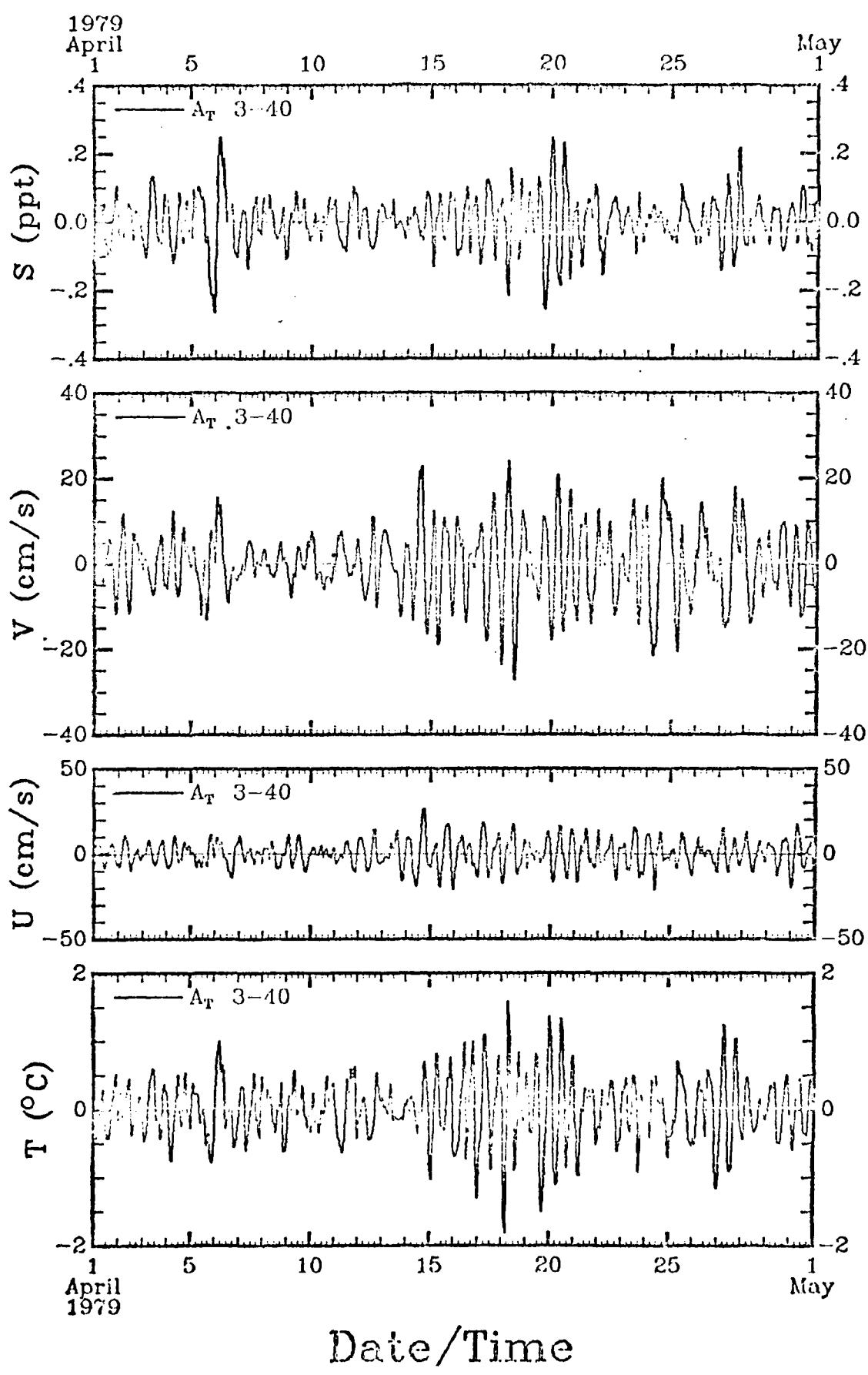
3-40 HRBP Data for Each Instrument

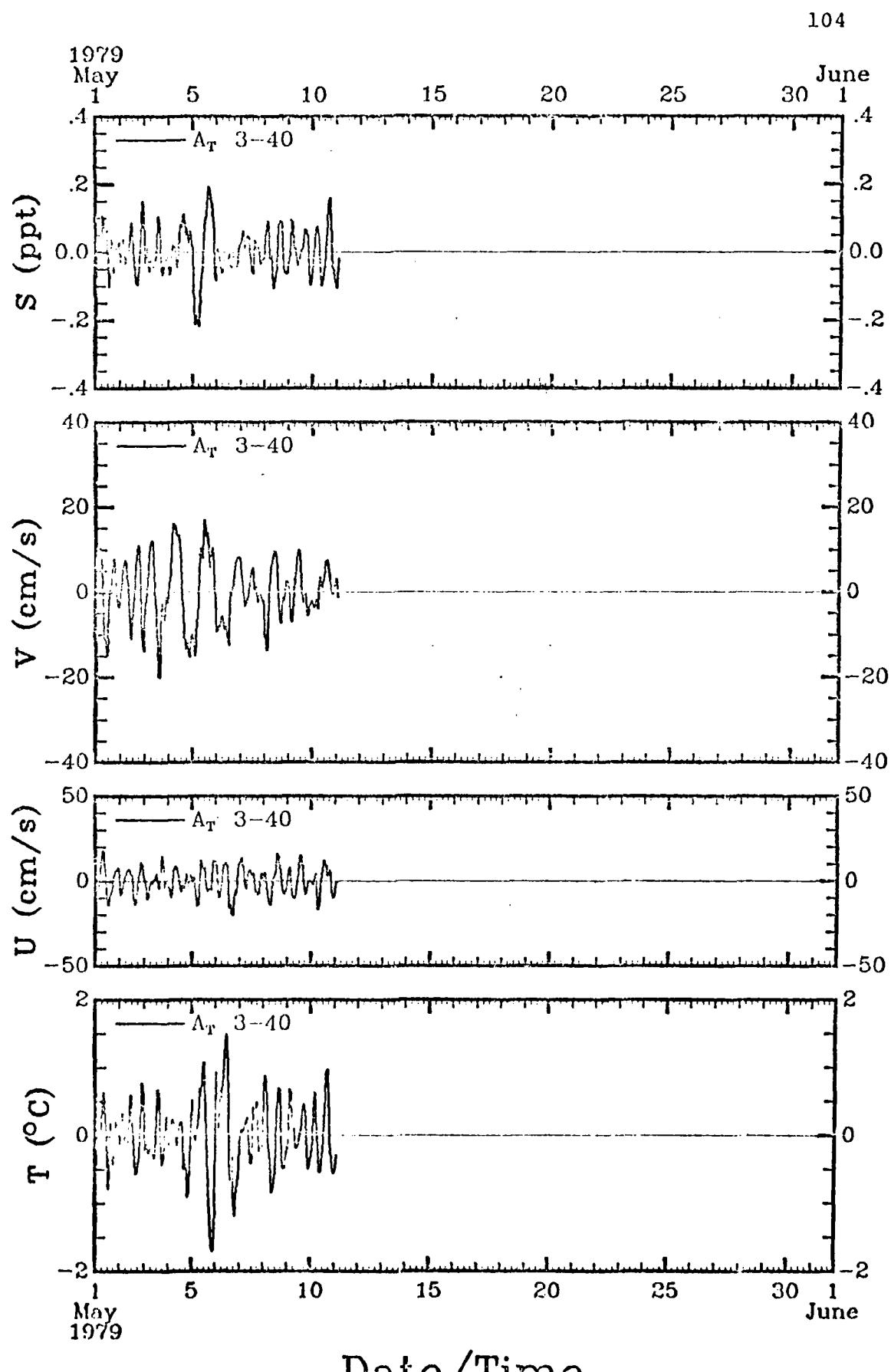
Figures 30 through 39 show the 3-40 HRBP current meter data separately by month for each instrument. The scale factors for similar data are not the same for all instruments in this section. Note that the bandpass operation removes the mean value.



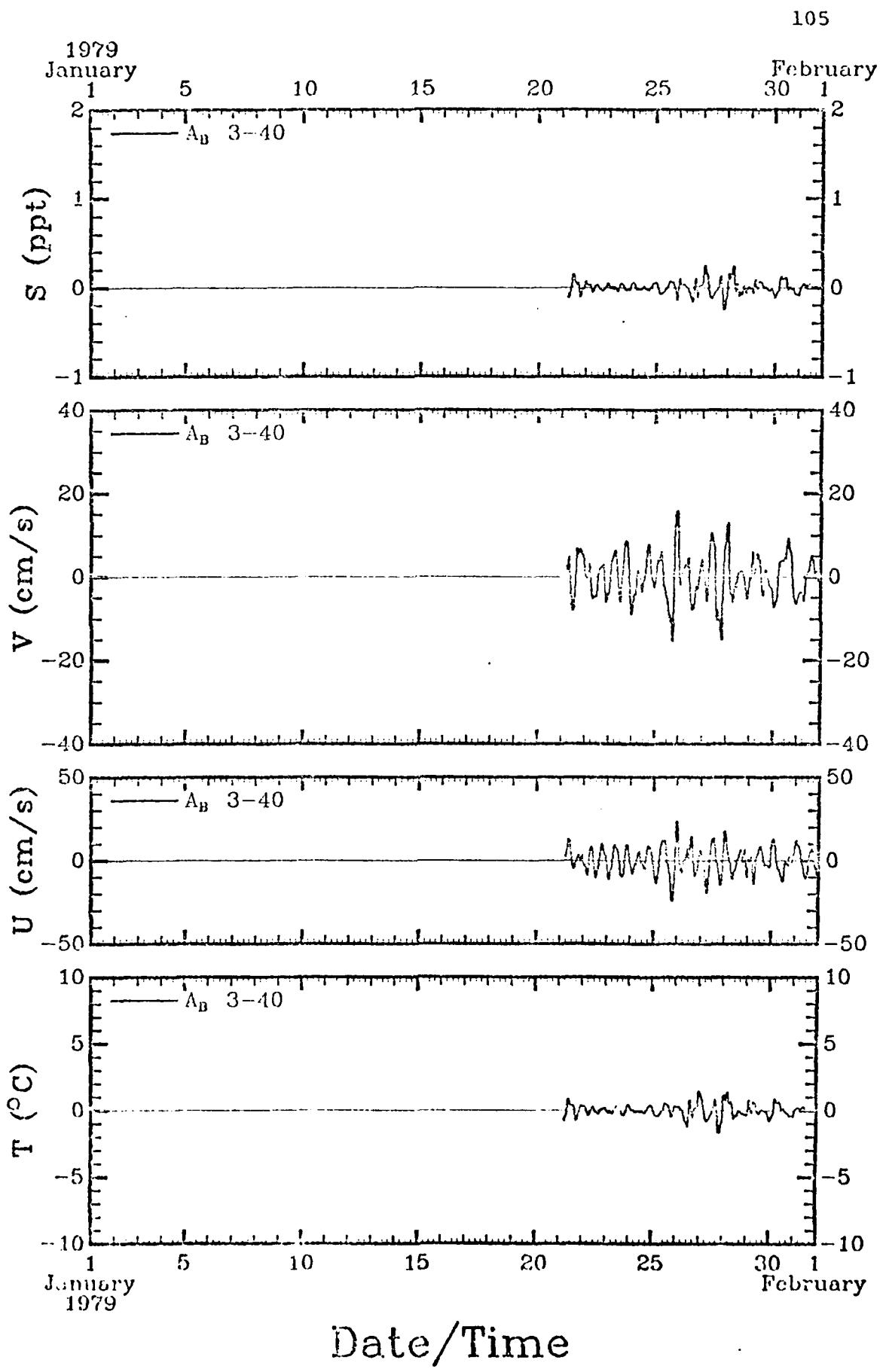


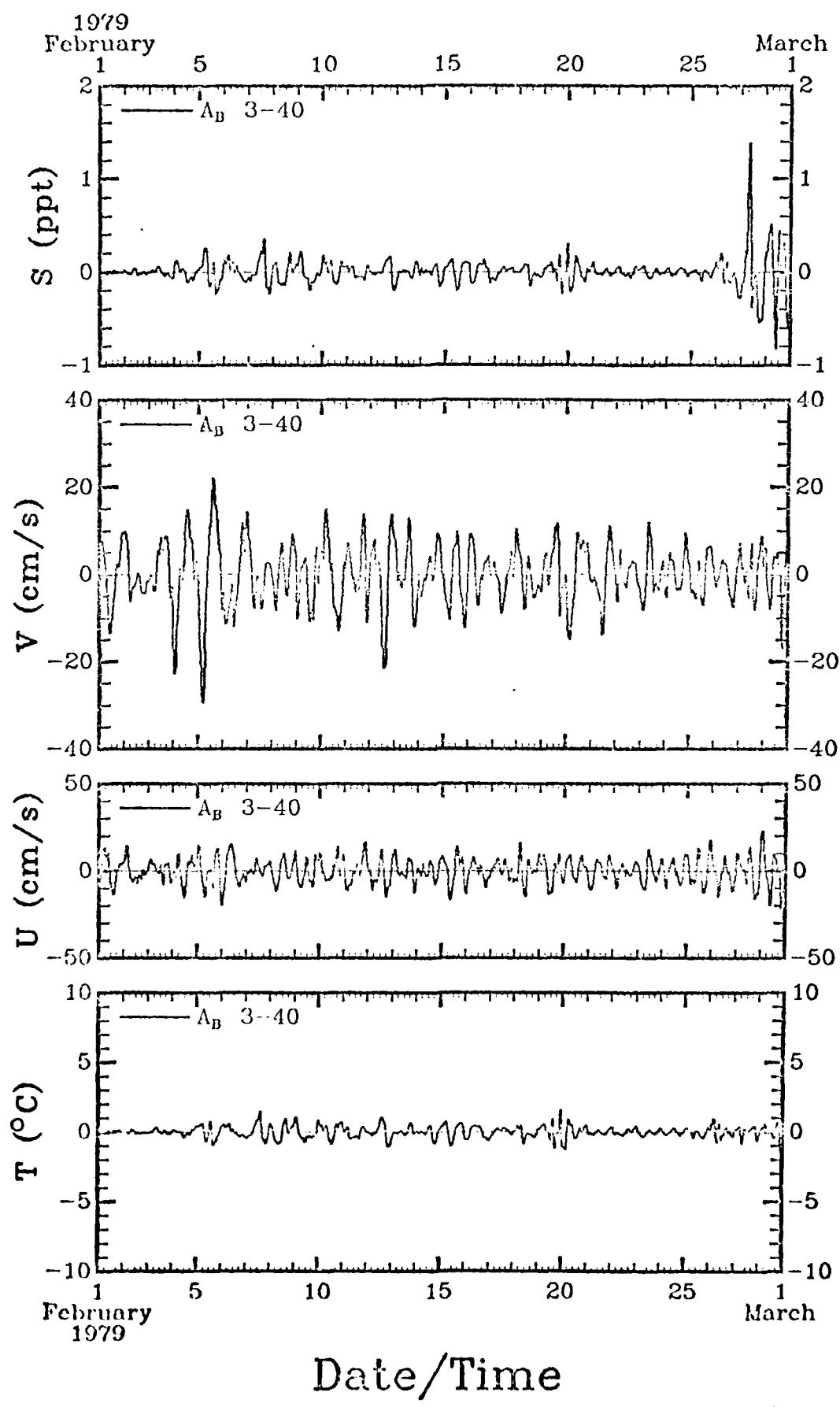


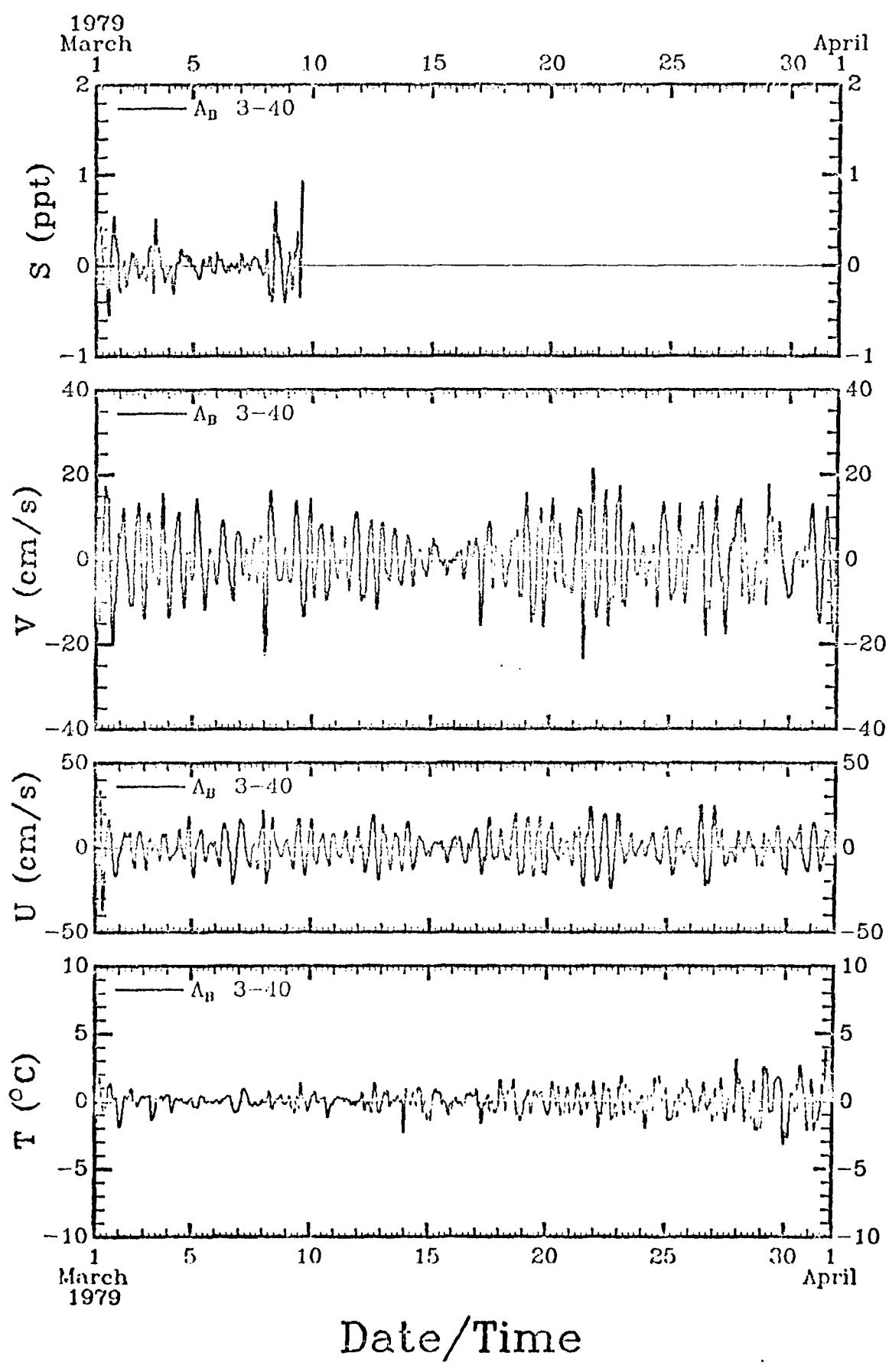




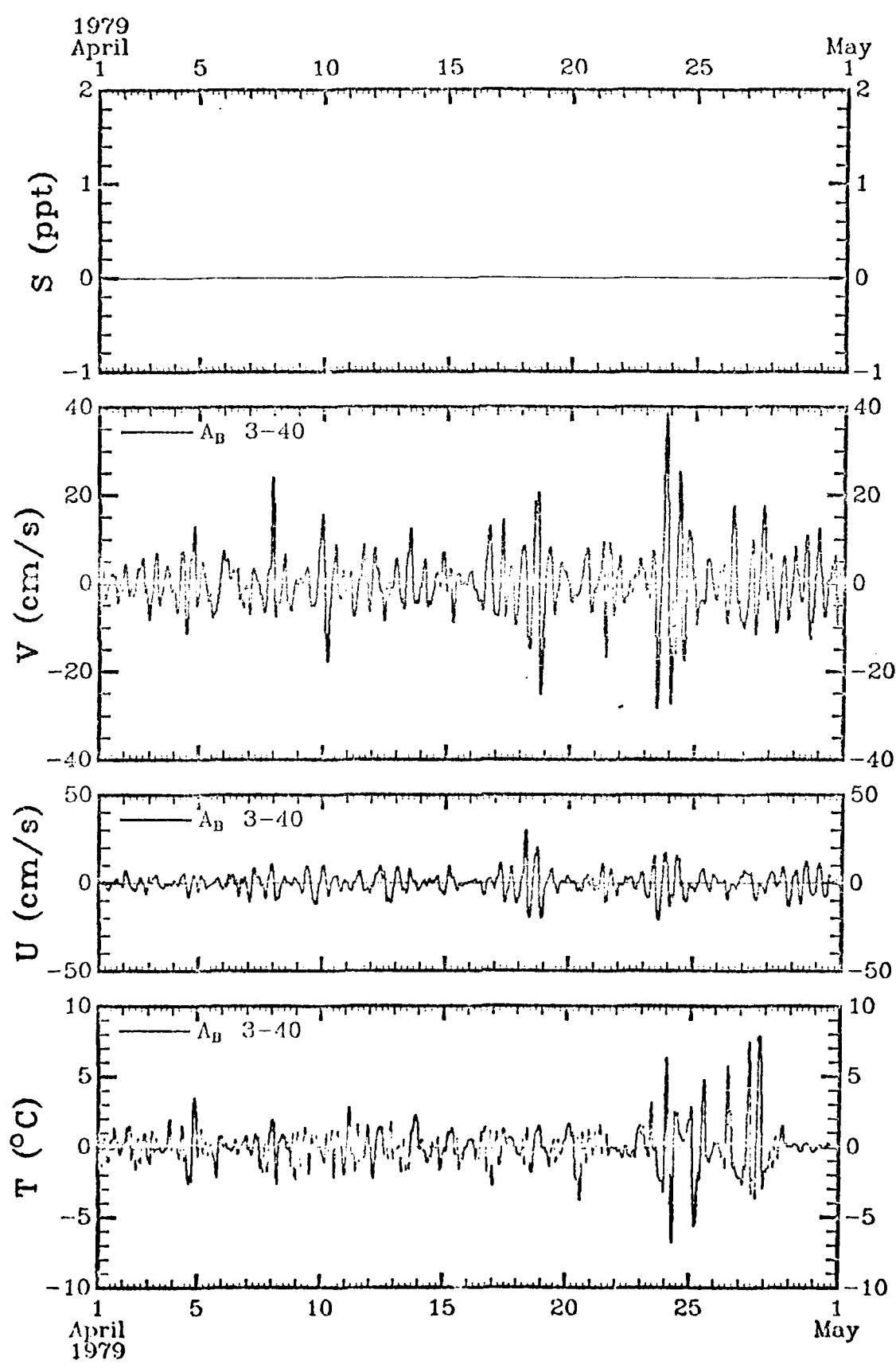
Date/Time



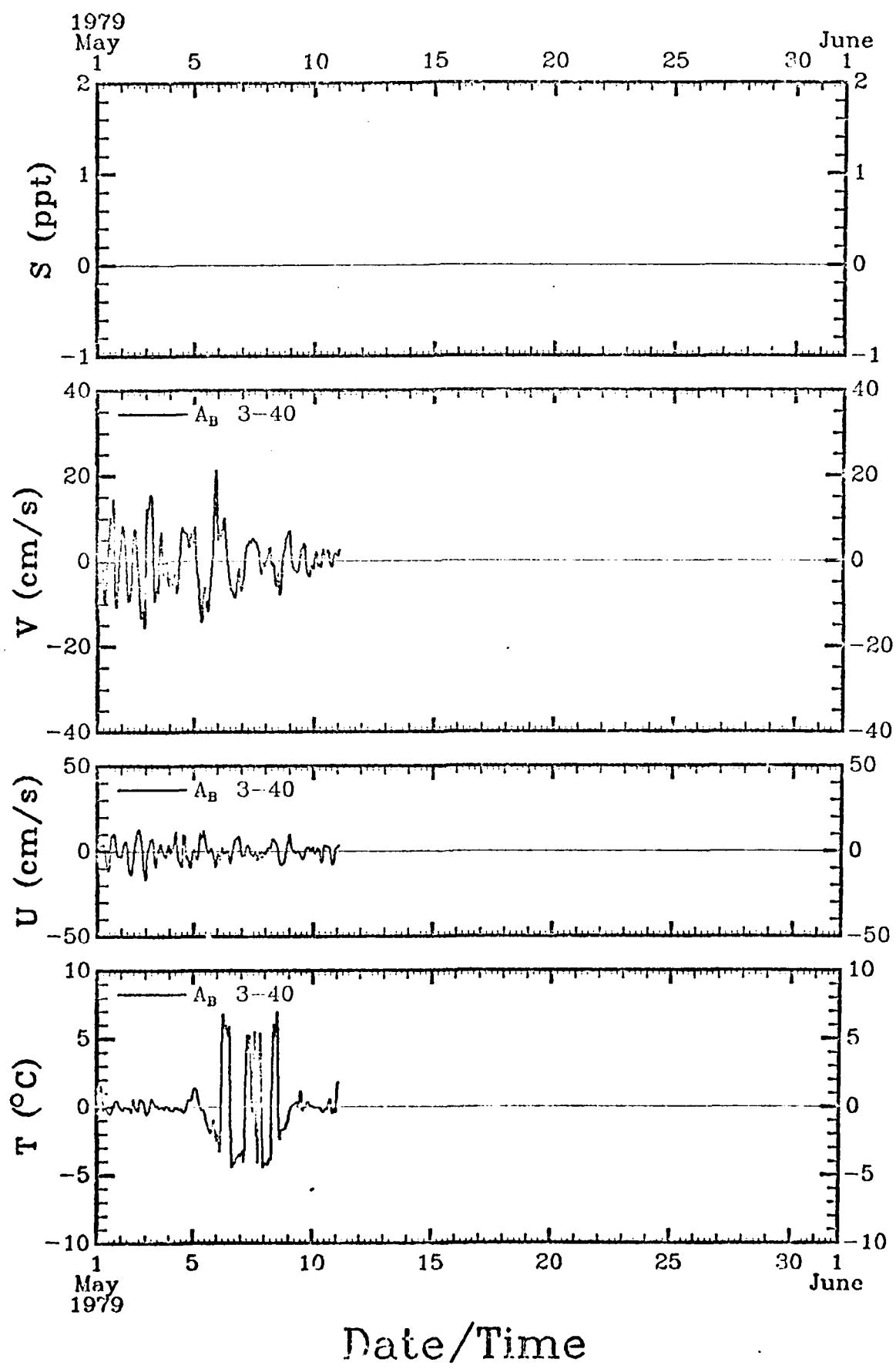


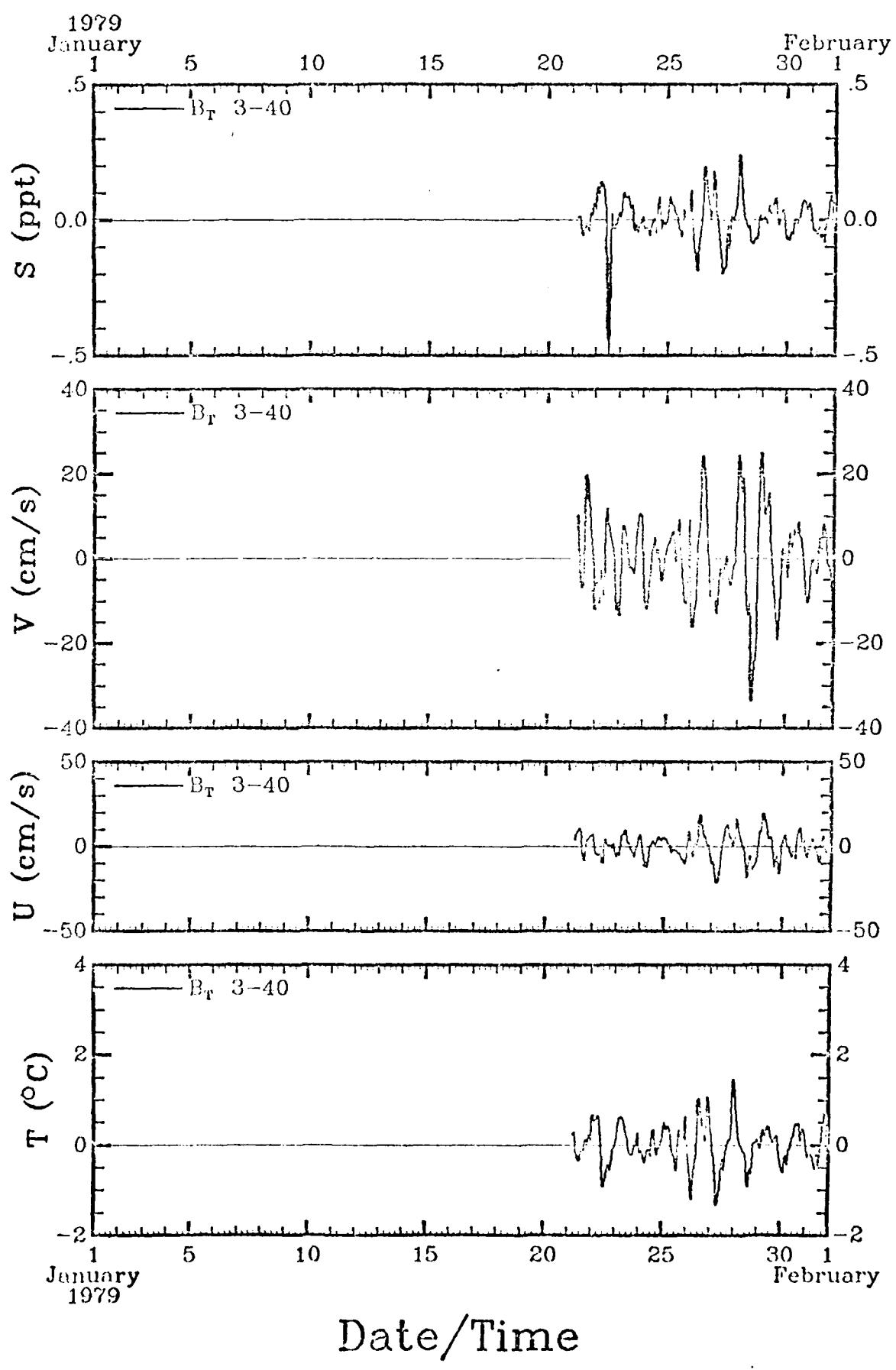


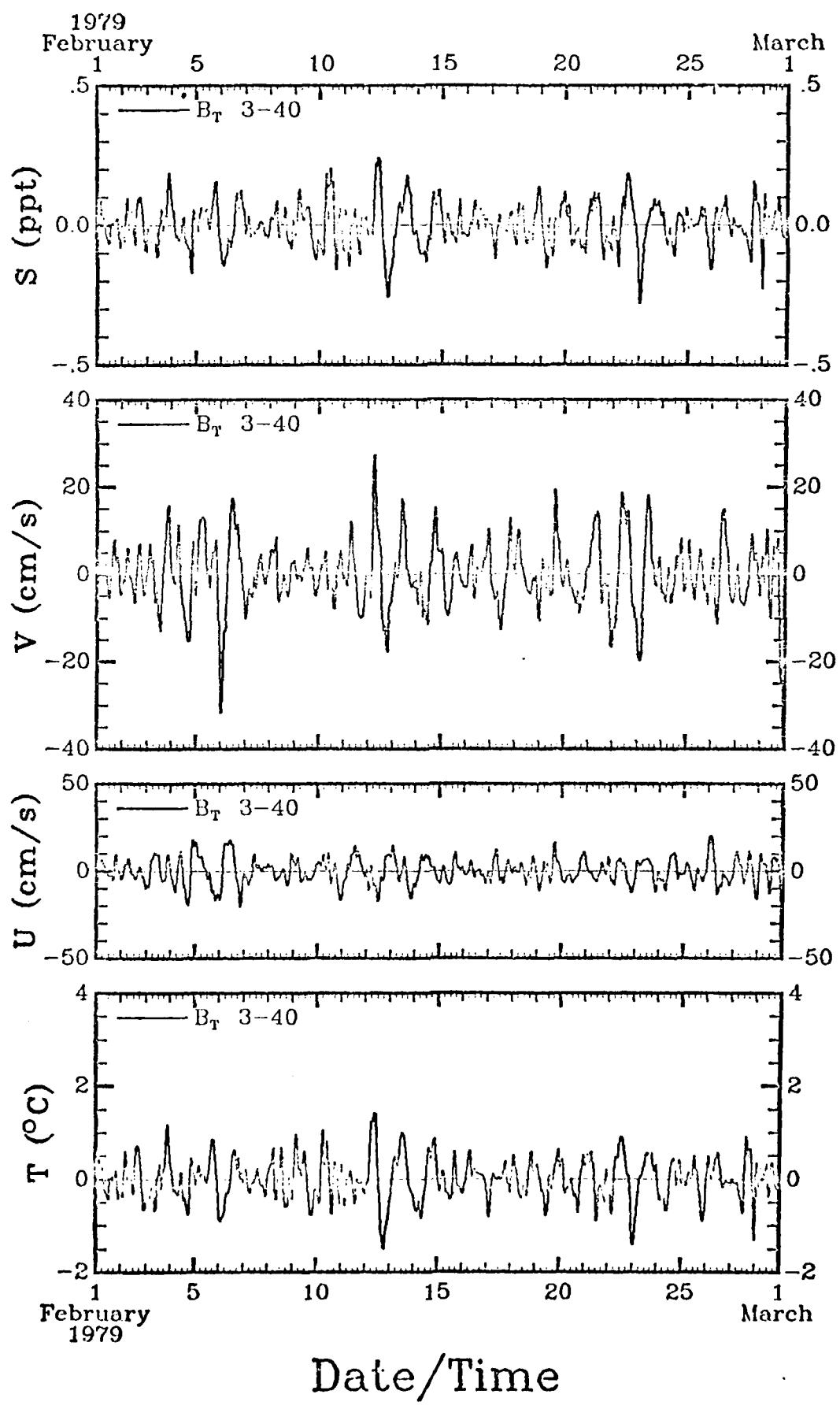
108

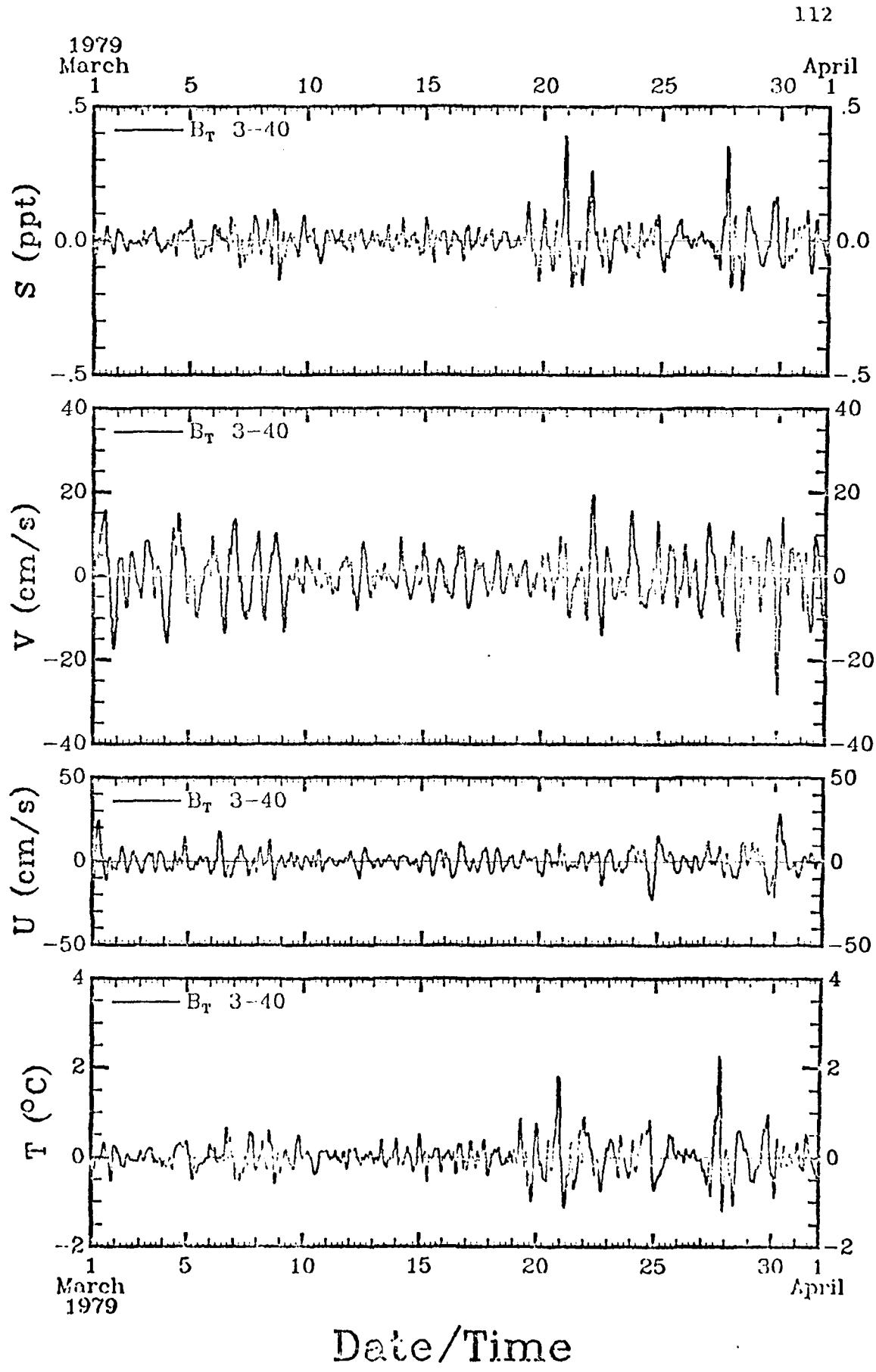


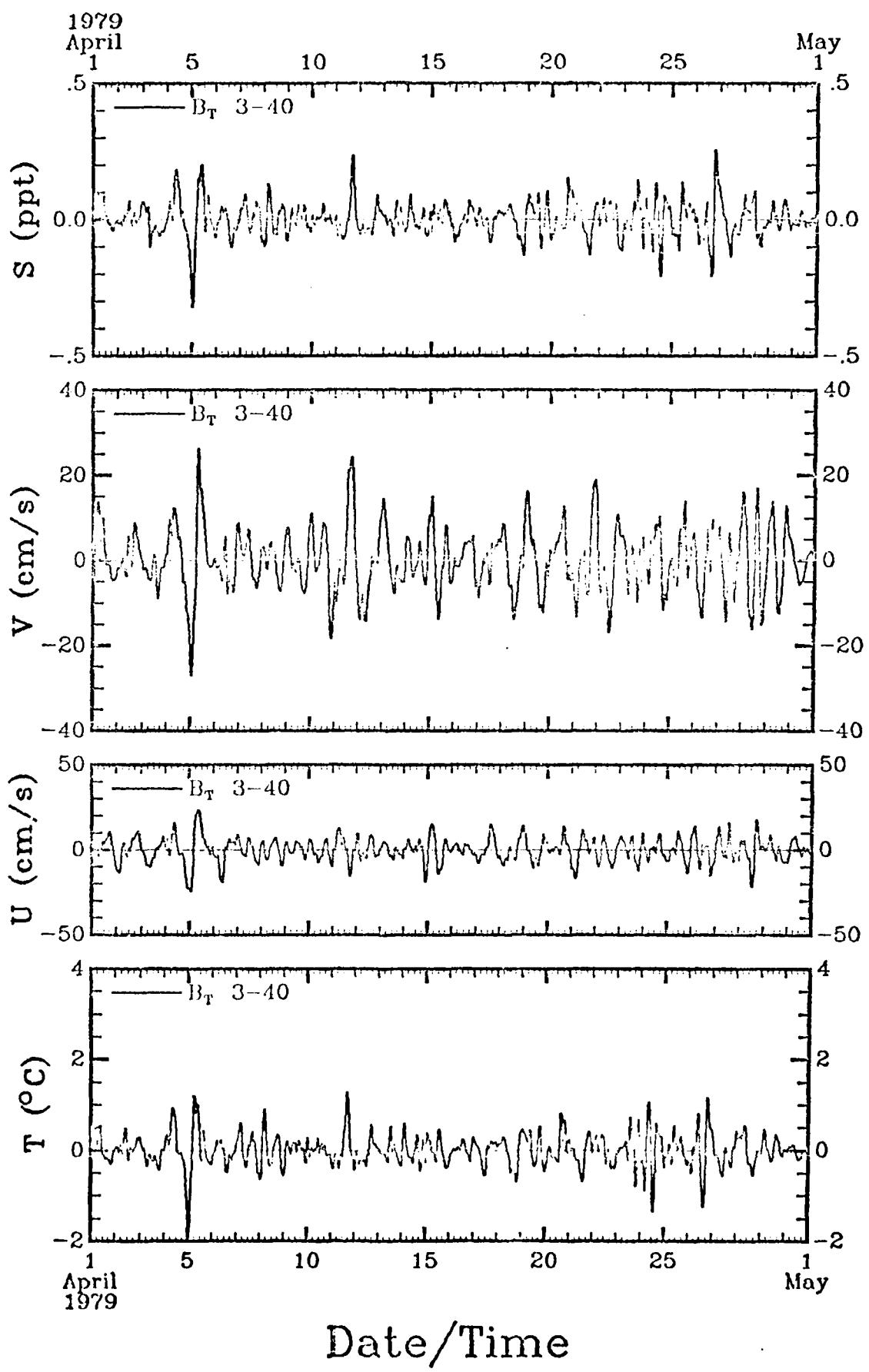
Date/Time

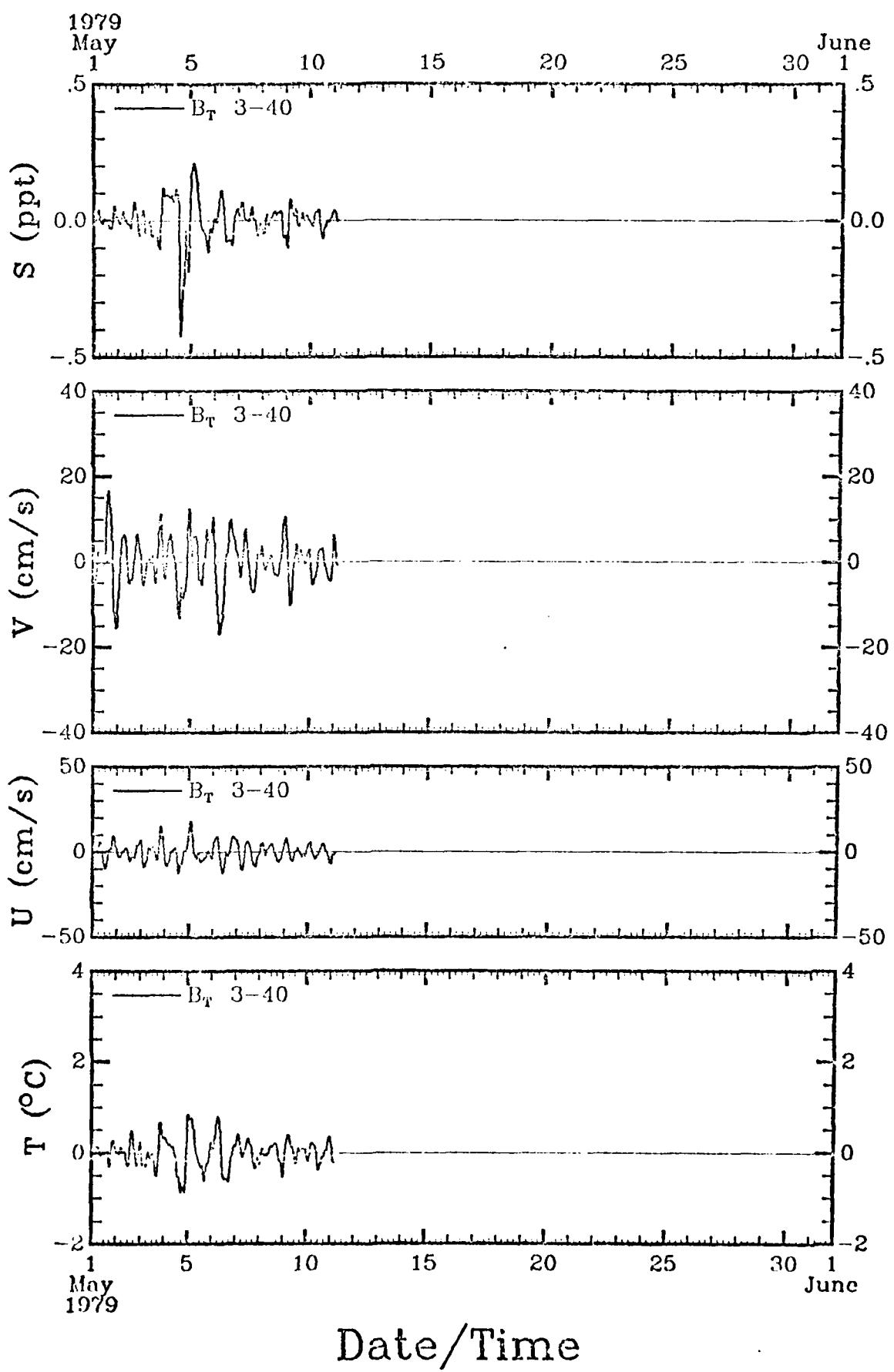


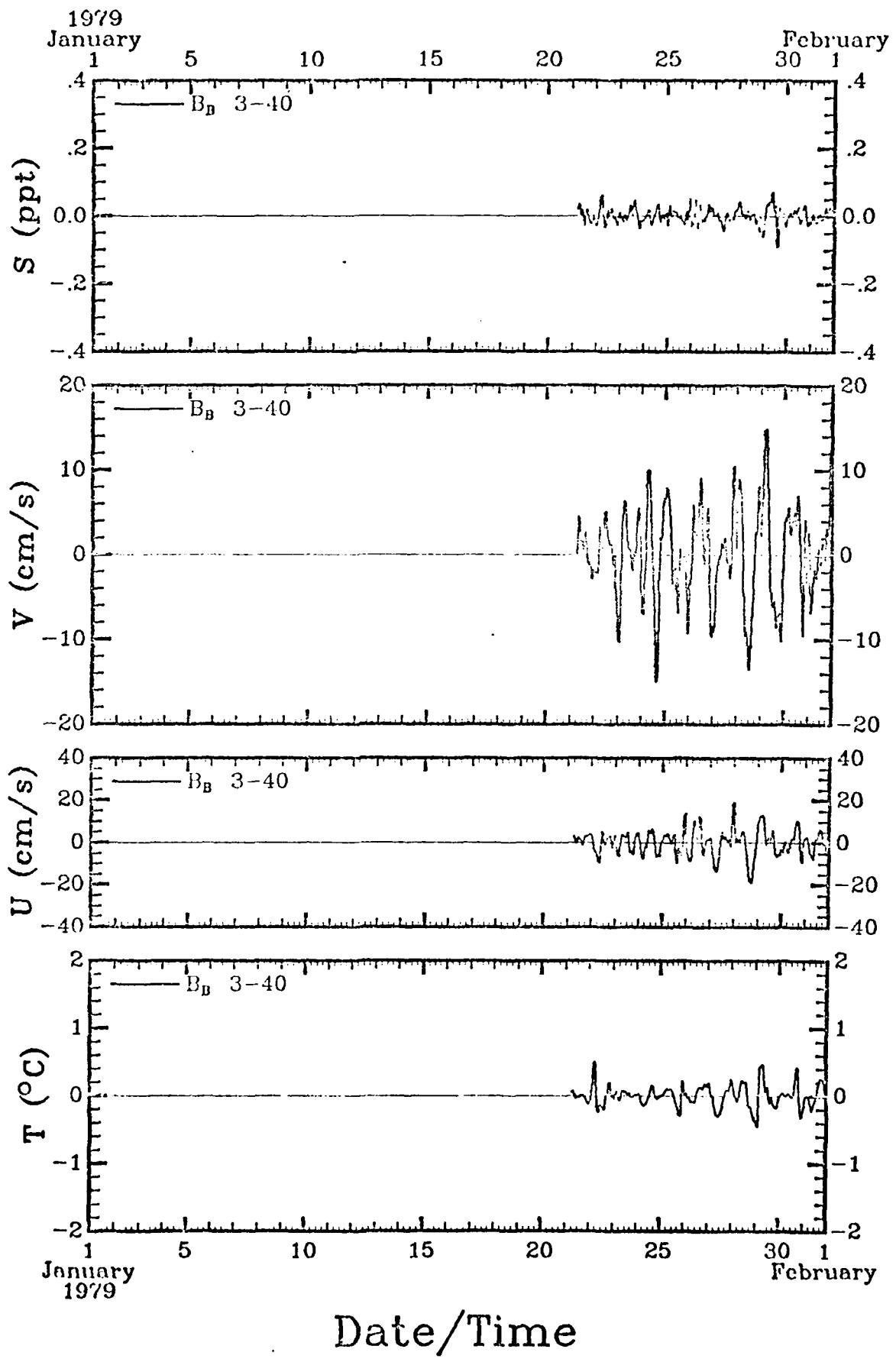


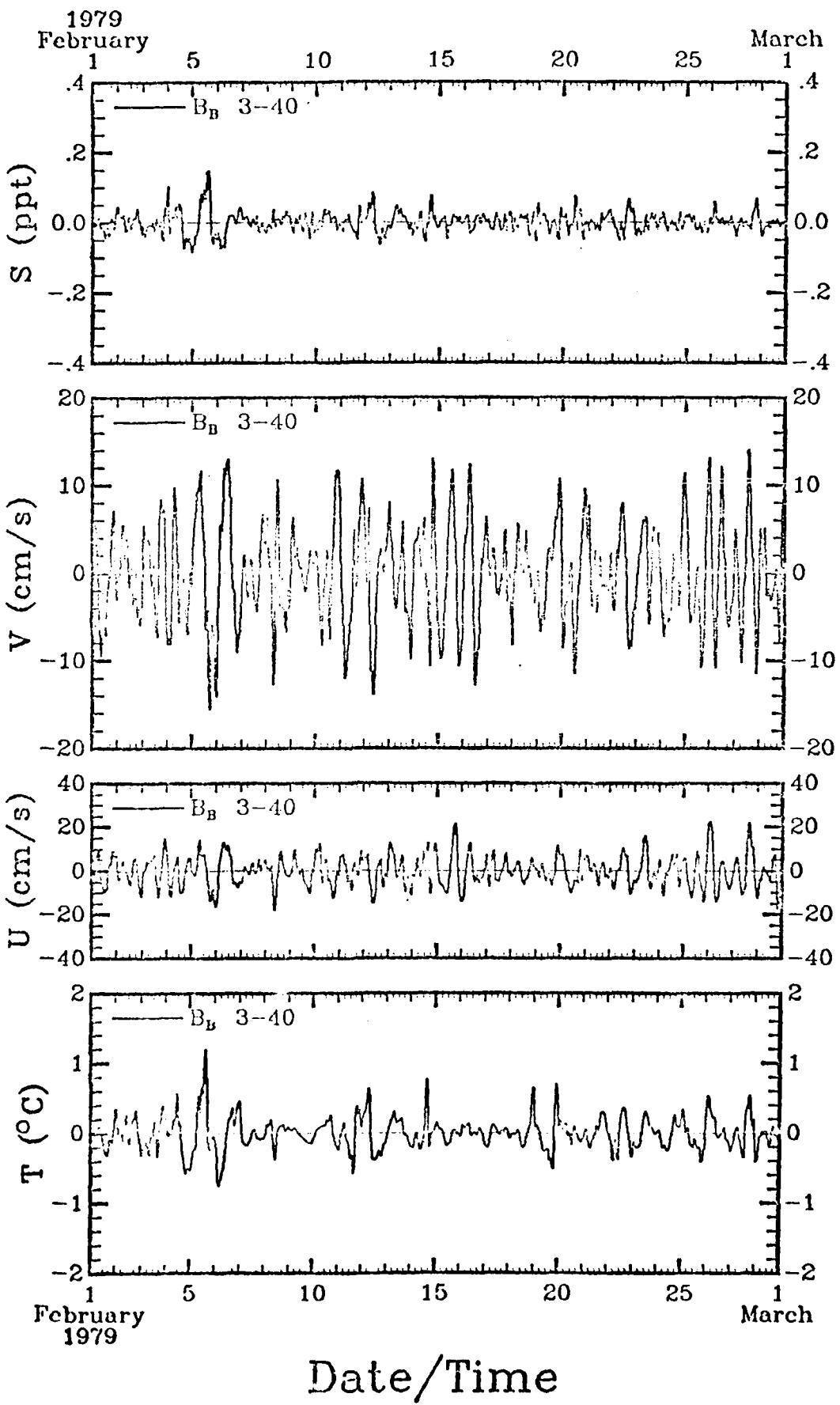


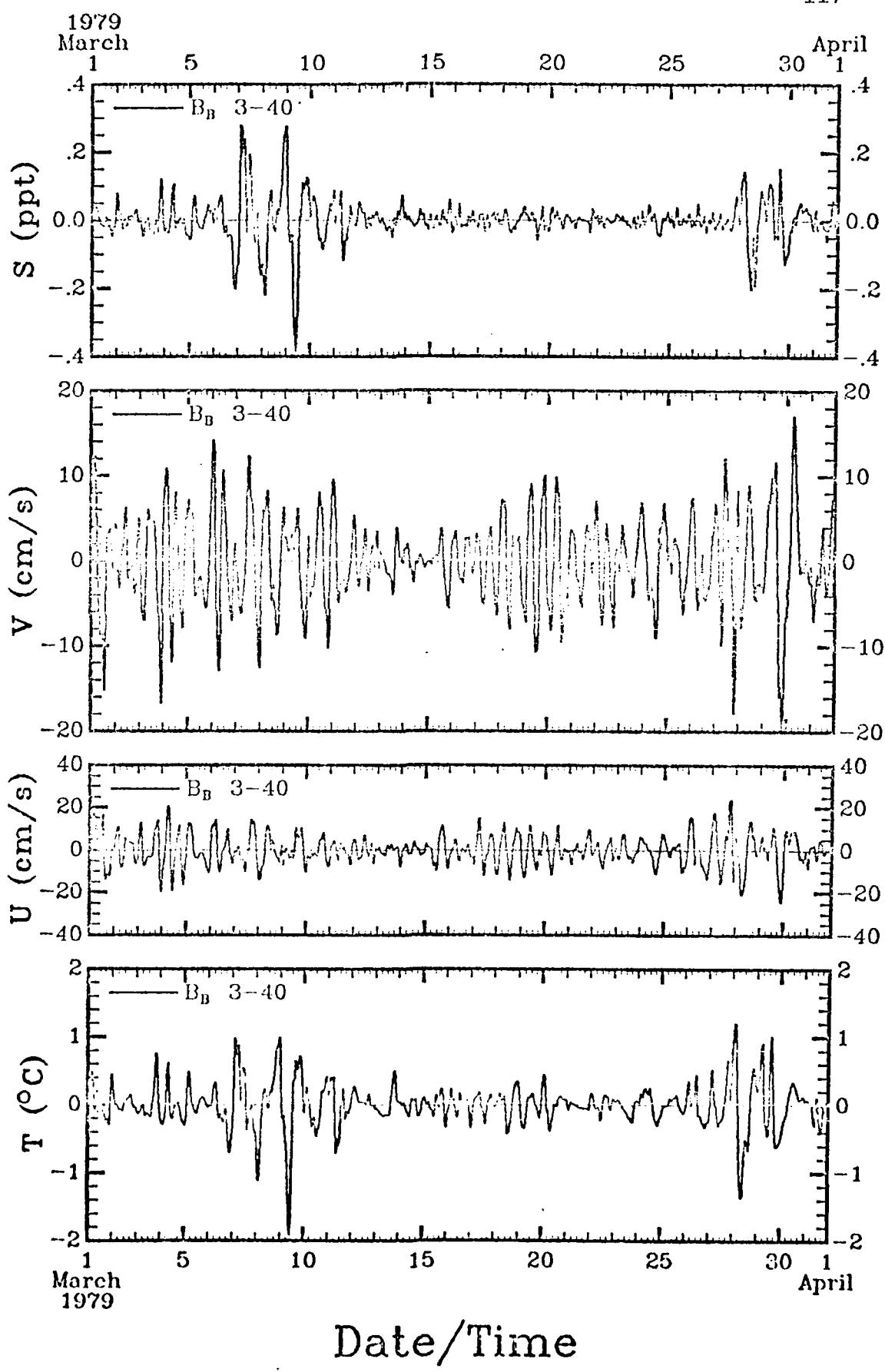


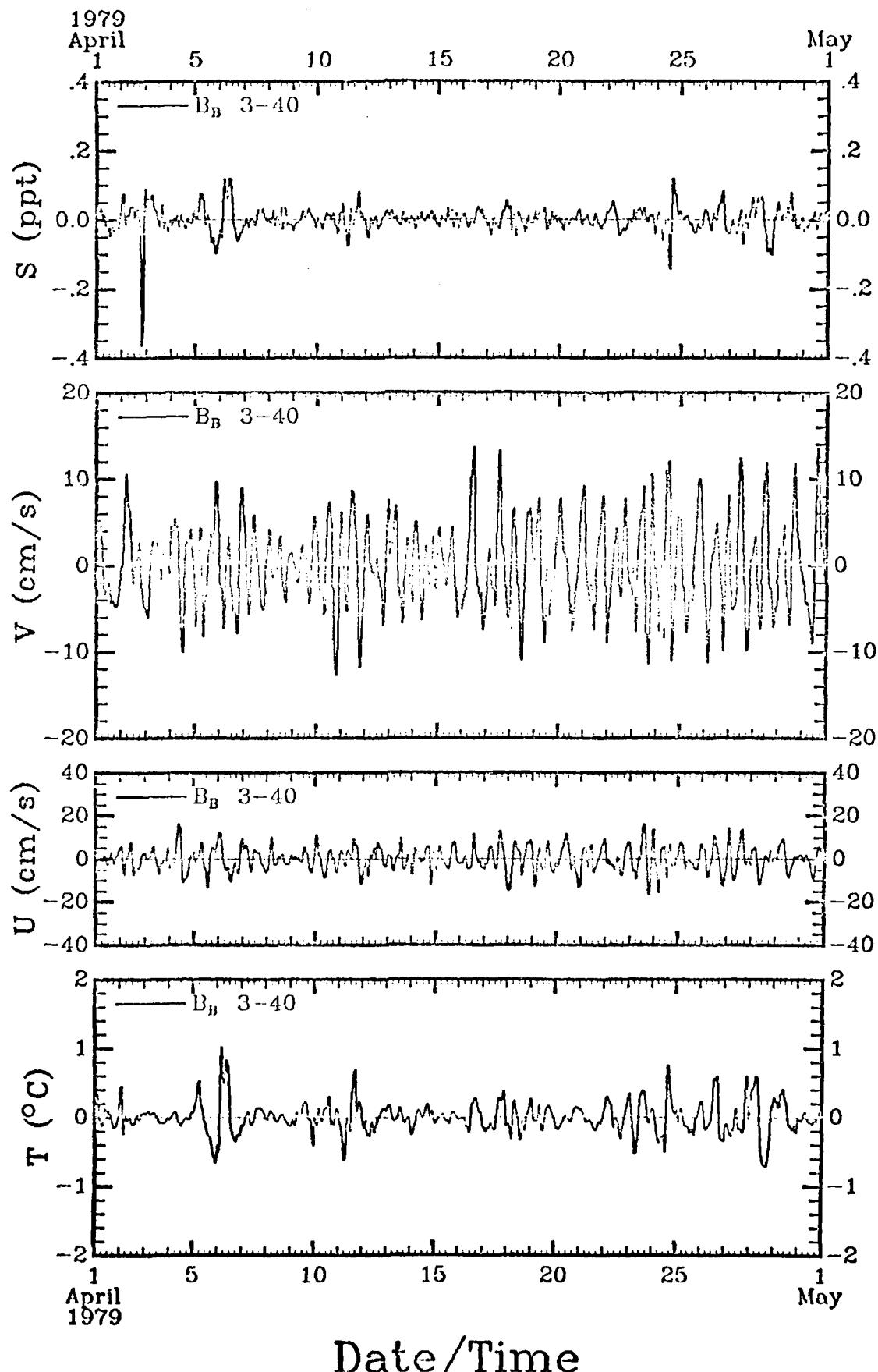


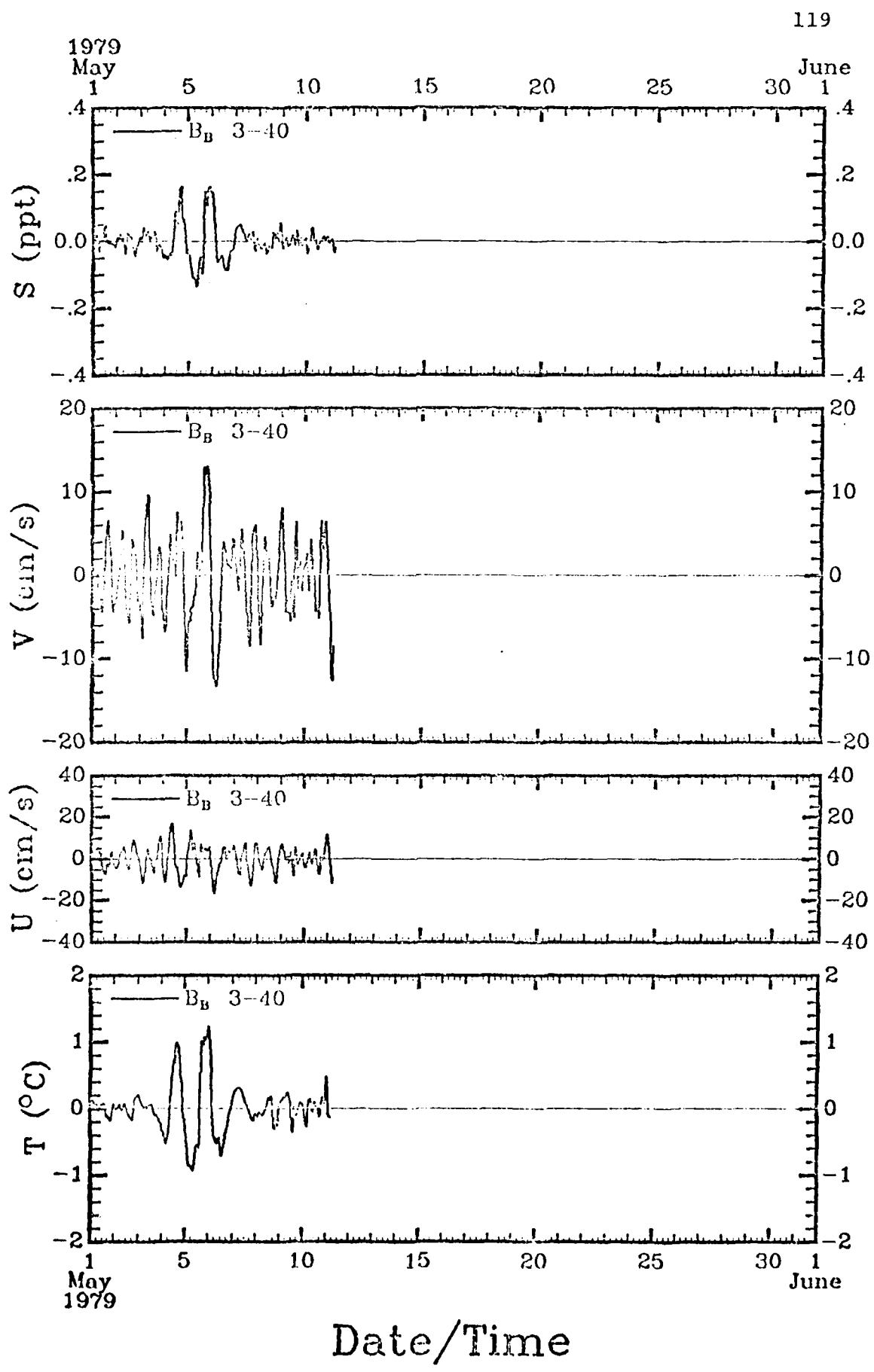


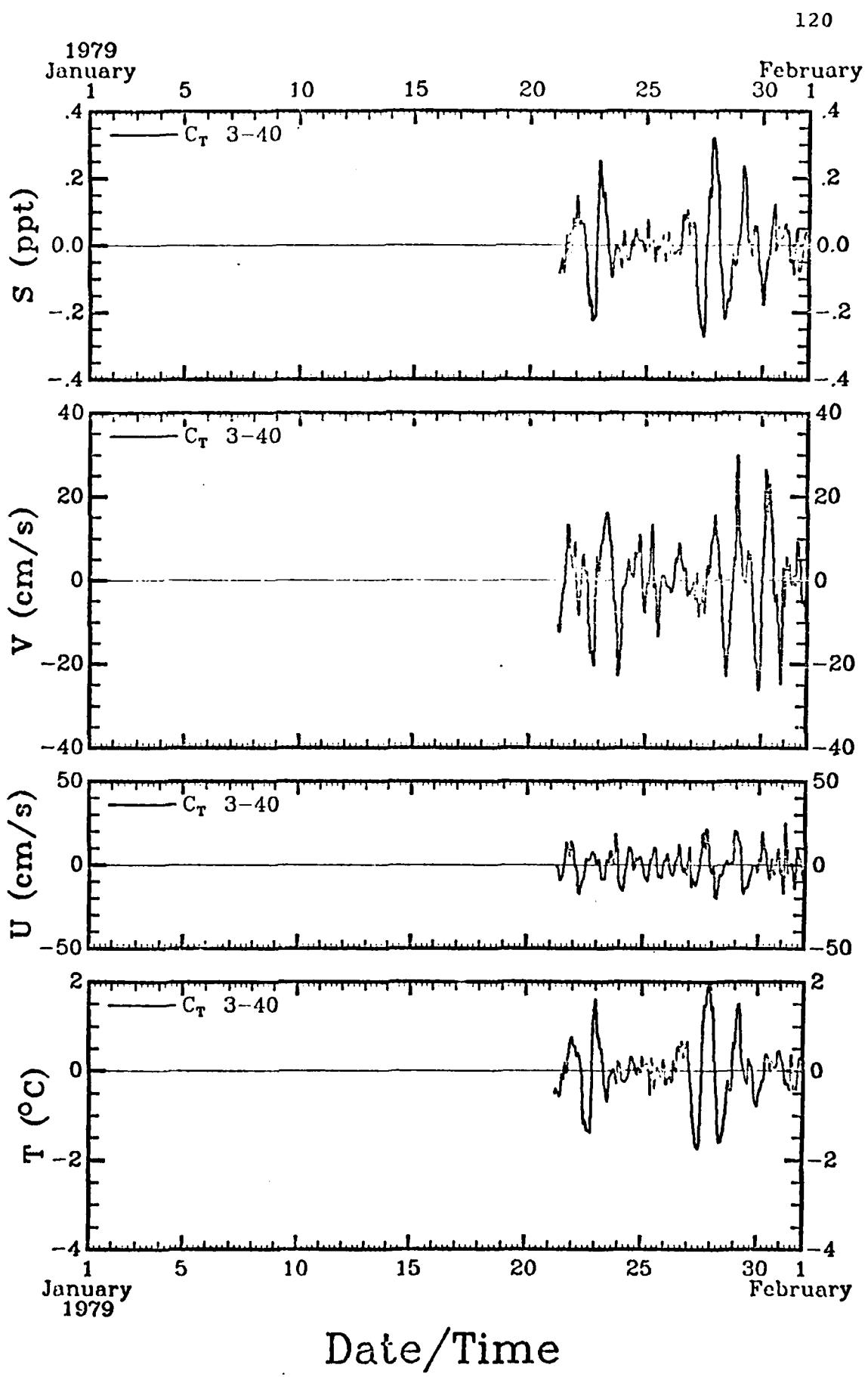


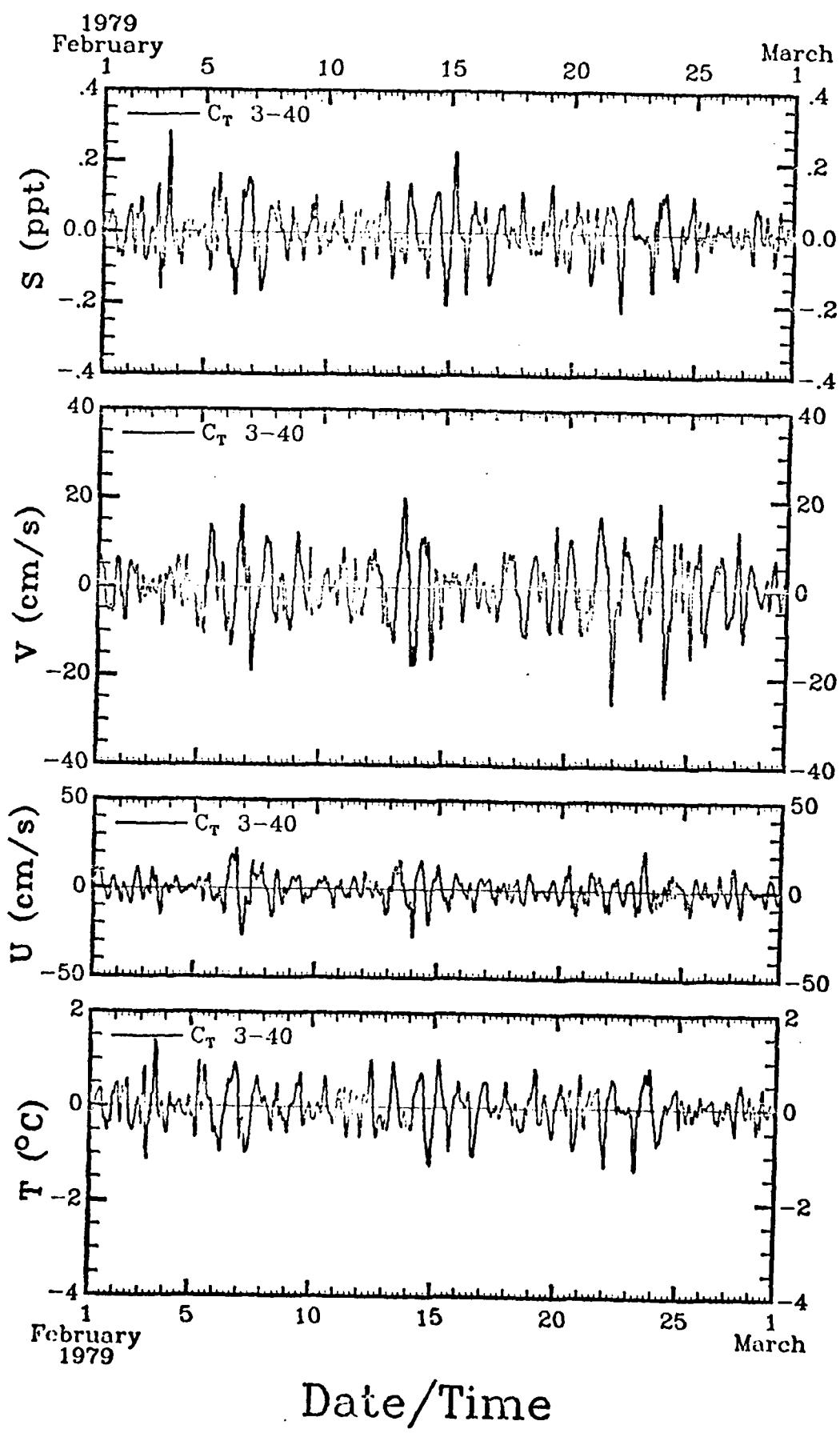


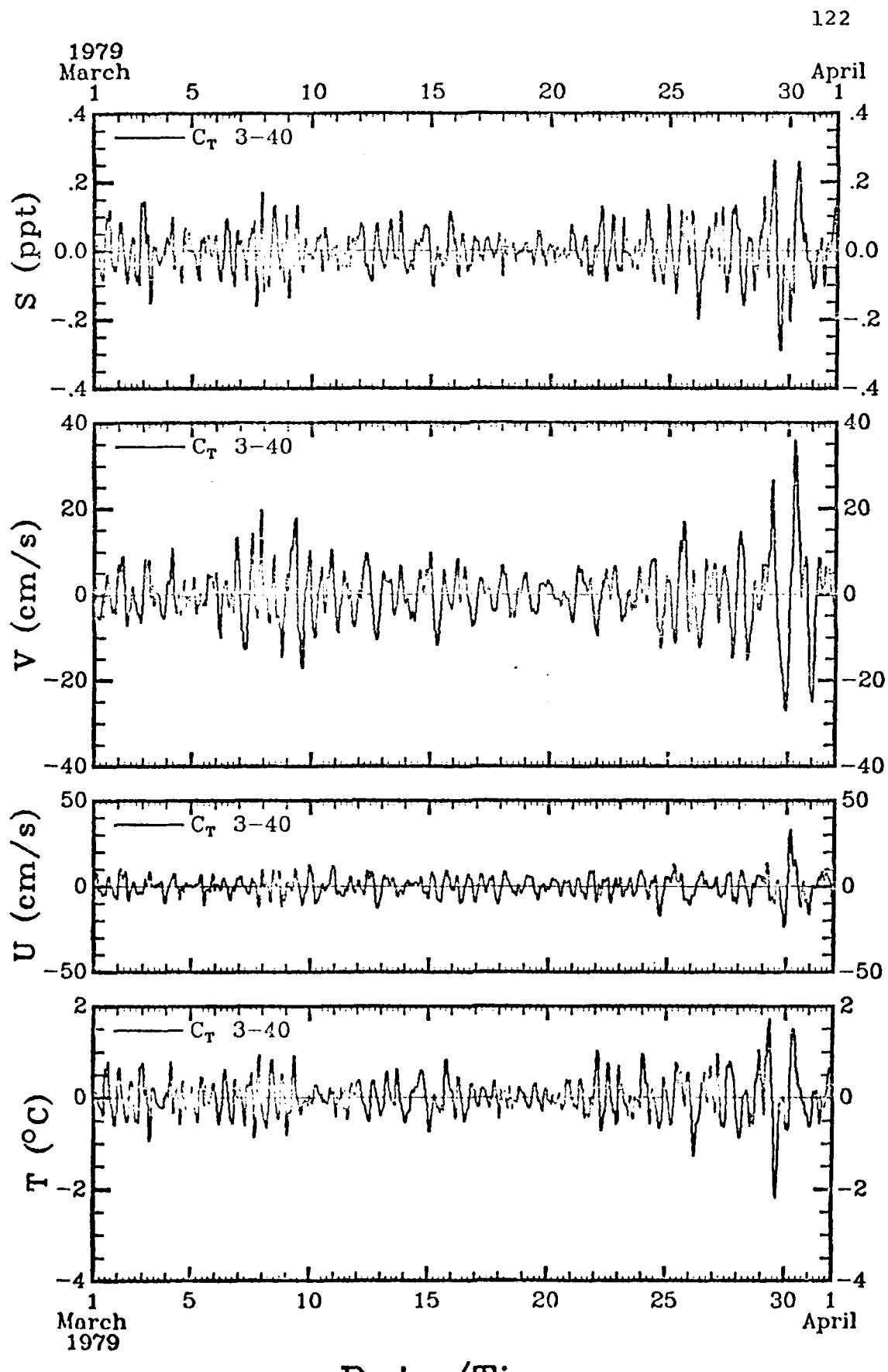


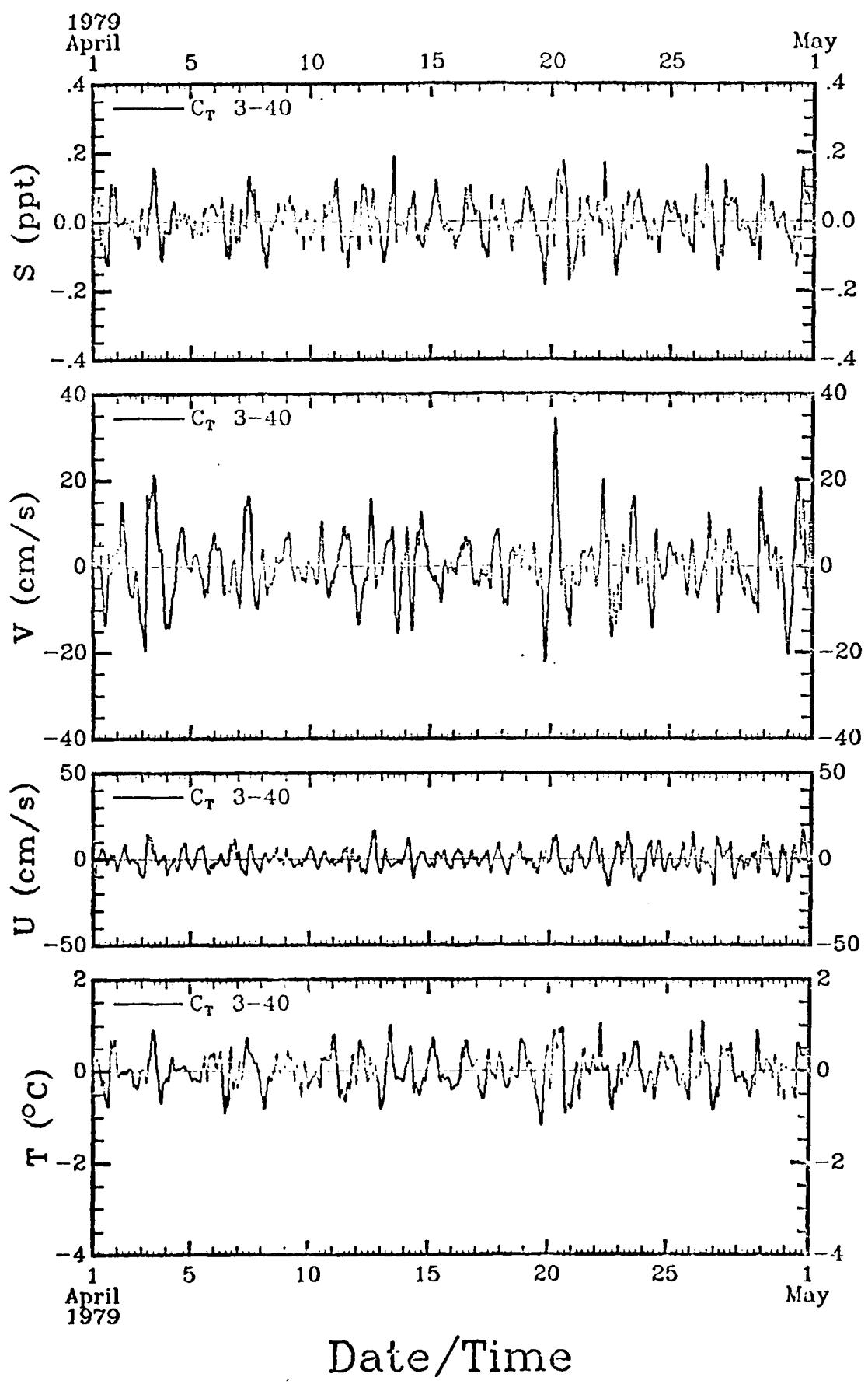




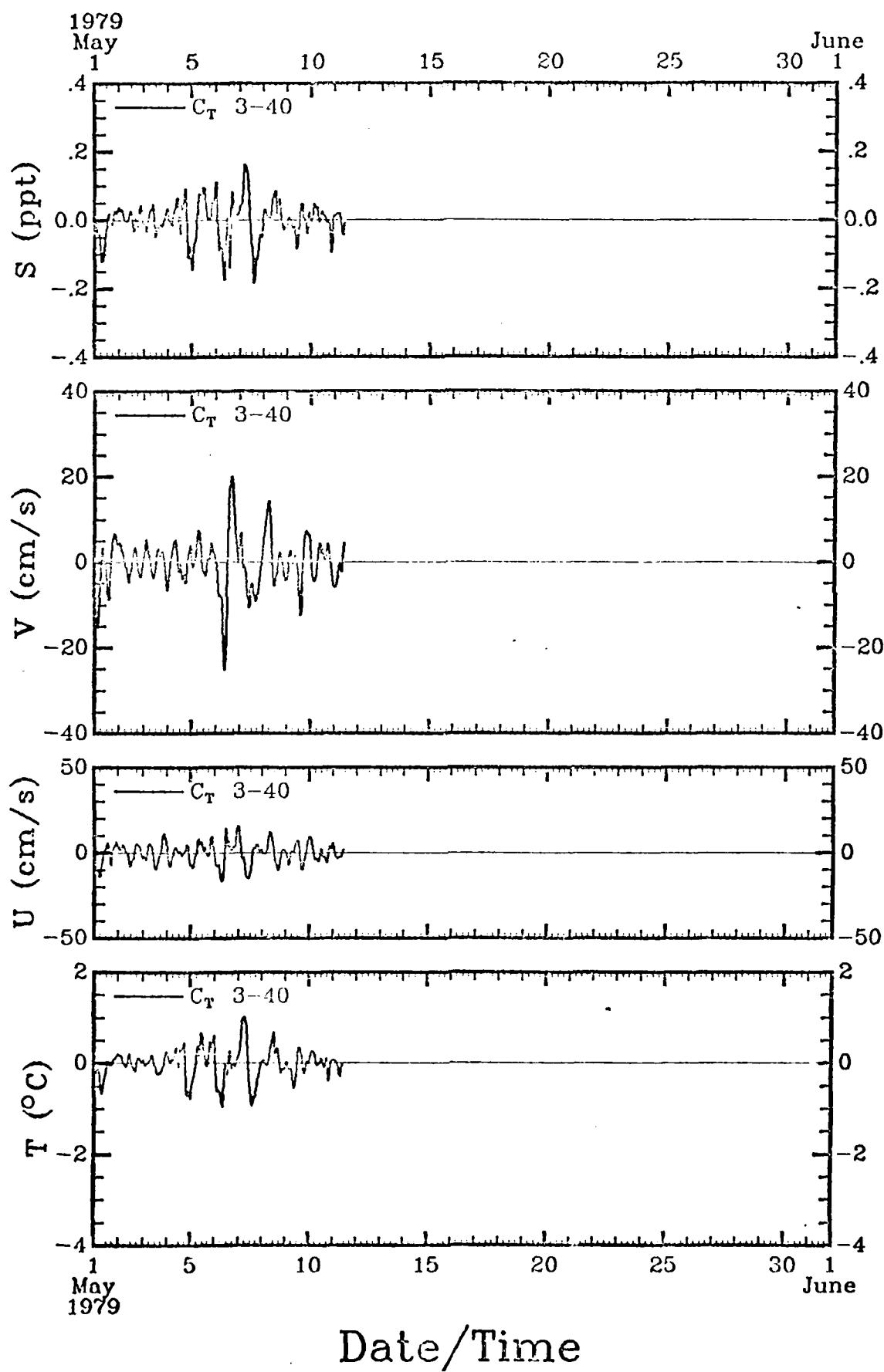




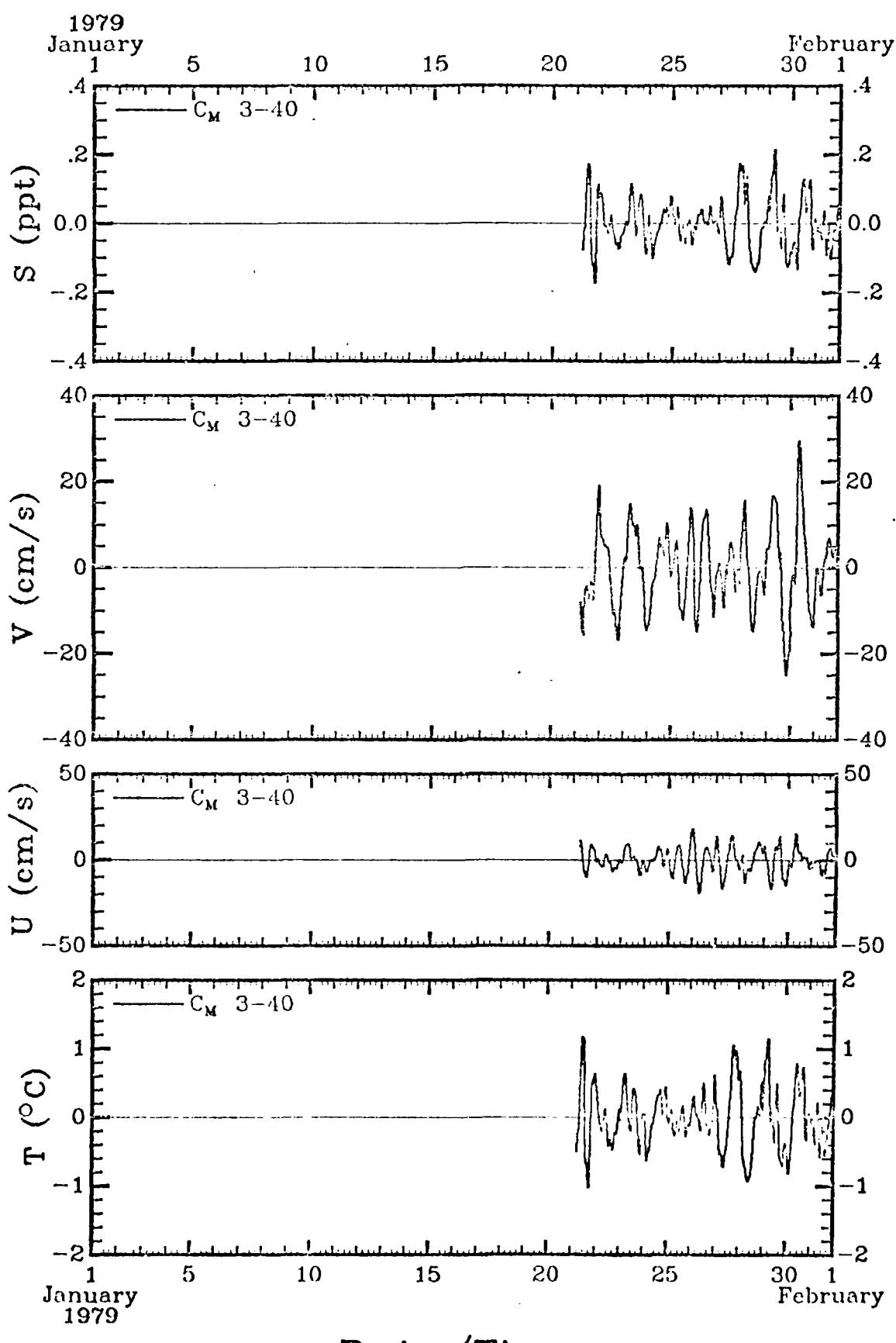




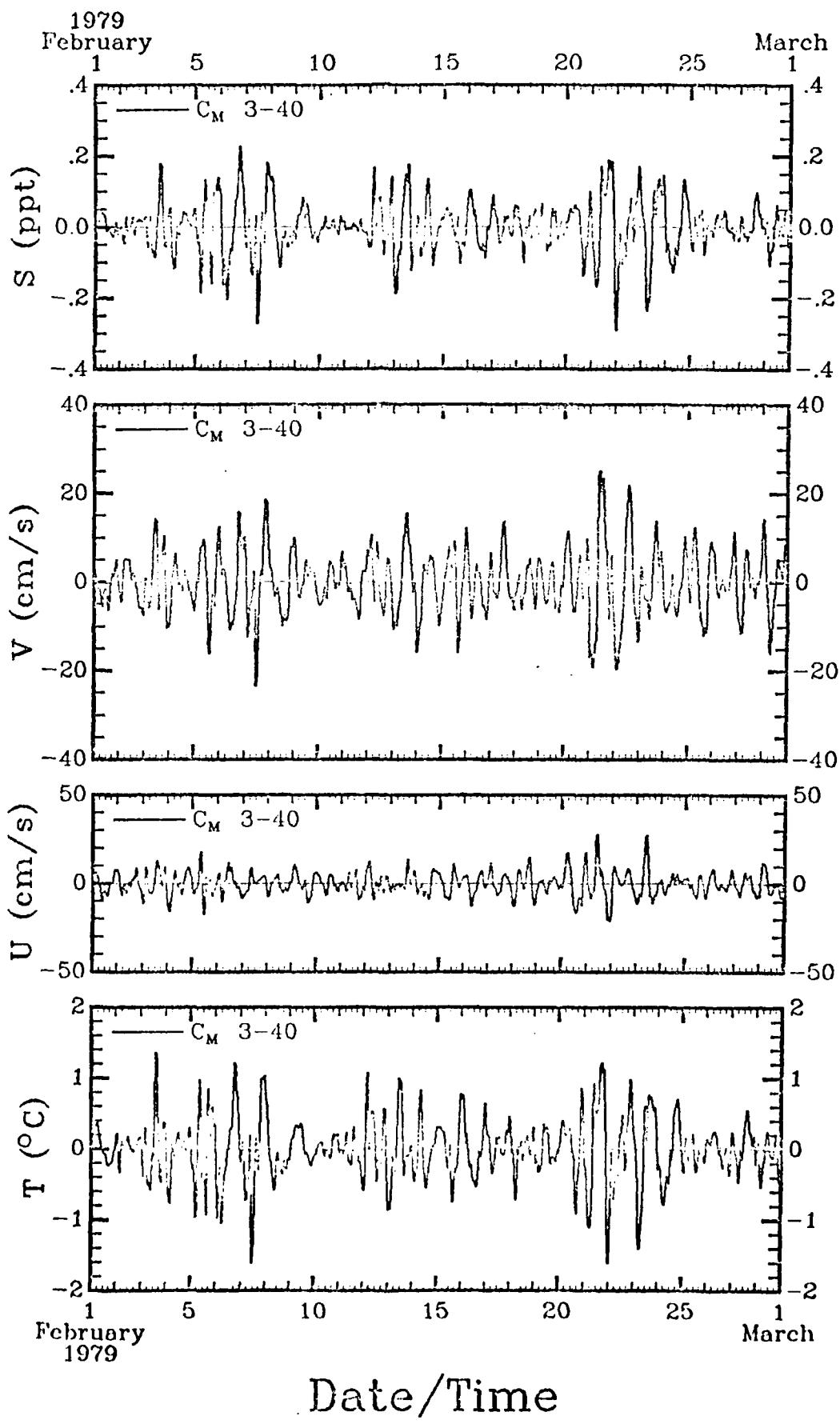
124

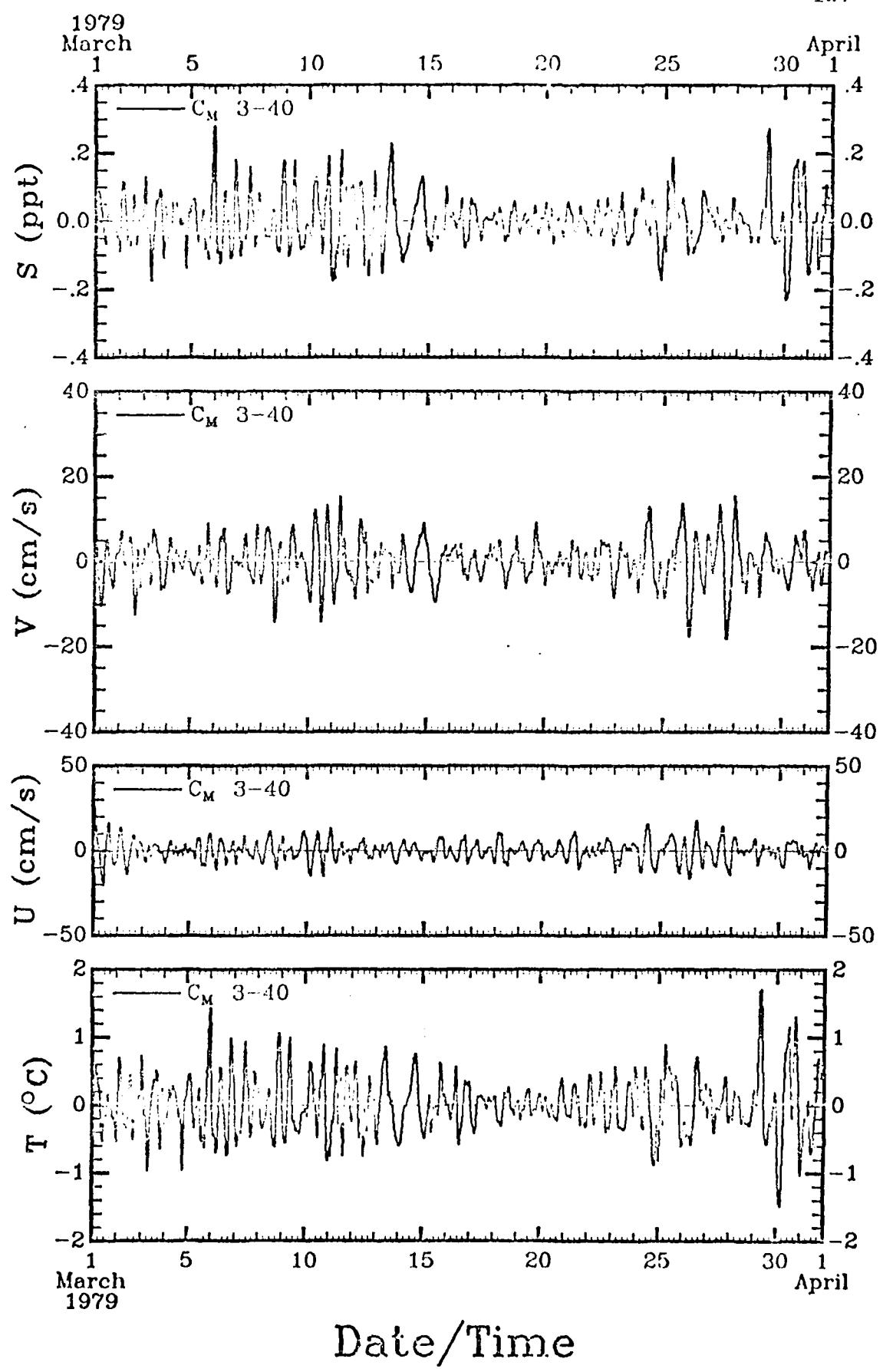


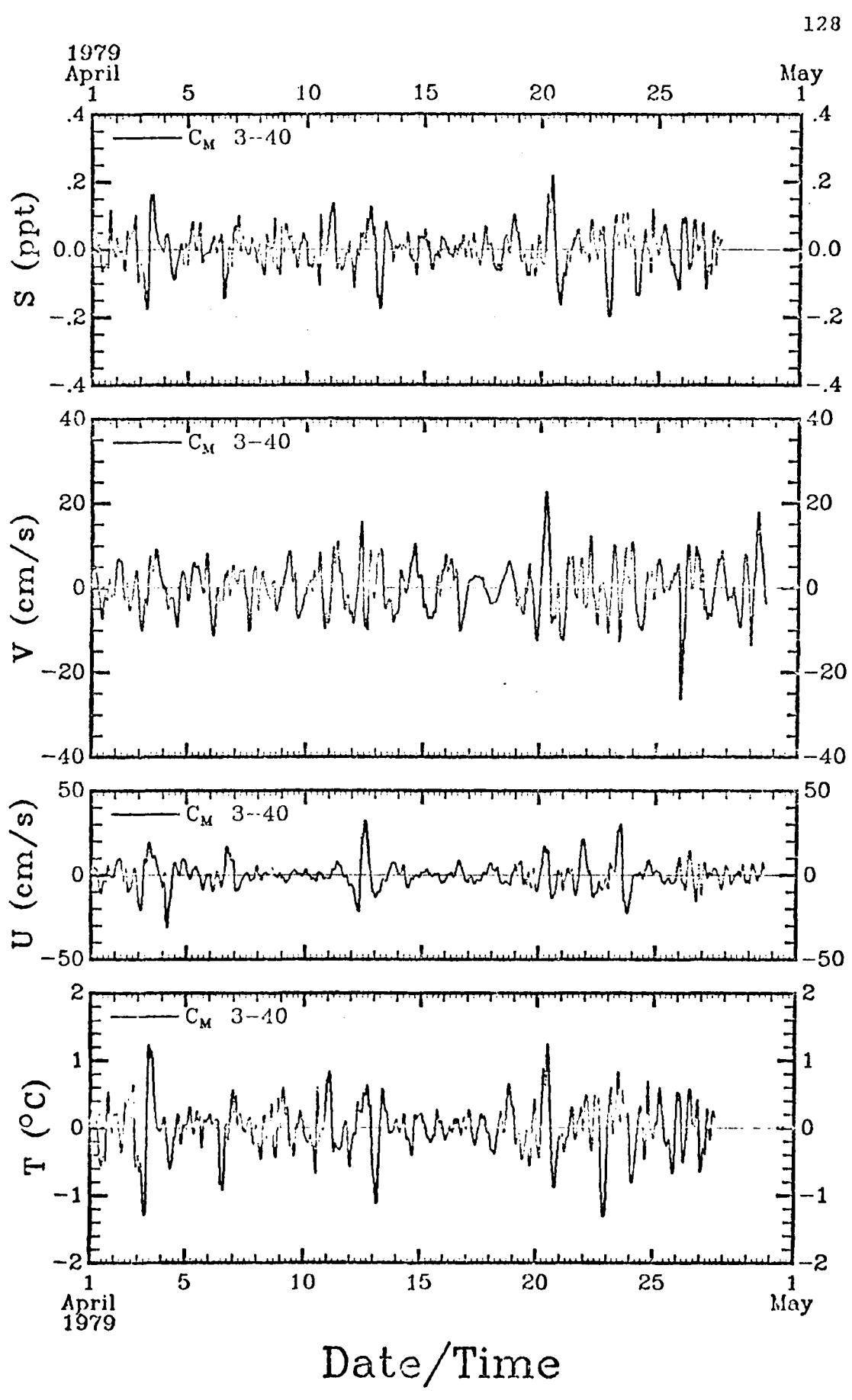
125

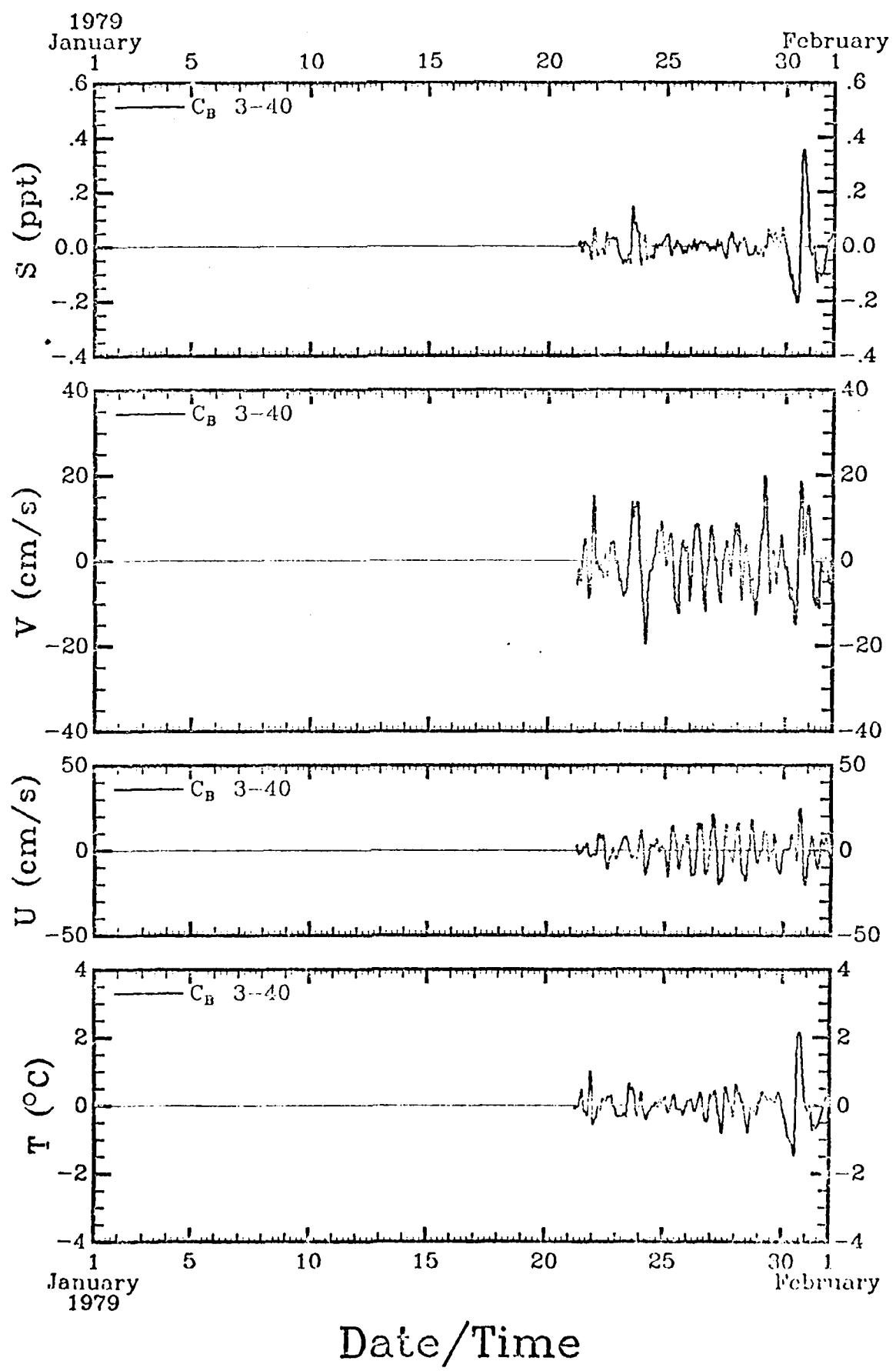


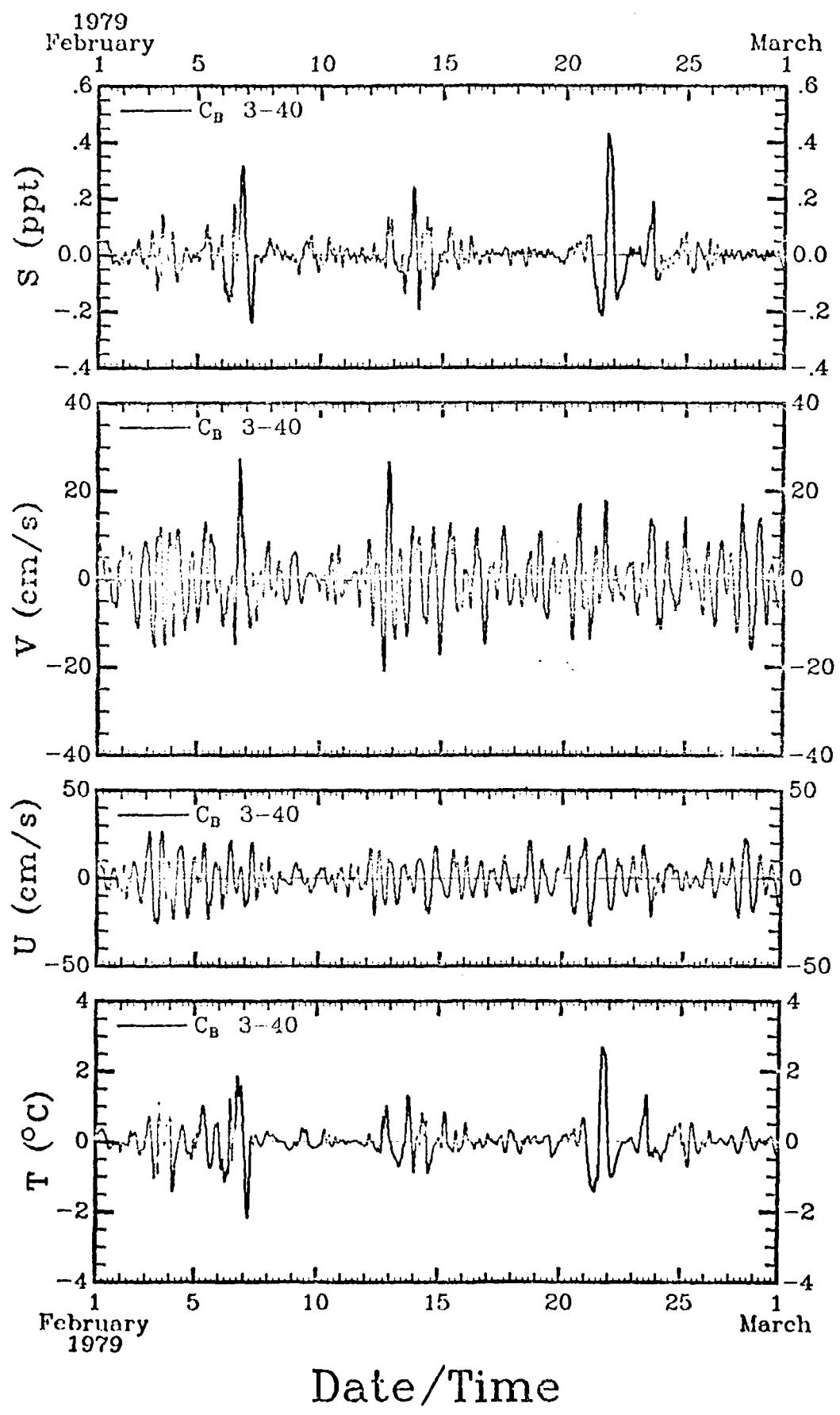
Date/Time

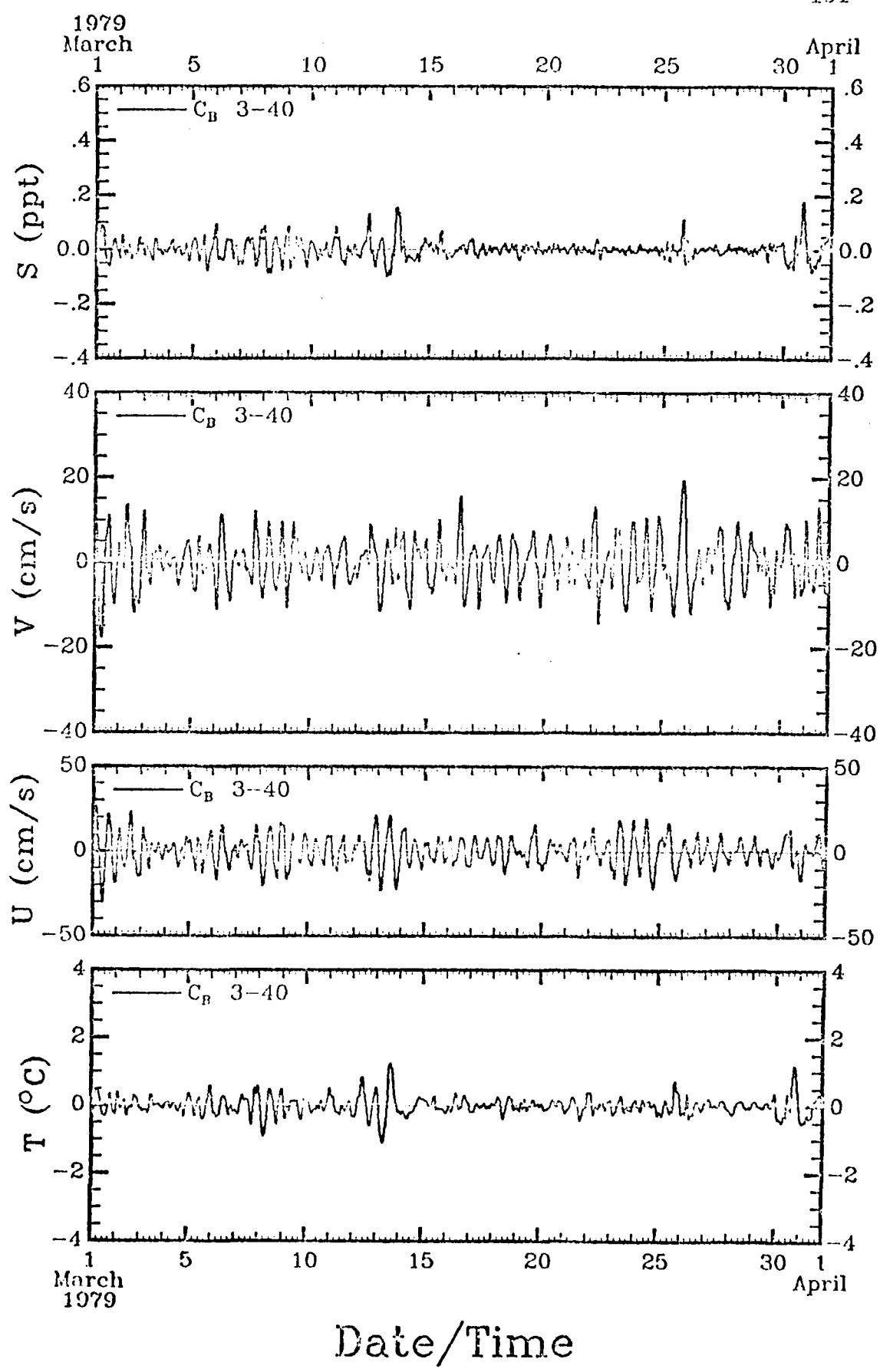


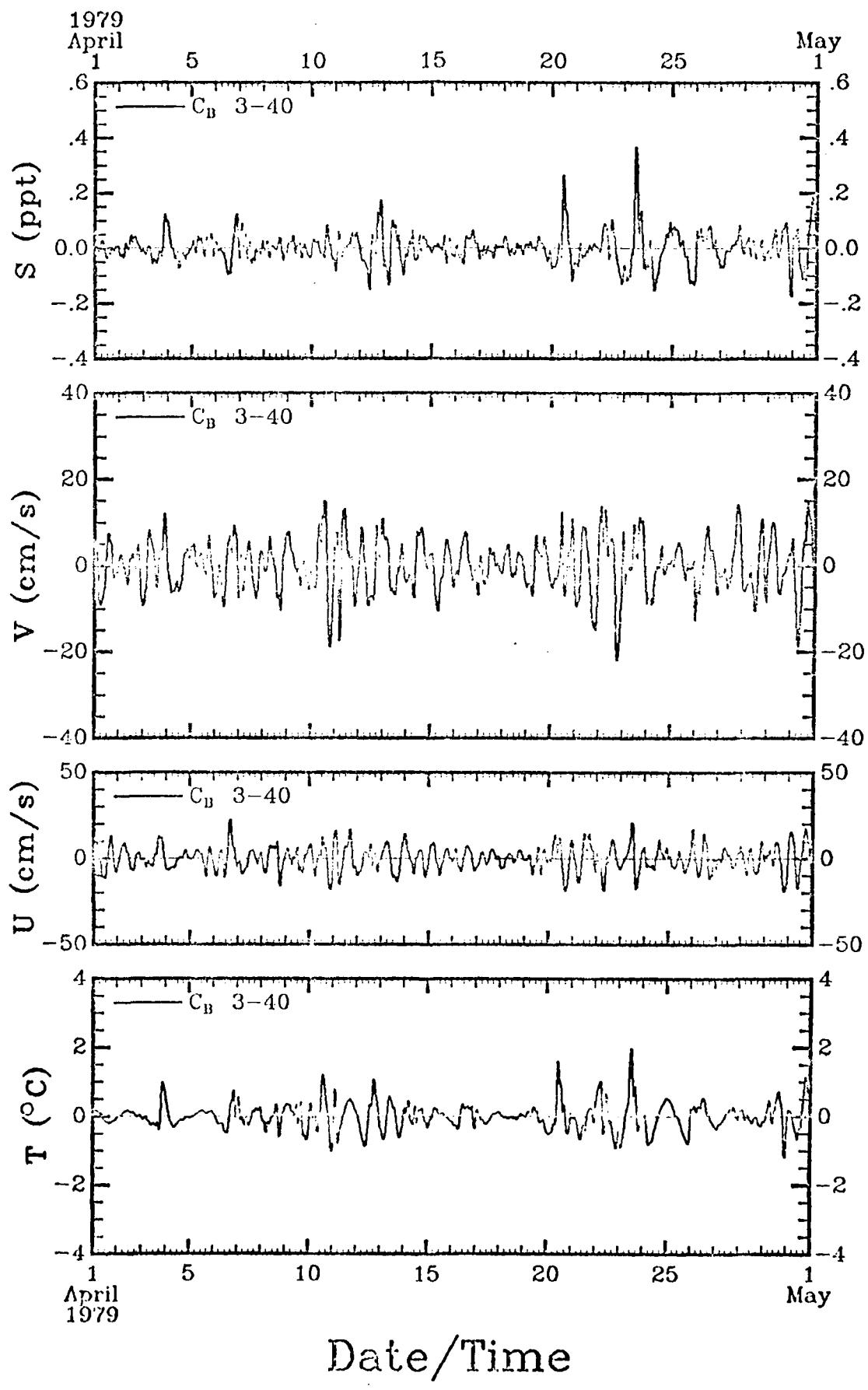


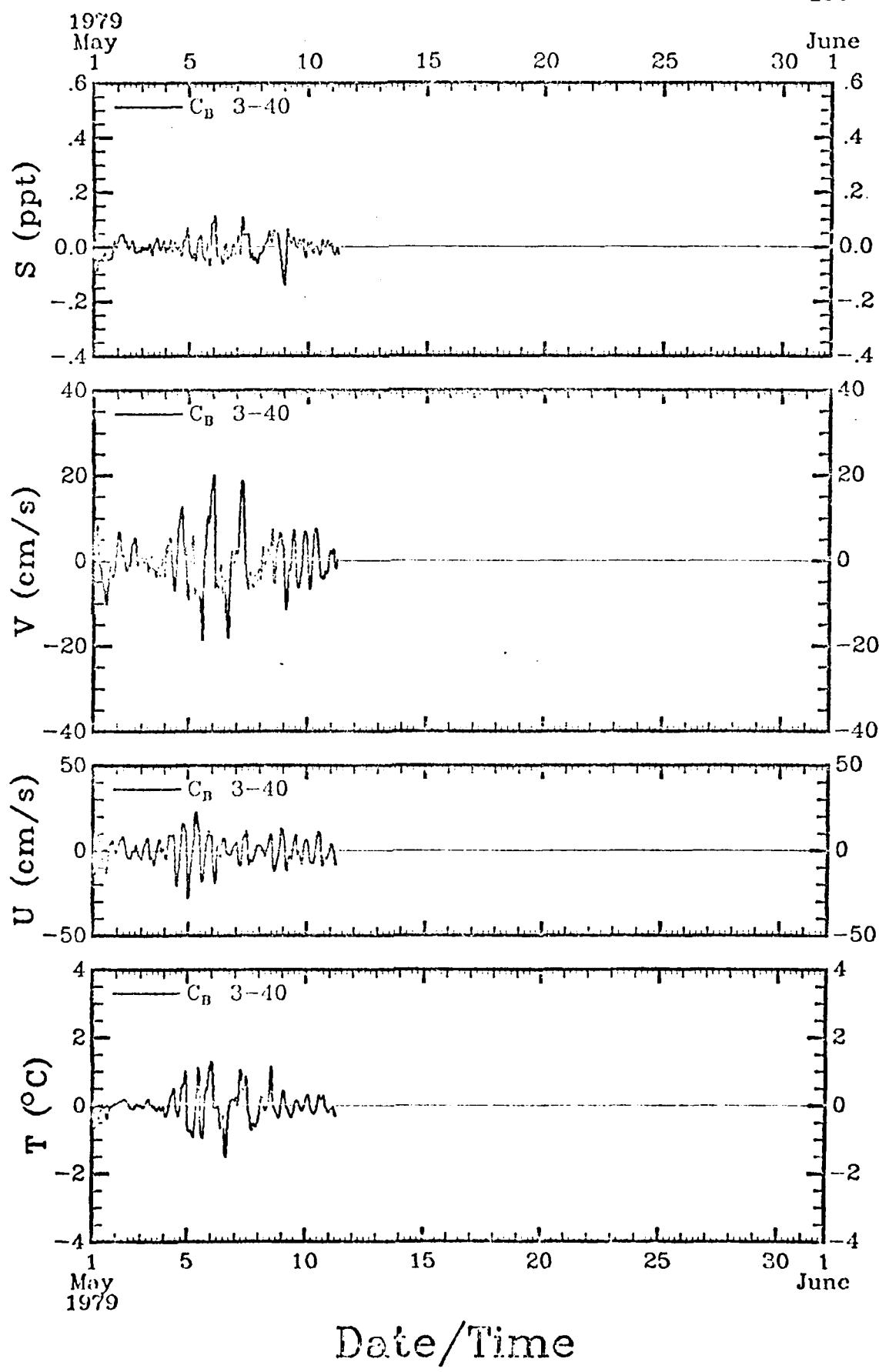


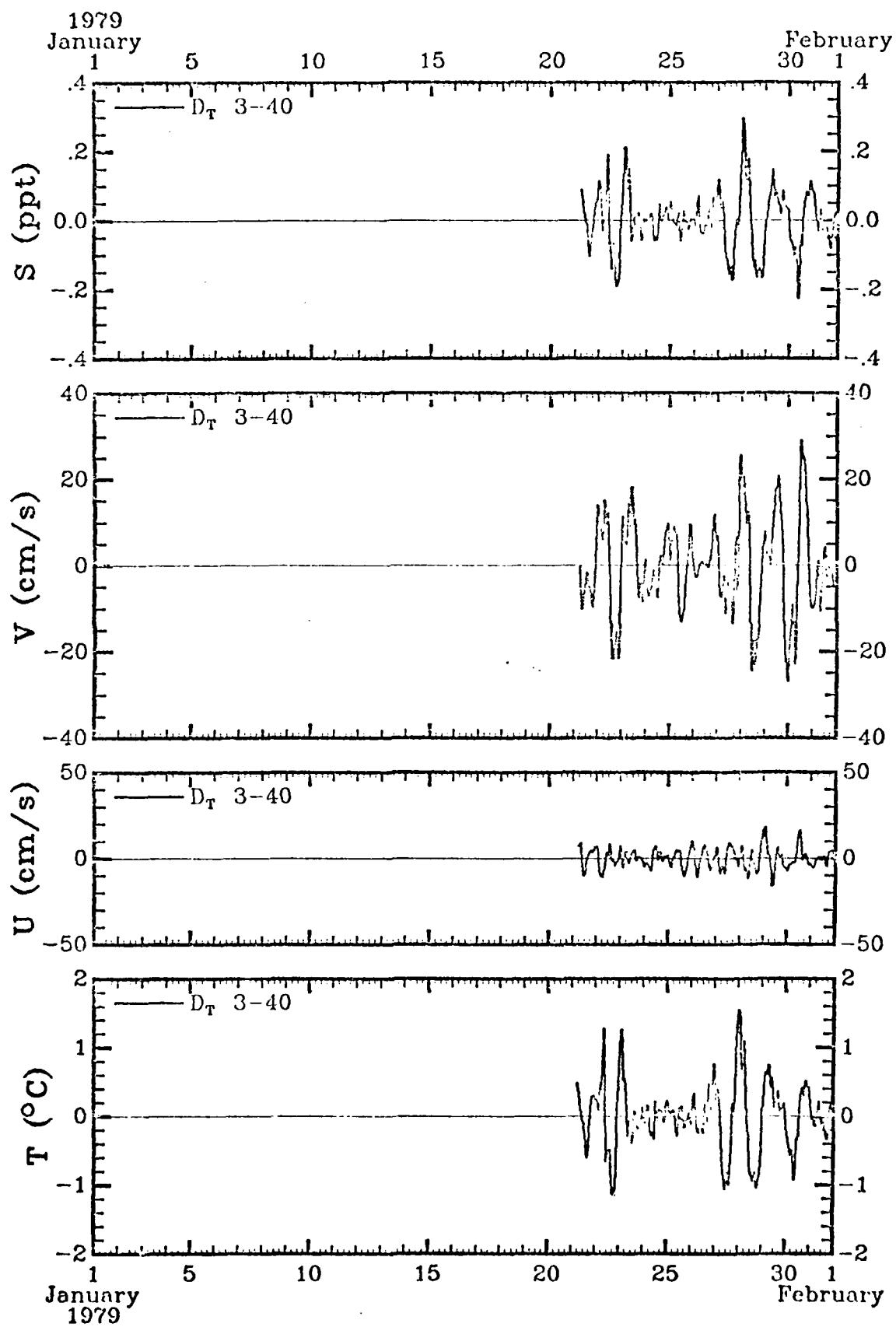




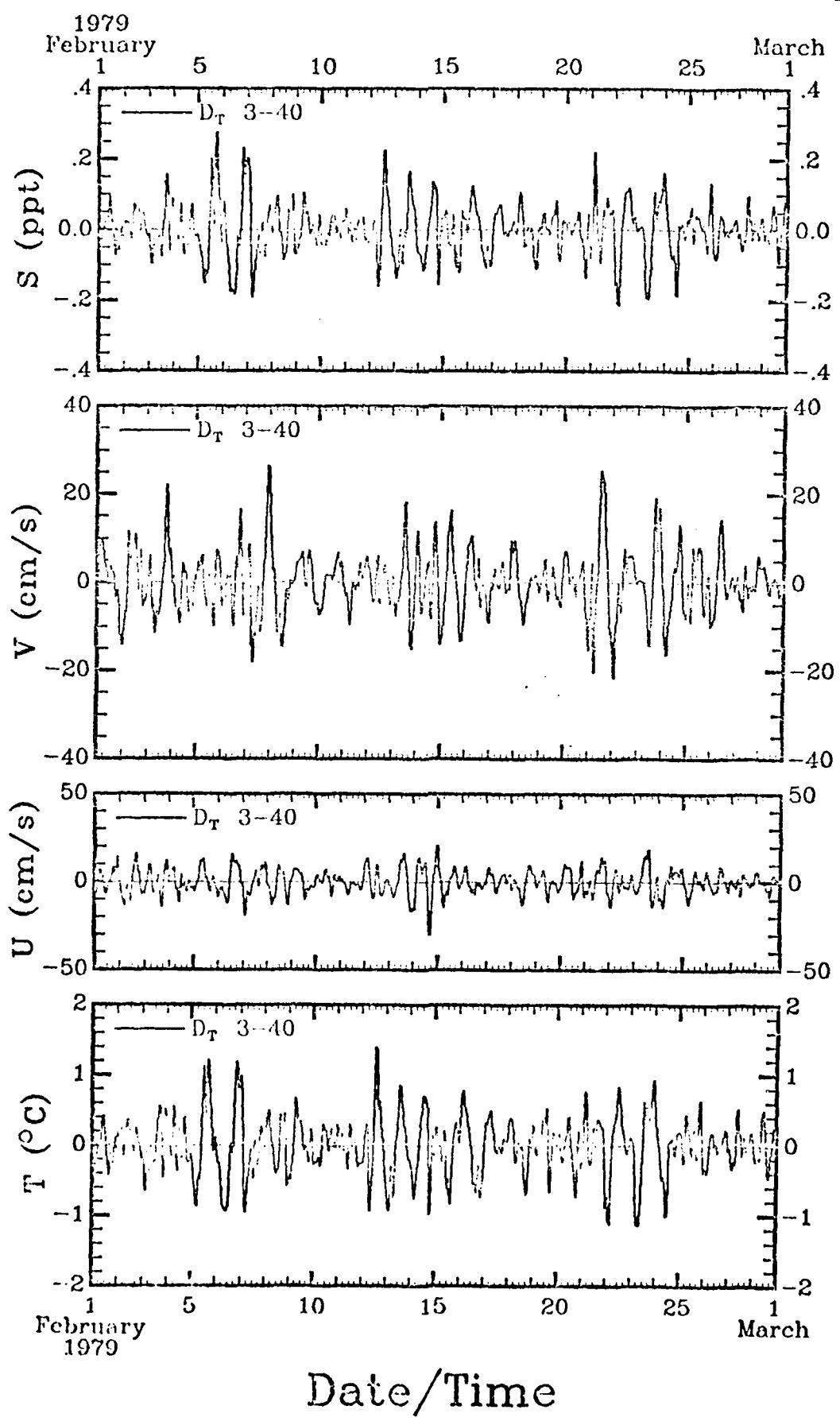




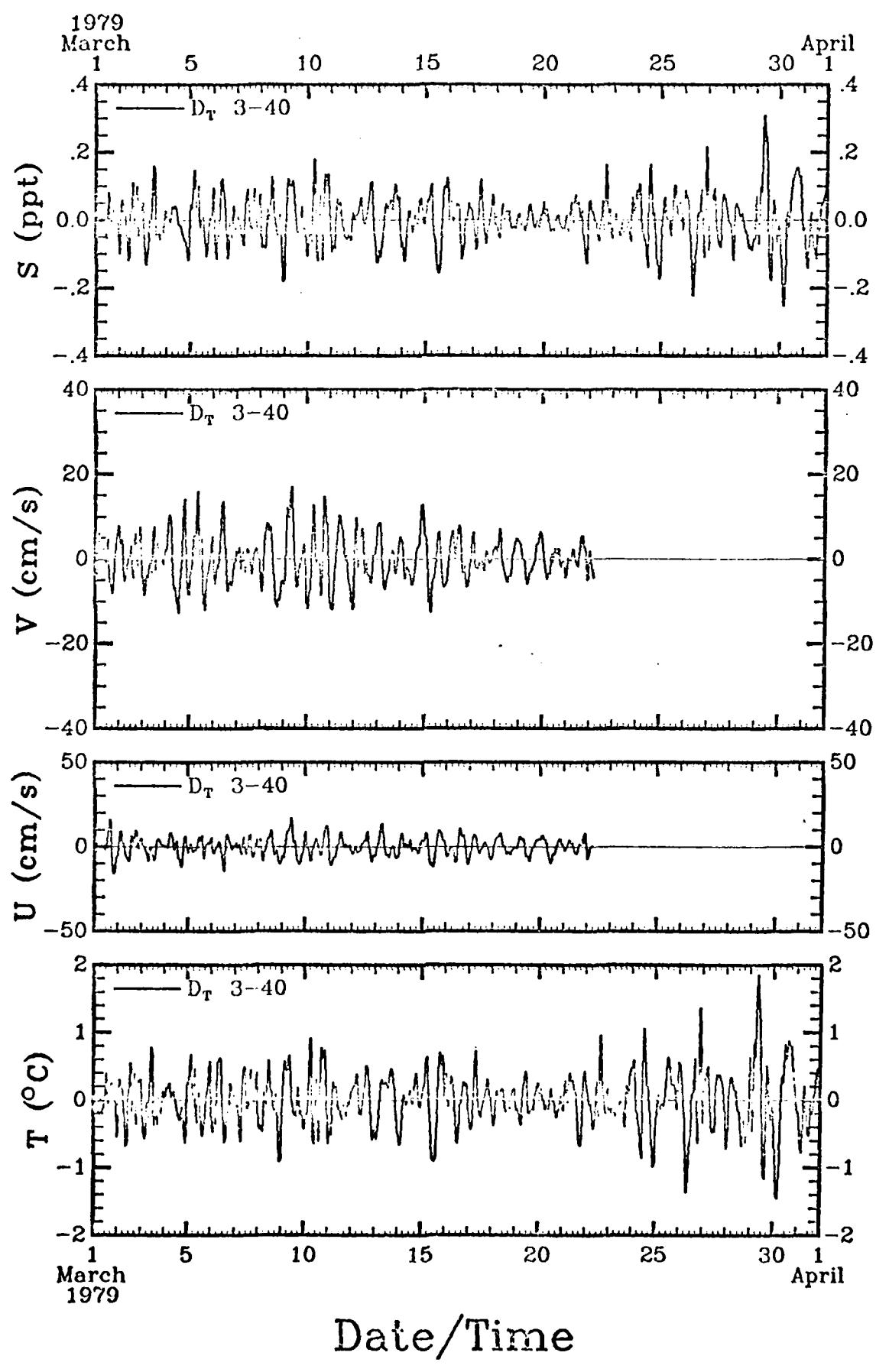


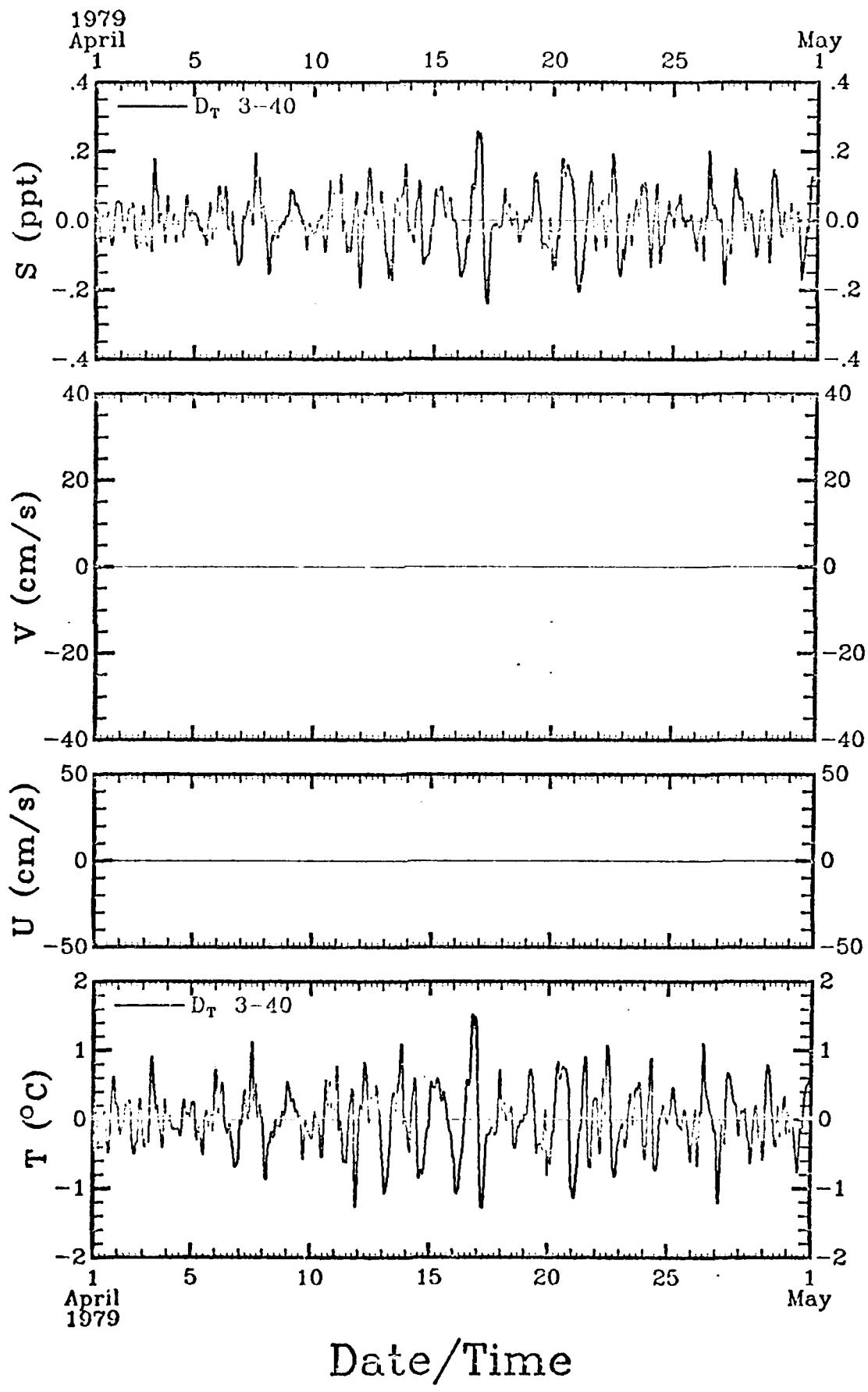


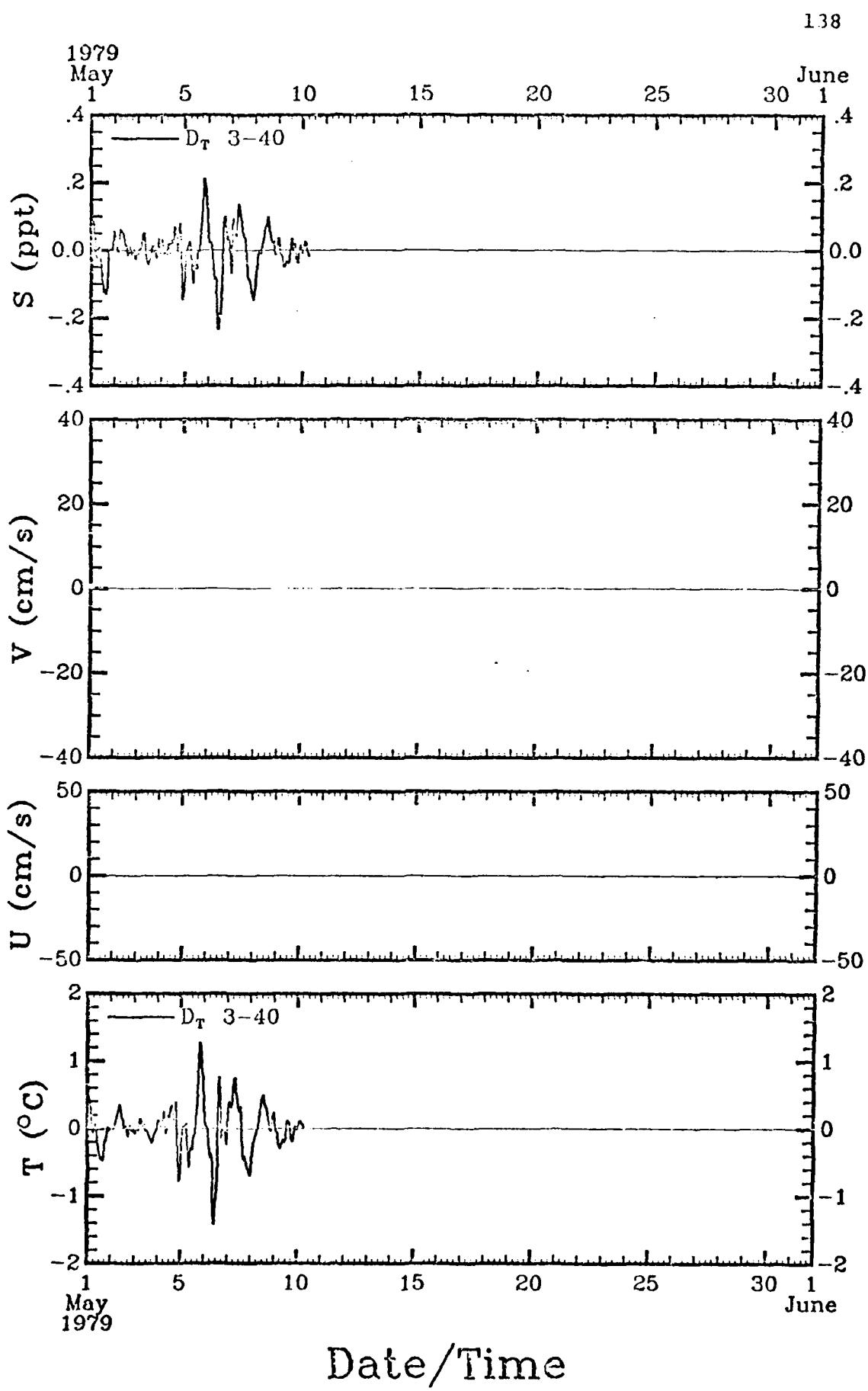
Date/Time

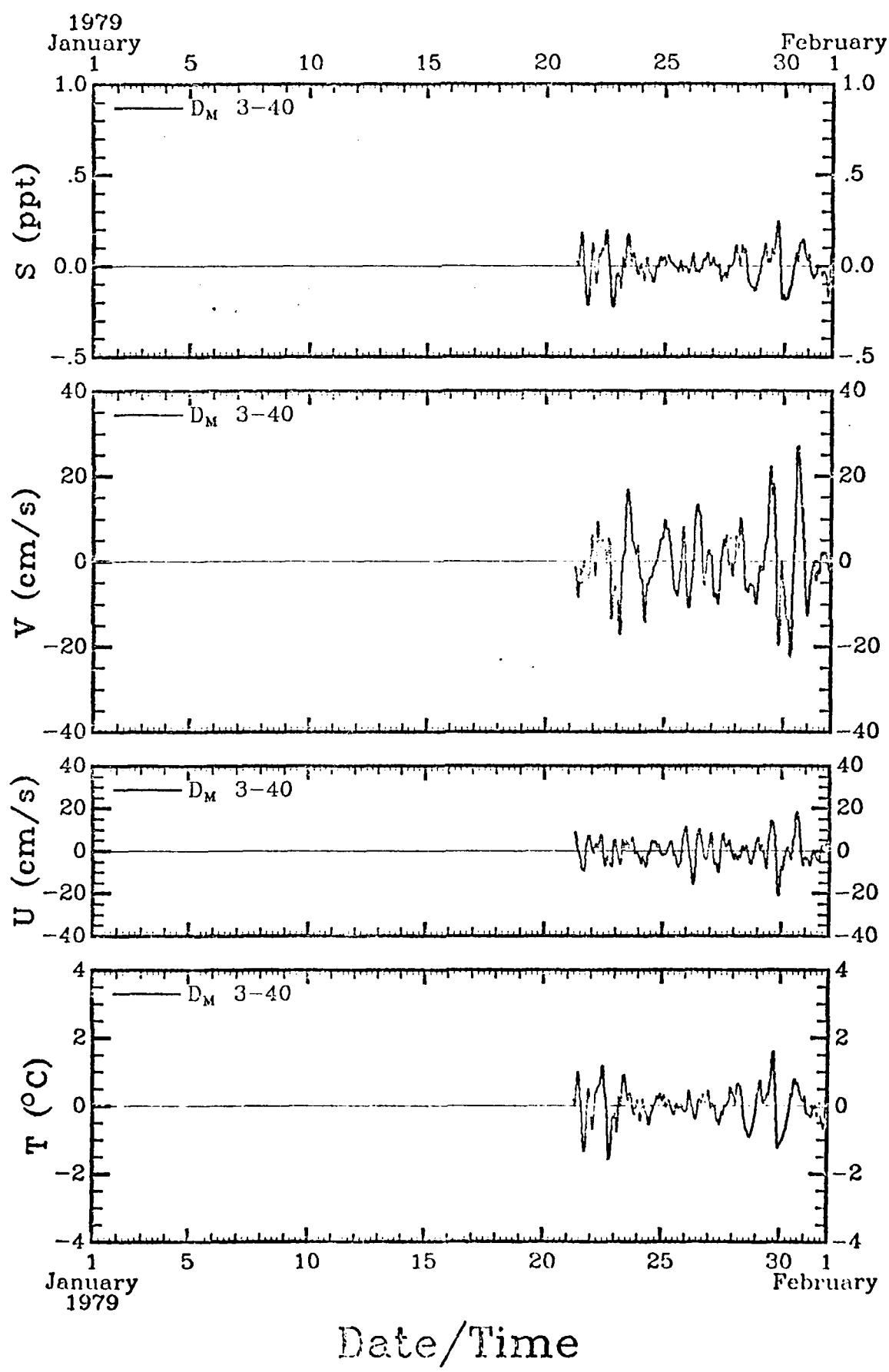


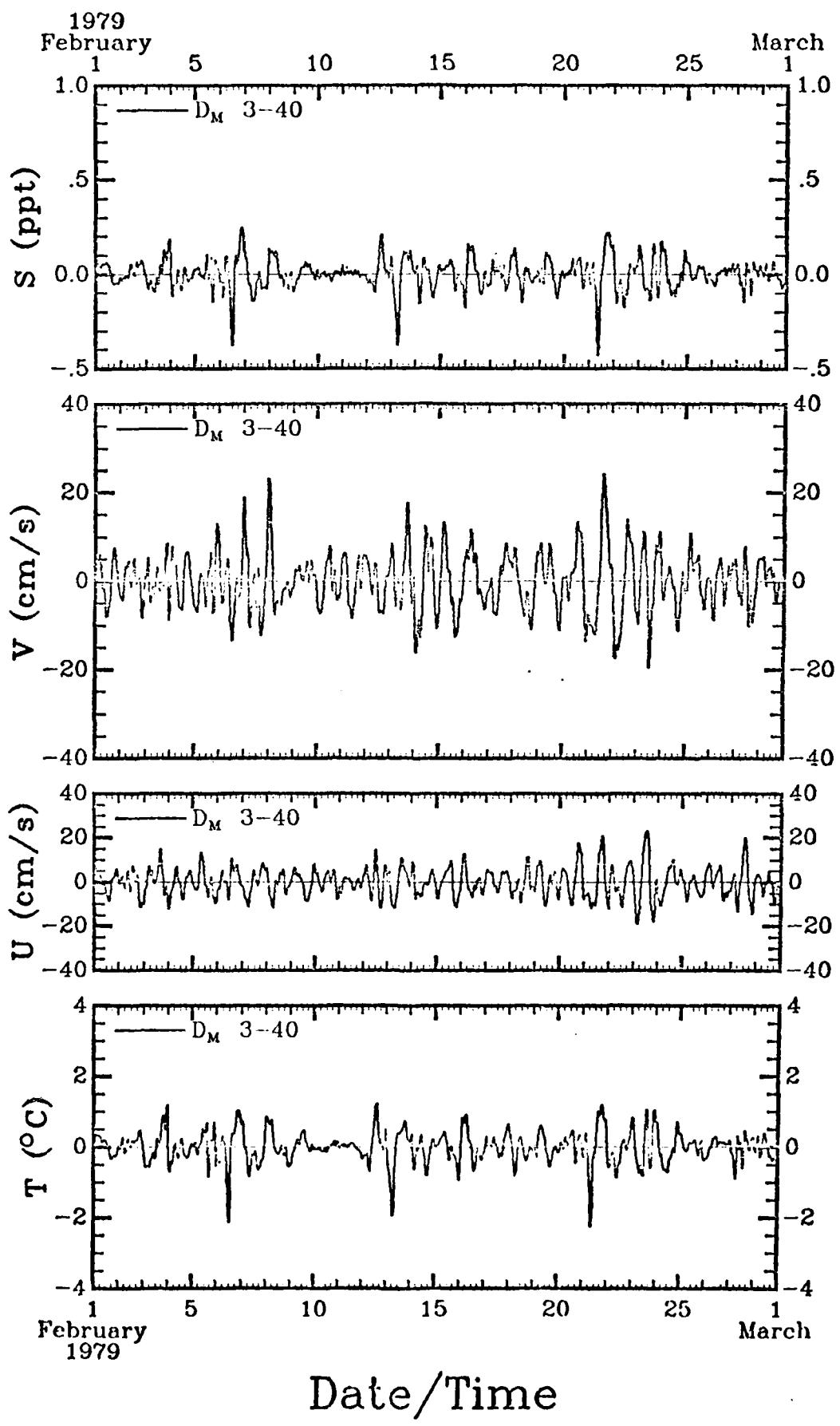
136

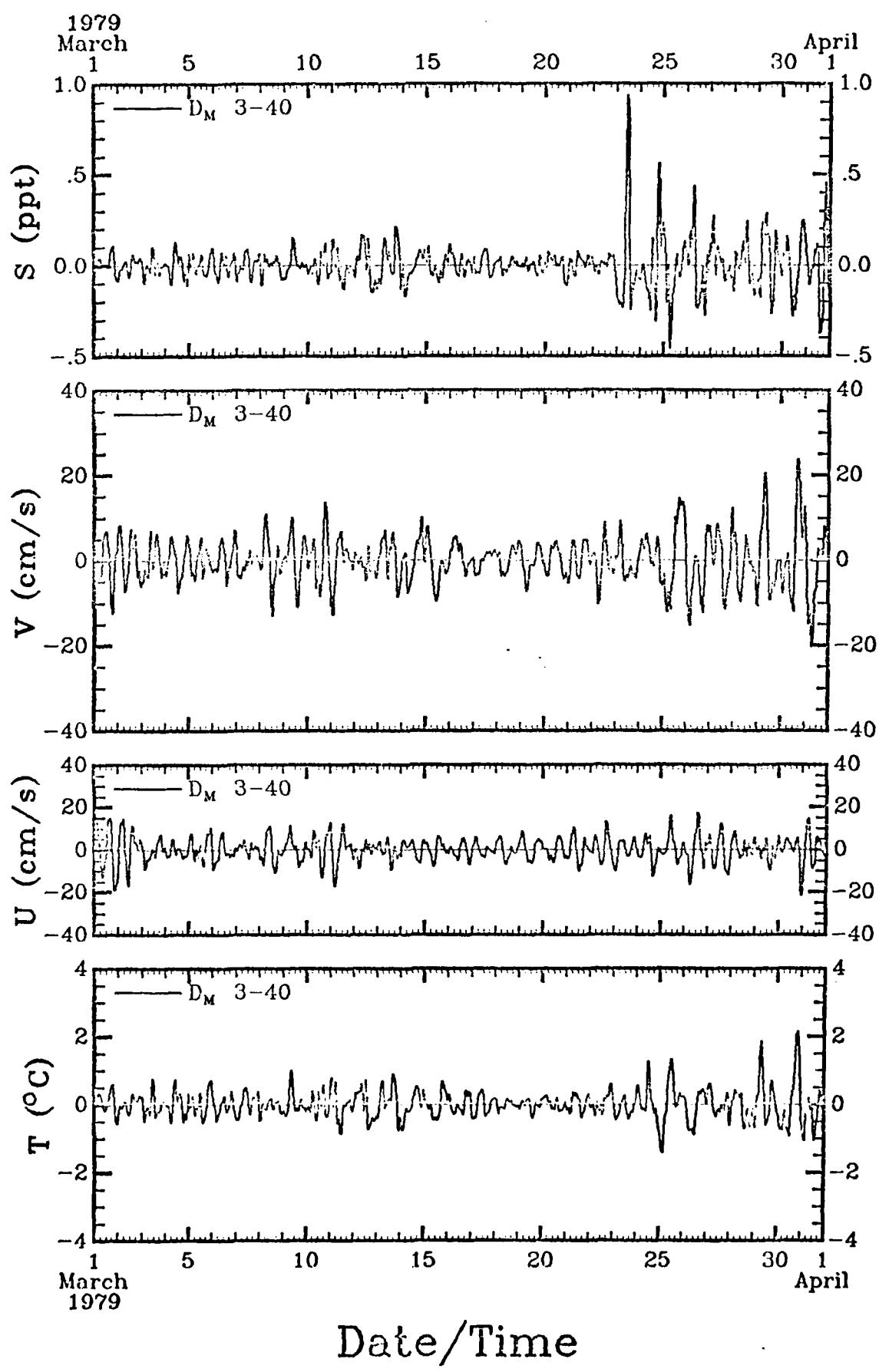


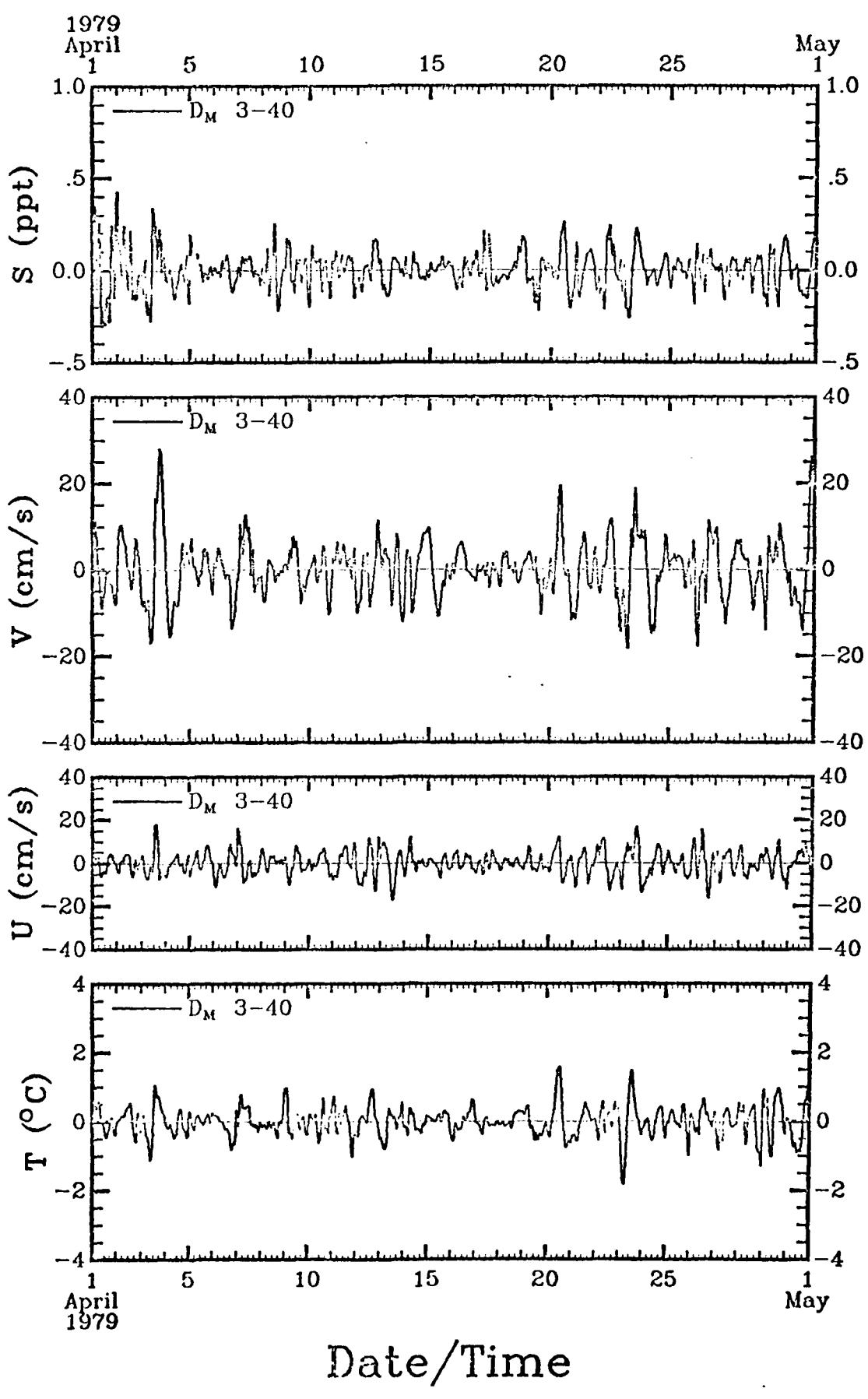


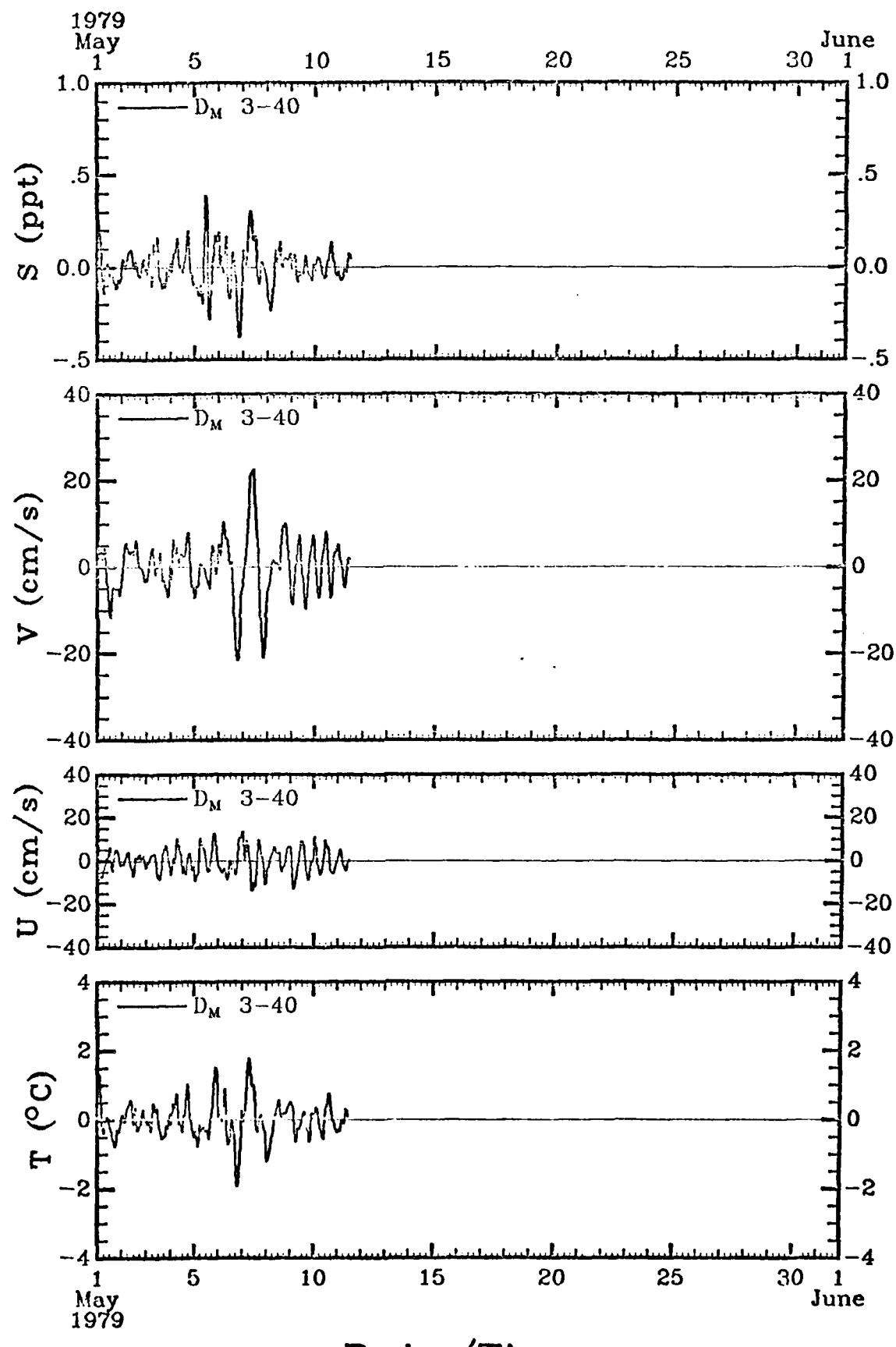




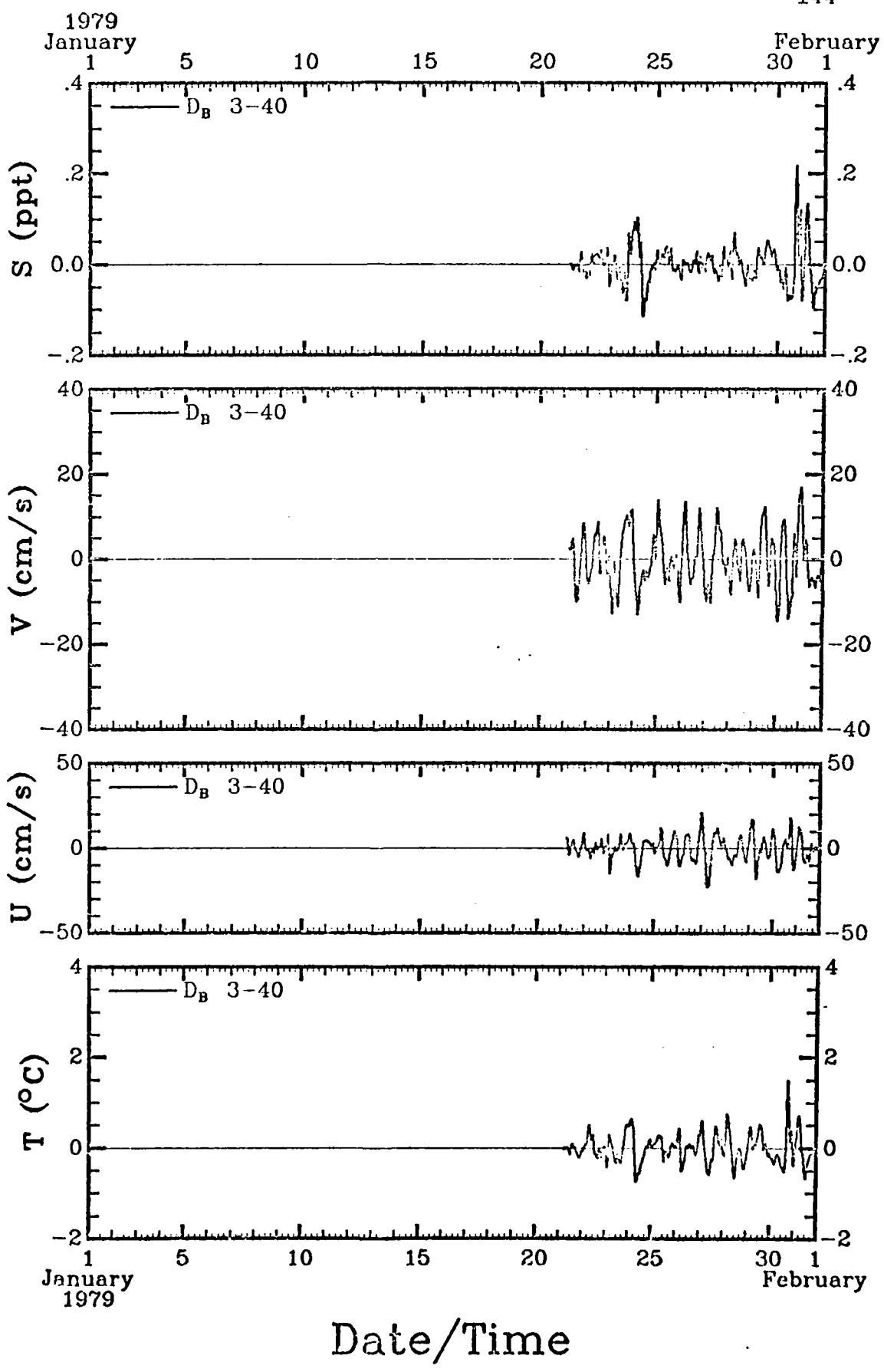


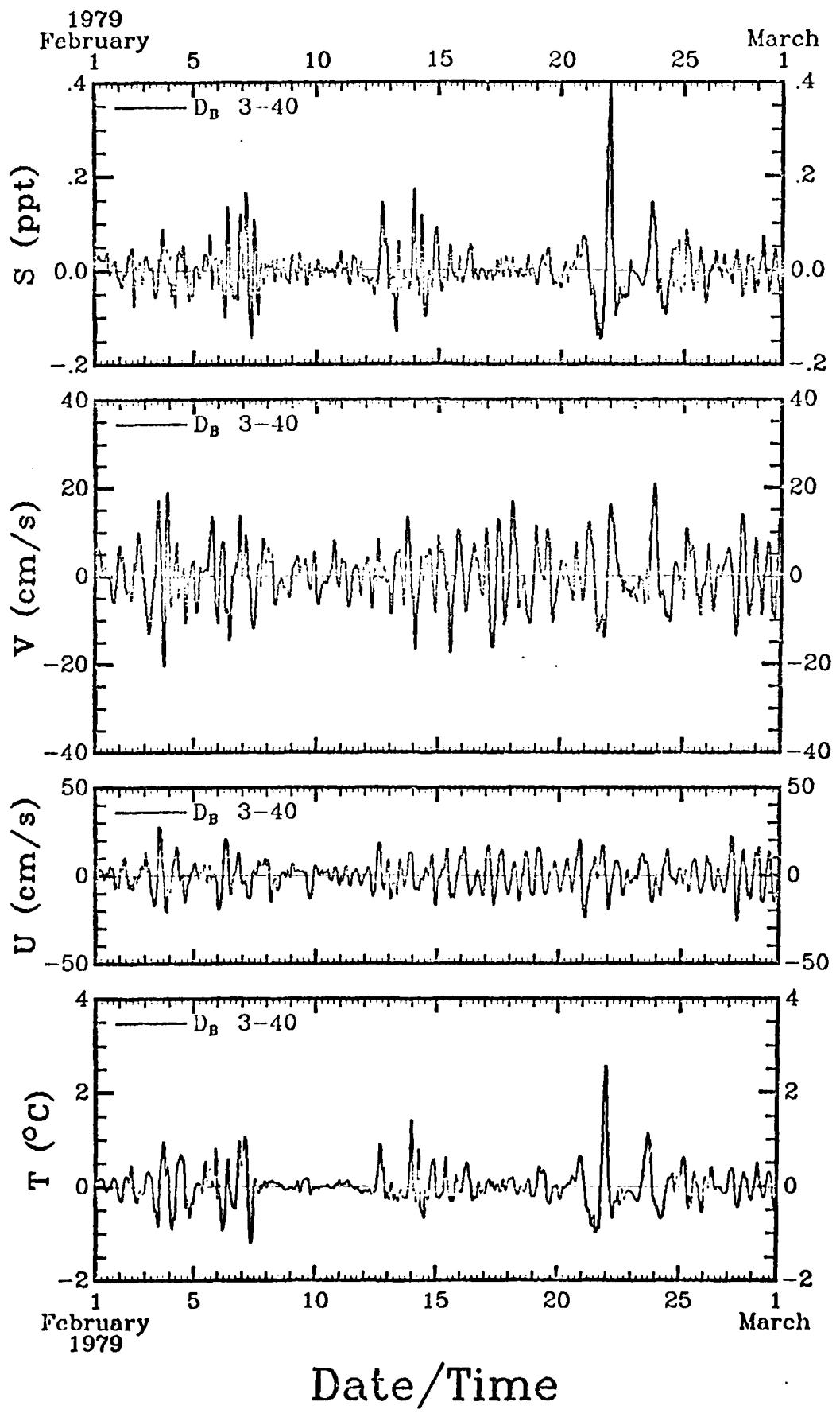


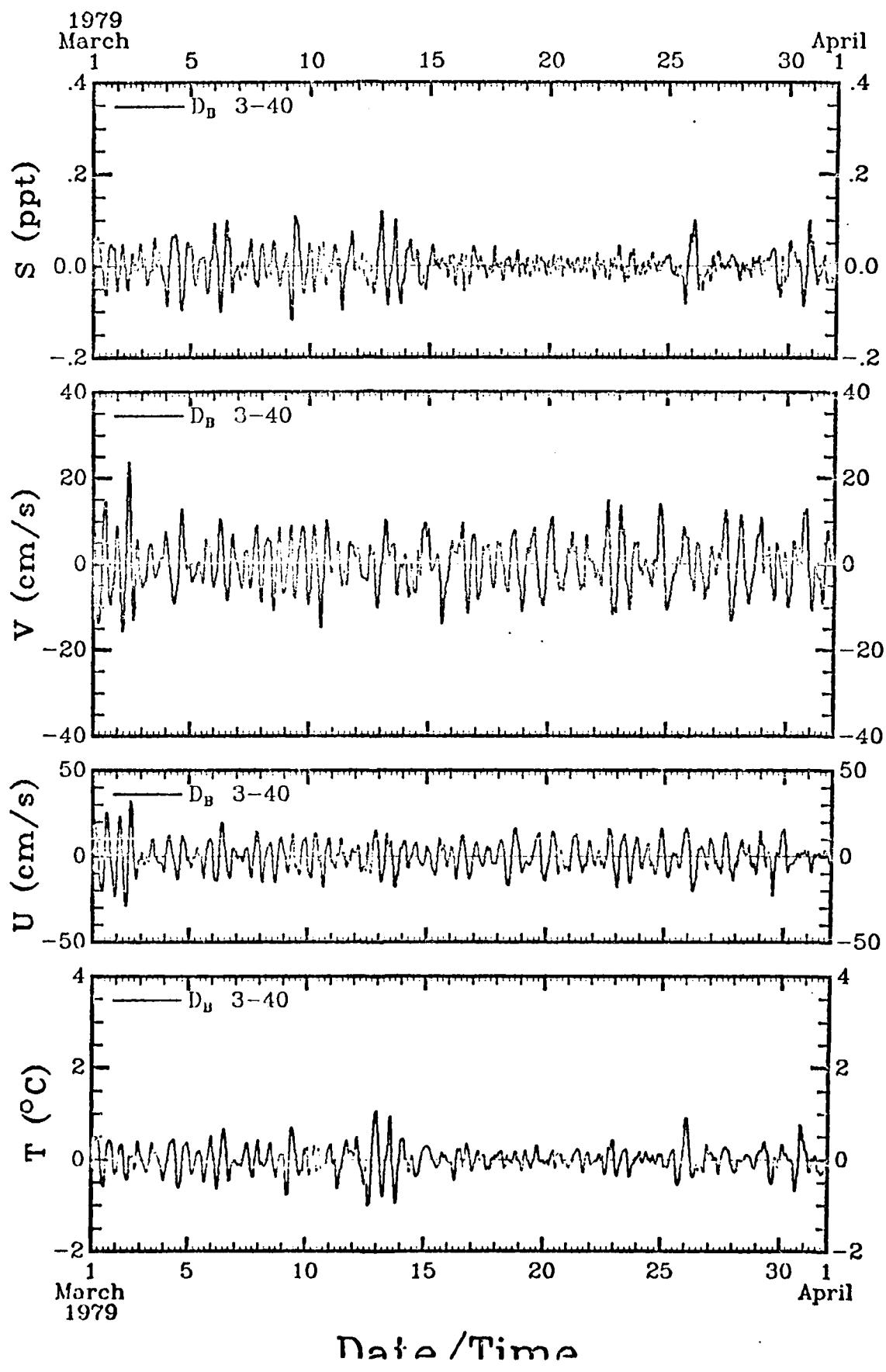


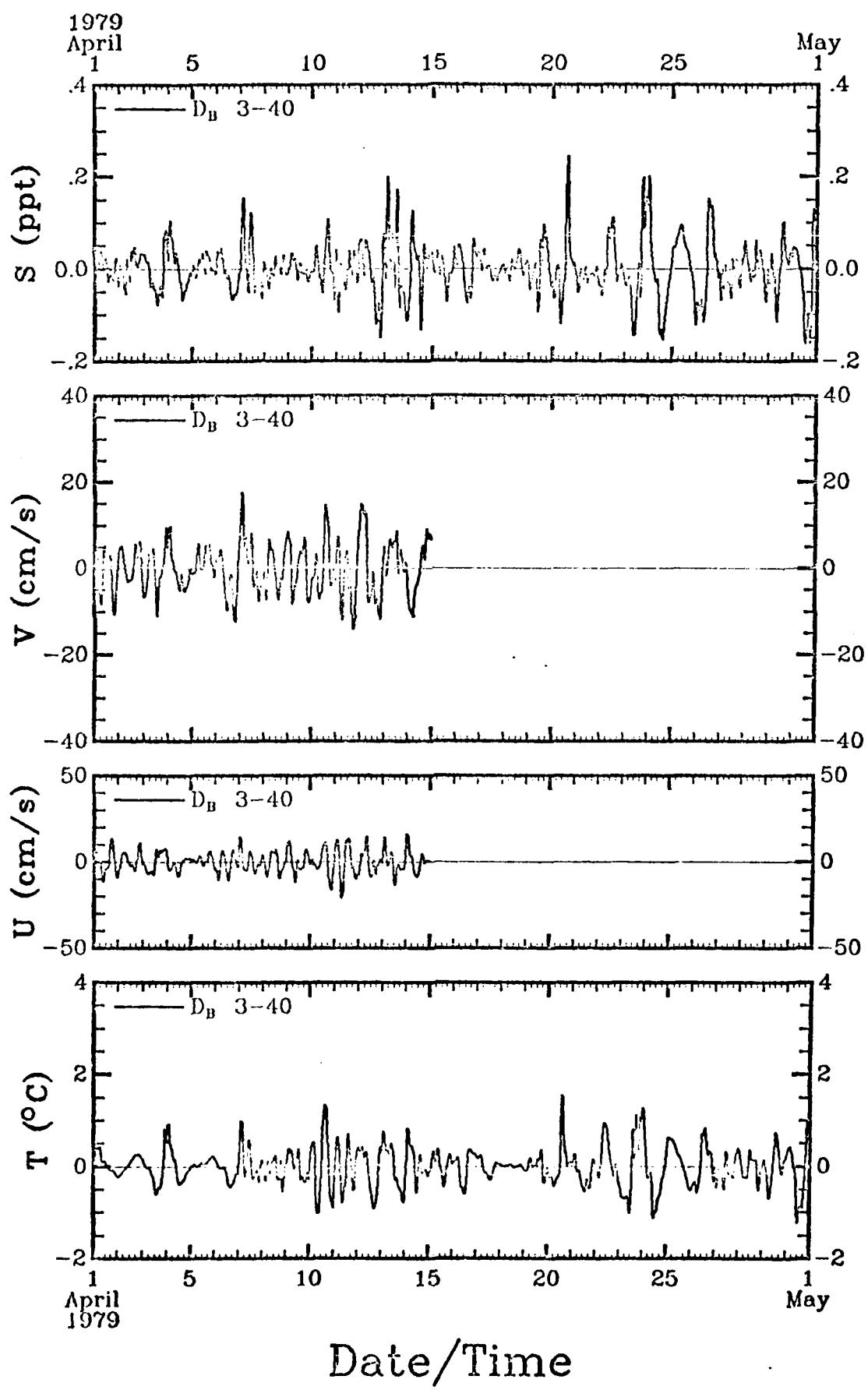


Date/Time

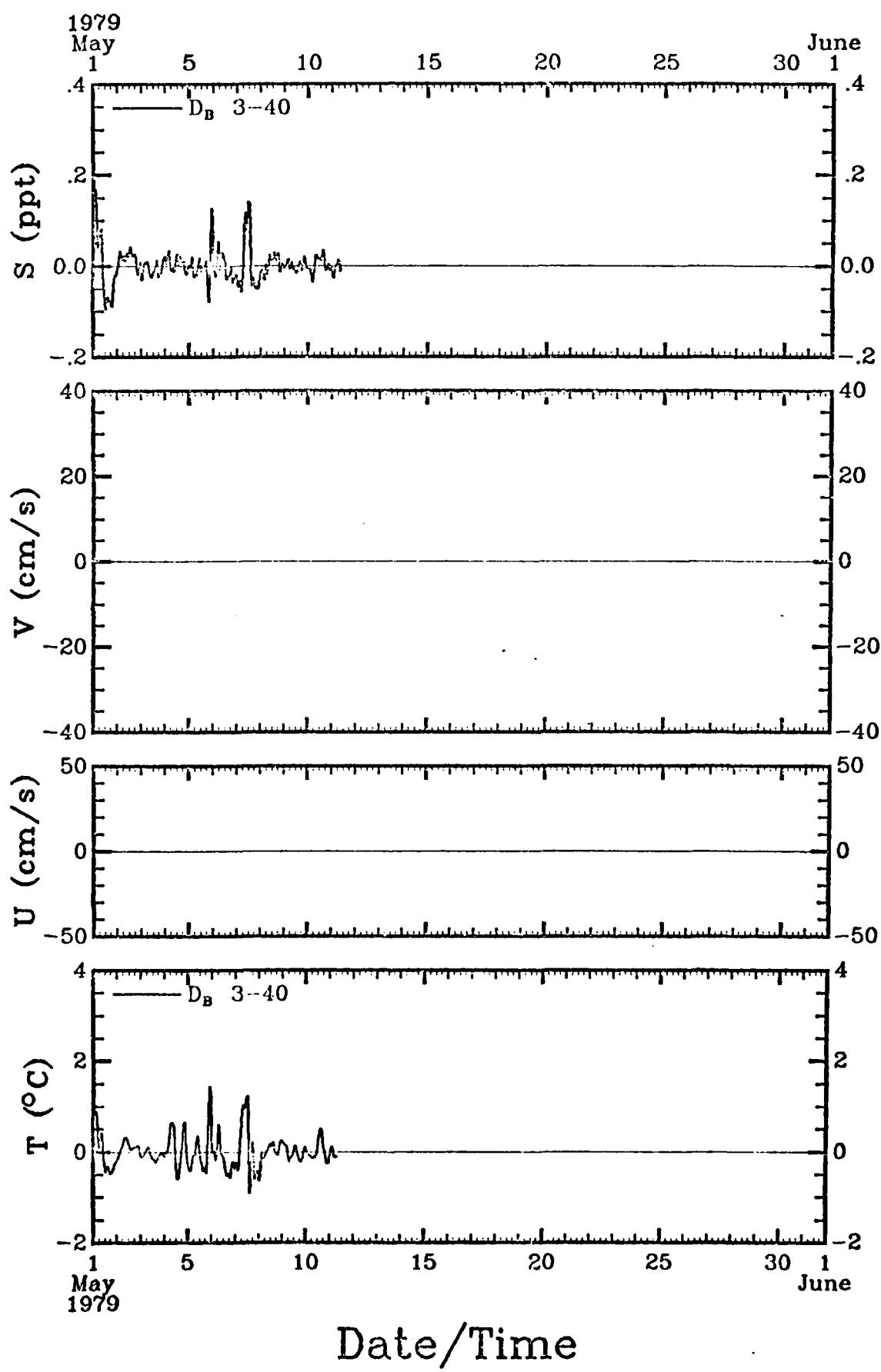








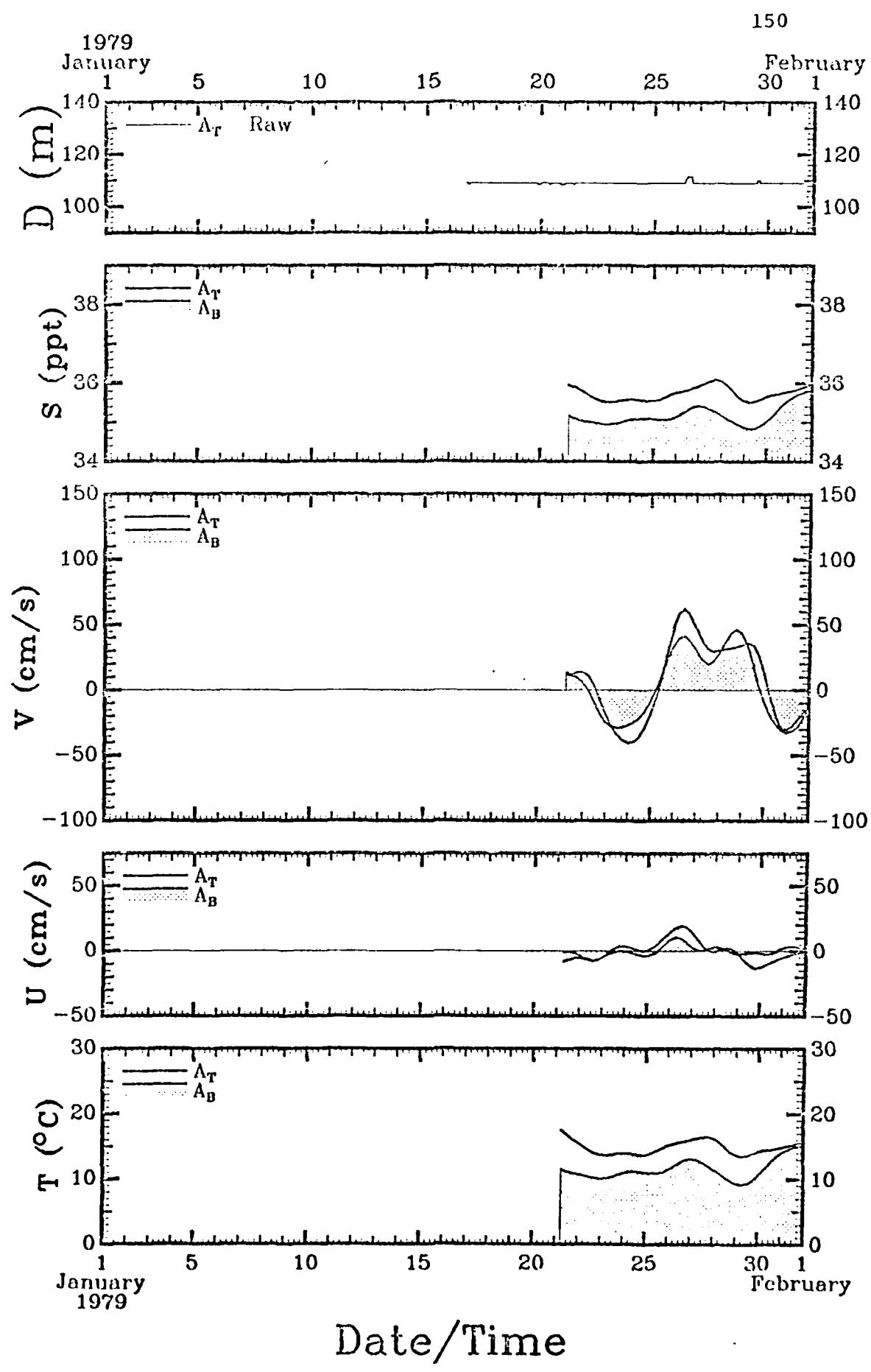
148

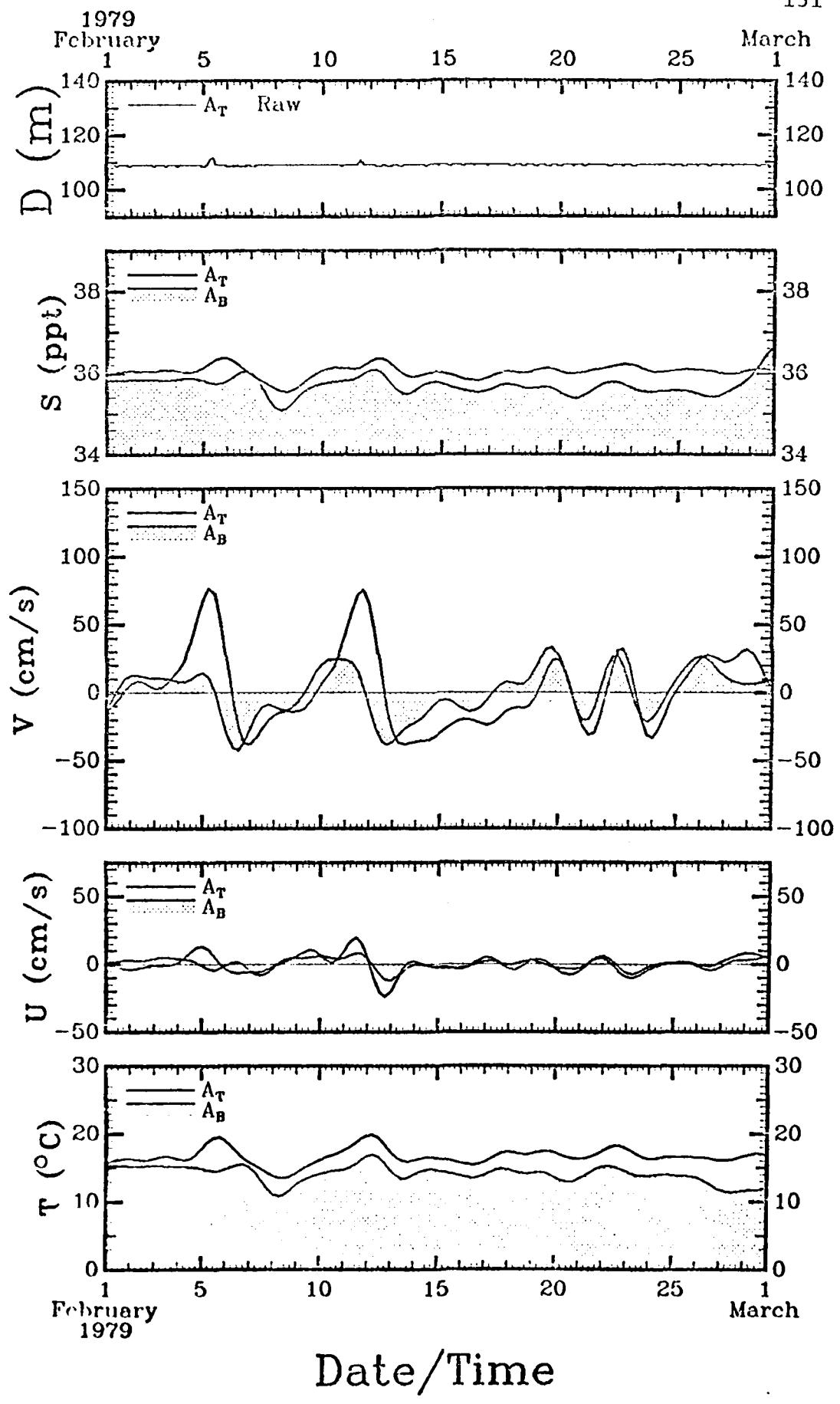


SECTION 5

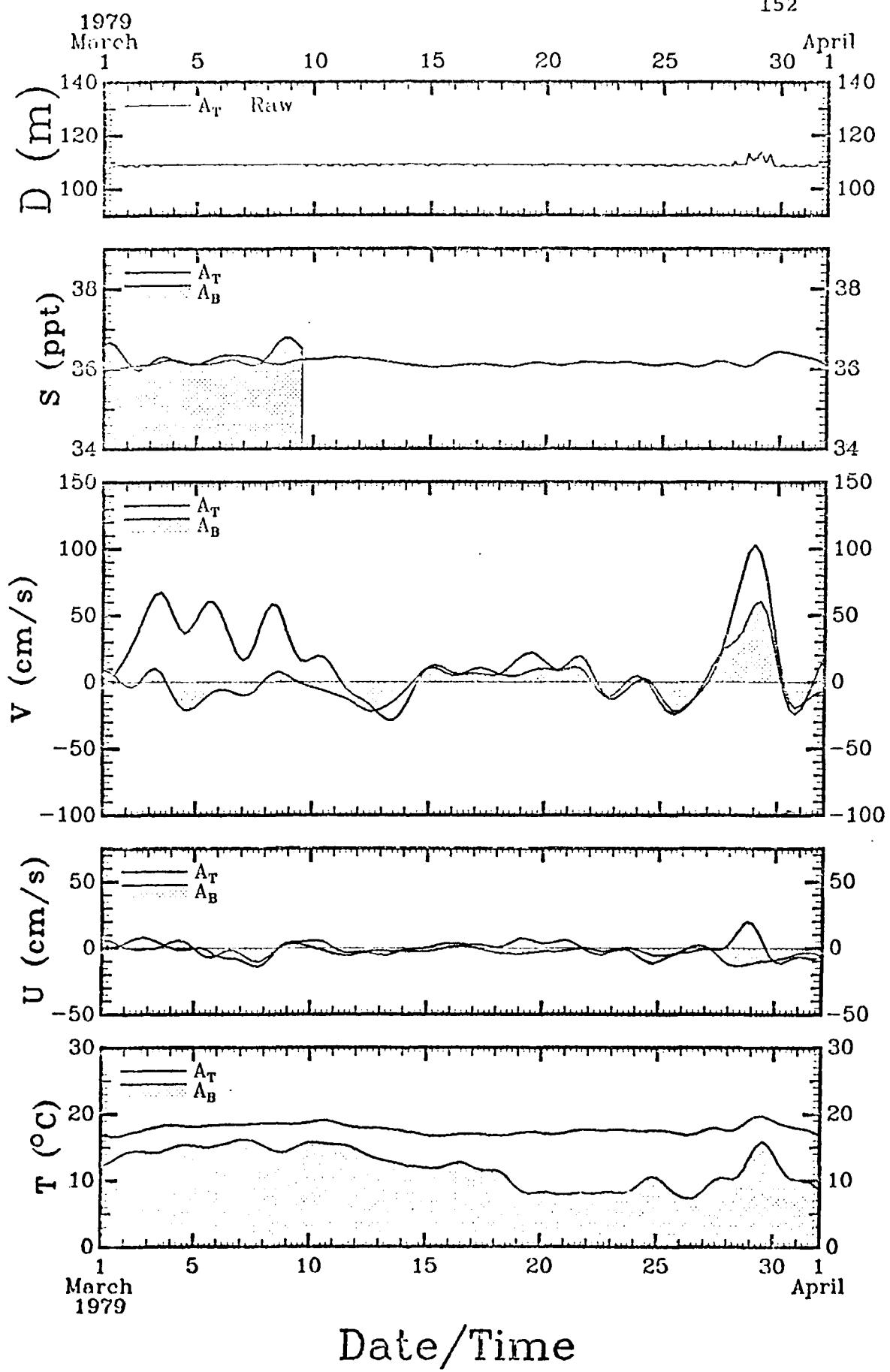
40 HRLP Data for Each Mooring

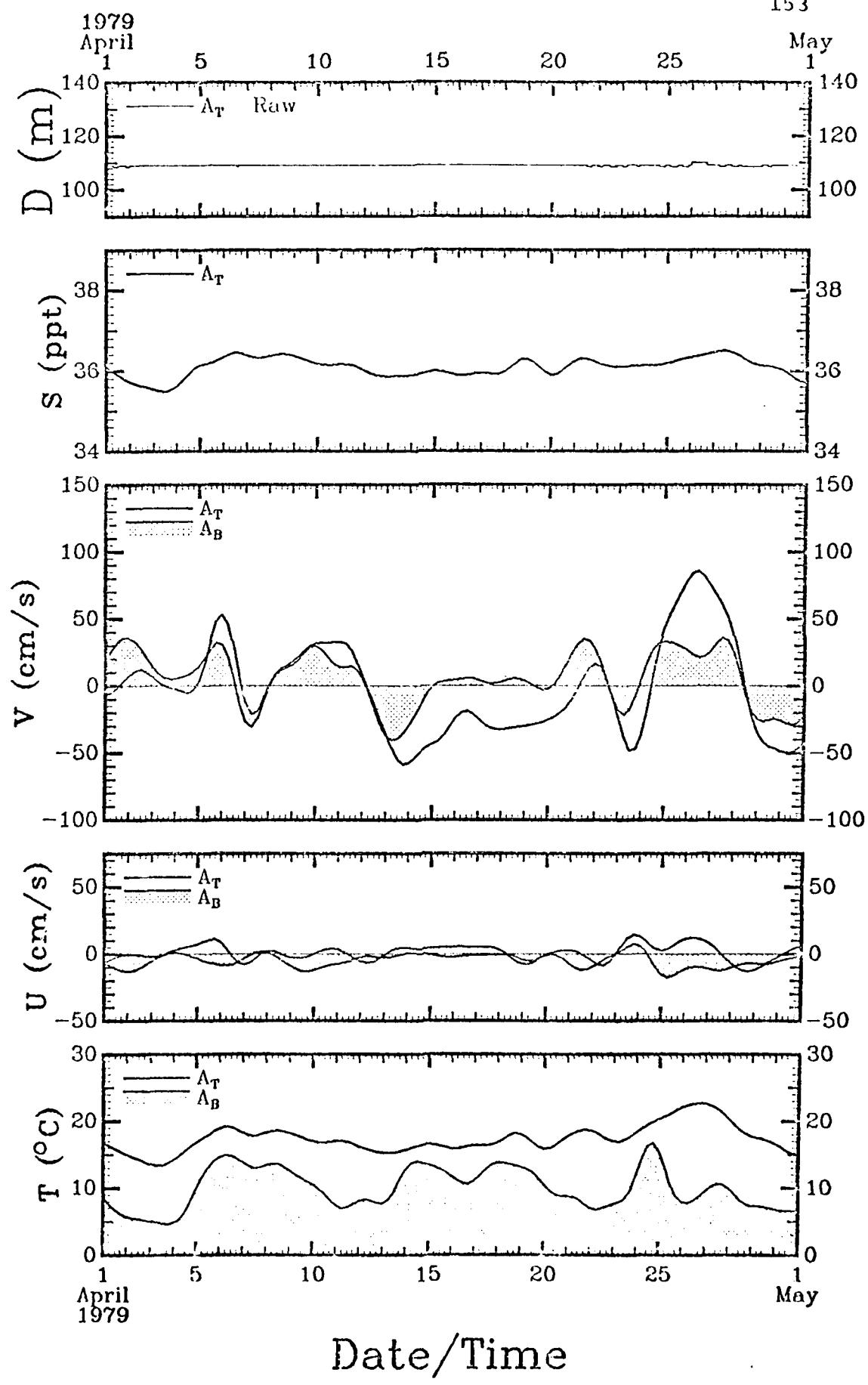
Figures 40 through 43 show the raw pressure data (converted to depth units) and the 40 HRLP current meter data by month for each mooring, superimposing similar data from each instrument on the mooring. Common scaling is used in this section.

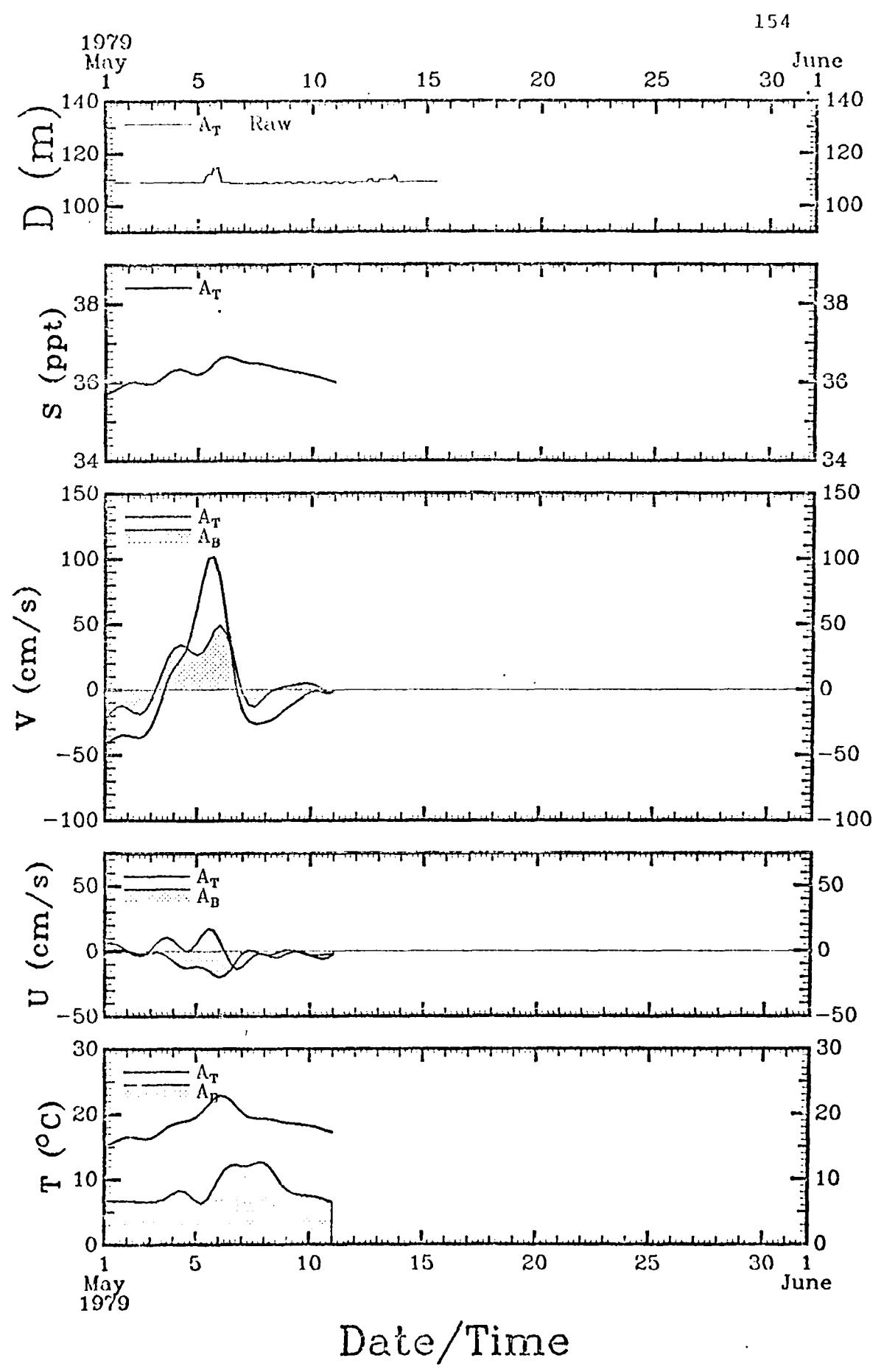


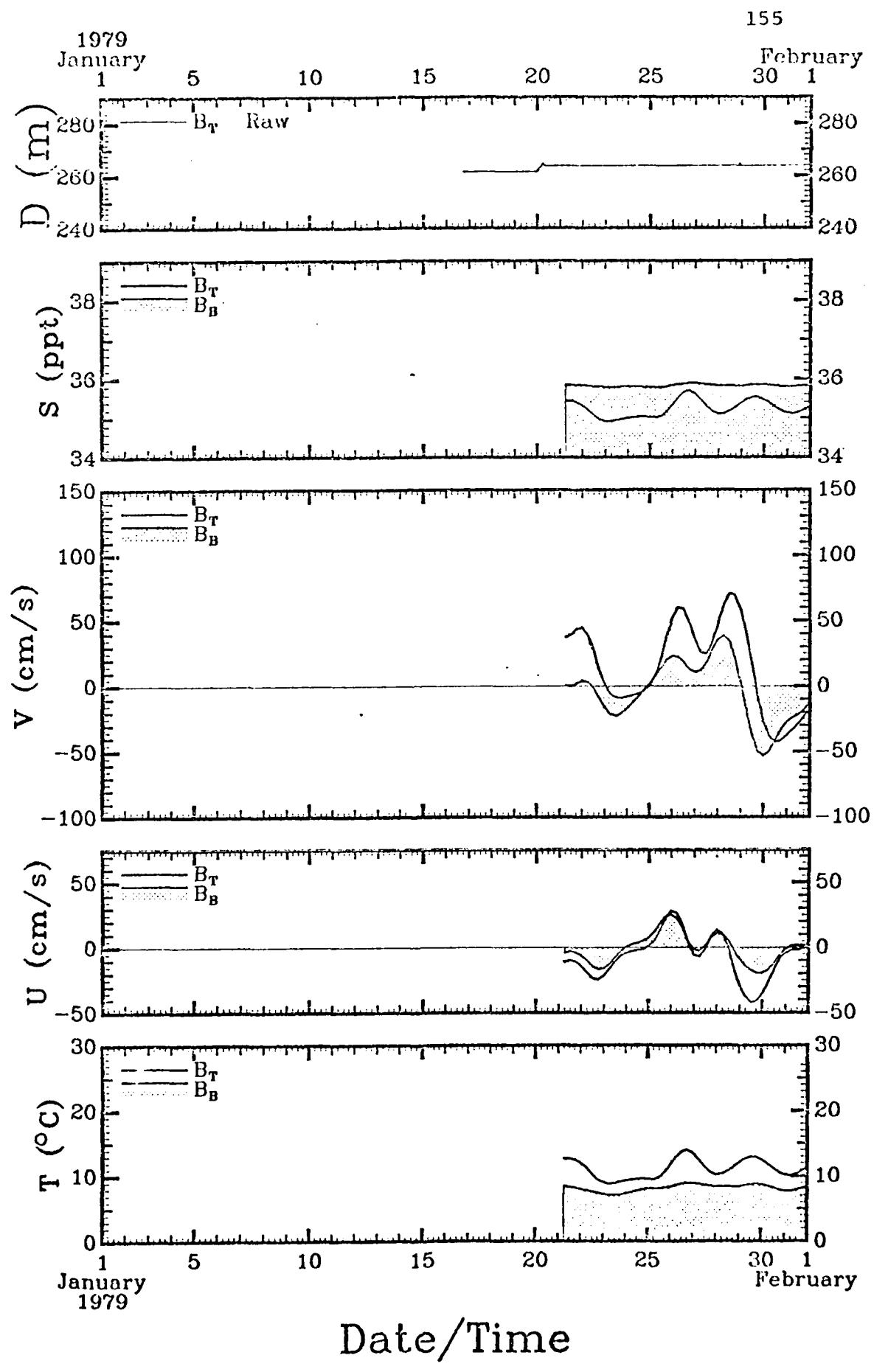


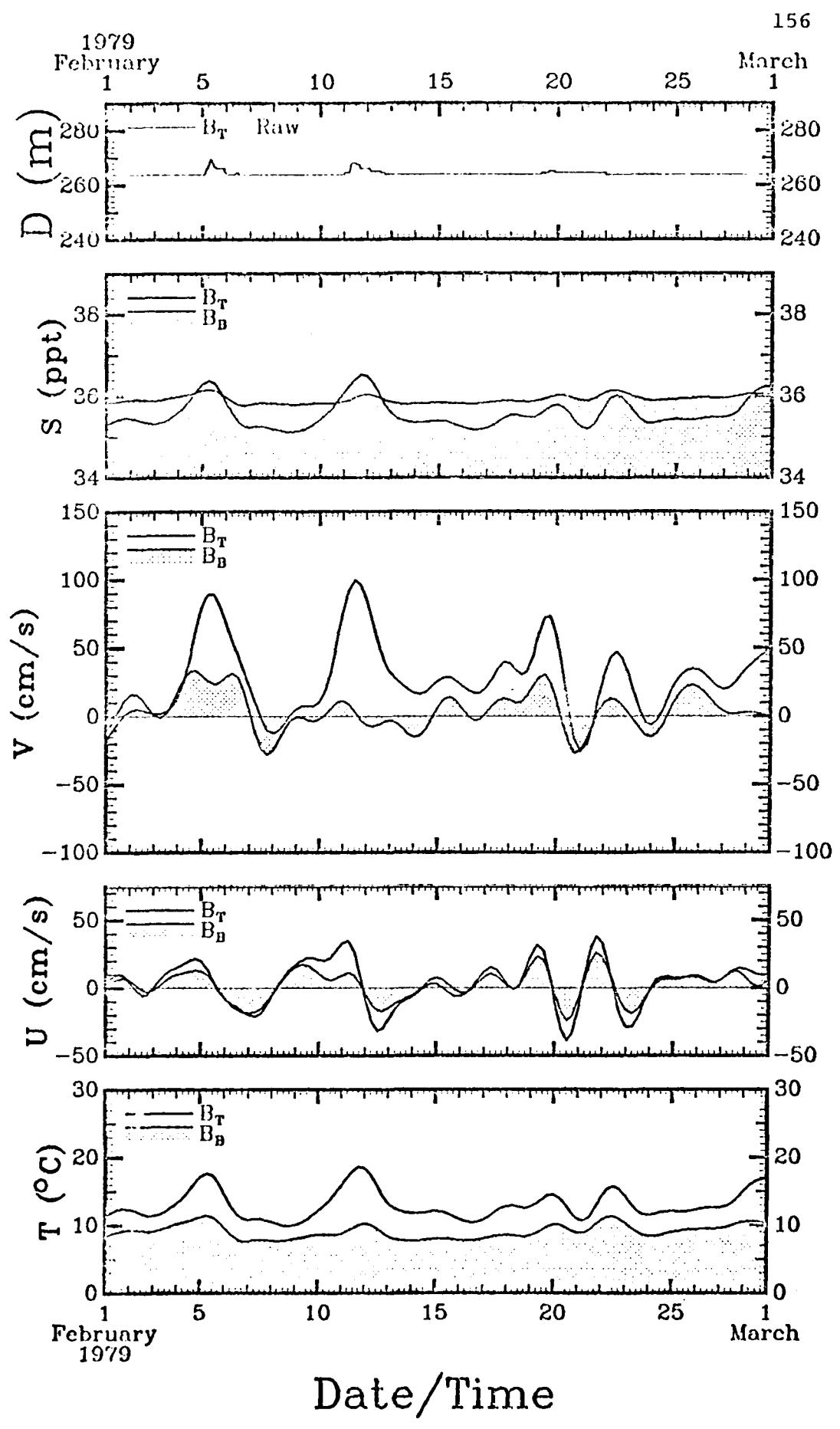
152

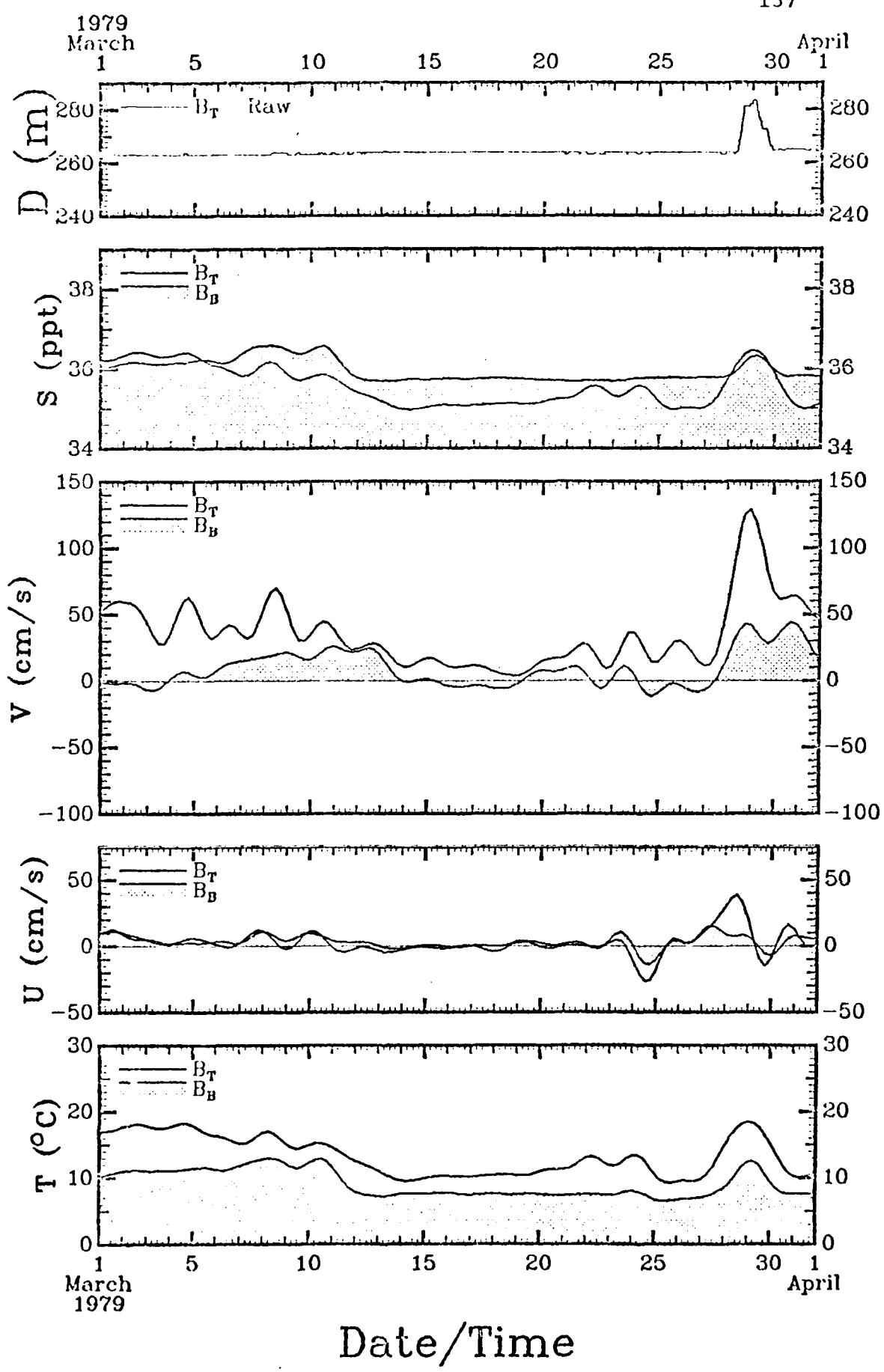


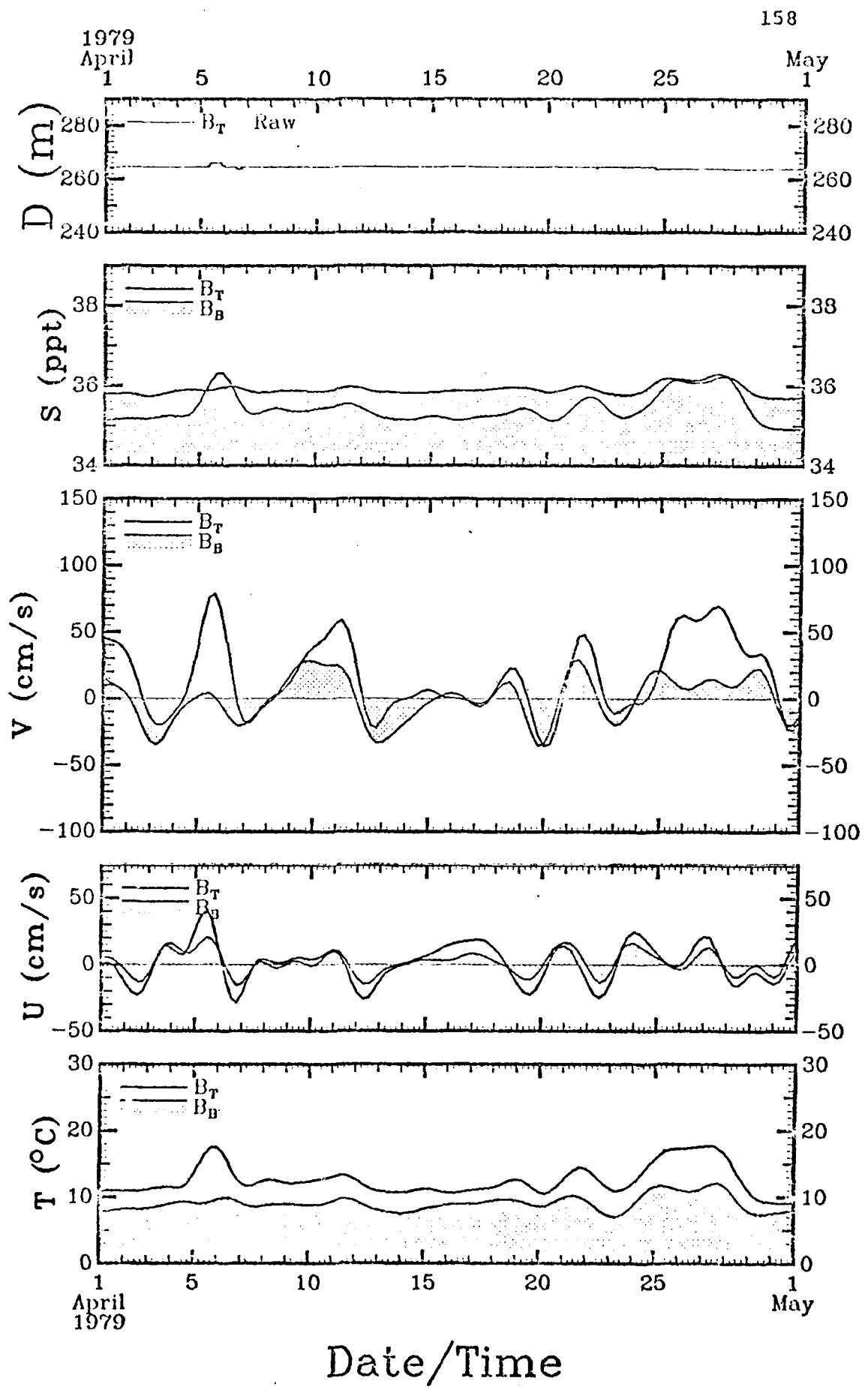




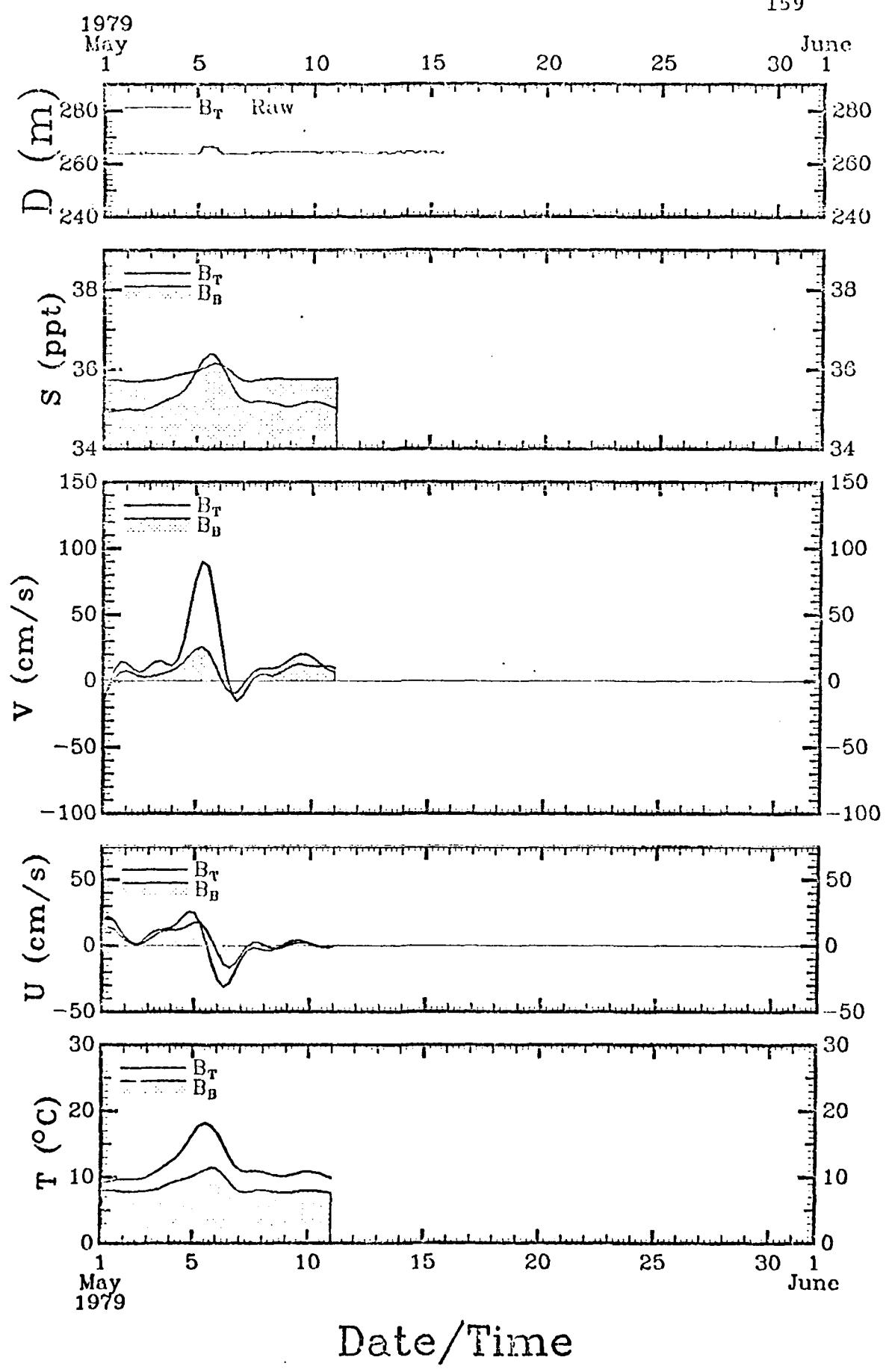


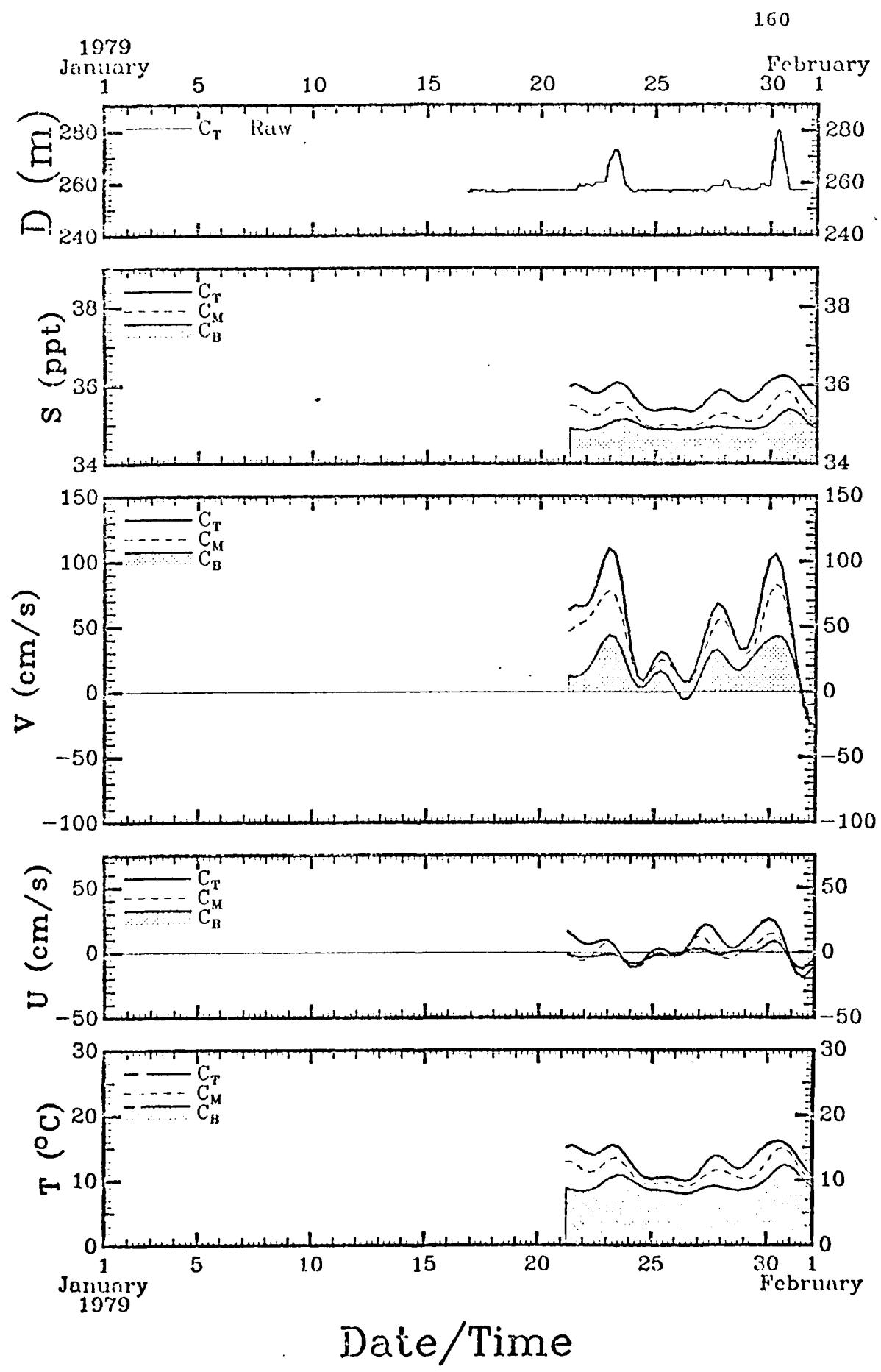


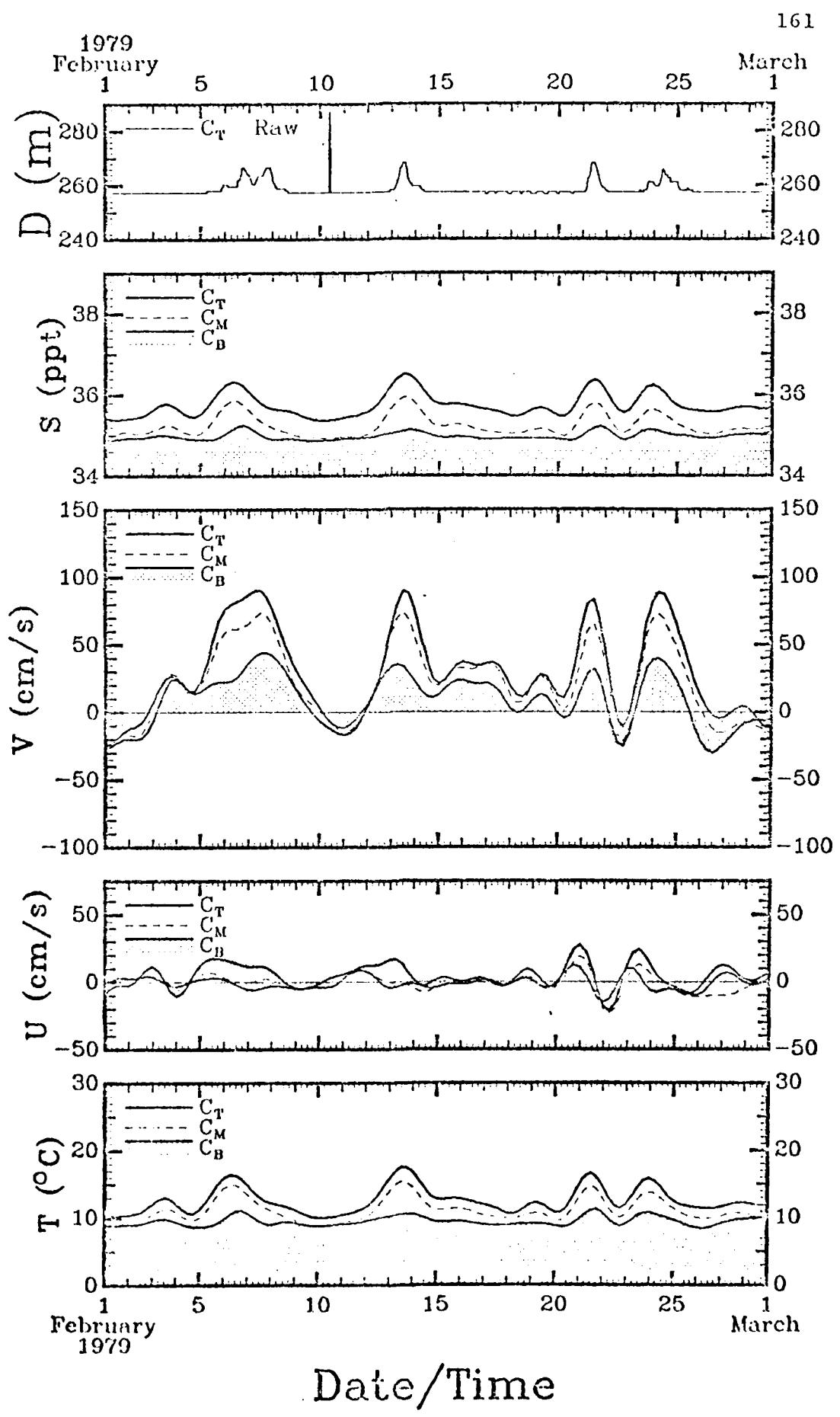


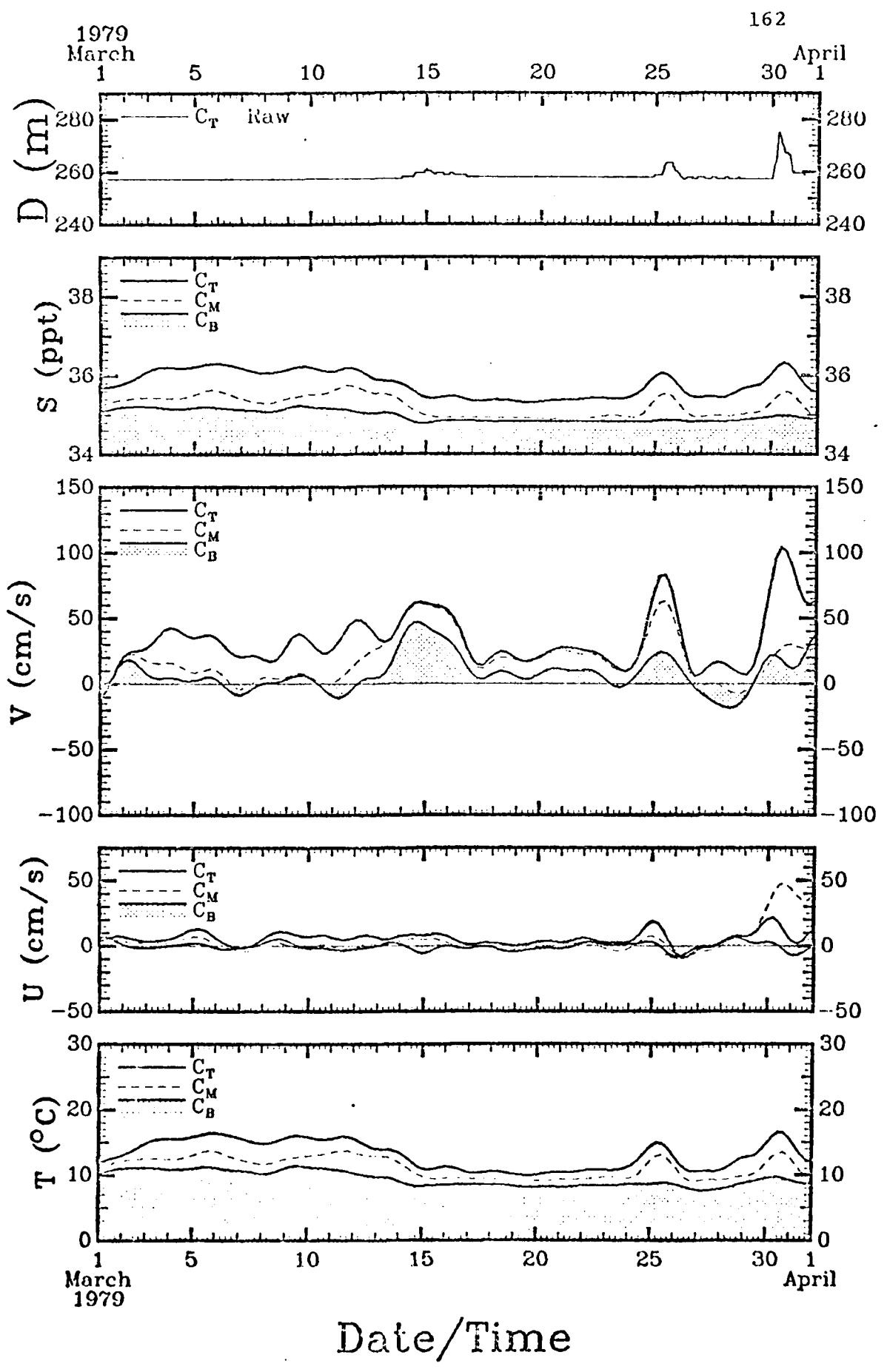


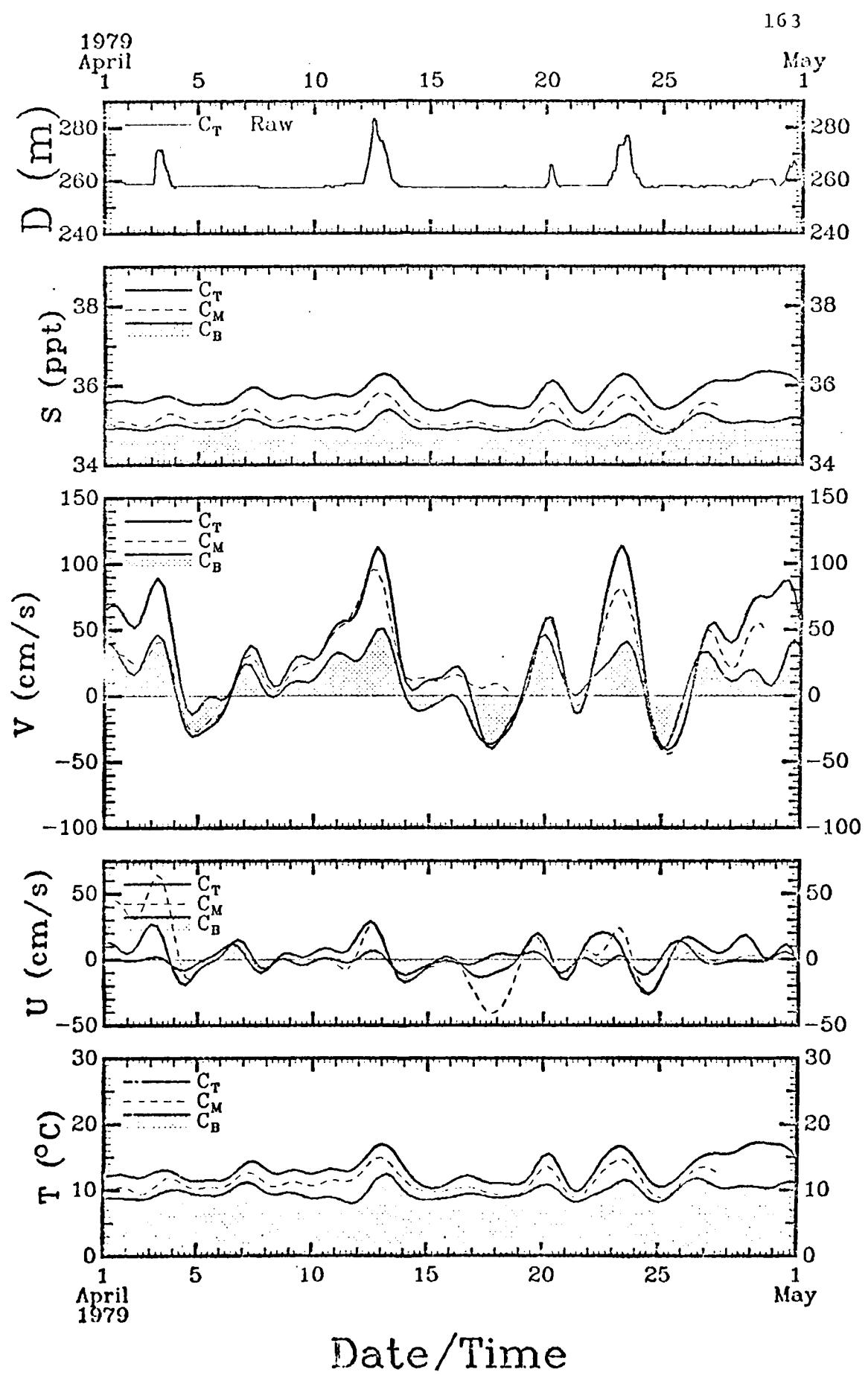
159

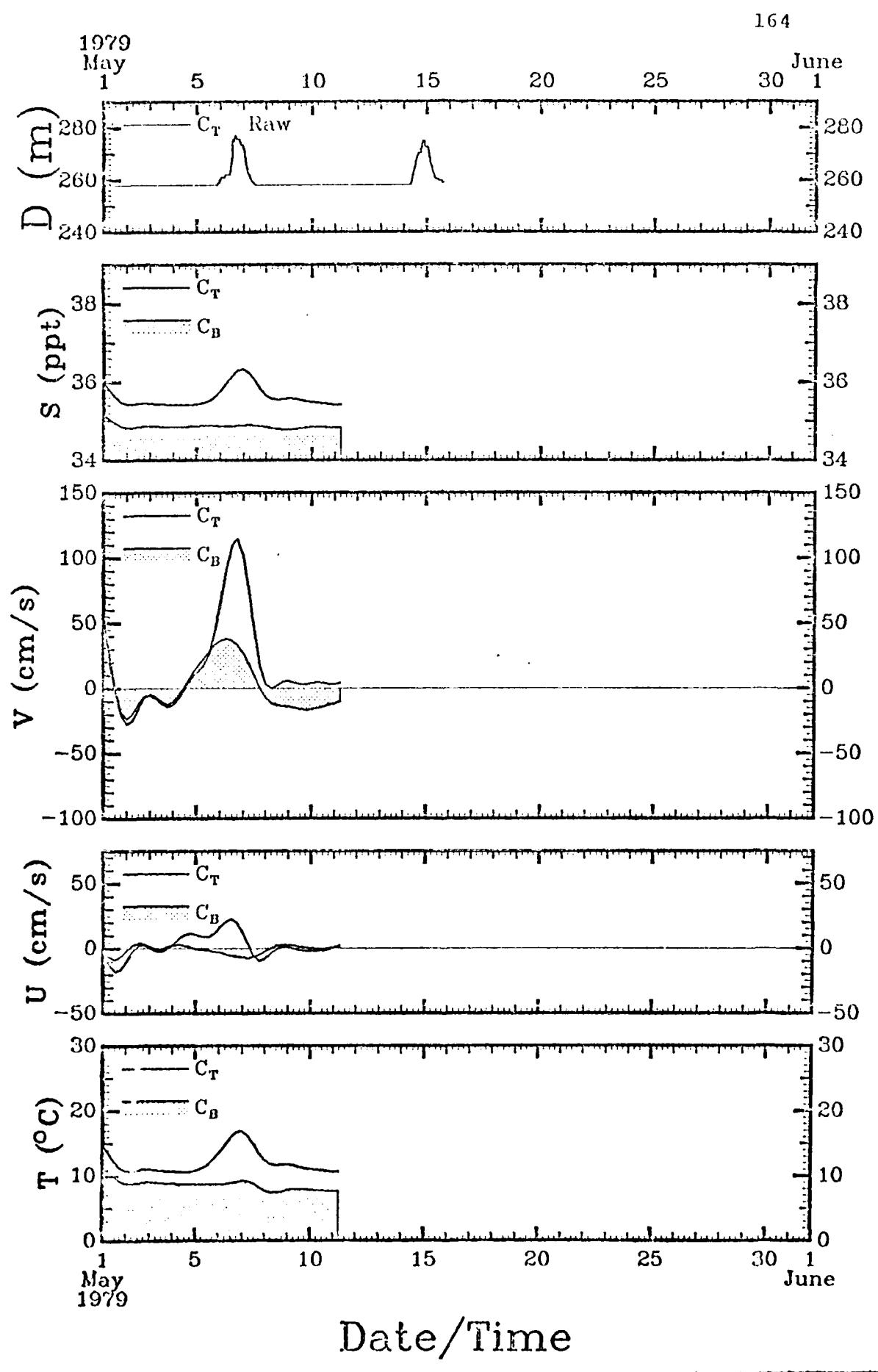


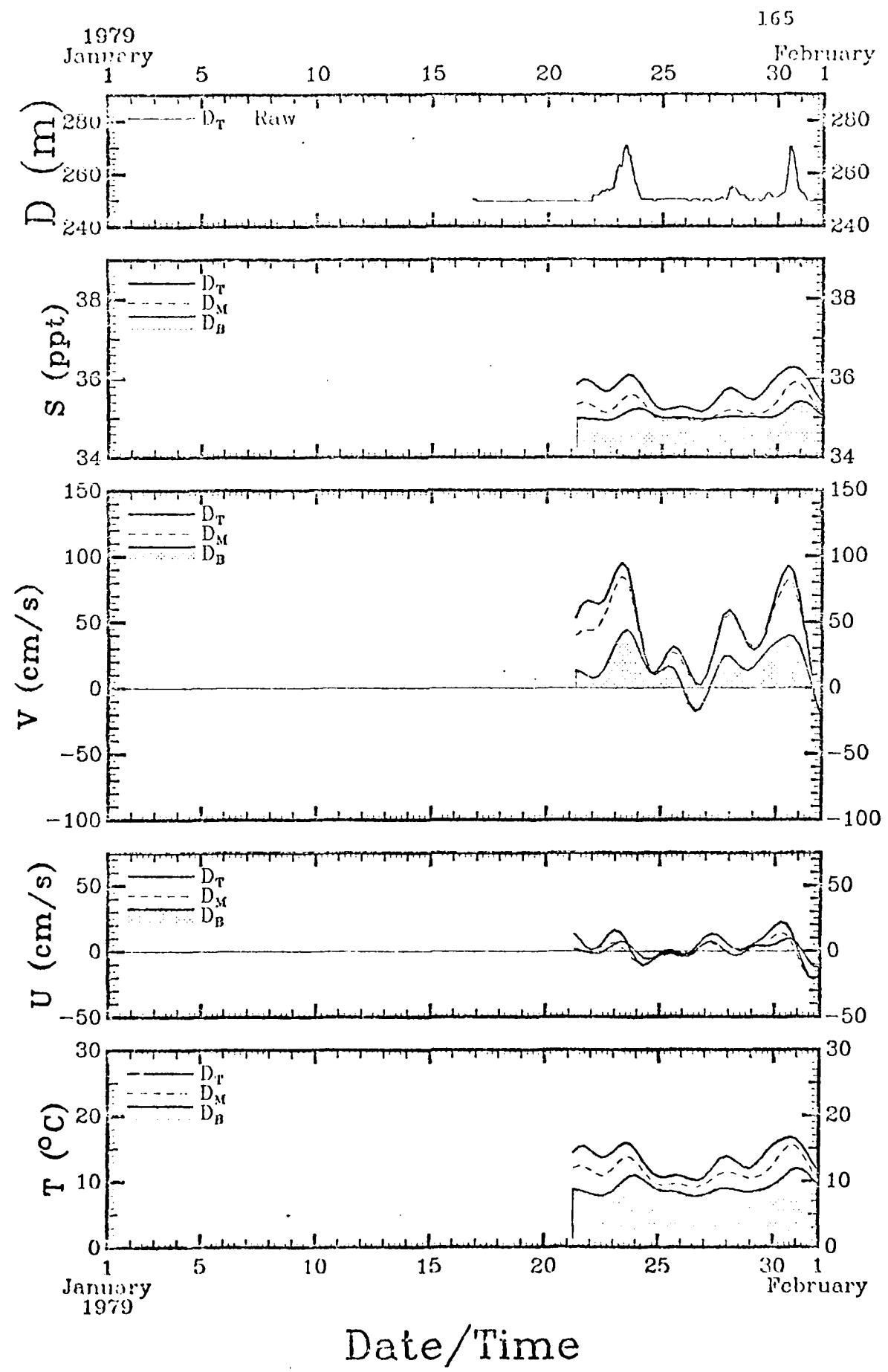


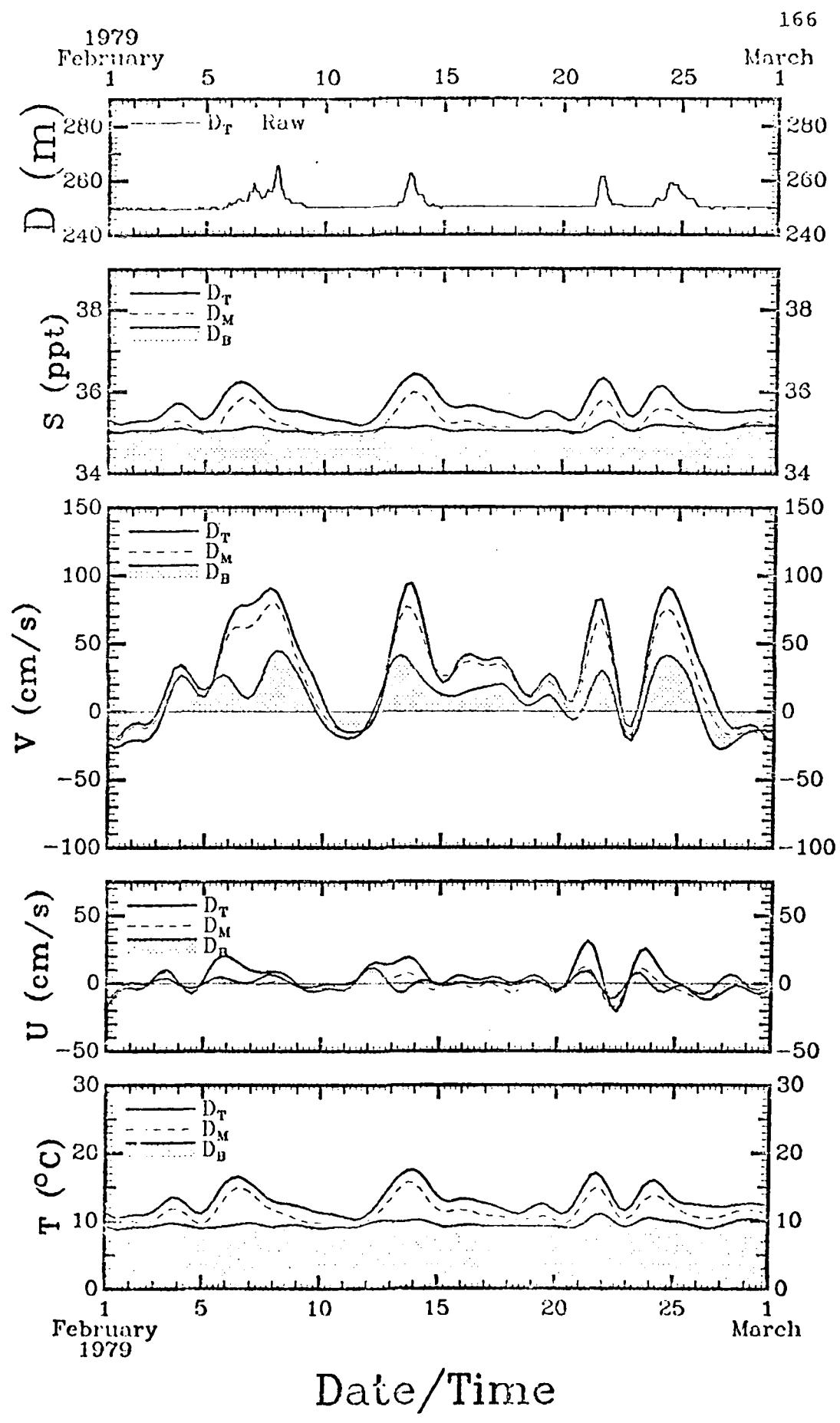


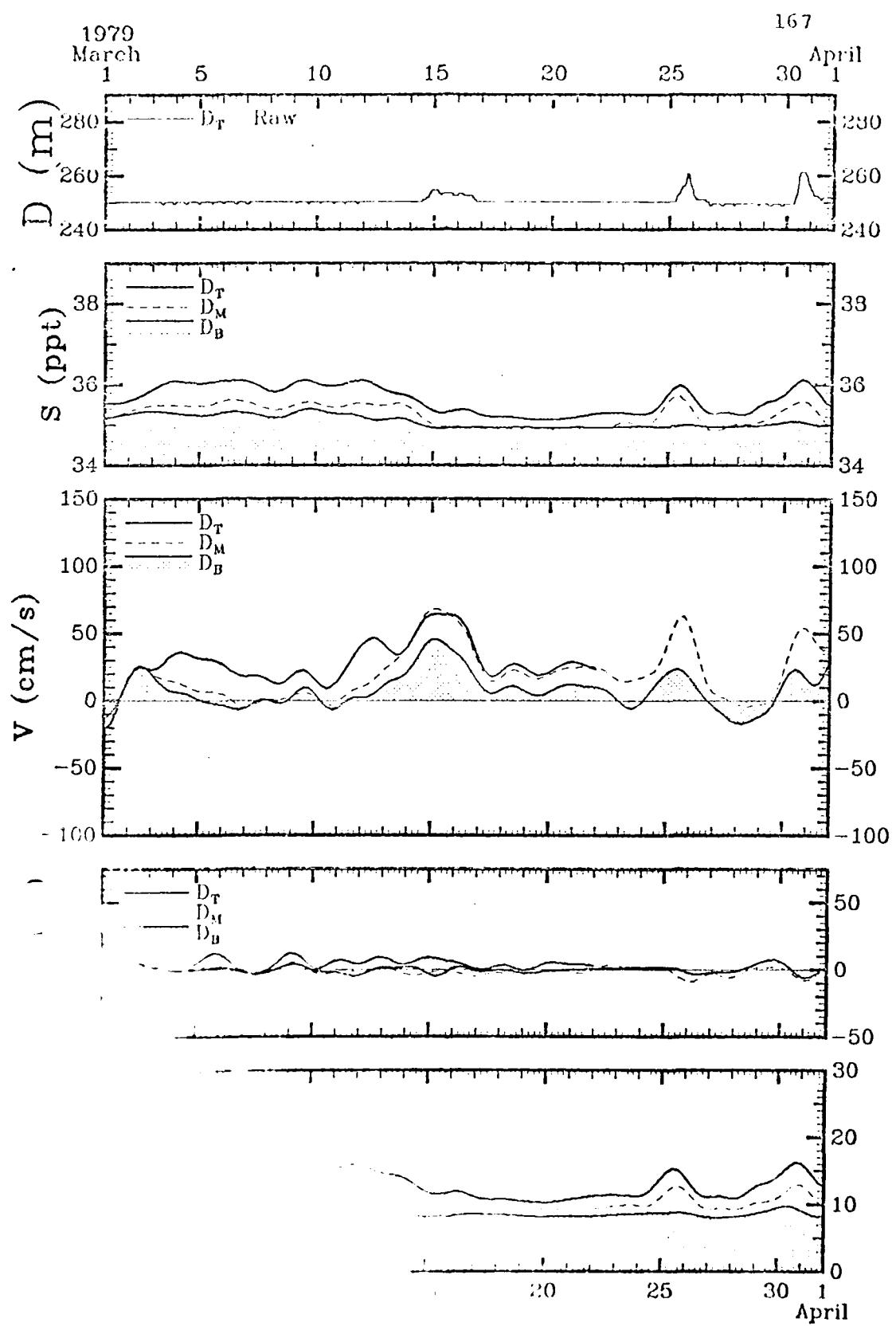




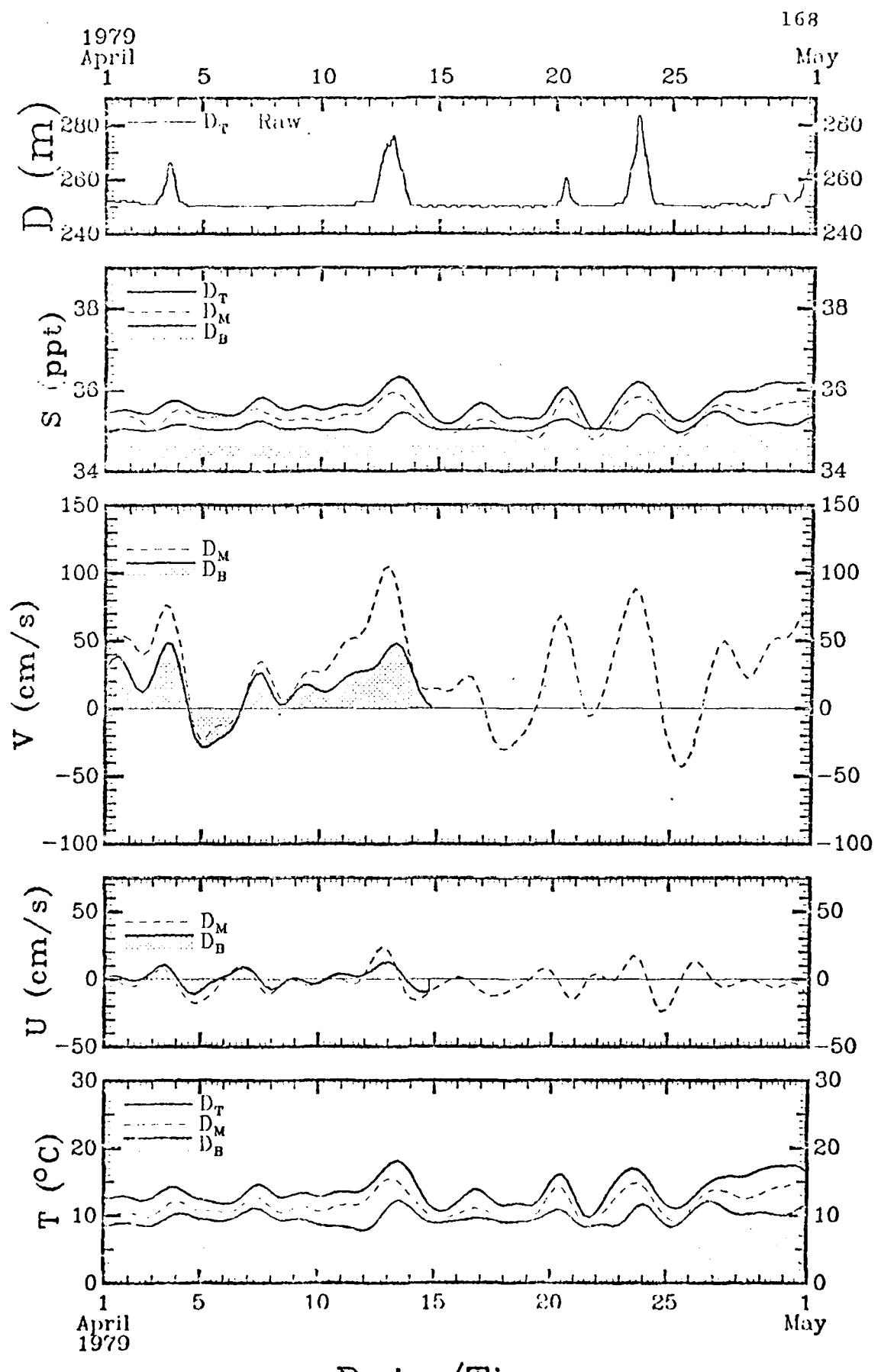


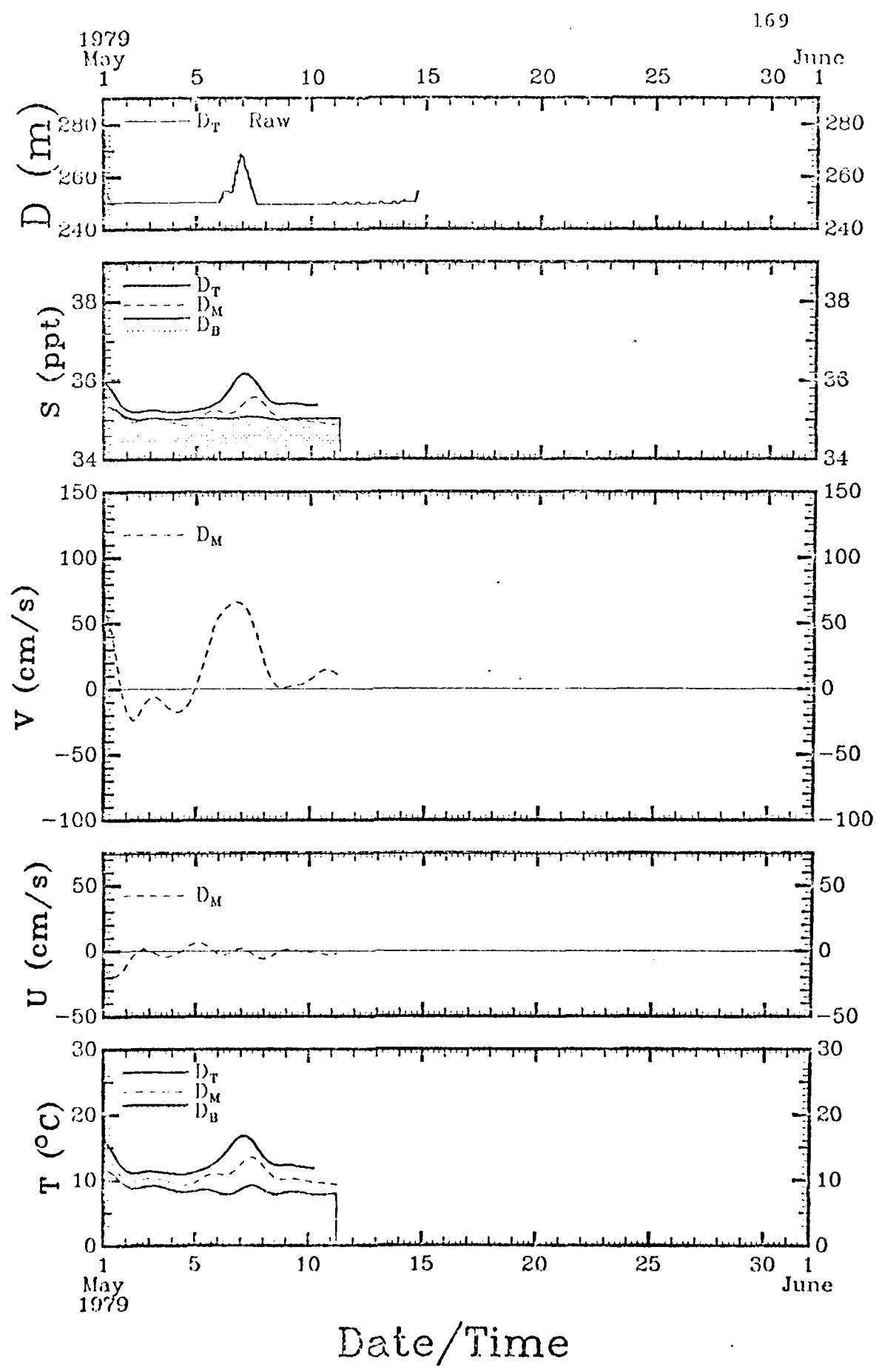






time

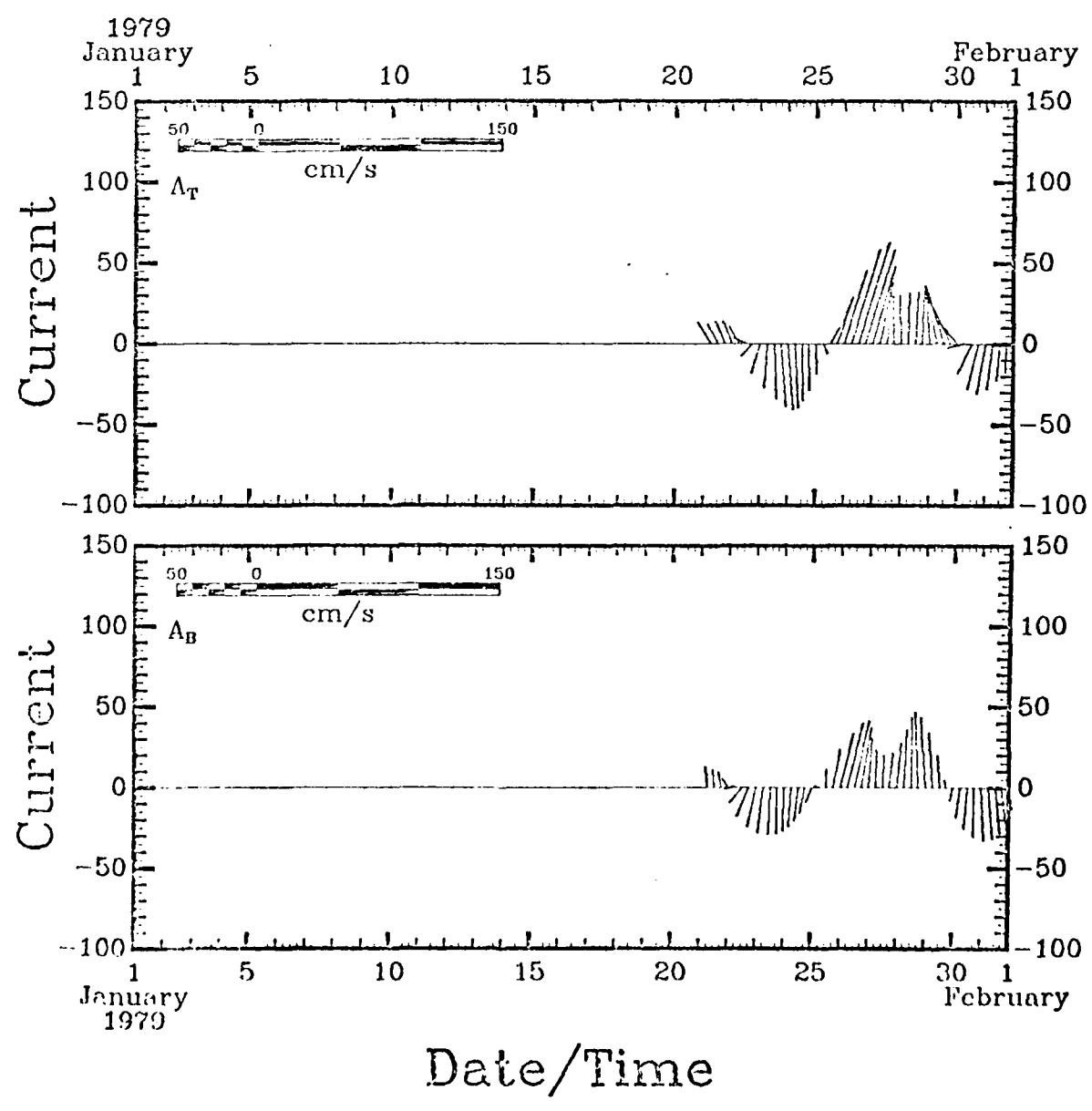


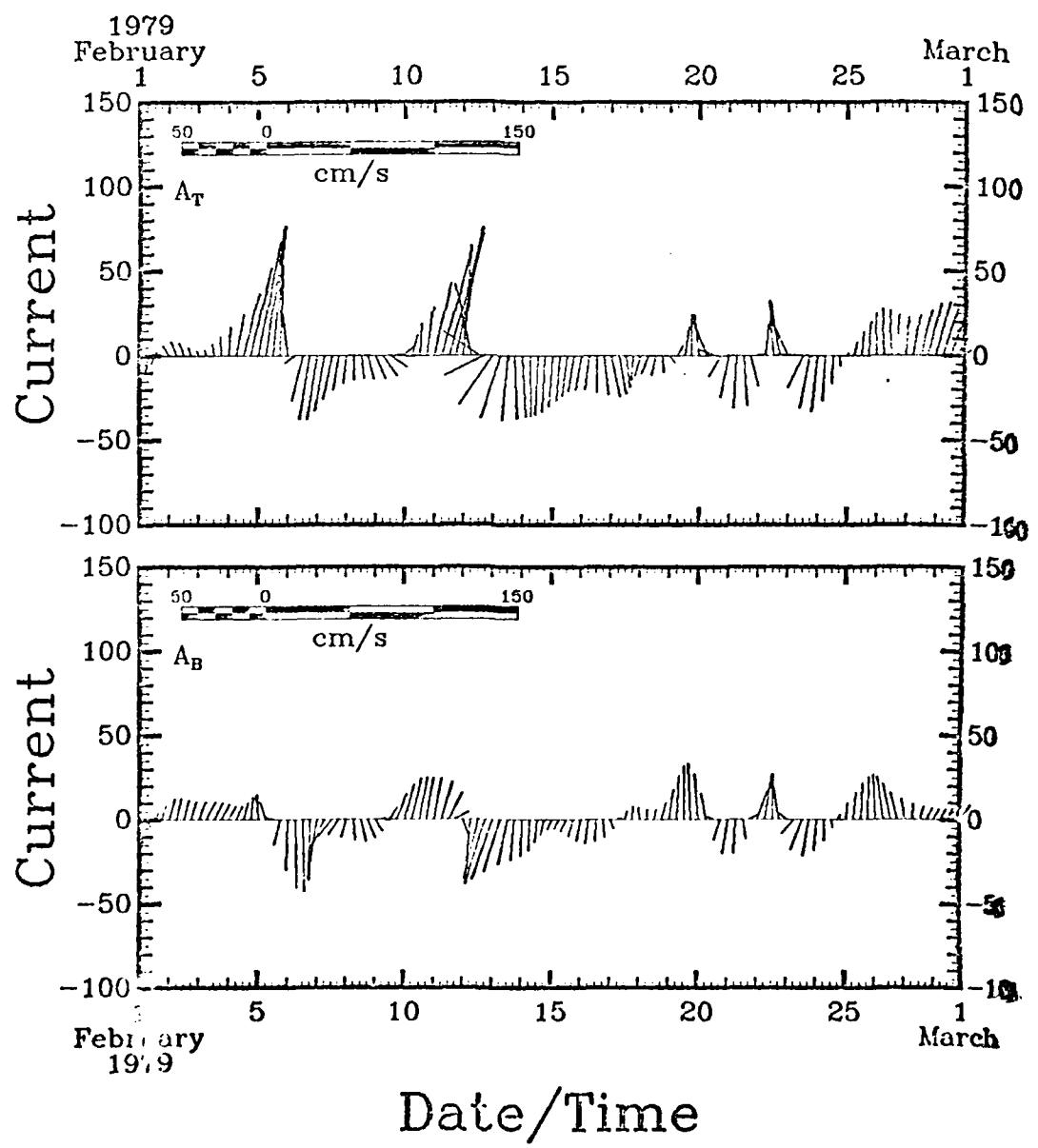


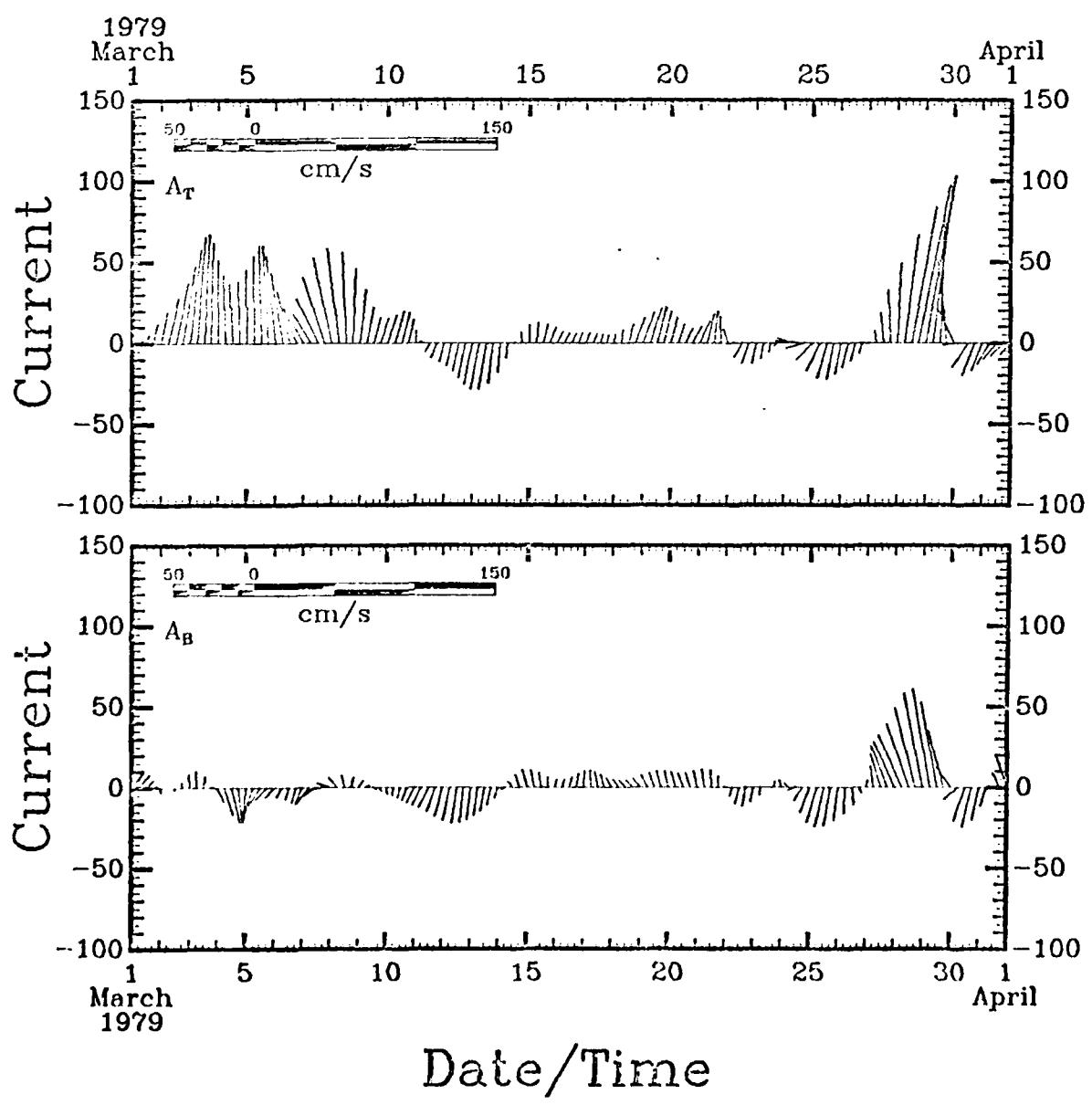
SECTION 6

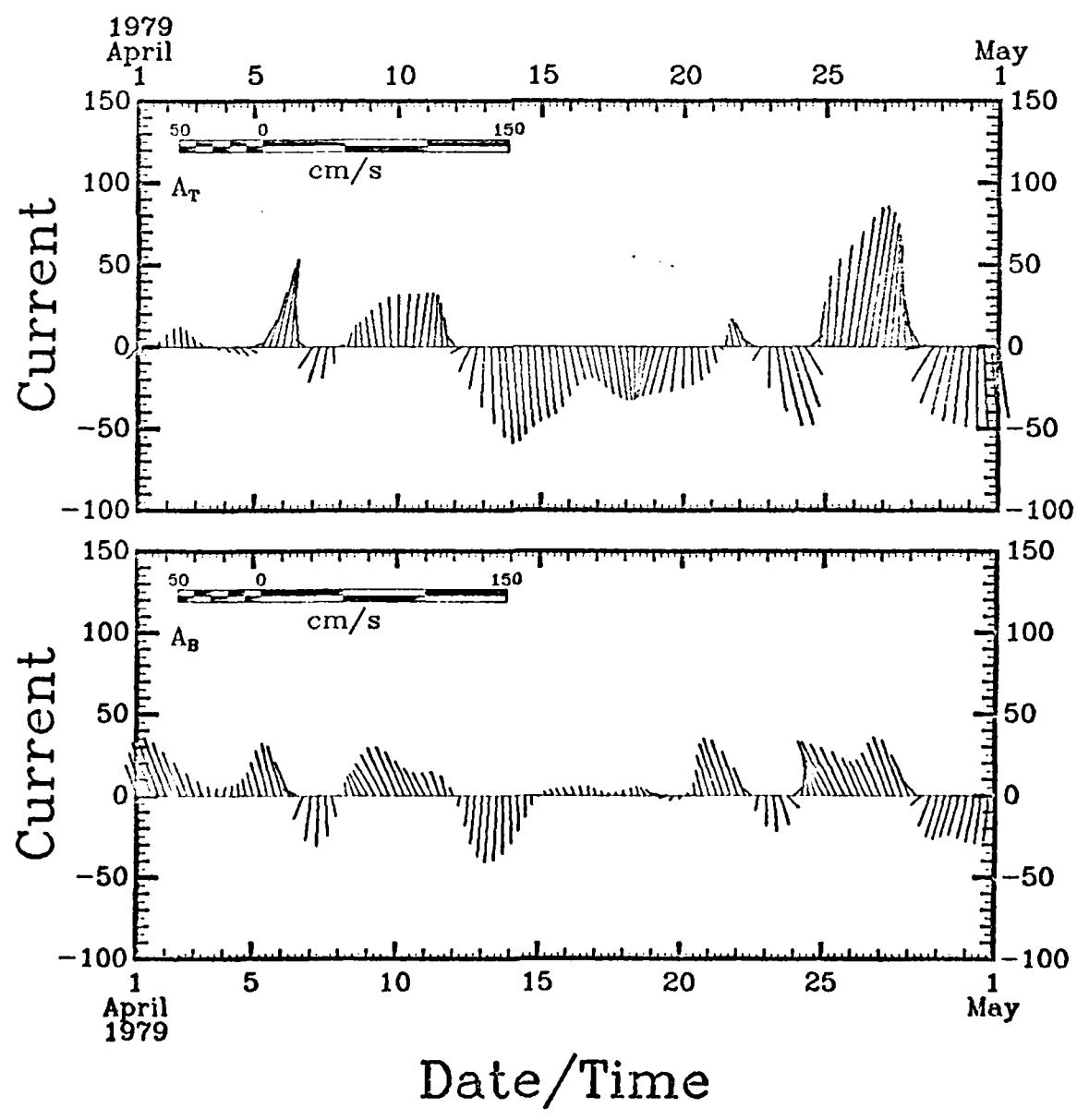
40 HRLP Current Vector "Stick" Plots for Each Mooring

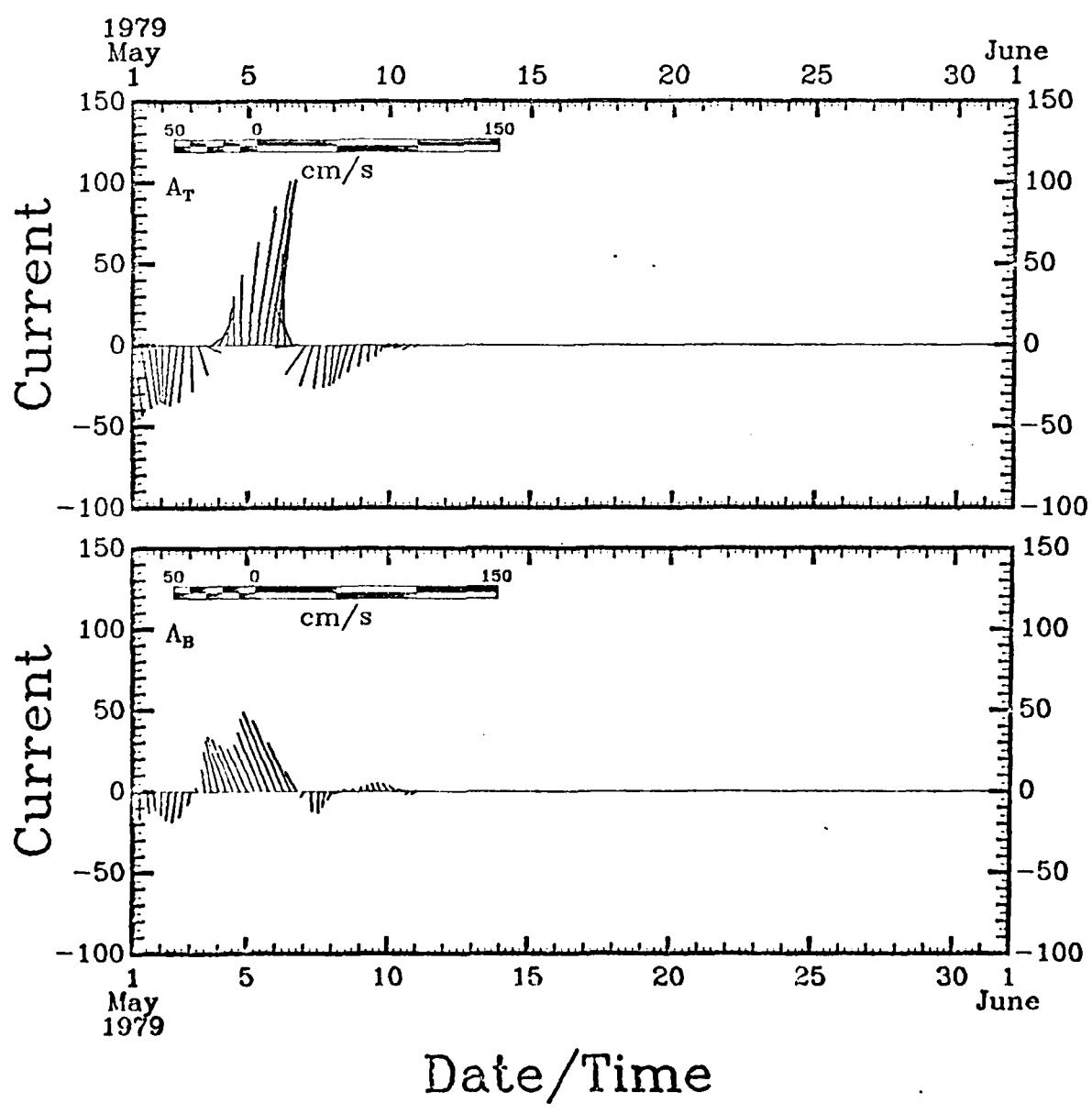
Figures 44 through 47 show the 40 HRLP current vectors in "stick" format by month for each mooring. Vectors pointing toward the top of the page correspond to flow in the downstream (34°T) direction. Common scaling is used in this section.

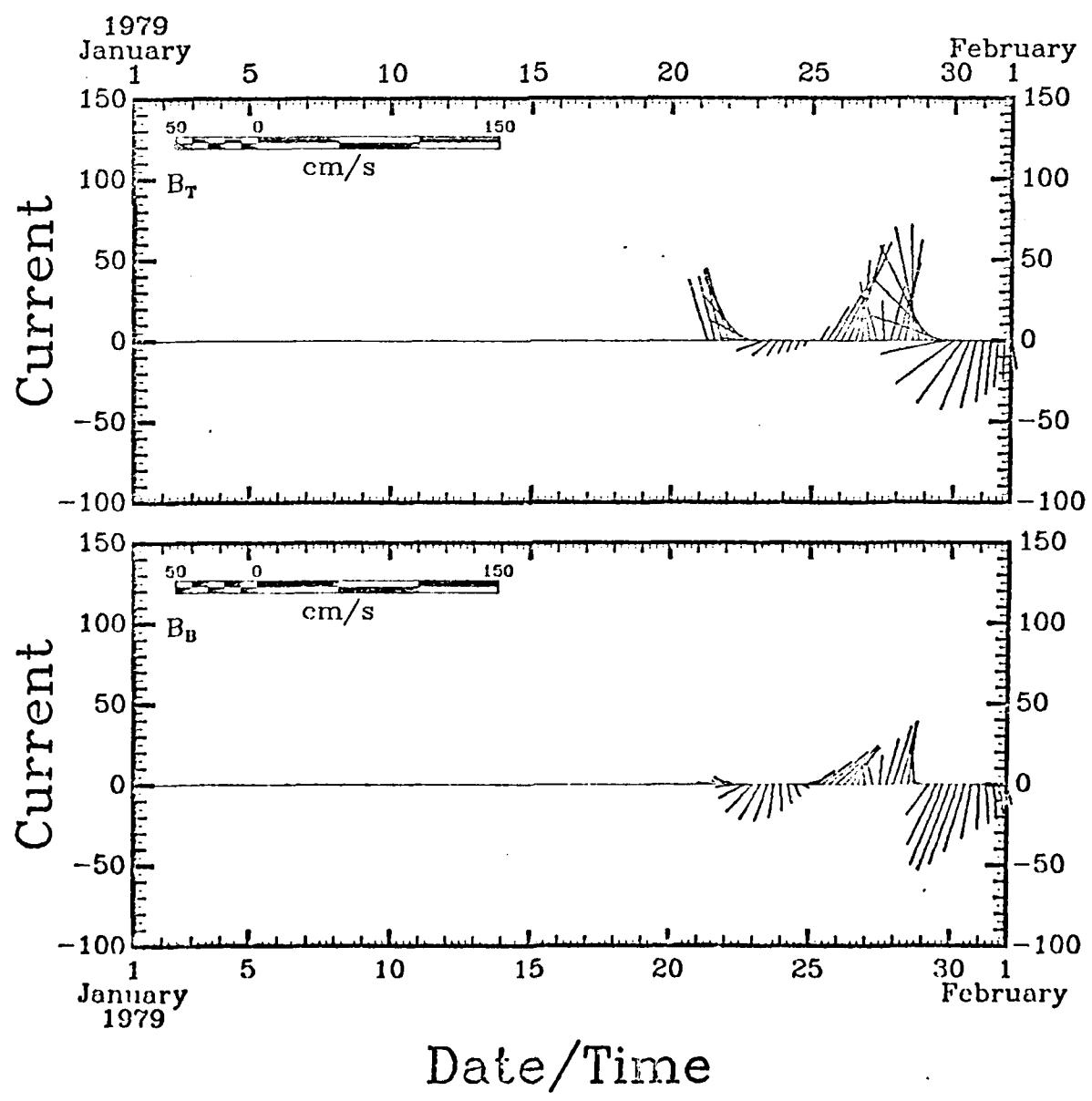


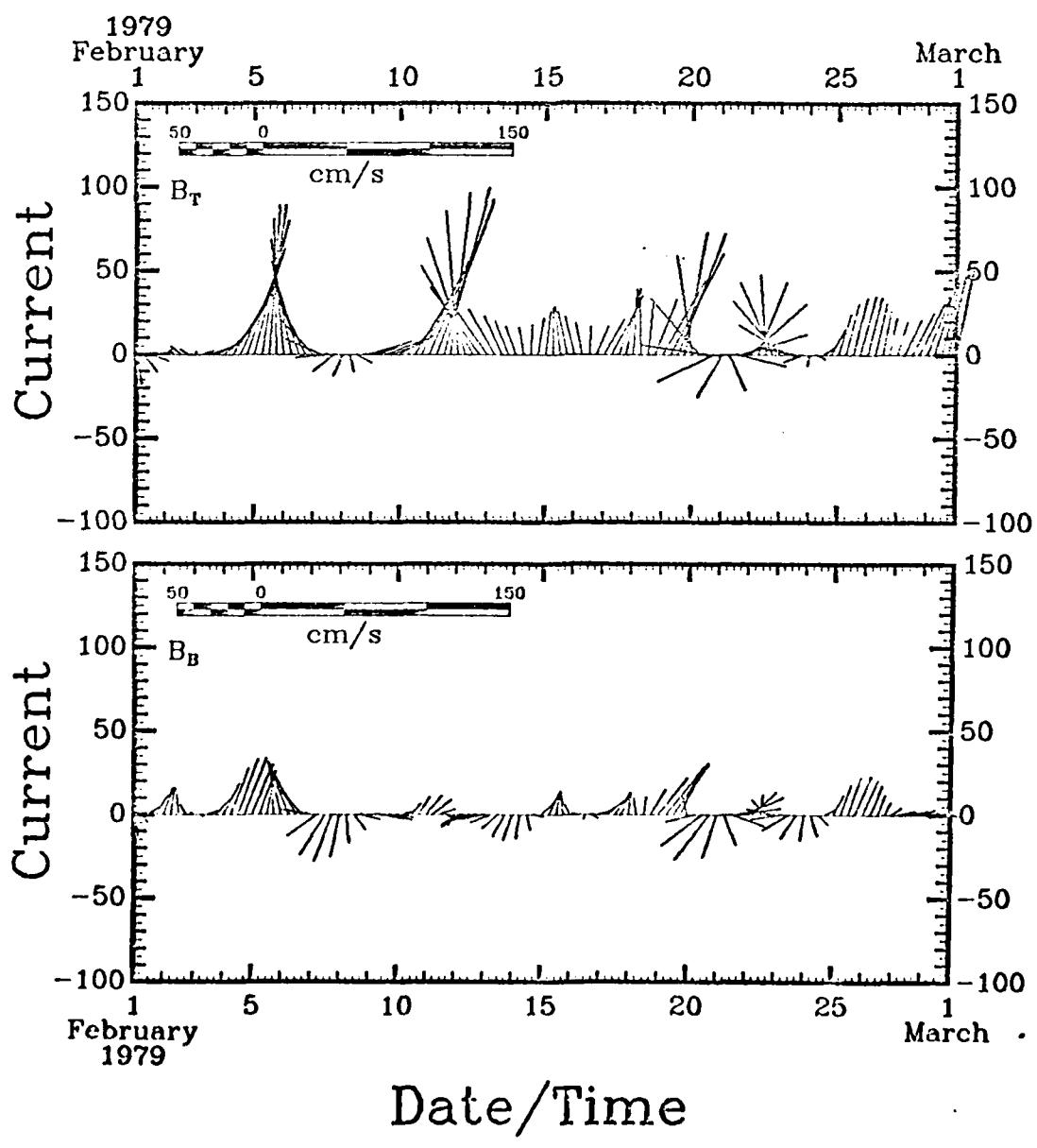


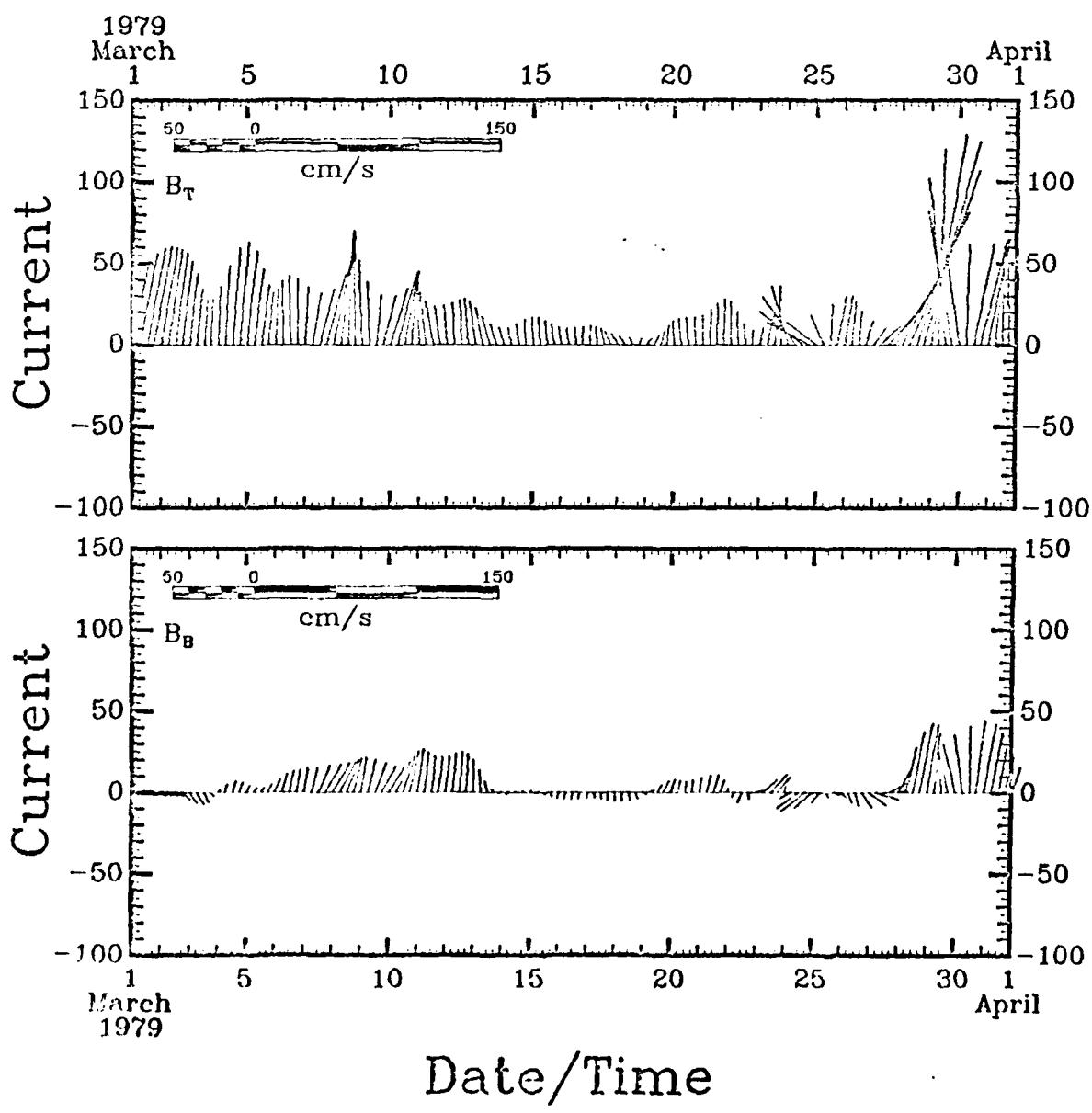


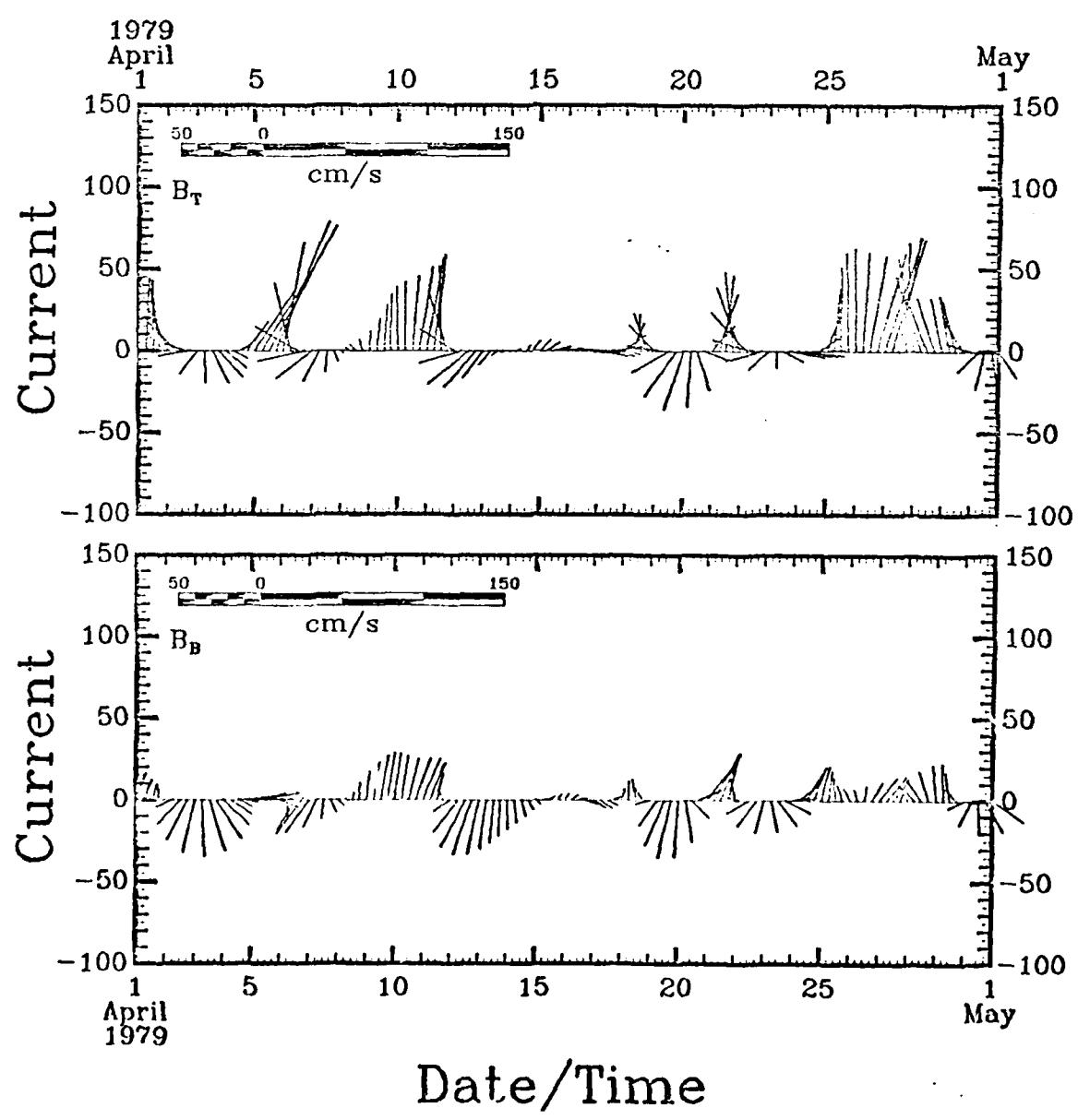


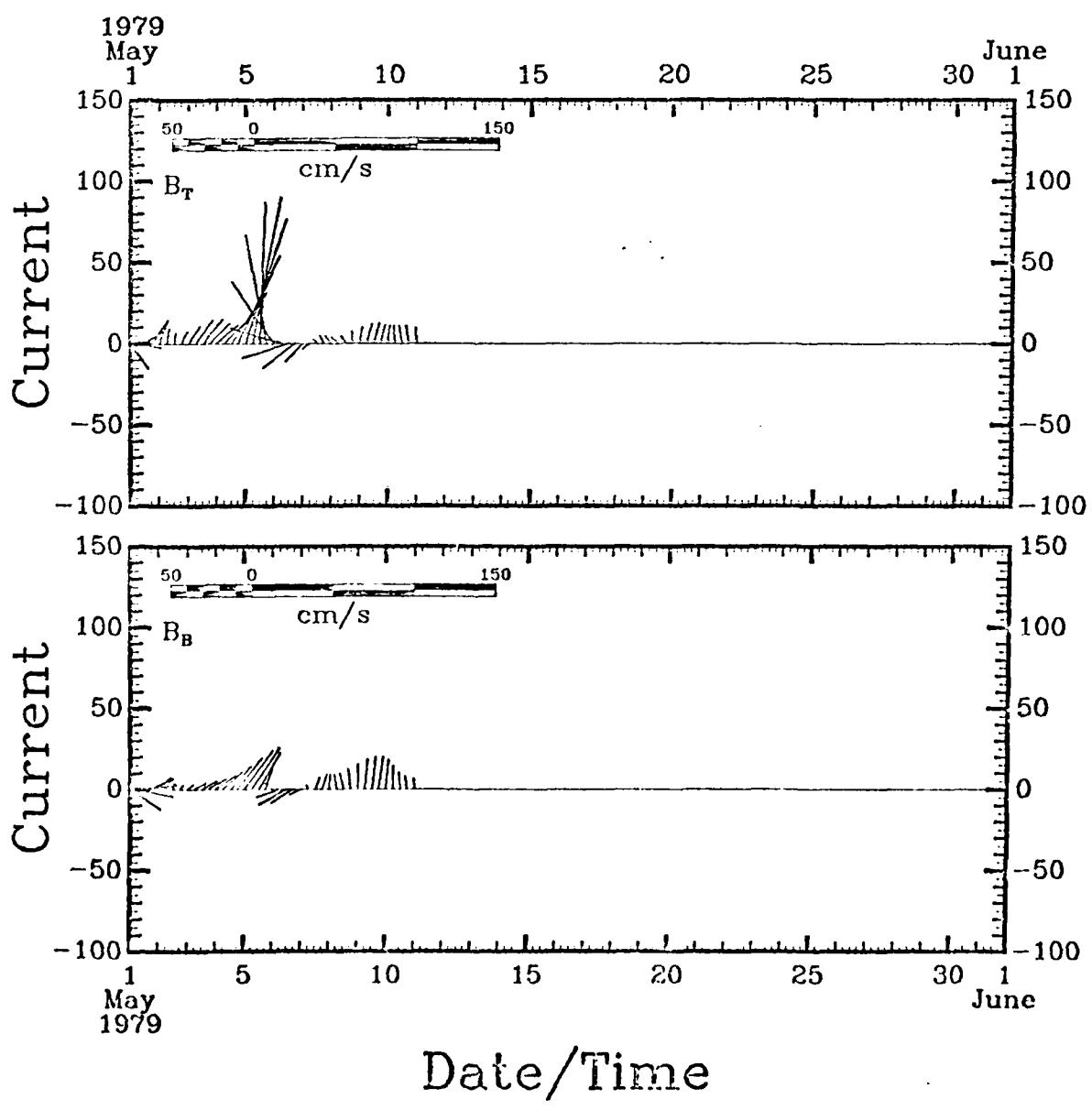












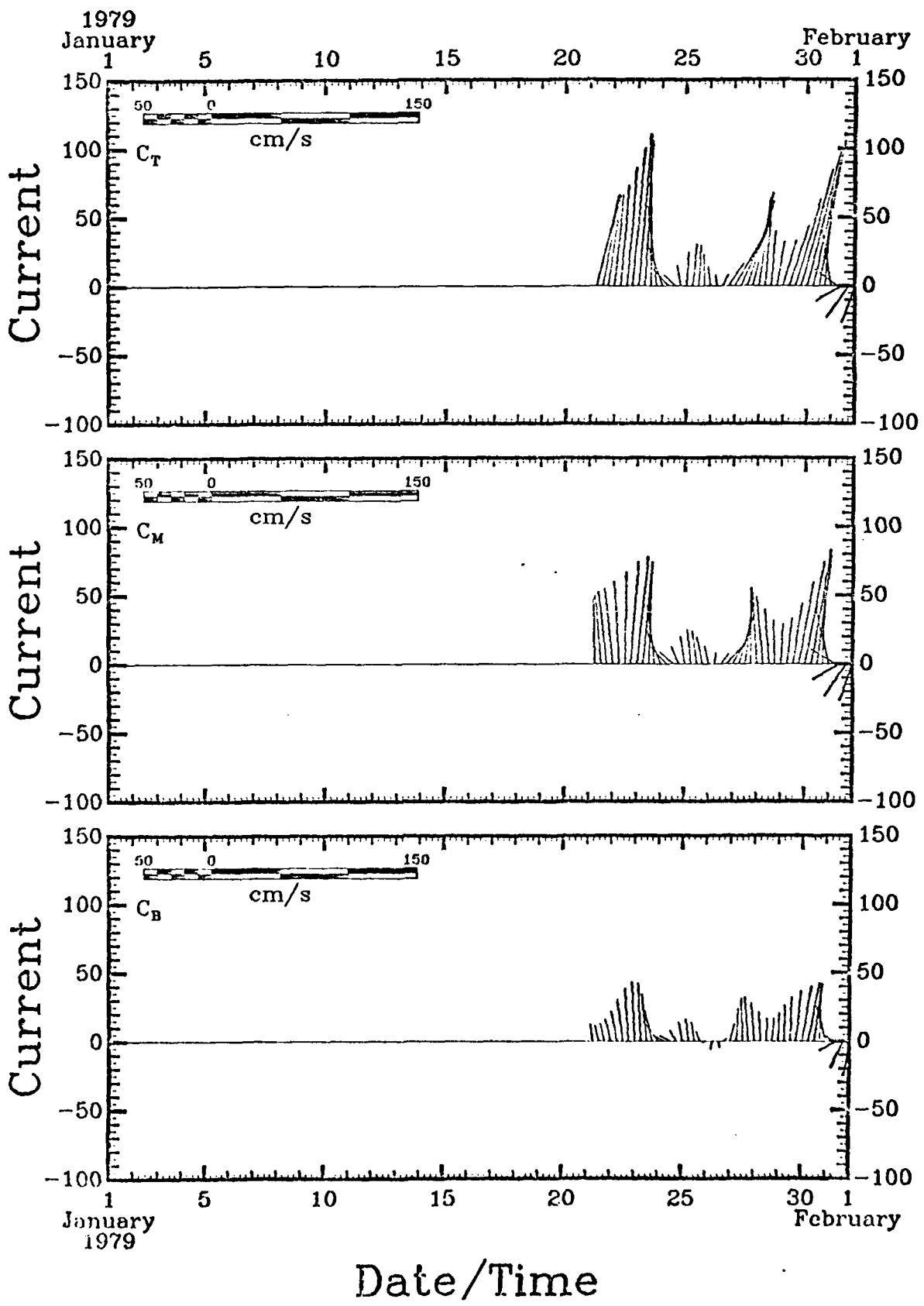
0-A088 069

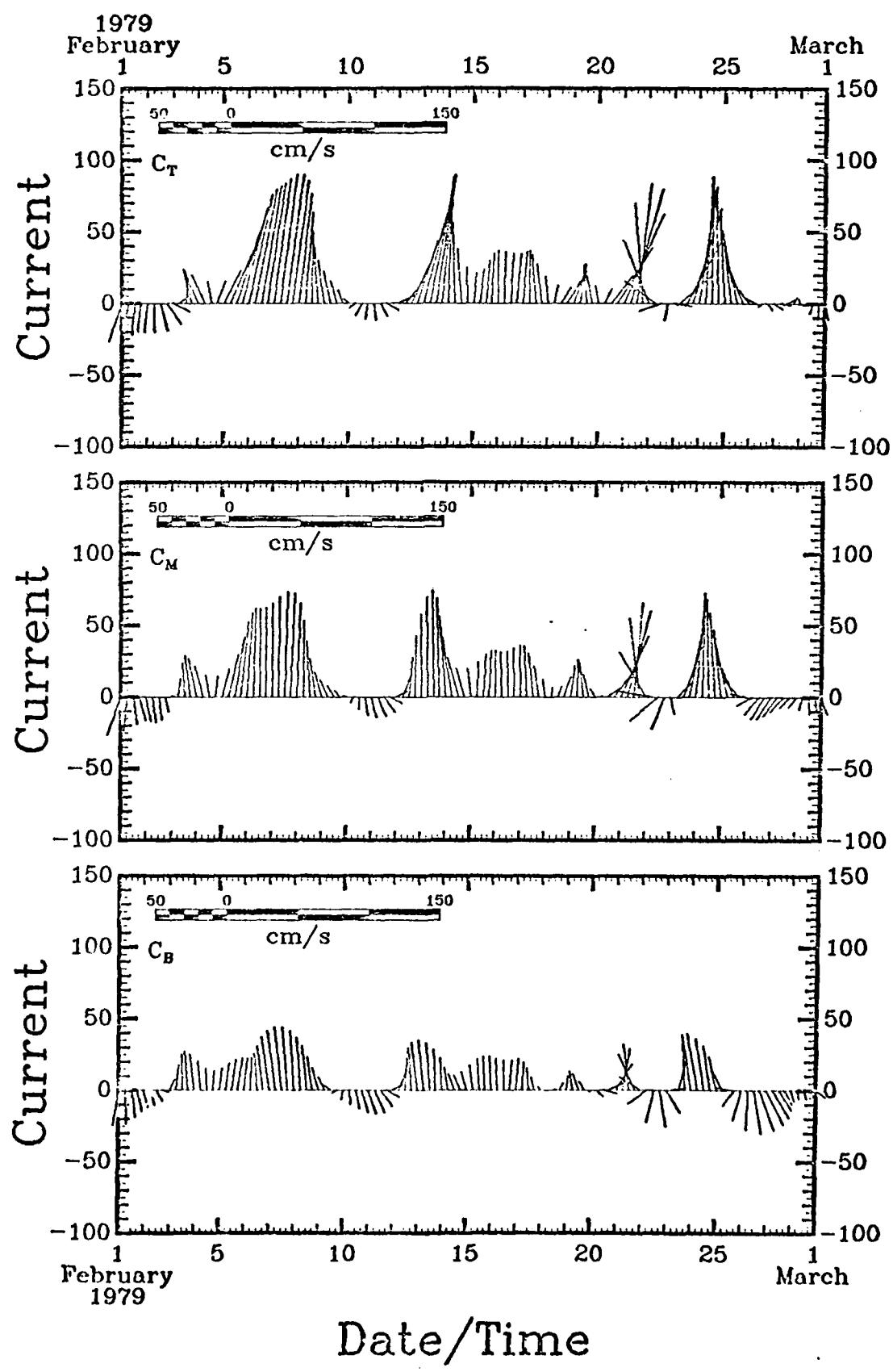
TEXAS A AND M UNIV COLLEGE STATION DEPT OF OCEANOGRAPHY F/0 B/S
THE GULF STREAM MEANDERS EXPERIMENT, CURRENT METER, ATMOSPHERIC--ETC(U)
JUL 80 D A BROOKS, J M BANE, R L COHEN N00014-77-C-0354
TAMU-REF-80-7-T NL

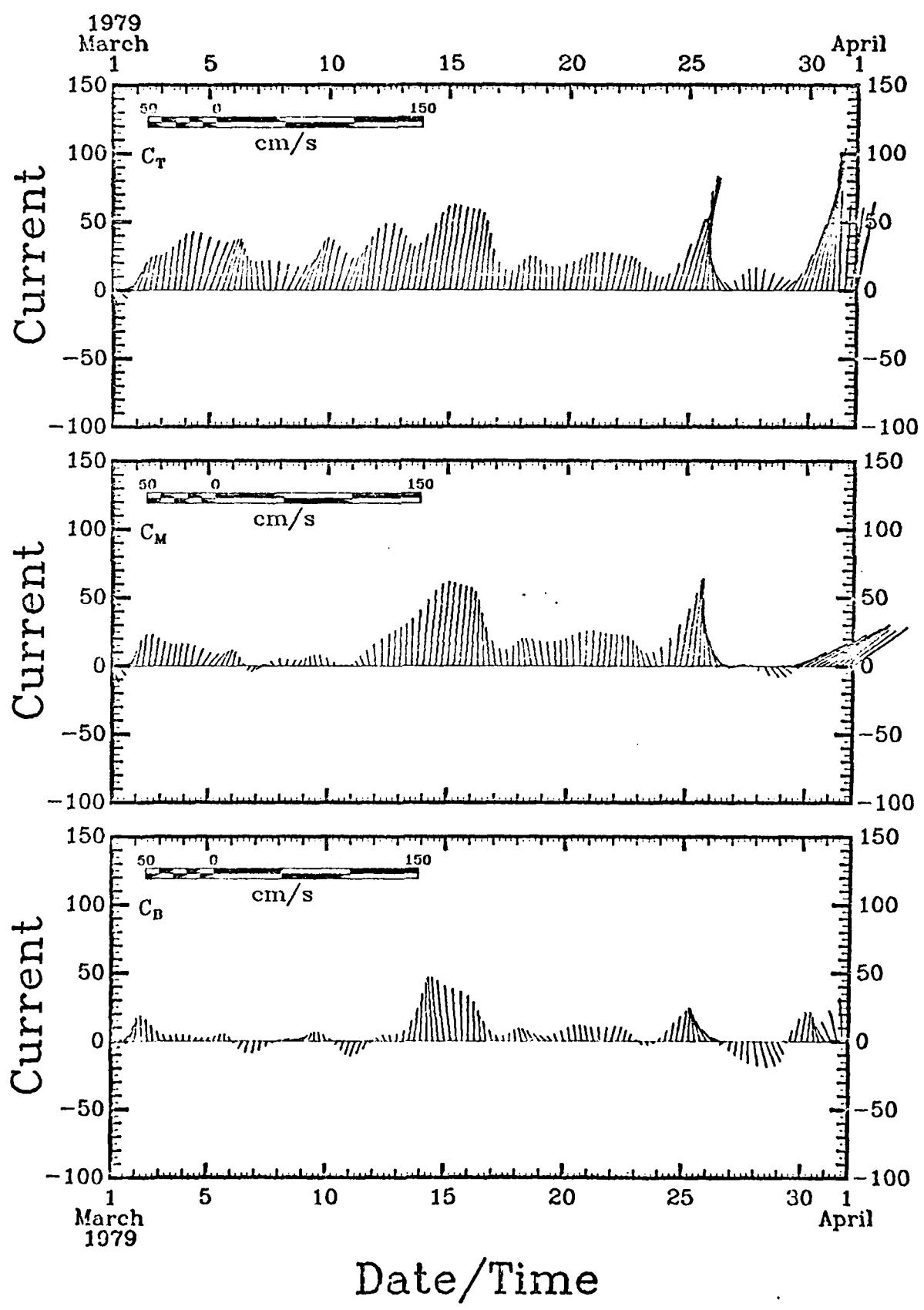
UNCLASSIFIED

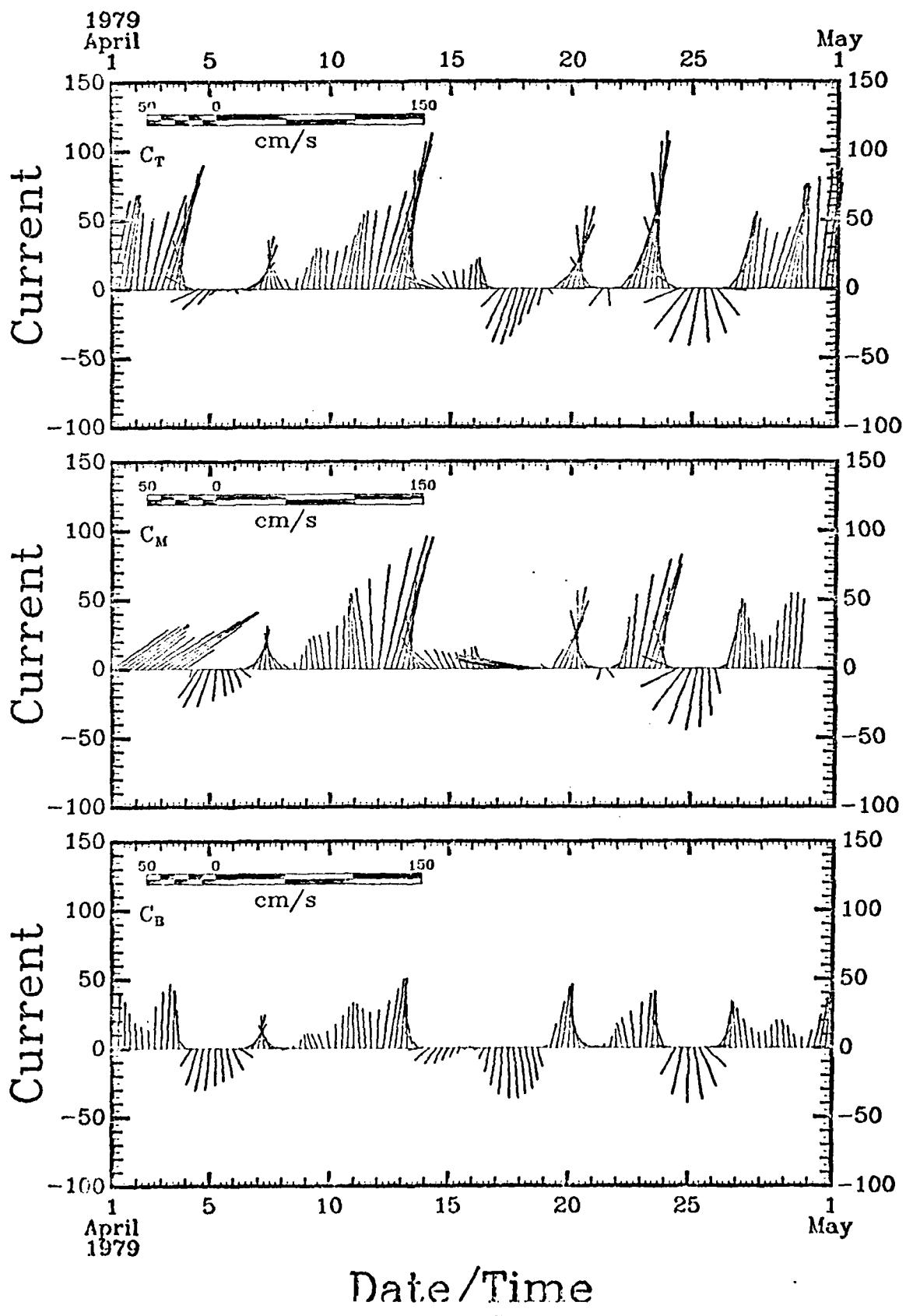
3 of 3
S-6669

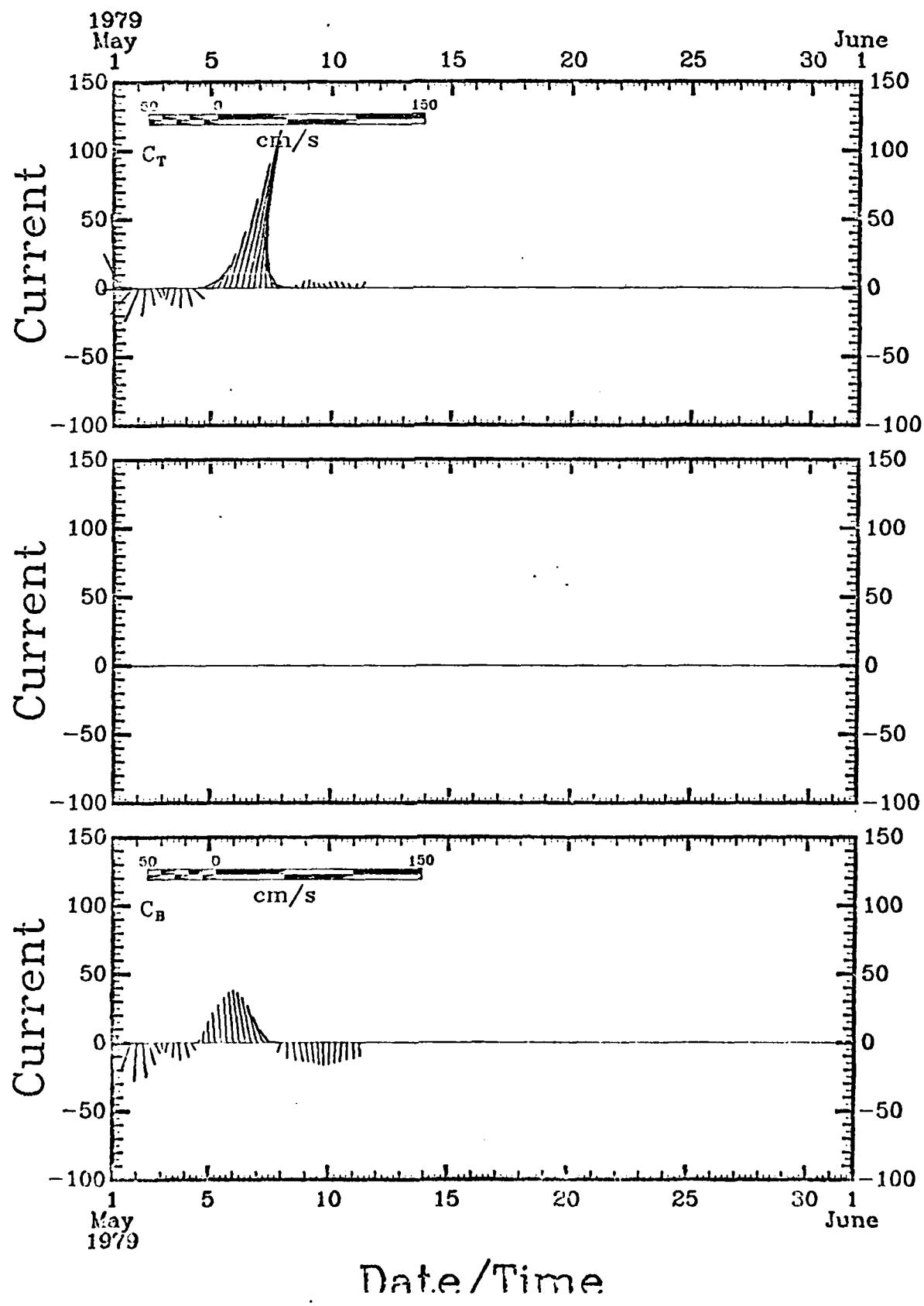
END
DATE
FILED
9-80
DTIC

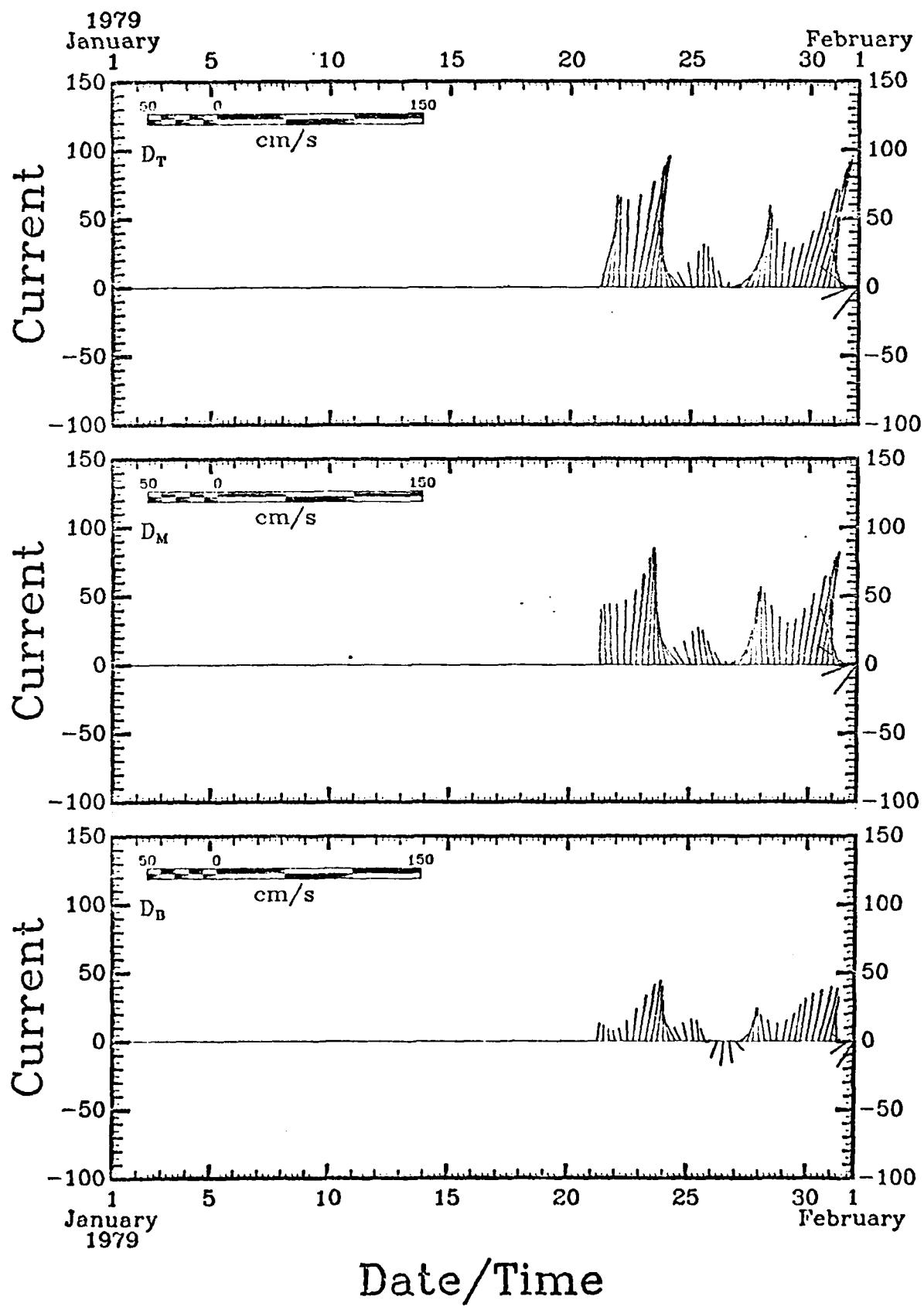


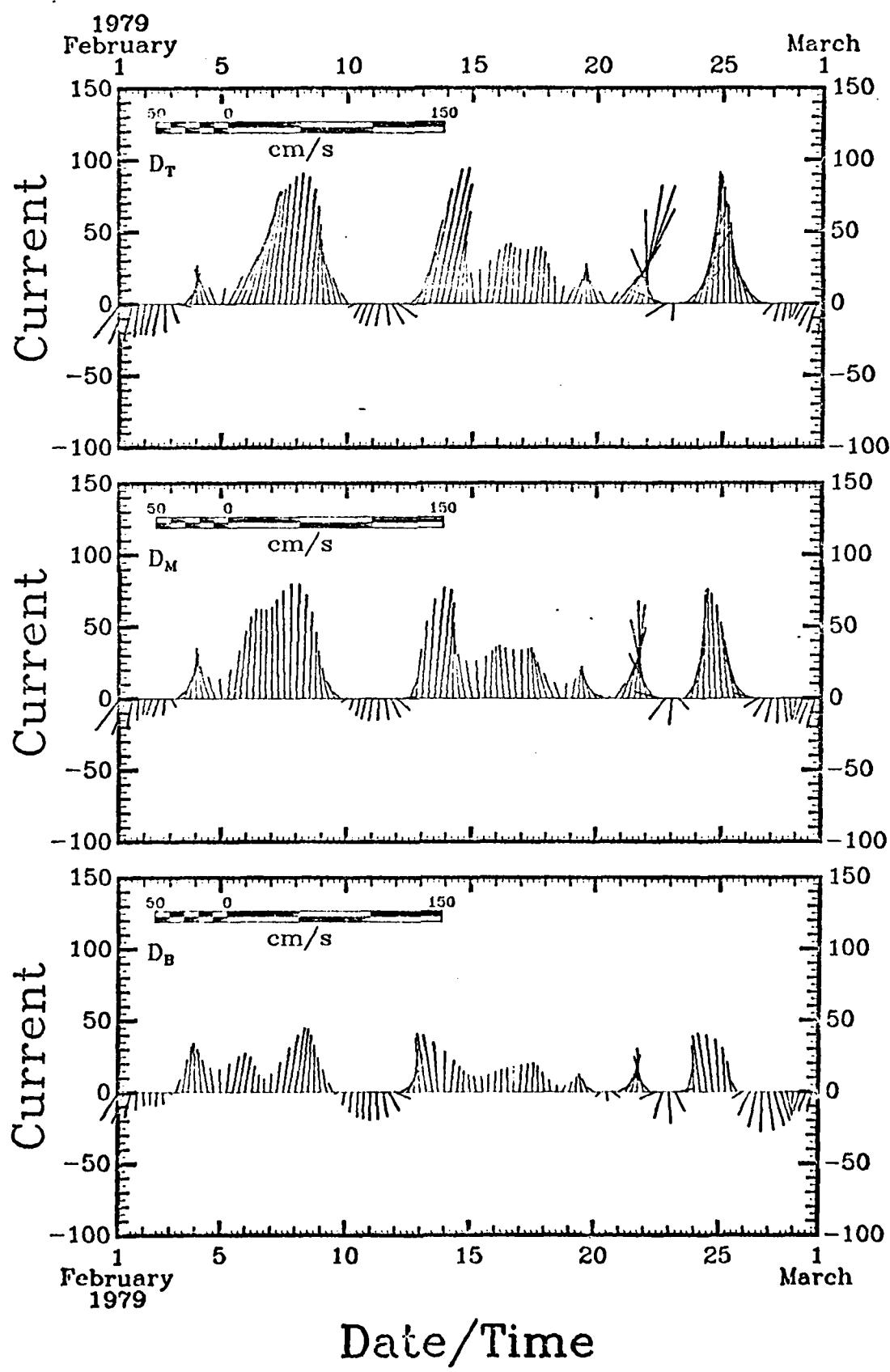


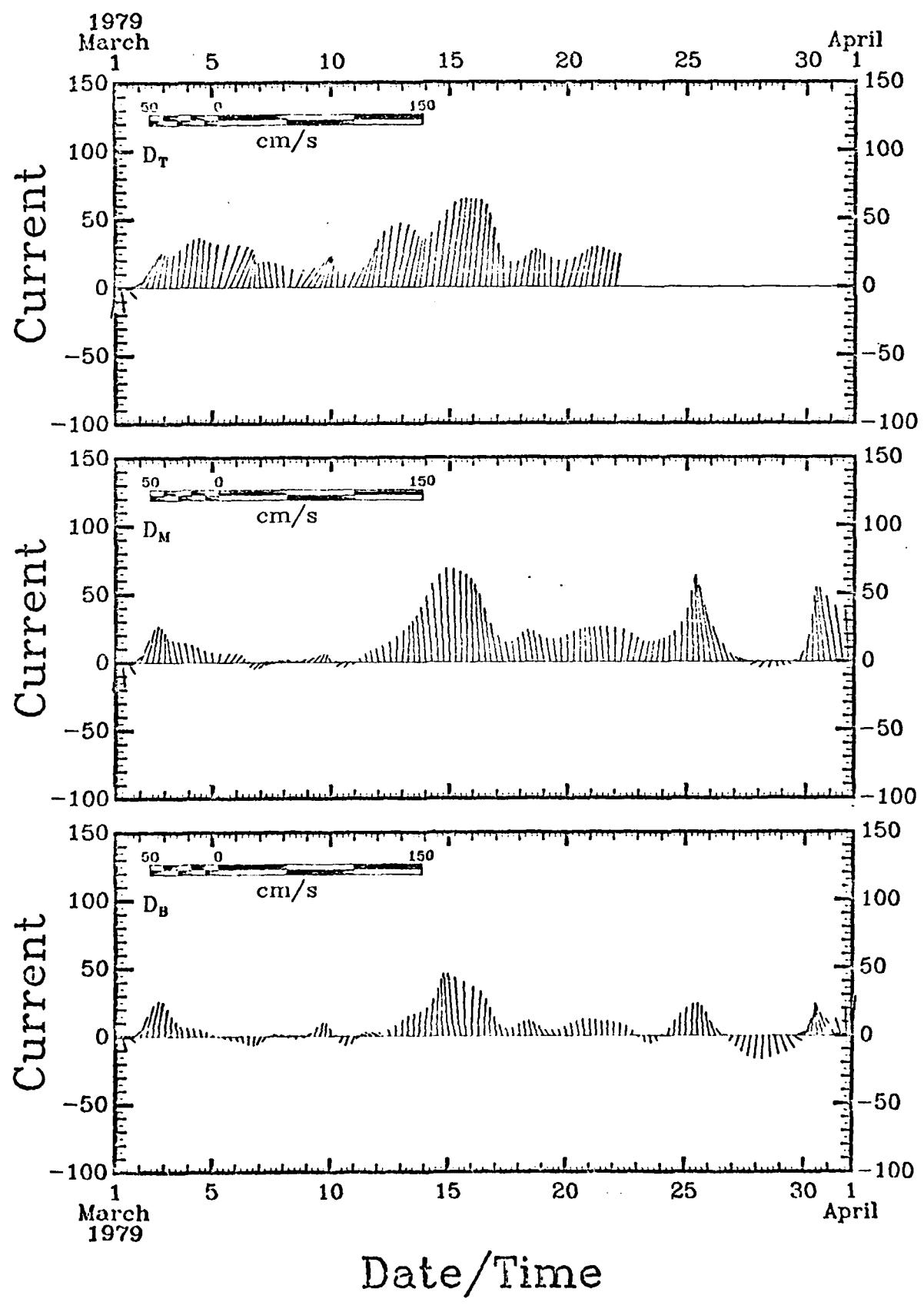


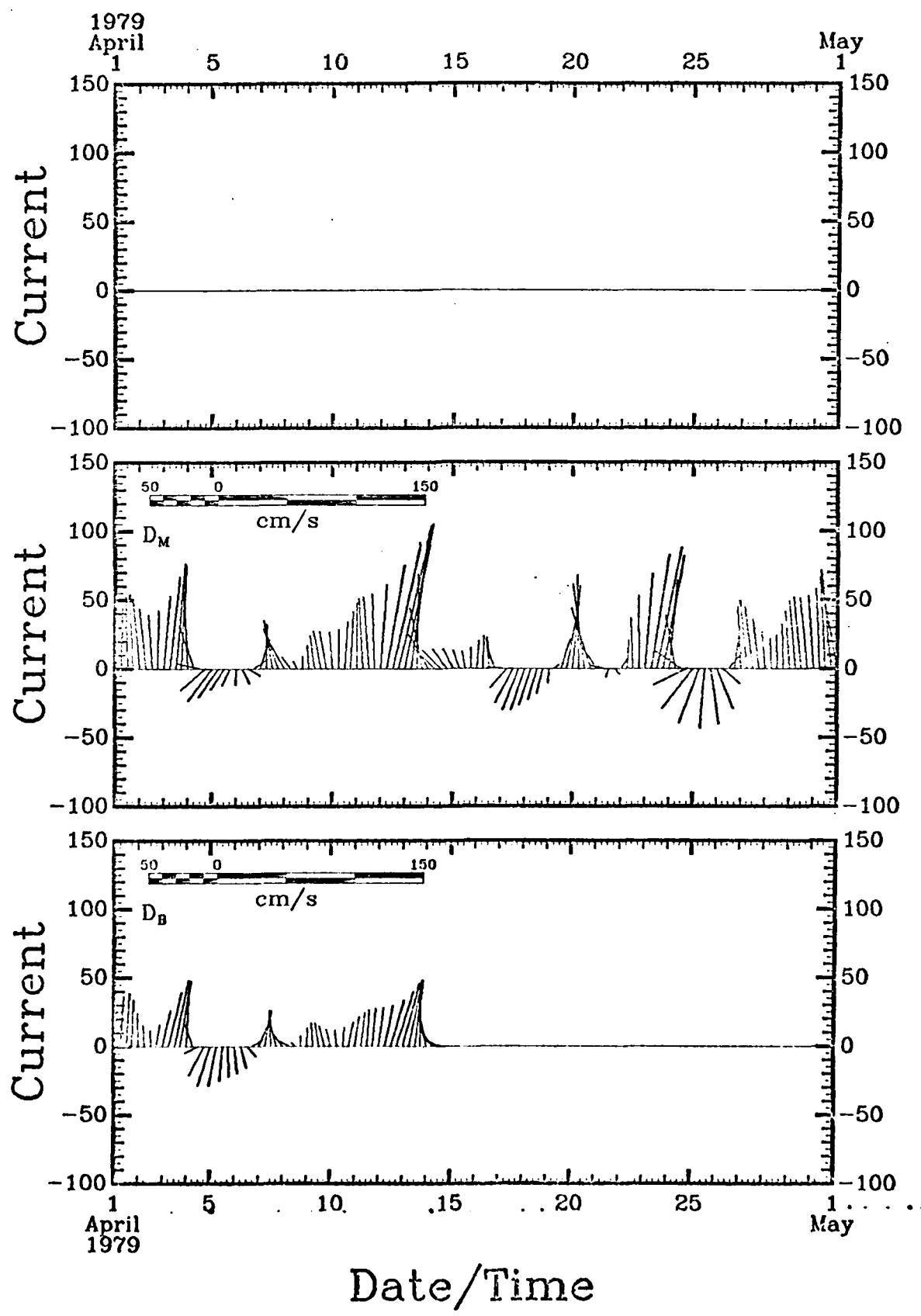


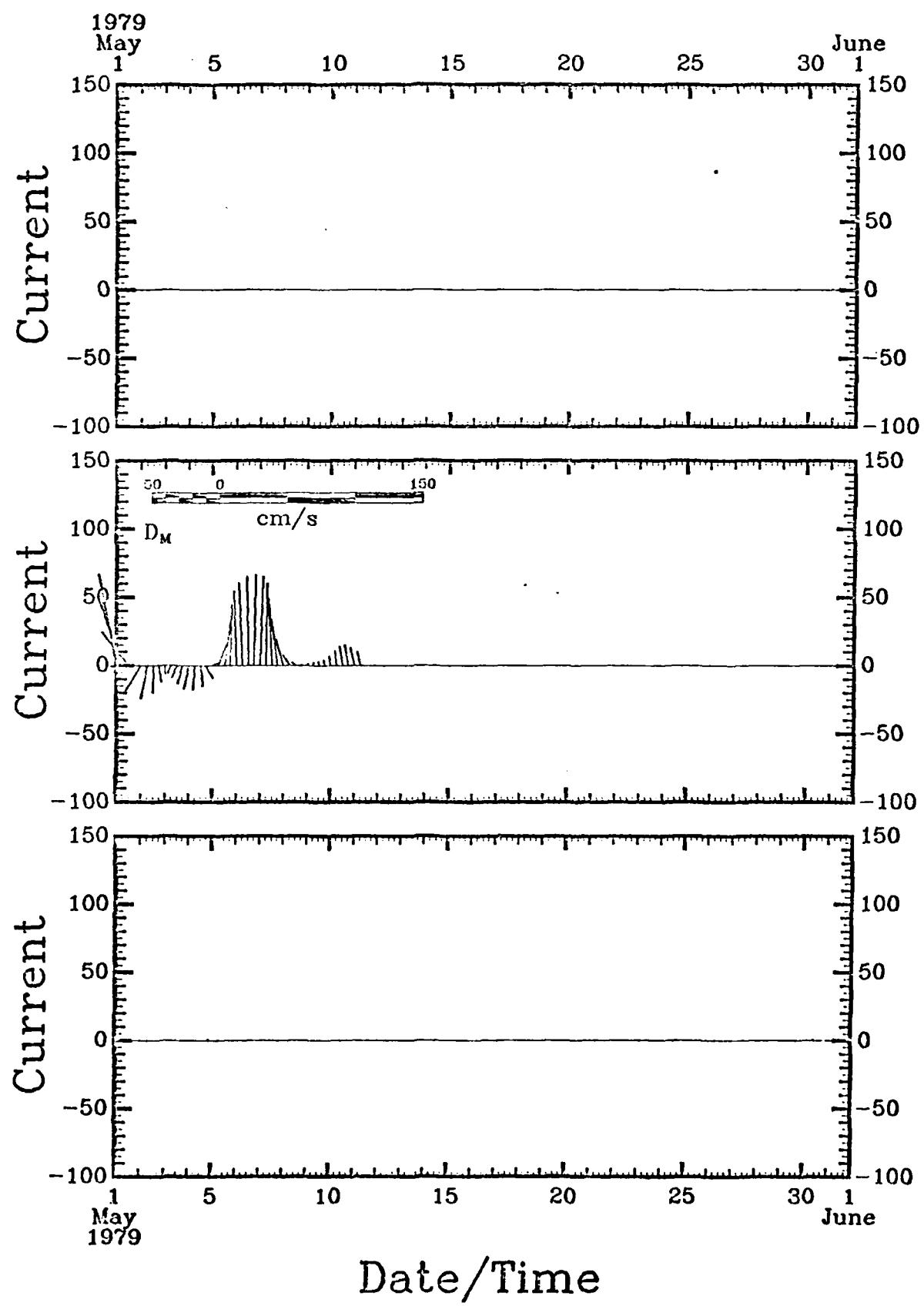










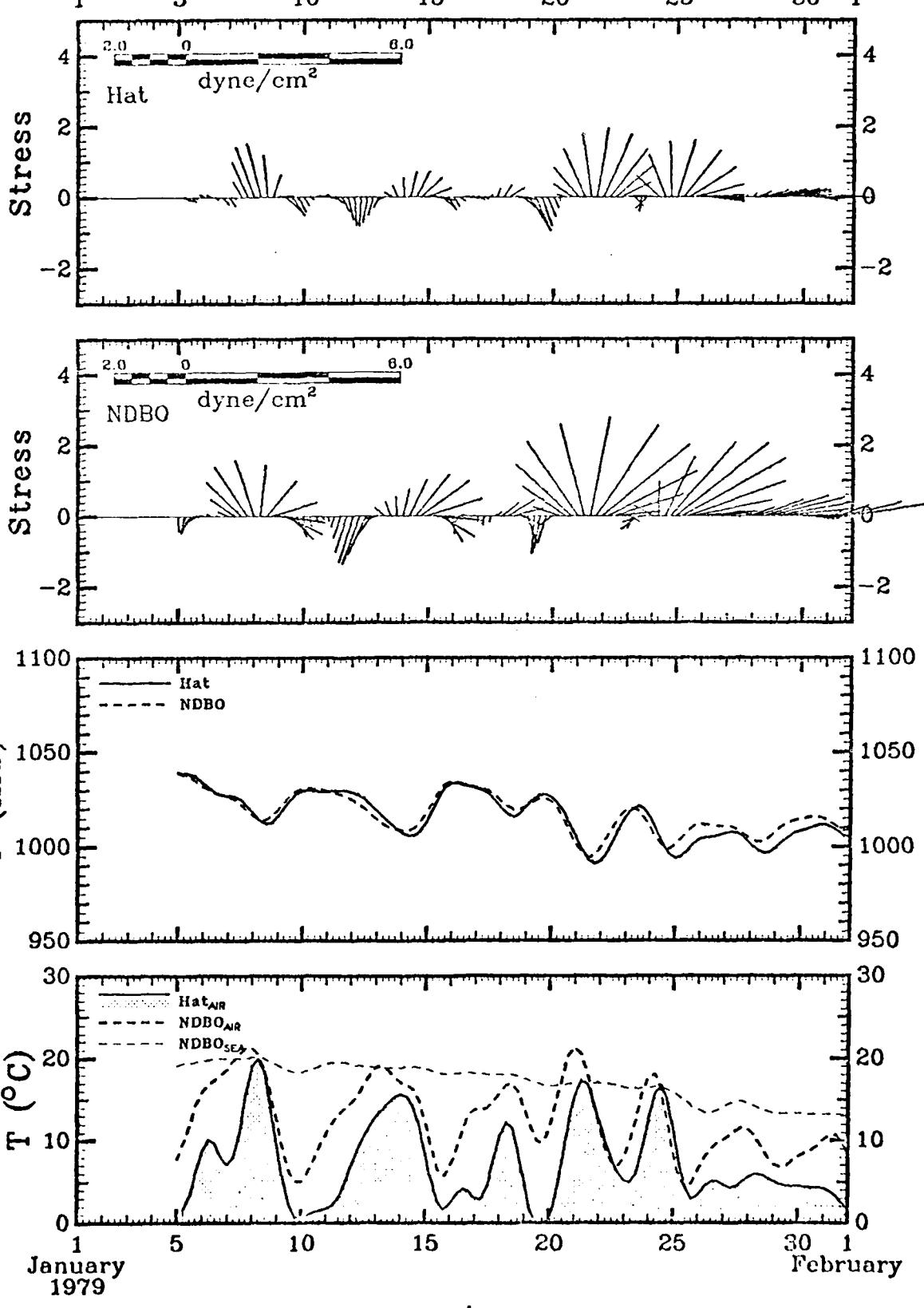


SECTION 7

40 HRLP Atmospheric Data from Cape Hatteras and NDB0 Buoy 41004

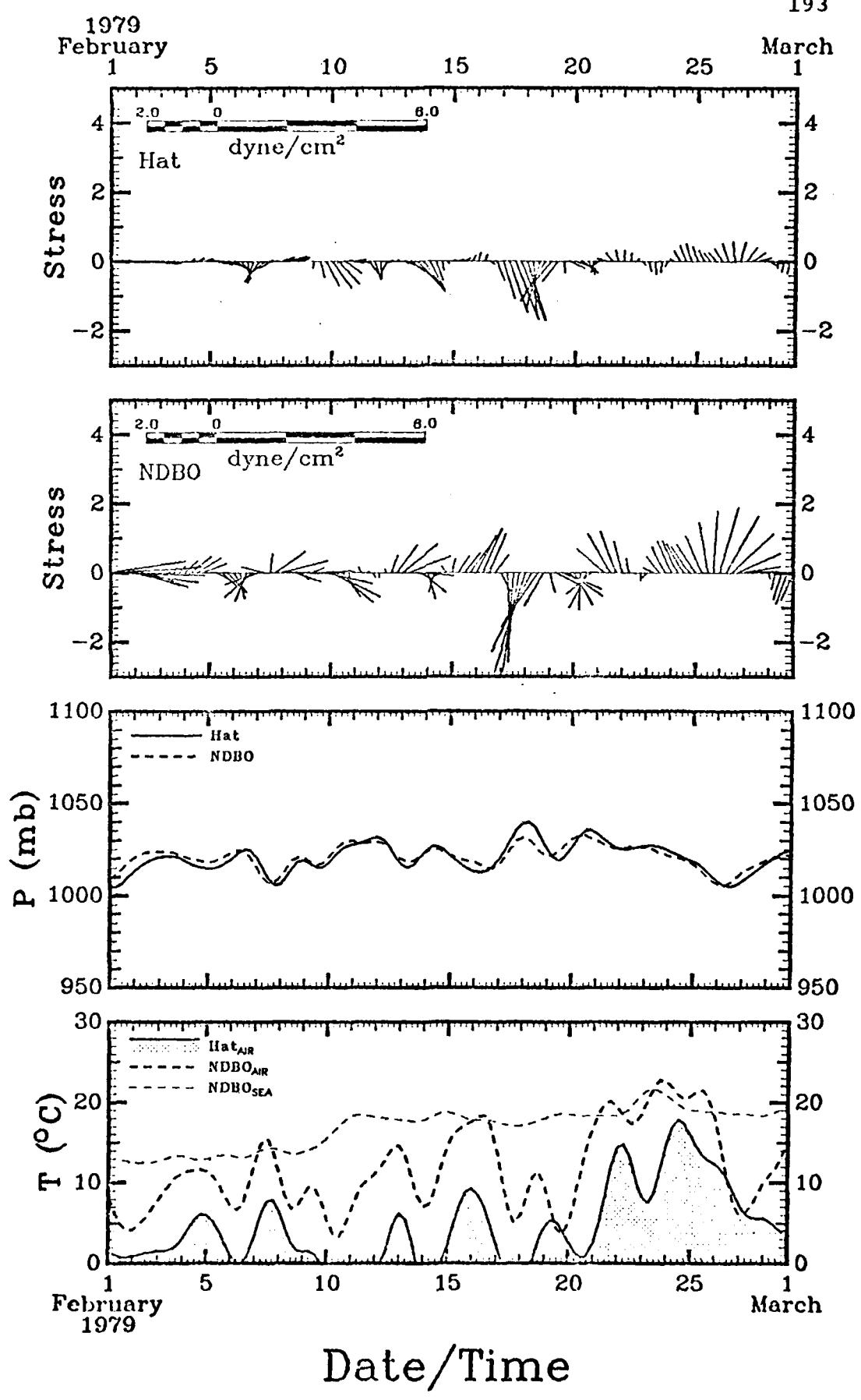
Figure 48 shows by month the 40 HRLP wind stress vector "sticks", the atmospheric pressure, and the air and sea temperatures at Cape Hatteras and the NDB0-4 buoy (see Fig. 1). Vectors pointing toward the top of the page correspond to flow in the downstream (34°T) direction. Common scaling is used in this section.

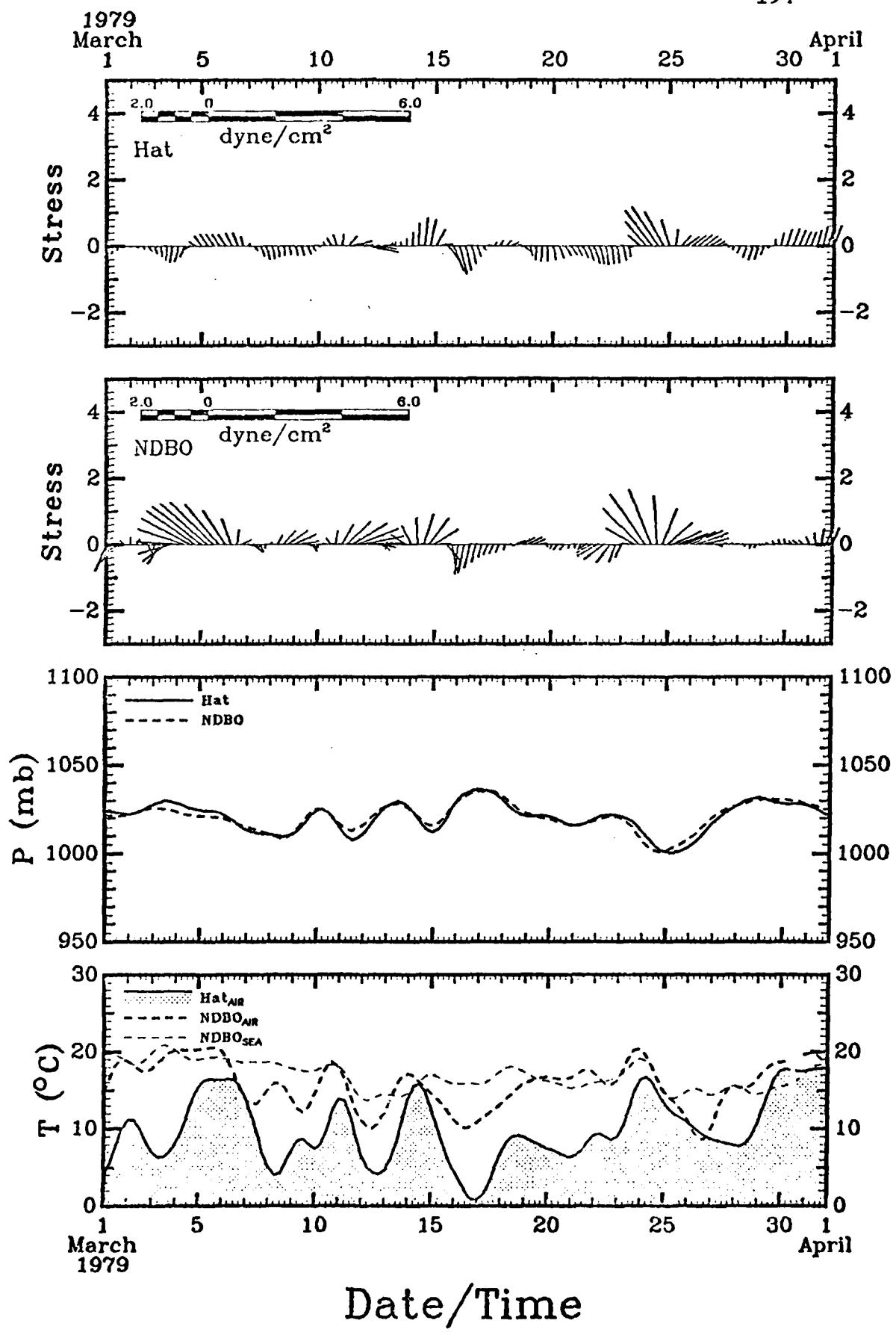
192

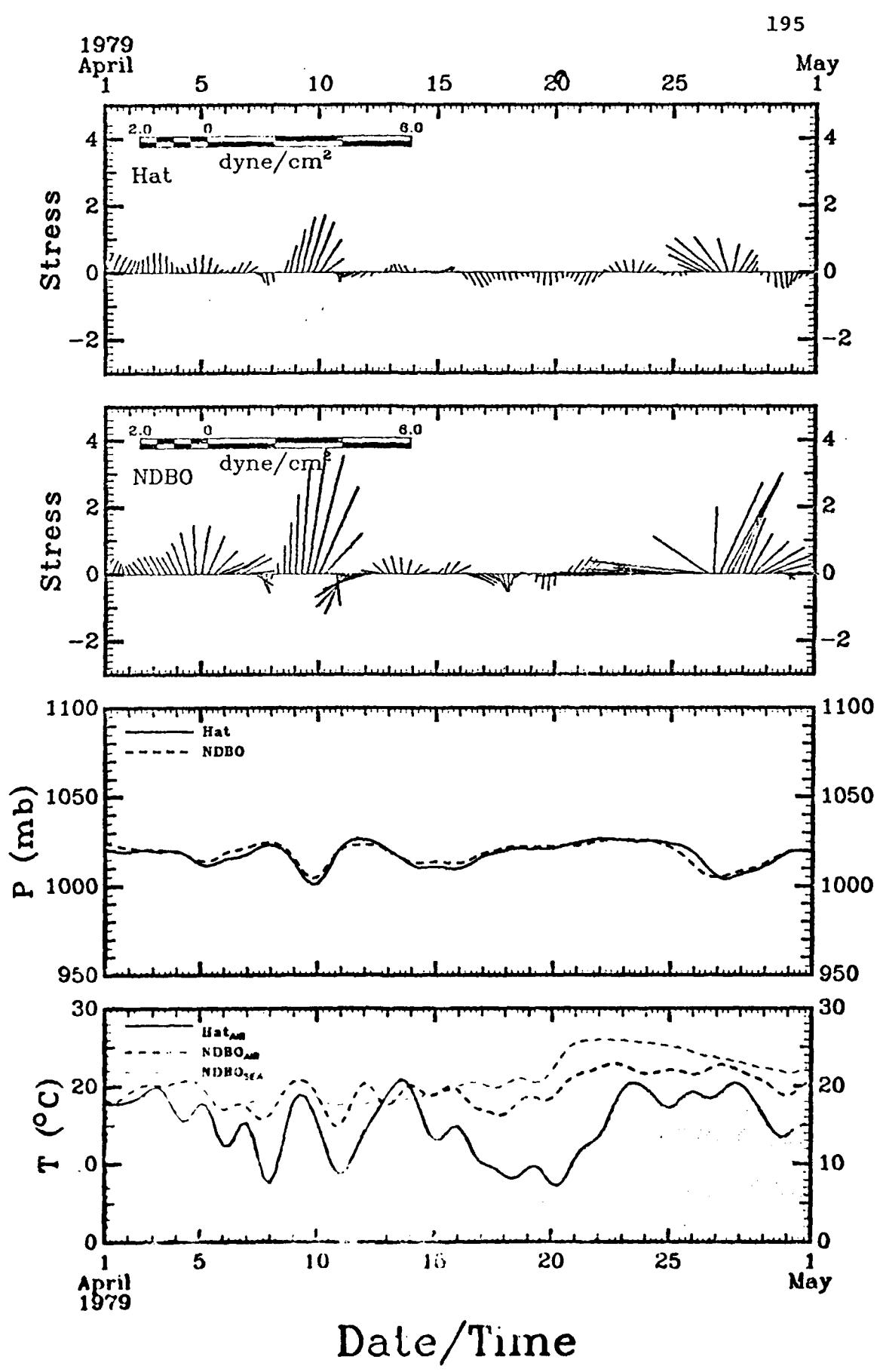
1979
JanuaryFebruary
30 1

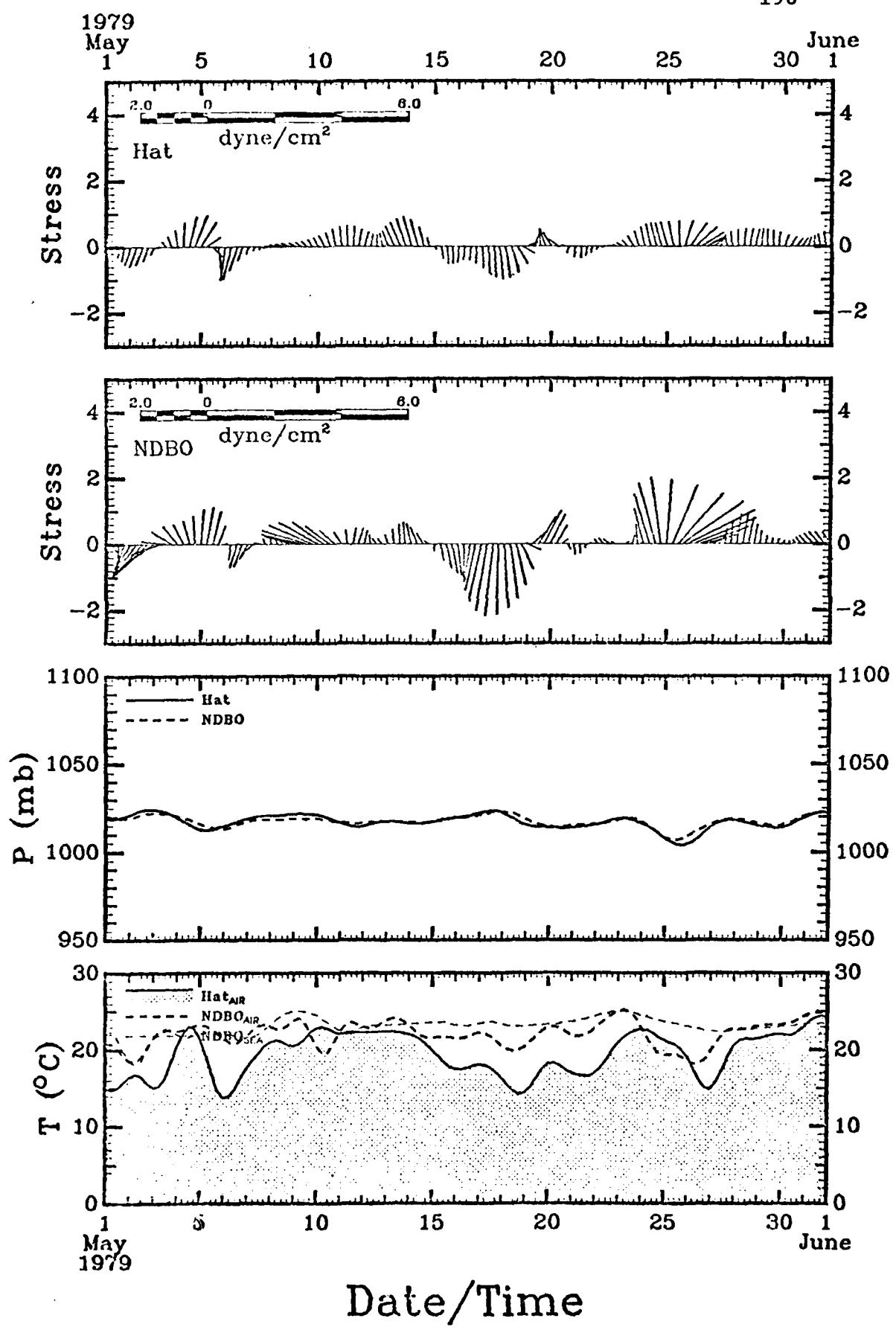
Date/Time

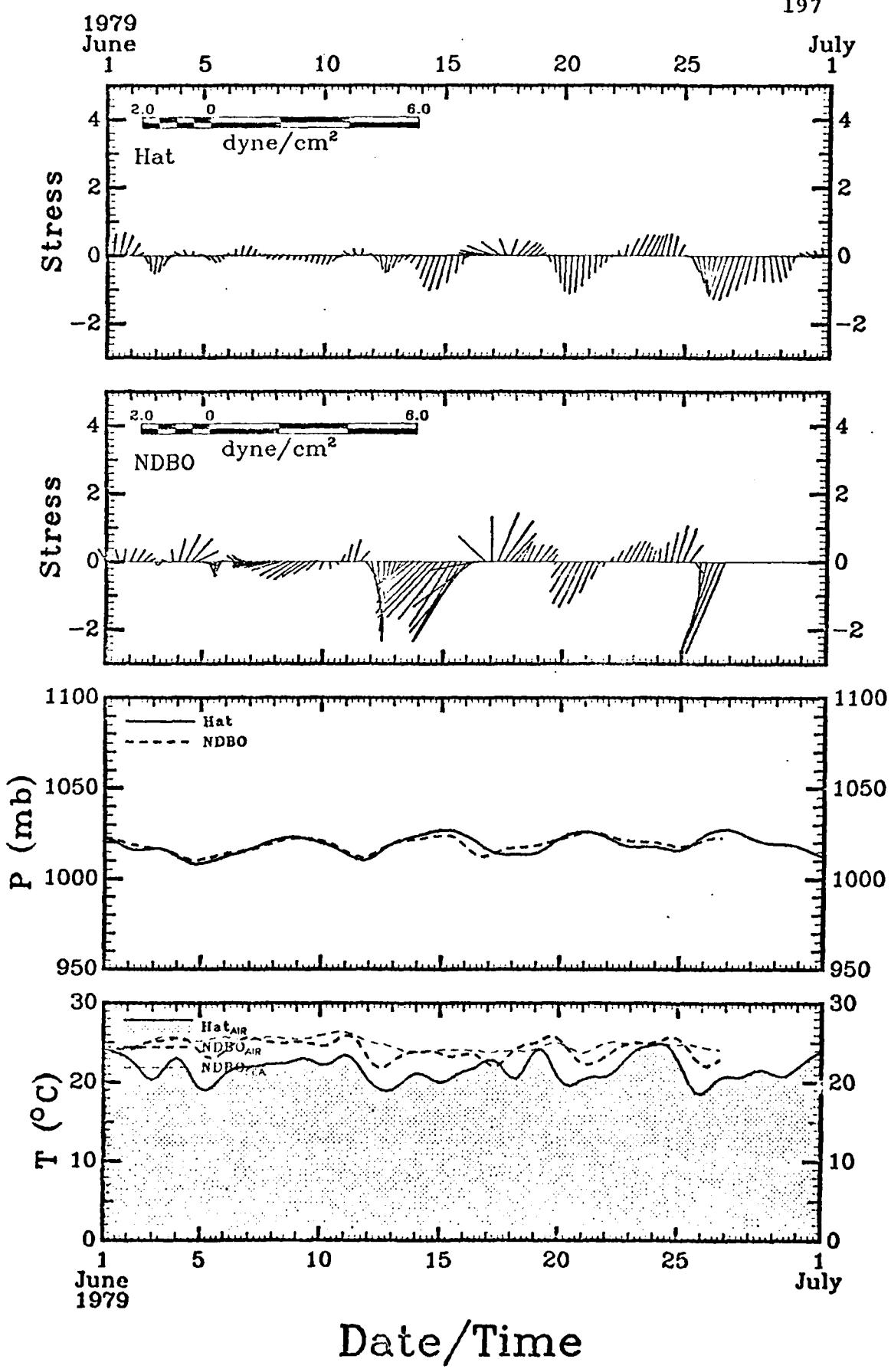
193



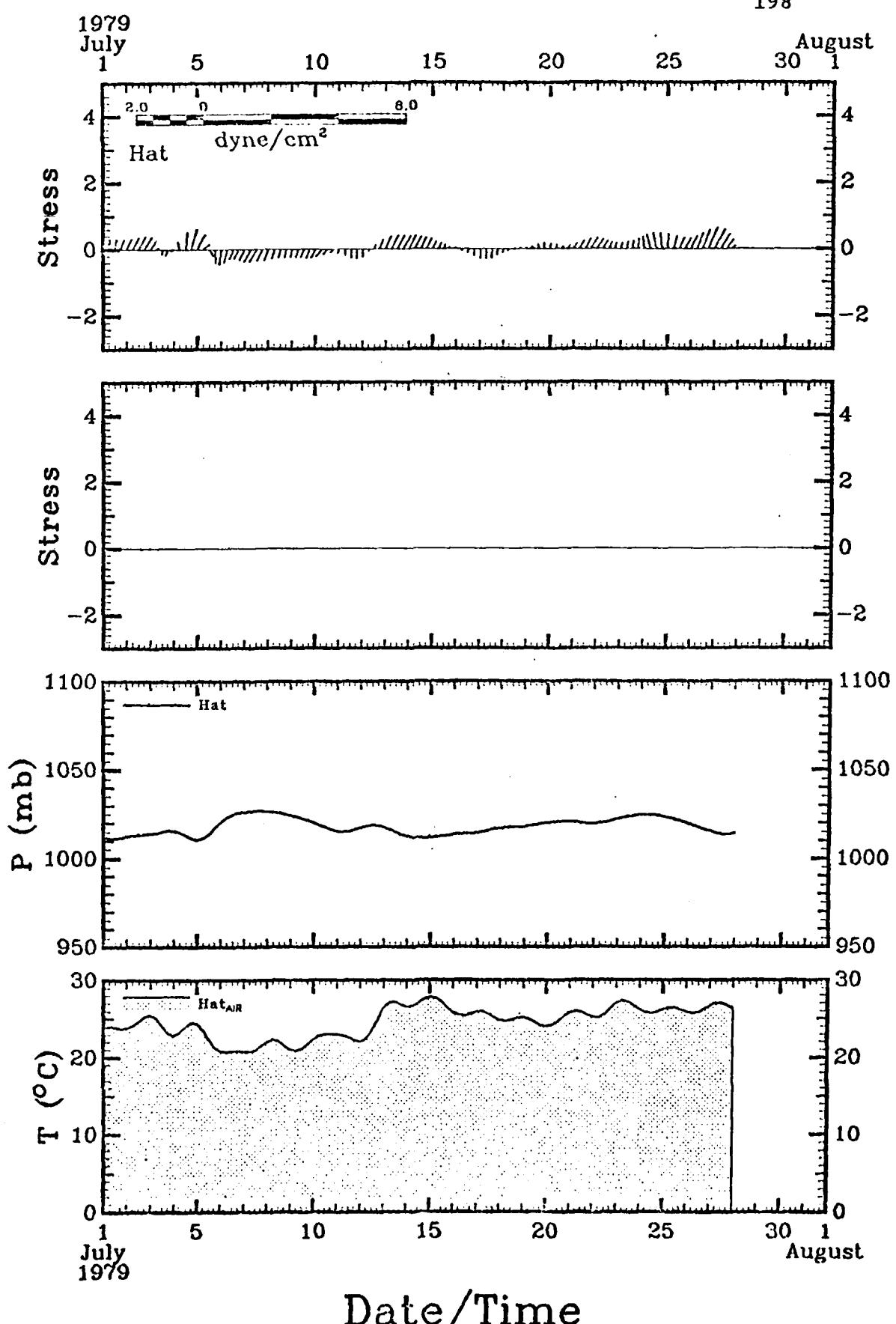








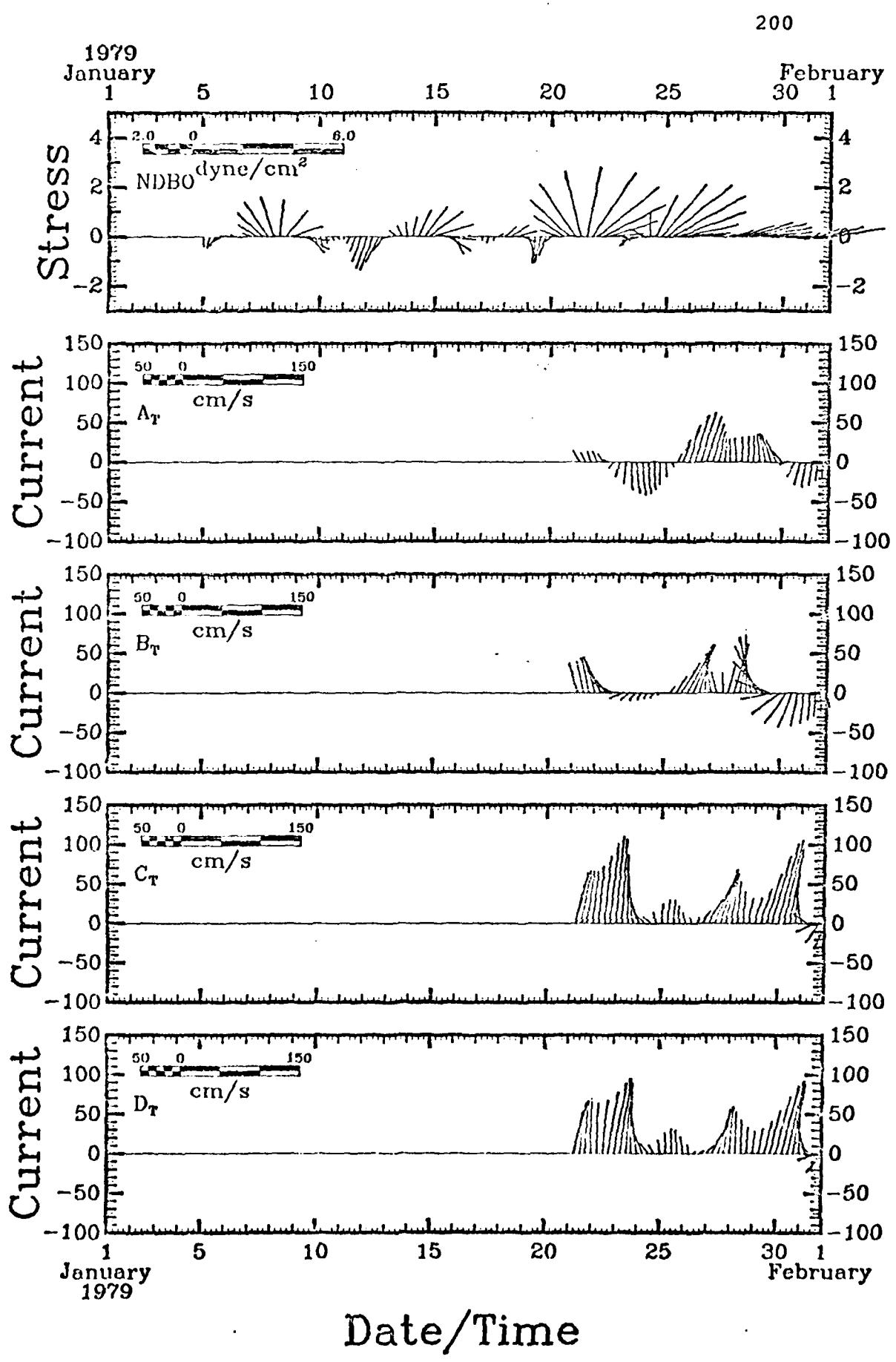
198

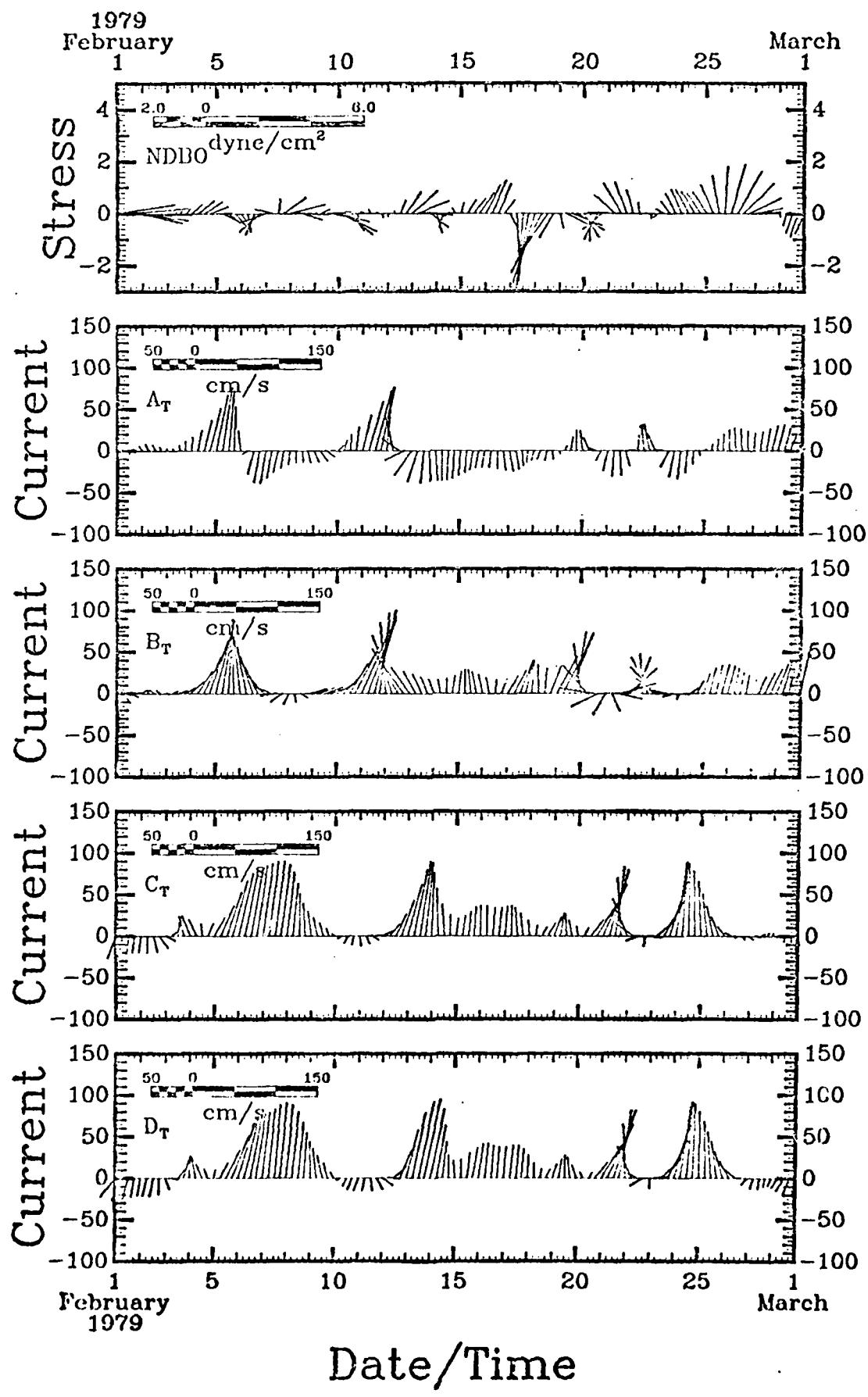


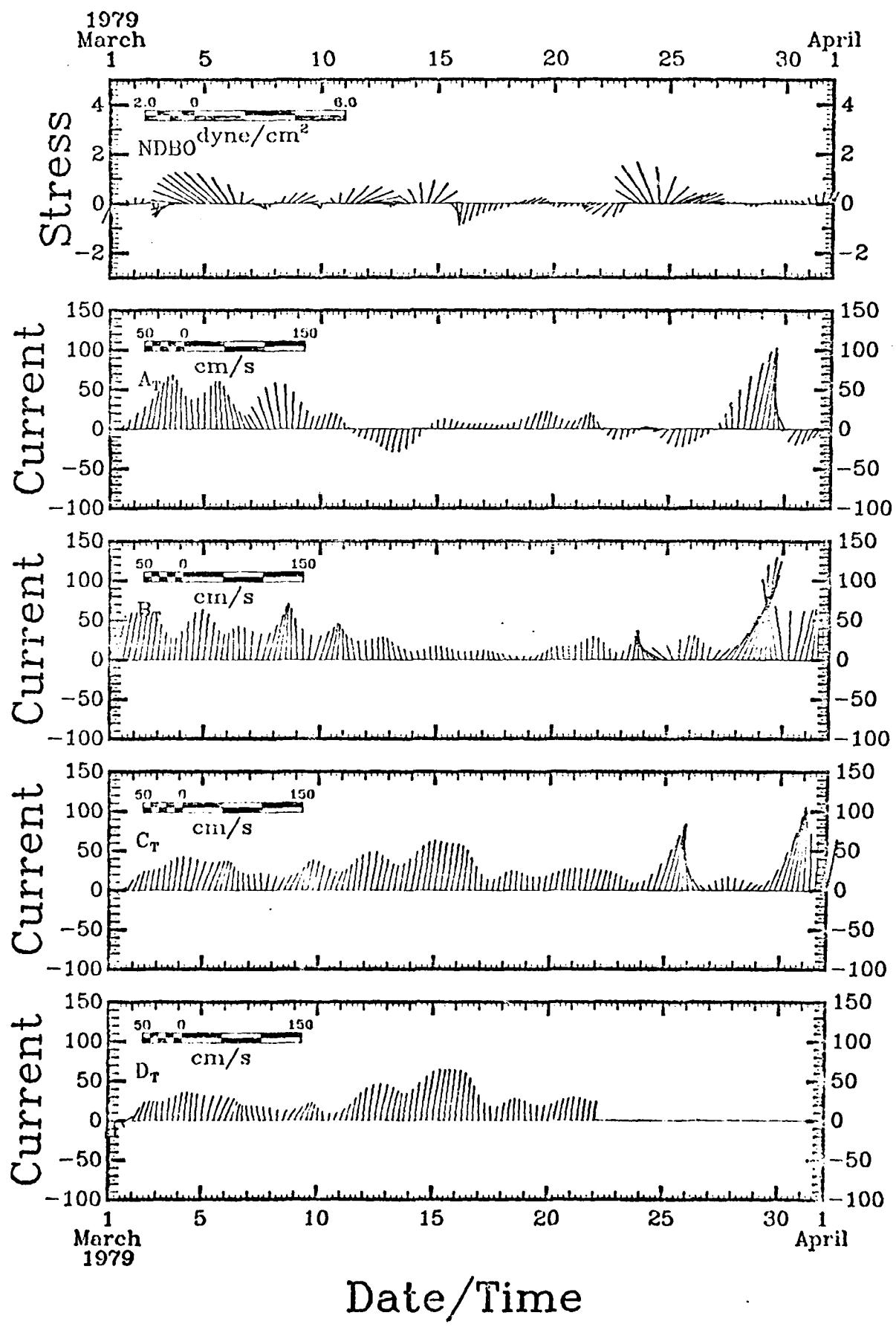
SECTION 8

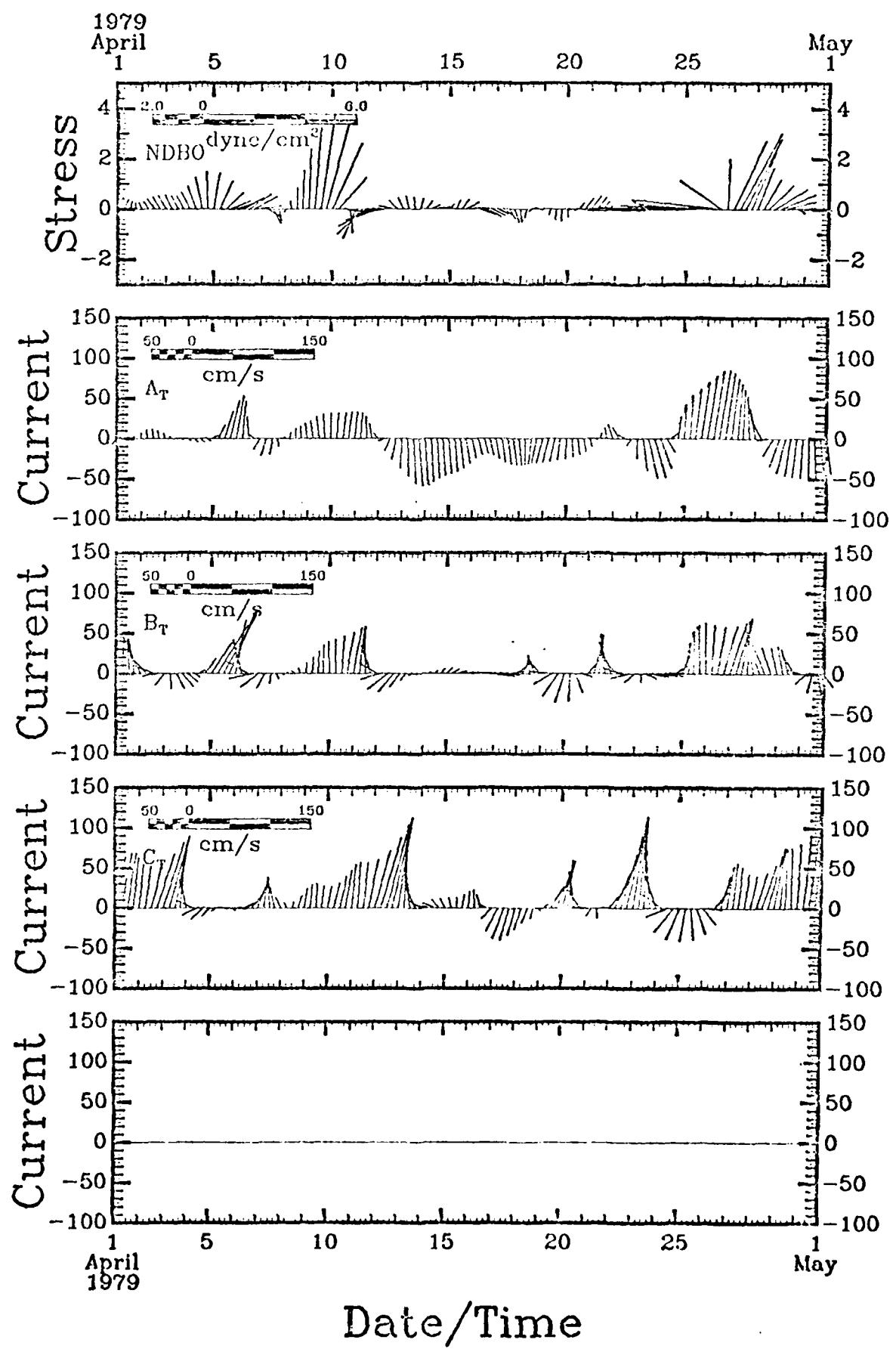
Comparison of 40 HRLP Wind Stress and Current Vector "Sticks"

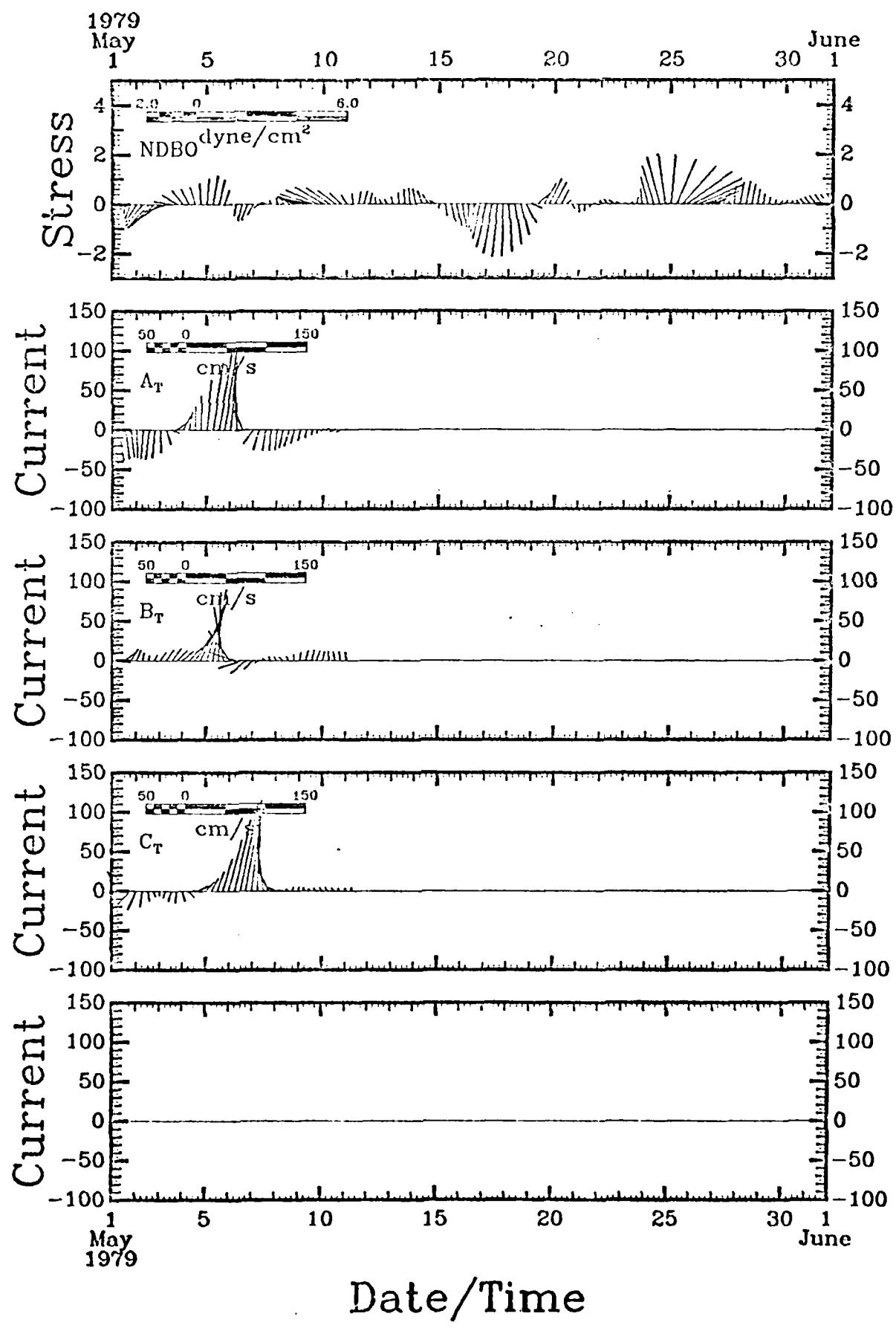
Figure 49 shows by month the 40 HRLP NDB0-4 wind stress vector "sticks" and the 40 HRLP current vector "sticks" for the topmost instrument on each mooring. Vectors pointing toward the top of the page correspond to flow in the downstream (34°T) direction. Common scaling is used in this section. Very little correlation is evident between the wind stress and currents.

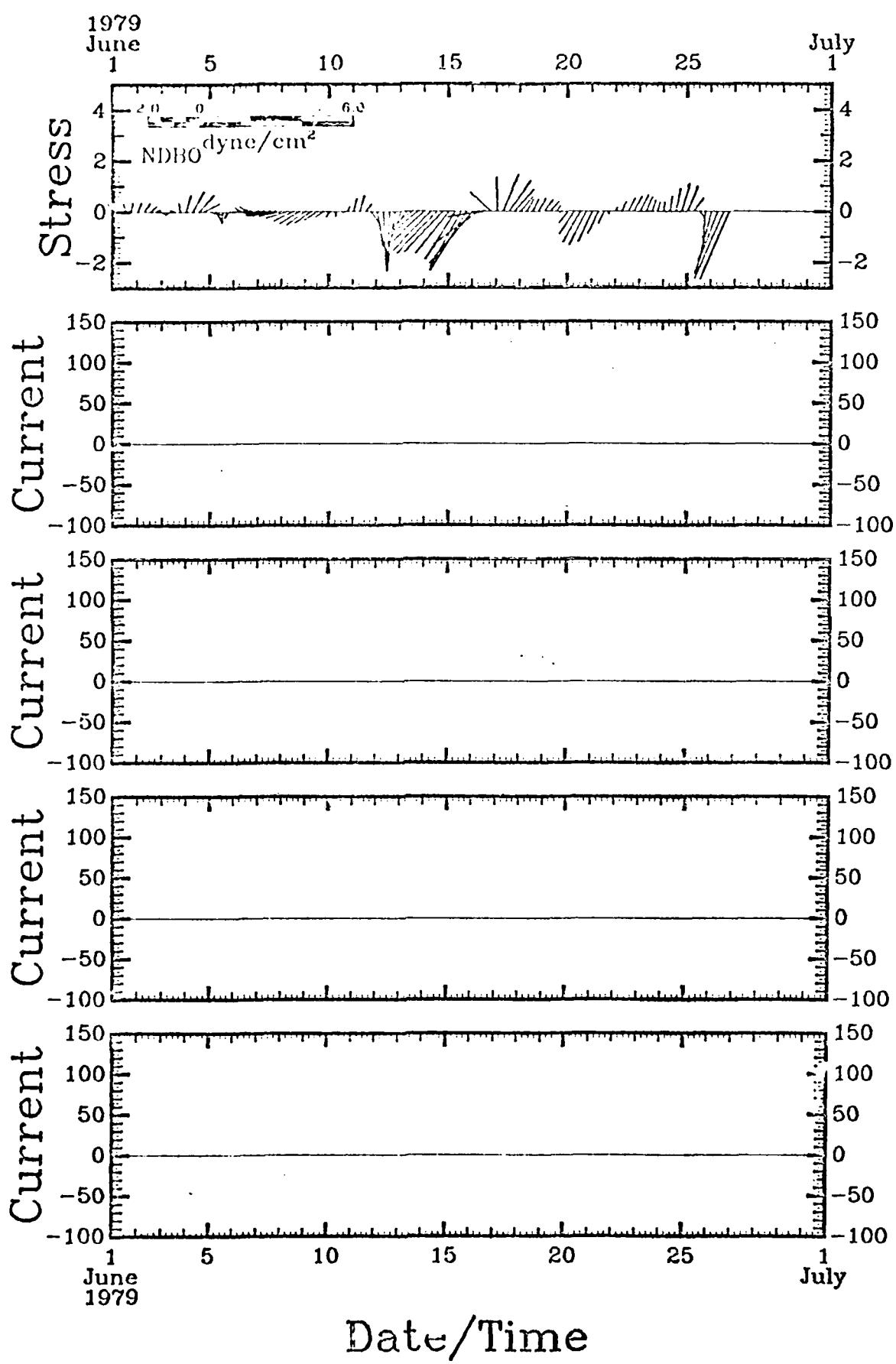








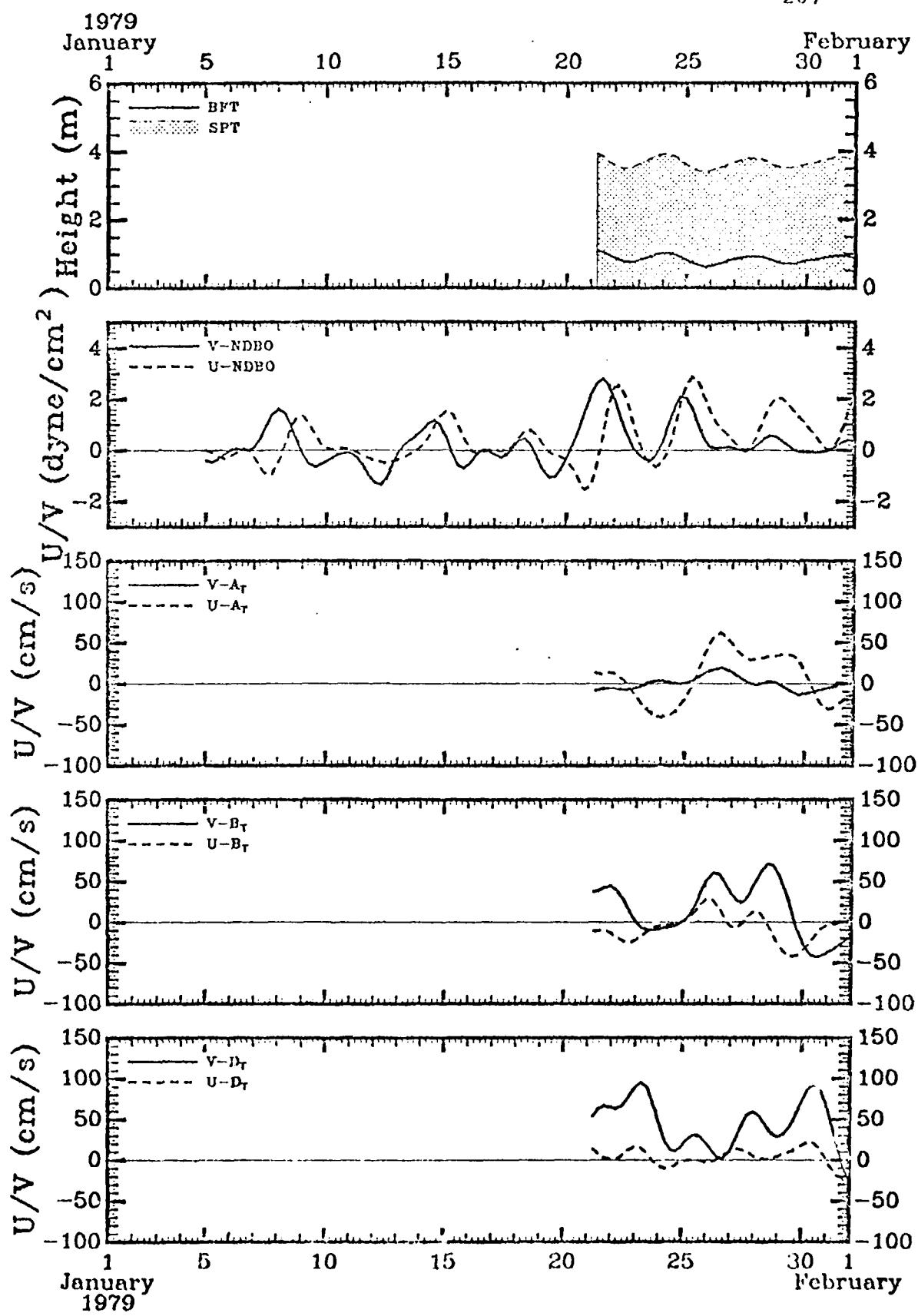




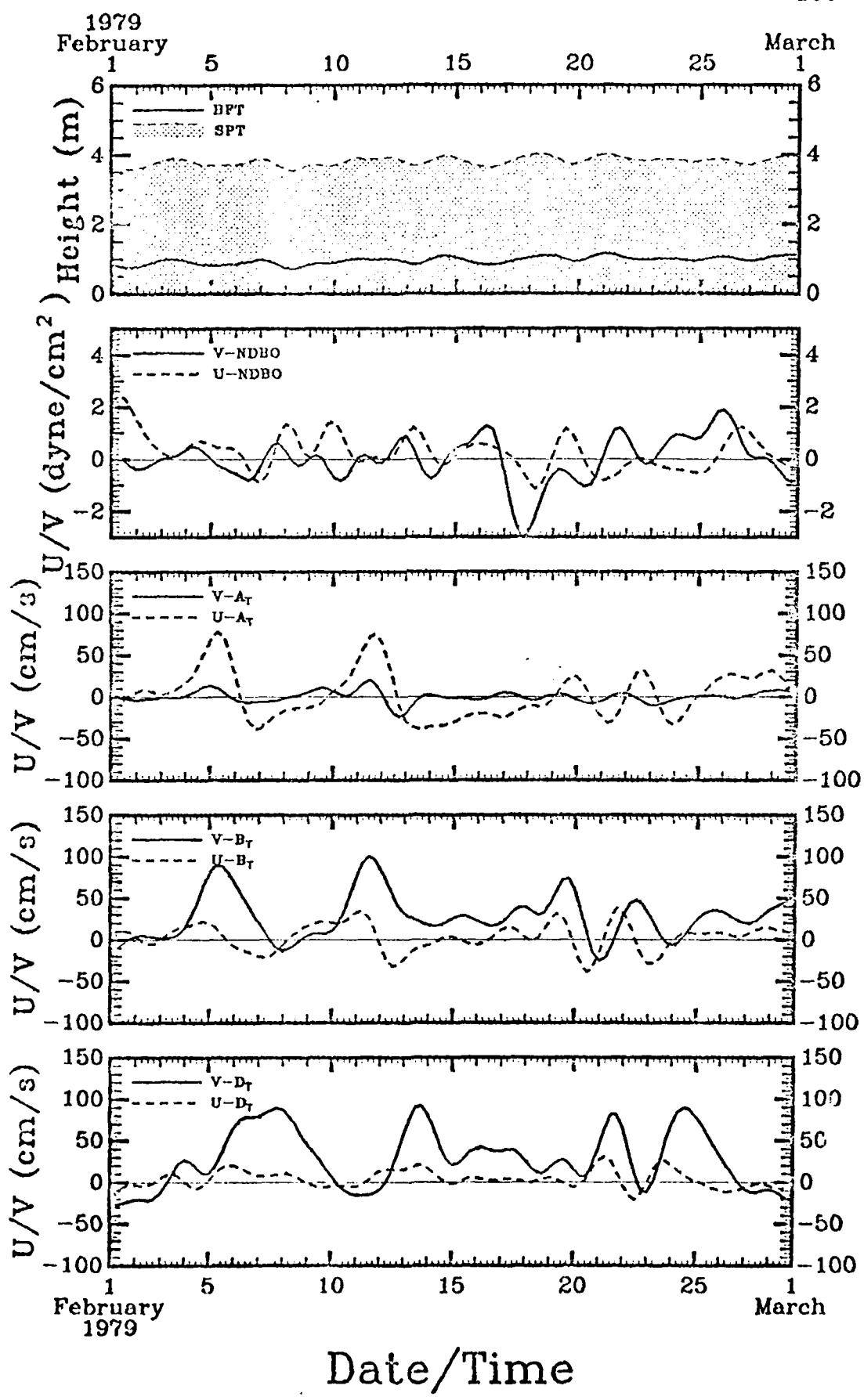
SECTION 9

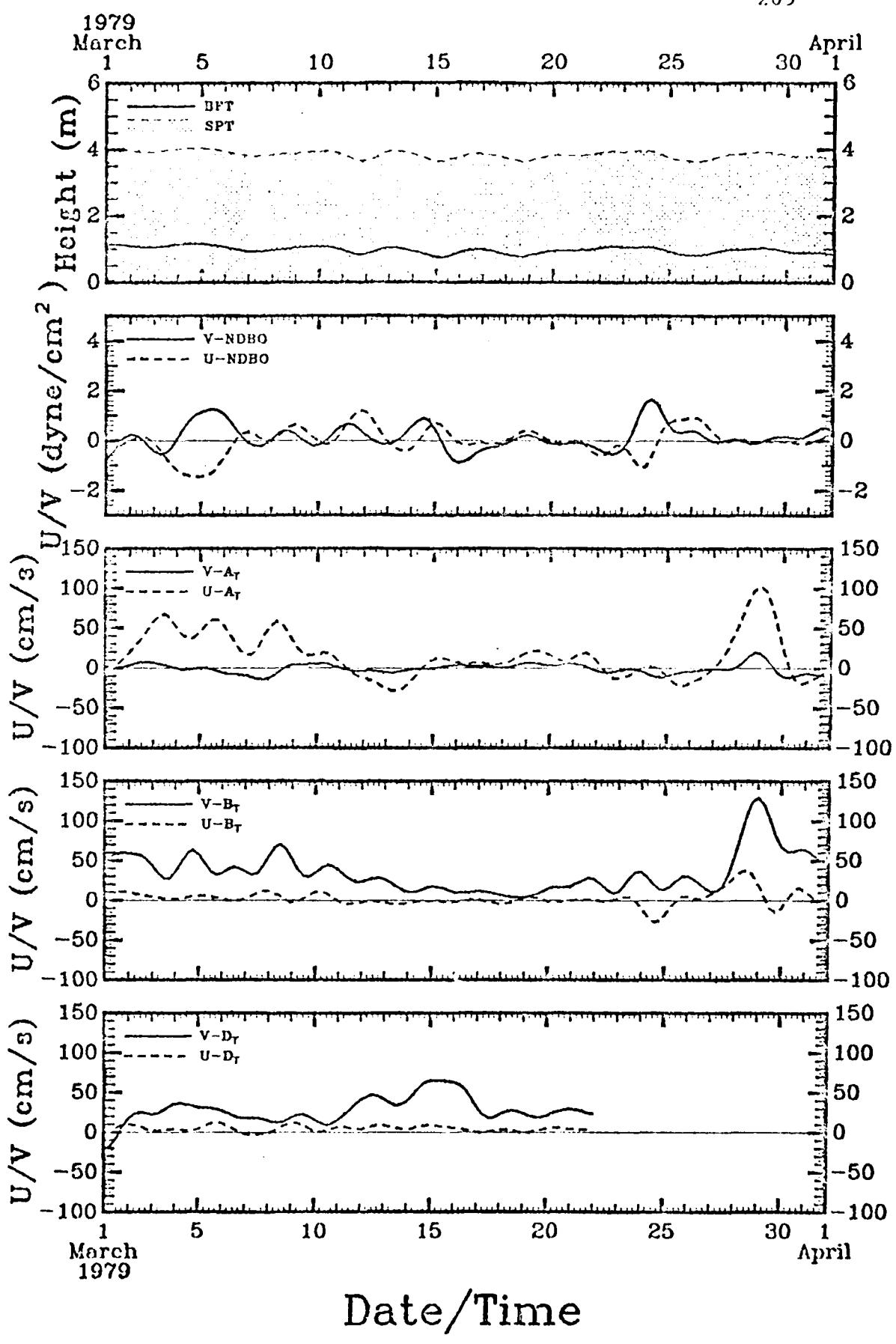
40 HRLP Sea Level Height, Wind Stress, and Current Velocity Components

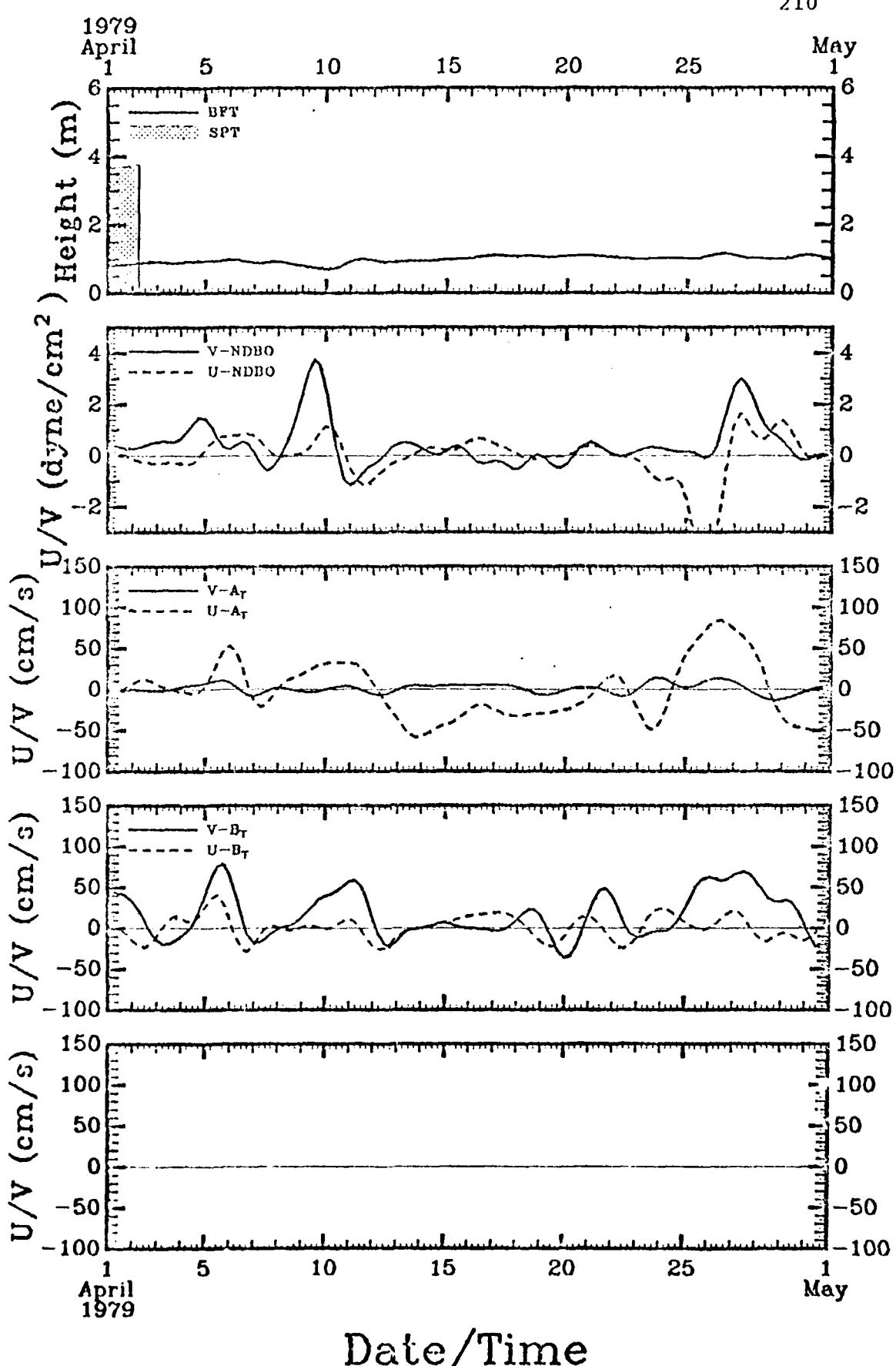
Figure 50 shows by month the adjusted sea level height at Beaufort (BFT) and at Southport (SPT), the u/v (offshore/downstream) components of Hatteras wind stress, and the u/v current vector components at the topmost instruments on the A, B and D moorings.

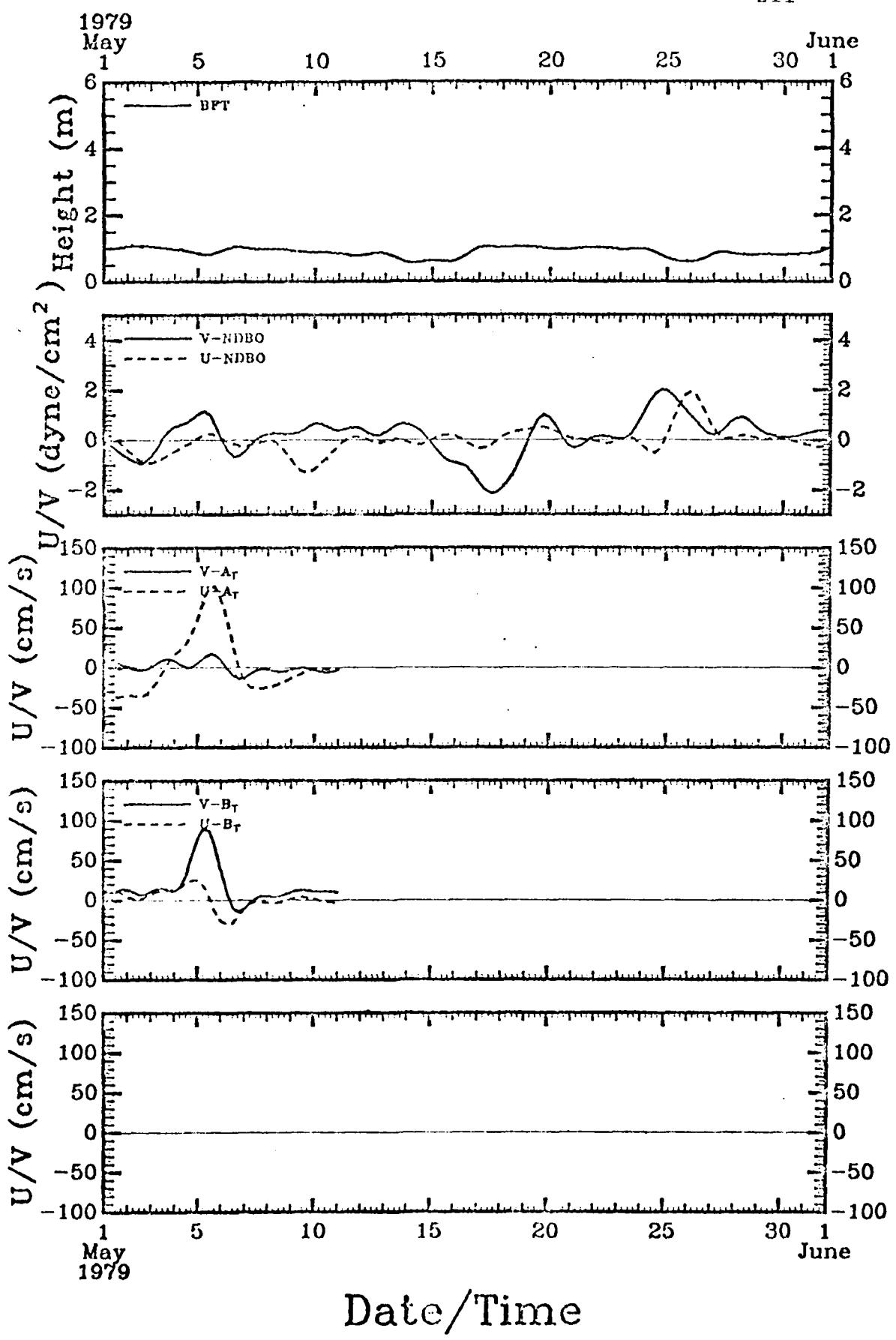


Date/Time









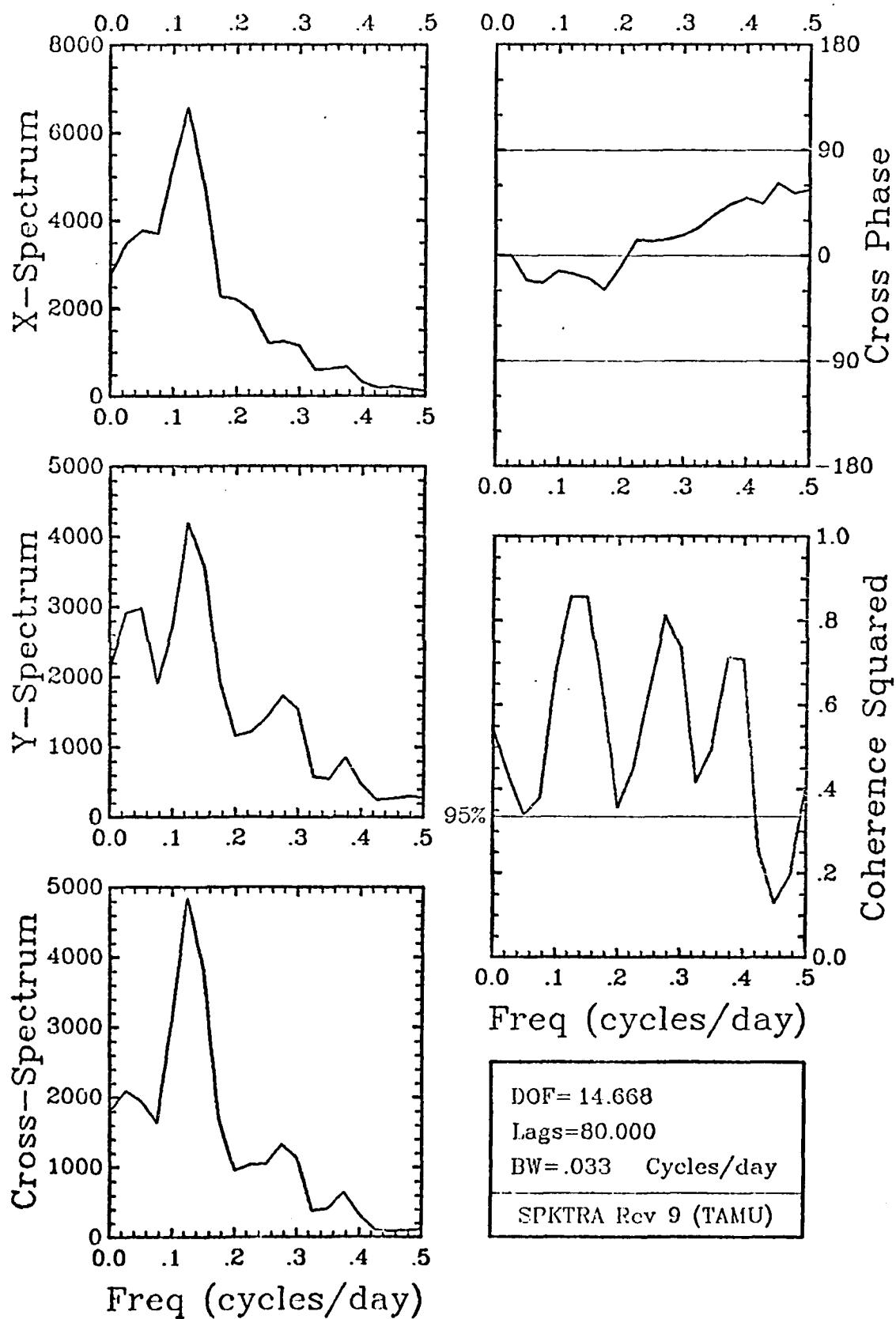
SECTION 10

Spectrum Calculations for Various Combinations of 40 HRLP Data Sets

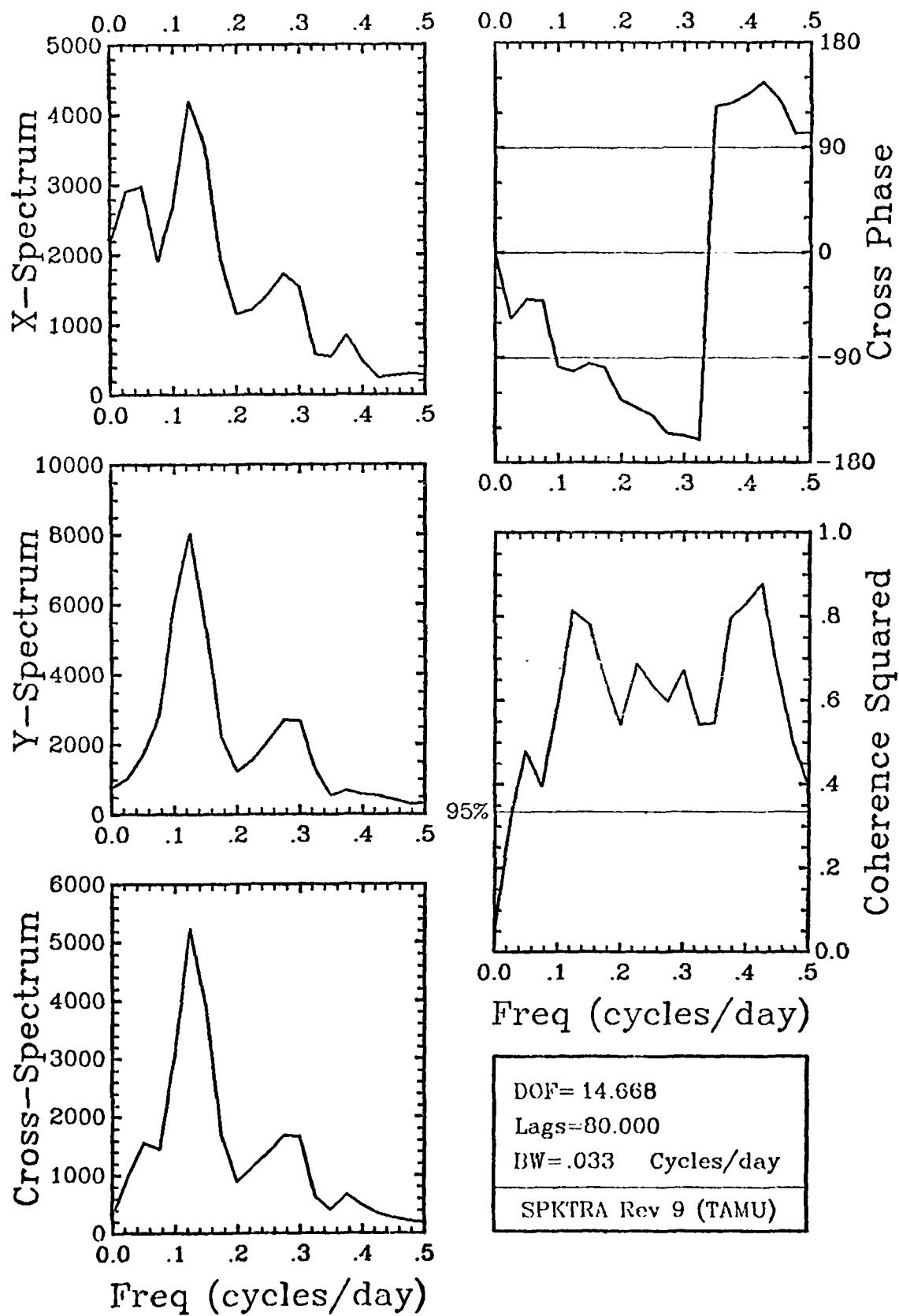
Figures 51 through 98 show spectrum, cross-spectrum, phase, and coherence squared calculations for selected pairs of 40 HRLP current components, Hatteras and NDBO wind stress components, "adjusted" (barometrically corrected) sea level, and various combinations thereof. The naming convention gives the "X" time series first and the "Y" time series second. Currents are identified by mooring letter, and instrument position on the mooring is given by subscript letter. The phase convention is such that negative phase values mean the "Y" series lags the "X" series. The spectrum ordinate units in all cases are variance units per cycle per day (CPD), where the variance units are those appropriate for the time series in question. Root-mean-square estimates of a variable in a particular frequency band can be obtained by multiplying the spectrum estimate in that band by the effective bandwidth (0.033 CPD in all cases) and taking the square root of the product. The 95% significance level for coherence squared, the level below which would fall 95% of the coherence estimates between truly uncorrelated variates, is shown by a horizontal line on the coherence graphs. Spectrum estimates nominally possess 15 degrees of freedom (DOF), although some variation in this number, accepted in favor of maintaining the bandwidth invariant, results from differing record lengths. For 15 DOF, the 95% confidence interval on the phase

estimate in a particular frequency band is approximately \pm (27, 18, 12) degrees for a coherence squared value of (0.4, 0.6, 0.8) in that band.

A remarkable feature apparent in this set of figures is the near-independence of the current and wind stress fluctuations for periods longer than several days.

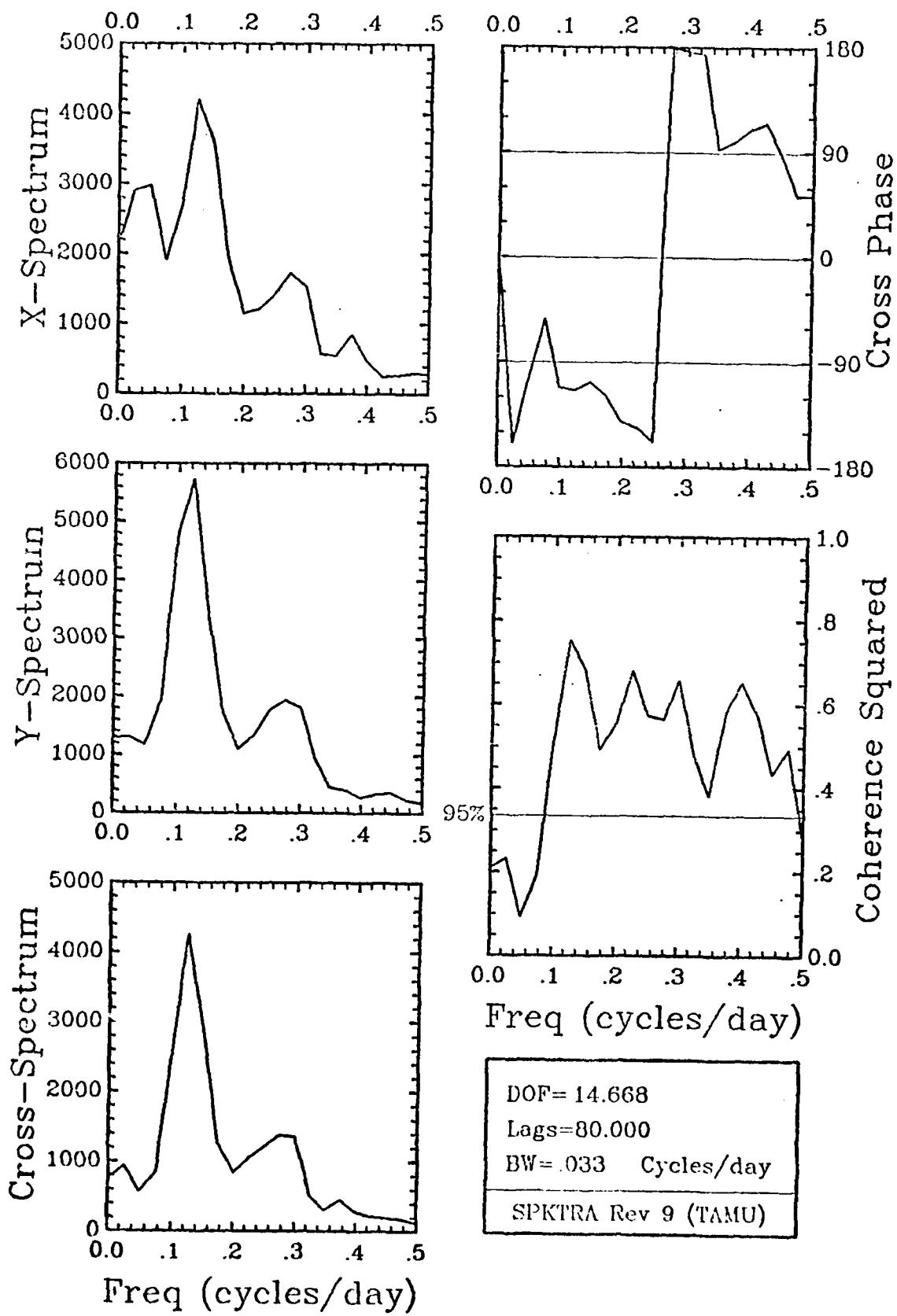


$A_T V / B_T V$ winter 40 HR LP



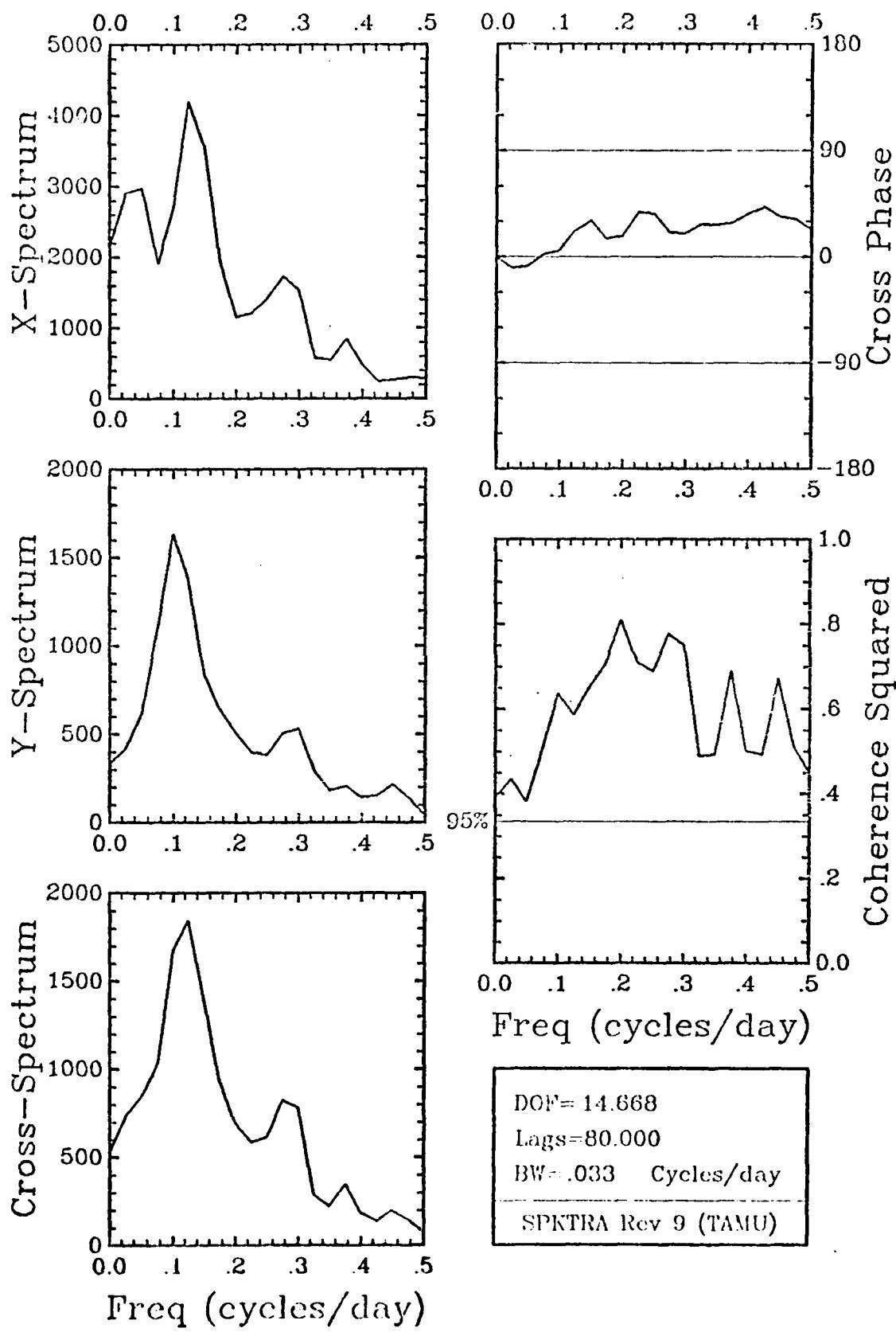
DOF = 14.668
Lags = 80.000
BW = .033 Cycles/day
SPKTRA Rev 9 (TAMU)

B_TV / C_TV winter 40 HR LP



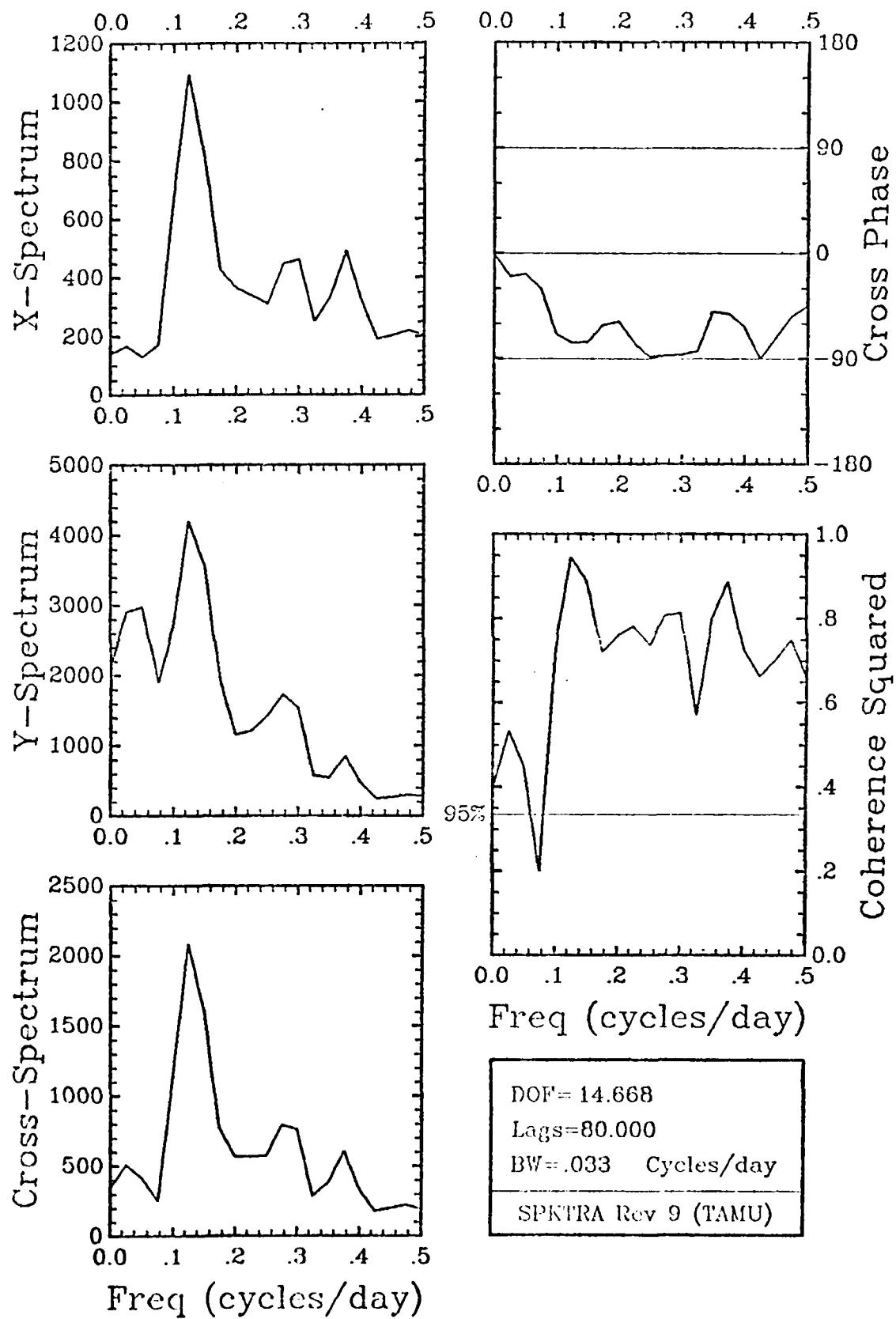
DOF = 14.668
Lags = 80.000
BW = .033 Cycles/day
SPKTRA Rev 9 (TAMU)

$B_T V / D_M V$ winter 40 HR LP

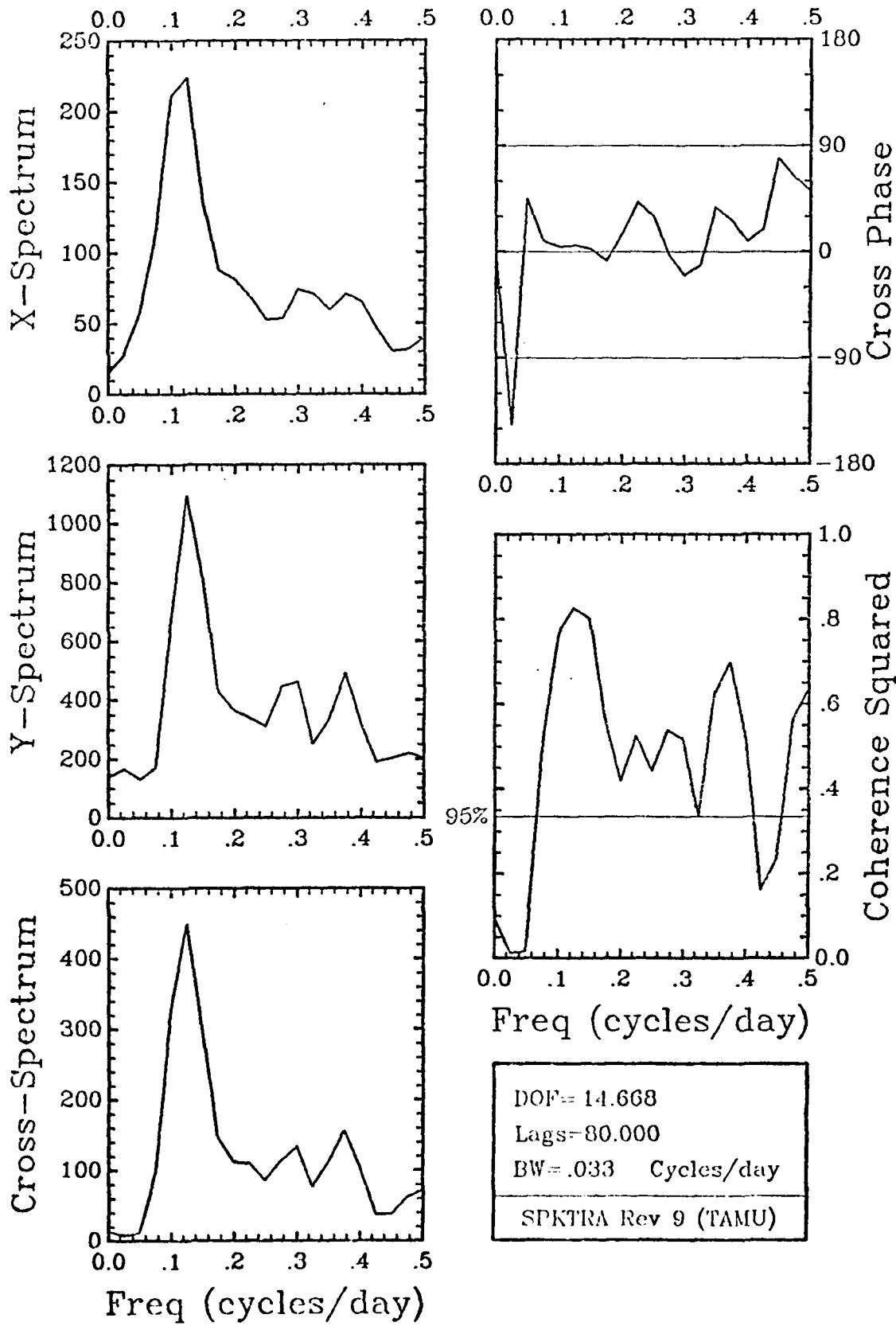


DOF = 14.668
Lags = 80.000
BW = .033 Cycles/day
SPKTRA Rev 9 (TAMU)

$B_T V / B_B V$ winter 40 HR LP

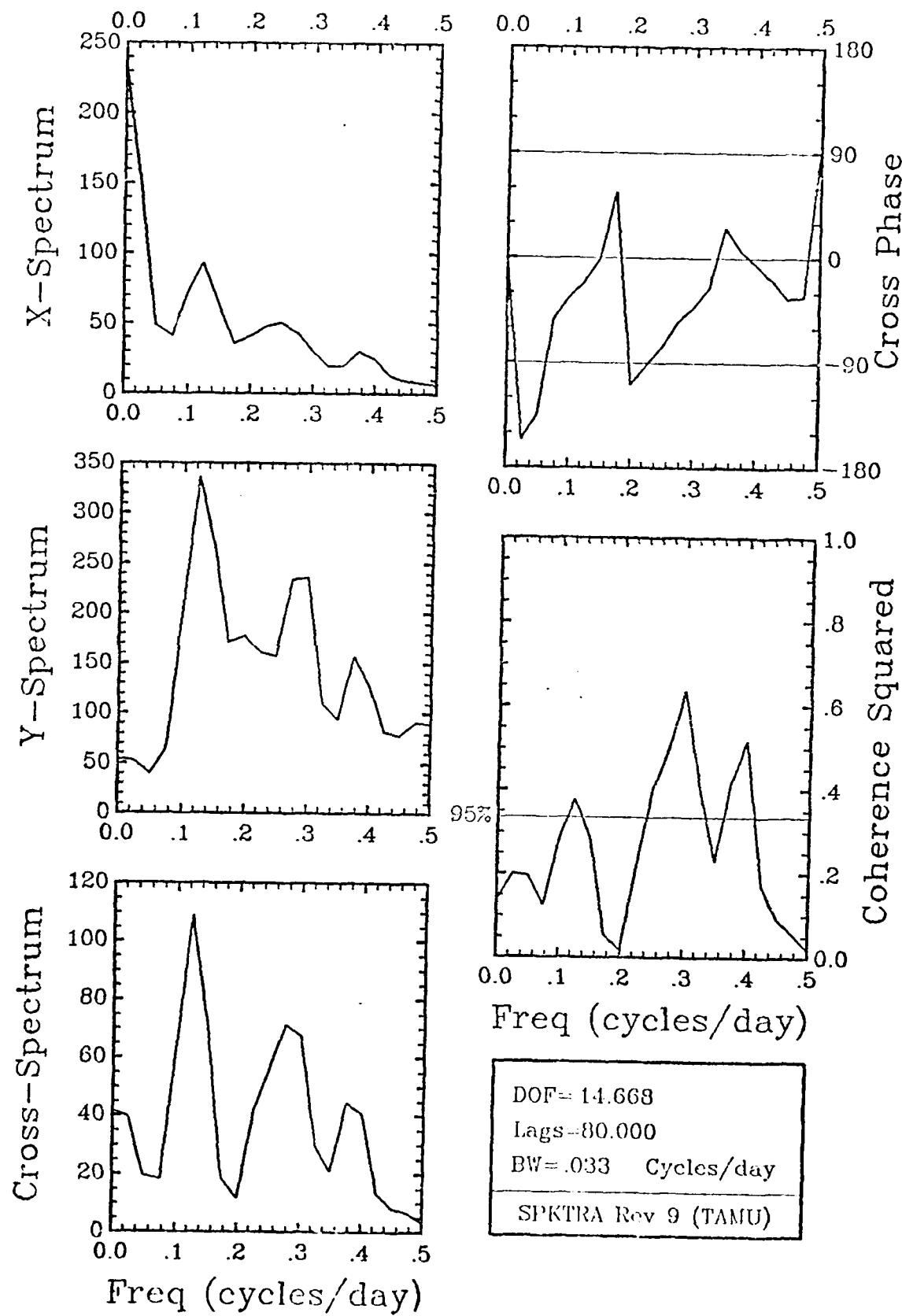


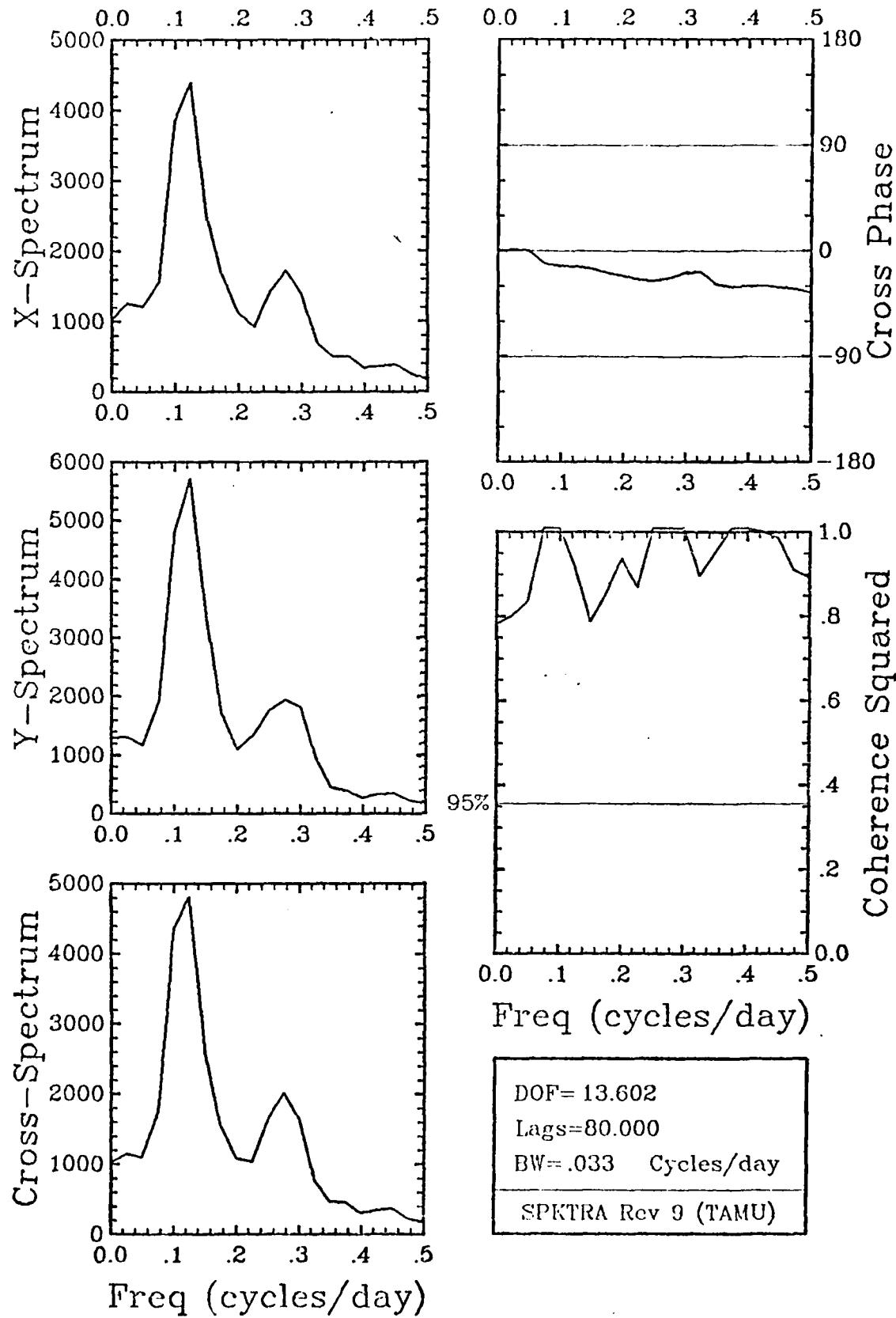
$B_T U / B_T V$ winter 40 HR LP



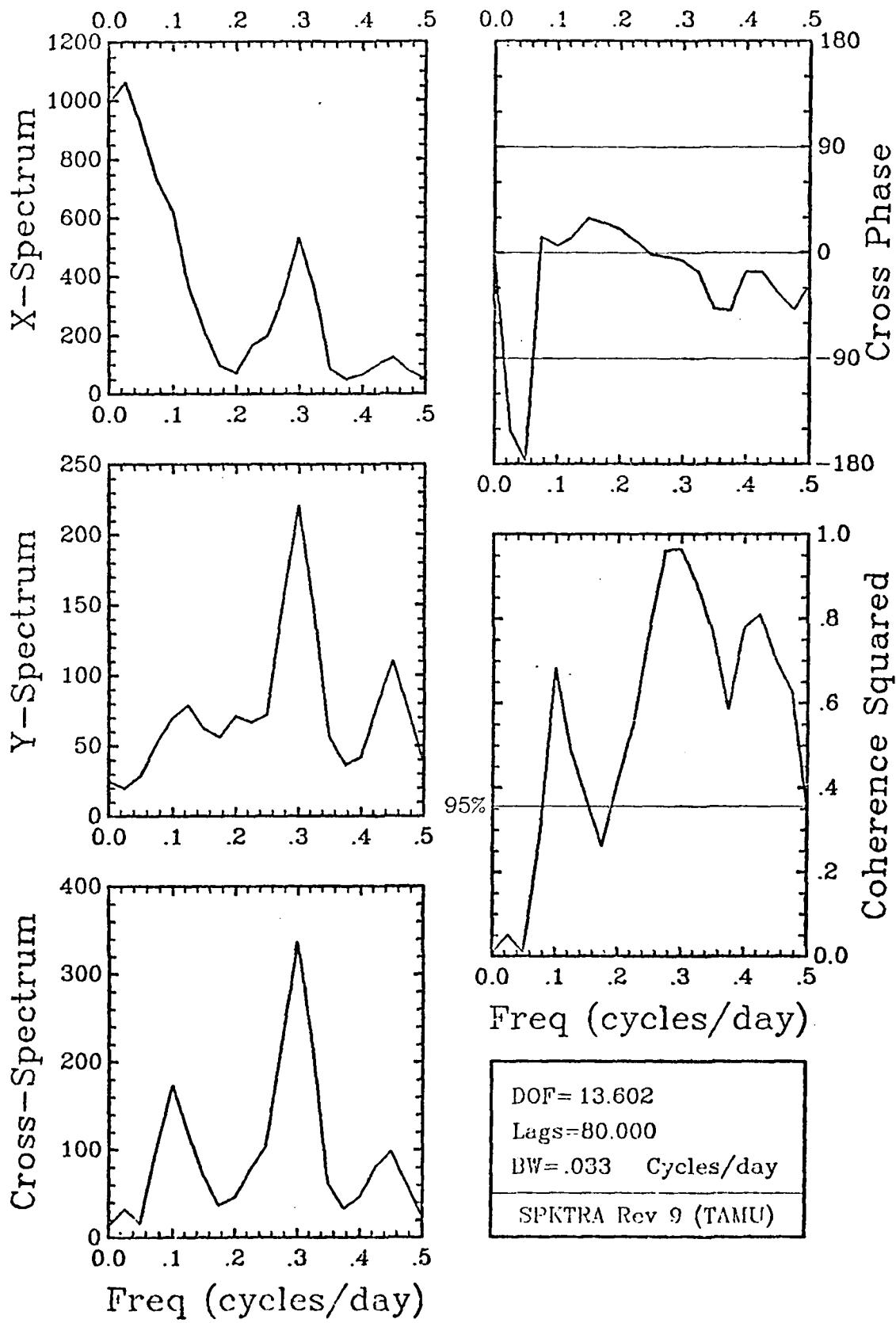
A_TU / B_TU winter 40 HR LP

220

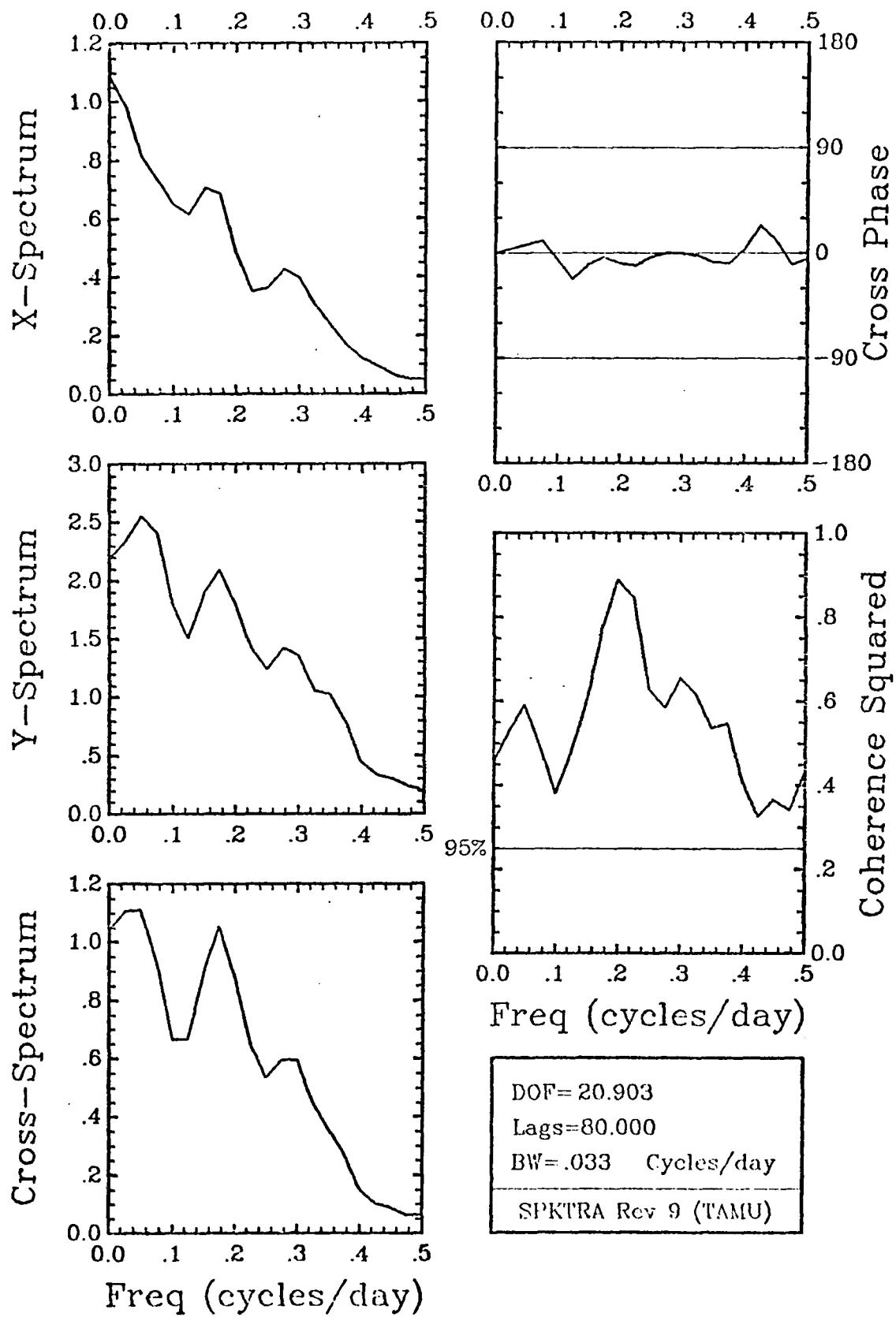
A_BU / B_BU winter 40 HR LP



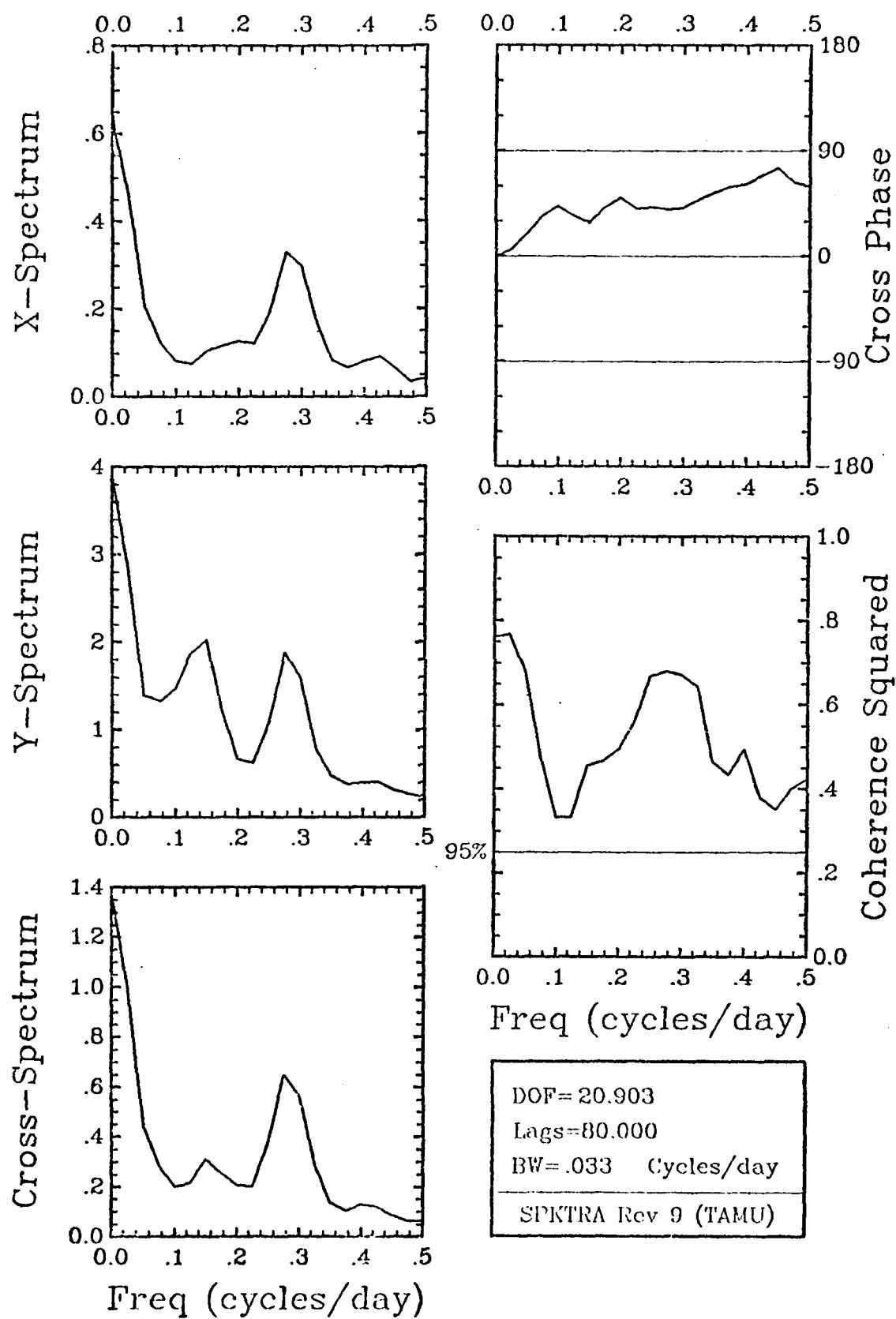
$C_M V / D_M V$ winter 40 HR LP



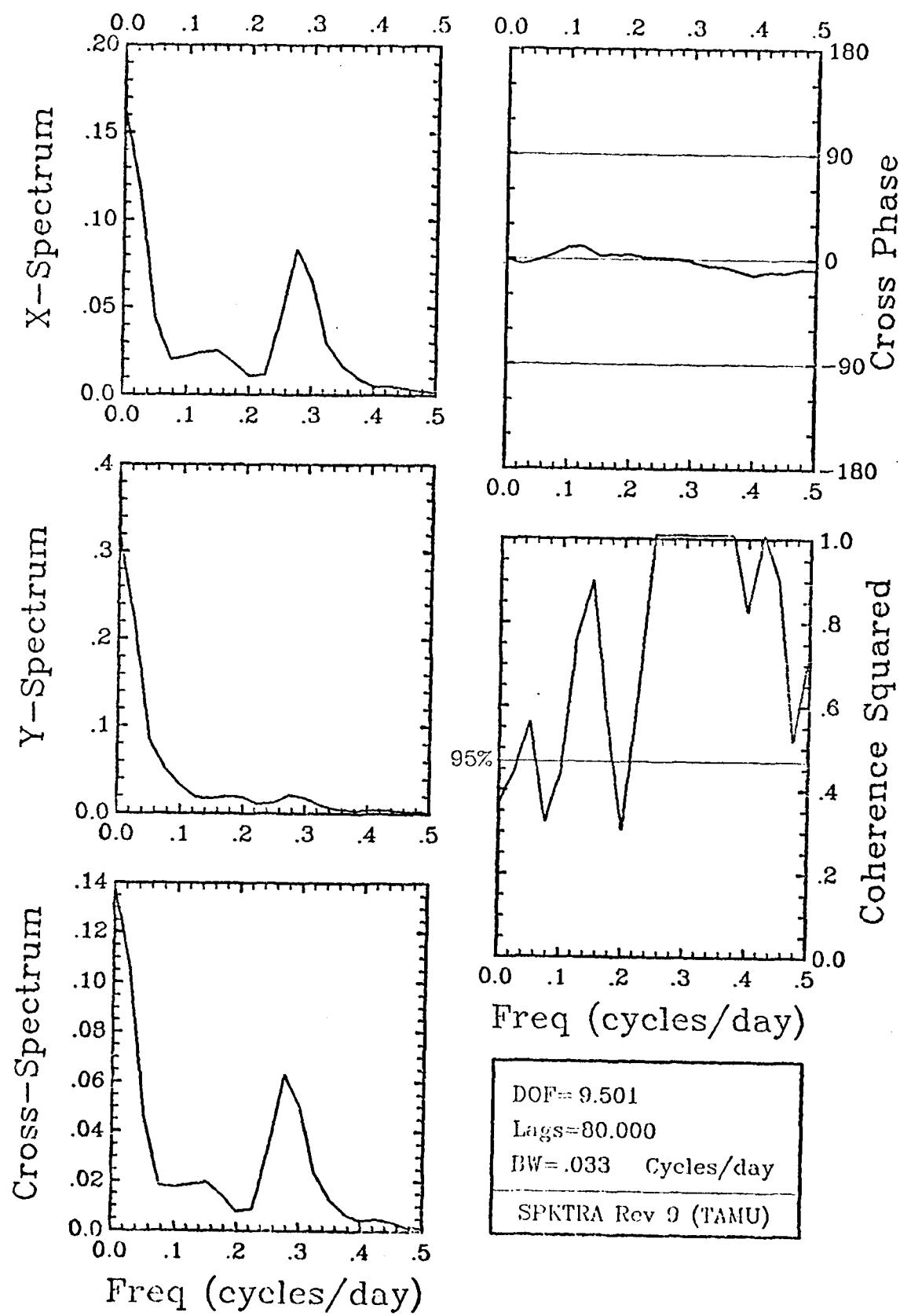
$C_M U / D_M U$ winter 40 HR LP



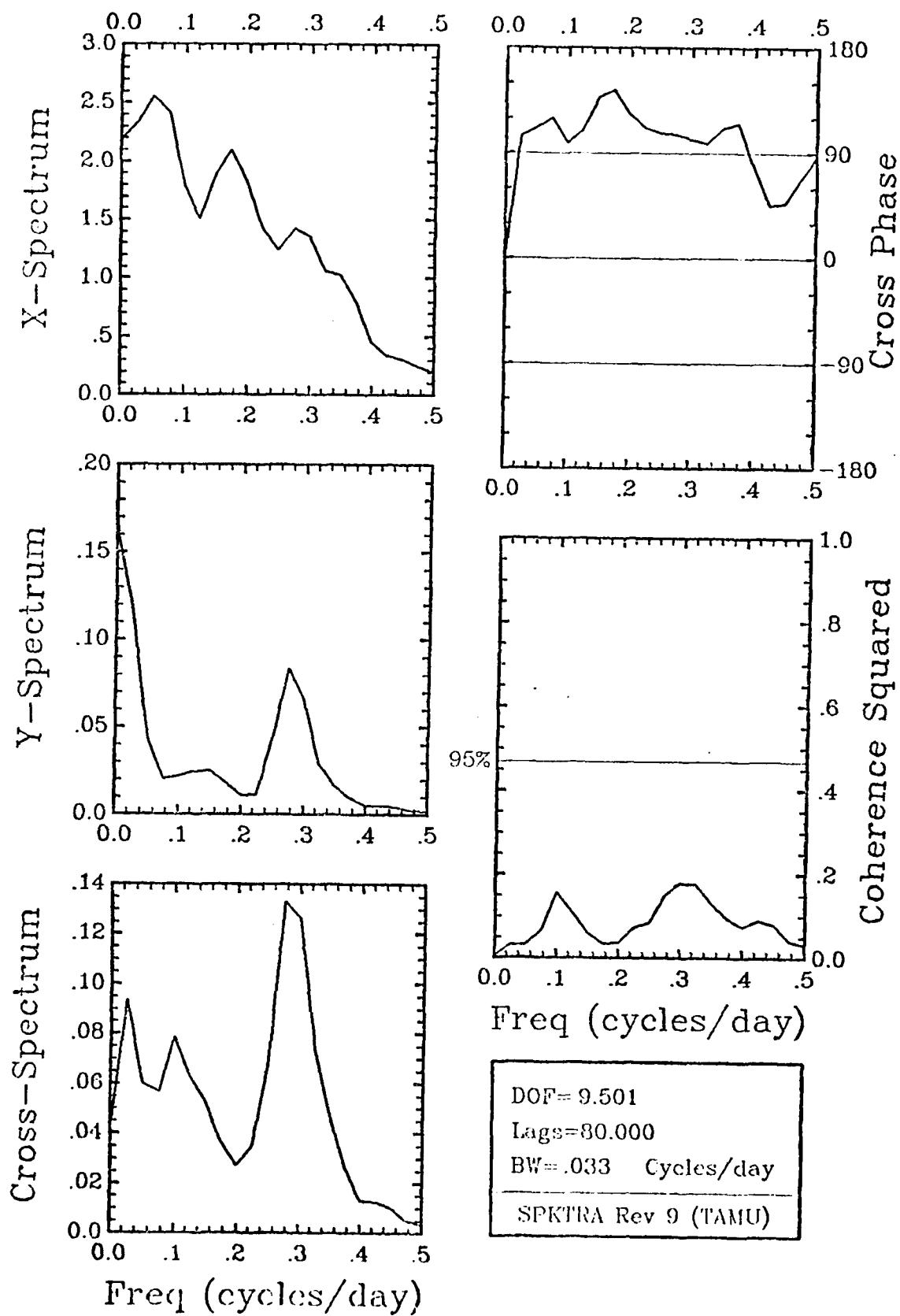
V-Stress_{HLAT} / V-Stress_{NDBO} Winter 40 HR LP



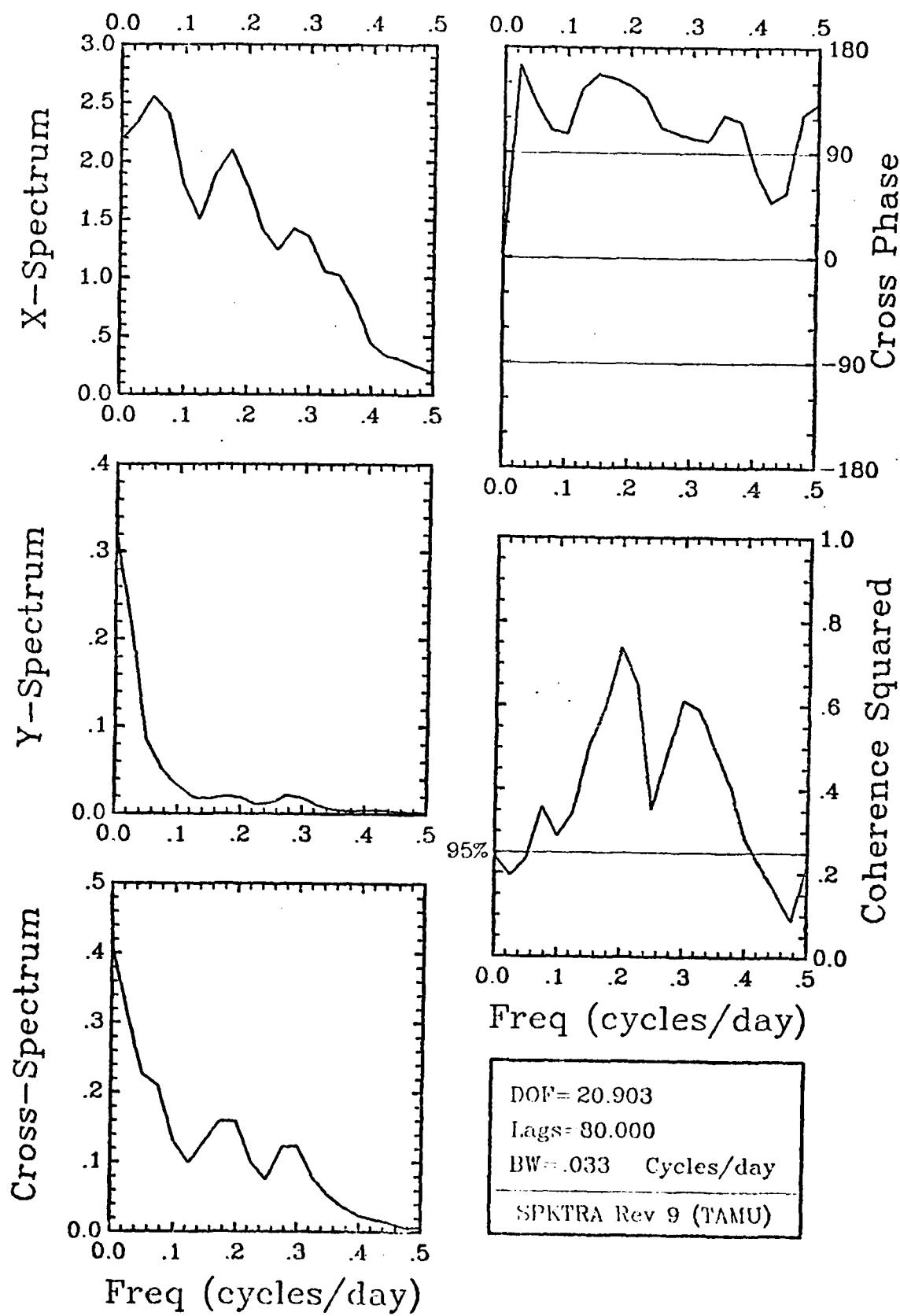
U-Stress_{IIAT} / U-Stress_{NDBO} Winter 40 HR LP



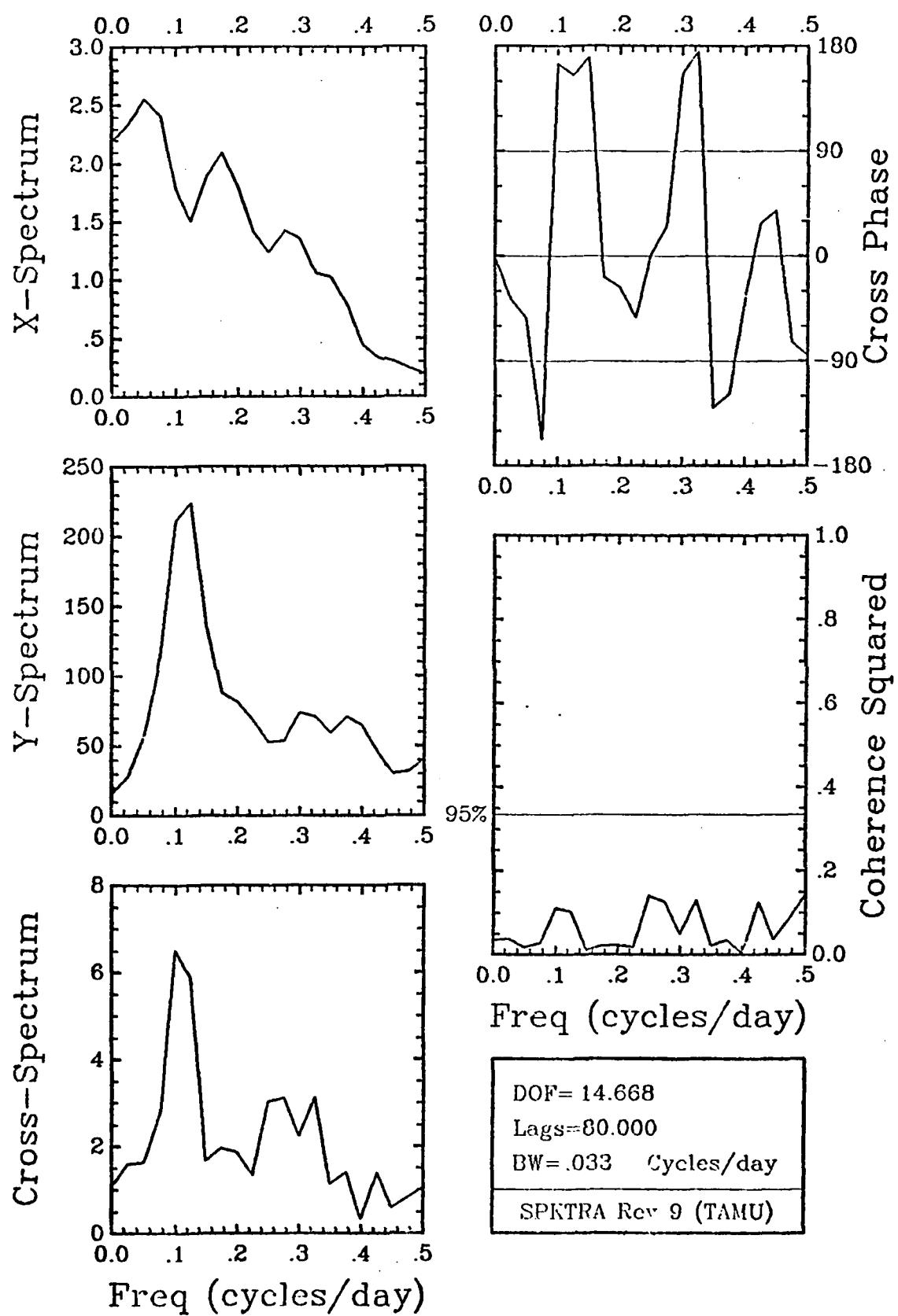
ADJ SL_{SPT} / ADJ SL_{BFT} Winter 40 HR LP



V-Stress_{NDBO} / ADJ SL_{SPT} Winter 40 HR LP



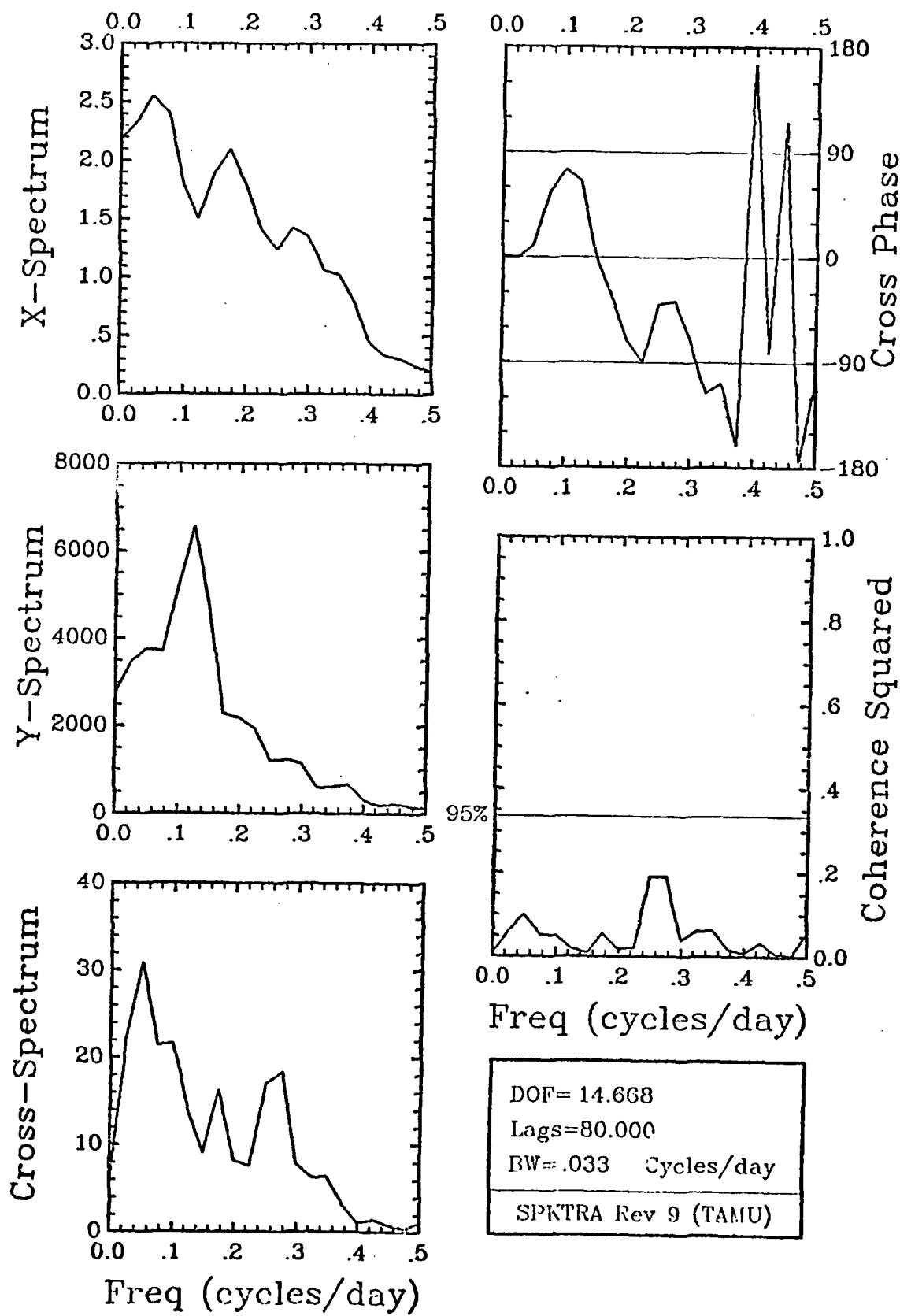
V-Stress_{NDBO} / ADJ SL_{BFT} Winter 40 HR LP



DOF = 14.668
Lags = 80.000
BW = .033 Cycles/day
SPKTRA Rev 9 (TAMU)

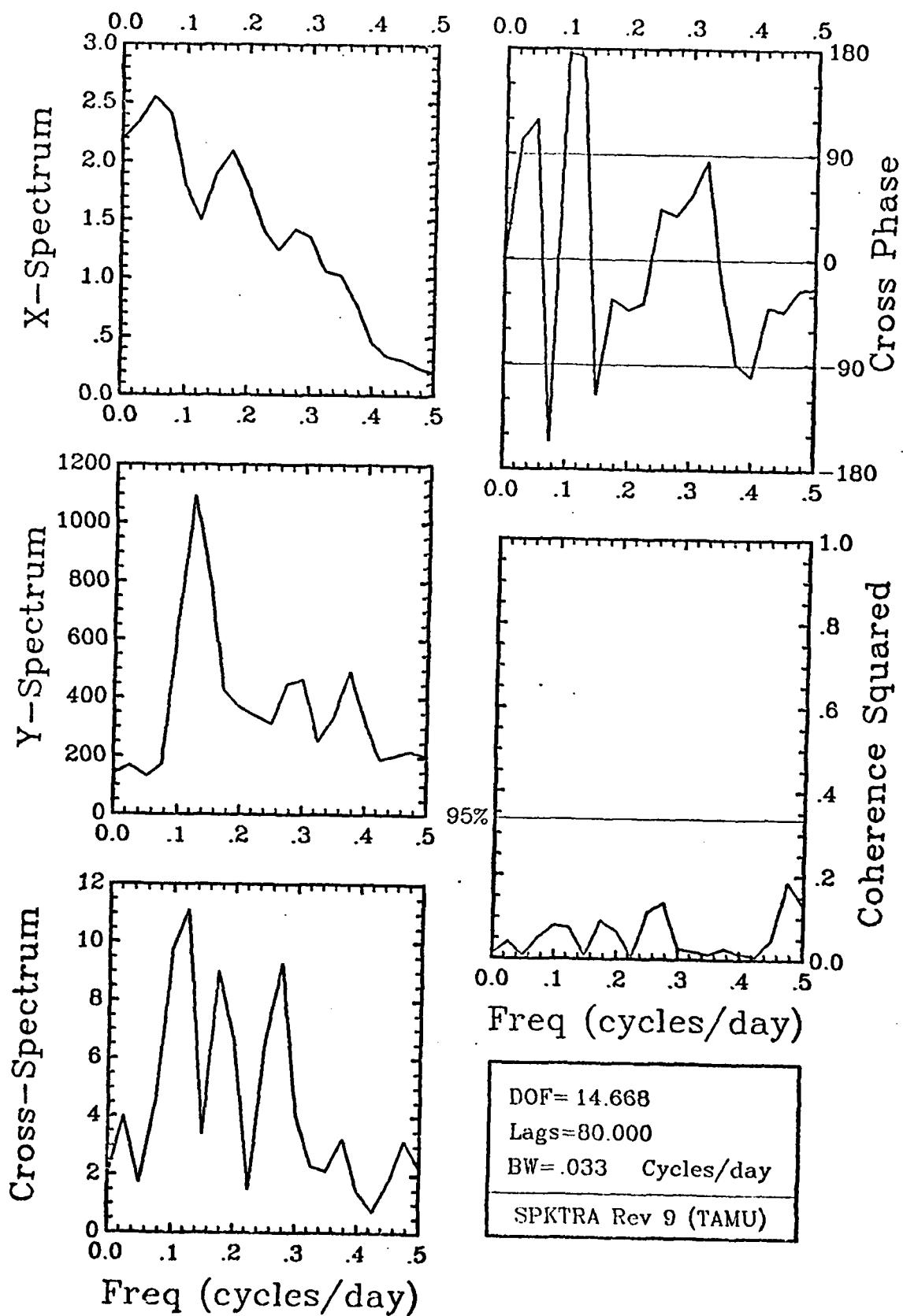
V-Stress_{NDBO} / A_TU

Winter 40 HR LP

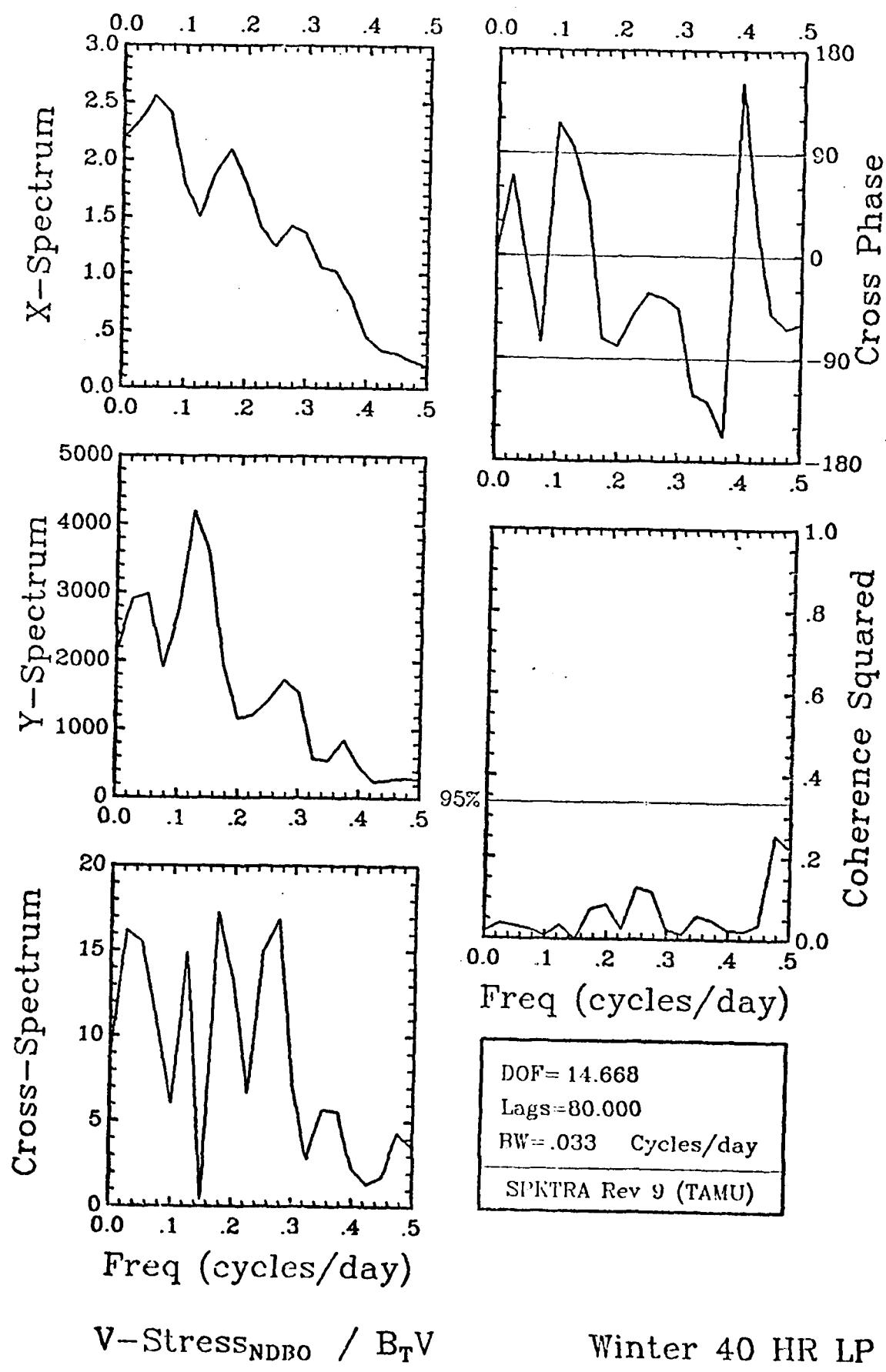


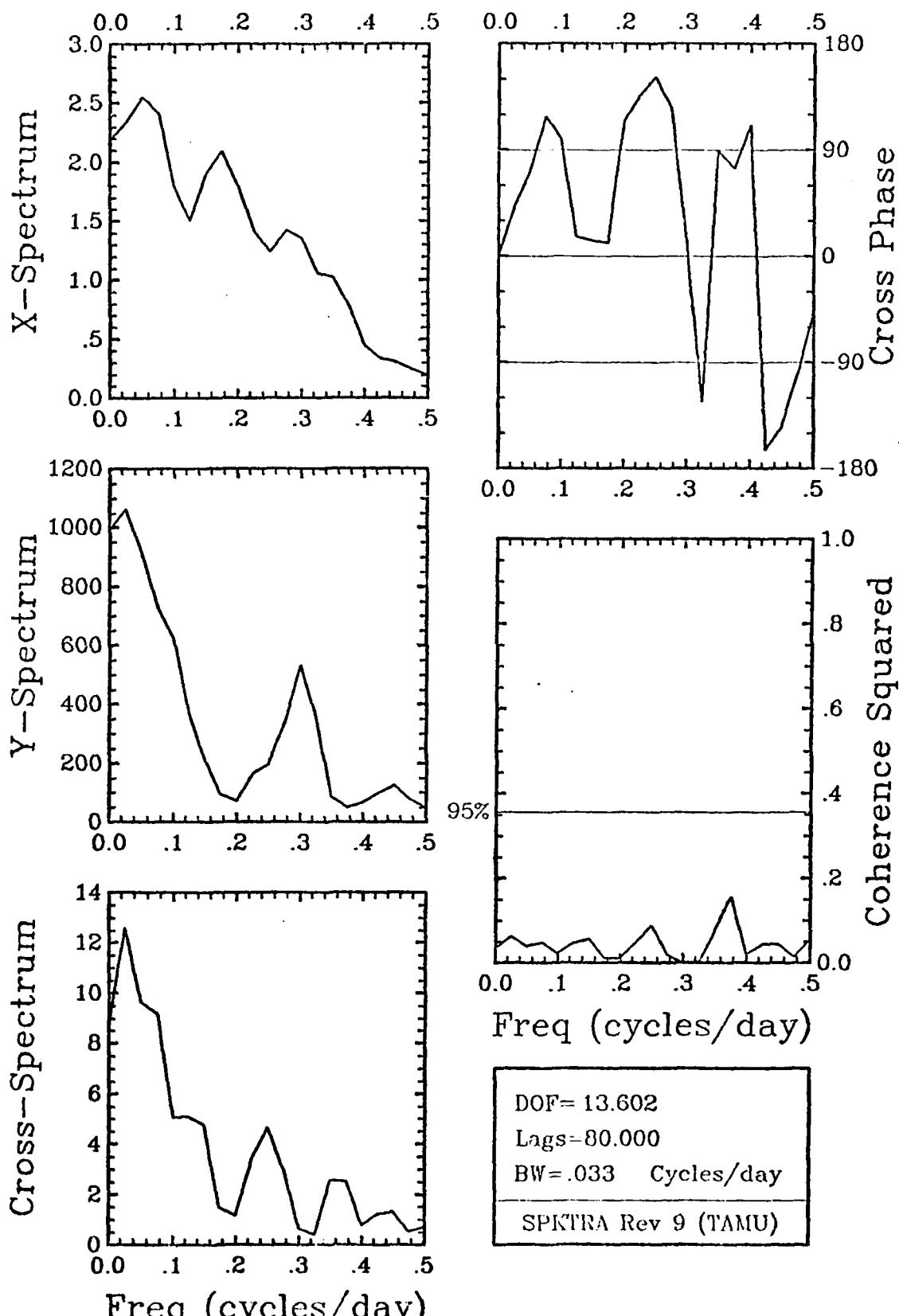
$V - \text{Stress}_{\text{NDBO}} / A_T V$

Winter 40 HR LP

V-Stress_{NDBO} / B_TU

Winter 40 HR LP

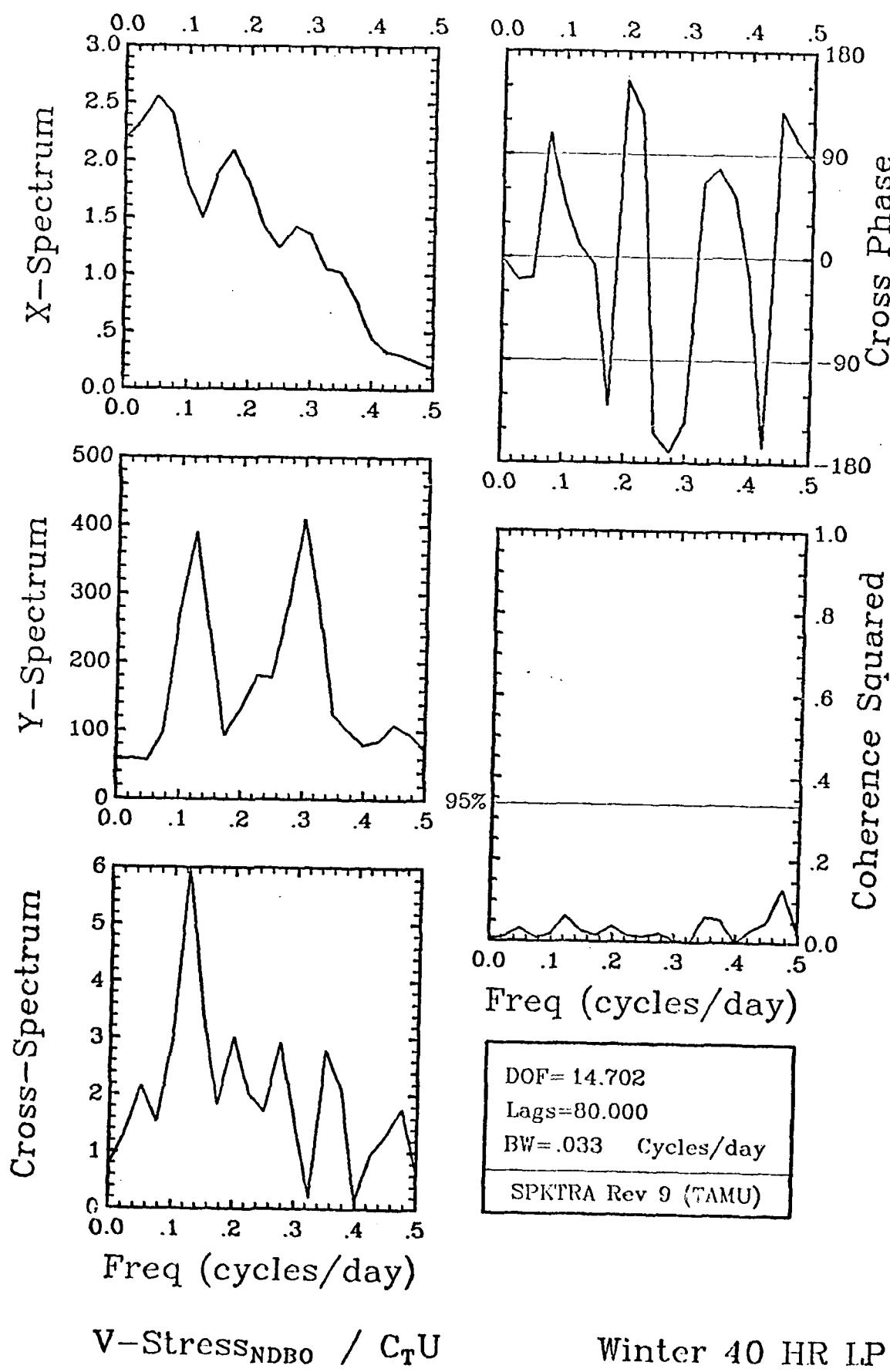


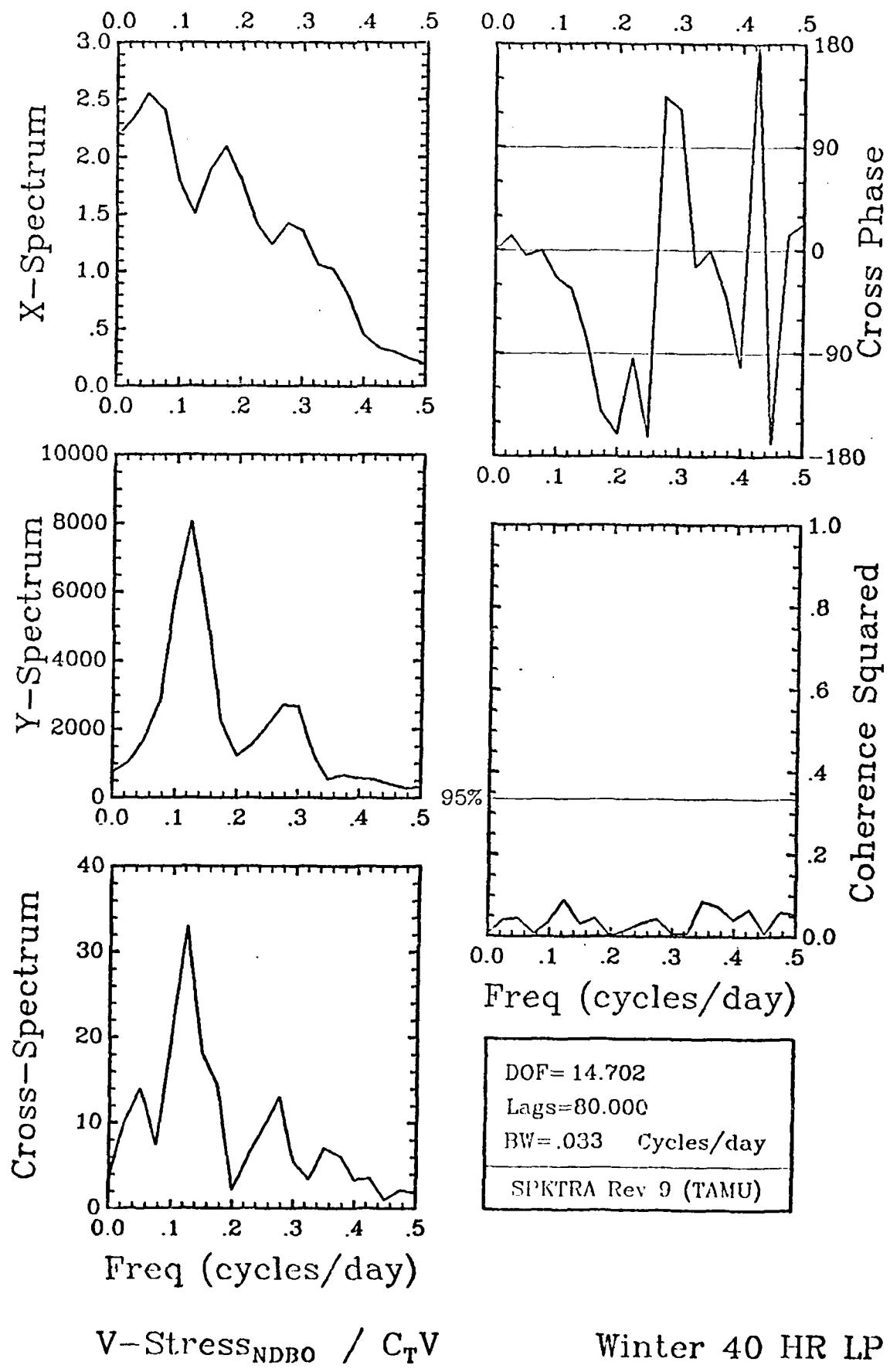


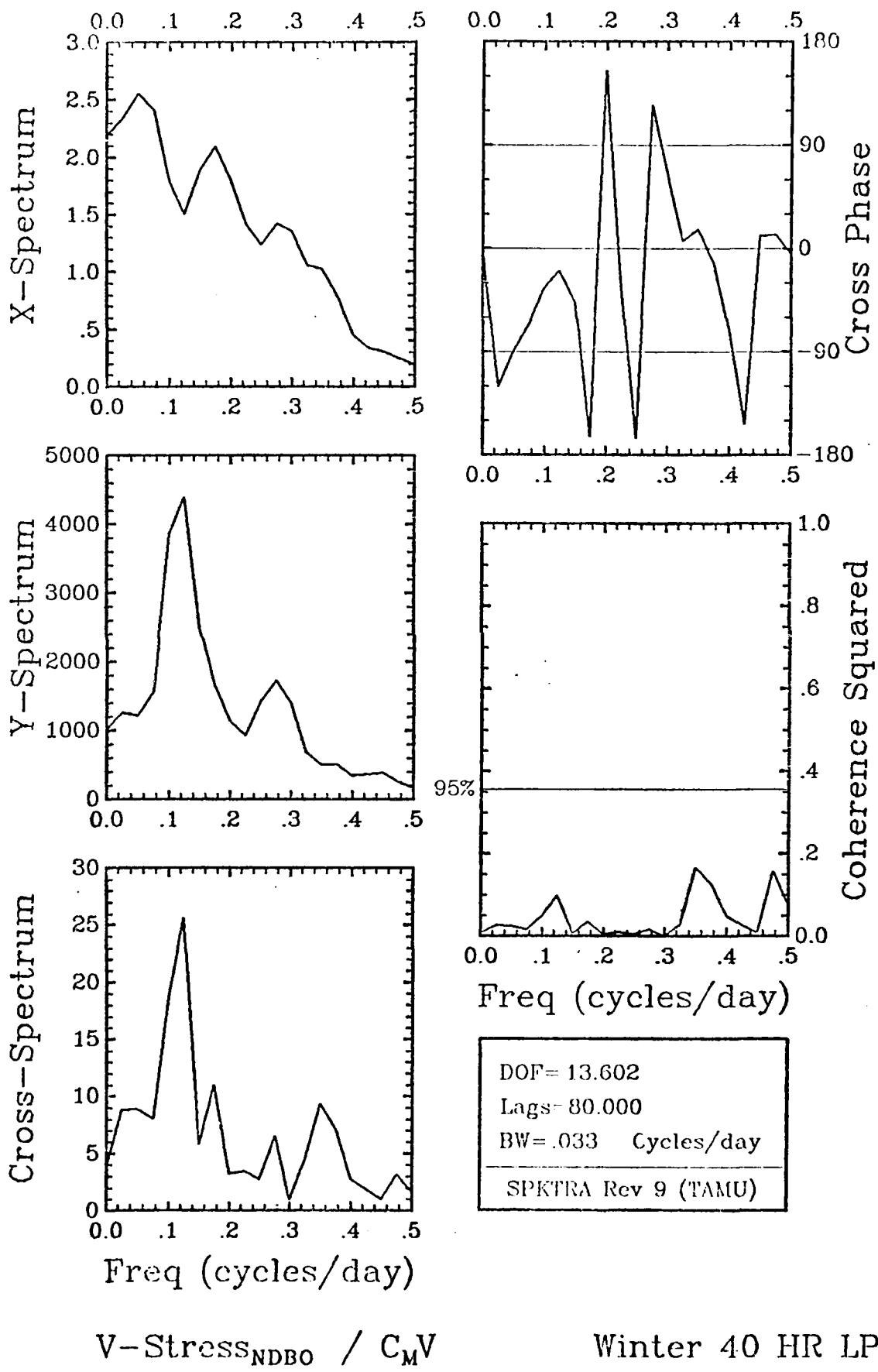
DOF = 13.602
Lags = 80.000
BW = .033 Cycles/day
SPKTRA Rev 9 (TAMU)

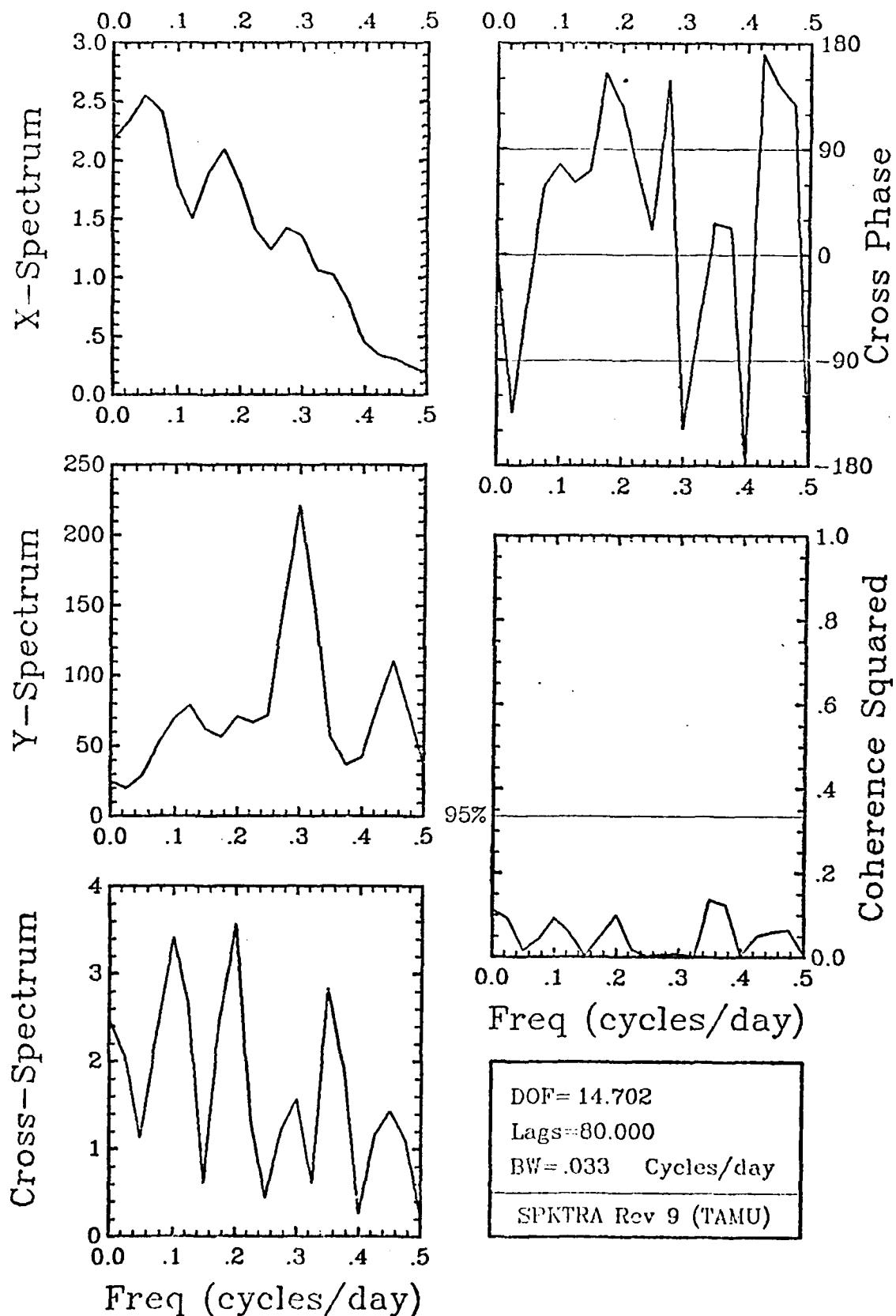
V-Stress_{NDBO} / C_MU

Winter 40 HR LP





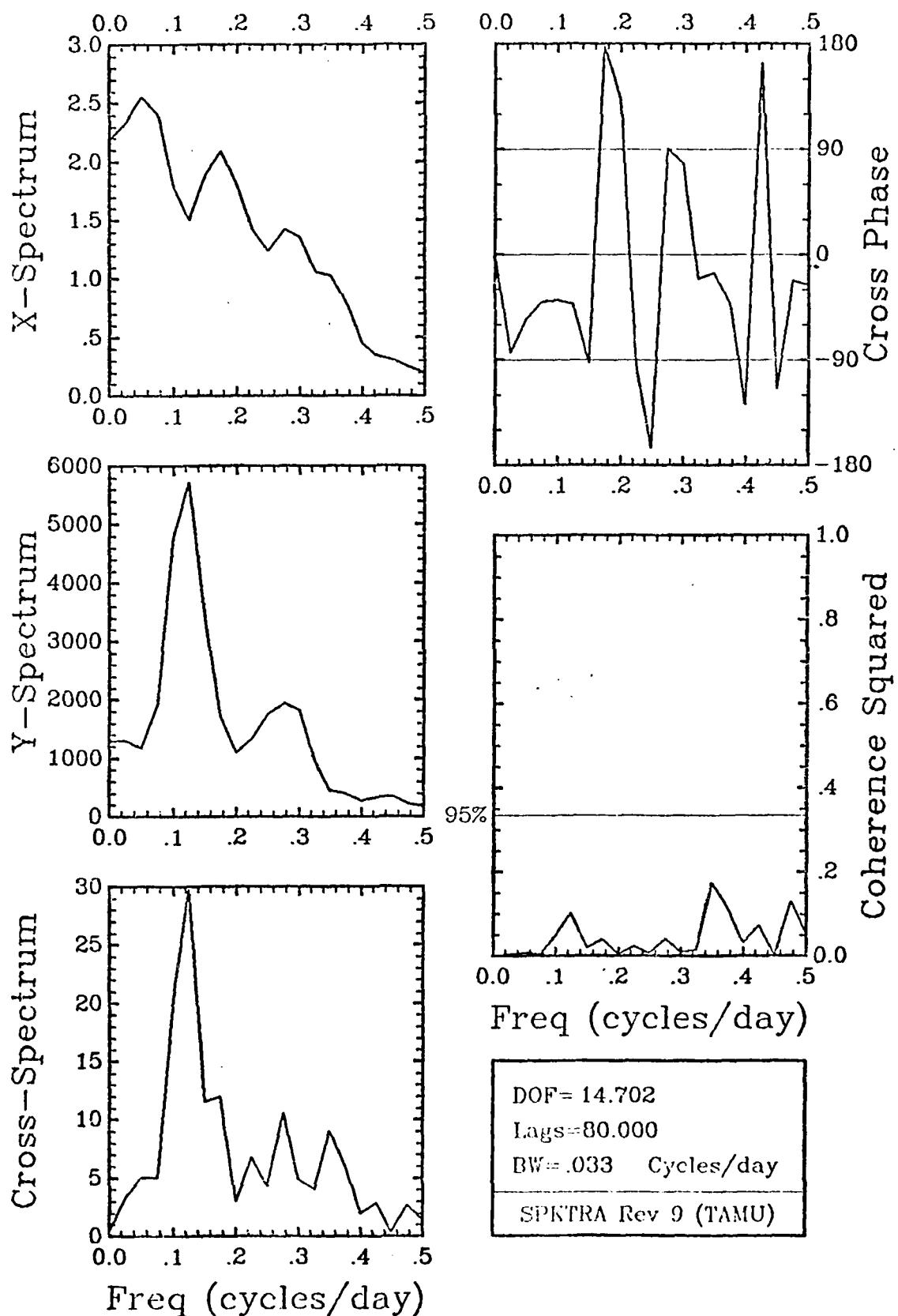




DOF = 14.702
Lags = 80.000
BW = .033 Cycles/day
SPKTRA Rev 9 (TAMU)

V-Stress_{NDBO} / D_MU

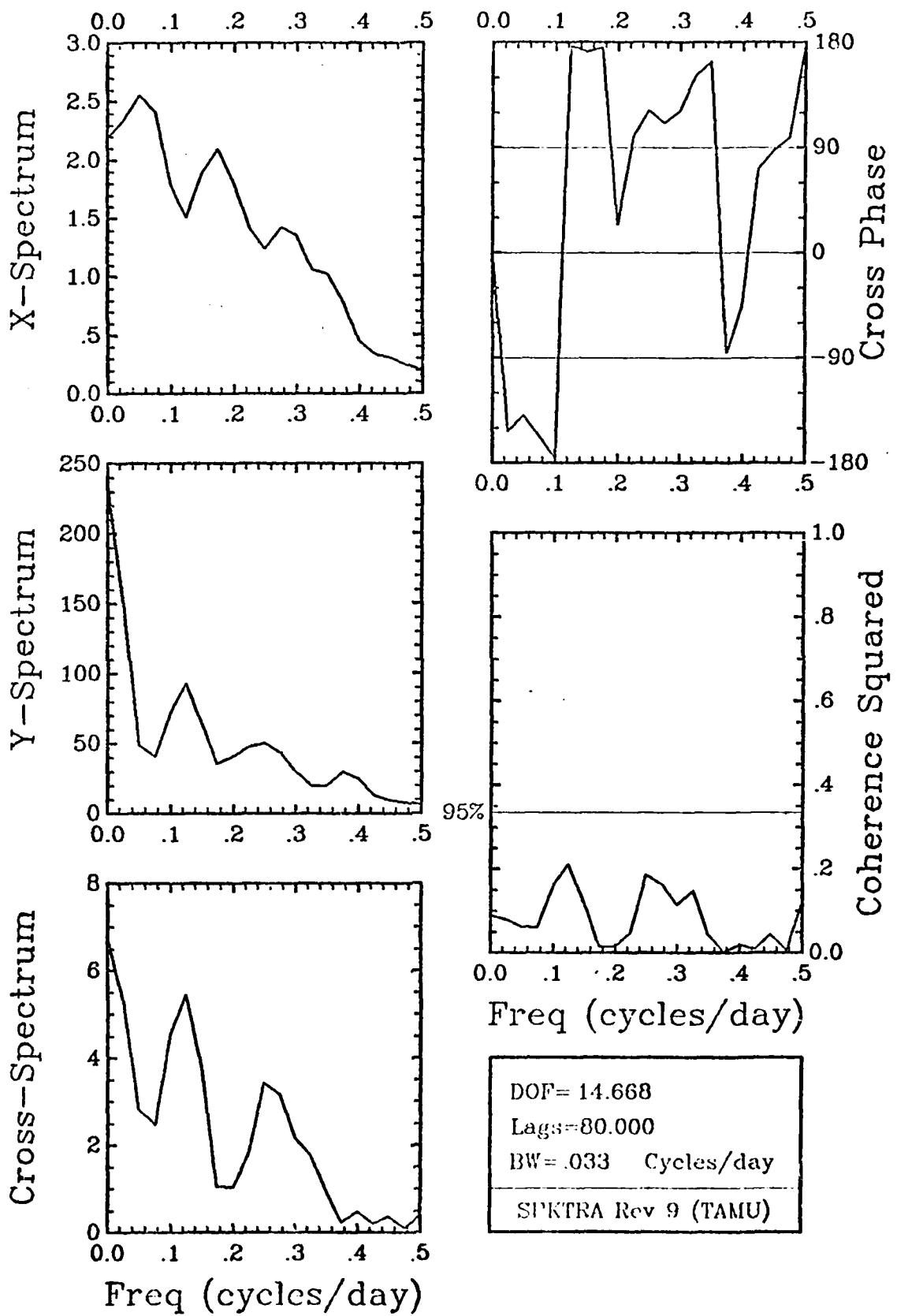
Winter 40 HR LP



DOF = 14.702
Lags = 80.000
BW = .033 Cycles/day
SPKTRA Rev 9 (TAMU)

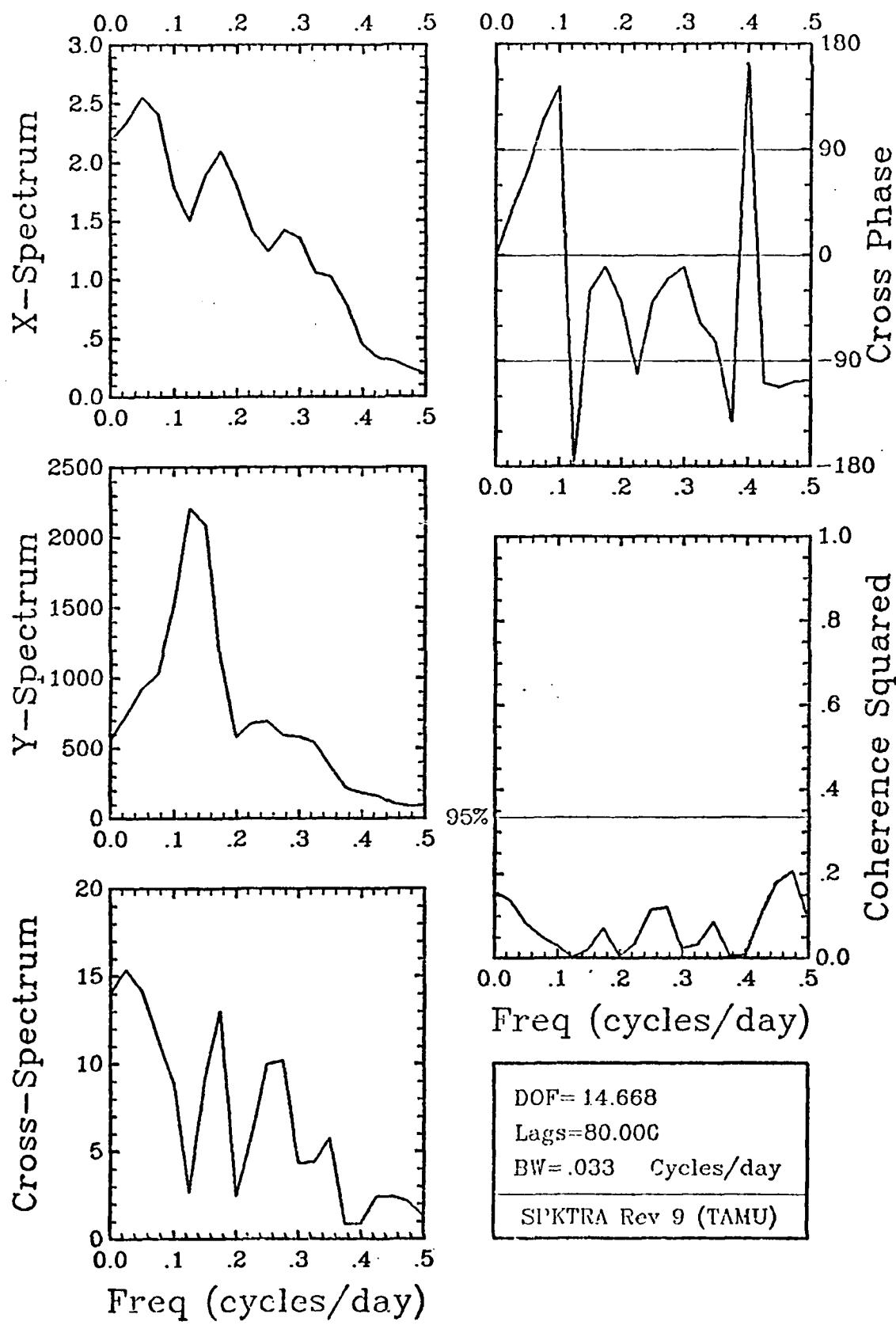
V-Stress_{NDBO} / D_MV

Winter 40 HR LP

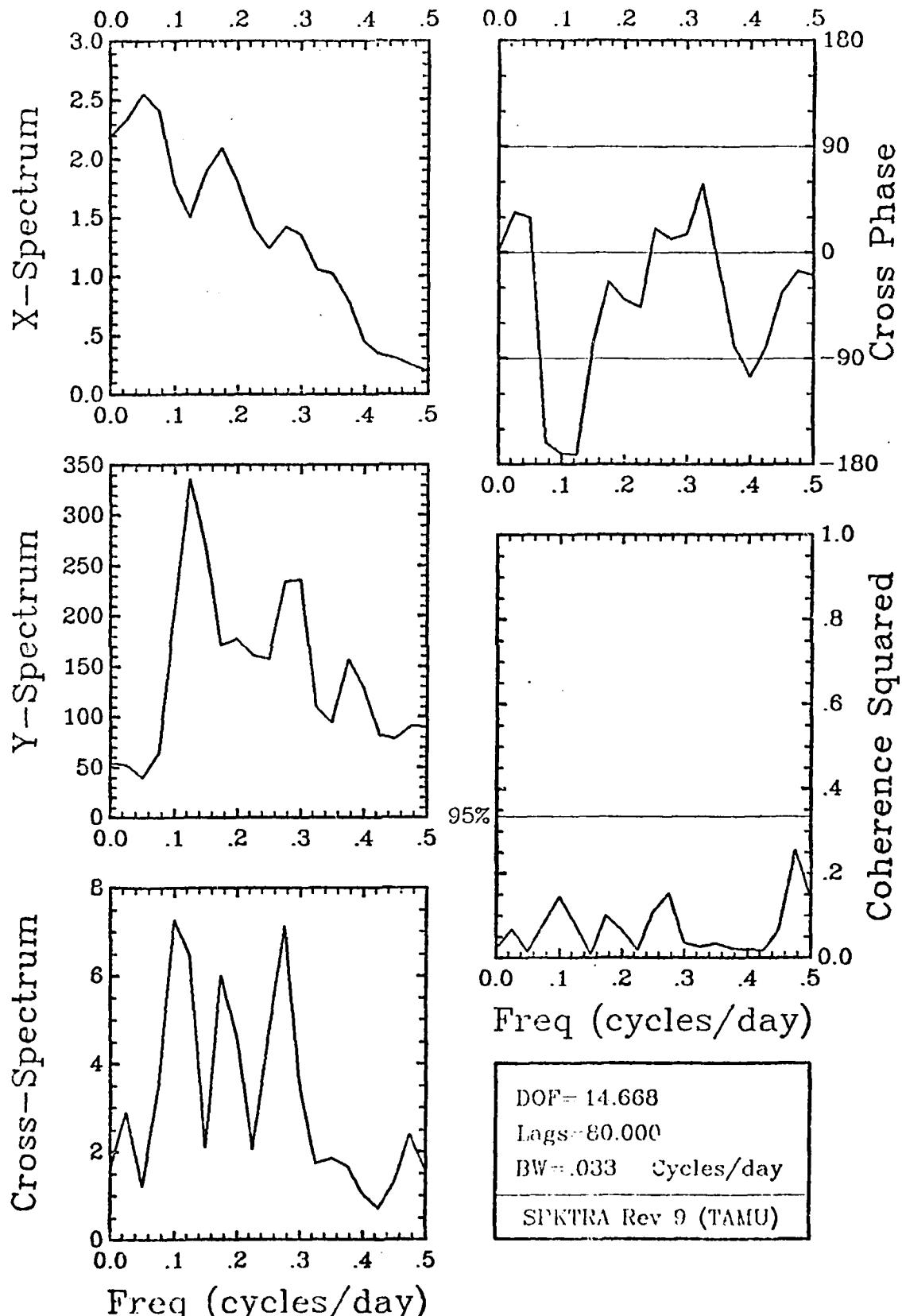


V-Stress_{NDBO} / A_B U

Winter 40 HR LP

V-Stress_{NDBO} / A_BV

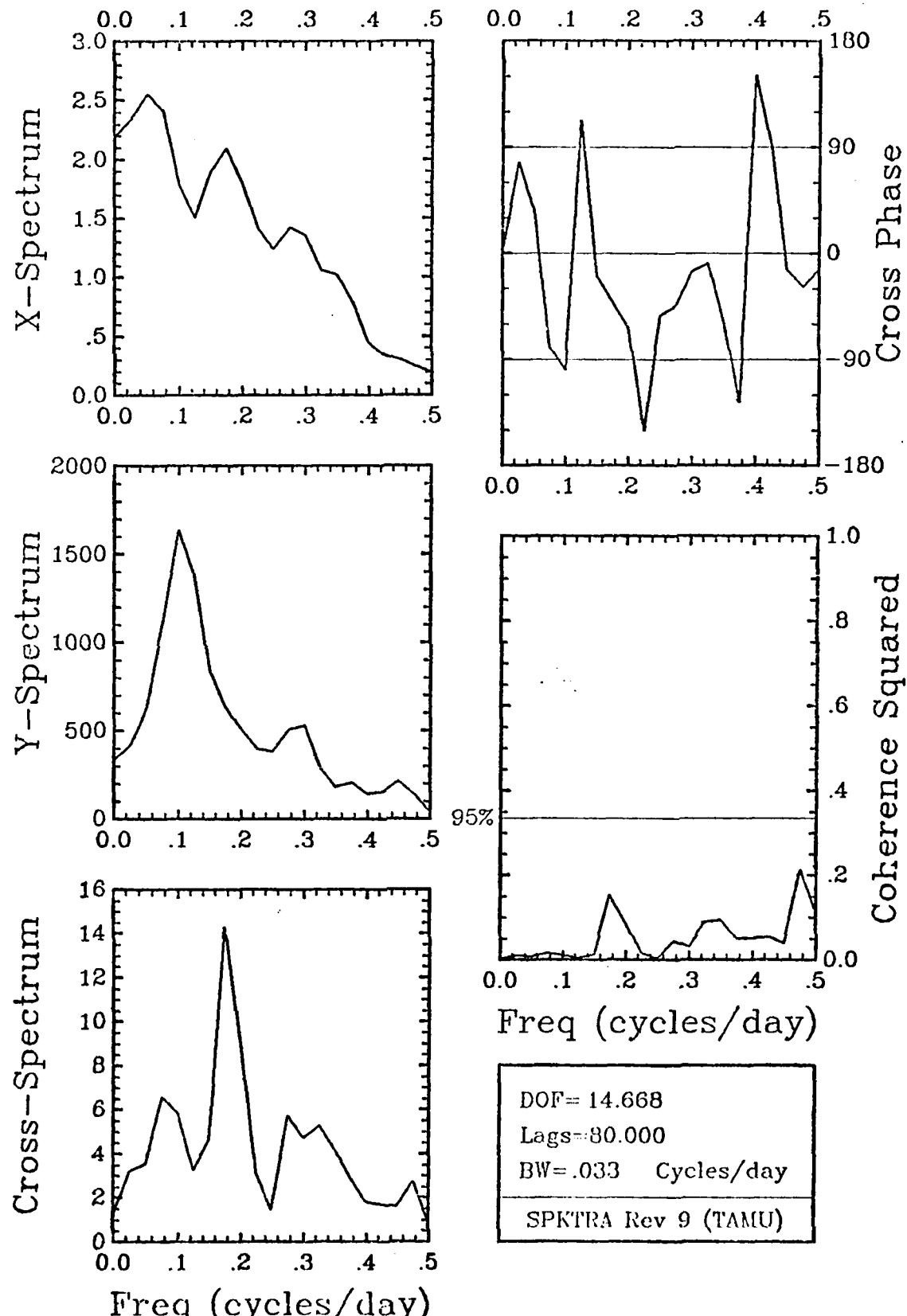
Winter 40 HR



DOF = 14.668
Lags = 80.000
BW = .033 Cycles/day
SPIKTRA Rev 9 (TAMU)

V-Stress_{NDBO} / B_BU

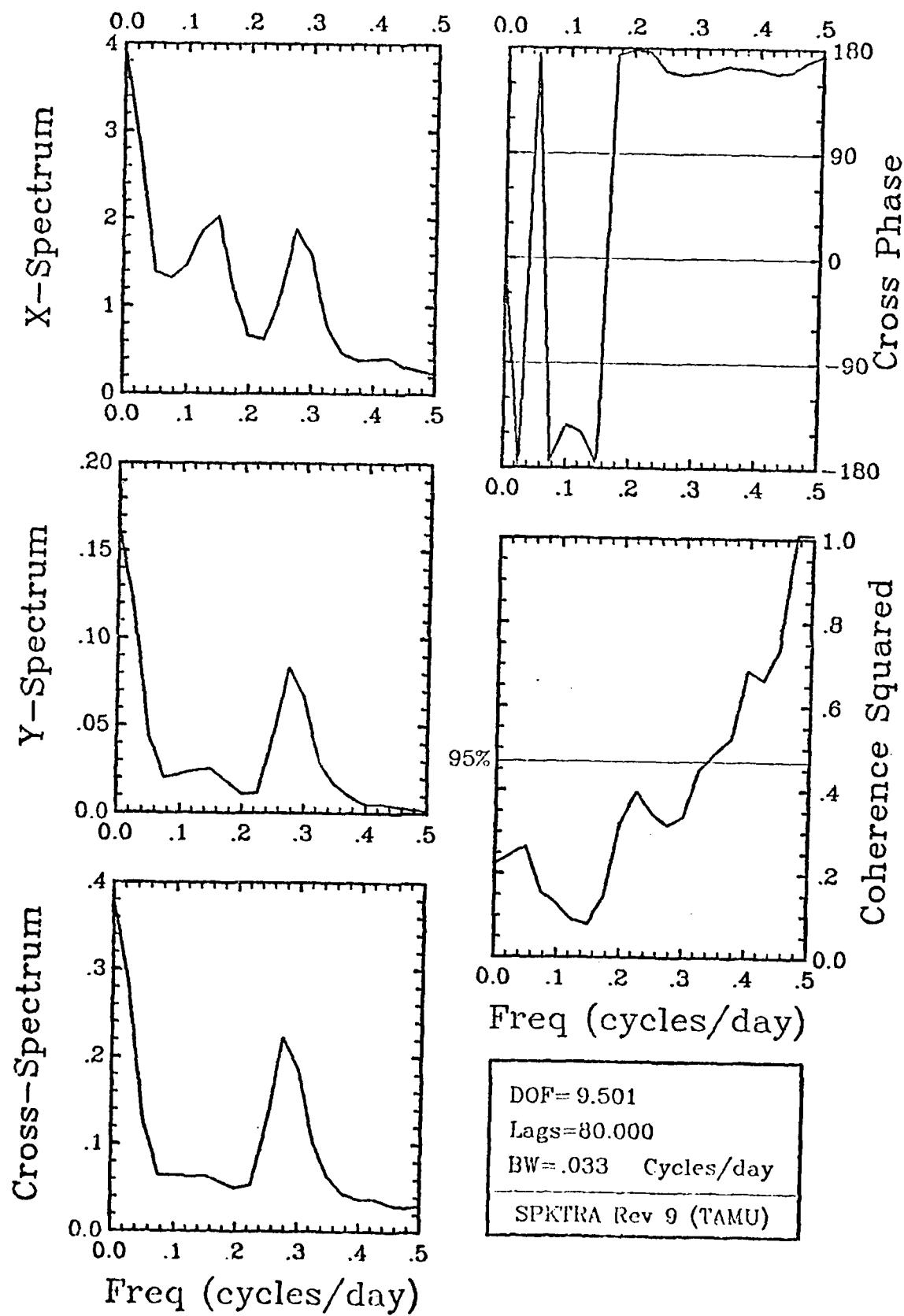
Winter 40 HR LP



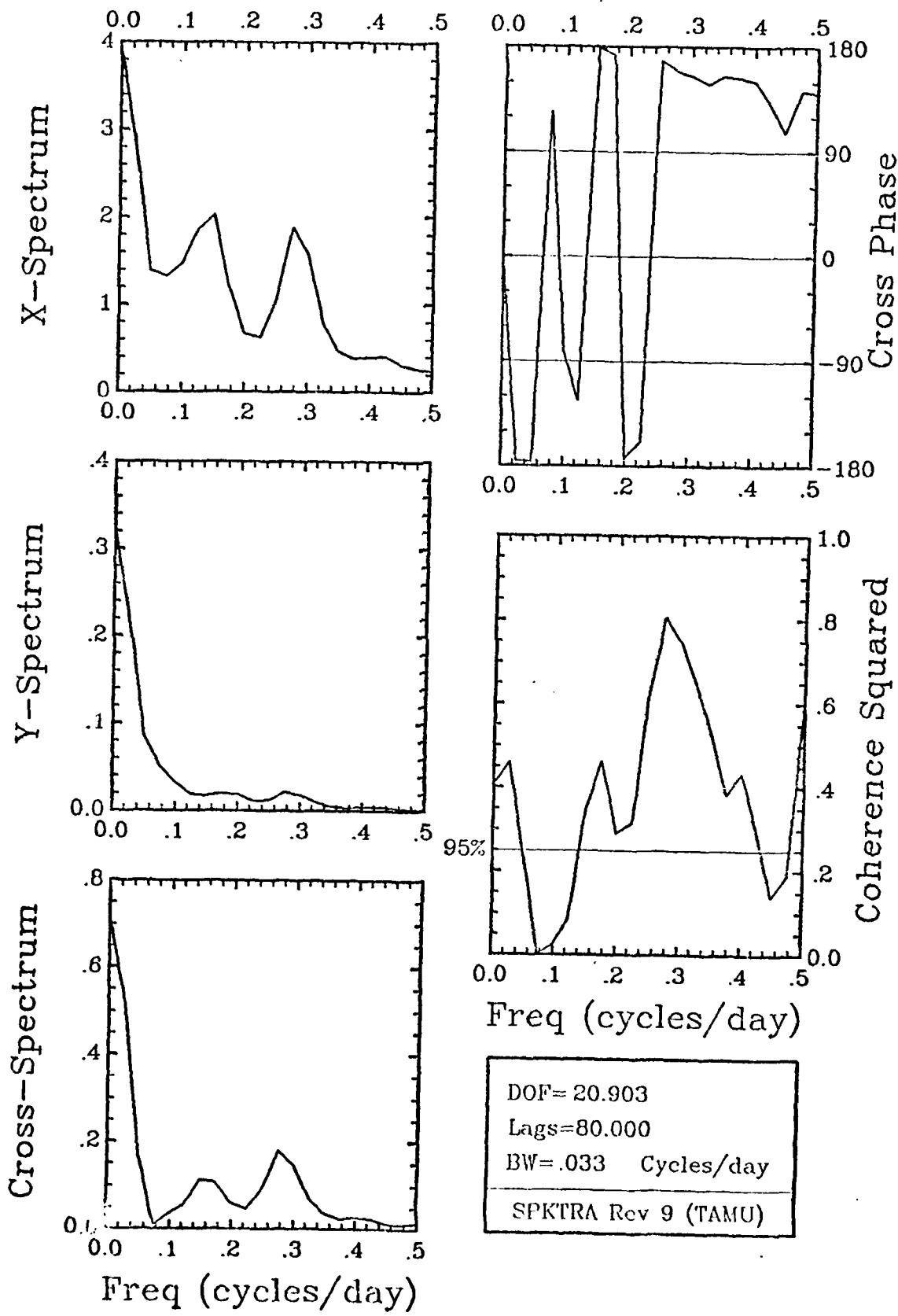
DOF = 14.668
Lags = 80.000
BW = .033 Cycles/day
SPKTRA Rev 9 (TAMU)

V-Stress_{NDBO} / B_BV

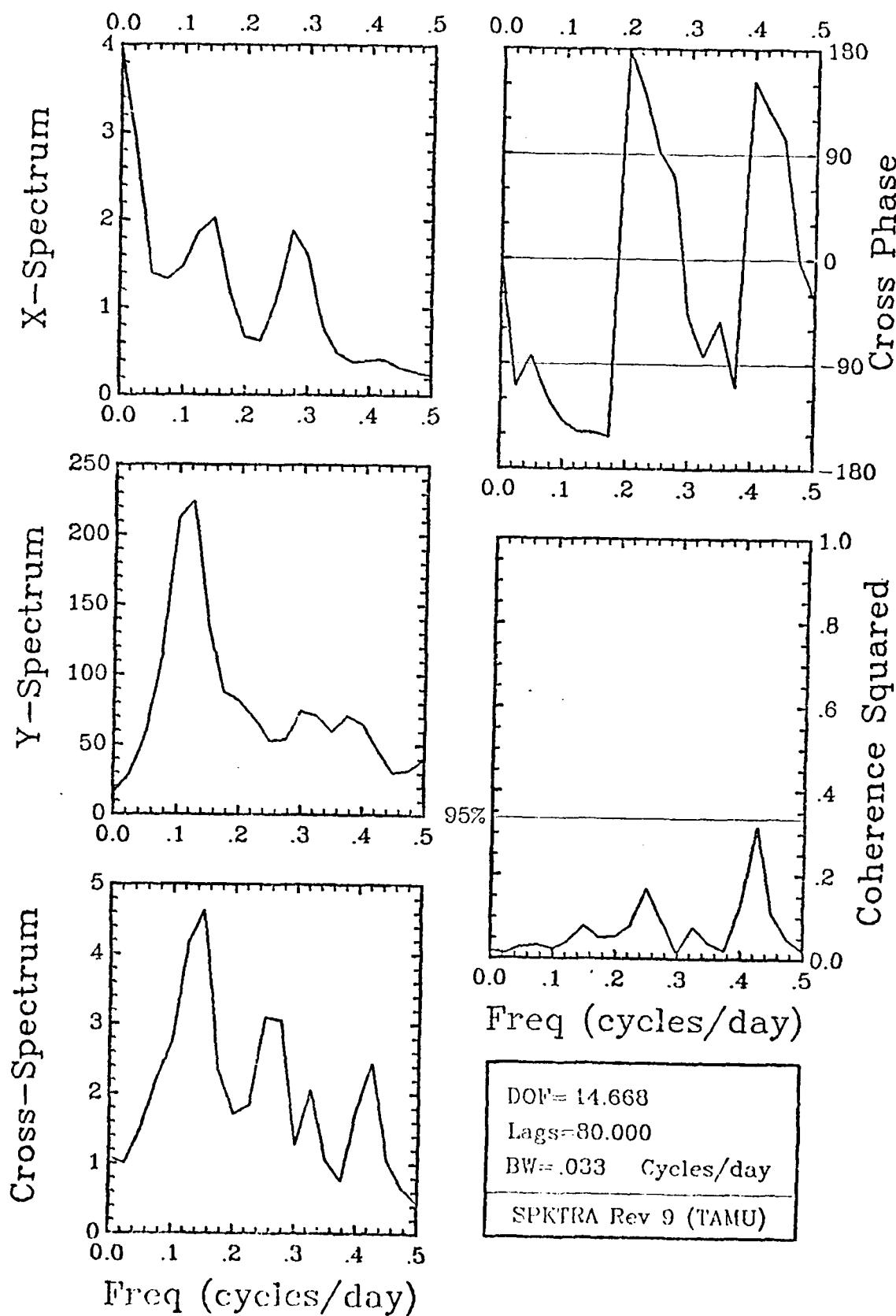
Winter 40 HR LP



U-Stress_{NDBO} / ADJ SL_{SPT} Winter 40 HR LP



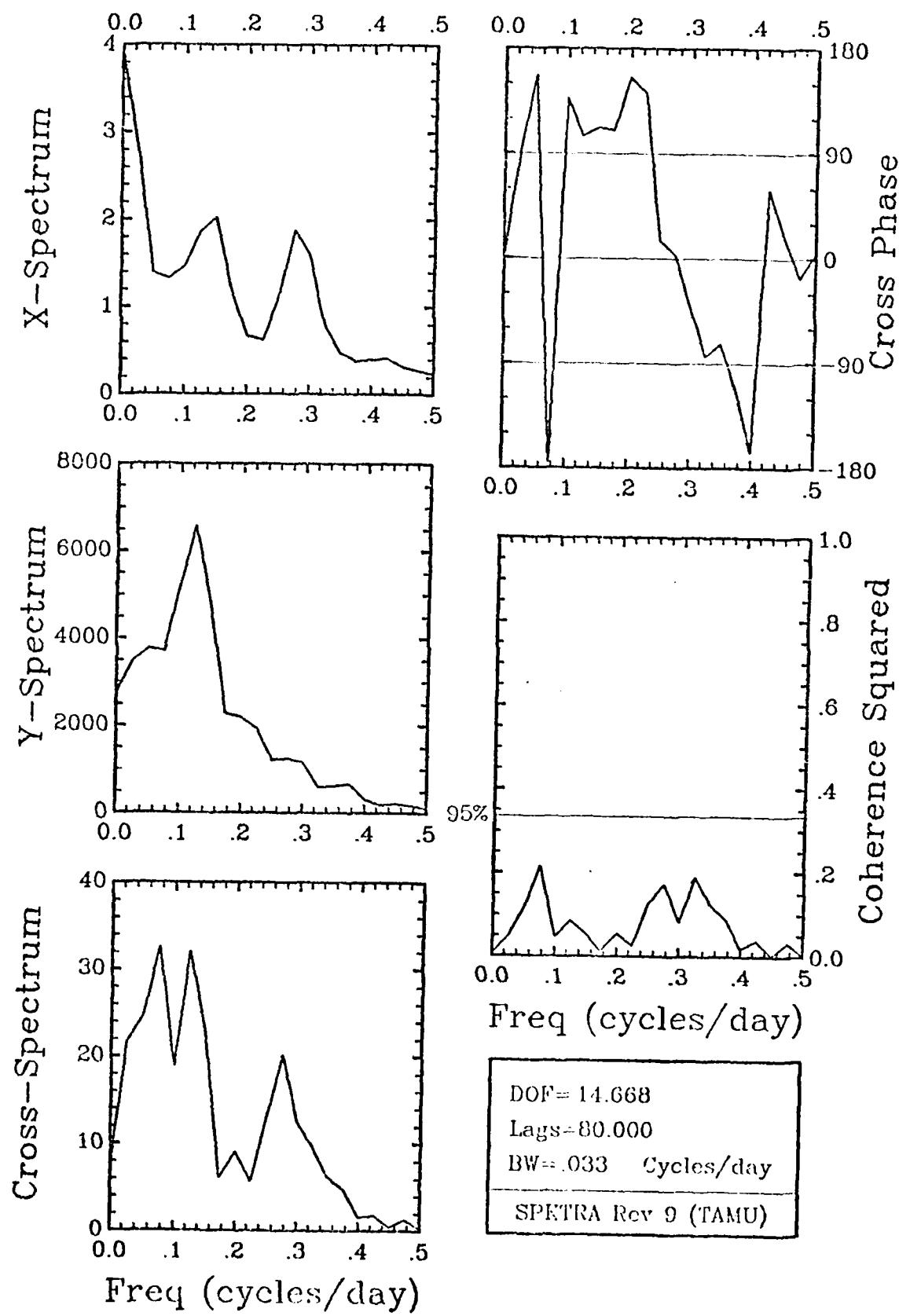
U-Stress_{NDBO} / ADJ SL_{BFT} Winter 40 HR LP



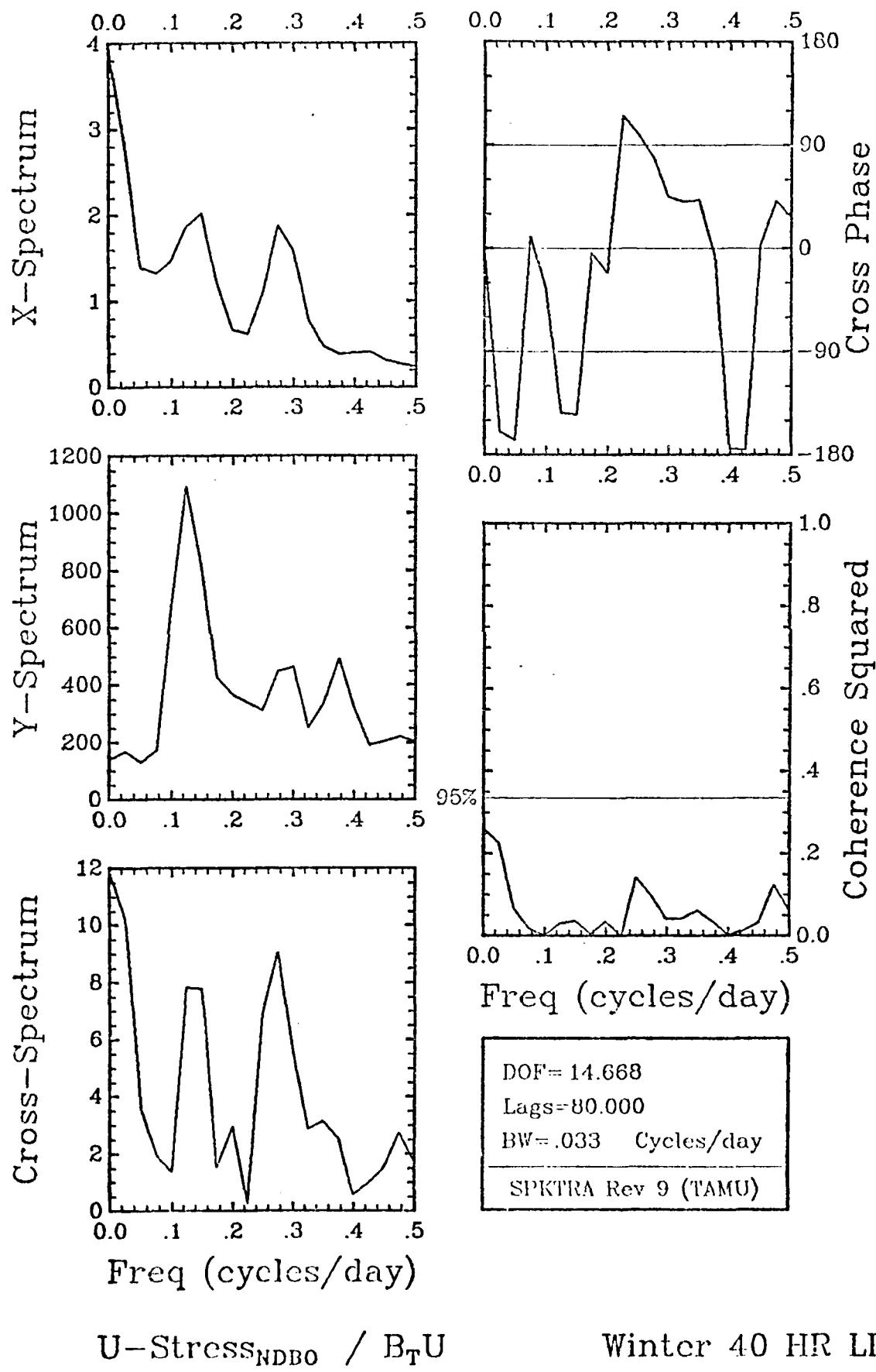
DOF = 14.668
Lags = 80.000
BW = .033 Cycles/day
SPKTRA Rev 9 (TAMU)

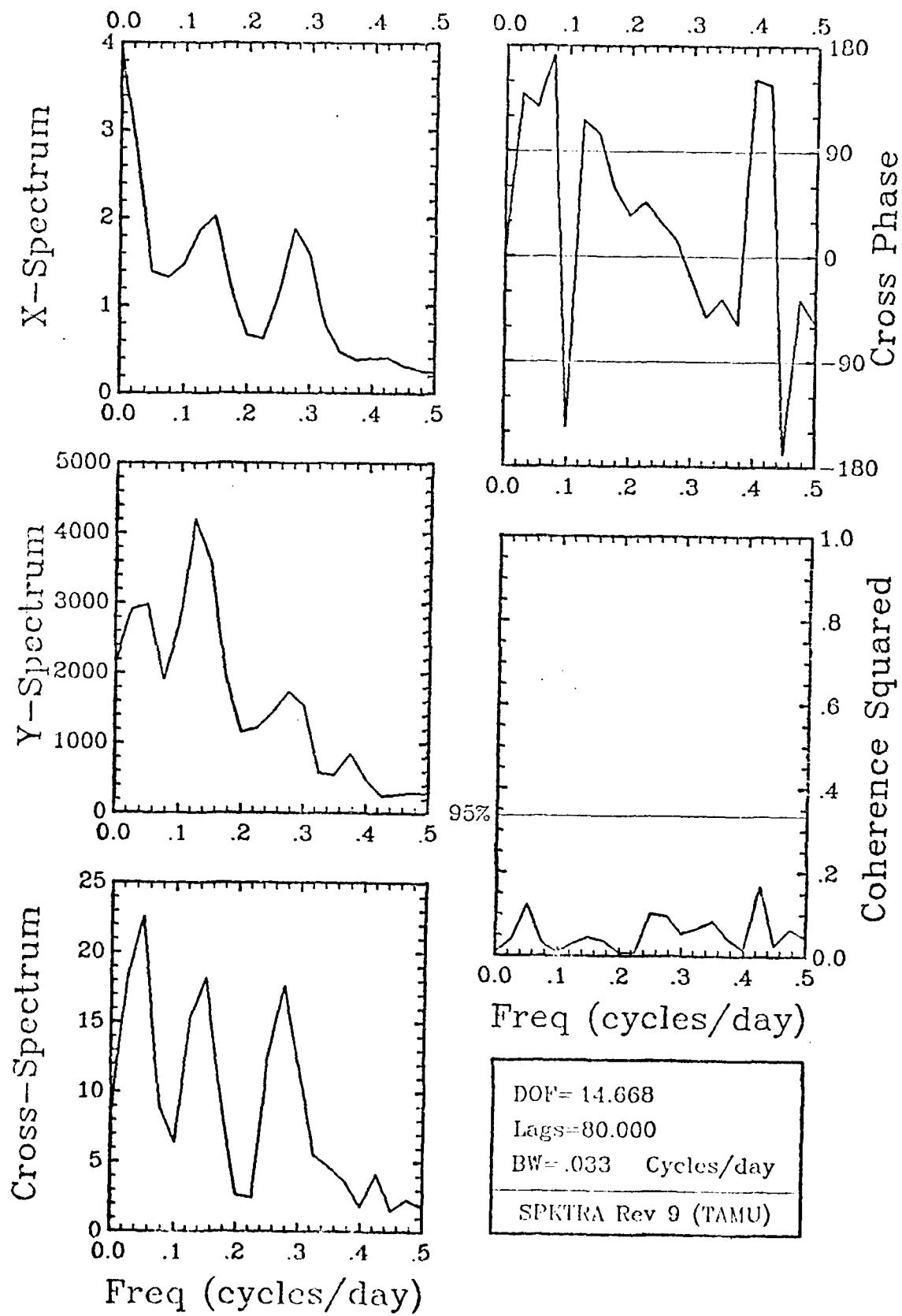
U-Stress_{NDBO} / A_TU

Winter 40 HR LP

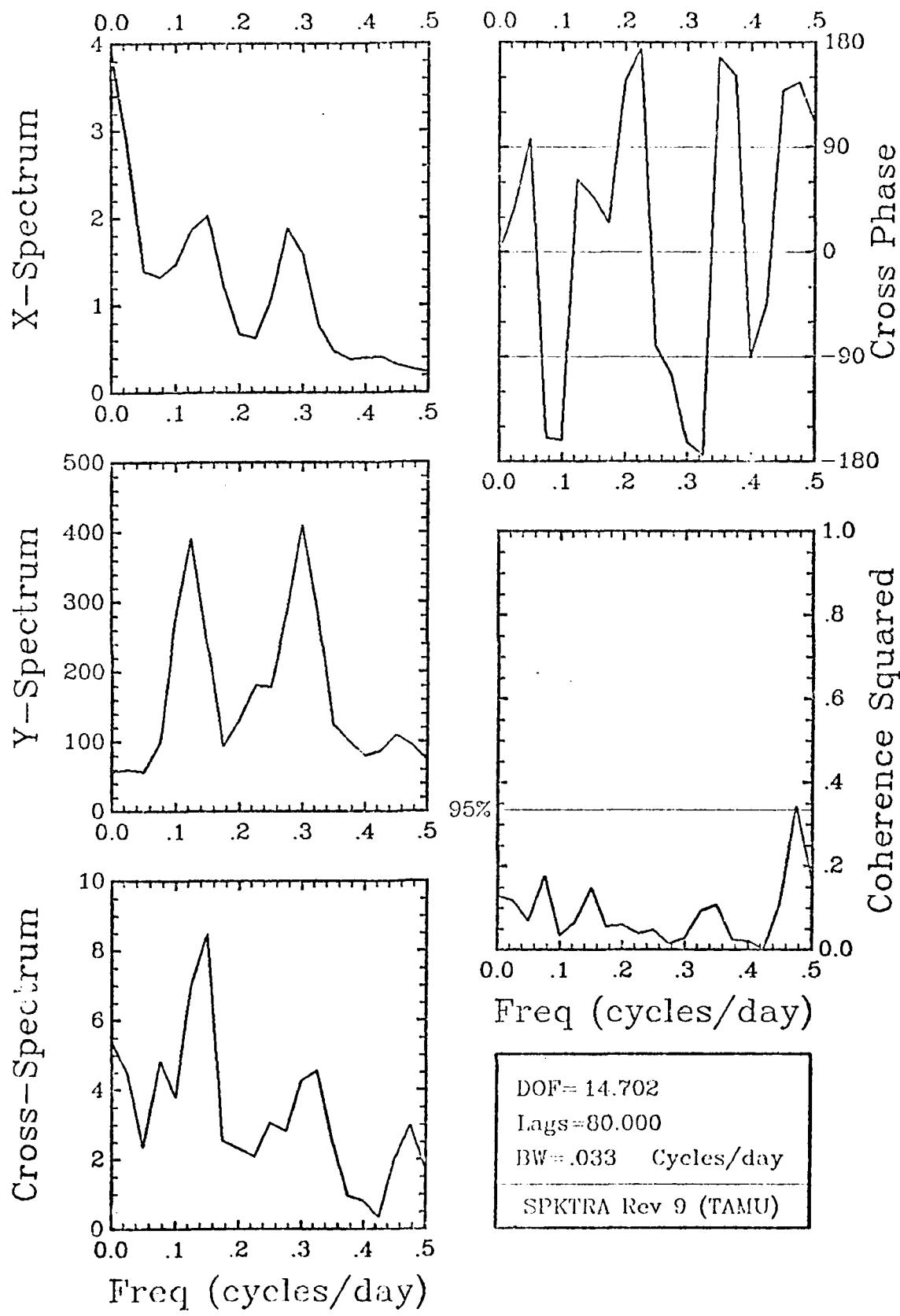
U-Stress_{NDBO} / A_TV

Winter 40 HR LP



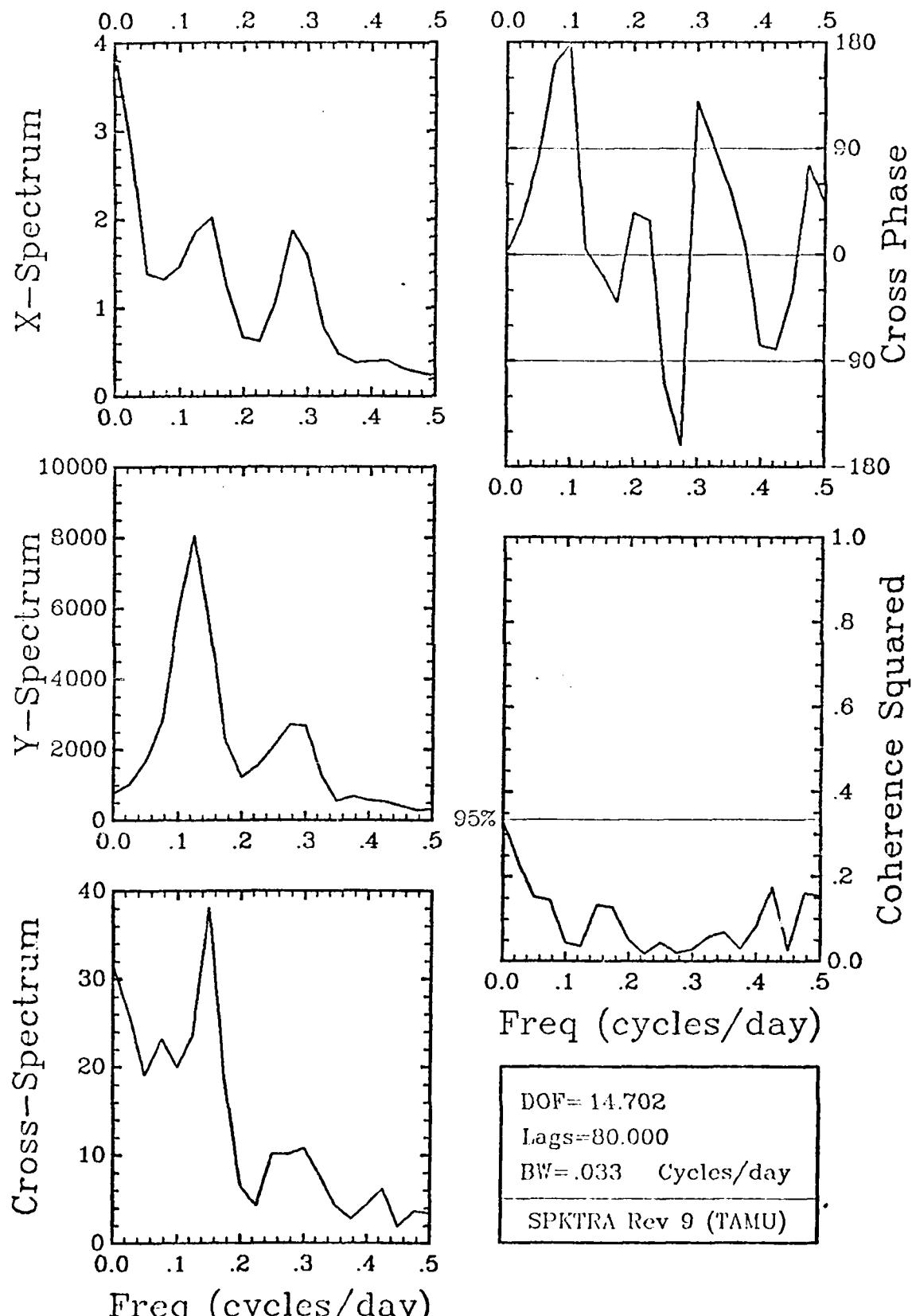
U-Stress_{NDBO} / B_TV

Winter 40 HR LP



U--Stress_{NDBO} / C_TU

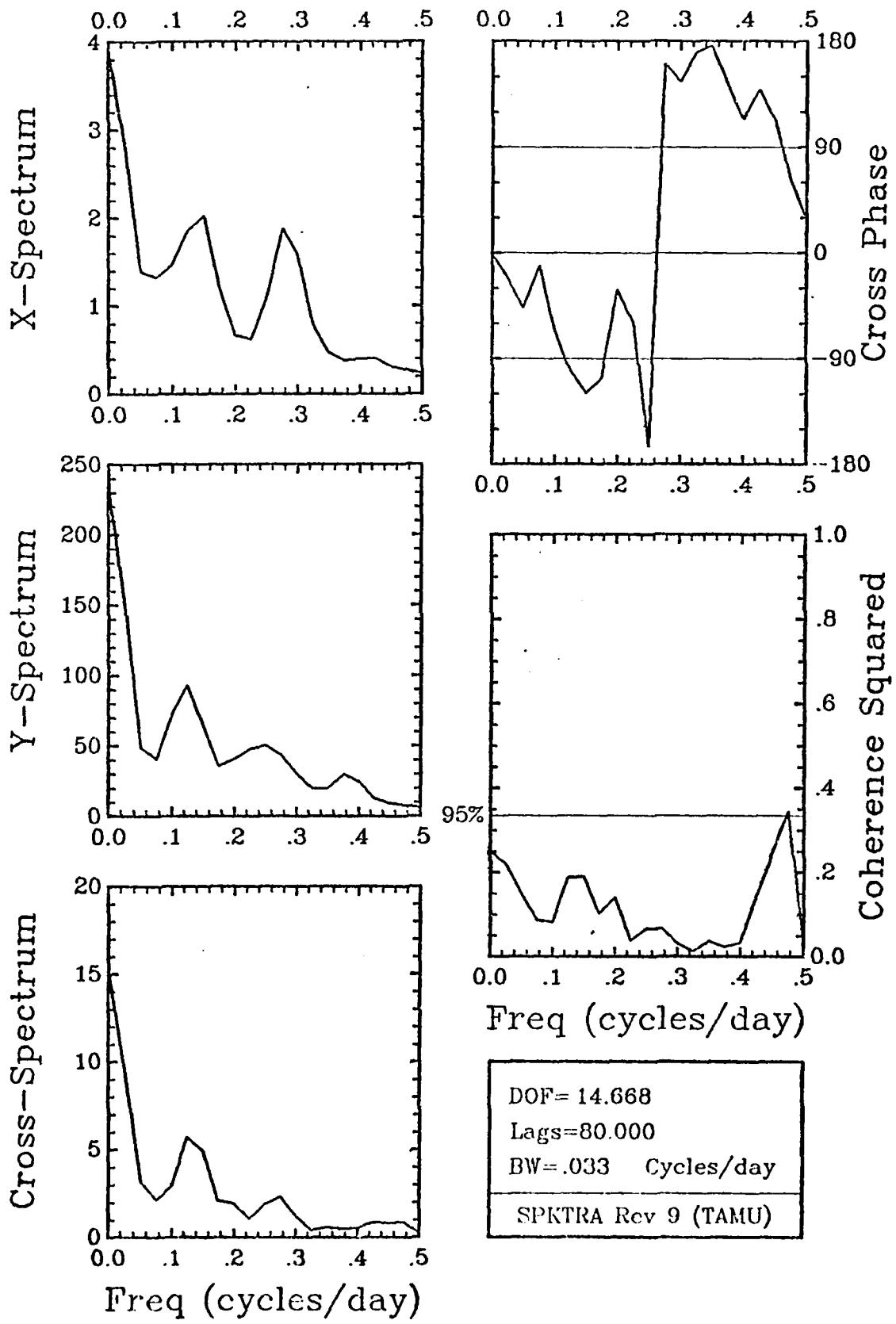
Winter 40 HR LP



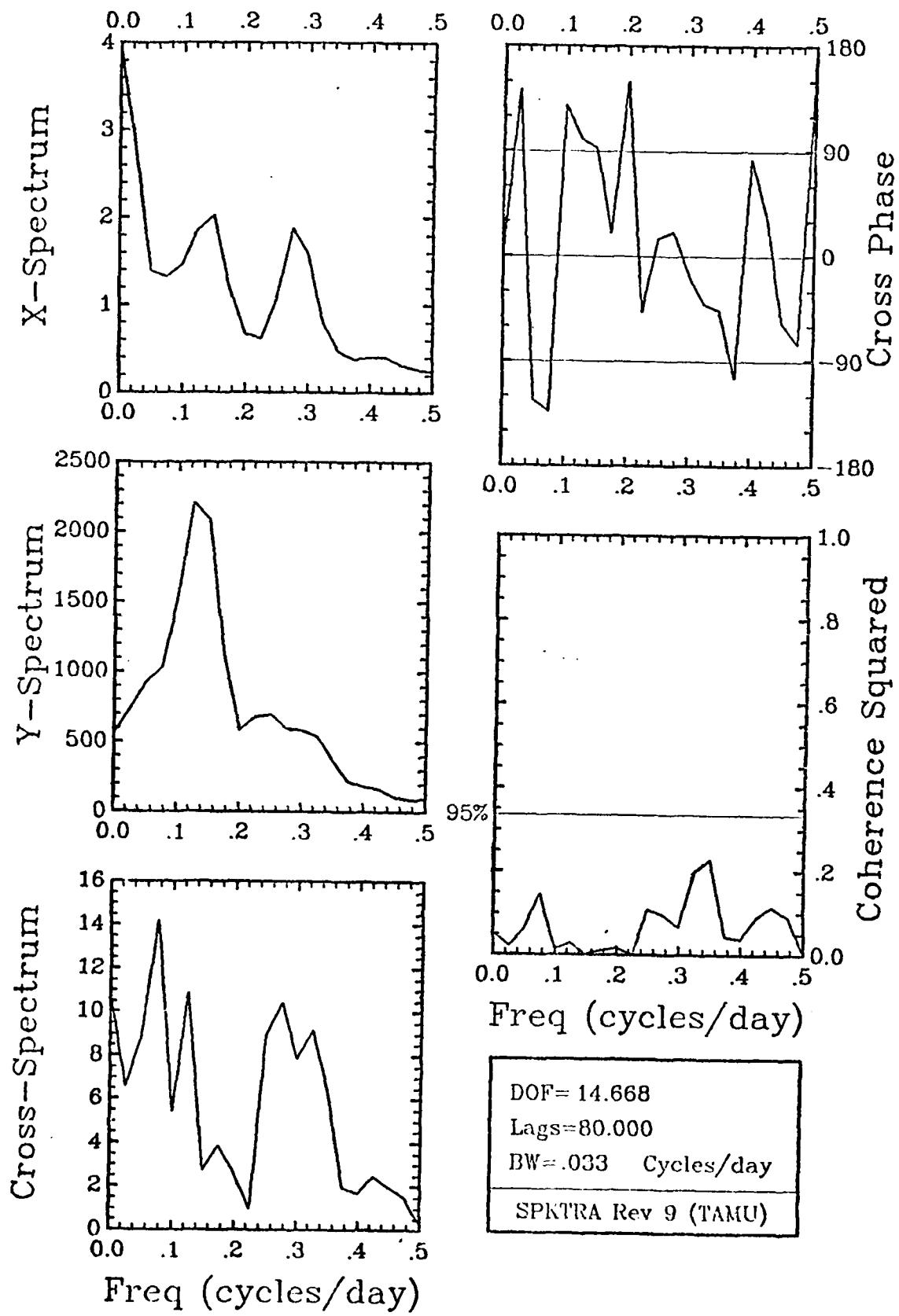
DOF = 14.702
Lags = 80.000
BW = .033 Cycles/day
SPKTRA Rev 9 (TAMU)

U-Stress_{NDBO} / C_TV

Winter 40 HR LP



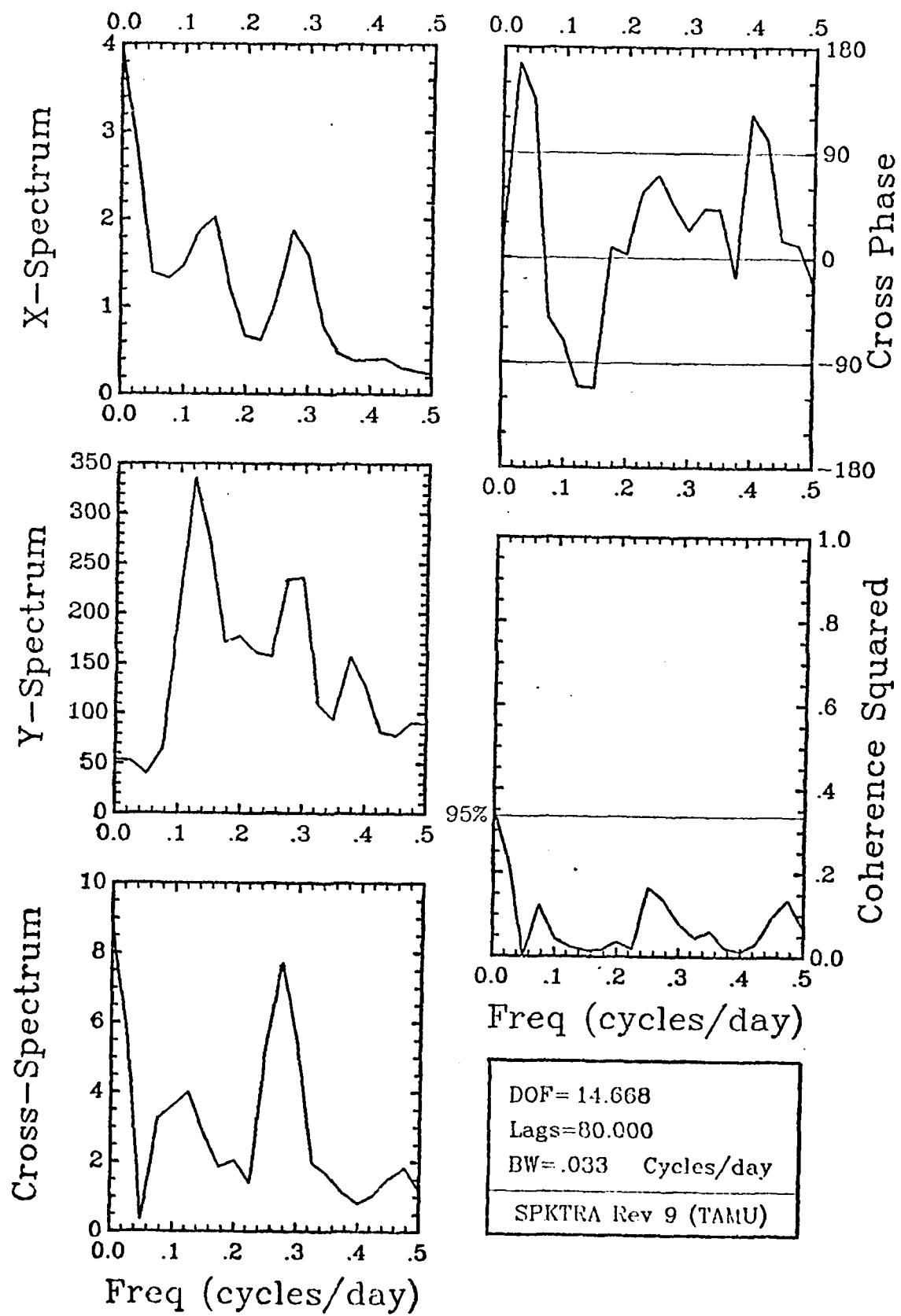
DOF = 14.668
Lags = 80.000
BW = .033 Cycles/day
SPKTRA Rev 9 (TAMU)



DOF = 14.668
Lags = 80.000
BW = .033 Cycles/day
SPKTRA Rev 9 (TAMU)

U-Stress_{NDBO} / A_BV

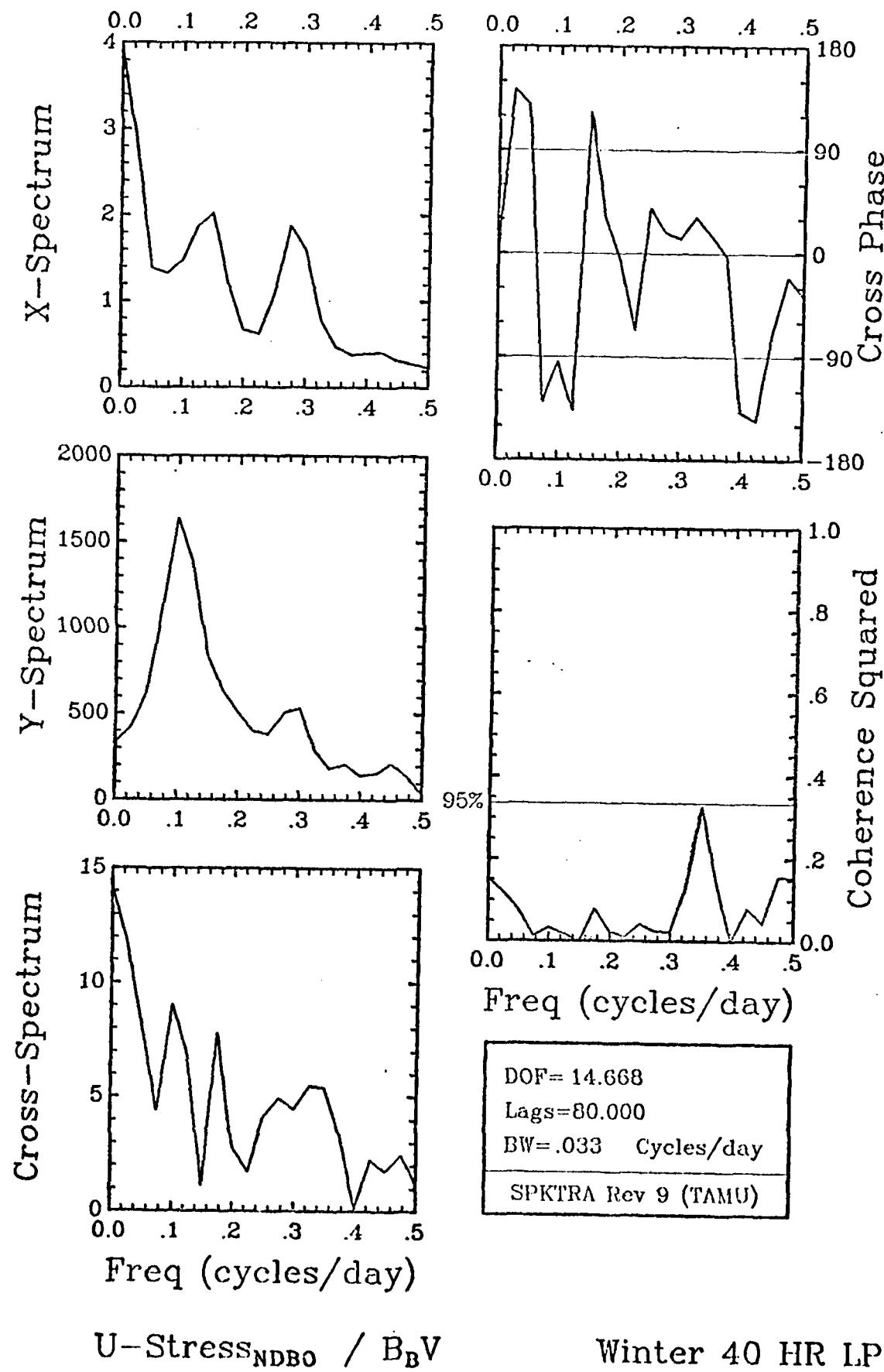
Winter 40 HR LP

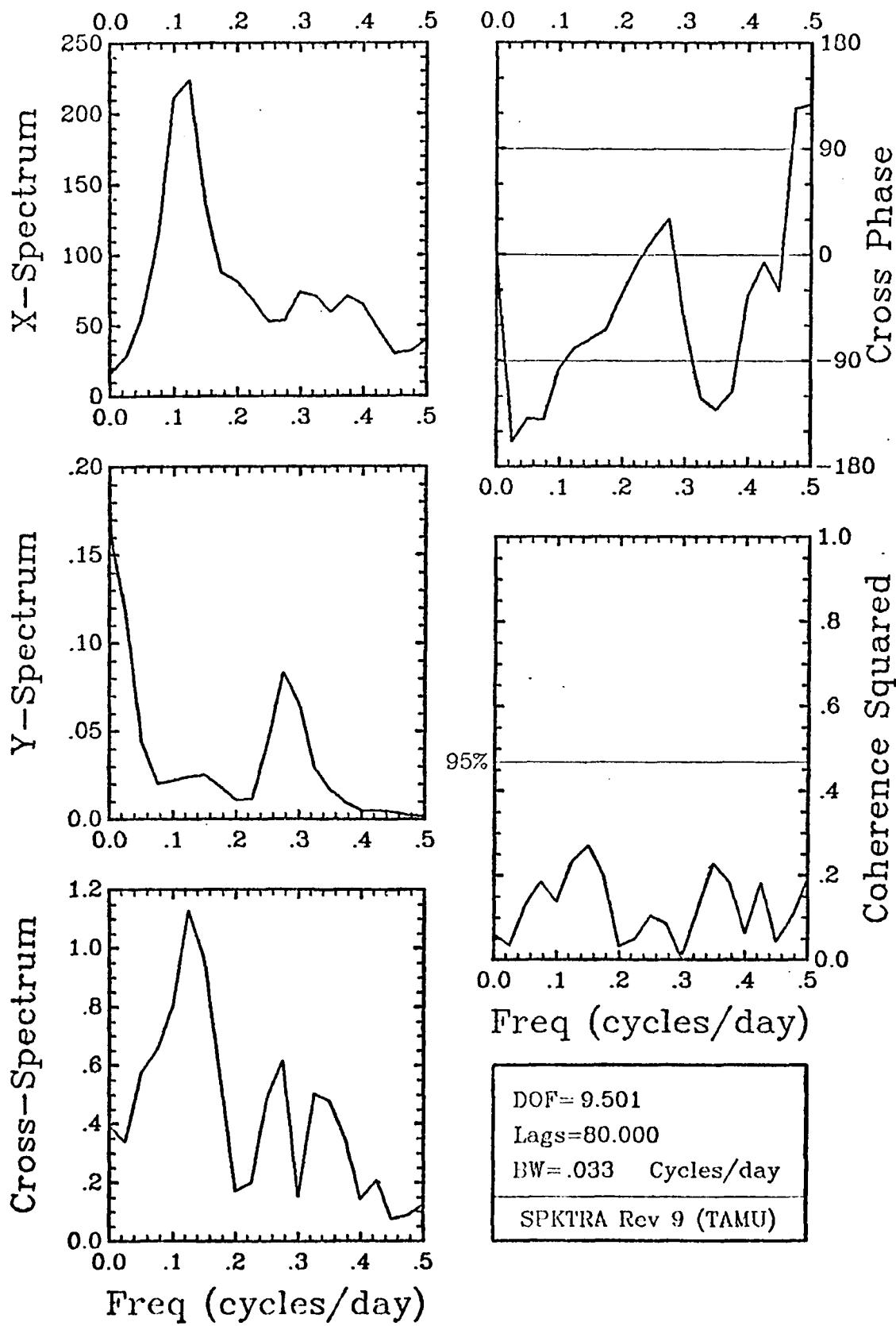


DOF = 14.668
Lags = 80.000
BW = .033 Cycles/day
SPKTRA Rev 9 (TAMU)

U-Stress_{NDBO} / B_BU

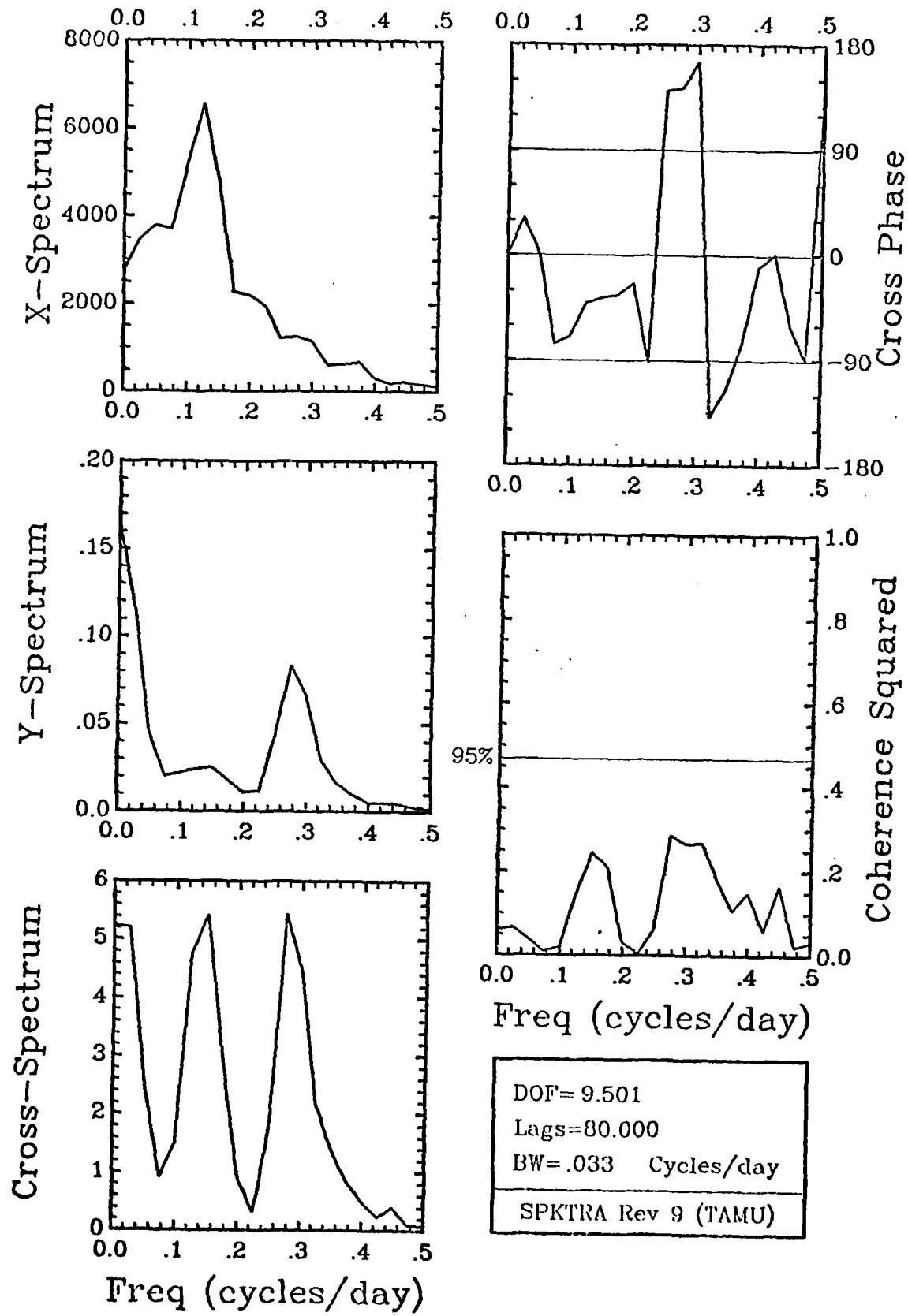
Winter 40 HR LP



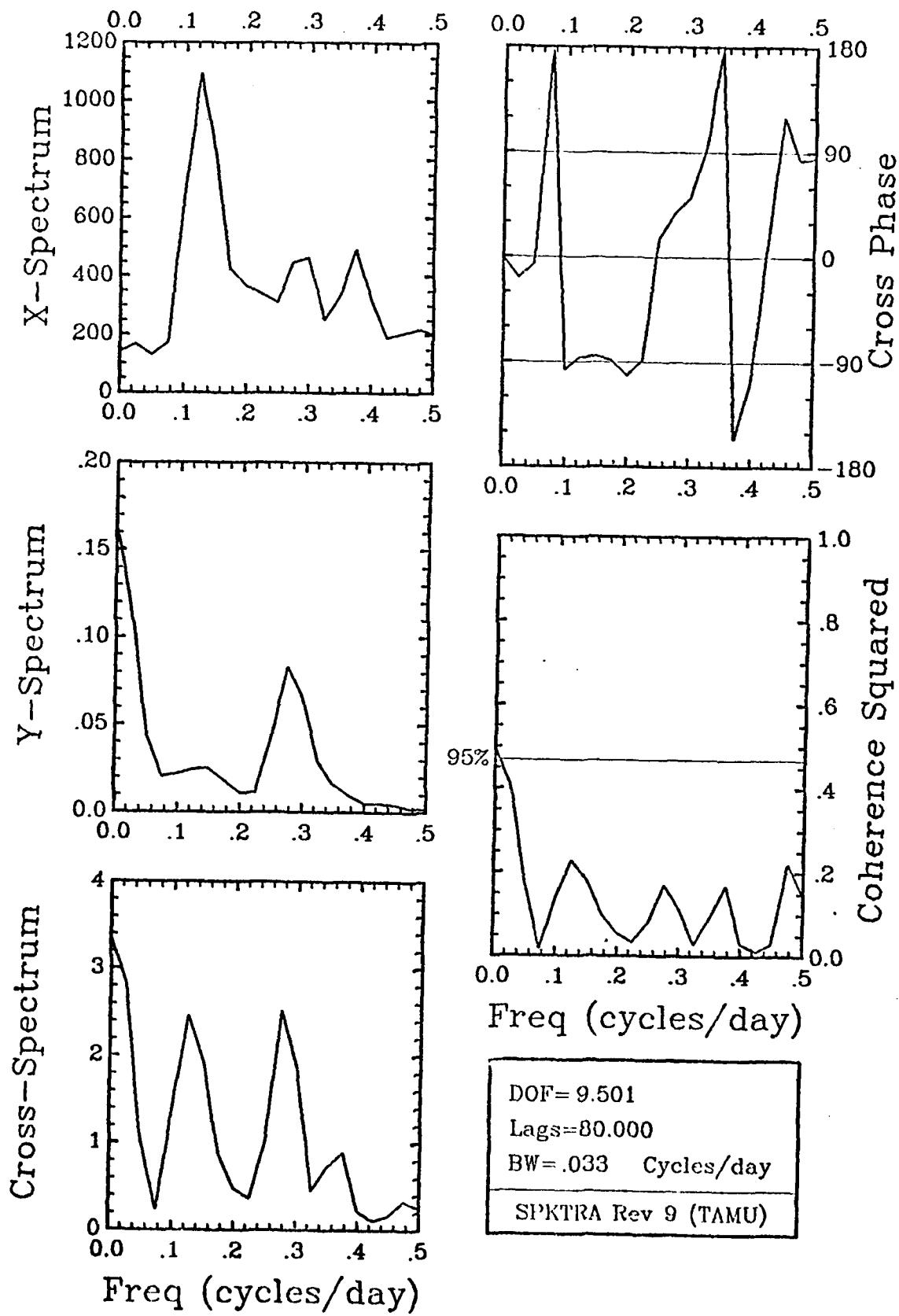


DOF = 9.501
Lags = 80.000
BW = .033 Cycles/day
SPKTRA Rev 9 (TAMU)

A_TU / ADJ SL_{SPT} Winter 40 HR LP

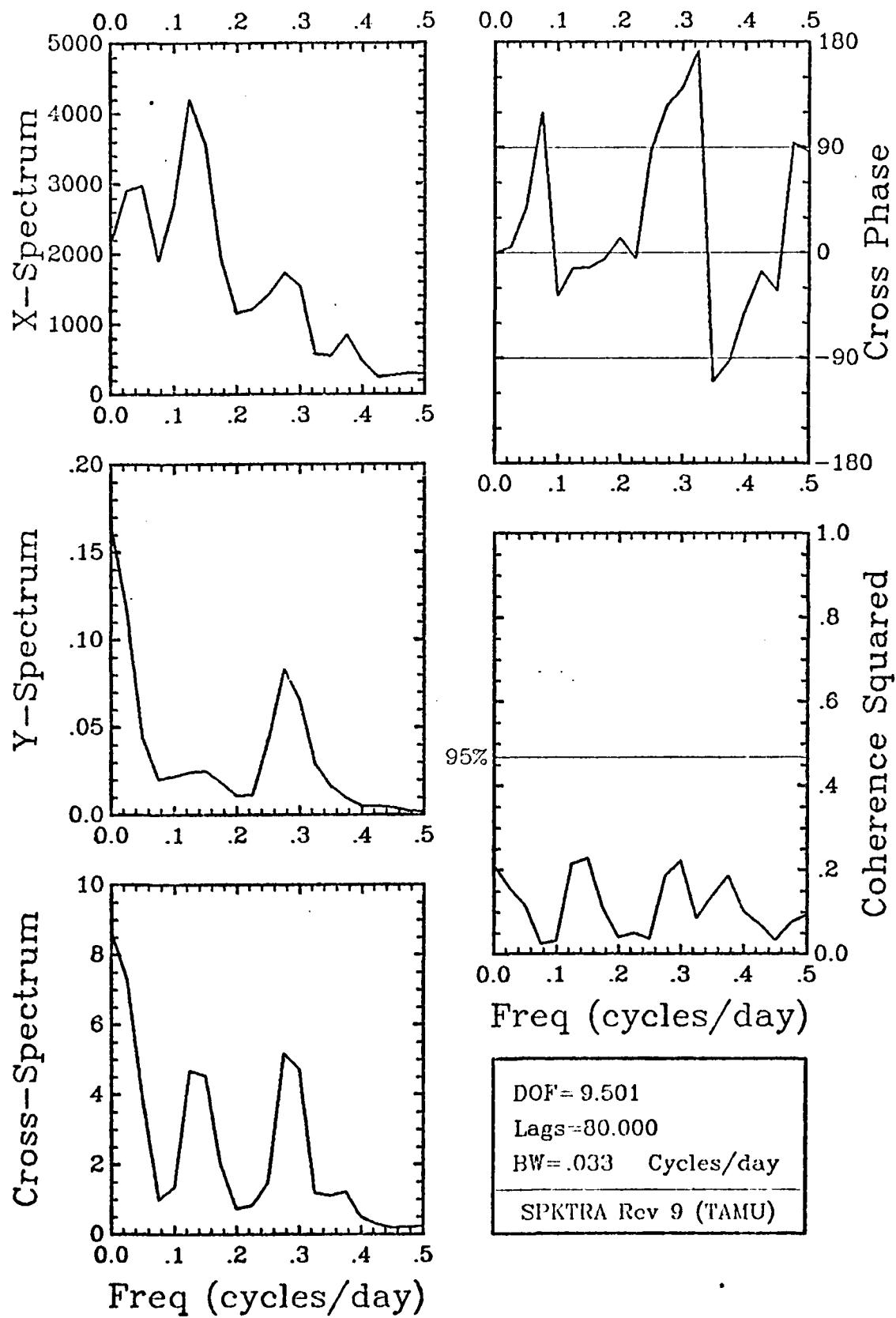


$A_T V / ADJ \text{ SL}_{SPT}$ Winter 40 HR LP

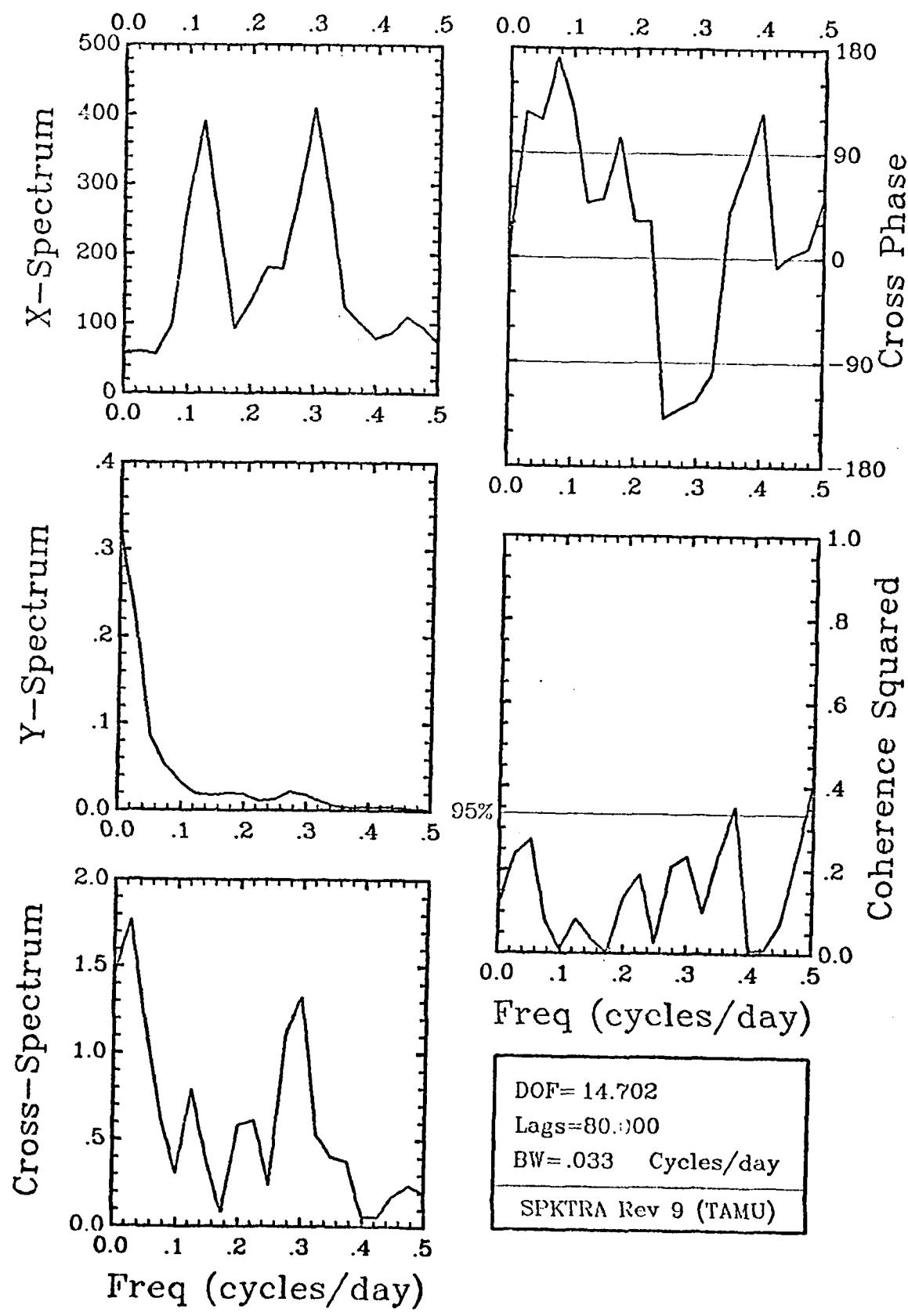


DOF = 9.501
Lags = 80.000
BW = .033 Cycles/day
SPKTRA Rev 9 (TAMU)

B_TU / ADJ SL_{SPT} Winter 40 HR LP

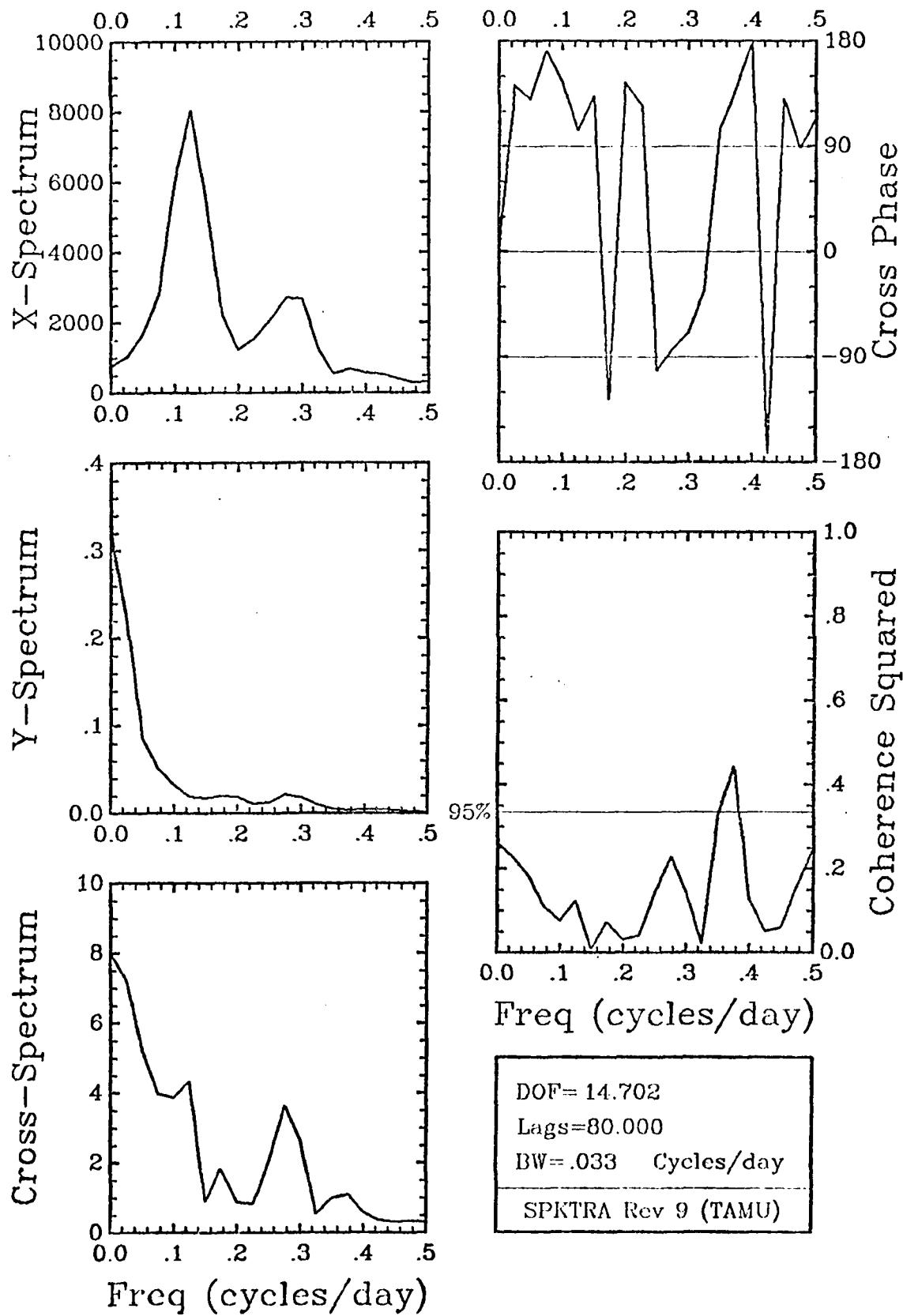


$B_T V / ADJ \text{ SL}_{SPT}$ Winter 40 HR LP



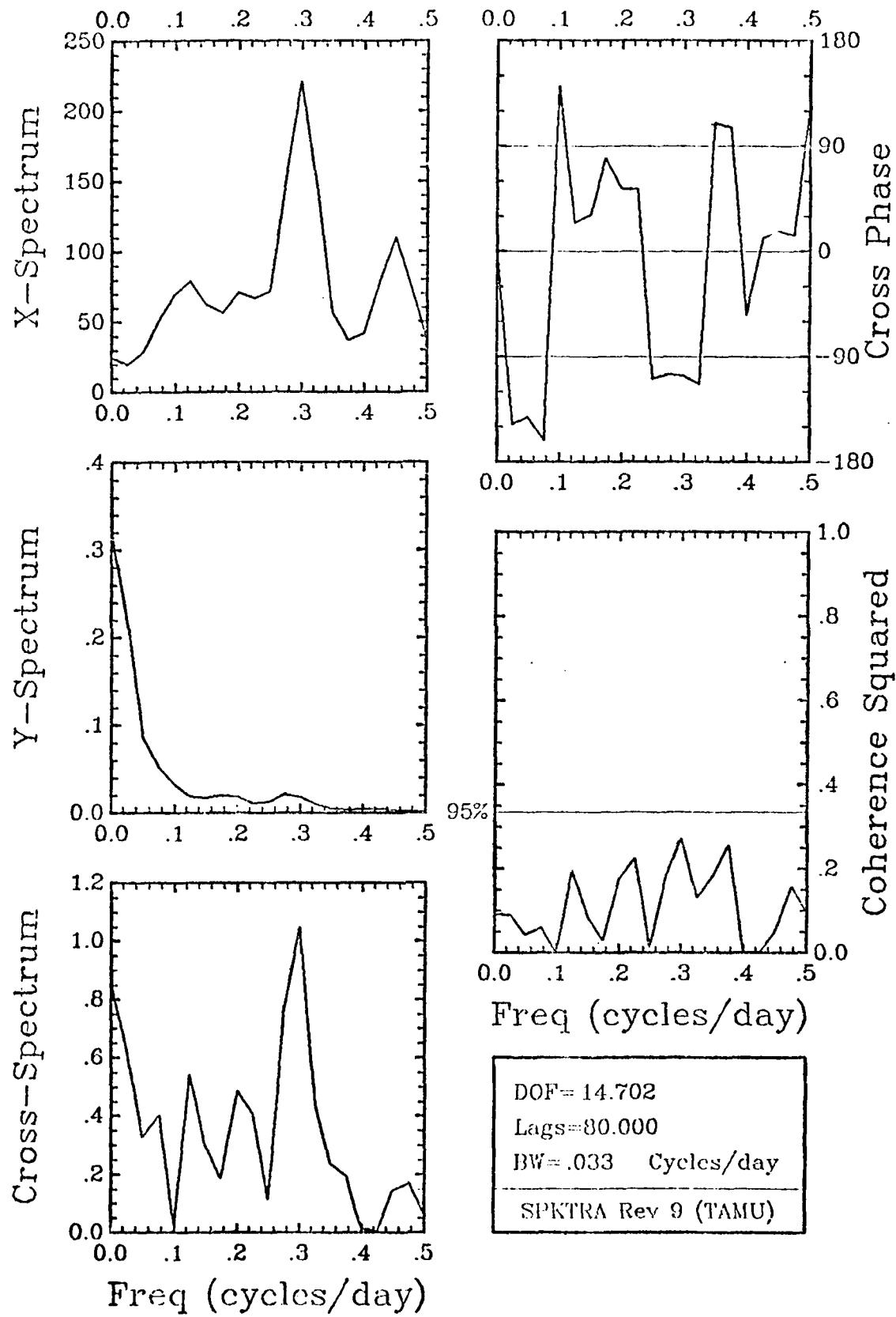
DOF = 14.702
Lags = 80.000
BW = .033 Cycles/day
SPKTRA Rev 9 (TAMU)

$C_T U / ADJ \text{ SL}_{BFT}$ Winter 40 HR LP

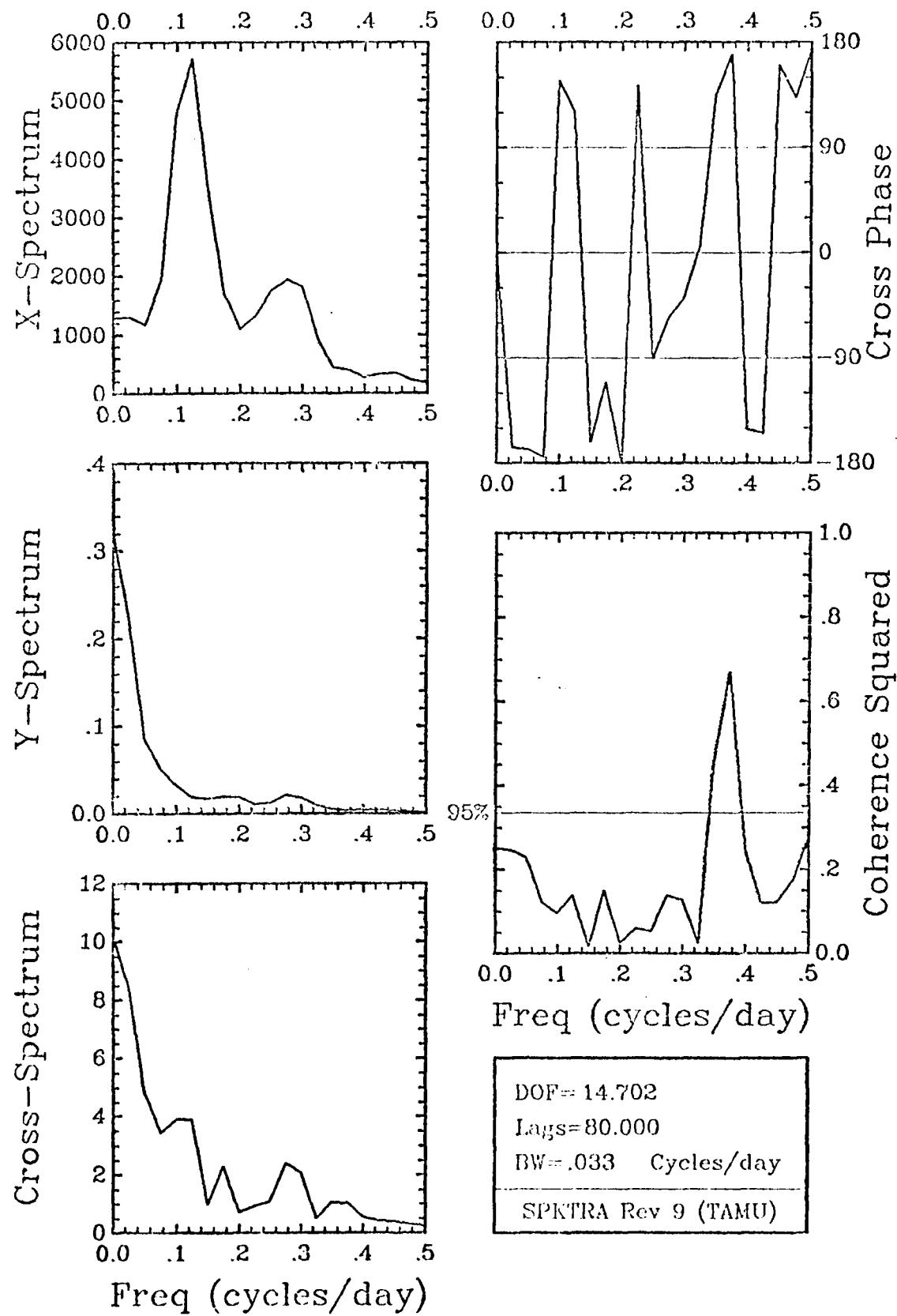


DOF = 14.702
Lags = 80.000
BW = .033 Cycles/day
SPKTRA Rev 9 (TAMU)

C_TV / ADJ SL_{BFT} Winter 40 HR LP



D_MU / ADJ SL_{BFT} Winter 40 HIR LP



DOF = 14.702
Lags = 80.000
BW = .033 Cycles/day
SPKTRA Rev 9 (TAMU)

D_MV / ADJ SL_{BFT} Winter 40 HR LP

Acknowledgments

The Gulf Stream Meanders Experiment was supported by the National Science Foundation, grant numbers OCE 77-25682 and OCE 79-06710; and by the office of Naval Research, contract number N-00014-77-C-0354. The successful deployment and recovery of current meter moorings was in large part due to the efforts of Mr. Paul Blankinship, aided by Messrs. David Leech and Mitch Malpass. We extend our appreciation to Captain Herb Bennett and the crew of the R/V *Endeavor* for expert service at sea. The delicate task of Aanderaa data tape transcription was greatly aided by Mr. Lawrence Ives, who designed and built an interface device for the purpose. Innumerable details associated with carrying out this project were attended to by graduate students at Texas A&M University, the University of North Carolina, and North Carolina State University, without whose help this experiment would not have been possible. The computer graphics and text editing software utilized in this report were implemented by Mr. Tom Reid, who also expertly directed the tedious file maintenance and data editing chores. Ms. Florace Kling painstakingly typed the tables, and Ms. Laura Haines endured the prototype stages of the computer text editing procedure. We thank Dr. Richard Legeckis of NOAA/NESS for providing us with the satellite cover photo, which makes the motivation for this experiment clear in an instant.

References

- Brooks, D. A., 1976 (Editor): Fast and EaSy Time Series Analysis at NCSU. Technical Report, Center for Marine and Coastal Studies, North Carolina State University, Raleigh.
- Brooks, D. A. and J. M. Bane, Jr., 1980: Gulf Stream meanders: Observations of their formation, structure, propagation, and energetics from Charleston to Cape Hatteras. *J. Phys. Oceanogr.* (submitted).
- Brooks, D. A., J. M. Bane, Jr., and M. J. Ignaszewski, 1980: The Gulf Stream meanders Experiment. Hydrographic Data Report, R/V Endeavor cruises EN-031 and EN-037. Texas A&M University, Rep. 80-1-T, 145 pp.
- Düing, W., 1973: Observations and first results from project SYNOPS 71. Technical Report No. UM-RSMAS-73010, University of Miami, Florida, 134 pp.
- Lee, T. N. and R. L. Shutts, 1977: Technical program for Aanderaa current meter moorings on continental shelves. University of Miami, Technical Report No. TR-77-5.
- Institute of Oceanography of Great Britain and Unesco, 1971: *World Oceanographic Table*, Volume 1. NIO, Wormley, England, 128

Richardson, W. S., W. J. Schmitz, Jr., and P. P. Niiler, 1969: The velocity structure of the Florida Current from the Straits of Florida to Cape Fear. *Deep-Sea Res.*, 16 (Suppl.), 225-231.

Webster, R., 1961a: A description of Gulf Stream meanders off Onslow Bay. *Deep-Sea Res.*, 9, 130-143.

_____, 1961b: The effect of meanders on the kinetic energy balance of the Gulf Stream. *Tellus*, 13, 392-401.

Weyl, P. K., 1964: On the change in electrical conductance of seawater with temperature. *Limnol. Oceanogr.*, 9, 75-78.

SECURITY CLASSIFICATION OF THIS PAGE (If Data Entered)

READ INSTRUCTIONS
BEFORE COMPLETING FORM

REPORT DOCUMENTATION PAGE		
1. REPORT NUMBER 80-7-T	2. GOVT ACCESSION NO. AD-A088 669	3. RECIPIENT'S CATALOG NUMBER
4. TITLE (and Subtitle) THE GULF STREAM MEANDERS EXPERIMENT Current Meter, Atmospheric, and Sea Level Data Report for the January to May, 1979 Mooring Period		5. TYPE OF REPORT & PERIOD COVERED Data Report
7. AUTHOR(s) David A. Brooks, John M. Bane, Robert L. Cohen, Paul Blankinship		6. PERFORMING ORG. REPORT NUMBER B. CONTRACT OR GRANT NUMBER(s) ONR: N-00014-77-C-0354 NSF: OCE79-06710 **see block 18
9. PERFORMING ORGANIZATION NAME AND ADDRESS Texas A&M University Department of Oceanography College Station, TX 77843		10. PROGRAM ELEMENT, PROJECT, TASK AREA & WORK UNIT NUMBERS
11. CONTROLLING OFFICE NAME AND ADDRESS Office of Naval Research 800 N. Quincy Street Arlington, VA 22217		12. REPORT DATE July 1980
14. MONITORING AGENCY NAME & ADDRESS (if different from Controlling Office)		13. NUMBER OF PAGES 264
		15. SECURITY CLASS. (of this report) Unclassified
		15a. DECLASSIFICATION/DOWNGRADING SCHEDULE
16. DISTRIBUTION STATEMENT (of this Report) Approved for public release, distribution unlimited		
17. DISTRIBUTION STATEMENT (of the abstract entered in Block 20, if different from Report)		
18. SUPPLEMENTARY NOTES ** Jointly sponsored by NSF and ONR		
19. KEY WORDS (Continue on reverse side if necessary and identify by block number) Current meters, Gulf Stream, Meanders		
20. ABSTRACT (Continue on reverse side if necessary and identify by block number) Current, sea level, and atmospheric data from the Gulf Stream region off North Carolina for the period January - May 1979 are documented in this data report.		

END

DATE

FILMED

9-80

DTIC